



HAL
open science

Nanosystèmes hybrides pour la délivrance intestinale

Annalisa Rosso

► **To cite this version:**

Annalisa Rosso. Nanosystèmes hybrides pour la délivrance intestinale. Pharmacology. Université de Lyon, 2020. English. NNT : 2020LYSE1288 . tel-03461285

HAL Id: tel-03461285

<https://theses.hal.science/tel-03461285v1>

Submitted on 1 Dec 2021

HAL is a multi-disciplinary open access archive for the deposit and dissemination of scientific research documents, whether they are published or not. The documents may come from teaching and research institutions in France or abroad, or from public or private research centers.

L'archive ouverte pluridisciplinaire **HAL**, est destinée au dépôt et à la diffusion de documents scientifiques de niveau recherche, publiés ou non, émanant des établissements d'enseignement et de recherche français ou étrangers, des laboratoires publics ou privés.



N° d'ordre NNT : 2020LYSE1288

THESE de DOCTORAT DE L'UNIVERSITE DE LYON

opérée au sein de
l'Université Claude Bernard Lyon 1

**Ecole Doctorale EDISS 205
(Ecole Doctorale Interdisciplinaire Sciences-Santé)**

**Spécialité de doctorat : Sciences pharmaceutiques
Discipline : Pharmacotechnie et Biopharmacie**

Soutenue publiquement le 16/12/20, par :
Annalisa ROSSO

Hybrid nanosystems for enhanced intestinal delivery

Nanosystèmes hybrides pour la délivrance intestinale

Devant le jury composé de :

DAVID Laurent, Professeur, Université de Lyon	Président
LUCIANI Paola, Professeur, Université de Bern	Rapporteuse
VAN NOSTRUM Cornelus F. Rene, Professeur, Université de Utrecht	Rapporteur
GOYCOOLEA Francisco, Professeur, Université de Leeds	Examineur
MARLOW Maria, Professeur, Université de Nottingham	Examinatrice
NANCEY Stephane, Professeur-Praticien Hospitalier, Université de Lyon	Examineur
BRIANCON Stéphanie, Professeur, Université de Lyon	Directrice de thèse
LOLLO Giovanna, Maître de conférences, Université de Lyon	Co-directrice de thèse

Université Claude Bernard – LYON 1

Administrateur provisoire de l'Université	M. Frédéric FLEURY
Président du Conseil Académique	M. Hamda BEN HADID
Vice-Président du Conseil d'Administration	M. Didier REVEL
Vice-Président du Conseil des Etudes et de la Vie Universitaire	M. Philippe CHEVALLIER
Vice-Président de la Commission de Recherche	M. Jean-François MORNEX
Directeur Général des Services	M. Pierre ROLLAND

COMPOSANTES SANTE

Département de Formation et Centre de Recherche en Biologie Humaine	Directrice : Mme Anne-Marie SCHOTT
Faculté d'Odontologie	Doyenne : Mme Dominique SEUX
Faculté de Médecine et Maïeutique Lyon Sud - Charles Mérieux	Doyenne : Mme Carole BURILLON
Faculté de Médecine Lyon-Est	Doyen : M. Gilles RODE
Institut des Sciences et Techniques de la Réadaptation (ISTR)	Directeur : M. Xavier PERROT
Institut des Sciences Pharmaceutiques et Biologiques (ISBP)	Directrice : Mme Christine VINCIGUERRA

COMPOSANTES & DEPARTEMENTS DE SCIENCES & TECHNOLOGIE

Département Génie Electrique et des Procédés (GEP)	Directrice : Mme Rosaria FERRIGNO
Département Informatique	Directeur : M. Behzad SHARIAT
Département Mécanique	Directeur M. Marc BUFFAT
Ecole Supérieure de Chimie, Physique, Electronique (CPE Lyon)	Directeur : Gérard PIGNAULT
Institut de Science Financière et d'Assurances (ISFA)	Directeur : M. Nicolas LEBOISNE
Institut National du Professorat et de l'Education	Administrateur Provisoire : M. Pierre CHAREYRON
Institut Universitaire de Technologie de Lyon 1	Directeur : M. Christophe VITON
Observatoire de Lyon	Directrice : Mme Isabelle DANIEL
Polytechnique Lyon	Directeur : Emmanuel PERRIN
UFR Biosciences	Administratrice provisoire : Mme Kathrin GIESELER
UFR des Sciences et Techniques des Activités Physiques et Sportives (STAPS)	Directeur : M. Yannick VANPOULLE
UFR Faculté des Sciences	Directeur : M. Bruno ANDRIOLETTI

A mio padre

“What I love about science is that as you learn, you don’t really get answers. You just get better questions.”

John Green

Acknowledgments

This PhD has been a demanding but rewarding journey. I want to take a moment to thank all the ones who helped me along the way.

First and foremost, I would like to thank my thesis advisor, Giovanna. During these years you have taught me a lot, both professionally and humanly. I know that dealing with me can be hard, but you never gave up on me and tried to find a way with your patience to meet the challenges together. I will always be grateful for your dedication to me, to this work and for your wise advises. Being your first PhD student has been a big responsibility and a great pleasure, I hope I made you proud.

I would like to express my sincere thanks to my thesis advisor, Pr. Stéphanie Briançon for welcoming me in her laboratory and for her insight and guidance over the course of my PhD studies. To my reviewers, Pr. Paola Luciani and Pr. Rene van Nostrum, thank you for your time and attention in reading and considering my thesis work. And to my jury, Pr. Francisco Goycoolea, Pr. Maria Marlow, Pr. Stephane Nancey, thank you for evaluating this work and for your professional input. To Pr. Laurent David thanks not only for presiding the jury but also for your time and feedback at each stage of my PhD.

I would like to acknowledge the EDISS doctoral school for funding my thesis fellowship.

Thanks to Alexandra and Ofelia for believing in me and fostering my development as a scientist. A great thanks to Yves, Eyad, Claire, David, Samira and Nouredine for the opportunity to work with them. Your suggestions pushed me to see this work from different perspectives, and to implement my knowledge and research plan.

Jacqueline, this PhD would not have been the same without all mice and nice moments spent together. I am grateful for your enthusiasm and your help.

Thanks to Ana Grenha for welcoming in her laboratory in Portugal and to Filipa for all they have taught me with patience and good spirit.

I want to thank Stephane Giraud, Renno Touffic and Isabelle Coste, for involving me in their project and give me the opportunity to broaden my knowledge.

Thank to Isabelle Kerzaon, Hay De Bettignies Anne-Emmanuelle and Dijoux Franca Marie Genevieve for the chance to teach with them and for the pleasant hours spent together during the TP. My sincere thanks also goes to Barbara Stella for the help in finding this PhD and for the enthusiasm for research you conveyed me.

This work would have not been the same without the Lagepp team. I would like to acknowledge Nadia, Jean-Pierre, Maria, Sebastien, Quentin, Cynthia and Délphine for their technical help and for creating an enjoyable environment in the lab. Géraldine, thanks for your support and dynamism, many things wouldn't have worked out without your help!

To the GePharm group, thanks for sharing your scientific expertise, coffees and patisseries during our morning journal club sessions.

A huge thanks to my PhD friends, Margaux, Ben, Francisco, Sabine, Geoffrey, Amanda and Elena, always ready to help and smile at me when needed and able to cheer me up when I was feeling upset, inside and outside the lab. All our laughs, tears, crazy adventures and Friday night dances will always have a special place in my heart.

To the Italian crew, who is growing day after day. Andrea, Flavia, Letizia, Francesca, Alice, Alvia, Serena, Beatrice, Mathieu, Ilaria, Yoann, Mattia, Daniele, you made me feel home!

Thank you Valentina, not only for collaborating with me on the project, but also for being an example for me and for your inner enthusiasm which spiced things up!

Wei, it was a great pleasure to sit next to you for the last three years. Marine and Julien thanks for sharing part of this PhD adventure, Caco-2 cells and fluorescent measurements are not much of a secret any more. To the master 1 students Soraya, Etienne, Idriss and Chucky, working with you was a great pleasure. Doctor Hamid your smiley saba7 al khayr has been one of the pillar of this PhD.

Jorge, three years have passed and it seems like yesterday we were using Sephadex columns and eating eclairs on the quai to cheer us up. Thanks for being so confident on my future as a researcher, and so proud of me for what I have accomplished during this PhD.

I especially thank my family. Babbo. Thanks for believing in me and giving me the possibility to be where I am. Because of you, I have the vision to reach for my dreams, and the grit to push through the challenges that are in my way. This accomplishment is for you.

Mamma. Thank you for unconditional love, for guiding me when I need advice, and for being there when I need a shoulder to cry on. The example that you set inspires me to be my best self.

Nonno Marco and Chiara, thanks for simply being there for me, all the time.

Thank to my grandmas, nonna Pasqua and nonna Marghe, who are guiding me from above. I hold you in my heart.

To Alessandro, my genius brother who can fix anything and achieve everything he has dreamt of. I am extremely proud of the man you have become.

Many thanks also to my roommate and travel companion Armelle, who lightened my evenings with her infectious lust for life in the year spent together. To Giulia, Katia and Martina, despite the distance you were there for holding me together and giving me smiles.

Lastly, thank to you Mohamad. Your love and patience are the backbone of this PhD thesis. Thank for standing me, for encouraging me in the toughest of times and for celebrating by my side in the best of times. Thanks for making me feel special, thanks for making me strong.

Table of contents

Abstract	5
List of Figures	7
List of Tables.....	11
List of abbreviations	12
General introduction.....	15
Hypothesis and aim of the thesis	16
Bibliographical review	19
Chapter I: The oral route of administration: physiological barriers and drug delivery technologies	21
I.1 Oral drug delivery	21
I.2 Biological challenges in oral drug delivery: how to overcome intestinal barriers	25
I.3 Lipid-based drug delivery systems.....	28
I.4 Nanoemulsions.....	31
I.5 Self-emulsifying drug delivery systems.....	41
I.6 Hybrid nanosystems for intestinal delivery.....	46
I. References.....	58
Experimental section	77
Chapter II: Development and structural characterization of dried nanoemulsion for oral drug delivery	79
II. Abstract.....	81
II.1. Introduction.....	81
II.2. Materials and methods.....	83
II.2.1. Materials	83
II.2.2. Nanoemulsion preparation.....	83
II.2.3. Physicochemical and morphological measurements	83
II.2.4. Tacrolimus-loaded nanoemulsion development	85
II.2.5. <i>In vitro</i> NE stability and release study of tacrolimus in simulated GI fluids.....	86
II.2.6. Drying techniques.....	86
II.2.7. Statistical analysis.....	87
II.3. Results and discussion	87
II.3.1. Design and development of nanoemulsion.....	87
II.3.2. Influence of formulation: ternary diagram and mixture design	88
II.3.3. Physicochemical and morphological characterization of optimized nanoemulsions.....	91
II.3.4. Tacrolimus-loaded nanoemulsion formulation and physicochemical characterization.....	92
II.3.5. Stability and <i>in vitro</i> release of tacrolimus-loaded nanoemulsion in simulated GI fluids	93
II.3.6. Conversion into dry solid powders	94
II.3.7. Structural characterization of nanoemulsions in colloidal suspension and reconstituted following drying processes.....	101
II.4. Conclusion	105
II. References.....	106
II. Supplementary Information	110

Chapter III: Nanocomposite sponges for enhancing intestinal residence time following oral administration.....	113
III. Abstract	115
III.1. Introduction	115
III.2. Material and methods	117
III.2.1. Materials.....	117
III.2.2. Process of nanoemulsions formulation.....	117
III.2.3. Physico-chemical characterization of nanoemulsions.....	118
III.2.4. Mucins-nanoemulsions interaction.....	119
III.2.5. Preparation of chitosan sponges and nanoemulsion incorporation process.....	120
III.2.6 Microscopy observations of sponges: scanning electron microscopy (SEM) and optical images.....	120
III.2.7. Rehydration and water uptake capacity.....	121
III.2.8. Rheological characterization	121
III.2.9. <i>In vitro</i> release studies	121
III.2.10. <i>In vitro</i> cell viability studies	122
III.2.11. <i>In vivo</i> biodistribution study of fluorescent NE-loaded sponges following oral administration.....	122
III.2.12. Statistical analysis	123
III.3. Results and discussion.....	123
III.3.1. Nanoemulsions formulation, physicochemical characterization, and stability.....	123
III.3.2. Mucopenetrating properties of nanoemulsions.....	124
III.3.3. Development of chitosan and nanoemulsion-loaded chitosan sponges.....	126
III.3.4. Sponges rehydration: water uptake capacity	128
III.3.5. Rheological analysis.....	129
III.3.6. <i>In vitro</i> release studies	130
III.3.7. <i>In vitro</i> cytotoxicity	133
III.3.8. <i>In vivo</i> biodistribution and transit studies in mice.....	134
III.4. Conclusions	136
III. References	137
III. Supplementary information.....	142
Chapter IV: Supersaturable self-microemulsifying delivery systems enhance oral bioavailability of a benzimidazole derivative anticancer drug.....	145
IV. Abstract	147
IV.1. Introduction	147
IV.2. Materials and methods	149
IV.2.1. Materials.....	149
IV.2.2. Solubility studies of BI.....	149
IV.2.3. Development of SMEDDS formulations	150
IV.2.4. SMEDDS characterization	151
IV.2.5. Stability studies in simulated gastrointestinal fluids	152
IV.2.6. <i>In vitro</i> studies on Caco-2 cells.....	153

IV.2.7. <i>In vivo</i> pharmacokinetic study.....	154
IV.2.8. Statistical analysis	156
IV.3. Results and discussion.....	156
IV.3.1. Solubility studies.....	156
IV.3.2. SMEDDS optimization through mixture design	157
IV.3.3. Supersaturable SMEDDS formulation and optimisation	159
IV.3.4. Determination of self-emulsification time	161
IV.3.5. BI loading in SMEDDS and S-SMEDDS	161
IV.3.6. Stability studies in simulated gastrointestinal fluids	162
IV.3.7 Cytotoxicity assessment of the SMEDDS and S-SMEDDS formulations.....	164
IV.3.8 <i>In vitro</i> transepithelial permeability and cellular uptake studies.....	165
IV.3.9 Pharmacokinetic studies.....	166
IV.4. Conclusions	168
IV. References.....	169
IV. Supplementary information.....	173
Chapter V. General discussion	175
V.1 Formulation and characterization	175
V.1.1 Nanosystems.....	176
V.1.2 Conversion of the nanoemulsions in solid dosage forms	178
V.1.3 Polymer hybrid nanosystems: nanocomposite sponges and S-SMEDDS	179
V.1.4 Highlights on the nanoemulsion structure	182
V.2 <i>In vitro</i> and <i>in vivo</i> evaluation	184
V.2.1 Considerations on stability in simulated gastrointestinal fluids	184
V.2.2 Insights into release mechanisms	186
V.2.3 Evaluation of the cytocompatibility of the developed formulations.....	189
V.2.4 Observations on developed nanoparticles cellular uptake and intestinal permeability	189
V.2.5 Considerations on nanosystems mucopenetrating ability.....	190
V.2.6 Combination of mucoadhesion and mucopenetration and analysis of the <i>in vivo</i> biodistribution following oral administration.....	191
V.2.7 Analysis of the SMEDDS and S-SMEDDS <i>in vivo</i> behaviour.....	192
V.2.8 Perspectives on the evaluation of system digestion.....	193
V. References	194
Conclusions	203
Résumé substantiel	205
Annexes.....	211

Abstract

Oral delivery of drugs and biologics has challenged the development of hybrid delivery devices that combine nanoparticles and polymeric systems. Such combination allows to merge the technological advantages of the two formulations and to improve their pharmaceutical performance which is usually limited by multifaceted biological challenges.

The aim of the present work was the development of hybrid polymeric-lipid systems based on nanoemulsions (NEs) loaded into a chitosan sponges and supersaturable self-microemulsifying drug delivery systems (S-SMEDDS). Both systems were designed for improving intestinal residence time following oral administration and to increase local or systemic drug absorption.

In the first part of this thesis, mucopenetrating NEs have been designed and optimized by mean of an experimental design. Stable NEs showing a droplet size of 100 nm and a neutral surface charge were obtained. NEs were efficiently dried using spray-drying and freeze-drying overcoming major challenges related with the production of dry powders from oil based systems. Then, an original structural characterization of NEs, with an in-depth focus on the NE shell crystalline and fluid nature was performed via X-ray diffraction, differential scanning calorimetry (DSC) and a novel polarity-sensitive fluorophore. NEs proved to be non-toxic on Caco-2 cells at concentration higher than 1 mg/mL, while a time- and concentration-dependent inhibition of cell viability was observed on HCT 116 cells being the threshold of toxicity at 313 $\mu\text{g}\cdot\text{mL}^{-1}$ after 24 h. The NEs mucopenetrating potential was confirmed by the absence of surface affinity and thermodynamic interactions with mucins, together with the rapid diffusion in a preformed mucins network. The natural polymer chitosan was used as mucoadhesive macrosystem to load mucopenetrating NEs and prepare nanocomposite sponges by freeze-drying. The sponge matrix allowed to sustainably release NEs in simulated biorelevant fluids (FaSSIF-V2) showing 28% release in 2 h followed by a plateau at 50% until 72 h. Moreover, *in vivo* intestinal residence time was enhanced for sponges compared to NE alone when orally administered to mice.

As a second part of this work, SMEDDS intended for the solubility and bioavailability enhancement of a hydrophobic anticancer model benzoimidazole drug were formulated and optimized. The hydroxypropyl cellulose (HPC) polymer was added as precipitation inhibitor to create supersaturable SMEDDS (S-SMEDDS). S-SMEDDS improved drug loading and system stability in simulated intestinal fluids compared to SMEDDS. Systems enhanced epithelial permeability in intestinal Caco-2 cell monolayers via a transient and reversible opening of tight junctions. Moreover, plasmatic drug concentrations in mice after oral gavage indicated that S-SMEDDS provided sustained drug absorption up to 24 h, 4.5-fold higher AUC and slower elimination rate compared to free drug dispersion in HPC, thanks to their ability in maintaining the drug in a supersaturated state over time.

Overall, this thesis provided an extensive investigation on hybrid formulation strategies aimed at overcoming the biological hurdles for intestinal delivery. The combination of nanosystems with additional delivery approaches proved to be a winning strategy for a complete control over oral administration in view of both local and systemic treatment.

Résumé

L'administration orale de médicaments a nécessité le développement de systèmes de délivrance hybrides, qui combinent des nanoparticules avec des systèmes polymériques. Une telle association permet de combiner les avantages technologiques des deux formulations et ainsi d'améliorer leurs performances pharmaceutiques.

Ce travail de thèse a pour objectif de développer deux types de systèmes hybrides polymères-lipides. Le premier système incorpore des nanoémulsions (NE) au sein d'une éponge de chitosan. Le second repose sur les systèmes auto-émulsionnables sursaturables (S-SMEDDS). Les deux systèmes ont été conçus pour prolonger la durée de rétention intestinale et ainsi augmenter l'absorption locale ou systémique des médicaments.

La première partie de ces travaux de thèse met en avant les études de formulation des NE et leur optimisation au moyen d'un plan d'expériences. Les NE obtenues étaient stables et mesuraient 100 nm en taille. Les NE ont été efficacement séchées en utilisant les technologies de spray-drying et de lyophilisation. Ensuite, une caractérisation physico-chimique de la structure des NE a été effectuée (diffraction à rayons X, calorimétrie à balayage différentiel et par le biais d'un nouveau fluorophore sensible à la polarité). La couche de surfactants était fluide, sa nature cristalline ou amorphe dépendant des conditions environnementales. Les NE se sont révélées cytocompatibles sur cellules Caco-2 à une concentration supérieure à 1 mg.mL^{-1} . L'absence d'affinité de surface avec les mucines, ainsi que la diffusion rapide dans un réseau de mucines préformées ont confirmé que les NE possèdent des propriétés muco-pénétrantes. Les NE ont ensuite été mélangées avec du chitosan, un polymère naturel qui possède des propriétés muco-adhésives, et des éponges hybrides chitosane-NE ont été préparées par lyophilisation. La matrice de l'éponge a permis la libération soutenue des NE dans des fluides intestinaux simulés (FaSSIF-V2). De plus, les études de biodistribution *in vivo* ont démontré que les éponges prolongeaient la durée de rétention intestinale des NE par rapport aux NE seules, lorsqu'elles étaient administrées par voie orale à des souris.

La deuxième partie de la thèse visait à formuler et optimiser des SMEDDS destinés à améliorer la solubilité d'un médicament anticancéreux hydrophobe modèle, appartenant à la classe des benzimidazoles. Le polymère hydroxypropylcellulose (HPC) a été ajouté comme inhibiteur de précipitation pour créer des SMEDDS sursaturables (S-SMEDDS). Les S-SMEDDS augmentent le taux d'encapsulation du médicament et la stabilité du système dans les liquides intestinaux simulés comparé aux SMEDDS. Les systèmes augmentent la perméabilité intestinale grâce à l'ouverture réversible des jonctions serrées, comme observé sur des monocouches de cellules Caco-2. Enfin, l'administration par gavage oral à des souris a démontré que les S-SMEDDS augmentaient le temps de circulation plasmatique, grâce à leur capacité à maintenir le médicament dans un état sursaturé au fil du temps.

Dans l'ensemble, cette thèse présente une étude approfondie des systèmes de délivrance hybrides pour le ciblage intestinal. La combinaison de nanosystèmes et de polymères s'est avérée une stratégie intéressante pour permettre un contrôle complet de l'administration orale des médicaments dans la perspective d'un traitement local ou systémique.

List of Figures

Chapter I

Fig. 1 Physiological barriers to oral delivery.

Fig. 2 Mechanisms of action of delivery devices used for oral drug delivery. Common approaches include facilitation of transcellular transport, opening up of paracellular transport, mucopenetration, mucoadhesion, physical insertion and enzyme inhibition. Fig. adapted from Brown et al. (2020).

Fig. 3 LBDDS types.

Fig. 4 Methods of nanoemulsion formulation: A) high energy methods: high-pressure homogenization, microfluidization and ultrasonication, B) low energy methods: phase inversion temperature (PIT), phase inversion composition (PIC), emulsion phase inversion (EPI).

Fig. 5 Schematic diagram of most common instability mechanisms that occur in food emulsions: creaming, sedimentation, flocculation, coalescence, Ostwald ripening and phase inversion.

Fig. 6 The spray-drying process.

Fig. 7 Freeze-drying cycle, showing shelf, product and condenser temperatures, chamber pressure and product behaviour during the freezing and drying steps.

Fig. 8 Schematic representation of the proposed mechanism for spontaneous emulsification.

Fig. 9 Different types of hybrid nanosystems deriving from the combination of nanoparticles and polymers: self-emulsifying polymer hybrid systems and matrix structured hybrid systems or polymeric nanocomposites.

Fig. 10 Several types of nanocomposite systems for oral drug delivery, classified on the base of their micro- or macro-structure.

Fig. 11 Illustration of the supersaturation mechanism. The drug delivery ability of conventional dosage form, which dissolve in the GI fluids, is limited by the drug solubility in the fluids (green line). While SMEDDS/SNEDDS disperse the drug in their excipients providing high solubilized drug concentrations. Changes in the environmental conditions (pH, dilution, digestion) can reduce their solubilisation capacity, letting the drug in a supersaturated state and consequently the drug precipitate (red line). The addition of precipitation inhibitors (PI) allows to maintain the drug in its supersaturated state for longer time, delaying drug precipitation (blue line). Reproduced with modification from Brouwers et al. (2009) [276].

Chapter II

Fig. 1 Effect of water titration (phosphate buffer 5 mM, pH 7.4) on the viscosity (black line) and electrical conductivity (grey line) of NE at 80 °C.

Fig. 2 (A) Ternary phase diagram at SMR = 2.5. The green area corresponds to formulations in the solid state, the two blue areas to formulations in the liquid state. The dark blue region corresponds to formulations containing NE. The trapezoid-shaped area is the selected reduced ROI for refined analysis. (B and C) Pseudoternary phase diagram at SMR = 2.5. Contour plots of the predicted droplet mean size (B) and PdI (C) in the triangle defined by the lower bounds of mass fractions of oil, water and Smix (SMR = 2.5) with design points (●), check points (▲) and optimized formulations (□). The composition of selected optimized formulation (14) is indicated by black lines. The red line corresponds to SOR = 2.

Fig. 3 Microscopy images of NE: (A and B) TEM of blank NE, (C and D) Cryo-TEM of blank NE, (E and F) Cold TEM of loaded-NE. All images are at magnification of 200 nm and 100 nm.

Fig. 4 *In vitro* release profiles of tacrolimus from solutions and loaded NE in SGF (pH 1.2) or FaSSIF-V2 (pH 6.5). Mean \pm SD, n = 3. SGF: simulated gastric fluid in presence of sodium lauryl sulfate (SLS 0.5% w/v); FaSSIF-V2: simulated intestinal fluid in fasted state.

Fig. 5 SEM images of spray-dried NE at different NE and MD concentrations (% w/v). NE:MD = (A) 5:10; (B) 10:10; (C) 15:10.

Fig. 6 Particle size and polydispersity index (PDI) of (A) re-hydrated spray-dried NE at different NE and MD concentrations (% w/v); (B) re-hydrated freeze-dried NE at different NE and TR concentrations (% w/v).

Fig. 7 Visual appearance of NE cakes and TEM images of NE after lyophilization. (A) blank NE without cryoprotectant; NE at different concentrations of TR (% w/v): (B) blank NE:TR = 13.5:2.5; (C) tacrolimus-NE:TR = 13.5:2.5; (D) blank NE: TR = 3.4:5.

Fig. 8 (1 and 2) DSC thermograms of: (A) Pure S1 powder, (B) S1 in water solution, (C) mixture of S1 and S2 (SMR = 2.5), (D) mixture of S1 and MCT, (E) oil phase: S1, S2 and MCT, (F) blank NE, (G) freeze-dried blank NE powder and (H) freeze-dried blank NE re-suspended in water. Analysis performed from $-80\text{ }^{\circ}\text{C}$ to $80\text{ }^{\circ}\text{C}$ at a $10\text{ }^{\circ}\text{C}\cdot\text{min}^{-1}$ rate. Data corresponding to the second cooling (1) and third heating (2) steps. (3) DSC thermogram of blank NE. Step 1: heating scan from $+20\text{ }^{\circ}\text{C}$ to $+160\text{ }^{\circ}\text{C}$; step 2: cooling scan from $+80\text{ }^{\circ}\text{C}$ to $-80\text{ }^{\circ}\text{C}$; step 3: heating scan from $-80\text{ }^{\circ}\text{C}$ to $+80\text{ }^{\circ}\text{C}$. (4) XRPD patterns of: (A) S1 as powder, (B) S1 in water, (C) mixture of dry S1 and S2 (SMR = 2.5), (D) blank NE in colloidal suspension, (E) blank NE after complete water evaporation, (F) freeze-dried blank NE powder.

Fig. 9 (A) Effect of temperature on fluorescence emission of Dioll-NE; (B) Generalized Polarization of probes inserted in Dioll-NE as a function of temperature.

Fig. 10 Representation of the NE structure.

Chapter III

Fig. 1 A) Z-stacks of NE penetration (red) in the mucin layer (10% w/v, 600 μm thickness) at time point 10 and 180 min; B) total fluorescence signal of NE in the mucin layer (10% w/v) as a function of time as determined by image analysis software.

Fig. 2 Formulation process of A) chitosan (CH) sponges and B) nanoemulsion-loaded chitosan (CH-NE) sponges and their aspect after re-hydration. CH-NE A: sponge at low CH concentration (CH 0.1%- NE 2.5% w/w), CH-NE C: sponge at high CH concentration (CH 1%- NE 10% w/w). CH: chitosan ($550\text{ kg}\cdot\text{mol}^{-1}$, DA 4%); NE: nanoemulsion.

Fig. 3 SEM images of CH and CH-NE sponges. I: CH A; II: CH-NE A; III: CH B; IV: CH-NE C as defined in Table 1. 1: sample surface at low magnification (scale bar:400 μm); 2: sample surface at higher magnification (scale bar:100 μm); 3: Bulk of the sponge sample at intermediate magnification (scale bar:200 μm); 4 Bulk of the sponge sample at high magnification (scale bar:20 μm).

Fig. 4 Optical images of CH B and CH-NE sponges (CH-NE B and CH-NE C). The z-axis values 535 μm , 146 μm and 90 μm represent the maximum depth of the pores on the sponge surface.

Fig. 5 A) Water uptake capacity of CH A sponge at pH 5, 5.5 and 7.5 in both PBS and FaSSIF-V2; B) Water uptake capacity of CH-NE A sponge at pH 5, 5.5 and 7.5 in both PBS and FaSSIF-V2.

Fig. 6 Variation of G' and G'' moduli and loss tangents of rehydrated CH and CH-NE sponges (PBS pH 7.5) at different CH and NE concentrations at an angular frequency $\omega = 1 \text{ rad}\cdot\text{s}^{-1}$.

Fig. 7 A) NEs release (Nile Red-loaded NE (NR-NE), $20 \mu\text{g}\cdot\text{mL}^{-1}$) from the nanocomposite sponge CH-NE A in PBS and FaSSIF-V2 at pH 5, 5.5 and 7.5 up to 24 h; destructive release study to evaluate the effect of pH and release medium; B) NEs release (curcumin-loaded NEs (CCM-NEs), CCM $50 \mu\text{g}\cdot\text{mL}^{-1}$) from nanocomposite sponges at different NEs and CH concentrations in FaSSIF-V2 at pH 7.5 up to 24 h, pH 5.5 up to 48 h and pH 5 up to 72 h; cumulative release study to evaluate the effect of chitosan and nanoemulsions concentration.

Fig. 8 Cell viability of HCT-116 and Caco-2 cells after exposure to blank NE for 3h and 24h. Statistical data analysis: $p < 0.05 = *$; $p < 0.01 = **$; $p < 0.001 = ***$; $\geq 0.05 = \text{not significant}$.

Fig. 9 A) Fluorescent images of mice whole body; B) representative *ex vivo* fluorescence images of intestines of mice sacrificed at 1, 2, 3, 4 and 6 h after oral administration of nanoemulsions (NE), CH-NE mixture (Mixture), CH-NE sponge (Sponge).

Fig. 10 A) Contents of nanoemulsion (NE), NE-loaded chitosan mixture (Mixture), NE-loaded chitosan sponge (Sponge) in different parts of the intestinal tract following oral administration at time 1, 2, 3, 4 and 6 h; B) Dissection scheme of the mouse GI tract. Statistical data analysis in supplementary information Fig. S6.

Chapter IV

Fig. 1 A) BI chemical structure and pKa values; B) Maximum solubility of BI in various excipients expressed in $\text{mg}\cdot\text{mL}^{-1}$.

Fig. 2 A) Ternary phase diagram of SMEDDS composed of Miglyol® 812, Kolliphor® RH40 and Transcutol® HP/ EtOH (50/50). Red dots correspond to unsuitable formulations. Blue dots correspond to formulations having a nanometric size and PDI lower than 0.3. Green dots correspond to the feasibility domain showing microemulsion droplets of around 20 nm and PDI lower than 0.1. The selected formulation is highlighted with a black circle (F12, size 19 nm, PDI 0.1); B) Pseudoternary phase diagram. Contour plots of the predicted droplet mean size in the triangle defined by the lower and upper bounds of mass fractions of oil, surfactant and co-solvents with the selected optimized formulation (F12) indicated by a black circle.

Fig. 3 A) Formulation of S-SMEDDS; B) Physicochemical properties of blank supersaturable SMEDDS (S-SMEDDS).

Fig. 4 Stability studies of BI-loaded SMEDDS c, S-SMEDDS I and S-SMEDDS II microemulsions in A) simulated gastric fluids (SGF) and B) simulated intestinal fluids (SIF) up to 3h. Stability was evaluated by mean of DLS analysis.

Fig. 5 Physicochemical properties of BI-loaded SMEDDS c and S-SMEDDS I and II following pH adjustment from acid (time point 0 min) to alkaline (from time point 10 min to 360 min).

Fig. 6 A) Viability of Caco-2 cells after incubation with blank SMEDDS, blank S-SMEDDS, drug-loaded SMEDDS, drug-loaded S-SMEDDS, free drug solution in EtOH for 24 h. Data are shown as mean \pm SD, $n = 3$. Statistical data analysis: $p < 0.05 = *$; $p < 0.01 = **$; $p < 0.001 = ***$; $\geq 0.05 = \text{not significant}$. B) TEER values of Caco-2 monolayer after incubation with DiD-labelled SMEDDS and S-SMEDDS ($1 \text{ mg}\cdot\text{mL}^{-1}$). C) Confocal microscope images of fixed and stained Caco-2 cell monolayers grown on transwell membranes for 21 days prior to 2 h and 4 h exposure to DiD-labelled SMEDDS and

DiD-labelled S-SMEDDS I (red). Fixed cells were stained with DAPI (blue nuclei) and Phalloidin-iFluor™ 488 Conjugate (green tight junctions). Scale bar: 30 μm .

Fig. 7 Plasma concentrations vs time profile after oral administration of A) drug dispersion in HPC and SMEDDS c (up to 6 h) and B) S-SMEDDS I and S-SMEDDS II (up to 24 h).

Chapter V

Fig. 1 Comparison between the two developed nanosystems, nanoemulsions (NE) and SMEDDS, as for their formulation process, composition and physicochemical attributes.

Fig. 2 Comparison between the two developed hybrid nanosystems, nanocomposite sponges and supersaturable SMEDDS, as for their formulation process, composition, physicochemical and structural attributes.

Fig. 3 Characteristics of the NE shell.

Fig. 4 Suggestion of the loading of nanoemulsion (NE), nanocomposite sponge and S-SMEDDS in enteric capsules.

Fig. 5 Summary of the mechanisms of NE release from the nanocomposite sponges of different composition, expressed as NE/CH ratio (CH-NE A: NE/CH ratio 25, CH-NE C: NE/CH ratio 10, CH-NE B: NE/CH ratio 2.5).

Fig. 6 Combination of mucoadhesion and mucopenetration properties in nanocomposite sponges.

List of Tables

Chapter I

Table 1 Marketed or in clinical trials oral LBDDS.

Table 2 Examples of spray-dried and freeze-dried NE.

Table 3 Comparison and conceptual differences between self-emulsifying drug delivery systems on the base of the Lipid Formulations Classification System (LFCS) by Pouton. (PdI : polydispersity index).

Table 4 Examples of solid SEDDS.

Table 5 Nanocomposites targeting the small intestine.

Table 6 Nanocomposites targeting the colon.

Table 7 Examples of supersaturable SEDDS.

Chapter II

Table 1 Mixture design and size distribution results.

Table 2 Compatibility of NE with different concentration of maltodextrin (MD) “–” “No separation; “+” Light separation, with very thin upper cream layer; “+++” Obvious separation, with upper creamed layer. % expressed as% w/v.

Table 3 Characteristics of spray-dried NE powders.

Table 4 List of TR and NE concentrations used in the freeze-thawing study of blank NE in presence of different TR concentrations. NE original size = 103.9 ± 2.7 nm; PdI = 0.20.

Table 5 Characteristics of freeze-dried NE powders.

Table 6 DSC analysis from -80 °C to $+160$ °C at a 10 °C·min⁻¹ heating rate. NE were analyzed at the second heating scan.

Chapter III

Table 1 Formulated chitosan (CH) and nanoemulsion-loaded chitosan (CH-NE) sponges.

Table 2 Physicochemical characteristics of blank and loaded nanoemulsions (NEs). NR-NE: Nile Red-loaded NE; CCM-NE: Curcumin-loaded NE.

Chapter IV

Table 1 Composition and physicochemical properties of SMEDDS in the feasibility domain composed of Miglyol® 812, Kolliphor® RH40, Transcutol® HP and EtOH.

Table 2 Physicochemical properties of blank and BI-loaded microemulsion and encapsulation efficiency in SMEDDS, s-SMEDDS I and s-SMEDDS II by HPLC analysis. *drug precipitation.

Table 3 Pharmacokinetic parameters of BI following oral administration to mice.

List of abbreviations

Abs: absorbance
API: Active Pharmaceutical Ingredient
AUC: area under the curve
BCS: Biopharmaceutical Classification System
BSA: bovine serum albumin
CCM: curcumin
CH: chitosan
CH-NE: nanoemulsion-loaded chitosan nanocomposite sponges
CLSM: Confocal Laser Scanning Microscopy
 C_{max} : maximum plasma concentration
CMC: carboxymethylcellulose
Cryo-TEM: cryogenic-transmission electron microscopy
DA: degree of acetylation
DAPI: 4',6-Diamidino-2-Phenylindole, Dihydrochloride
DCM: dichloromethane
DiD: 1,1'-dioctadecyl-3,3',3'-tetramethylindodicarbocyanine, 4-chlorobenzene sulfonate salt or DiIc18(5) solid
DL: drug loading
DLS: dynamic Light Scattering
DMEM: dulbecco's modified Eagle's medium
DMSO: dimethyl sulfoxide
DSC: differential scanning calorimetry
DSS: dextran sulfate sodium
EE: encapsulation efficiency
Em: emission
EPI: emulsion phase inversion
ESI: electrospray ionization
EtOH: ethanol
Eudragit®: Poly (methyl methacrylate) derivative
Ex: excitation
FaSSIF-V2: simulated intestinal fluid in fasted state
FBS: foetal bovine serum
FDA: Food and Drug Administration
GI: gastrointestinal
GMP: Good Manufacturing Practices
GP: generalized polarization parameter
HBSS: Hanks' Balanced Salt solution
HCl: hydrochloric acid
HLB: Hydrophilic Lipophilic Balance
HPC: hydroxypropyl cellulose

HPLC: high performance liquid chromatography
HPMC: hydroxypropyl methylcellulose
IBD: inflammatory bowel diseases
ICH: International Conference on Harmonisation
ITC: Isothermal Titration Calorimetry
KCl: potassium chloride
KH₂PO₄: potassium dihydrogen phosphate
LBDDS: lipid-based drug delivery systems
LC-MS: liquid chromatography-mass spectrometry
LFCS: Lipid Formulations Classification System
LNC: lipid nanocapsules
LOD: detection limit
LOQ: quantification limit
MC: methyl cellulose
MCT: medium chain triglycerides
MD: Maltodextrin
MeOH: methanol
MRT: mean residence time
MTS: 3-(4,5-dimethylthiazol-2-yl)-5-(3-carboxymethoxyphenyl)-2-(4-sulfophenyl)-2H-tetrazolium
MTT: 3-(4,5-dimethylthiazol-2-yl)-2,5-diphenyltetrazolium
M_w: molecular weight
Na₂HPO₄·2H₂O: Di-sodium hydrogen orthophosphate dihydrate
NaCl: Sodium chloride
NaOH: sodium hydroxide
NaTC: sodium taurocholate
NE: nanoemulsion
NiMDS: Nanoparticle-in-Microparticle Delivery System
NLC: nanostructured lipid carrier
NP: nanoparticles
NR: Nile Red
o/w: oil-in-water
PAA: poly (acrylic acid)
P_{app}: apparent permeability coefficient
PBS: phosphate buffer saline
PCL: polycaprolactone
PDE: Permitted Daily Exposure
PdI: polydispersity index
PEG: polyethylene glycol
PEG-b-PCMA: poly(ethylene glycol)-b-poly(cholesterol methacrylate)
PET: polyethylene terephthalate
PFA: paraformaldehyde
PgP: P-glycoprotein

PI: precipitation inhibitors
PIC: phase inversion composition
PIT: phase inversion temperature
PLGA: poly(lactic-co-glycolic acid)
PVA: polyvinyl alcohol
PVP: polyvinylpyrrolidone
ROS: reactive oxygen species
RPB: High-Gravity Rotating Packed Bed
S1: Polyoxyethylene(40) stearate; Myri® 52
S2: oleoyl polyoxyl-6 glycerides; Labrafil® M1944CS
SDS: sodium dodecyl sulphate
SEDDS: self-emulsifying drug delivery systems
SEM: scanning electron microscopy
SGF: simulated gastric fluid
SIF: simulated intestinal fluids
SLN: solid lipid nanoparticles
SLS: Sodium Lauryl Sulfate
SMEDDS: self-microemulsifying drug delivery systems
Smix: surfactant mixture
SMR: Surfactant Mass Ratio
SNEDDS: self-nanoemulsifying drug delivery systems
Soluplus®: polyvinyl caprolactam–polyvinyl acetate–polyethylene glycol graft copolymer
SOR: surfactant to oil ratio
S-SMEDDS: supersaturable self-microemulsifying drug delivery systems
 $t_{1/2}$: elimination half-life
TEER: transepithelial electrical resistance
TEM: transmission electron microscopy
T_g: glass transition temperature
TGA: thermogravimetric analysis
T_{max}: time to reach the maximum plasma concentration
TPGS: D- α -Tocopherol polyethylene glycol 1000 succinate
TR: Trehalose
w/o: water-in-oil
XRPD: X-ray powder diffraction

General introduction

Oral delivery is considered the favoured route of administration for both local and systemic delivery of a wide range of Active Pharmaceutical Ingredients (APIs). Advantages arise from the intestinal extensive surface area for drug absorption and induction of mucosal immunity, the possibility of self-administration which ameliorate patient compliance, and the low production costs [1–3].

However, oral drug delivery faces major obstacles related to drug precipitation or degradation in the harsh gastric medium, and low intestinal residence time and inefficient absorption due to intestinal peristalsis, rapid clearance, digestion process, mucus and epithelial barriers [4].

In this frame, the use of nanoparticles proved to be a promising approach to modulate drug absorption or enhance drug local therapeutic efficacy following oral administration. By leveraging mechanism of passive (mucopenetration, bioadhesion to the inflamed intestinal area, enhanced paracellular or transcellular transport) or active targeting, a variety of nanosystems have been developed [5].

Among them, lipid-based drug delivery systems (LBDDS), namely nanoemulsions (NE) and self-emulsifying drug delivery systems, are attractive candidates because of their ability to increase solubility and permeability of poorly water soluble drugs thus enhancing bioavailability [6–8]. NE are thermodynamically unstable colloidal dispersions consisting of two immiscible liquids (water and oil), with one of the liquids being dispersed as nanometric droplets in the other liquid and stabilized by a surfactant shell [9,10]. NE can be produced by both high and low energy methods and their stability can be improved by conversion in solid dosage forms through freeze- or spray-drying [11,12]. Self-emulsifying drug delivery systems are anhydrous pre-concentrates of NEs and microemulsions able to spontaneously form nano- (SNEDDS) or microemulsions (SMEDDS) upon dispersion in intestinal intraluminal fluids [13]. As with NE, their conversion in solid dosage form has been proposed to improve their stability [14].

Despite the several technological advances, some biological challenges, such as poor stability, improvable drug loading, modulation of drug release, short intestinal residence time, are still preventing these delivery strategies from meeting the many therapeutic requirements [15].

The pressing need for improved technologies to serve clinical needs has led to design of novel delivery platforms based on the combination of conventional delivery systems [16]. Notably, nanoparticles and polymers were combined in a single delivery device as a hybrid nanosystem. The polymer was integrated in the form of 3D network in which the nanoparticles were embedded as in the case of the matrix structured hybrid systems, also referred to as polymeric nanocomposites, or in the form of solution/dispersion in which the nanodroplets were suspended as in the case of the self-emulsifying polymer hybrid systems. The synergy between nanosystem and polymer offers the possibility of a precise control over drug delivery enhancing drug therapeutic efficacy and minimising side effects [17].

Hypothesis and aim of the thesis

In the present work, hybrid polymeric nanosystems have been tailored to improve intestinal delivery. Firstly, we assumed that the intestinal mucus barrier could be targeted to refine and prolong intestinal delivery. By designing mucopenetrating nanoparticles able to efficiently cross the mucus layer, the associated drug will attain the underlying epithelium. By embedding such nanoparticles inside chitosan sponges able to adhere to the mucus layer, the intestinal residence time of the active will be increased. This will lead to enhanced drug therapeutic efficacy in a future systemic or local delivery. Secondly, we hypothesized that the use of precipitation inhibitor associated to SMEDDS will increase drug loading and stability in the GI tract. By adding such PI to SMEDDS also the intestinal permeability can be altered resulting in an increase of the transcellular and/or the paracellular drug transport. The intestinal absorption will be maximised and the drug blood circulation will be prolonged.

The main aim of this PhD work was to design hybrid polymeric nanosystems to improve intestinal drug delivery. Two different hybrid nanosystems were designed: i) polymeric nanocomposites made of nanoemulsions (NEs) loaded into chitosan (CH) sponges and ii) supersaturable S-SMEDDS by combination of conventional SMEDDS with the polymeric precipitation inhibitor hydroxypropylcellulose (HPC).

To reach this aim, specific objectives were:

1. to prepare, optimize and physicochemically characterize the nanosystems, NE and SMEDDS;
2. to combine the nanosystems with polymers (CH or HPC) to obtain their hybrid counterparts, nanocomposite sponge and S-SMEDDS;
3. to evaluate *in vitro* stability and release profile in simulated GI fluids, mucopenetrating ability, cytocompatibility and intestinal permeability on Caco-2 cells;
4. to study *in vivo* biodistribution and pharmacokinetic profile after oral administration to mice.

The manuscript is divided in two parts: a bibliographical review (Chapter I) and an experimental section that is further divided in 3 chapters (Chapter II, III and IV).

Chapter I includes a bibliographic report describing the main challenges in the oral administration of drug and biologics and the advantages offered by delivery devices. A focus on the technological aspects of lipid-based drug delivery systems and in particular of nanoemulsions and self-emulsifying drug delivery systems (SEDDS) is provided. Then, the role of hybrid formulations in ameliorating the technological and pharmacological performance of the conventional delivery strategies is discussed.

Chapter II is dedicated to the formulation aspects of nanoemulsions. The process of nanoemulsion preparation, optimisation and physicochemical characterisation is presented. A proof-of-concept of the feasibility of converting NE in solid dosage forms is provided. Lastly, the influence of the NE composition on its structure is highlighted. This part includes an original research article published in the journal *Colloids and Surfaces A*, <https://doi.org/10.1016/j.colsurfa.2020.124614>.

Chapter III focuses on the design of nanocomposite sponges. Firstly, the *in vitro* evaluation of the NE mucopenetrating performance and cytocompatibility is presented. Then, the NE loading in chitosan sponges loading of NE in chitosan sponges and the *in vivo* evaluation of the nanocomposite ability to increase the residence time in the mouse intestine are described. Results were submitted to the Journal of Controlled Release.

Chapter IV is devoted to the design of SMEDDS and S-SMEDDS. The work presents the process of system optimisation, the evaluation of stability in the gastrointestinal environment, the effect on the intestinal permeability and the evaluation of the pharmacokinetic profile *in vivo* after oral administration to mice. The work was submitted to the Drug Delivery and Translational Research journal.

References

- [1] A.A. Date, J. Hanes, L.M. Ensign, Nanoparticles for oral delivery: Design, evaluation and state-of-the-art, *J. Control. Release.* 240 (2016) 504–526. doi:10.1016/j.jconrel.2016.06.016.
- [2] L.M. Ensign, R. Cone, J. Hanes, Oral drug delivery with polymeric nanoparticles: The gastrointestinal mucus barriers, *Adv. Drug Deliv. Rev.* 64 (2012) 557–570. doi:10.1016/j.addr.2011.12.009.
- [3] P. Long, Q. Zhang, M. Xue, G. Cao, C. Li, W. Chen, F. Jin, Z. Li, R. Li, X. Wang, W. Ge, Tomato lectin-modified nanoemulsion-encapsulated MAGE1-HSP70/SEA complex protein vaccine: Targeting intestinal M cells following peroral administration, *Biomed. Pharmacother.* 115 (2019) 108886. doi:10.1016/j.biopha.2019.108886.
- [4] B. Homayun, X. Lin, H.-J. Choi, Challenges and Recent Progress in Oral Drug Delivery Systems for Biopharmaceuticals, *Pharmaceutics.* 11 (2019) 129. doi:10.3390/pharmaceutics11030129.
- [5] T.D. Brown, K.A. Whitehead, S. Mitragotri, Materials for oral delivery of proteins and peptides, *Nat. Rev. Mater.* 5 (2020) 127–148. doi:10.1038/s41578-019-0156-6.
- [6] T. Lindmark, Y. Kimura, P. Artursson, Absorption enhancement through intracellular regulation of tight junction permeability by medium chain fatty acids in Caco-2 cells., *J. Pharmacol. Exp. Ther.* 284 (1998) 362–9.
- [7] K. Koga, Y. Kusawake, Y. Ito, N. Sugioka, N. Shibata, K. Takada, Enhancing mechanism of Labrasol on intestinal membrane permeability of the hydrophilic drug gentamicin sulfate, *Eur. J. Pharm. Biopharm.* 64 (2006) 82–91. doi:10.1016/j.ejpb.2006.03.011.
- [8] H. Park, E. Ha, M. Kim, Current Status of Supersaturable Self-Emulsifying Drug Delivery Systems, *Pharmaceutics.* 12 (2020) 365. doi:10.3390/pharmaceutics12040365.
- [9] D.J. McClements, Nanoemulsions versus microemulsions: terminology, differences, and similarities, *Soft Matter.* 8 (2012) 1719–1729. doi:10.1039/C2SM06903B.
- [10] N. Anton, T.F. Vandamme, Nano-emulsions and micro-emulsions: Clarifications of the critical differences, *Pharm. Res.* 28 (2011) 978–985. doi:10.1007/s11095-010-0309-1.
- [11] D.J. McClements, J. Rao, Food-Grade Nanoemulsions: Formulation, Fabrication, Properties, Performance, Biological Fate, and Potential Toxicity, *Crit. Rev. Food Sci. Nutr.* 51 (2011) 285–330. doi:10.1080/10408398.2011.559558.
- [12] T.W. Wong, P. John, Advances in Spray Drying Technology for Nanoparticle Formation, in: *Handb. Nanoparticles, 2015: pp. 1–16.* doi:10.1007/978-3-319-13188-7_18-1.
- [13] T. Vasconcelos, F. Araújo, C. Lopes, A. Loureiro, J. das Neves, S. Marques, B. Sarmento, Multicomponent self nano emulsifying delivery systems of resveratrol with enhanced pharmacokinetics profile, *Eur. J. Pharm. Sci.* 137 (2019). doi:10.1016/j.ejps.2019.105011.
- [14] B. Singh, S. Beg, R.K. Khurana, P.S. Sandhu, R. Kaur, O.P. Katare, Recent Advances in Self-Emulsifying Drug Delivery Systems (SEDDS), *Crit. Rev. Ther. Drug Carrier Syst.* 31 (2014) 121–185. doi:10.1615/CritRevTherDrugCarrierSyst.2014008502.
- [15] C. Desfrancois, R. Auzély, I. Texier, Lipid nanoparticles and their hydrogel composites for drug delivery: A review, *Pharmaceutics.* 11 (2018). doi:10.3390/ph11040118.
- [16] S. Merino, C. Martín, K. Kostarelos, M. Prato, E. Vázquez, Nanocomposite Hydrogels: 3D Polymer–Nanoparticle Synergies for On-Demand Drug Delivery, *ACS Nano.* 9 (2015) 4686–4697. doi:10.1021/acsnano.5b01433.
- [17] E. Taipaleenmäki, B. Städler, Recent Advancements in Using Polymers for Intestinal Mucoadhesion and Mucopenetration, *Macromol. Biosci.* 20 (2020) 1900342. doi:10.1002/mabi.201900342.

Bibliographical review

Chapter I: The oral route of administration: physiological barriers and drug delivery technologies

I.1 Oral drug delivery

Oral delivery is considered the preferred route of administration, encompassing over 50% of FDA approvals [1] since it offers several advantages, such as the possibility of self-administration, flexibility in dosage regimen which ameliorate patient compliance, and the avoidance of sterile conditions for oral products manufacture reducing production costs [2]. The oral route is of interest for physiological reasons, offering an extensive surface area (300–400 m²) for drug absorption and induction of mucosal immunity [3,4]. Regardless of the clear advantages offered by the oral route, the therapeutic efficacy of several hydrophobic and hydrophilic drugs and biologics (peptides, proteins and nucleic acids) is limited by their poor aqueous solubility and/or permeability and chemical/enzymatic stability [5].

In an attempt to overcome these challenges, APIs have been encapsulated within orally administrable delivery devices, namely macro-scaffolds, micro- and nanoparticulate systems. The objective was to protect APIs from the harsh conditions of the gastrointestinal (GI) environment and to release them at the target site [6,7].

Oral drug delivery can target stomach, small intestine and colon. The interest in gastric delivery lies in the enhancement in efficacy of drugs that are mainly absorbed in the stomach and in the treatment of *Helicobacter pylori* infections that can lead to gastric ulcers or chronic gastritis [8,9]. When the target is the small intestine, the goal is to achieve enhanced API absorption through the mucosal wall into the systemic circulation [10,11]. Finally, drug delivery to the colon aims at improving local delivery to colorectal tissues or at providing macromolecules systemic uptake by minimising previous absorption in the GI tract [12,13].

In the design of delivery systems for an effective intestinal delivery, the main biological barriers to overcome can be divided into biochemical-luminal, cellular, immune and absorption-activity related barriers [14] (Fig. 1). In the following paragraphs, an introduction to the structure, physiology and biological barriers of the intestinal tract is presented. The main strategies to challenge them are also described.

I.1.1 Structure of the intestine

The intestine, or bowel, is a winding muscular tube extending from the stomach to the anus, grossly divided in small and large intestine [15]. Throughout its length four tissue layers can be identified: the mucosa, the submucosa, the muscularis externa and the serosa. The mucosa is in turn subdivided into epithelium, lamina propria and muscularis mucosae [16].

The small intestine includes duodenum, jejunum, and ileum. [17]. Its lumen is arranged in plicae circulares, villi and microvilli that together increase the absorptive surface of the small intestine by 600- to 1000-fold for a total of 250 to 400 m². Within each villus are an arteriole and a venule that contribute to a network of capillaries for blood uptake and a lacteal, a lymphatic capillary aimed at the absorption of lipid components. In between the villi are the crypts of Lieberkühn, invaginations where pluripotent intestinal epithelial stem cells reside, responsible for the replacement of the epithelium every 3 to 6 days [18]. The small intestine predominant cell type are the enterocytes, goblet cells, M cells,

enteroendocrine, Paneth and stem cells [18-22]. Besides, the large intestine is divided into four main regions: cecum, colon, rectum, and anus. The cecum represents a small portion of the large intestine; the peculiarity is the small appendix that attaches to it, which contains lymphoid tissue, suggesting an immunological function. In contrast with the small intestine, the colon epithelium does not present villi and microvilli but invaginations named intestinal glands. The colon mucosa is a simple columnar epithelium made mostly of enterocytes and goblet cells [23,24]. The normal colonic microflora of humans is extremely large and complex. The composition of this bacterial population is affected by host-mediated factors, microbial factors, microbial interactions, and environmental factors [25].

I.1.2 Biological barriers to intestinal delivery

I.1.2.1 Biochemical-luminal barriers

The biochemical-luminal barriers of stomach and intestine are the first biological hurdle for orally administered drugs. In the stomach these barriers are represented by the harsh gastric medium where the low pH (pH 1–2.5) can affect drug solubility causing precipitation [26], and the gastric enzymes such as pepsin and gelatinase that can degrade active compounds [27,28]. Once in the intestine, the peristalsis and rapid clearance can prevent complete drug absorption and affect the permanence of delivery devices. During the fed state, segmentation and peristalsis propel the food bolus through the small intestine and into the colon for a mean transit time of 84 min in small intestine and 14-24 h in the large one. When food is ingested, the transit is interrupt, thus increasing mucosal contact time and allowing more efficient absorption of nutrients, electrolytes and water [18,21]. The drug intake in fed conditions could thus seem advantageous to enhance oral bioavailability, particularly in the case of highly lipophilic Biopharmaceutical Classification System (BCS) Class II drugs. However, co-administration with food has to be monitored to avoid sub-therapeutic plasma drug concentrations or problematic effects for the drugs with a narrow therapeutic index [29].

Luminal fluids can constitute a further obstacle for oral drug delivery [18]. If on one side the overall availability of fluids is a prerequisite for dissolution and absorption of hydrophilic molecules, it is also the main cause for drug precipitation and reduced pharmacological activity of poorly water-soluble drugs administered at high doses [30]. Instead, the colon has a reduced luminal fluid volume in an almost neutral environment, supplemented by a higher viscosity of the luminal content, due to the higher water-absorbing capacity [31]. This limit drug absorption representing a further obstacle.

The impact of digestion is essential to the understanding of the fate of delivery devices, especially lipid-based ones. Lipid nanosystems composed of digestible excipients are processed in the intestine by biliary salts and pancreatic enzymes, and the loaded active is absorbed together with dietary fats. Conversely, non-digestible nanoparticles are transported intact across the intestinal epithelium [32].

Barriers to oral delivery

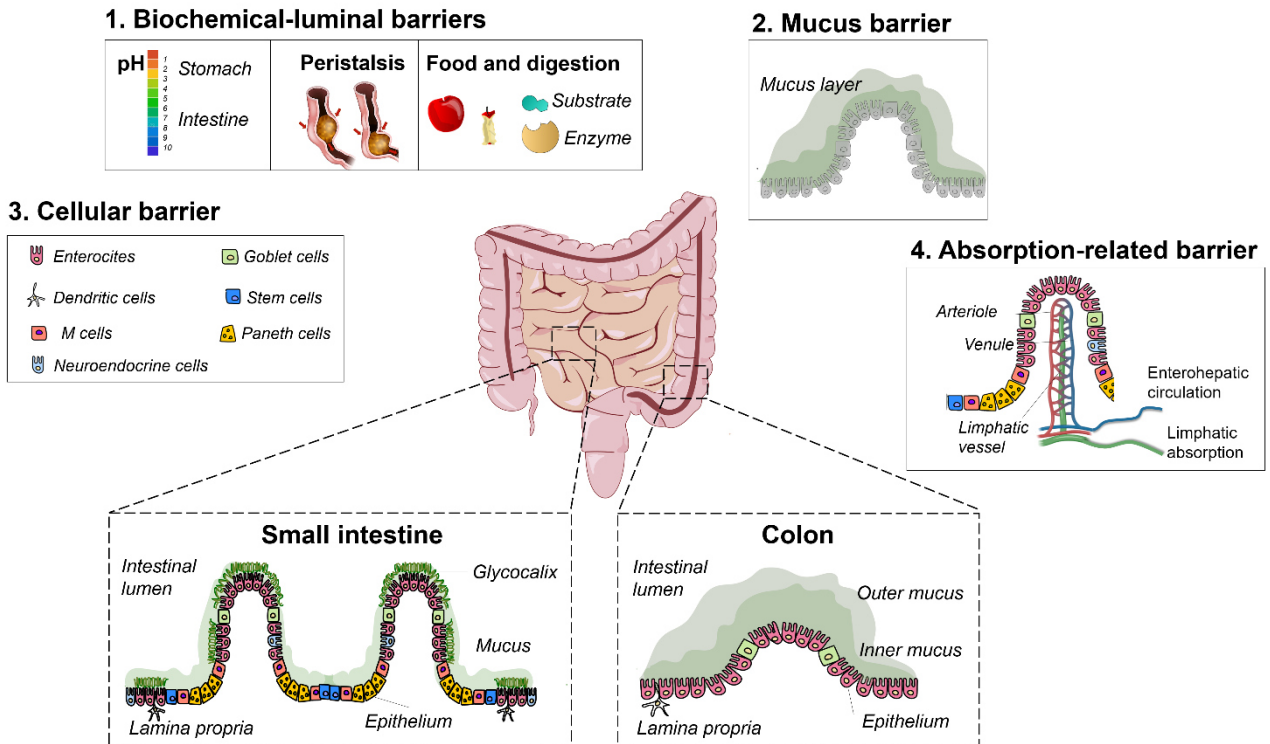


Fig. 1 Physiological barriers to oral delivery.

I.1.2.2 Mucins layer barrier

Mucins are glycosylated proteins produced by epithelial cells which line the entirety of the intestinal tract to protect the mucosa from pathogens and mechanical stresses [33]. They can be divided into secreted and transmembrane mucins. The transmembrane mucins are present in the small intestine where they form a coating layer on the enterocytes surface known as the glycocalyx [34]. The glycocalyx enables the attachment of normal flora, limits colonisation by pathogens and acts as size-selective diffusion barrier for bacteria, viruses and nanoparticles [35]. Besides, the secreted mucins constitute the lubricant mucus layer. Mucus is secreted by the goblet cells and typically contains up to 95% of water, mucins, sloughed cells, bacteria, lipids, salts, proteins, macromolecules and cellular debris [20]. Mucins form the skeleton of the intestinal mucus and give it its gel-like properties. They are mainly composed of negatively charged glycoproteins that take turn to hydrophobic cysteine-rich domains creating a structured network with mesh size of 200-500 nm in which pathogens are trapped via multiple low-affinity interactions [34]. The overall mucus surface is anionic, fostering interactions with polycations. Mucus thickness, turnover and pH vary depending on their location in the GI tract of mucus membrane. The pH ranges between 5.5 and 7.5 in the small intestine, while values around 7 are normally recorded in the colon [36,37]. Thickness is highly dependent on digestive activity, dietary and physio-pathological conditions. If the colon has a two-layered system with an inner mucus layer of around 100-400 μm in thickness and an outer one 300-700 μm thick, the small intestine possess one single and discontinuous layer of around 50 to 450 μm [21]. The small intestinal mucus is not anchored to the epithelial surface and moves with the peristaltic waves in a distal direction. While, the inner firm mucus layer of the colon adheres firmly to the epithelium surface by transmembrane domain and cannot be remove by simple

shear [22]. By acting as a size-exclusion filter, the mucus constitutes a barrier for poorly soluble drugs and nanosystems, challenging the quest for smarter delivery devices [37,38].

I.1.2.3 Immune barrier

The small intestine provides the largest immune barrier between epithelial surface and body interior, making the induction of mucosal immunity by oral administration convenient, highly efficient and long-lasting [39]. Both the small and large intestines have essential immunological roles. In the small intestine the M cells in Peyer's patches sample antigens from the gut lumen, while the large intestine is rich in innate immune cells such as macrophages and neutrophils that enable the immune system activation occurring through the production of mucosal antibodies immunoglobulin A (IgA) and systemic antibodies and T-cell-mediated response [14,21]. Because of these reasons oral vaccination is an attractive therapeutic strategy, counting seven live oral vaccines approved by the FDA [40].

I.1.2.4 Cellular barrier

Mucosal cells form a continuous monolayer regulating the passage of molecules and particles from the apical surface facing the lumen to the basolateral compartment. Several cell types can compose the mucosa. Enterocytes, aimed at nutrients absorption, are the predominant cell type. In the small intestine, each enterocyte presents at its luminal surface thousands of microvilli, actin-based membrane protrusions which appear as a striated brush border, serving at increasing the absorptive surface area [18]. M cells in Peyer's patches which are relatively less protected by mucus secretions and drug efflux transporters like P-glycoprotein (PgP), are a common delivery target for nanoparticles [19]. Paracellular transport between adjacent cells is restricted by tight-junction protein complexes, adherent junctions and desmosomes [41,42]. Transport across the cellular barrier, referred to as transcellular transport, is a passive mechanism for highly lipophilic molecules, while large molecules and nanoparticles are actively internalized by enterocytes or M cells via a pinocytosis mechanism resulting from either micropinocytosis, clathrin-mediated endocytosis, caveolae-mediated endocytosis or clathrin- and caveolae-independent processes [43]. Further hurdle is the expulsion back in the lumen by efflux pumps expressed on the apical membrane of enterocytes, as the PgP, reducing drug absorption and bioavailability [44].

I.1.2.5 Absorption-related barriers

The absorption of APIs and/or delivery systems into systemic circulation occurs through the portal vein or the lymphatic system [29]. The lumen of the small intestine is arranged in plicae circulares, villi and microvilli that together increase the absorptive surface of the small intestine by 600- to 1000-fold for a total of 250 to 400 m². Within each villus are an arteriole and a venule that contribute to a network of capillaries for blood uptake and a lacteal, a lymphatic capillary that is mainly aimed at the absorption of lipid-containing chylomicrons, lipid-soluble vitamins and lipid-based systems. In between the villi are the crypts of Lieberkühn, invaginations where pluripotent intestinal epithelial stem cells reside, responsible for the replacement of the epithelium every 3 to 6 days [18]. While the colon epithelium does not present villi, but has invaginations (intestinal glands) and hence the available area for the absorption is much smaller [45]. Shortcomings deriving from the enterohepatic circulation of APIs,

namely first-pass metabolism, bile secretion/elimination, altered pharmacokinetics and pharmacodynamics, make the lymphatic the preferred route of absorption [17].

I.2 Biological challenges in oral drug delivery: how to overcome intestinal barriers

Several systems presenting different degrees of complexity have been developed to target specific intestinal portions. The main approach exploits peculiarities of the intestinal tract and distinctive features of small and large intestine for smart drug delivery.

One of the major goals in drug delivery to the small intestine is to increase the efficiency absorption and systemic bioavailability. In parallel with technology solutions for the treatment of systemic diseases, the small intestine can be targeted for oral local vaccination purposes and for the management of local conditions such as infection, chronic inflammations, diarrhoea, enzyme deficiency and injury [46]. Instead, colon targeted drug delivery is highly desirable for the local treatment of several disorders such as inflammatory bowel diseases (IBD) and colon cancer and for systemic delivery due to the presence of lower levels of digestive enzymes and bile salts than small intestine and the protracted residence time (up to 24 h) [46]. Initially, for a more efficient intestinal delivery, macro-scaled like enteric capsules and pellets were developed to simply avoid degradation in the gastric acidic environment and to modulate the release of the loaded active at desired pH in duodenum (pH 4–5.5.0), jejunum (pH 5.5–7.0), ileum (pH 7.0–7.5) or colon (pH 6–6.7) [47]. Other commonly exploited GI features intended mostly for a smart colon targeting were i) transit time via time-controlled release system releasing the drug after a predetermined lag time, ii) pressure as the intense colonic peristalsis can promote drug release, and iii) microflora for the enzyme-controlled degradation by colonic anaerobic bacteria of polymer-based delivery platforms [48–50]. Then, further insight into intestinal barriers allowed the design of delivery approaches with additional functionalities including facilitation of paracellular and transcellular transport, enzyme inhibition, mucopenetration, mucoadhesion and physical insertion [51] (Fig. 2).

One of the first reported strategies to promote transcellular transport has been the creation of prodrugs [52]. By conjugating propranolol to dendrimers the drug solubility was increased and Pgp efflux protein transporters was bypassed leading to an enhancement in absorption and bioavailability [53]. Prodrugs have also been exploited as colon-targeting strategies. Thanks to the covalent linkage to a carrier (amino acids, polysaccharides, polymers, cyclodextrins), the prodrug remained intact through stomach and small intestine and released the active moieties in the colon, following enzymatic hydrolysis [54]. An exemplary case is that of sulfasalazine, a prodrug consisting of mesalazine as active ingredient linked through an azo-bound to the carrier molecule sulfapyridine, for the treatment of inflammatory bowel disease (IBD) [55].

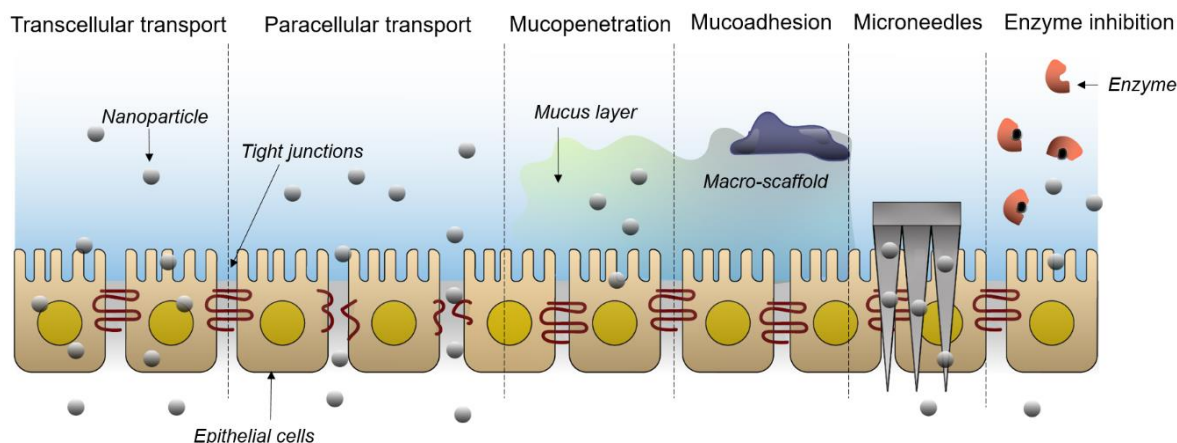


Fig. 2 Mechanisms of action of delivery devices used for oral drug delivery. Common approaches include facilitation of transcellular transport, opening up of paracellular transport, mucopenetration, mucoadhesion, physical insertion and enzyme inhibition. Fig. adapted from Brown et al. (2020) [38].

Nanoparticles, such as polymeric, inorganic, micellar and liposomal nanosystems, offered several advantages for the oral delivery of drugs and biologics [51]. Among them, lipid based nanosystems can increase the paracellular or transcellular permeability by opening tight junctions or by increasing membrane fluidity notably when they contain medium chain fatty acids and lysophospholipids [56,57]. Moreover, the presence of specific surfactants as vitamin E TPGS (d- α -Tocopheryl polyethylene glycol 1000 succinate), Pluronic (poloxamer) and Kolliphors (Polyoxyl castor oil) in their shell, enable them to inhibit efflux transporters by altering the transporter structure or by changing the transporter expression [58]. Further formulation strategies have been addressed to exploit intraluminal fluids as aqueous phase for nano- and microemulsion formation in situ through self-emulsifying drug delivery systems (SEDDS) [59]. Also several vehicles have been developed for oral vaccination purposes aiming at delivering vaccines to the inductive site in gut-associated lymphoid tissue (GALT) [39,40,60,61]. However, the efficient targeting of the intestinal epithelium is often hampered by the presence of the mucus layer [4]. To overcome the mucus barrier the nanoparticle surface has been coated with hydrophilic neutrally charged polymers such as polyethylene glycol (PEG) [62], poly(2-alkyl-2-oxazolines) (POZ) [63], polydopamine (PDA) [64], dextran-containing polymers [65] and poly-(*N*-(2-hydroxypropyl) methacrylamide) (PHPMA) [66] in order to minimize interactions with mucus. Also nanoemulsions have been rendered mucopenetrating by incorporation of PEGylated surfactants in the NE shell [67,68]. Alternatively, oppositely charged polyelectrolytes such as polyacrylic acid (PAA) and chitosan (CH) [69] or zwitterionic polymers such as dilaurylphosphatidylcholine lipids [70] has been included to create nanoparticles that mimic viruses mucopenetrating attitude. Further mucopenetrating strategy is particle decoration with mucolytic enzymes like papain, however the disintegration of the mucus resulting in a temporary loss of mucus protective activity and in pathogens free entry make it not ideal for oral drug delivery [71].

Nanoparticles for colon delivery have been designed to passively target the site of inflammation [72]. Nanoemulsions were coated with mucoadhesive polymers such as pectin and carrageenan to maximise interactions with mucins [73]. Cationic nanosystems were designed to adhere to the negatively charged mucus, whose production is increased in Crohn's disease, leading to a thicker mucus layer in ulcerated

areas [74]. While anionic nanoparticles were designed to adhere to inflamed tissue via electrostatic interaction with positively charged proteins, namely eosinophil protein and transferrin, that are overexpressed in inflamed colon sections of IBD patients [75]. Site-specific delivery into the colon was also achieved via nanoparticles that disintegrated preferentially at high colonic pH levels. Budesonide-loaded nanospheres prepared using polymeric mixtures of poly(lactic-co-glycolic acid (PLGA) and pH-sensitive polymer Eudragit® S100 (Poly (methyl methacrylate) derivative) showed higher colon levels and specific adhesion to the ulcerated and inflamed mucosal tissue of the rat colon [76]. Further colon delivery strategy took advantage of the high levels of reactive oxygen species (ROS) produced at the site of colonic inflammation by designing nanoparticles that degrades selectively in response to ROS [77]. Together with all abovementioned strategies based on a passive targeting mechanism, nanosystem (and loaded-drug) absorption has been achieved through active targeting by functionalising the particle surface with ligands which specifically interact with different cells, transporters and disease sites [78]. Neonatal Fc receptors (FcRn), lectins, vitamins present on enterocytes have been explored as targets for nanoparticles delivery of insulin or paclitaxel, while M cells and dendritic cells have been targeted for oral vaccination purposes [78]. Recently, nanostructured lipid carrier (NLC) has been proved to have an inherent targeting potential for enteroendocrine cells without external ligand modification, offering a novel platform for the treatment of diabetes [79]. Lastly, nanoparticles were prepared to actively target the inflamed colon by using ligands coupled to their surface since the expression of receptors, adhesion molecules and proteins can be altered on the cellular surface of colonic tissues under inflammatory conditions [80].

As an alternative to nanoparticle, several macrosystems have been developed. Wafers, also referred to as thin films or intestinal patches, are mucoadhesive platform intended to increase the retention time of delivered actives specifically in the upper small intestine. In recent years, water-insoluble, enteric and pH-sensitive polymers, fragrances, absorption enhancer, buffer substances and preservatives have been included in their design to create multi-layered intelligent tunable platforms [81]. pH-responsive hydrogels and beads have been developed for protecting the cargo in the stomach and release it in intestinal basic pH [82]. These systems are frequently composed of polysaccharides such as carboxymethyl cellulose, alginate, pectin, and chitosan that confer them mucoadhesive or bioadhesive properties for enhanced residence time and sustained API release [14,33]. pH sensitive hydrogels made of cross-linked polymers able to shrink at low pH and to swell at higher pH such as alginate hydrogels were specifically used for colon targeting purposes [83]. Alternatively, hydrogels and scaffolds were designed as enzyme-controlled delivery platforms that are specifically degraded by colonic anaerobic bacteria, notably azoreductase, glycosidases, esterases and amidases [84]. Microneedles, primarily intended for transdermal and intradermal applications [85,86], have recently seen application in intestinal drug delivery. Examples are the ‘robotic’ RaniPill™ to delivery biologic therapies developed by Rani Therapeutics that successfully completed phase 1 of the first-in-human safety study [87] and the luminal unfolding microneedle injector for macromolecule drugs as insulin designed by Traverso et al. that proved its efficacy in *ex vivo* human and *in vivo* swine studies [88].

Among all oral delivery systems able to cope with the abovementioned barriers, lipid-based nanoparticles have received much attention in recent decades. In the next sections the advantages and technological challenges of these lipid based system and in particular of nanoemulsion and self-emulsifying drug delivery systems will be presented.

I.3 Lipid-based drug delivery systems

Lipid-based drug delivery systems (LBDDS) is a wide-ranging designation for formulations containing a dissolved or suspended drug in lipid excipients. These excipients are oils to improve drug dissolution, surfactants to aid emulsification/solubilisation and co-solvents to favour solvation/dispersion. They are usually composed of fatty acids or lipophilic hydrocarbon chains linked to a hydrophilic group like glycerol, polyglycerol or polyalcohol. The melting range, solubilisation capacity, and miscibility properties of the excipient are defined by the fatty acid chain length and degree of unsaturation. The amphiphilicity or dual polar and non-polar nature of oils and surfactants is characterized by the Hydrophilic Lipophilic Balance (HLB), a measure of the degree to which they are hydrophilic or lipophilic. The relative proportions of each of these materials dictate both solubility and metabolic effects of the drug and stability of the formulation [89].

LBDDS confer a range of biopharmaceutical, pharmaceutical and commercial advantages. The primary benefit is in increases in dissolution and intestinal solubility for lipophilic, poorly water soluble drugs, but it is also becoming increasingly clear that they may provide advantages in enhancing permeability and, under some circumstances, in avoiding first pass metabolism [90]. Hence they have become attractive candidates for the preparation of pharmaceuticals, as well as diagnostics, vaccines, and nutraceuticals [91–94]. They can be administered in a with a range of different finished dose forms (softgels, hard capsules or lipid multiparticulates) and also provide a platform for product life extension.

I.3.1 Classification LBDDS

LBDDS include a wide range of nanosystems that can be classified as: i) vesicular systems such as liposomes and niosomes, ii) fluid emulsified systems such as nanoemulsions (NE), microemulsions and self-emulsifying drug delivery systems (SEDDS), and iii) solid lipid particulate systems such as solid lipid nanoparticles (SLN), nanostructured lipid carrier (NLC) and lipid nanocapsules (LNC) (Fig. 3).

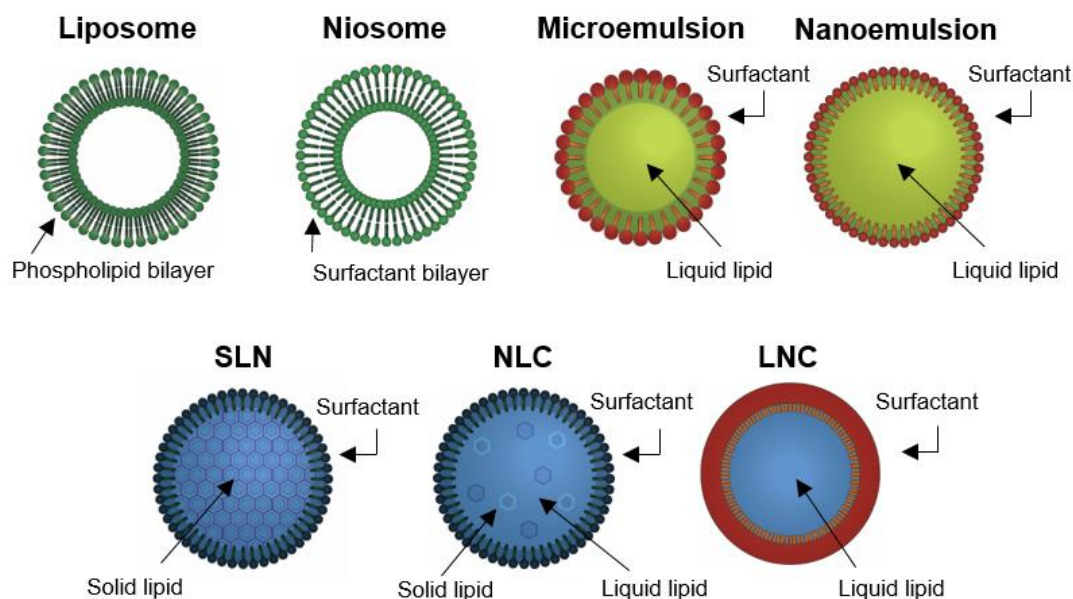


Fig. 3 LBDDS types.

The several LBDDS differ from their structural properties [95]. Liposomes and niosomes are vesicles made of a lipid bilayer of phospholipids and of non-ionic surfactants, respectively. SLN, also known as nanosphere, are nanostructures composed of lipids which are solid at room and physiological temperature and surfactants [96]. NLC share similar structures to SLN, except that the solid lipid core is replaced by a mixture of solid lipids and liquid oil [97]. While LNC exhibit a typical core-shell structure, being the external shell made of solid lipids and emulsifying agents, and the core of liquid oils [98]. Nanoemulsions are thermodynamically unstable colloidal dispersion consisting of two immiscible liquids, with one of the liquids being dispersed as small spherical droplets in the other liquid (oil-in-water, O/W or water-in-oil, W/O). NE droplets size in the nm range (generally below 300 nm) provides numerous advantages regarding stability towards aggregation compared to conventional emulsions, whose droplets are in the μm range [99]. Microemulsions are thermodynamically stable, monophasic and optically clear isotropic colloidal dispersions consisting of small particles (comprised of oil, surfactant, co-surfactant) dispersed within an aqueous medium [100]. Lastly, self-emulsifying nano- and microemulsions are a further category of lipid based systems, as discussed in detail in section I.5.

I.3.2 LBDDS in the clinic

LBDDS accounts for 2–4% of commercialised pharmaceutical formulations [101]. The LBDDS transfer to the clinic dates back to 1983 with Sandimmune (Sandoz) containing cyclosporine A, the first self-emulsifying microemulsion formulation approved by the FDA for transplant rejection. From then onwards, several LBDDS formulations have been marketed for a total of 36 different self-emulsifying formulations FDA approved for the oral route [101] (table 1). Clinical trials studying SEDDS, liposomes, lipid crystal nanoparticle and NE are ongoing showing promising results (table 1) as highlighted by the recent success of a Phase 1b clinical study of iCo's oral Amphotericin B delivery system (iCo 019) which began on December 9 2019 and will be an alternative to the marketed parenteral liposomal and emulsion formulations (AmBisome[®], Amphomul[®]) [102,103].

Orally administered NE and SEDDS, being the subject of this thesis, will be described in detail in the next sections (I.4 and I.5).

Table 1 Marketed or in clinical trials oral LBDDS.

Type of LBDDS	API	Indication	Product/Company	Phase/ ClinicalTrial.gov identifier
SEDDS in soft gelatin capsule	Cyclosporin	Immunosuppressant	Sandimmune®/Novartis	Marketed (1983)
SMEDDS in soft gelatin capsule	Cyclosporin	Immunosuppressant	Neoral®/Novartis	Marketed (1995)
SEDDS IV in hard gelatin capsule	Cyclosporin	Immunosuppressant	Gengraf®/AbbVie	Marketed (2000)
SNEDDS in soft gelatin capsule	Ritonavir	HIV antiviral	Norvir®/AbbVie	Marketed (1996)
SEDDS in Soft gelatin capsule	Saquinavir	HIV antiviral	Fortovase®/Roche	Marketed (1997). Discontinued
SEDDS IV in soft gelatin capsule	Amprenavir	HIV antiviral	Agenerase®/GlaxoSmithKline	Marketed (1999). Discontinued
oil in soft gelatin capsule	Valproic acid	Antiepileptic	Depakene®/AbbVie	Marketed (1978)
oil in soft gelatin capsule	Calcitriol	Calcium regulator	Rocaltrol®/Roche	Marketed (1978)
SEDDS IV in soft gelatin capsule	Bexarotene	Antineoplastic	Targretin®/Ligand	Marketed (1999)
oil in soft gelatin capsule	Tretinoin	Acute promyelocytic leukemia	Vesanoid®/Roche	Marketed (1995)
SEDDS in soft gelatin capsule	Tipranavir	HIV antiviral	Aptivus®/Boehringer Ingelheim	Marketed (2005)
SMEDDS as oral solution	Sirolimus	Immunosuppressant	Rapamune®/ Pfizer	Marketed (1999)
SMEDDS in hard gelatin capsule	Fenofibrate	Anti-Hyper Lipoproteinemic	Lipofen®/ Kowa Pharmaceuticals	Marketed (2006)
SEDDS in soft gelatin capsule	Nintedanib	Pulmonary fibrosis	Ofev®/ Boehringer Ingelheim Pharmaceuticals	Marketed (2014)
SMEDDS in soft gelatin capsule	Calcifediol	Hyperparathyroidism	Rayaldee™/ OPKO Health	Marketed (2016)
Liposome	Iron	Iron deficiency and anemia	Sucrosomial® iron/ Alesco srl	Marketed (2010)
Liposome	Insulin	Type 1 and 2 Diabetes	HDV-I/ Diasome Pharmaceuticals	Type 2: Phase 3/ NCT00521378 (Completed 2009); Type 1: Phase 2b/ NCT02794155 (Completed 2019)
Liposomal gel	Lidocaine	Anesthetic	Brazilian University of Campinas	Phase 1/ NCT01425840 (completed 2011)
Lipid-crystal nanoparticle	Amphotericin B	Vulvovaginal Candidiasis	CAMB/MAT2203/ Matinas BioPharma Nanotechnologies	Phase 2/ NCT02971007 (completed 2018)
Lipid crystal nanoparticle	Amphotericin B	Mucocutaneous candidiasis	CAMB/MAT2203/ Matinas BioPharma Nanotechnologies	Phase 2/ NCT02629419 (Active, not recruiting 2019)
Nanoemulsion	Curcumin	Reduction in aromatase inhibitor-induced symptoms	City of Hope Medical Center	Phase -/ NCT03865992 (Recruiting 2020)
Nanoemulsion	Methotrexate	Left Ventricular Remodeling After STEMI	ddMTX-LDE/InCor Heart Institute	Phase 2-3/ NCT03516903 (Recruiting 2020)
SEDDS	Amphotericin B	Visceral Leishmaniasis	iCo 010/019/ iCo Therapeutics	Phase 1-2/ ACTRN12619001762145 (Suspended 2019)
Emulsion	Elemene	Antitumoral	BeiJing Yijiyi Medicine Techonoloy Co.	Phase -/ NCT03166553(Recruiting 2016)

I.4 Nanoemulsions

Since their first article using the term “*nanoemulsion*” appeared in 1996 [104], NE have been widely exploited as delivery systems for oral administration because of: i) high entrapment efficiency of hydrophobic drugs, ii) characteristic dynamic microstructure which results in better drug solubilizing capacity and rapid and free drug diffusion, iii) possibility to be formulated into different dosage forms with ease of manufacture and scale-up [94,95,105].

NE applications range from food [106] to pharmaceutical industry. They are ideal vehicles for hydrophobic drugs like antiosteoporotics [107], antidiabetics [108,109], antivirals [110,111], anti-inflammatories [112] and antihypertensives [113]. In addition, NE have been developed for the oral delivery of hydrophilic proteins as insulin in the form of insulin-phospholipid complex and bovine serum albumin (BSA). The encapsulation within these systems did not alter the bioactivity, specificity and conformational structure of the protein [114,115]. Vaccine delivery via NE has been explored by targeting receptors on intestinal epithelial M cells to induce anti-tumor immune protection. [39].

Because of all these reasons, the design of NE is an attractive field of research. In the following paragraphs we will shed light on the current state of NE as for their formulation process, physicochemical and structural characteristics and related technological challenges.

I.4.1 Formulation methods

The adequate selection of manufacturing techniques and system components allows the formulation of NE with required physicochemical characteristics [116]. NE can be formulated by either high- or low-energy approaches (Fig. 4). The high-energy approaches exploit mechanical devices, while in the low-energy ones no external energy is furnished to the system and the droplets formation is spontaneous under precise system conditions [117].

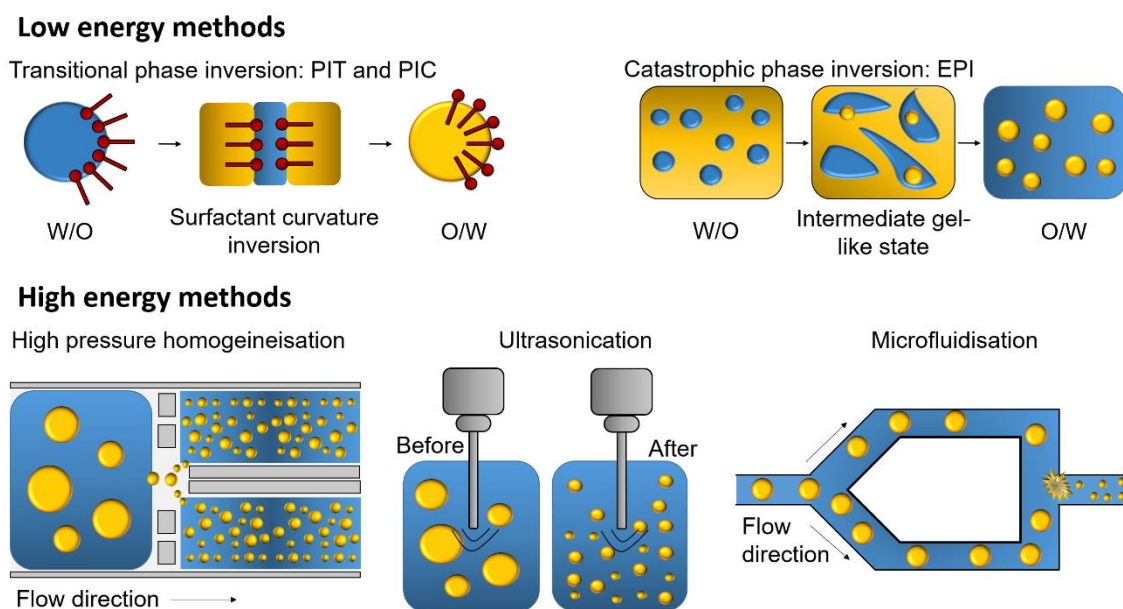


Fig. 4 Methods of nanoemulsion formulation : Low energy methods: phase inversion temperature (PIT), phase inversion composition (PIC), emulsion phase inversion (EPI). High energy methods: high-pressure homogenization, microfluidization and ultrasonication.

I.4.1.1 High energy

High energy approaches rely on the generation of extreme disruptive forces to facilitate the oil phase disruption in smaller droplets and to exceed the restorative tendency that would lead to droplet coalescence. The size of the formed NE droplets is highly dependent on homogenizer type, energy intensity, temperature and system composition (surfactant type, viscosity, interfacial tension) [118]. High-pressure homogenization, microfluidization and ultrasonication are the most commonly used high energy methods for O/W NE production [119–122]. Major limitations to the exploitation of high energy approaches are the extreme heat generated that may cause decomposition of actives or surfactants and the high cost of the equipment, that are currently restricting industrial scale-up and commercialization [123]. Worthy of mention is the use of high shear mixers notably the Ultra-Turrax®, as economic, easy and rapid alternative approach for nanoemulsion formulation. This technique is the classic procedure for the emulsion and microemulsion preparation, but if applied to nanoemulsion having an optimized oil and surfactant amount (surfactant to oil ratio, SOR) it can lead to fine NE droplet size refinement [112,124].

I.4.1.2 Low energy

Low energy methods can be classed as spontaneous emulsification or phase inversion methods.

The process of spontaneous emulsification, also referred to as self-emulsification, implies the rapid diffusion of water-miscible solvent and surfactant molecules from the organic to the aqueous phase without changes in the surfactant spontaneous curvature [125]. Self-micro- and nanoemulsifying drug delivery systems (SMEDDS and SNEDDS) rely on this mechanism to generate oil in water (O/W) micro or nanoemulsions, in which hydrophobic drugs are dispersed, upon direct dispersion in the GI tract [126]. Insights will be given in section I.5. Besides, if modifications of the surfactant spontaneous curvature during emulsification are involved the methods are referred to as transitional phase inversion ones. The surfactant curvature inversion depends on a change in formulation parameters, notably the temperature in the phase inversion temperature (PIT) method, or the composition of oil and aqueous phases in the phase inversion composition (PIC).

In the PIT method the phase inversion involves the transformation of an emulsion from the W/O to the O/W type or vice-versa through an intermediate bi-continuous phase thanks to changes in the surfactant physicochemical properties with temperature [127,128]. In recent years several NE have been formulated by PIT aiming at the delivery of hydrophobic actives such as isohexadecane [129] and mineral oil [130]. Moreover, the PIT method has been used as a template for the production of other nanoparticles, namely the LNC by Benoit research group [131]. A limitation of the technique is the range of exploitable surfactants that is usually restricted to thermosensitive polyoxyethylene non-ionic surfactants, in which the temperature variation modifies the hydration of the poly(oxyethylene) chains, consequently increasing their solubility and changing their curvature [116].

In the PIC method an alteration in the composition such as the salt concentration leads to the phase inversion. An example of NE preparation by the PIC is the one of lidocaine-loaded NE. Initially, a W/O emulsion containing a high salt concentration is prepared. Upon dilution with water the ionic strength is reduced and the salt ions are not sufficient enough to screen electrical charge on the surfactant head groups leading to changes in the surfactant curvature from negative to positive and transition from W/O to O/W system [132].

Further method for NE production is the emulsion phase inversion (EPI) method. The EPI relies on a different type of phase inversion called catastrophic, in which the NE formation is triggered by changes in conditions such as the ratio between dispersed and continuous phases. Water is progressively titrated over a mixture of oil and hydrophilic surfactants under continuous stirring leading to the transformation of a W/O in a hydrogel-like intermediate multiple emulsion and finally in a stable O/W emulsion [94]. The method has been widely explored for the delivery of natural products having antitumor activity, nutraceuticals, vitamins and for the formulation of NE composed of food-grade ingredients [94,133,134]. The main drawbacks associated with low energy methods are the limited types of oils and emulsifiers that can be used and the need for large amount of surfactants for droplet stabilization that can cause biomembrane fluidization [123]. Sometimes formulating nanoemulsions by low-energy approaches requires the presence of co-surfactants (such as short and medium-chain alcohols) or co-solvents (such as polyols like propylene glycol, glycerol, and sorbitol). Organic solvents are usually removed by evaporation, but residuals can remain in the final product, causing potential toxic effects and limiting the NE large-scale production and wide application [117].

I.4.1.3 Novel formulation approaches

In addition to traditional methods, novel approaches for the nanoemulsion production include bubble bursting, evaporative ripening, microfluidic and High-Gravity Rotating Packed Bed methods.

The bubble bursting method, in which nanosized oil droplets are formed by bubble collapse following the bubbling of a gas through an oil/water/surfactant mixture, has been proved to be adaptable to NE production providing an energy-efficient platform with potential up-scalability for applications in drug delivery, food production and materials science [135].

Microfluidics by making use of intersecting microchannels induce the precipitation of components as nanoparticles on the base of the 'anti-solvent approach', offering the advantages of high reproducibility, ease of optimization and scalability under Good Manufacturing Practices (GMP) conditions [136]. In a recent work a staggered herringbone micromixer was used to develop castor oil nanoemulsions showing excellent dispersion quality and reproducibility [137].

Lastly, High-Gravity Rotating Packed Bed (RPB) has been proposed as an alternative to facilitate the industrial production of drug-loaded NE by decreasing the surfactant content in the formulation. In the preparation of NE made of glycerol triacetate/RH-40/1, 2-propanediol, the use of RPB allowed to reduce the amount of mixed surfactants of 75% compared to self-emulsification method and to obtain stable and highly monodispersed 13 nm droplets able to efficiently permeate Caco-2 cells [123].

I.4.2 Stability in nanoemulsions

Emulsions and nanoemulsions are kinetically stable but thermodynamically unstable systems that are prone to separation over time. The physicochemical mechanisms causing destabilization of emulsions include flocculation, coalescence, gravitational separation and Ostwald ripening (Fig. 5).

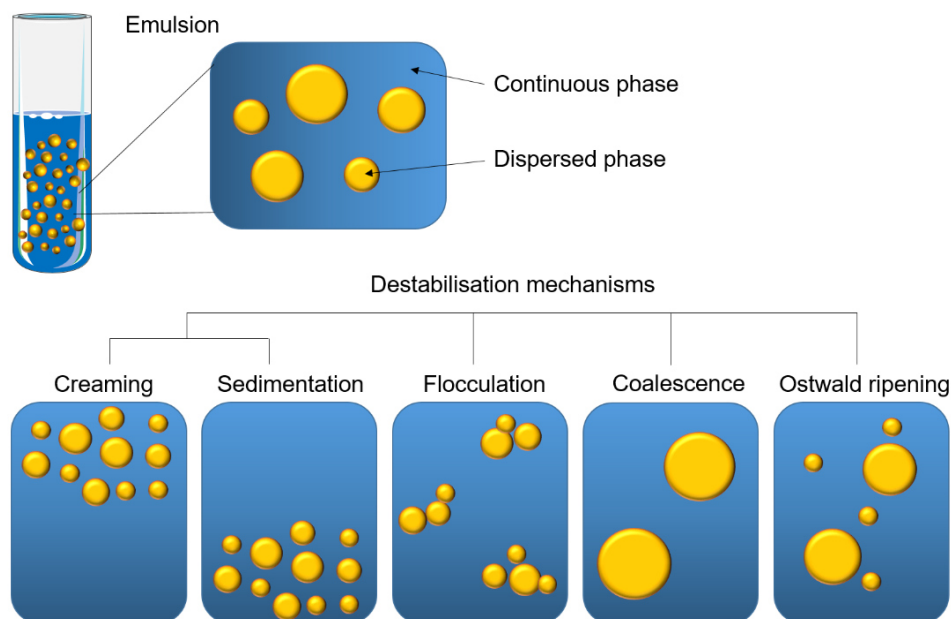


Fig. 5 Schematic diagram of most common instability mechanisms that occur in food emulsions: creaming, sedimentation, flocculation, coalescence, Ostwald ripening and phase inversion.

Flocculation is a reversible process in which droplets come closer to each other due to attractive interactions, while coalescence implies the irreversible merging of several droplets in a bigger one. In contrast to conventional emulsions, nanoemulsions have much better stability to coalescence and flocculation because of the small droplet size and the steric stabilisation which minimize colloidal interactions [138]. The small-sized droplets together with Brownian motion also slow down nanoemulsion gravitational separation, occurring through creaming or sedimentation [133].

Accordingly, Ostwald ripening is the main mechanism of NE instability. Ostwald ripening is the process of mass transfer from small to large droplets driven by the magnitude of Laplace pressure [139]. An increase in the system polydispersity typically leads to higher tendency for Ostwald ripening. Also, instability increases at higher temperature due to changes in solubility and diffusivity and at higher ionic strength of the continuous phase since ions shield the nanoparticle surface charge reducing the Debye length for significant repulsion between droplets [139,140]. Ostwald ripening rate can be slowed down by selecting oil phase components with a very low water-solubility, such as long chain triglycerides [141]. The use of mixed emulsifiers has been recently suggested to retard the rate of Ostwald ripening by i) decreasing the interfacial tension, ii) decreasing the diffusion coefficient of the oil molecules through the shell by increasing the shell thickness, iii) increasing the mechanical strength or lastly iv) opposing the state of thermodynamical instability that creates when droplets have a different interfacial composition via the restriction of emulsifier transfer. The last usually occurs when using a highly water soluble surfactant, able to migrate between droplets, and a highly lipophilic one, which always stays attached to the NE core [142]. Moreover, a negative or positive surface charge confers nanoparticle stability thanks to enhanced electrostatic repulsive forces [143]. When non-ionic surfactants are used, the steric stabilisation of droplets has to be maximized through the fine control over system composition and formulation process [144].

I.4.3 Conversion in solid dosage forms

Further to the physicochemical processes of destabilisation previously discussed, chemical hurdles such as microbiological contamination, degradation by hydrolysis, loss of the drug pharmacological activity and technological hurdles such as reduced shelf-life, difficulty in transport, storage, scalability can affect the NE full-scale exploitation. Therefore, the stability improvement is a primary concern for these drug delivery systems. The most promising strategy to achieve preparations with shelf life of several years is to eliminate the water out of the aqueous suspensions to obtain dry powders, that can be easily reconstituted in water at a later stage/time or directly *in vivo* at the site of administration.

The development of solid dosage form using drying process can be conducted by various technologies, namely oven/tray, fluidized bed, band, turbo tray, centrifugation, pneumatic, cyclone, drum, vacuum, filter, spray-drying and freeze-drying methods [145].

I.4.3.1 Spray-drying

Spray-drying is a method for the production of powders from solutions, suspensions or dispersions by atomization into a hot drying gas medium, usually air [146]. Spray-drying is mostly considered as a dehydration process aimed to prolong the lifespan of the product, but it can also be used as a method of formulation itself as it allows the micro- and nano-encapsulation of drugs, biologics, chemicals and food bioactive ingredients within a protective matrix [121,147–149].

Several dispersed systems such as emulsions, liposomes or nanocapsules were successfully spray-dried with preservation of their structure using drying auxiliaries such as hydroxypropylmethylcellulose (HPMC) and lactose [150,151]. In more recent years, the feasibility of spray-drying NE has started to be explored, highlighting the benefits of dehydrating the nanodroplets compared to conventional emulsions in terms of dry powder physical properties [152,153] and therapeutic efficacy [154].

The spray-drying process involves the atomization of the feed liquid into the dry chamber through an atomizer or a nozzle that breaks it in fine droplets, followed by the droplets dispersion in a flowing air stream for drying, with the aid of a compressed gas (Fig 6). As soon as the contact with the drying air occurs, the liquid starts evaporate from the droplet surface, developing a significant gradient concentration that is counterbalanced by the movement of nanoparticles and additives from the edge of the droplet to its centre. Consequently, a dried crust is formed at the droplet surface and the surface becomes immobilized. The dry particles are then separated from the drying gas by means of a cyclone that deposits them in a glass collector situated in the bottom of the device [146].

The main advantages of this technique are its being rapid, continuous, single-step, reproducible, scalable and cost-effective. Moreover, it allows the fine control of particle size, shape, morphology and release of the loaded active, it is applicable to both hydrophilic and hydrophobic molecules and provides high encapsulation efficiency [146].

Major challenges are the complete collection of dry particles that leads to low process yields and the obtainment of dry particles having regular spherical shape, low surface fat content, small size that easily re-dispersed in water while maintaining the original physicochemical properties and guarantying the active chemical stability and biological activity.

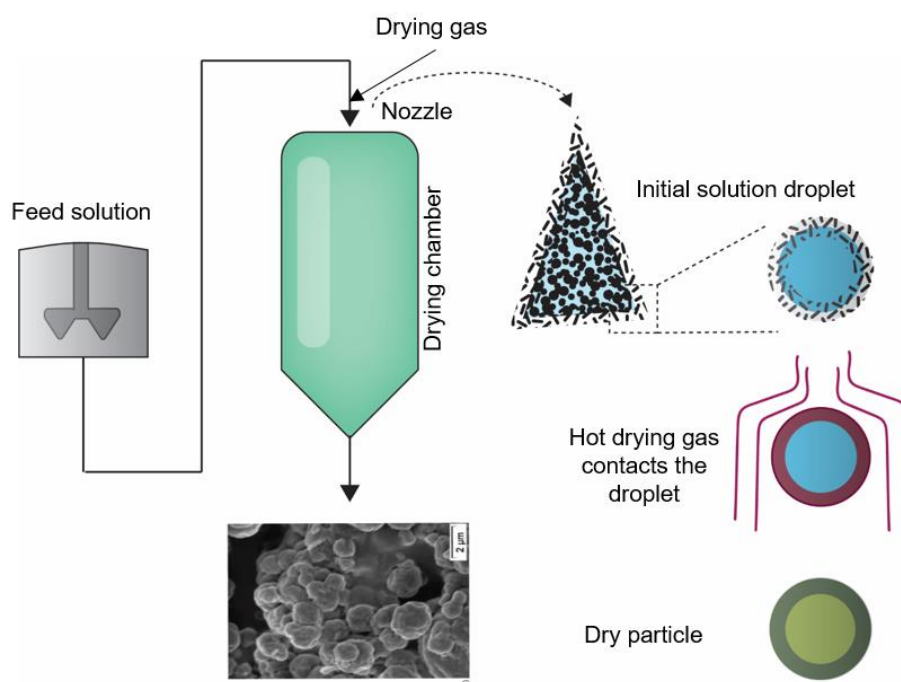


Fig. 6 The spray-drying process.

Both formulation parameters, such as feed composition, viscosity, solvent type, solids concentration and processing parameters, such as inlet and outlet temperature, sample feed rate, atomizer pressure, drying gas flow rate can be tuned to obtain dry products with desired properties, namely smooth and spherical morphology, minimisation of powder stickiness, small dry particle size and to ensure the recovery of NE physicochemical properties after re-hydration [147,152,155].

Feed nanoemulsions can be supplemented with drying excipients, also referred to as wall materials, to protect against drying stress, facilitate powder collection and improve powder re-dispersion.

Exploitable excipients include sugars as sucrose, lactose, mannitol, maltodextrin and polysaccharides namely gum arabic, whey protein, modified starch, hydroxypropyl beta cyclodextrins, polyvinyl alcohol (PVA), polyvinylpyrrolidone (K30-PVP and K90-PVP), hydroxypropylcellulose (HPC), hydroxypropylmethylcellulose (HPMC) [152,153,155–157].

Li et al. evaluated the impact of modified starch, maltodextrin, hydroxypropyl beta cyclodextrins, arabic gum and whey protein at several concentrations and NE: excipient ratio on dry particle morphology, homogeneity and size. When using arabic gum or whey protein at concentration of 15% in ratio 4:1 of NE: excipient, dry nanoparticles with spherical shape and smooth surfaces were obtained. These particles were rapidly re-dispersed in about 5 min with minimal alteration of NE size (< 150 nm) and PDI (< 0.2) [156].

The use of high atomization pressure, small nozzle diameter and low solid concentration feed generally renders smaller dry particles [147]. However, conventional spray-drying is limited for producing particles with characteristic dimension below $1 \mu\text{m}$ because of the atomization technology employed and the generation of a turbulent gas flow. The production of dry particles in the nanometer range is feasible when using newer technologies such as the nano-spray-dryer [153,158,159]. Nano-spray drying has been used for encapsulation of vitamin E-loaded NE in presence of whey protein leading to dry particles in the nm range completely recovering their physicochemical attributes when re-hydrated [153]

and for the solidification of eugenol-loaded NE in absence of drying excipient obtaining spray-dried particles of 200–500 nm which rapidly rehydrated without adversely affecting the antimicrobial activity of eugenol [159]. Examples of spray-dry NE are listed in table 2.

I.4.3.2 Freeze-drying

Freeze-drying, also known as lyophilization, is a dehydration technique based on the removal of water from the system by sublimation under vacuum, at low pressure and at low temperature, leading to an anhydrous product [160]. In the case of polymeric nanoparticles, lipid-based nanosystems (i.e. NLC and liposomes) and macro-emulsions the freeze-drying technique has been widely explored, but its application in the NE domain is still laborious and challenging [161]. Some recent unsuccessful attempts to prepare freeze-dried NE has suggested the use of better performing approaches, less expensive and time consuming, for the production of dry NE [121,162]. However, the benefits of this technique such as the possibility of fine control over the process, the superior product quality and the low temperature that makes it exploitable for thermosensitive drug, are still making it an attractive research subject [161]. A typical freeze-drying cycle consists of three stages: freezing, primary drying and secondary drying. Firstly, samples are freeze at a temperature below the product glass transition temperature (T_g) concentrating the solid content in between the growing ice crystals. Then, ice is removed by sublimation at a pressure below the vapour pressure of the ice and at gradually increasing temperature. Finally, secondary drying allows the elimination of the remaining water by desorption and it usually operates at low pressure and temperature higher than the primary drying step but always below the excipients melting point (Fig. 7). The obtained dried cakes are usually sealed to avoid humidity absorption from the environment during storage [161].

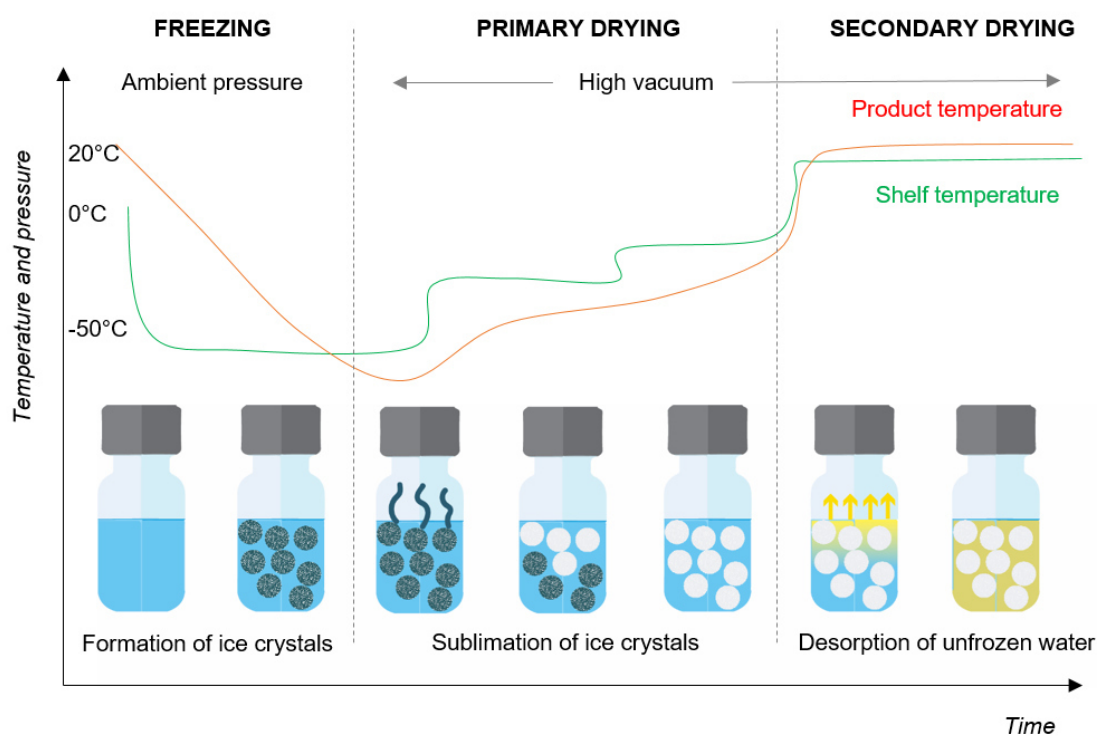


Fig. 7 Freeze-drying cycle, showing shelf, product and condenser temperatures, chamber pressure and product behaviour during the freezing and drying steps.

The main technological challenge is the avoidance of product disruption during the process caused by the several type of stress, notably freezing and dehydration stresses. For a dry NE to be alimentary or pharmaceutically exploitable, it shall comply with the following prerequisites: i) the preservation of the primary chemical and physical characteristics of the product (elegant cake appearance, short reconstitution time, nearly unmodified particle size distribution, lack of drug leakage, unchanged activity of the encapsulated drug), ii) an acceptable residual moisture content, and iii) long-term stability. Droplets aggregation or irreversible fusion and destabilisation caused by the high particulate concentration and the mechanical forces generated during ice crystallization and drying can be avoided by adding special excipient with a protective role against the freezing (cryoprotectant) or drying stress (lyoprotectants) [120]. The exploitable stabilizers range from poly(vinyl alcohol), hydroxypropyl- β -cyclodextrin, poly(vinyl pyrrolidone), gelatine, glycine to sugars as trehalose, sucrose, glucose, lactose, maltose, sorbitol and mannitol [163]. In most published work on NE, an efficient drying was achieved while using trehalose, mannitol or lactose at concentrations ranging from 5 to 20% [164–167]. The level of stabilization generally depends on cryoprotectant concentrations, sugar/lipid nanosystem ratio [166], time and way of the cryoprotectant addition [164], composition and structure of the nanosystem [168,169] and freezing-rate [170,171]. The analysis of literature results reports that up to date no conventional NE could be freeze-dried in absence of stabilizers without alteration of its physicochemical properties after reconstitution [121,162,172] (table 2).

As final proof of the process performance the freeze-dried cakes are reconstituted in water or in biorelevant fluids to assess the re-suspended particles physicochemical characteristics. Reconstitution can be done by hand shaking, vortex or sonication. Li et al observed that when sonication was used the NE size significantly increased while vortexing and hand-shaking did not have any impact, and they concluded that because of its technical convenience hand-shaking should be the method of choice for NE reconstitution [164].

The different types of freeze-dried NE reported in the literature are summarized in table 2.

Ledet et al. reported that the lyophilisation of NE composed of corn oil, Span-80, Tween-80 and loaded with the γ -tocotrienol (GT3), a radioprotective agent intended for the oral administration in case of nuclear accident or exposure to high radiations. The freeze-drying of these NE in presence of lactose prevented GT3 degradation without modification of the NE physicochemical properties [167]. Freeze-drying has also been applied for the solidification of NE loaded with functional food ingredients, as in the case of krill oil NE containing long-chain (ω 3) polyunsaturated fatty acids (LC-(ω 3)-PUFA) [121], and hydrophobic drugs like curcumin and paclitaxel [119,166]. Lastly, lyophilized NE has been used in the in the biotechnology field, mainly as carriers for genes or as adjuvants for vaccine formulations. Studies reported by Orr et al. proved the efficient drying of NE destined be used as an adjuvant for a vaccine formulation, without alteration of the system physicochemical properties and maintenance of immunological activity and resulting protective efficacy against *Mycobacterium tuberculosis* [120,165].

Table 2 Examples of spray-dried and freeze-dried NE.

NE composition and preparation method	Solid carrier	API	Size, Pdl, ζ -potential) before (B) and after (A)	Main achieved advantage	Ref.
Spray drying					
Vitamin E acetate, Kolliphor® ELP. Spontaneous emulsification	Maltodextrin (Md), whey protein (WP)	Vitamin E acetate	B: 84.9 nm, 0.12 A: 140.6 nm, 0.17 (Md); 110.3 nm, 0.27 (WP)	Efficient encapsulation of NE in dry 800 nm particles with preservation of NE physicochemical properties by Nano spray-drying	[153]
Vitamin E acetate, Kolliphor® ELP. Spontaneous emulsification	Arabic gum or whey protein	Vitamin E acetate	B: 84 nm, 0.11 A: < 150 nm, < 0.20	Efficient encapsulation of NE in 2 μ m dry particles showing fast reconstitution, no alteration of NE properties and preservation of vitamin E acetate integrity	[156]
Sodium caseinate and sunflower oil. Microfluidization	Mixture of lactose or 70:30 lactose: sucrose (23.9% w/w)	–	B: 154 nm A: 151 nm (70:30 lactose: sucrose)	Reduced surface free fat content and better morphological properties of NE spray-dried with lactose:sucrose than with pure lactose because of lower crystallization on dry particle surface	[152]
Sodium caseinate and sunflower oil. Microfluidization	Lactose (57.7% w/w)	–	B: - A: around 150 nm	Dry NE crystallized more quickly than emulsions. Lactose increased crystallization rate causing particle aggregation and irregular shape.	[157]
Vegetable oil, Span® 85, Tween® 80. High pressure homogenization	Maltodextrin (3% w/w)	–	B: 110 nm A: 158 nm, Pdl low, -16.4 mV (110 °C, pump rate of 30%)	Importance of processing parameters. High temperature (130°C) and lower pump rate led to increase in droplet size (> 180 nm)	[155]
Algae oil, saponin, β -sitosterol, γ -oryzanol, sodium azide. Ultrasonication	–	Omega-3 (ω -3) polyunsaturated fatty acids	B: 158 nm, 0.21 A: unaffected	Dry powders showed excellent reconstitution, stability over 30-day storage, maximization of fishy off-flavour and oxidative stability.	[122]
Gum Arabic, ethanol, lecithin. UltraTurrax®	–	Eugenol	B: 110 nm, 0.18, -45 mV A: 319.2 nm, 0.47, -56.5 mV	Spherical, smooth, 300-500 nm NE powders by nano spray-drying. No eugenol leakage and preservation of antimicrobial efficacy.	[159]
Capryol® 90, Kolliphor® RH40 and Transcutol® P. Spontaneous emulsification	Lactose (2% w/v)	Curcumin	-	Spherical agglomerated dry particles with smooth surface. Improved oral bioavailability of curcumin in dry NE compared to free drug.	[154]
Lactoferrin (Lf), Omega-3 (ω -3) polyunsaturated fatty acids. High-pressure homogenization	–	Omega-3 (ω -3) polyunsaturated fatty acids	B: 156.7 nm, 0.14, +41.7 mV (Lf 4% w/w) A: -	Smooth defined particles smaller than 500 nm. Loss of Lf secondary structure after nano spray-drying.	[121]

Maltodextrin, whey protein concentrate, gum Arabic, krill oil. Microfluidization and UltraTurrax®	—	Krill oil (Omega-3 (ω 3) polyunsaturated fatty acids)	B: 157.3 nm, -25 mV (2% oil) and -48 mV (4% oil) A: -	Wrinkled, spherical, 1.77 μ m dry particles. Good encapsulation efficiency (70%) and oxidative stability, high <i>in vitro</i> bioaccessibility (80%) during 2 h <i>in vitro</i> gastro-intestinal digestion.	[162]
Freeze-drying					
Soybean oil, Lipoid E-80®, Pluronic® F68, Tween® 80, glycerine, sodium oleate. High-pressure homogenization.	Trehalose or maltose (20%).	Bufadienolides	B: 43.5 nm, 0.10, -19.7 mV A: unvaried	Powders stability up to 3 months, no change in particle size and no drug leakage. Better reconstitution by manual shaking over sonication.	[164]
Poloxamer® 188 and glycerol, 1,2-dimyristoyl-sn-glycero-3-phosphocholine (DMPC), squalene. Microfluidisation.	Trehalose (5% w/v)	Mycobacterium tuberculosis (Mtb) vaccine	B: 70 nm, < 0.10, -13 mV A: 80 nm, < 0.10, -15 mV	Efficient drying of co-valied ID93 proteins and glucopyranosyl lipid adjuvant (GLA)-NE without impairing immunological activity and protective efficacy against Mtb.	[165]
Gum Arabic, ethanol, lecithin. UltraTurrax®	-	Eugenol	B: 110 nm, 0.18, -45 mV A: 528 nm, 0.41, -60 mV	Comparison with nano spray-drying: freeze-drying bad technique for NE stabilisation	[159]
Corn oil, Span® 80, Tween® 80. High pressure homogenization	Lactose (5:1 lactose: NE)	γ -tocotrienol (GT3)	B: 130 nm, 0.10, -30 mV A: 150 nm, 0.22, -40 mV	Lyophilization prevented GT3 degradation.	[167]
DL- α -tocopheryl acetate, soybean oil, Polysorbate coated with hyaluronic acid. Microfluidization	Mannitol (5% w/v)	Paclitaxel	B: - A: 80 nm, 0.20, -37 mV	Dry NE reduced tumour growth and showed less toxicity in tumour-transplanted mice compared to free drug.	[119]
Miglyol® 812, Epikuron® 145V Rotaevaporation of ethanol and acetone	Trehalose (5 and 10% w/w)	Curcumin	B: 200 nm, \leq 0.20, -30 mV A: unvaried	No loss in effectivity upon reconstitution. Efficient prevention of melanoma re-incidence and metastasis. Exploitable for the oral route.	[173]
Poloxamer® 188 and glycerol, 1,2-dimyristoyl-sn-glycero-3-phosphocholine (DMPC), squalene. Microfluidisation.	Disaccharide, glycine, mannitol, trehalose, sucrose	Mtb vaccine	B: 89 nm A: 108 nm	Continuation of [165]. Methodical screening of stabilizing conditions and drying excipients. Stability and maintenance of biological activity of dry NE in heat stress condition storage for 30 days at 50°C.	[120]
Maltodextrin, whey protein, gum arabic, krill oil. Microfluidization and UltraTurrax®	—	Omega-3 (ω 3) polyunsaturated fatty acids	B: 157.3 nm, -25 mV (2% oil) and -48 mV (4% oil) A: -	7-fold increment in particle size, good encapsulation efficiency (60%) and oxidative stability. Spray-drying recommended over freeze-drying.	[162]
Lactoferrin (Lf) and Omega-3 (ω -3) polyunsaturated fatty acids. High-pressure homogenization	—	Omega-3 (ω -3) polyunsaturated fatty acids	B: 156.7 nm, 0.134, +41.7 mV (at Lf 4% w/w) A: -	Comparison with nano spray-drying: freeze-drying bad technique for NE stabilisation.	[121]

I.5 Self-emulsifying drug delivery systems

Self-emulsifying systems are isotropic mixtures of oils, surfactants and hydrophilic co-solvents which spontaneously form nano- or microemulsions upon dispersion in an aqueous phase [59,174].

Self-emulsifying systems are broadly classified into four types according to the Lipid Formulations Classification System (LFCS) proposed by Pouton C.W. et al. [175]. Type I are simple oils that need to be digested in order to form mixed micelles; type II are mixtures of lipids and water-insoluble surfactants (HLB <12), known as self-emulsifying drug delivery systems (SEDDS); type III are lipid formulations containing oil, water-soluble surfactants (HLB >12) and co-solvents; and type IV are lipid formulations that do not contain oil and are based on water-soluble surfactants and co-solvents.

In this thesis, a major focus on type III formulations, namely self-nanoemulsifying drug delivery systems (SNEDDS) and self-microemulsifying drug delivery systems (SMEDDS), is given.

SNEDDS correspond to LFCS type III A and generate nanoemulsions, which are two-phases kinetically stable systems. Instead, SMEDDS correspond to LFCS type III B and form microemulsions, which are one-phase thermodynamically stable systems. Their main characteristics are summarized in table 3.

Table 3 Comparison and conceptual differences between self-emulsifying drug delivery systems on the base of the Lipid Formulations Classification System (LFCS) by Pouton. (PdI : polydispersity index).

		SNEDDS	SMEDDS
Definition		Anhydrous pre-concentrate of nanoemulsion that upon dilution with aqueous phase produce nanoemulsion droplets of 50-250 nm	Anhydrous pre-concentrate of microemulsion that upon dilution with aqueous phase produce microemulsion droplets of <100 nm
Method of preparation		Spontaneous emulsification	Spontaneous emulsification
LFCS type		III A	III B
Typical composition (% w/w)	Triglycerides or mixed glycerides	40-80	<20
	Surfactants	20-40 (HLB > 11)	20-50 (HLB > 11)
	Co-solvents	0-40	20-50
Significance of digestibility		Possibility of inhibition of digestion	Probable absorption without digestion
		Nanoemulsion	Microemulsion
Size		50-250 nm	10-100 nm
PdI		< 0.2	< 0.1
Shape		Spherical	Spherical, lamellar
Appearance		Turbid (Tyndall effect)	Transparent
Stability		Thermodynamically unstable, kinetically stable	Thermodynamically stable
Destabilizing process		Ostwald ripening	Dilution, temperature change

Several advantages can be offered by SMEDDS/SNEDDS compared to conventional emulsified systems.

SMEDDS/SNEDDS are anhydrous pre-concentrates of NEs and microemulsions and consequently they can cope up with stability and formulation related issues of colloidal suspensions, such as poor palatability, unsuitability for delivery through hard or soft gelatin capsule, physical and chemical stability and long-term storage [176]. Besides they offer the benefit of higher solubilisation ability for hydrophobic drugs and possibility of higher administration doses than NE [177]. They can inhibit the

P-gp efflux and increase the permeability by opening tight junctions [178-181]. Moreover, when containing alcohol esters of unsaturated long chain fatty acids they facilitate the drug lymphatic route of uptake thus enhancing the bioavailability [182].

Their production occurs through the mechanism of self-emulsification, also known as spontaneous emulsification, when aqueous and organic phases are brought into contact. The amphiphilic molecules initially present in the organic phase rapidly diffuse in the aqueous phase to minimize the interfacial tension at monolayer curvatures. This leads to interfacial turbulence and oil droplet formation [116]. The proposed mechanism is illustrated in Fig. 8.

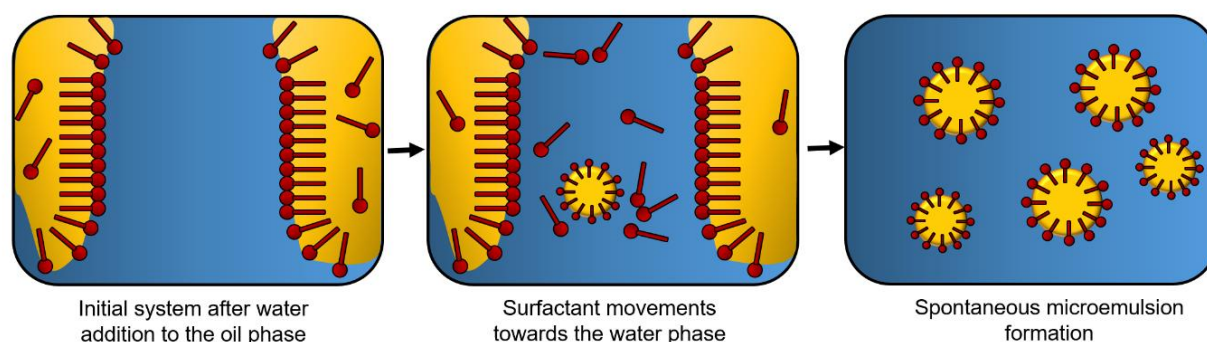


Fig. 8 Schematic representation of the proposed mechanism for spontaneous emulsification.

SEDDS were initially designed for the delivery of hydrophobic actives such as antioxidants, alkaloids, anticancer, immunosuppressant, anti-hypertensive, antiviral, antifungal and antiprotozoal drugs [183]. Then their scope was broadened to hydrophilic macromolecular drugs such as peptides, proteins, polysaccharides and DNA-based drugs [184]. For the loading in the lipophilic phase of SEDDS the macromolecules were firstly dissolved in amphiphile-like phospholipids, solidified and then the solid dispersion was mixed with SEDDS excipients [185]. Alternatively, the drug lipophilicity was increased via the hydrophobic ion pairing technique, consisting in the creation of complexes between hydrophilic drug and oppositely charged lipophilic auxiliary agents [186]. An example is given by insulin, whose complexation with dimyristoyl phosphatidylglycerol (DMPG) by ion pairing previous loading in SNEDDS led to increased permeability and many folds reduced enzymatic degradation [187]. SEDDS have been exploited for oral vaccination purposes. Bernkop-Schnürch A. research group encapsulated bovine serum albumin (BSA) as model antigen into SEDDS containing monophosphoryl lipid A (MPLA) as adjuvant and demonstrated the ability of the system to induce systemic and mucosal immune response following oral administration to mice [92]. SMEDDS have also a potential as colon-targeted delivery systems, as proved by the folate-modified SMEDDS which efficiently delivered curcumin on colon cancer cells after specific binding to folate receptors [188].

1.5.1 Technological challenges

Despite the popularity of SEDDS, there have been some challenges associated with their formulation, packaging and stability. The drawbacks related to the formulation process include the small range of exploitable excipients, the inadequate solubility of drug in the system components and consequently the sub-optimal drug loading [189]. The shortcomings of the packaging reside in the filling in soft gelatine capsules in the industrial production that requires expensive machinery and resources, in the transfer of volatile co-solvents into the capsule shell causing the precipitation of the drug and in the gelatine itself

that if of animal origin can be a medical and religious concern [189]. For all these reasons, substitutes for gelatine like HPMC-based capsules might be the best packaging choice [190].

Furthermore, stability issues, namely the leakage of liquid SEDDS from hard capsules, the oxidation of unsaturated lipids and the polymorphism of lipid components, can limit storage and exploitability of SEDDS [191]. One of the main reported innovations to pave the way for SEDDS with improved technological characteristics is the conversion of liquid SEDDS in solid dosage form, as discussed in the next paragraph.

1.5.2 Solid SEDDS

In the aim of improving SEDDS stability ameliorating drug oral absorption and bioavailability, liquid SEDDS can be converted into solid systems through numerous techniques including capsule filling, melt granulation, extrusion-spheronization, spray-congealing, spray drying, freeze-drying [192,193] or absorbed onto inert carriers and subsequently formulated into free-flowing powders, granules, pellets, tablets, microspheres and nanoparticles [194,195]. In addition to the enhanced system stability, advantages of solid SEDDS are low production costs, ease of transport, handling and storage, precise drug dosing and improved patient compliance [177]. Upon oral administration solid SEDDS firstly disintegrate and then self-emulsify following the same fate as liquid SEDDS. It is therefore fundamental that the drying step does not impair the system properties and that droplets physicochemical characteristics are preserved after re-hydration [196].

The different methods used for the conversion of liquid SEDDS to solid SEDDS and exhaustive examples of their application are summarized in table 4. Among them the spray-drying is the preferred SEDDS solidification method at the industrial scale because of the ease of manufacturing and scale-up. Besides, it provides significant amelioration in dissolution rate, physicochemical characteristics, and stability of the active leading to enhanced biopharmaceutical performance [197,198]. The freeze-drying on the other side is still an open challenge, with only few reported examples in the literature. The associated advantages, notably aseptic conditions, high water content removal and applicability to heat-sensitive compounds, make it a promising solidification alternative to explore [199].

Noteworthy, solid SEDDS have recently been prepared using the three-dimensional printing (3DP) technology. Advantages are the feasibility of solidify in absence of a solid-phase carrier and the fine control of the system geometrical shape (cylindrical, prism, torus and cube) which allows to modulate and control dispersion and digestion rates [200].

Table 4 Examples of solid SEDDS.

SEDDS composition	Solid carrier	Active	Main achieved advantage	Ref.
Spherical crystalline technology				
castor oil, Kolliphor® RH40, 1,2-propanediol	-	Puerarin	No alteration in particle size (19.66 nm), rapid re-dispersion within 60 s and 27-fold and 23-fold improvement of oral bioavailability compared to free drug and liquid SMEDDS.	[201]
castor oil, Kolliphor® RH40, and 1,2-propylene glycol	1:2 of ethyl cellulose: Eudragit S100	Osthole	No SMEDDS changes in terms of morphology, particle size, ζ-potential. Sustained drug release in rabbits. Bioavailability increase by 205% and 152% compared to free drug and liquid SMEDDS	[202]
Adsorption onto a solid carrier				
Capmul® MCM, Tween® 20, tetraglycol	Mannitol, lactose, Sylysia, Aerosil	Atorvastatin calcium	Solid SMEDDS improve oral bioavailability (101%) compared to liquid system	[203]
Capmul® MCM, castor oil, Kolliphor® EL, Kolliphor® RH 40	amorphous silica and Neusilin® US2	Resveratrol	Successful adsorption on Neusilin® US2 and tableting without loss of SMEDDS self-microemulsifying ability	[204]
Hot melt extrusion				
Capric/caprylic triglycerides, Plurol®, Transcutol® HP	HPMCAS, HPC, MCC, talc, colloidal silicon dioxide	Carvedilol	pH dependent effect: rapid and complete microemulsion reconstitution and drug release at pH 6.8, whereas avoided in acidic conditions.	[205]
Extrusion spheronisation				
Tween® 80, PEG 400, Capmul® MCM C8	microcrystalline cellulose	Gliclazide	Solid SMEDDS pellets released the drug in 20 min and reduced significantly plasma glucose levels in albino mice compared to the marketed product.	[206]
Wet granulation				
Capmul® MCM EP, castor oil, Kolliphor® RH 40, PEG 400	Neusilin® US2, HPMC and PVP K30	Carvedilol	Granulation followed by compression into tablets. Preservation of self-microemulsifying properties (size 57 nm, PdI 0.4), high drug loading (65% w/w) and complete drug release in (45 min at pH 6.8, 10 min at pH 1.2).	[207]
Spray-congealing				
Cremophor® EL, Poloxamer 188, PEG 4000 as	Gelucire® 50/13	Glibenclamide	Spray congealed microparticles increased the drug solubilisation of five times. These microparticles showed self-dispersibility within 60 min and micelles dimensions around 360 nm.	[208]
Spray-drying				

Cremophor® RH, Labrasol® , ethyl oleate	mannitol, lactose, maltodextrin, dextran 40, PVP K30 and acacia	Nimodipine	Enhanced drug solubilisation and reduced drug precipitation in gastric fluids via SMEDDS solidified with dextran 40, maltodextrin and PVP K30	[209]
sulfuraphane, Kolliphor® EL, acconon CC6	Soluplus®	Curcumin	More favourable release profiles when compared to the conventional hydrophobic adsorbents	[197]
castor oil, Tween® 80, and Plurol® diisostearique	calcium silicate	Metotrexate	Significantly increased bioavailability compared to the drug powder and drug protection from light-induced degradation	[210]
Miglyol® 812, Cremophor® EL and PEG-600	Aerosil 200	Piperine	Unaltered self-emulsification performance of liquid SMEDDS (size 22.12 ± 0.88 nm, PDI 0.185 ± 0.03). Improved permeation in rat intestine compared with a pure drug	[211]
Lauroglycol® FCC (320 mg) Tween® 80 (1200 mg) and Transcutol® P	Neusilin US2	Canagliflozin	Significantly higher drug plasma concentrations via solid SMEDD and enhanced anti-diabetic activity	[198]
Capryol® 90, Transcutol® HP, Cremophor® EL, Soluplus®	Aerosil 200	Dutasteride	Solid SMEDDS tablets bioequivalence with commercialized drug soft gelatin capsules in beagle dogs	[212]
Freeze-drying				
Kolliphor® HS15, Transcutol® HP, Labrafil® M 1944 CS	Sucrose	Lornoxicam	Enhanced drug solubility and bioavailability than marketed tablets	[193]
Capryol™ 90, Miglyol® 812, Cremophor® RH 40, Transcutol® HP	Trehalose	Febuxostat	Rapid redispersion in 20 s and preservation of liquid SNEDDS physicochemical properties	[199]
Capmul® MCM C8, Tween® 60, PEG 200	Mannitol	Adefovir dipivoxil	Solid SNEDDS enhanced drug absorption in rat intestine compared to free drug and reduced drug pH-dependent variability	[213]

I.6 Hybrid nanosystems for intestinal delivery

The design of smart LBDDS, and more in general of advanced nano- and macro-systems, have addressed various technological and biological challenges, as highlighted in section I.2.

Despite the achievements of these delivery strategies, the development of a product with the ability of delivering drug molecules at a specific target and according to patients' needs is still an avenue to explore. Recently, nanoparticles have been combined with polymers to create hybrid nanosystems.

The different types of hybrid nanosystems can be categorized based on their architecture and surface chemistry. The polymer can be integrated in the form of i) a 3D network in which the nanoparticles are embedded as in the case of the matrix structured hybrid systems, also referred to as polymeric nanocomposites, or ii) a solution/dispersion in which the nanodroplets are suspended as in the case of the self-emulsifying polymer hybrid systems (Fig. 9). The integration of two distinct materials into one formulation results in unique physicochemical and biological properties that neither one of the two building blocks can achieve independently. Advantages arise from the superior capabilities in improving system mechanical strength, modulating drug release kinetics, assisting site-specific drug targeting, increasing drug stability and enhancing drug loading [214]. The main characteristics and applications of polymeric nanocomposites and self-emulsifying polymer hybrids will be presented in the next two sections.

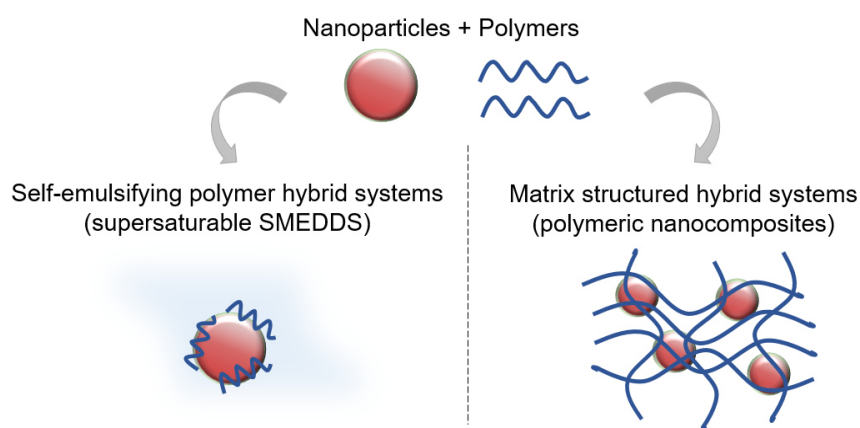


Fig. 9 Different types of hybrid nanosystems deriving from the combination of nanoparticles and polymers: self-emulsifying polymer hybrid systems and matrix structured hybrid systems or polymeric nanocomposites.

I.6.1 Polymeric nanocomposites

Nanocomposites are hybrid delivery devices composed of at least one nano-scale phase, including a variety of lipid, polymeric and inorganic nanocarriers, that are dispersed in a polymeric matrix [82].

After the discovery of the first polymer nanocomposites made of nylon-6/clay to be used in the automobile sector by the Toyota research group back in early 1990s, the nanocomposites' unique properties allowed their use in the manufacture of electronics, aeronautics, medical equipment, as components for solar and fuel cells, electrolytes for batteries, thin-film capacitors, and as biomaterials for delivery purposes [215]. Their application in the context of oral delivery is fairly new and rather promising. Orally administered nanocomposites can have a semi-solid or solid nature and present different shapes and sizes (in the macro or micro scale range) depending on composition and formulation process used. Nanocomposite macro-systems include hydrogels, aerogels, sponges, films, microneedles,

tablets and capsules. While micro-systems, defined as microparticles, comprise microspheres, microgels and microcapsules (Fig.10).

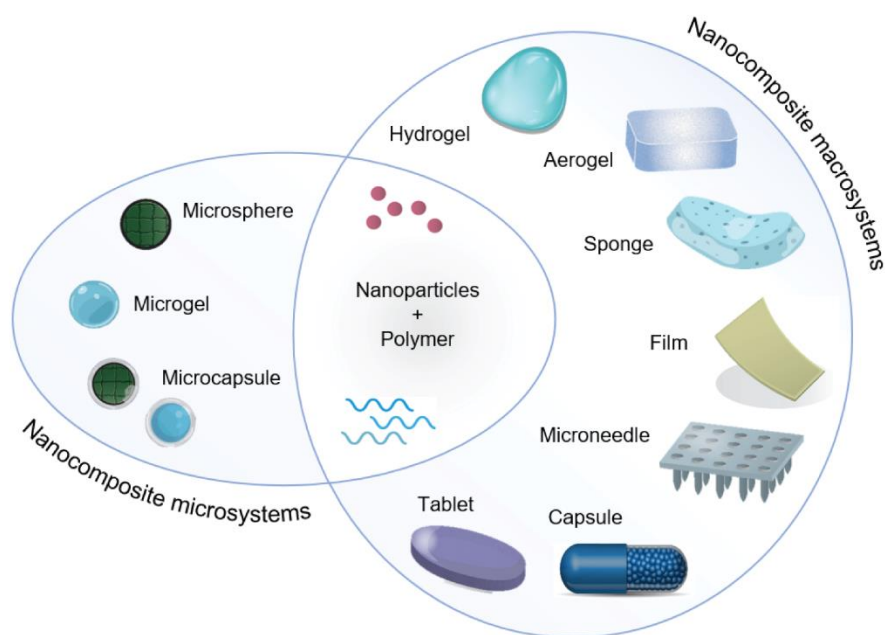


Fig. 10 Several types of nanocomposite systems for oral drug delivery, classified on the base of their micro- or macro-structure.

The most know and widely explored type of macro-systems are nanocomposite hydrogels, semi- solid dosage forms made of a cross-linked 3D network with the ability to swell and retain a large fraction of water within their structure [216]. These hydrogels are commonly made of polymers such as chitosan, alginate, cellulose, xanthan, dextran, carrageenan, polycaprolactone (PCL), carboxymethylcellulose (CMC) and hydroxypropylmethylcellulose (HPMC) [33,82,214].

Several types of nanostructures, namely polymeric, metallic, carbon-based and lipid nanoparticles have been immobilized in hydrogels, resulting in a plethora of composite systems [82]. The embedding of nanosystems occurs mostly via post-insertion of the nanoparticles in a pre-formed hydrogel matrix, or by mixing the nanoparticles with the monomer solution, followed by gelation *in situ* [217,218].

The huge progress that has been made in the field in recent years has led to the development of hydrogel nanocomposites with tailored physical properties and custom-made functionalities.

The incorporation of nanoparticles allowed hydrogels to transport hydrophobic drugs, to target specific parts of the GI tract, to promote the response to a specific physiological-pathological stimulus and to release the nanosystem on-demand. On the other hand, the presence of the hydrogel matrix conferred to nanoparticles higher stability, ensured protection from physical and enzymatic degradation, and guaranteed the sustained release of the loaded cargo, thus providing the attributes necessary for their clinical applications [82].

Because of the fluid and hydrated nature, hydrogels can face practical concerns such as the limited stability during storage, the fast dissolution and burst drug release at certain pH ranges that could lead to poor pharmaceutical performance. Thus, hydrogels have been used as building blocks for the preparation of solid dosage forms, notably aerogels and films [219–224]. Nanocomposite in the form of tablets and capsules have also been developed [10,23].

Ranging from the macro to the micro scale, formulation scientist attention has focused on the design of nanocomposite microparticles, including microsphere, microgels and microcapsules. Thanks to their small size, which is commonly lower than 1000 μm , these systems offer the advantage of easy passage through the intestine and of better coverage of the wide intestinal surface area compared to conventional macrosystems [225]. The loading of the nanoparticles commonly occurs by mixing with the monomer solution, followed by gelation. In composite microspheres, the polymeric matrix in which nanoparticles are embedded, can possess solid or semi-solid nature depending on the formulation process [226-228]. While microgels, also called hydrogel microparticle, possess a semi-solid swollen matrix structure, which facilitates the loading of nanocarriers and tunes their release [62,229]. The sustained release is achieved via i) stimuli-responsive polymers that change under external signals, notably changes in temperature, pH, pressure as for conventional hydrogels, ii) modulation of particle size, since larger particles guarantee larger diffusion distances and smaller surface per volume compared to smaller particles, iii) adjustment of hydrogel mesh size, being the release profile slower for smaller mesh sizes, iv) chemical interactions between particles and matrix, since strong attraction delay the release [225]. Microspheres or microgels have been converted into microcapsules by deposition of a surface coating layer. The purpose of the coating ranges from the protection against degradation in the acidic pH of the stomach, to the avoidance of a burst release particles or loaded-drug, and to the amelioration of system mucoadhesive properties aimed at increasing the residence time in the GI tract [11,230,231]. Because of the tunability in their structural and physicochemical properties, nanocomposites can be designed to target specific portions of the intestinal tract. This has enabled to distinguished between a delivery to the small intestine aiming at increasing systemic drug absorption or allowing for oral local vaccination, and a delivery to the colon aiming at the local treatment of inflammatory bowel diseases (IBD) and colon cancer.

1.6.1.1 Targeting the small intestine

Hybrid nanosystems targeting the small intestine have been proposed as a new class of biomaterials unleashing unique synergistic properties with significant potential to smartly bypass intestinal barriers and improve drug delivery efficiency.

The main purpose in the design of intestinal-targeted hybrid systems has been to avoid gastric degradation and improve systemic bioavailability of hydrophobic APIs [11,232–236]. Besides, polymeric nanocomposites have been explored for hydrophilic proteins such as insulin leading to a major step forward their oral delivery that may revolutionize diabetes treatment [227,231]. Sodium dodecyl sulphate modified-metal-organic framework nanoparticles (Ins@MIL100/SDS) were embedded in microsphere composed of the enteric biodegradable methoxy poly(ethylene glycol)-block-poly(L-lactide) (mPEG-b-PLLA) polymer that protect them from rapid degradation under acidic conditions and specifically release them in the small intestine. The double encapsulation technology increased insulin intestinal absorption and plasma level while lowering blood glucose level with a relative pharmacological availability of 7.8% in diabetic rats [237]. Also antisense oligonucleotide loaded in nanoparticles were combined with chitosan-phytic acid multicompartimental capsules for cancer therapy or with alginate hydrogels Duchenne muscular dystrophy treatment [10,238]. While nanoparticles-in-microsphere oral system (NiMOS) containing the plasmid DNA vectors CMV- β and EGFPN1 were design for oral local vaccination purposes allowing prolonged residence in the small intestine and good transfection capability following oral administration to rats [239].

The exploitation of the mucus barrier for a targeted and sustain delivery has seen its application in mucoadhesive spray-dried HPMC microparticles and chitosan bilaminated films. In a new and more sophisticated technology, mucoadhesive alginate microparticles were embedded with mucopenetrating PEGylated nanoparticles in a failed attempt to achieve prolonged small intestinal retention while guaranteeing the reachment of the epithelium [62].

Lastly, nanocomposites were designed as functional foods able to locally control the rate of lipid digestion within the GI tract of people suffering from obesity or diabetes, opening the way for their use in the food industry [240].

Examples of nanocomposites targeting the small intestine are summarized in table 5.

Table 5 Nanocomposites targeting the small intestine.

SYSTEM					Interaction with the environment	Therapeutic application	Ref
Nanosystem			Matrix				
Type	Size, PdI, ζ -potential	API	Material	Type			
NLC	85.9 nm, 0.43	Amphotericin B	Alginate	Beads, 1.2 mm	pH dependent release in the intestine. NLC to enhance solubility and permeability, beads to target intestine	Systemic: fungal infections, leishmaniasis	[232]
NE	205.3 nm	Nobiletin	Alginate	Hydrogel	Hydrogel swelling at pH 7.4 (intestine). Enhanced drug loading, no drug digestion and precipitation	Systemic: inflammation, cancer, atherosclerosis	[233]
NLC	85.5 nm, 0.23	Quercetin	Alginate hydrogel beads	Beads, 1 mm	pH-dependent and sustained release in the intestine	Systemic: functional food, drug delivery.	[229]
NE	130 nm	-	Alginate or carrageenan	Microgel, 2.5-3 mm	pH-dependent intestinal delivery via microgel dissolution. No lipid digestion in stomach	Local: functional foods for obesity, diabetes patients	[240]
Pickering emulsion	45 nm	Curcumin	Sodium alginate	Hydrogel	pH-dependent intestinal delivery via hydrogel collapse	Systemic: reduce lipid digestion	[234]
Cationic core-shell NP	156 nm, 0.02	Antisense oligoribonucleotide	Alginate	Hydrogel	Increased intestinal adhesiveness. But laxative effect of alginate	Systemic: Duchenne muscular dystrophy	[238]
Gelatine nanoparticles	around 100 nm	Plasmid DNA vectors: CMV- β , EGFPN1	Poly(epsilon-caprolactone) microspheres	Microsphere 5.0 μ m	Intestinal NP release after microsphere degradation by lipases. Internalisation of NP in enterocytes	Local and systemic: therapeutic and vaccination	[239]
Chitosan nanoparticles	192.9 nm, 0.26, +30.9 mV	Antisense oligonucleotide	Chitosan, phytic acid	Multicompartimental capsule, 10 mm	Mucoadhesion in the intestine. Small capsules for delivery to small intestine, and large capsules for colon-targeted delivery	Local and systemic: Cancer	[10]
PEG-based lipid-polymer hybrid vesicles	147 nm, 0.20, -14 mV	-	Alginate	Microgel, 229 μ m	Mucopenetration NP, mucoadhesion hydrogel	Systemic: enhance bioavailability	[62]
SLN	117-192 nm, 0.27	Ibuprofene	Dextran methacrylate	Hydrogel	Sustained drug release	Systemic and/or local	[219]
Nanoparticle (drug nanonization)	724 nm, 0.14	Indinavir	Alginate, chitosan, Eudragit	Nanoparticle-in-Microparticle Delivery System	Increased intestinal residence. Mucoadhesive microparticles. Time-controlled NP release	Systemic: HIV treatment.	[235]
Bovine serum albumin NP	192.7 nm, 0.37, -39.5 mV	Exenatide	Eudragit L, HPMC	Microparticles 1 to 15 μ m	Bioadhesion in intestine (HPMC), gastro-resistance (Eudragit L), lymphatic uptake (dextran)	Systemic: Diabetes	[226]

NP (drug nanonization)	166 nm, 0.51, -61 mV.	Darunavir and Ritonavir	Alginate-chitosan, Eudragit RPLO and S100	Beads	gastro-resistance (Eudragit s100)	Systemic: HIV treatment.	[11]
Carboxylation chitosan-grafted NP	200 nm	Coumarine-6 and insulin	Chitosan-EDTA and ethylcellulose	Bilaminated film, 20 μ m thick	Mucoadhesion and pH dependent release in intestine. Reversible opening of tight junction	Systemic: protein drugs via oral administration	[224]
Graphene quantum dot NP	4–6 nm, -9.6 mV pH 7.4	Naproxen	Carboxymethylcellulose	Beads	pH-sensitive delivery in intestine, reduced GIT irritation induced by NPX	Systemic and local: anti-inflammatory	[241]
Graphene quantum dot NP	15.3 nm	Sodium salicylate	Chitosan, carboxymethylcellulose	Beads	pH-sensitive release in the intestine	Systemic: anti-inflammatory	[230]
i) Alginate NP, ii) alginate-stearic acid NP, iii) alginate-C18 NP	522.5 nm, 0.74, -35.7 mV	Insulin	Alginate and chitosan-oleic acid	Beads	Targeted intestinal delivery. Increased blood insulin level. Decreased intestinal glucose absorption	Systemic: oral insulin delivery	[231]
Benzenetricarboxylic acid nanoparticle	132.8 nm, -18.3 mV	Insulin	mPEG-b-PLLA	Microsphere, 3-5 μ m	NP release in small intestine. Enhanced plasma insulin levels in diabetic rats and lowered blood glucose levels	Systemic: oral insulin delivery	[237]
PCEC micelles	20 nm, <0.20	Docetaxel	MPEGMA, PECA	Hydrogel	pH responsiveness for small intestine targeting. 10-fold higher drug bioavailability, inhibition of tumour growth	Systemic: breast cancer therapy	[236]
Chitosan-coated liposomes	363 nm, 0.32, +23 mV	Insulin	Hydroxypropyl methylcellulose acetate succinate	Microparticles, 19 \pm 1 μ m	Mucoadhesion of NP. Gastro-resistance. Enhanced intestinal paracellular permeability	Systemic: oral insulin delivery	[227]

I.6.1.2 Targeting the colon

Hybrid nanosystems possessing specific colon targeting attributes were designed to improve the biopharmaceutical performance of conventional colonic delivery devices.

Several hybrid nanosystems were developed for a local drug delivery to treat cancer or for systemic and mucosal immunisation, achieving colonic targeted delivery by a pH-dependent dissolution, pH-dependent swelling or transit time-dependent mechanism [23,242–244]. Alginate coated with Eudragit S100 embedded with liposomes were exploited for the local delivery of the anticancer alkaloid capsaicin aiming at the local treatment of colon carcinoma. Specific and sustained colonic delivery was ensured by specific drug release at pH of 7 thanks to the pH dependent dissolution of the Eudragit coating [245]. Besides, systemic absorption through targeted colon delivery was achieved via the loading of PLGA nanoparticle in Eudragit FS30D microspheres intended to induce both rectal and vaginal immunity. Thanks to the pH-dependent release mechanism, ascribable to the Eudragit FS30D dissolution in the upper colon, the vaccine encapsulated in the nanoparticles was specifically delivered to the large intestinal mucosa inducing colorectal immunity in mice [246].

Colon-targeted nanocomposites have received significant attention for their potential to treat IBD, which predominantly affects the colon [247]. The presence of the macrosystem also ensured the long-term delivery, benefit that is fundamental for patients suffering from chronic diseases requiring multiple dosage regimes [248]. These nanocomposites mainly exploited the altered physio-pathological conditions of the inflamed intestinal tract, achieving a colonic targeted delivery via a passive mechanism of bioadhesion, mucoadhesion, specific enzymatic degradation and size-dependent accumulation or via an active mechanism based on the interaction with specific receptors [249–253]. Chitosan-alginate hydrogel beads containing folate-functionalised nanoparticles for IBD treatment were designed to target folate receptors that are over-expressed in inflammatory responses. After oral administration to dextran sulfate sodium (DSS)-induced colitis mice colitis symptoms were significantly alleviated and colitis wound healing was accelerated [249]. Alternatively, a hierarchical structured (nano-in-nano-in-micro) system containing negatively charged hyaluronic acid on the nanoparticle surface was designed to bind to positively charged proteins which accumulate on enterocytes due to destruction and increased discontinuity of the mucus layer. *In vivo* studies in DSS-induced colitis mice proved that the nanocomposite efficiently protected, transported and released the loaded drug locally to inflamed sites of intestine, contributing to superior therapeutic efficacy and significantly reduced systemic drug exposure [253].

Examples of nanocomposites for colon delivery are enlisted in table 6.

Table 6 Nanocomposites targeting the colon.

SYSTEM					Interaction with the environment	Therapeutic application	Ref
Nanophase			Matrix				
Type	Size, PdI, ζ -potential	API	Material	Type			
Liposomes	-	Bee Venom Peptide	Alginate, Eudragit S100	Beads 1 mm	pH and time dependent release	Local delivery: several treatments	[13]
Liposomes coated with Chitosan.	190 nm	5-ASA	Eudragit S100	Microsphere 100 μ m	Dissolution-dependent release	Local delivery: inflammations	[242]
PLGA NP	300-400 nm	FITC-BSA and TLR-agonist peptides	Eudragit FS30D or L100-55	Microsphere 50 μ m	pH dependent release (Eudragit FS30D soluble above pH 7 - terminal ileum)	Systemic delivery: mucosal immunization	[254]
AuNP	2-5 nm	5-ASA and Ornidazole	HPMC	Tablet	release determined by swelling at pH higher than 7	Local delivery: inflammations	[23]
Graphene Oxide nanosheets		Curcumin	PVA+GO-NN-GO	Hydrogel	release determined by swelling at different pH	Local delivery: colon cancer	[244]
Liposomes	284 nm, -61 mV	Capsaicin	Alginate, Eudragit S100	Beads 1 mm	release determined by the pH thanks to the Eudragit coating	Local delivery: colon carcinoma	[243]
Folate-functionalised PLGA-PLA NPs	246 nm, -29 mV	6-shogaol	Alginate, Chitosan	Beads 1 mm	Active drug targeting to folate receptors over-expressed in inflammatory responses	Local delivery: UC wound healing	[249]
Nanogels	115 nm, 18 mV	siRNA-anti TNF α	MAA+NVP polymer, trypsin GRRRGK peptide	Microgel lyophilized of < 30 μ m	degradation of microgel by trypsin in the intestine. Accumulation of nanogel in inflamed area	Local delivery: inflammation, TNF overexpression	[250]
DMDDO-Crosslinked (Xr), non-crosslinked (Non-Xr) micelles	Xr: 121 nm, 0.27; Non-Xr: 115 nm, 0.46	Resveratrol	Chitosan-carballylic acid	Hydrogel	Mucoadhesion and chitosan degradation by the colon microflora	Local delivery: IBD	[251]
Nanoparticle	-	antisense oligonucleotide	Chitosan-Alginate	Hydrogel	The hydrogel specific release of particles in the colon	Local delivery: IBD, Colon-targeting	[252]
Silicon-NPs coated with hyaluronic acid (HA) loaded with nanogels	Psi-HA: 200 nm, 0.11, -30 mV	Budesonide	hydroxypropyl methylcellulose acetate succinate	Microparticle, 35 μ m	HA target NP at intestinal inflammation site, pH dependent degradation of and release	Local delivery: IBD	[253]
Gelatin NPs containing siRNA	200 nm	Plasmid DNA expressing IL10	poly(epsilon-caprolactone)	Microparticle	Intestine release after PCL degradation due to lipase	Local delivery: IBD	[228]
Double emulsion	366 nm	Tripeptide Lys-Pro-Val (KPV)	Alginate and chitosan	Hydrogel	Mucoadhesion to inflamed area. pH-dependent release	Local delivery: IBD	[255]

1.6.2 Self-emulsifying polymer hybrid systems

During past few years, the exploitation of new functional excipients and the selection of specific lipids/surfactant combinations have allowed SEDDS to overcome several biological barriers [256–271]. However, despite these several improvements there still are some challenges that can be hardly faced by SEDDS alone. Notably, the SEDDS toxicity due to the presence of large quantity of surfactants (60% w/w) that can increase the chances of GI irritation and lead to poor toleration during chronic use [196]. Secondly, the precipitation of the active *in vivo* because of the loss of the system solubilisation capacity and the creation of a supersaturated drug state as a result of sharp pH changes, dilution of the formulation with body fluids, or digestion of the solubilizing excipients [59]. Precipitation occurs in three main steps, supersaturation, nucleation, and crystal growth, and results in compromised bioavailability [272]. To prevent this, SEDDS can be combined with polymers to create hybrid systems able to cope with conventional SEDDS limitations. The main class of self-emulsifying-polymer hybrids are the supersaturable SEDDS.

1.6.2.1 Supersaturable SEDDS

Supersaturable formulations are able to induce a supersaturated drug concentration when exposed to the aqueous environment of the GI tract and maintain the supersaturated state for a time long enough to guarantee complete drug absorption [273]. A thermodynamically unstable, supersaturated solution of a drug is usually generated when the solubility of the drug in the system excipients is exceeded, leading to drug precipitation [274]. To benefit from the supersaturated state for increasing absorption, precipitation has to be retarded or avoided. This can be achieved by increasing drug solubility by addition of solubilizing agents such as surfactants, co-solvents, cyclodextrins that reduce the degree of supersaturation [275] or by adding in the formulation precipitation inhibitors that maintain a highly supersaturated state of the drug *in vivo* (Fig. 11) [276].

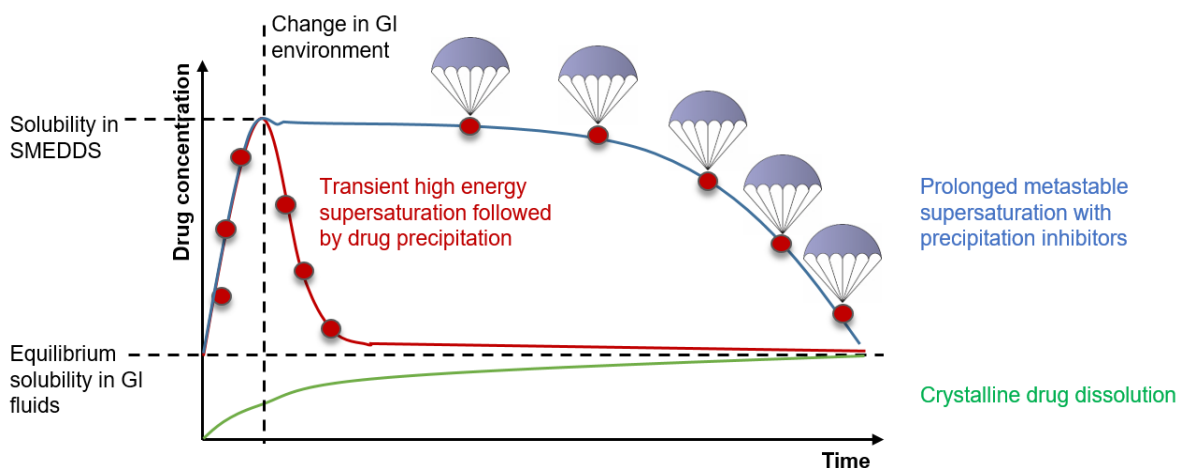


Fig. 11 Illustration of the supersaturation mechanism. The drug delivery ability of conventional dosage form, which dissolve in the GI fluids, is limited by the drug solubility in the fluids (green line). While SMEDDS/SNEDDS disperse the drug in their excipients providing high solubilized drug concentrations. Changes in the environmental conditions (pH, dilution, digestion) can reduce their solubilisation capacity, letting the drug in a supersaturated state and consequently the drug precipitate (red line). The addition of precipitation inhibitors (PI) allows to maintain the drug in its supersaturated

state for longer time, delaying drug precipitation (blue line). Reproduced with modification from Brouwers et al. (2009) [274].

The addition of precipitation inhibitors has made SEDDS efficient at overcoming challenges related to the harsh intestinal intraluminal environment, notably the dilution-dependent drug precipitation [277–279], the pH-driven supersaturation [280,281] and the degradation by digestion [282], resulting in improved drug bioavailability. PI were included in SEDDS to reduce the surfactant amount by replacing surfactants thus decreasing the system toxicity [283–285]. Moreover, PI enhanced the intestinal permeability, as was the case for the positively charged Eudragit® E PO that provided strong electrostatic interactions with epithelial cells improving transcellular transport [181].

The most commonly used precipitation inhibitors (PI) are polymeric PIs such as D- α -Tocopherol polyethylene glycol 1000 succinate (TPGS), Poloxamers, Kolliphor® EL, HPMC, HPMC-AS, HPC, CMC, MC, cellulose, acetate phthalate, alginic acid, HEC, Na-CMC, arabic gum, PVP, PVP-VA, PVA, PAA, several Eudragit® (polymethacrylate-based copolymers) and Soluplus® (polyvinyl caprolactam–polyvinyl acetate–polyethylene glycol graft copolymer) [59].

Facile synthesis approaches are utilized to fabricate self-emulsifying-polymer hybrids, mainly consisting in the addition of the PI to the SEDDS pre-concentrate, followed by gentle physical mixing and/or heating to produce a uniform sample [59]. The concentration of PI added is excipient- and system-dependent, but frequently ranges from 0.5-5 % w/w. The different methods of PI addition depend upon the solubility of the PI in the S-SEDDS. PIs can be dissolved in the SEDDS lipid phase as in the case of soluble PI such as Poloxamer 407 [286] or they can be suspended in the SEDDS lipid phase when the PIs are not soluble in lipids as for HPMC [277] and HPC-L [280], Soluplus® [284]. Alternatively, PIs can be dissolved in soluble solvent and then mixed with the lipid phase. An example is the case of HPMC or Soluplus® that were firstly suspended in ethanol or a mixture of water and ethanol, then added to SEDDS mixture and spray dried [287]. Lastly, the PIs powder can be blended with solid SEDDSs, as done by Quan et al. who successfully solidified SEDDS by solvent evaporation and then mixed the SEDDS powder with Soluplus® [278].

The PIs ability to prevent drug precipitation from lipid formulations has been well established, however it still is unknown whether the site of action of the PIs is in the aqueous phase, the lipid phase or at the interface. The PI process of stabilisation can involve several mechanisms that can coexist and complement each other. H-bonds and hydrophobic interactions between polymers and drugs can inhibit nucleation and crystal growth, while the selection of polymers of high rigidity and high molecular weight helps to better absorb the drug crystals and prolong the supersaturated state [273]. Furthermore, being the rate of crystal growth proportional to the diffusion rate in the medium, an enhancement in the system viscosity via PI addition can positively impact drug precipitation [280,282].

The number of designed S-SEDDS has exponentially increased in the past few years. Some of the most representative examples are summarised in table 7.

For sustained delivery purposes, S-SEDDS were converted in solid dosage forms. The matrix used for the solidification acts as release controlling agent and helps in modulating release after re-hydration in situ. Some matrix-type solid S-SEDDS such as spherical granules and pellets were developed, offering the benefits of both absorption improvement and sustained release of drug [59].

As an alternative to the supersaturation approach, SEDDS were formulated as matrix structured systems aiming at a sustained and targeted drug delivery at the intestinal site. The formulation method involves the addition of the SEDDS pre-concentrate in polymers' porous matrix. Since the formation of the nano- or microparticles occurs in situ in the GI tract, these matrix systems cannot be defined as nanocomposites and we mentioned them below as a separate category. A first strategy relied on the production of matrix-embedded SMEDDS as solid dosage forms. Baek et al. loaded SMEDDS in a gelatin matrix and spray-dried them as microparticles leading to controlled dutasteride absorption [288]. These formulations differ from conventional SMEDDS solid dosage forms since the polymeric matrix is aimed to a technological or biological activity and it does not simply act as solidifying excipient. Matrix structured SMEDDS were also formulated as sponges by freeze-drying. SMEDDS were embedded in alginate or HPMC porous matrix, allowing to enhance drug loading, to form microemulsion droplets in situ and to prolong drug release [289,290]. While in an effort to achieve a targeted delivery composite SMEDDS were designed as hydrogels. Examples are offered by the SMEDDS-Eudragit® S100 hydrogels that enabled targeted simvastatin release at pH of 7 in the distal ileum region [291] and the SEDDS alginate beads that ensured pH-dependent gamma-oryzanol release in the small intestine [292].

Table 7 Examples of supersaturable SEDDS.

Type	Precipitation inhibitor	Size, Pdl, ζ -potential	API	Outcome/advantage	Ref
S-SNEDDS	HPMC (5% w/w)	213 nm, 0.47	Trans-resveratrol	Reduced drug precipitation, improved intestinal permeability and oral bioavailability	[277]
S-SEDDS	PVP (5% w/v)	114 nm, < 0.40, -4.2 mV	Cyclosporine A	Apparent concentration–time profile comparable to that of conventional SEDDS with reduced use of oil, surfactant, and co-solvent	[283]
S-SMEDDS	HPC-L (5% w/w)	195 nm, 0.22, +57 mV	Raloxifene hydrochloride	pH-modified S-SMEDDS formulation B (phosphoric acid): inhibition of drug precipitation, increased the solubility and dissolution rate. Compatibility with hard gelatin capsule.	[280]
S-SEDDS	Soluplus® (6% w/v)	68.6 nm, 0.32, -1.8 mV	Tacrolimus	Four times lower oil, surfactant, and co-solvent content but release rate and pharmacokinetic parameters comparable to SEDDS.	[284]
Super-SSEDDS	Soluplus® (15% w/w)	132.8 nm, 0.19	Fenofibrate	Suppression of drug precipitation. Improvement of oral relative bioavailability of 40% compared to conventional solid SEDDS.	[278]
S-SEDDS	HPMC (5% w/w)	266 nm, 0.36, -33.8 mV	Krill oil	Potent hypotriglyceridemic effect, enhanced nutraceutical properties of krill oil.	[293]
SEDDS	Vit E TPGS (20% w/w)	18.8 nm (TPGS), 193 nm (Labrasol)	Indomethacin or probucol	TPGS inhibit precipitation and achieve high drug supersaturation levels. Raman spectroscopy to study precipitation.	[294]
S-SNEDDS	PVP/VA 64 (20% w/w)	47.3 nm	Simvastatin	Drug loading of 200%, precipitation inhibitory effect during <i>in vitro</i> lipolysis compared to SNEDDS.	[282]
S-SMEDDS	Poloxamer 407 (7% w/w)	110 nm, 0.31	Valsartan	pH-independent, rapid, and high dissolution, in situ permeability and <i>in vivo</i> PK. Tween 80: P-gp inhibitory effect.	[180]
S-SNEDDS	Soluplus®, Poloxamer407 (5% w/w)	62.2 nm, 0.25	carvedilol	Inhibition of drug precipitation at basic intestinal pH, improved bioavailability (397.41%) compared to commercial capsules	[281]
S-SNEDDS	HPMC K4M (2% w/w)	25.60 nm, -10.2 mV	Luteolin	Inhibition of drug precipitation, more excellent <i>in vitro</i> dissolution and <i>in vivo</i> drug oral bioavailability in rats when compared to both SNEDDS and drug suspension.	[279]
S-SMEDDS	PVP K30 (0.5%, w/w)	44.3 nm, -23.1 mV	Ellagic acid	Enhanced API <i>in vivo</i> antioxidant ability	[295]
S-SEDDS	HPMC (5%, w/w)	114 nm, 0.46	Ginger extract	Enhanced dissolution, prolonged systemic exposure with three-fold higher oral bioavailability in rats (100 mg/kg) than free extract and hepatoprotective function.	[285]
S-SEDDS	Poloxamer 407 (10% w/w)	221.4 nm, 0.51	Silymarin	PI effect concentration and type-dependent: Poloxamer 407 > HP β CD, HPMCP, Eudragit L100.. Enhanced oral bioavailability <i>in vivo</i> in Rabbits	[286]
S-SMEDDS	Poloxamer 407 10%, w/w)	121.2 nm, 0.21	Valsartan	Concentration dependent PI effect. Enhanced dissolution in SGF (pH 1.2) of granules and Tablets. Improved oral bioavailability in rat (1.8-fold >than Diovan®, 10 mg/kg).	[296]
S-SMEDDS	Eudragit® E PO (1, 3, or 5% w/w)	21.8 nm, 0.21	Curcumin	Inhibition of drug precipitation in SGF. Reduction of Caco-2 cell toxicity. Higher permeability across the Caco-2 monolayer by paracellular (tight junction opening) and transcellular (PI positive charge) transport. Improved bioavailability in rats.	[181]

I. References

- [1] FDA, Drug Approvals and Databases, (2020). <https://www.fda.gov/drugs/development-approval-process-drugs/drug-approvals-and-databases>.
- [2] A.A. Date, J. Hanes, L.M. Ensign, Nanoparticles for oral delivery: Design, evaluation and state-of-the-art, *J. Control. Release.* 240 (2016) 504–526. doi:10.1016/j.jconrel.2016.06.016.
- [3] J. Holmgren, C. Czerkinsky, Mucosal immunity and vaccines, *Nat. Med.* 11 (2005) S45. doi:10.1038/nm1213.
- [4] L.M. Ensign, R. Cone, J. Hanes, Oral drug delivery with polymeric nanoparticles: The gastrointestinal mucus barriers, *Adv. Drug Deliv. Rev.* 64 (2012) 557–570. doi:10.1016/j.addr.2011.12.009.
- [5] Y. Liu, F. Wang, Z. Shah, X. Cheng, M. Kong, C. Feng, X. Chen, Nano-polyplex based on oleoyl-carboxymethyl-chitosan (OCMCS) and hyaluronic acid for oral gene vaccine delivery, *Colloids Surfaces B Biointerfaces.* 145 (2016) 492–501. doi:10.1016/j.colsurfb.2016.05.035.
- [6] X. Han, Y. Lu, J. Xie, E. Zhang, H. Zhu, H. Du, K. Wang, B. Song, C. Yang, Y. Shi, Z. Cao, Zwitterionic micelles efficiently deliver oral insulin without opening tight junctions, *Nat. Nanotechnol.* 1 (2020). doi:10.1038/s41565-020-0693-6.
- [7] C. He, H. Yue, L. Xu, Y. Liu, Y. Song, C. Tang, C. Yin, siRNA release kinetics from polymeric nanoparticles correlate with RNAi efficiency and inflammation therapy via oral delivery, *Acta Biomater.* 103 (2020) 213–222. doi:10.1016/j.actbio.2019.12.005.
- [8] N.A.H. Abou Youssef, A.A. Kassem, M.A.E. EL-Massik, N.A. Boraie, Development of gastroretentive metronidazole floating raft system for targeting *Helicobacter pylori*, *Int. J. Pharm.* 486 (2015) 297–305. doi:10.1016/j.ijpharm.2015.04.004.
- [9] K.-M. Hwang, C.-H. Cho, N.-T. Tung, J.-Y. Kim, Y.-S. Rhee, E.-S. Park, Release kinetics of highly porous floating tablets containing cilostazol, *Eur. J. Pharm. Biopharm.* 115 (2017) 39–51. doi:10.1016/j.ejpb.2017.01.027.
- [10] T. Kim, J.U. Kim, K. Yang, K. Nam, D. Choe, E. Kim, I.-H. Hong, M. Song, H. Lee, J. Park, Y.H. Roh, Nanoparticle-Patterned Multicompartmental Chitosan Capsules for Oral Delivery of Oligonucleotides, *ACS Biomater. Sci. Eng.* 4 (2018) 4163–4173. doi:10.1021/acsbiomaterials.8b00806.
- [11] R. Augustine, D.L. Ashkenazi, R.S. Arzi, V. Zlobin, R. Shofti, A. Sosnik, Nanoparticle-in-microparticle oral drug delivery system of a clinically relevant darunavir/ritonavir antiretroviral combination, *Acta Biomater.* 74 (2018) 344–359. doi:10.1016/j.actbio.2018.04.045.
- [12] N. Iglesias, E. Galbis, M. Díaz-Blanco, R. Lucas, E. Benito, M.-V. De-Paz, Nanostructured Chitosan-Based Biomaterials for Sustained and Colon-Specific Resveratrol Release, *Int. J. Mol. Sci.* 20 (2019) 398. doi:10.3390/ijms20020398.
- [13] L. Xing, C. Dawei, X. Liping, Z. Rongqing, Oral colon-specific drug delivery for bee venom peptide: development of a coated calcium alginate gel beads-entrapped liposome, *J. Control. Release.* 93 (2003) 293–300. doi:10.1016/j.jconrel.2003.08.019.
- [14] B. Homayun, X. Lin, H.-J. Choi, Challenges and Recent Progress in Oral Drug Delivery Systems for Biopharmaceuticals, *Pharmaceutics.* 11 (2019) 129. doi:10.3390/pharmaceutics11030129.
- [15] A.M.C. Faria, A.C. Gomes-Santos, J.L. Gonçalves, T.G. Moreira, S.R. Medeiros, L.P.A. Dourado, D.C. Cara, Food components and the immune system: From tonic agents to allergens, *Front. Immunol.* 4 (2013) 102. doi:10.3389/fimmu.2013.00102.
- [16] D.M. Denbow, *Gastrointestinal Anatomy and Physiology*, in: *Sturkie's Avian Physiol.* Sixth Ed., Elsevier Inc., 2015: pp. 337–366. doi:10.1016/B978-0-12-407160-5.00014-2.
- [17] Q. Fu, J. Sun, X. Ai, P. Zhang, M. Li, Y. Wang, X. Liu, Y. Sun, X. Sui, L. Sun, X. Han, M. Zhu, Y. Zhang, S. Wang, Z. He, Nimodipine nanocrystals for oral bioavailability improvement: Role of mesenteric lymph transport in the oral absorption, *Int. J. Pharm.* 448 (2013) 290–297. doi:10.1016/j.ijpharm.2013.01.065.
- [18] N. Volk, B. Lacy, *Anatomy and Physiology of the Small Bowel*, *Gastrointest. Endosc. Clin. N. Am.* 27 (2017) 1–13. doi:10.1016/j.giec.2016.08.001.
- [19] A. des Rieux, V. Fievez, I. Théate, J. Mast, V. Pr at, Y.-J. Schneider, An improved in vitro model of human intestinal follicle-associated epithelium to study nanoparticle transport by M cells, *Eur. J. Pharm. Sci.* 30 (2007) 380–391. doi:10.1016/j.ejps.2006.12.006.
- [20] M.E. V. Johansson, D. Ambort, T. Pelaseyed, A. Sch utte, J.K. Gustafsson, A. Ermund, D.B.

- Subramani, J.M. Holmén-Larsson, K.A. Thomsson, J.H. Bergström, S. van der Post, A.M. Rodríguez-Piñero, H. Sjövall, M. Bäckström, G.C. Hansson, Composition and functional role of the mucus layers in the intestine, *Cell. Mol. Life Sci.* 68 (2011) 3635–3641. doi:10.1007/s00018-011-0822-3.
- [21] J.S. Dutton, S.S. Hinman, R. Kim, Y. Wang, N.L. Allbritton, Primary Cell-Derived Intestinal Models: Recapitulating Physiology, *Trends Biotechnol.* 37 (2019) 744–760. doi:10.1016/j.tibtech.2018.12.001.
- [22] M.E. V. Johansson, G.C. Hansson, Keeping Bacteria at a Distance, *Science* (80-.). 334 (2011) 182–183. doi:10.1126/science.1213909.
- [23] R. Das, D. Das, P. Ghosh, S. Dhara, A.B. Panda, S. Pal, Development and application of a nanocomposite derived from crosslinked HPMC and Au nanoparticles for colon targeted drug delivery, *RSC Adv.* 5 (2015) 27481–27490. doi:10.1039/C5RA02672E.
- [24] H. Li, J.P. Limenitakis, T. Fuhrer, M.B. Geuking, M.A. Lawson, M. Wyss, S. Brugiroux, I. Keller, J.A. Macpherson, S. Rupp, B. Stolp, J. V. Stein, B. Stecher, U. Sauer, K.D. McCoy, A.J. Macpherson, The outer mucus layer hosts a distinct intestinal microbial niche, *Nat. Commun.* 6 (2015) 8292. doi:10.1038/ncomms9292.
- [25] C.D. Davis, J.A. Milner, Gastrointestinal microflora, food components and colon cancer prevention, *J. Nutr. Biochem.* 20 (2009) 743–752. doi:10.1016/j.jnutbio.2009.06.001.
- [26] C. Stillhart, D. Dürr, M. Kuentz, Toward an Improved Understanding of the Precipitation Behavior of Weakly Basic Drugs from Oral Lipid-Based Formulations, *J. Pharm. Sci.* 103 (2014) 1194–1203. doi:10.1002/jps.23892.
- [27] G.A. Ruiz, M. Opazo-Navarrete, M. Meurs, M. Minor, G. Sala, M. van Boekel, M. Stieger, A.E.M. Janssen, Denaturation and in Vitro Gastric Digestion of Heat-Treated Quinoa Protein Isolates Obtained at Various Extraction pH, *Food Biophys.* 11 (2016) 184–197. doi:10.1007/s11483-016-9429-4.
- [28] J. Huang, Q. Shu, L. Wang, H. Wu, A.Y. Wang, H. Mao, Layer-by-layer assembled milk protein coated magnetic nanoparticle enabled oral drug delivery with high stability in stomach and enzyme-responsive release in small intestine, *Biomaterials.* 39 (2015) 105–113. doi:10.1016/j.biomaterials.2014.10.059.
- [29] M. Koziolok, S. Alcaro, P. Augustijns, A.W. Basit, M. Grimm, B. Hens, C.L. Hoad, P. Jedamzik, C.M. Madla, M. Maliepaard, L. Marciani, A. Maruca, N. Parrott, P. Pávek, C.J.H. Porter, C. Reppas, D. van Riet-Nales, J. Rubbens, M. Stelova, N.L. Trevaskis, K. Valentová, M. Vertzoni, D.V. Čepo, M. Corsetti, The mechanisms of pharmacokinetic food-drug interactions – A perspective from the UNGAP group, *Eur. J. Pharm. Sci.* 134 (2019) 31–59. doi:10.1016/j.ejps.2019.04.003.
- [30] M. Vertzoni, P. Augustijns, M. Grimm, M. Koziolok, G. Lemmens, N. Parrott, C. Pentafragka, C. Reppas, J. Rubbens, J. Van Den Abeele, T. Vanuytsel, W. Weitschies, C.G. Wilson, Impact of regional differences along the gastrointestinal tract of healthy adults on oral drug absorption: An UNGAP review, *Eur. J. Pharm. Sci.* 134 (2019) 153–175. doi:10.1016/j.ejps.2019.04.013.
- [31] S. Amidon, J.E. Brown, V.S. Dave, Colon-Targeted Oral Drug Delivery Systems: Design Trends and Approaches, *AAPS PharmSciTech.* 16 (2015) 731–741. doi:10.1208/s12249-015-0350-9.
- [32] P.M. van Hasselt, G.E.P.J. Janssens, T.K. Slot, M. van der Ham, T.C. Minderhoud, M. Talelli, L.M. Akkermans, C.J.F. Rijcken, C.F. van Nostrum, The influence of bile acids on the oral bioavailability of vitamin K encapsulated in polymeric micelles, *Journal of Controlled Release* 133 (2009) 161–168. doi: 10.1016/j.jconrel.2008.09.089.
- [33] E. Taipaleenmäki, B. Städler, Recent Advancements in Using Polymers for Intestinal Mucoadhesion and Mucopenetration, *Macromol. Biosci.* 20 (2020) 1900342. doi:10.1002/mabi.201900342.
- [34] T. Pelaseyed, J.H. Bergström, J.K. Gustafsson, A. Ermund, G.M.H. Birchenough, A. Schütte, S. van der Post, F. Svensson, A.M. Rodríguez-Piñero, E.E.L. Nyström, C. Wising, M.E. V. Johansson, G.C. Hansson, The mucus and mucins of the goblet cells and enterocytes provide the first defense line of the gastrointestinal tract and interact with the immune system, *Immunol. Rev.* 260 (2014) 8–20. doi:10.1111/imr.12182.
- [35] W.W. Sun, E.S. Krystofiak, A. Leo-Macias, R. Cui, A. Sesso, R. Weigert, S. Ebrahim, B. Kachar, Nanoarchitecture and dynamics of the mouse enteric glycocalyx examined by freeze-etching

- electron tomography and intravital microscopy, *Commun. Biol.* 3 (2020) 5. doi:10.1038/s42003-019-0735-5.
- [36] S.G. Nugent, Intestinal luminal pH in inflammatory bowel disease: possible determinants and implications for therapy with aminosalicylates and other drugs, *Gut.* 48 (2001) 571–577. doi:10.1136/gut.48.4.571.
- [37] K. Netsomboon, A. Bernkop-Schnürch, Mucoadhesive vs. mucopenetrating particulate drug delivery, *Eur. J. Pharm. Biopharm.* 98 (2016) 76–89. doi:10.1016/j.ejpb.2015.11.003.
- [38] T.D. Brown, K.A. Whitehead, S. Mitragotri, Materials for oral delivery of proteins and peptides, *Nat. Rev. Mater.* 5 (2020) 127–148. doi:10.1038/s41578-019-0156-6.
- [39] P. Long, Q. Zhang, M. Xue, G. Cao, C. Li, W. Chen, F. Jin, Z. Li, R. Li, X. Wang, W. Ge, Tomato lectin-modified nanoemulsion-encapsulated MAGE1-HSP70/SEA complex protein vaccine: Targeting intestinal M cells following peroral administration, *Biomed. Pharmacother.* 115 (2019) 108886. doi:10.1016/j.biopha.2019.108886.
- [40] S. Ma, L. Wang, X. Huang, X. Wang, S. Chen, W. Shi, X. Qiao, Y. Jiang, L. Tang, Y. Xu, Y. Li, Oral recombinant *Lactobacillus* vaccine targeting the intestinal microfold cells and dendritic cells for delivering the core neutralizing epitope of porcine epidemic diarrhea virus, *Microb. Cell Fact.* 17 (2018) 20. doi:10.1186/s12934-018-0861-7.
- [41] B.M. Denker, S.K. Nigam, Molecular structure and assembly of the tight junction, *Am. J. Physiol. Physiol.* 274 (1998) F1–F9. doi:10.1152/ajprenal.1998.274.1.F1.
- [42] X. Han, Y. Lu, J. Xie, E. Zhang, H. Zhu, H. Du, K. Wang, B. Song, C. Yang, Y. Shi, Z. Cao, Zwitterionic micelles efficiently deliver oral insulin without opening tight junctions, *Nat. Nanotechnol.* 1 (2020). doi:10.1038/s41565-020-0693-6.
- [43] J. Zhao, M.H. Stenzel, Entry of nanoparticles into cells: the importance of nanoparticle properties, *Polym. Chem.* 9 (2018) 259–272. doi:10.1039/C7PY01603D.
- [44] H. Lian, Z. He, Z. Meng, Rational design of hybrid nanomicelles integrating mucosal penetration and P-glycoprotein inhibition for efficient oral delivery of paclitaxel, *Colloids Surfaces B Biointerfaces.* 155 (2017) 429–439. doi:10.1016/j.colsurfb.2017.04.045.
- [45] N. Rouge, P. Buri, E. Doelker, Drug absorption sites in the gastrointestinal tract and dosage forms for site-specific delivery, *Int. J. Pharm.* 136 (1996) 117–139. doi:10.1016/0378-5173(96)85200-8.
- [46] M. Durán-Lobato, Z. Niu, M.J. Alonso, Oral Delivery of Biologics for Precision Medicine, *Adv. Mater.* 32 (2020) 1901935. doi:10.1002/adma.201901935.
- [47] J.A.C. Barbosa, M.M. Al-Kaurashi, A.M. Smith, B.R. Conway, H.A. Merchant, Achieving gastroresistance without coating: Formulation of capsule shells from enteric polymers, *Eur. J. Pharm. Biopharm.* 144 (2019) 174–179. doi:10.1016/j.ejpb.2019.09.015.
- [48] A. Gazzaniga, P. Iamartino, G. Maffione, M.E. Sangalli, Oral delayed-release system for colonic specific delivery, *Int. J. Pharm.* 108 (1994) 77–83. doi:10.1016/0378-5173(94)90418-9.
- [49] D.R. Friend, New oral delivery systems for treatment of inflammatory bowel disease, *Adv. Drug Deliv. Rev.* 57 (2005) 247–265. doi:10.1016/j.addr.2004.08.011.
- [50] T. Takaya, C. Ikeda, N. Imagawa, K. Niwa, K. Takada, Development of a Colon Delivery Capsule and the Pharmacological Activity of Recombinant Human Granulocyte Colony-stimulating Factor (rhG-CSF) in Beagle Dogs, *J. Pharm. Pharmacol.* 47 (1995) 474–478. doi:10.1111/j.2042-7158.1995.tb05834.x.
- [51] T.D. Brown, K.A. Whitehead, S. Mitragotri, Materials for oral delivery of proteins and peptides, *Nat. Rev. Mater.* 5 (2020) 127–148. doi:10.1038/s41578-019-0156-6.
- [52] G. Fuhrmann, A. Grotzky, R. Lukić, S. Matoori, P. Luciani, H. Yu, B. Zhang, P. Walde, A.D. Schlüter, M.A. Gauthier, J.-C. Leroux, Sustained gastrointestinal activity of dendronized polymer–enzyme conjugates, *Nat. Chem.* 5 (2013) 582–589. doi:10.1038/nchem.1675.
- [53] A. D’Emanuele, R. Jevprasesphant, J. Penny, D. Attwood, The use of a dendrimer-propranolol prodrug to bypass efflux transporters and enhance oral bioavailability, *J. Control. Release.* 95 (2004) 447–453. doi:10.1016/j.jconrel.2003.12.006.
- [54] D. Kim, S. Hong, S. Jung, Y. Jung, Y.M. Kim, Synthesis and Evaluation of N-Nicotinoyl-2-{2-(2-Methyl-5-Nitroimidazol-1-yl)Ethoxy}-D,L-Glycine as a Colon-Specific Prodrug of Metronidazole, *J. Pharm. Sci.* 98 (2009) 4161–4169. doi:10.1002/jps.21720.
- [55] M.A. Peppercorn, P. Goldman, The role of intestinal bacteria in the metabolism of

- salicylazosulfapyridine., *J. Pharmacol. Exp. Ther.* 181 (1972) 555–62. <http://www.ncbi.nlm.nih.gov/pubmed/4402374>.
- [56] T. Lindmark, Y. Kimura, P. Artursson, Absorption enhancement through intracellular regulation of tight junction permeability by medium chain fatty acids in Caco-2 cells., *J. Pharmacol. Exp. Ther.* 284 (1998) 362–9. <http://www.ncbi.nlm.nih.gov/pubmed/9435199>.
- [57] K. Koga, Y. Kusawake, Y. Ito, N. Sugioka, N. Shibata, K. Takada, Enhancing mechanism of Labrasol on intestinal membrane permeability of the hydrophilic drug gentamicin sulfate, *Eur. J. Pharm. Biopharm.* 64 (2006) 82–91. doi:10.1016/j.ejpb.2006.03.011.
- [58] B.M. Johnson, W.N. Charman, C.J.H. Porter, An in vitro examination of the impact of polyethylene glycol 400, pluronic P85, and vitamin E d- α -tocopheryl polyethylene glycol 1000 succinate on P-glycoprotein efflux and enterocyte-based metabolism in excised rat intestine, *AAPS PharmSci.* 4 (2002) 193–205. doi:10.1208/ps040440.
- [59] H. Park, E. Ha, M. Kim, Current Status of Supersaturable Self-Emulsifying Drug Delivery Systems, *Pharmaceutics.* 12 (2020) 365. doi:10.3390/pharmaceutics12040365.
- [60] S. Jain, H. Harde, A. Indulkar, A.K. Agrawal, Improved stability and immunological potential of tetanus toxoid containing surface engineered bilosomes following oral administration, *Nanomedicine Nanotechnology, Biol. Med.* 10 (2014) 431–440. doi:10.1016/j.nano.2013.08.012.
- [61] C. Primard, N. Rochereau, E. Luciani, C. Genin, T. Delair, S. Paul, B. Verrier, Traffic of poly(lactic acid) nanoparticulate vaccine vehicle from intestinal mucus to sub-epithelial immune competent cells, *Biomaterials.* 31 (2010) 6060–6068. doi:10.1016/j.biomaterials.2010.04.021.
- [62] E. Taipaleenmäki, G. Christensen, E. Brodskij, S.A. Mouritzen, N. Gal, S. Madsen, M.S. Hedemann, T.A. Knudsen, H.M. Jensen, S.L. Christiansen, F.V. Sparsø, B. Städler, Mucopenetrating polymer – Lipid hybrid nanovesicles as subunits in alginate beads as an oral formulation, *J. Control. Release.* 322 (2020) 470–485. doi:10.1016/j.jconrel.2020.03.047.
- [63] T.M.M. Ways, W.M. Lau, K.W. Ng, V. V. Khutoryanskiy, Synthesis of thiolated, PEGylated and POZylated silica nanoparticles and evaluation of their retention on rat intestinal mucosa in vitro, *Eur. J. Pharm. Sci.* 122 (2018) 230–238. doi:10.1016/j.ejps.2018.06.032.
- [64] B. Poinard, S. Kamaluddin, A.Q.Q. Tan, K.G. Neoh, J.C.Y. Kah, Polydopamine Coating Enhances Mucopenetration and Cell Uptake of Nanoparticles, *ACS Appl. Mater. Interfaces.* 11 (2019) 4777–4789. doi:10.1021/acsami.8b18107.
- [65] Y. Song, Y. Shi, L. Zhang, H. Hu, C. Zhang, M. Yin, L. Chu, X. Yan, M. Zhao, X. Zhang, H. Mu, K. Sun, Synthesis of CSK-DEX-PLGA Nanoparticles for the Oral Delivery of Exenatide to Improve Its Mucus Penetration and Intestinal Absorption, *Mol. Pharm.* 16 (2019) 518–532. doi:10.1021/acs.molpharmaceut.8b00809.
- [66] M. Liu, J. Zhang, X. Zhu, W. Shan, L. Li, J. Zhong, Z. Zhang, Y. Huang, Efficient mucus permeation and tight junction opening by dissociable ‘mucus-inert’ agent coated trimethyl chitosan nanoparticles for oral insulin delivery, *J. Control. Release.* 222 (2016) 67–77. doi:10.1016/j.jconrel.2015.12.008.
- [67] M.J. Santander-Ortega, M. Plaza-Oliver, V. Rodríguez-Robledo, L. Castro-Vázquez, N. Villaseca-González, J. González-Fuentes, E.L. Cano, P. Marcos, M. V. Lozano, M.M. Arroyo-Jiménez, PEGylated Nanoemulsions for Oral Delivery: Role of the Inner Core on the Final Fate of the Formulation, *Langmuir.* 33 (2017) 4269–4279. doi:10.1021/acs.langmuir.7b00351.
- [68] S. Zaichik, C. Steinbring, M. Jelkmann, A. Bernkop-Schnürch, Zeta potential changing nanoemulsions: Impact of PEG-corona on phosphate cleavage, *Int. J. Pharm.* 581 (2020) 119299. doi:10.1016/j.ijpharm.2020.119299.
- [69] M. Abdulkarim, N. Agulló, B. Cattoz, P. Griffiths, A. Bernkop-Schnürch, S.G. Borros, M. Gumbleton, Nanoparticle diffusion within intestinal mucus: Three-dimensional response analysis dissecting the impact of particle surface charge, size and heterogeneity across polyelectrolyte, pegylated and viral particles, *Eur. J. Pharm. Biopharm.* 97 (2015) 230–238. doi:10.1016/j.ejpb.2015.01.023.
- [70] W. Shan, X. Zhu, W. Tao, Y. Cui, M. Liu, L. Wu, L. Li, Y. Zheng, Y. Huang, Enhanced Oral Delivery of Protein Drugs Using Zwitterion-Functionalized Nanoparticles to Overcome both the Diffusion and Absorption Barriers, *ACS Appl. Mater. Interfaces.* 8 (2016) 25444–25453. doi:10.1021/acsami.6b08183.

- [71] C. Menzel, A. Bernkop-Schnürch, Enzyme decorated drug carriers: Targeted swords to cleave and overcome the mucus barrier, *Adv. Drug Deliv. Rev.* 124 (2018) 164–174. doi:10.1016/j.addr.2017.10.004.
- [72] S. Hua, E. Marks, J.J. Schneider, S. Keely, Advances in oral nano-delivery systems for colon targeted drug delivery in inflammatory bowel disease: Selective targeting to diseased versus healthy tissue, *Nanomedicine Nanotechnology, Biol. Med.* 11 (2015) 1117–1132. doi:10.1016/j.nano.2015.02.018.
- [73] G.B. Celli, Y. Liu, Y. Dadmohammadi, R. Tiwari, K. Raghupathi, W. Mutilangi, A. Abbaspourrad, Instantaneous interaction of mucin with pectin- and carrageenan-coated nanoemulsions, *Food Chem.* 309 (2019) 125795. doi:10.1016/j.foodchem.2019.125795.
- [74] H.-K. Han, H.-J. Shin, D.H. Ha, Improved oral bioavailability of alendronate via the mucoadhesive liposomal delivery system, *Eur. J. Pharm. Sci.* 46 (2012) 500–507. doi:10.1016/j.ejps.2012.04.002.
- [75] A. Beloqui, R. Coco, M. Alhouayek, M.Á. Solinís, A. Rodríguez-Gascón, G.G. Muccioli, V. Préat, Budesonide-loaded nanostructured lipid carriers reduce inflammation in murine DSS-induced colitis, *Int. J. Pharm.* 454 (2013) 775–783. doi:10.1016/j.ijpharm.2013.05.017.
- [76] A. Makhlof, Y. Tozuka, H. Takeuchi, pH-Sensitive nanospheres for colon-specific drug delivery in experimentally induced colitis rat model, *Eur. J. Pharm. Biopharm.* 72 (2009) 1–8. doi:10.1016/j.ejpb.2008.12.013.
- [77] D.S. Wilson, G. Dalmaso, L. Wang, S. V. Sitaraman, D. Merlin, N. Murthy, Orally delivered thioketal nanoparticles loaded with TNF- α -siRNA target inflammation and inhibit gene expression in the intestines, *Nat. Mater.* 9 (2010) 923–928. doi:10.1038/nmat2859.
- [78] Y. Xu, N. Shrestha, V. Préat, A. Beloqui, Overcoming the intestinal barrier: A look into targeting approaches for improved oral drug delivery systems, *J. Control. Release.* 322 (2020) 486–508. doi:10.1016/j.jconrel.2020.04.006.
- [79] N. Shrestha, O. Bouttefeux, K. Vanvarenberg, P. Lundquist, J. Cunarro, S. Tovar, G. Khodus, E. Andersson, Å. V. Keita, C. Gonzalez Dieguez, P. Artursson, V. Préat, A. Beloqui, The stimulation of GLP-1 secretion and delivery of GLP-1 agonists via nanostructured lipid carriers, *Nanoscale.* 10 (2018) 603–613. doi:10.1039/C7NR07736J.
- [80] B. Xiao, H. Laroui, S. Ayyadurai, E. Viennois, M.A. Charania, Y. Zhang, D. Merlin, Mannosylated bioreducible nanoparticle-mediated macrophage-specific TNF- α RNA interference for IBD therapy, *Biomaterials.* 34 (2013) 7471–7482. doi:10.1016/j.biomaterials.2013.06.008.
- [81] K. Kirsch, U. Hanke, W. Weitschies, An overview of intestinal wafers for oral drug delivery, *Eur. J. Pharm. Biopharm.* 114 (2017) 135–144. doi:10.1016/j.ejpb.2017.01.003.
- [82] S. Merino, C. Martín, K. Kostarelos, M. Prato, E. Vázquez, Nanocomposite Hydrogels: 3D Polymer–Nanoparticle Synergies for On-Demand Drug Delivery, *ACS Nano.* 9 (2015) 4686–4697. doi:10.1021/acs.nano.5b01433.
- [83] R.M. Talukder, R. Fassihi, Development and in-vitro evaluation of a colon-specific controlled release drug delivery system, *J. Pharm. Pharmacol.* 60 (2008) 1297–1303. doi:10.1211/jpp/60.10.0005.
- [84] V.. Sinha, R. Kumria, Microbially triggered drug delivery to the colon, *Eur. J. Pharm. Sci.* 18 (2003) 3–18. doi:10.1016/S0928-0987(02)00221-X.
- [85] A.H. Sabri, Y. Kim, M. Marlow, D.J. Scurr, J. Segal, A.K. Banga, L. Kagan, J.B. Lee, Intradermal and transdermal drug delivery using microneedles – Fabrication, performance evaluation and application to lymphatic delivery, *Adv. Drug Deliv. Rev.* (2019). doi:10.1016/j.addr.2019.10.004.
- [86] A. Sabri, J. Ogilvie, J. McKenna, J. Segal, D. Scurr, M. Marlow, Intradermal Delivery of an Immunomodulator for Basal Cell Carcinoma; Expanding the Mechanistic Insight into Solid Microneedle-Enhanced Delivery of Hydrophobic Molecules, *Mol. Pharm.* (2020) acs.molpharmaceut.0c00347. doi:10.1021/acs.molpharmaceut.0c00347.
- [87] C. Hale, Rani Therapeutics completes first- in-human safety study of its robotic biologic pill, *Rani Ther.* (2019). <https://clinicaltrials.gov/ct2/show/record/NCT03798912?view=record>.
- [88] A. Abramson, E. Caffarel-Salvador, V. Soares, D. Minahan, R.Y. Tian, X. Lu, D. Dellal, Y. Gao, S. Kim, J. Wainer, J. Collins, S. Tamang, A. Hayward, T. Yoshitake, H.-C. Lee, J. Fujimoto, J.

- Fels, M.R. Frederiksen, U. Rahbek, N. Roxhed, R. Langer, G. Traverso, A luminal unfolding microneedle injector for oral delivery of macromolecules, *Nat. Med.* 25 (2019) 1512–1518. doi:10.1038/s41591-019-0598-9.
- [89] C.W. Pouton, Formulation of poorly water-soluble drugs for oral administration: Physicochemical and physiological issues and the lipid formulation classification system, *Eur. J. Pharm. Sci.* 29 (2006) 278–287. doi:10.1016/j.ejps.2006.04.016.
- [90] C.J.H. Porter, N.L. Trevaskis, W.N. Charman, Lipids and lipid-based formulations: Optimizing the oral delivery of lipophilic drugs, *Nat. Rev. Drug Discov.* 6 (2007) 231–248. doi:10.1038/nrd2197.
- [91] G. Lou, G. Anderluzzi, S. Tandrup Schmidt, S. Woods, S. Gallorini, M. Brazzoli, F. Giusti, I. Ferlenghi, R. Johnson, C.W. Roberts, D.T. O’Hagan, B.C. Baudner, Y. Perrie, Delivery of self-amplifying mRNA vaccines by cationic lipid nanoparticles: The impact of cationic lipid selection, *J. Control. Release.* 155 (2020) 104743. doi:10.1016/j.jconrel.2020.06.027.
- [92] N. Lupo, V.N. Tkadlečková, M. Jelkmann, F. Laffleur, G. Hetényi, K. Kubová, A. Bernkop-Schnürch, Self-emulsifying drug delivery systems: In vivo evaluation of their potential for oral vaccination, *Acta Biomater.* 94 (2019) 425–434. doi:10.1016/j.actbio.2019.06.026.
- [93] N. Wang, M. Chen, T. Wang, Liposomes used as a vaccine adjuvant-delivery system: From basics to clinical immunization, *J. Control. Release.* 303 (2019) 130–150. doi:10.1016/j.jconrel.2019.04.025.
- [94] S. Mayer, J. Weiss, D.J. McClements, Vitamin E-enriched nanoemulsions formed by emulsion phase inversion: Factors influencing droplet size and stability, *J. Colloid Interface Sci.* 402 (2013) 122–130. doi:10.1016/j.jcis.2013.04.016.
- [95] N. Anton, J.-P. Benoit, P. Saulnier, Design and production of nanoparticles formulated from nano-emulsion templates—A review, *J. Control. Release.* 128 (2008) 185–199. doi:10.1016/j.jconrel.2008.02.007.
- [96] A. Zielńska, N.R. Ferreira, A. Feliczak-Guzik, I. Nowak, E.B. Souto, Loading, release profile and accelerated stability assessment of monoterpenes-loaded solid lipid nanoparticles (SLN), *Pharm. Dev. Technol.* 25 (2020) 832–844. doi:10.1080/10837450.2020.1744008.
- [97] T. Zhang, J. Chen, Y. Zhang, Q. Shen, W. Pan, Characterization and evaluation of nanostructured lipid carrier as a vehicle for oral delivery of etoposide, *Eur. J. Pharm. Sci.* 43 (2011) 174–179. doi:10.1016/j.ejps.2011.04.005.
- [98] T. Briot, E. Roger, N. Lautram, A. Verger, A. Clavreul, F. Lagarce, Development and in vitro evaluations of new decitabine nanocarriers for the treatment of acute myeloid leukemia, *Int. J. Nanomedicine.* Volume 12 (2017) 8427–8442. doi:10.2147/IJN.S147659.
- [99] N. Anton, T.F. Vandamme, Nano-emulsions and micro-emulsions: Clarifications of the critical differences, *Pharm. Res.* 28 (2011) 978–985. doi:10.1007/s11095-010-0309-1.
- [100] D.J. McClements, Nanoemulsions versus microemulsions: terminology, differences, and similarities, *Soft Matter.* 8 (2012) 1719–1729. doi:10.1039/C2SM06903B.
- [101] R. Savla, J. Browne, V. Plassat, K.M. Wasan, E.K. Wasan, Review and analysis of FDA approved drugs using lipid-based formulations, *Drug Dev. Ind. Pharm.* 43 (2017) 1743–1758. doi:10.1080/03639045.2017.1342654.
- [102] G. Cuddihy, E. Wasan, Y. Di, K. Wasan, The Development of Oral Amphotericin B to Treat Systemic Fungal and Parasitic Infections: Has the Myth Been Finally Realized?, *Pharmaceutics.* 11 (2019) 99. doi:10.3390/pharmaceutics11030099.
- [103] S. Sundar, K. Pandey, C.P. Thakur, T.K. Jha, V.N.R. Das, N. Verma, C.S. Lal, D. Verma, S. Alam, P. Das, Efficacy and Safety of Amphotericin B Emulsion versus Liposomal Formulation in Indian Patients with Visceral Leishmaniasis: A Randomized, Open-Label Study, *PLoS Negl. Trop. Dis.* 8 (2014) e3169. doi:10.1371/journal.pntd.0003169.
- [104] P. Calvo, J.L. Vila-Jato, M.J. Alonso, Comparative in vitro evaluation of several colloidal systems, nanoparticles, nanocapsules, and nanoemulsions, as ocular drug carriers, *J. Pharm. Sci.* 85 (1996) 530–536. doi:https://doi.org/10.1021/js950474.
- [105] T. Delmas, H. Piraux, A.C. Couffin, I. Texier, F. Vinet, P. Poulin, M.E. Cates, J. Bibette, How to prepare and stabilize very small nanoemulsions, *Langmuir.* 27 (2011) 1683–1692. doi:10.1021/la104221q.
- [106] J. Komaiko, D.J. McClements, Food-grade nanoemulsion filled hydrogels formed by

- spontaneous emulsification and gelation: Optical properties, rheology, and stability, *Food Hydrocoll.* 46 (2015) 67–75. doi:10.1016/j.foodhyd.2014.12.031.
- [107] B.M. Altaani, A.M. Almaaytah, S. Dadou, K. Alkhamis, M.H. Daradka, W. Hananeh, Oral Delivery of Teriparatide Using a Nanoemulsion System: Design, in Vitro and in Vivo Evaluation, *Pharm. Res.* 37 (2020) 80. doi:10.1007/s11095-020-02793-0.
- [108] H.-Y. Xu, C.-S. Liu, C.-L. Huang, L. Chen, Y.-R. Zheng, S.-H. Huang, X.-Y. Long, Nanoemulsion improves hypoglycemic efficacy of berberine by overcoming its gastrointestinal challenge, *Colloids Surfaces B Biointerfaces.* 181 (2019) 927–934. doi:10.1016/j.colsurfb.2019.06.006.
- [109] Y.-J. Li, X.-B. Hu, X.-L. Lu, D.-H. Liao, T.-T. Tang, J.-Y. Wu, D.-X. Xiang, Nanoemulsion-based delivery system for enhanced oral bioavailability and Caco-2 cell monolayers permeability of berberine hydrochloride, *Drug Deliv.* 24 (2017) 1868–1873. doi:10.1080/10717544.2017.1410257.
- [110] Q. Xu, A. Zhou, H. Wu, Y. Bi, Development and in vivo evaluation of baicalin-loaded W/O nanoemulsion for lymphatic absorption, *Pharm. Dev. Technol.* 24 (2019) 1155–1163. doi:10.1080/10837450.2019.1646757.
- [111] L. Wu, Y. Bi, H. Wu, Formulation optimization and the absorption mechanisms of nanoemulsion in improving baicalin oral exposure, *Drug Dev. Ind. Pharm.* 44 (2018) 266–275. doi:10.1080/03639045.2017.1391831.
- [112] R. Rutckeviski, F.H. Xavier, A.R.D.V. Morais, L. Amaral-Machado, E.D.N. Alencar, J. Genre, A.A. De Souza Araujo, E.S.T. Do Egito, Therapeutic bullfrog oil-based nanoemulsion for oral application: Development, characterization and stability, *Acta Pharm.* 69 (2019) 33–48. doi:10.2478/acph-2019-0001.
- [113] A. Khames, Formulation and Characterization of Eplerenone Nanoemulsion Liquisols, An Oral Delivery System with Higher Release Rate and Improved Bioavailability, *Pharmaceutics.* 11 (2019) 40. doi:10.3390/pharmaceutics11010040.
- [114] X.-B. Hu, T.-T. Tang, Y.-J. Li, J.-Y. Wu, J.-M. Wang, X.-Y. Liu, D.-X. Xiang, Phospholipid complex based nanoemulsion system for oral insulin delivery: preparation, in vitro, and in vivo evaluations, *Int. J. Nanomedicine.* Volume 14 (2019) 3055–3067. doi:10.2147/IJN.S198108.
- [115] H. Sun, K. Liu, W. Wang, B. Tang, J. Gu, J. Zhang, X. Mao, Q. Zou, H. Zeng, W. Liu, C. Guo, H. Li, Development and characterization of a novel nanoemulsion drug-delivery system for potential application in oral delivery of protein drugs, *Int. J. Nanomedicine.* 7 (2012) 5529. doi:10.2147/IJN.S36071.
- [116] D.J. McClements, Edible nanoemulsions: fabrication, properties, and functional performance, *Soft Matter.* 7 (2011) 2297–2316. doi:10.1039/C0SM00549E.
- [117] D.J. McClements, J. Rao, Food-Grade Nanoemulsions: Formulation, Fabrication, Properties, Performance, Biological Fate, and Potential Toxicity, *Crit. Rev. Food Sci. Nutr.* 51 (2011) 285–330. doi:10.1080/10408398.2011.559558.
- [118] S. Kentish, T.J. Wooster, M. Ashokkumar, S. Balachandran, R. Mawson, L. Simons, The use of ultrasonics for nanoemulsion preparation, *Innov. Food Sci. Emerg. Technol.* 9 (2008) 170–175. doi:10.1016/j.ifset.2007.07.005.
- [119] J.E. Kim, Y.J. Park, Paclitaxel-loaded hyaluronan solid nanoemulsions for enhanced treatment efficacy in ovarian cancer, *Int. J. Nanomedicine.* 12 (2017) 645–658. doi:10.2147/IJN.S124158.
- [120] R.M. Kramer, M.C. Archer, M.T. Orr, N. Dubois Cauwelaert, E.A. Beebe, P.W.D. Huang, Q.M. Dowling, A.M. Schwartz, D.M. Fedor, T.S. Vedvick, C.B. Fox, Development of a thermostable nanoemulsion adjuvanted vaccine against tuberculosis using a design-of-experiments approach, *Int. J. Nanomedicine.* 13 (2018) 3689–3711. doi:10.2147/IJN.S159839.
- [121] R. Nunes, B.D.A. Pereira, M.A. Cerqueira, P. Silva, L.M. Pastrana, A.A. Vicente, J.T. Martins, A.I. Bourbon, Lactoferrin-based nanoemulsions to improve the physical and chemical stability of omega-3 fatty acids, *Food Funct.* 11 (2020) 1966–1981. doi:10.1039/c9fo02307k.
- [122] X.-W. Chen, Y.-J. Chen, J.-M. Wang, J. Guo, S.-W. Yin, X.-Q. Yang, Phytosterol structured algae oil nanoemulsions and powders: improving antioxidant and flavor properties, *Food Funct.* 7 (2016) 3694–3702. doi:10.1039/C6FO00449K.
- [123] H.-R. Wu, C.-Q. Wang, J.-X. Wang, J.-F. Chen, Y. Le, Engineering of Long-Term Stable Transparent Nanoemulsion Using High-Gravity Rotating Packed Bed for Oral Drug Delivery,

- Int. J. Nanomedicine. Volume 15 (2020) 2391–2402. doi:10.2147/IJN.S238788.
- [124] J.F. Mendes, H.H.A. Martins, C.G. Otoni, N.A. Santana, R.C.S. Silva, A.G. Da Silva, M.V. Silva, M.T.S. Correia, G. Machado, A.C.M. Pinheiro, R.H. Piccoli, J.E. Oliveira, Chemical composition and antibacterial activity of *Eugenia brejoensis* essential oil nanoemulsions against *Pseudomonas fluorescens*, *LWT*. 93 (2018) 659–664. doi:10.1016/j.lwt.2018.04.015.
- [125] C. Solans, D. Morales, M. Homs, Spontaneous emulsification, *Curr. Opin. Colloid Interface Sci.* 22 (2016) 88–93. doi:10.1016/j.cocis.2016.03.002.
- [126] H. Liao, Y. Gao, C. Lian, Y. Zhang, B. Wang, Y. Yang, J. Ye, Y. Feng, Y. Liu, Oral absorption and lymphatic transport of baicalein following drug–phospholipid complex incorporation in self-microemulsifying drug delivery systems, *Int. J. Nanomedicine*. Volume 14 (2019) 7291–7306. doi:10.2147/IJN.S214883.
- [127] B. Heurtault, P. Saulnier, J.-P. Benoit, J.-E. Proust, B. Pech, J. Richard, Lipid nanocapsules, preparation process and use as medicines - US Patent US8057823B2, 2011. doi:10.1016/j.(73).
- [128] N. Anton, T.F. Vandamme, The universality of low-energy nano-emulsification, *Int. J. Pharm.* 377 (2009) 142–147. doi:10.1016/j.ijpharm.2009.05.014.
- [129] P. Izquierdo, J. Feng, J. Esquena, T.F. Tadros, J.C. Dederen, M.J. Garcia, N. Azemar, C. Solans, The influence of surfactant mixing ratio on nano-emulsion formation by the pit method, *J. Colloid Interface Sci.* 285 (2005) 388–394. doi:10.1016/j.jcis.2004.10.047.
- [130] D. Morales, C. Solans, J.M. Gutiérrez, M.J. Garcia-Celma, U. Olsson, Oil/Water Droplet Formation by Temperature Change in the Water/C 16 E 6 /Mineral Oil System, *Langmuir*. 22 (2006) 3014–3020. doi:10.1021/la052324c.
- [131] G. Lollo, K. Matha, M. Bocchiardo, J. Bejaud, I. Marigo, A. Virgone-Carlotta, T. Dehoux, C. Rivière, J.-P. Rieu, S. Briançon, T. Perrier, O. Meyer, J.-P. Benoit, Drug delivery to tumours using a novel 5-FU derivative encapsulated into lipid nanocapsules, *J. Drug Target.* 27 (2019) 634–645. doi:10.1080/1061186X.2018.1547733.
- [132] N. Sadurní, C. Solans, N. Azemar, M.J. García-Celma, Studies on the formation of O/W nano-emulsions, by low-energy emulsification methods, suitable for pharmaceutical applications, *Eur. J. Pharm. Sci.* 26 (2005) 438–445. doi:10.1016/j.ejps.2005.08.001.
- [133] D.J. McClements, Edible nanoemulsions: fabrication, properties, and functional performance, *Soft Matter*. 7 (2011) 2297–2316. doi:10.1039/C0SM00549E.
- [134] H. Ragelle, S. Crauste-Manciet, J. Seguin, D. Brossard, D. Scherman, P. Arnaud, G.G. Chabot, Nanoemulsion formulation of fisetin improves bioavailability and antitumour activity in mice, *Int. J. Pharm.* 427 (2012) 452–459. doi:10.1016/j.ijpharm.2012.02.025.
- [135] J. Feng, M. Roché, D. Vigolo, L.N. Arnaudov, S.D. Stoyanov, T.D. Gurkov, G.G. Tsutsumanova, H.A. Stone, Nanoemulsions obtained via bubble-bursting at a compound interface, *Nat. Phys.* 10 (2014) 606–612. doi:10.1038/nphys3003.
- [136] S. Streck, L. Hong, B.J. Boyd, A. McDowell, Microfluidics for the Production of Nanomedicines: Considerations for Polymer and Lipid-based Systems, *Pharm. Nanotechnol.* 7 (2019) 423–443. doi:10.2174/2211738507666191019154815.
- [137] J. Riewe, P. Erfle, S. Melzig, A. Kwade, A. Dietzel, H. Bunjes, Antisolvent precipitation of lipid nanoparticles in microfluidic systems – A comparative study, *Int. J. Pharm.* 579 (2020) 119167. doi:10.1016/j.ijpharm.2020.119167.
- [138] T. Tadros, P. Izquierdo, J. Esquena, C. Solans, Formation and stability of nano-emulsions, *Adv. Colloid Interface Sci.* 108–109 (2004) 303–318. doi:10.1016/j.cis.2003.10.023.
- [139] T. Delmas, H. Piraux, A.C. Couffin, I. Texier, F. Vinet, P. Poulin, M.E. Cates, J. Bibette, How to prepare and stabilize very small nanoemulsions, *Langmuir*. 27 (2011) 1683–1692. doi:10.1021/la104221q.
- [140] A. Patel, A. Mohanan, S. Ghosh, Effect of protein type, concentration and oil droplet size on the formation of repulsively jammed elastic nanoemulsion gels, *Soft Matter*. 15 (2019) 9762–9775. doi:10.1039/C9SM01650C.
- [141] Y. Li, S. Le Maux, H. Xiao, D.J. McClements, Emulsion-Based Delivery Systems for Tributyrin, a Potential Colon Cancer Preventative Agent, *J. Agric. Food Chem.* 57 (2009) 9243–9249. doi:10.1021/jf901836f.
- [142] D.J. McClements, S.M. Jafari, Improving emulsion formation, stability and performance using mixed emulsifiers: A review, *Adv. Colloid Interface Sci.* 251 (2018) 55–79.

- doi:10.1016/j.cis.2017.12.001.
- [143] A.B. Buya, B. Ucar, A. Beloqui, P.B. Memvanga, V. Pr at, Design and evaluation of self-nanoemulsifying drug delivery systems (SNEDDSs) for senicapoc, *Int. J. Pharm.* 580 (2020) 119180. doi:10.1016/j.ijpharm.2020.119180.
- [144] A. Nasr, A. Gardouh, M. Ghorab, Novel solid self-nanoemulsifying drug delivery system (S-SNEDDS) for oral delivery of olmesartan medoxomil: Design, formulation, pharmacokinetic and bioavailability evaluation, *Pharmaceutics*. 8 (2016). doi:10.3390/pharmaceutics8030020.
- [145] T.W. Wong, P. John, Advances in Spray Drying Technology for Nanoparticle Formation, in: *Handb. Nanoparticles*, 2015: pp. 1–16. doi:10.1007/978-3-319-13188-7_18-1.
- [146] A. Sosnik, K.P. Seremeta, Advantages and challenges of the spray-drying technology for the production of pure drug particles and drug-loaded polymeric carriers, *Adv. Colloid Interface Sci.* 223 (2015) 40–54. doi:10.1016/j.cis.2015.05.003.
- [147] E. Assadpour, S.M. Jafari, Advances in Spray-Drying Encapsulation of Food Bioactive Ingredients: From Microcapsules to Nanocapsules, *Annu. Rev. Food Sci. Technol.* 10 (2019) 103–131. doi:10.1146/annurev-food-032818-121641.
- [148] T. Nassar, A. Rom, A. Nyska, S. Benita, Novel double coated nanocapsules for intestinal delivery and enhanced oral bioavailability of tacrolimus, a P-gp substrate drug, *J. Control. Release.* 133 (2009) 77–84. doi:10.1016/j.jconrel.2008.08.021.
- [149] B.A. Morgan, M. Manser, M. Jeyanathan, Z. Xing, E.D. Cranston, M.R. Thompson, Effect of Shear Stresses on Adenovirus Activity and Aggregation during Atomization To Produce Thermally Stable Vaccines by Spray Drying, *ACS Biomater. Sci. Eng.* (2020). doi:10.1021/acsbomaterials.0c00317.
- [150] P. Goldbach, H. Brochart, A.A. Stamm, Spray-Drying of liposomes for a Pulmonary Administration. I. Chemical Stability of Phospholipids, *Drug Dev. Ind. Pharm.* 19 (1993) 2611–2622. doi:10.3109/03639049309047204.
- [151] P. Tewa-Tagne, S. Brian on, H. Fessi, Preparation of redispersible dry nanocapsules by means of spray-drying: Development and characterisation, *Eur. J. Pharm. Sci.* 30 (2007) 124–135. doi:10.1016/j.ejps.2006.10.006.
- [152] P.G. Maher, Y.H. Roos, M.A. Fenelon, Physicochemical properties of spray dried nanoemulsions with varying final water and sugar contents, *J. Food Eng.* 126 (2014) 113–119. doi:10.1016/j.jfoodeng.2013.11.001.
- [153] X. Li, N. Anton, C. Arpagaus, F. Belleiteix, T.F. Vandamme, Nanoparticles by spray drying using innovative new technology: The B uchi Nano Spray Dryer B-90, *J. Control. Release.* 147 (2010) 304–310. doi:10.1016/j.jconrel.2010.07.113.
- [154] L. Hu, Q. Hu, C. Yang, Spray-dried curcumin nanoemulsion: A new road to improvement of oral bioavailability of curcumin, *Pak. J. Pharm. Sci.* 31 (2018) 169–173.
- [155] H.H. Myat, G.C. Ritthidej, Impact of formulation parameters on physical characteristics of spray dried nanoemulsions and their reconstitutions, *Asian J. Pharm. Sci.* 11 (2016) 197–198. doi:10.1016/j.ajps.2015.11.038.
- [156] X. Li, N. Anton, T.M.C. Ta, M. Zhao, N. Messaddeq, T.F. Vandamme, Microencapsulation of nanoemulsions: novel Trojan particles for bioactive lipid molecule delivery., *Int. J. Nanomedicine.* 6 (2011) 1313–1325. doi:10.2147/ijn.s20353.
- [157] P.G. Maher, M.A.E. Auty, Y.H. Roos, L.M. Zychowski, M.A. Fenelon, Microstructure and lactose crystallization properties in spray dried nanoemulsions, *Food Struct.* 3 (2015) 1–11. doi:10.1016/j.foostr.2014.10.001.
- [158] A.M. Oliveira, K.L. Guimaraes, N.N. Cerize, A.S. Tunussi, J.G. Poco, Nano Spray Drying as an Innovative Technology for Encapsulating Hydrophilic Active Pharmaceutical Ingredients (API), *J. Nanomed. Nanotechnol.* 4 (2013). doi:10.4172/2157-7439.1000186.
- [159] Q. Hu, H. Gerhard, I. Upadhyaya, K. Venkitanarayanan, Y. Luo, Antimicrobial eugenol nanoemulsion prepared by gum arabic and lecithin and evaluation of drying technologies, *Int. J. Biol. Macromol.* 87 (2016) 130–140. doi:10.1016/j.ijbiomac.2016.02.051.
- [160] F. Franks, Freeze-drying of bioproducts: putting principles into practice, *Eur. J. Pharm. Biopharm.* 45 (1998) 221–229. doi:10.1016/S0939-6411(98)00004-6.
- [161] A.R.D.V. Morais,  .D.N. Alencar, F.H. Xavier J nior, C.M. De Oliveira, H.R. Marcelino, G. Barratt, H. Fessi, E.S.T. Do Egito, A. Elaissari, Freeze-drying of emulsified systems: A review,

- Int. J. Pharm. 503 (2016) 102–114. doi:10.1016/j.ijpharm.2016.02.047.
- [162] T.M. El-Messery, U. Altuntas, G. Altin, B. Özçelik, The effect of spray-drying and freeze-drying on encapsulation efficiency, in vitro bioaccessibility and oxidative stability of krill oil nanoemulsion system, *Food Hydrocoll.* 106 (2020). doi:10.1016/j.foodhyd.2020.105890.
- [163] W. Abdelwahed, G. Degobert, S. Stainmesse, H. Fessi, Freeze-drying of nanoparticles: Formulation, process and storage considerations, *Adv. Drug Deliv. Rev.* 58 (2006) 1688–1713. doi:10.1016/j.addr.2006.09.017.
- [164] F. Li, T. Wang, H.B. He, X. Tang, The properties of bufadienolides-loaded nano-emulsion and submicro-emulsion during lyophilization, *Int. J. Pharm.* 349 (2008) 291–299. doi:10.1016/j.ijpharm.2007.08.011.
- [165] M.T. Orr, R.M. Kramer, L. V. Barnes, Q.M. Dowling, A.L. Desbien, E.A. Beebe, J.D. Laurance, C.B. Fox, S.G. Reed, R.N. Coler, T.S. Vedvick, Elimination of the cold-chain dependence of a nanoemulsion adjuvanted vaccine against tuberculosis by lyophilization, *J. Control. Release.* 177 (2014) 20–26. doi:10.1016/j.jconrel.2013.12.025.
- [166] S. Guerrero, M. Inostroza-Riquelme, P. Contreras-Orellana, V. Diaz-Garcia, P. Lara, A. Vivanco-Palma, A. Cárdenas, V. Miranda, P. Robert, L. Leyton, M.J. Kogan, A.F.G. Quest, F. Oyarzun-Ampuero, Curcumin-loaded nanoemulsion: a new safe and effective formulation to prevent tumor recurrence and metastasis, *Nanoscale.* 10 (2018) 22612–22622. doi:10.1039/C8NR06173D.
- [167] G.A. Ledet, S. Biswas, V.P. Kumar, R.A. Graves, D.M. Mitchner, T.M. Parker, L.A. Bostanian, S.P. Ghosh, T.K. Mandal, Development of orally administered γ tocotrienol (GT3) nanoemulsion for radioprotection, *Int. J. Mol. Sci.* 18 (2017). doi:10.3390/ijms18010028.
- [168] C. Dulieu, D. Bazile, Influence of lipid nanocapsules composition on their aptness to freeze-drying., *Pharm. Res.* 22 (2005) 285–92. doi:10.1007/s11095-004-1196-0.
- [169] W. Abdelwahed, G. Degobert, H. Fessi, A pilot study of freeze drying of poly(epsilon-caprolactone) nanocapsules stabilized by poly(vinyl alcohol): Formulation and process optimization, *Int. J. Pharm.* 309 (2006) 178–188. doi:10.1016/j.ijpharm.2005.10.003.
- [170] M.J. Choi, S. Briançon, J. Andrieu, S.G. Min, H. Fessi, Effect of Freeze-Drying Process Conditions on the Stability of Nanoparticles, *Dry. Technol.* 22 (2004) 335–346. doi:10.1081/DRT-120028238.
- [171] M.K. Lee, M.Y. Kim, S. Kim, J. Lee, Cryoprotectants for freeze drying of drug nano-suspensions: Effect of freezing rate, *J. Pharm. Sci.* 98 (2009) 4808–4817. doi:10.1002/jps.21786.
- [172] Q. Hu, H. Gerhard, I. Upadhyaya, K. Venkitanarayanan, Y. Luo, Antimicrobial eugenol nanoemulsion prepared by gum arabic and lecithin and evaluation of drying technologies, *Int. J. Biol. Macromol.* 87 (2016) 130–140. doi:10.1016/j.ijbiomac.2016.02.051.
- [173] S. Guerrero, M. Inostroza-Riquelme, P. Contreras-Orellana, V. Diaz-Garcia, P. Lara, A. Vivanco-Palma, A. Cárdenas, V. Miranda, P. Robert, L. Leyton, M.J. Kogan, A.F.G. Quest, F. Oyarzun-Ampuero, Curcumin-loaded nanoemulsion: A new safe and effective formulation to prevent tumor recurrence and metastasis, *Nanoscale.* 10 (2018) 22612–22622. doi:10.1039/c8nr06173d.
- [174] T. Vasconcelos, F. Araújo, C. Lopes, A. Loureiro, J. das Neves, S. Marques, B. Sarmento, Multicomponent self nano emulsifying delivery systems of resveratrol with enhanced pharmacokinetics profile, *Eur. J. Pharm. Sci.* 137 (2019). doi:10.1016/j.ejps.2019.105011.
- [175] C.W. Pouton, C.J.H. Porter, Formulation of lipid-based delivery systems for oral administration: Materials, methods and strategies, *Adv. Drug Deliv. Rev.* 60 (2008) 625–637. doi:10.1016/j.addr.2007.10.010.
- [176] F.U. Rehman, K.U. Shah, S.U. Shah, I.U. Khan, G.M. Khan, A. Khan, From nanoemulsions to self-nanoemulsions, with recent advances in self-nanoemulsifying drug delivery systems (SNEDDS), *Expert Opin. Drug Deliv.* 14 (2017) 1325–1340. doi:10.1080/17425247.2016.1218462.
- [177] B. Singh, S. Beg, R.K. Khurana, P.S. Sandhu, R. Kaur, O.P. Katare, Recent Advances in Self-Emulsifying Drug Delivery Systems (SEDDS), *Crit. Rev. Ther. Drug Carrier Syst.* 31 (2014) 121–185. doi:10.1615/CritRevTherDrugCarrierSyst.2014008502.
- [178] O.M. Feeney, M.F. Crum, C.L. McEvoy, N.L. Trevaskis, H.D. Williams, C.W. Pouton, W.N. Charman, C.A.S. Bergström, C.J.H. Porter, 50 years of oral lipid-based formulations:

- Provenance, progress and future perspectives, *Adv. Drug Deliv. Rev.* 101 (2016) 167–194. doi:10.1016/j.addr.2016.04.007.
- [179] A. Beloqui, P.B. Memvanga, R. Coco, S. Reimondez-Troitiño, M. Alhouayek, G.G. Muccioli, M.J. Alonso, N. Csaba, M. de la Fuente, V. Préat, A comparative study of curcumin-loaded lipid-based nanocarriers in the treatment of inflammatory bowel disease, *Colloids Surfaces B Biointerfaces*. 143 (2016) 327–335. doi:10.1016/j.colsurfb.2016.03.038.
- [180] Y.T. Goo, S.H. Song, D.W. Yeom, B.R. Chae, H.Y. Yoon, C.H. Kim, S.Y. Park, T.H. Kang, S. Lee, Y.W. Choi, Enhanced oral bioavailability of valsartan in rats using a supersaturable self-microemulsifying drug delivery system with P-glycoprotein inhibitors, *Pharm. Dev. Technol.* 25 (2020) 178–186. doi:10.1080/10837450.2019.1683749.
- [181] P. Jaisamut, K. Wiwattanawongsa, P. Graidist, Y. Sangsen, R. Wiwattanapatapee, Enhanced Oral Bioavailability of Curcumin Using a Supersaturable Self-Microemulsifying System Incorporating a Hydrophilic Polymer; In Vitro and In Vivo Investigations, *AAPS PharmSciTech.* 19 (2018) 730–740. doi:10.1208/s12249-017-0857-3.
- [182] B.T. Griffin, C.M. O'Driscoll, A comparison of intestinal lymphatic transport and systemic bioavailability of saquinavir from three lipid-based formulations in the anaesthetised rat model, *J. Pharm. Pharmacol.* 58 (2006) 917–925. doi:10.1211/jpp.58.7.0006.
- [183] S. Rani, R. Rana, G.K. Saraogi, V. Kumar, U. Gupta, Self-Emulsifying Oral Lipid Drug Delivery Systems: Advances and Challenges, *AAPS PharmSciTech.* 20 (2019). doi:10.1208/s12249-019-1335-x.
- [184] A. Mahmood, A. Bernkop-Schnürch, SEDDS: A game changing approach for the oral administration of hydrophilic macromolecular drugs, *Adv. Drug Deliv. Rev.* 142 (2019) 91–101. doi:10.1016/j.addr.2018.07.001.
- [185] S. Venkata Ramana Rao, J. Shao, Self-nanoemulsifying drug delivery systems (SNEDDS) for oral delivery of protein drugs. I. Formulation development, *Int. J. Pharm.* 362 (2008) 2–9. doi:10.1016/j.ijpharm.2008.05.018.
- [186] J. Griesser, G. Hetényi, M. Moser, F. Demarne, V. Jannin, A. Bernkop-Schnürch, Hydrophobic ion pairing: Key to highly payloaded self-emulsifying peptide drug delivery systems, *Int. J. Pharm.* 520 (2017) 267–274. doi:10.1016/j.ijpharm.2017.02.019.
- [187] T. Karamanidou, K. Karidi, V. Bourganis, K. Kontonikola, O. Kammona, C. Kiparissides, Effective incorporation of insulin in mucus permeating self-nanoemulsifying drug delivery systems, *Eur. J. Pharm. Biopharm.* 97 (2015) 223–229. doi:10.1016/j.ejpb.2015.04.013.
- [188] G. Zhai, Zhang, Guo, Yu, Ji, Gao, Sun, A novel folate-modified self-microemulsifying drug delivery system of curcumin for colon targeting, *Int. J. Nanomedicine.* 7 (2012) 151. doi:10.2147/IJN.S27639.
- [189] S. Dokania, A.K. Joshi, Self-microemulsifying drug delivery system (SMEDDS)-challenges and road ahead, *Drug Deliv.* 22 (2015) 675–690. doi:10.3109/10717544.2014.896058.
- [190] M. Sherry Ku, W. Li, W. Dulin, F. Donahue, D. Cade, H. Benameur, K. Hutchison, Performance qualification of a new hypromellose capsule: Part I. Comparative evaluation of physical, mechanical and processability quality attributes of Vcaps Plus®, Quali-V® and gelatin capsules, *Int. J. Pharm.* 386 (2010) 30–41. doi:10.1016/j.ijpharm.2009.10.050.
- [191] L.A.D. Silva, E.R. Cintra, E.C.P. Alonso, G.L. Alves, E.M. Lima, S.F. Taveira, M.S.S. da Cunha-Filho, R.N. Marreto, Selection of excipients for the development of carvedilol loaded lipid-based drug delivery systems, *J. Therm. Anal. Calorim.* 130 (2017) 1593–1604. doi:10.1007/s10973-017-6380-7.
- [192] T. Yi, J. Wan, H. Xu, X. Yang, A new solid self-microemulsifying formulation prepared by spray-drying to improve the oral bioavailability of poorly water soluble drugs, *Eur. J. Pharm. Biopharm.* 70 (2008) 439–444. doi:10.1016/j.ejpb.2008.05.001.
- [193] F. Li, S. Song, Y. Guo, Q. Zhao, X. Zhang, W. Pan, X. Yang, Preparation and pharmacokinetics evaluation of oral self-emulsifying system for poorly water-soluble drug Lornoxicam, *Drug Deliv.* 22 (2015) 487–498. doi:10.3109/10717544.2014.885615.
- [194] J.H. Kang, D.H. Oh, Y.K. Oh, C.S. Yong, H.G. Choi, Effects of solid carriers on the crystalline properties, dissolution and bioavailability of flurbiprofen in solid self-nanoemulsifying drug delivery system (solid SNEDDS), *Eur. J. Pharm. Biopharm.* 80 (2012) 289–297. doi:10.1016/j.ejpb.2011.11.005.

- [195] V. Jannin, J. Musakhanian, D. Marchaud, Approaches for the development of solid and semi-solid lipid-based formulations, *Adv. Drug Deliv. Rev.* 60 (2008) 734–746. doi:10.1016/j.addr.2007.09.006.
- [196] B. Chatterjee, S. Hamed Almurisi, A. Ahmed Mahdi Dukhan, U.K. Mandal, P. Sengupta, Controversies with self-emulsifying drug delivery system from pharmacokinetic point of view, *Drug Deliv.* 23 (2016) 3639–3652. doi:10.1080/10717544.2016.1214990.
- [197] M.M. Kamal, A. Salawi, M. Lam, A. Nokhodchi, A. Abu-Fayyad, K.A. El Sayed, S. Nazzal, Development and characterization of curcumin-loaded solid self-emulsifying drug delivery system (SEDDS) by spray drying using Soluplus® as solid carrier, *Powder Technol.* 369 (2020) 137–145. doi:10.1016/j.powtec.2020.05.023.
- [198] D. Singh, A.P. Singh, D. Singh, A.K. Kesavan, S. Arora, A.K. Tiwary, N. Bedi, Enhanced oral bioavailability and anti-diabetic activity of canagliflozin through a spray dried lipid based oral delivery: a novel paradigm, *DARU, J. Pharm. Sci.* 28 (2020) 191–208. doi:10.1007/s40199-020-00330-3.
- [199] H.N. ElShagea, N.A. ElKasabgy, R.H. Fahmy, E.B. Basalious, Freeze-Dried Self-Nanoemulsifying Self-Nanosuspension (SNESNS): a New Approach for the Preparation of a Highly Drug-Loaded Dosage Form, *AAPS PharmSciTech.* 20 (2019). doi:10.1208/s12249-019-1472-2.
- [200] K. Vithani, A. Goyanes, V. Jannin, A.W. Basit, S. Gaisford, B.J. Boyd, A Proof of Concept for 3D Printing of Solid Lipid-Based Formulations of Poorly Water-Soluble Drugs to Control Formulation Dispersion Kinetics, *Pharm. Res.* 36 (2019) 102. doi:10.1007/s11095-019-2639-y.
- [201] G. Cheng, R. Hu, L. Ye, B. Wang, Y. Gui, S. Gao, X. Li, J. Tang, Preparation and In Vitro/In Vivo Evaluation of Puerarin Solid Self-Microemulsifying Drug Delivery System by Spherical Crystallization Technique, *AAPS PharmSciTech.* 17 (2016) 1336–1346. doi:10.1208/s12249-015-0469-8.
- [202] C. Sun, Y. Gui, R. Hu, J. Chen, B. Wang, Y. Guo, W. Lu, X. Nie, Q. Shen, S. Gao, W. Fang, Preparation and Pharmacokinetics Evaluation of Solid Self-Microemulsifying Drug Delivery System (S-SMEDDS) of Osthole, *AAPS PharmSciTech.* 19 (2018) 2301–2310. doi:10.1208/s12249-018-1067-3.
- [203] D.W. Yeom, H.Y. Son, J.H. Kim, S.R. Kim, S.G. Lee, S.H. Song, B.R. Chae, Y.W. Choi, Development of a solidified self-microemulsifying drug delivery system (S-SMEDDS) for atorvastatin calcium with improved dissolution and bioavailability, *Int. J. Pharm.* 506 (2016) 302–311. doi:10.1016/j.ijpharm.2016.04.059.
- [204] K. Bolko Seljak, I.G. German Ilić, M. Gašperlin, A. Zvonar Pobirk, Self-microemulsifying tablets prepared by direct compression for improved resveratrol delivery, *Int. J. Pharm.* 548 (2018) 263–275. doi:10.1016/j.ijpharm.2018.06.065.
- [205] L.A.D. Silva, S.L. Almeida, E.C.P. Alonso, P.B.R. Rocha, F.T. Martins, L.A.P. Freitas, S.F. Taveira, M.S.S. Cunha-Filho, R.N. Marreto, Preparation of a solid self-microemulsifying drug delivery system by hot-melt extrusion, *Int. J. Pharm.* 541 (2018) 1–10. doi:10.1016/j.ijpharm.2018.02.020.
- [206] H. Patel, N. Pandey, B. Patel, K. Ranch, K. Bodiwala, B. Vyas, Enhancement of in vivo hypoglycemic effect of gliclazide by developing self-microemulsifying pellet dosage form, *Futur. J. Pharm. Sci.* 6 (2020). doi:10.1186/s43094-020-00034-0.
- [207] J. Mandić, V. Pirnat, M. Luštrik, I. German Ilić, F. Vrečer, M. Gašperlin, A. Zvonar Pobirk, Solidification of SMEDDS by fluid bed granulation and manufacturing of fast drug release tablets, *Int. J. Pharm.* 583 (2020). doi:10.1016/j.ijpharm.2020.119377.
- [208] B. Albertini, M. Di Sabatino, C. Melegari, N. Passerini, Formulation of spray congealed microparticles with self-emulsifying ability for enhanced glibenclamide dissolution performance, *J. Microencapsul.* 32 (2015) 181–192. doi:10.3109/02652048.2014.985341.
- [209] T. Yi, J. Zhang, Effects of hydrophilic carriers on structural transitions and in vitro properties of solid self-microemulsifying drug delivery systems, *Pharmaceutics.* 11 (2019) 1–13. doi:10.3390/pharmaceutics11060267.
- [210] D.S. Kim, J.H. Cho, J.H. Park, J.S. Kim, E.S. Song, J. Kwon, B.R. Giri, S.G. Jin, K.S. Kim, H.G. Choi, D.W. Kim, Self-microemulsifying drug delivery system (SMEDDS) for improved oral delivery and photostability of methotrexate, *Int. J. Nanomedicine.* 14 (2019) 4949–4960.

doi:10.2147/IJN.S211014.

- [211] S.C. Patil, A.A. Tagalpallewar, C.R. Kokare, Natural anti-proliferative agent loaded self-microemulsifying nanoparticles for potential therapy in oral squamous carcinoma, *J. Pharm. Investig.* 49 (2019) 527–541. doi:10.1007/s40005-018-00415-x.
- [212] J.-S. Kim, E.-S. Ha, H. Park, D.H. Choi, M.-S. Kim, I. Baek, Pharmacokinetic Study of a Soft Gelatin Capsule and a Solid-Supersaturatable SMEDDS Tablet of Dutasteride in Beagle Dogs, *Eur. J. Drug Metab. Pharmacokinet.* 45 (2020) 235–241. doi:10.1007/s13318-019-00594-4.
- [213] S. Gupta, S. Chavhan, K.K. Sawant, Self-nanoemulsifying drug delivery system for adefovir dipivoxil: Design, characterization, in vitro and ex vivo evaluation, *Colloids Surfaces A Physicochem. Eng. Asp.* 392 (2011) 145–155. doi:10.1016/j.colsurfa.2011.09.048.
- [214] C. Desfrancois, R. Auzély, I. Texier, Lipid nanoparticles and their hydrogel composites for drug delivery: A review, *Pharmaceuticals*. 11 (2018). doi:10.3390/ph11040118.
- [215] N. Cheikhyoussef, A. Cheikhyoussef, Industrial polymer synthesis using supercritical carbon dioxide, in: *Green Sustain. Process Chem. Environ. Eng. Sci.*, 2020: pp. 435–453. doi:10.1016/B978-0-12-817388-6.00018-0.
- [216] S. Peers, P. Alcouffe, A. Montembault, C. Ladavière, Embedment of liposomes into chitosan physical hydrogel for the delayed release of antibiotics or anaesthetics, and its first ESEM characterization, *Carbohydr. Polym.* 229 (2020) 115532. doi:10.1016/j.carbpol.2019.115532.
- [217] J.P. Schillemans, E. Verheyen, A. Barendregt, W.E. Hennink, C.F. Van Nostrum, Anionic and cationic dextran hydrogels for post-loading and release of proteins, *Journal of Controlled Release*, 150 (2011) 266–271. doi: 10.1016/j.jconrel.2010.11.027.
- [218] P. Thoniyot, M.J. Tan, A.A. Karim, D.J. Young, X.J. Loh, Nanoparticle–Hydrogel Composites: Concept, Design, and Applications of These Promising, Multi-Functional Materials, *Adv. Sci.* 2 (2015) 1–13. doi:10.1002/advs.201400010.
- [219] M.A. Casadei, F. Cerreto, S. Cesa, M. Giannuzzo, M. Feeney, C. Marianecchi, P. Paolicelli, Solid lipid nanoparticles incorporated in dextran hydrogels: A new drug delivery system for oral formulations, *Int. J. Pharm.* 325 (2006) 140–146. doi:10.1016/j.ijpharm.2006.06.012.
- [220] N. Niknia, R. Kadkhodae, M.N. Eshtiaghi, Gum tragacanth-polyvinyl alcohol aerogel for oral delivery of silymarin, *Int. J. Biol. Macromol.* 157 (2020) 151–157. doi:10.1016/j.ijbiomac.2020.04.202.
- [221] M. Wang, Y. Ma, Y. Sun, S.Y. Hong, S.K. Lee, B. Yoon, L. Chen, L. Ci, J.-D. Nam, X. Chen, J. Suhr, Hierarchical Porous Chitosan Sponges as Robust and Recyclable Adsorbents for Anionic Dye Adsorption, *Sci. Rep.* 7 (2017) 18054. doi:10.1038/s41598-017-18302-0.
- [222] H.A. Hazzah, R.M. Farid, M.M.A. Nasra, M.A. EL-Massik, O.Y. Abdallah, Lyophilized sponges loaded with curcumin solid lipid nanoparticles for buccal delivery: Development and characterization, *Int. J. Pharm.* 492 (2015) 248–257. doi:10.1016/j.ijpharm.2015.06.022.
- [223] M.A.A. Kassem, A.N. ElMeshad, A.R. Fares, Lyophilized Sustained Release Mucoadhesive Chitosan Sponges for Buccal Bupirone Hydrochloride Delivery: Formulation and In Vitro Evaluation, *AAPS PharmSciTech.* 16 (2015) 537–547. doi:10.1208/s12249-014-0243-3.
- [224] F. Cui, C. He, L. Yin, F. Qian, M. He, C. Tang, C. Yin, Nanoparticles incorporated in bilaminated films: A smart drug delivery system for oral formulations, *Biomacromolecules*. 8 (2007) 2845–2850. doi:10.1021/bm070339e.
- [225] A.C. Daly, L. Riley, T. Segura, J.A. Burdick, Hydrogel microparticles for biomedical applications, *Nat. Rev. Mater.* 5 (2020) 20–43. doi:10.1038/s41578-019-0148-6.
- [226] L. Soudry-Kochavi, N. Naraykin, T. Nassar, S. Benita, Improved oral absorption of exenatide using an original nanoencapsulation and microencapsulation approach, *J. Control. Release*. 217 (2015) 202–210. doi:10.1016/j.jconrel.2015.09.012.
- [227] C. Costa, Z. Liu, J.P. Martins, A. Correia, P. Figueiredo, A. Rahikkala, W. Li, J. Seitsonen, J. Ruokolainen, S.-P. Hirvonen, A. Aguiar-Ricardo, M.L. Corvo, H.A. Santos, All-in-one microfluidic assembly of insulin-loaded pH-responsive nano-in-microparticles for oral insulin delivery, *Biomater. Sci.* 8 (2020) 3270–3277. doi:10.1039/D0BM00743A.
- [228] M.D. Bhavsar, M.M. Amiji, Oral IL-10 gene delivery in a microsphere-based formulation for local transfection and therapeutic efficacy in inflammatory bowel disease, *Gene Ther.* 15 (2008) 1200–1209. doi:10.1038/gt.2008.67.
- [229] R. Sun, Q. Xia, Nanostructured lipid carriers incorporated in alginate hydrogel: Enhanced

- stability and modified behavior in gastrointestinal tract, *Colloids Surfaces A Physicochem. Eng. Asp.* 574 (2019) 197–206. doi:10.1016/j.colsurfa.2019.04.082.
- [230] S. Javanbakht, A. Shaabani, Encapsulation of graphene quantum dot-crosslinked chitosan by carboxymethylcellulose hydrogel beads as a pH-responsive bio-nanocomposite for the oral delivery agent, *Int. J. Biol. Macromol.* 123 (2019) 389–397. doi:10.1016/j.ijbiomac.2018.11.118.
- [231] M. Alfatama, L.Y. Lim, T.W. Wong, Alginate–C18 Conjugate Nanoparticles Loaded in Tripolyphosphate-Cross-Linked Chitosan–Oleic Acid Conjugate-Coated Calcium Alginate Beads as Oral Insulin Carrier, *Mol. Pharm.* 15 (2018) 3369–3382. doi:10.1021/acs.molpharmaceut.8b00391.
- [232] J.P. Senna, T.N. Barradas, S. Cardoso, T.C. Castiglione, M.J. Serpe, K.G. de H. e. Silva, C.R.E. Mansur, Dual alginate-lipid nanocarriers as oral delivery systems for amphotericin B, *Colloids Surfaces B Biointerfaces.* 166 (2018) 187–194. doi:10.1016/j.colsurfb.2018.03.015.
- [233] L. Lei, Y. Zhang, L. He, S. Wu, B. Li, Y. Li, Fabrication of nanoemulsion-filled alginate hydrogel to control the digestion behavior of hydrophobic nobiletin, *LWT - Food Sci. Technol.* 82 (2017) 260–267. doi:10.1016/j.lwt.2017.04.051.
- [234] J. Xiao, C. Shi, Y. Li, Y. Pan, Q. Huang, Pickering emulsions immobilized within hydrogel matrix with enhanced resistance against harsh processing conditions and sequential digestion, *Food Hydrocoll.* 62 (2017) 35–42. doi:10.1016/j.foodhyd.2016.07.025.
- [235] J.C. Imperiale, P. Nejamkin, M.J. del Sole, C. E. Lanusse, A. Sosnik, Novel protease inhibitor-loaded Nanoparticle-in-Microparticle Delivery System leads to a dramatic improvement of the oral pharmacokinetics in dogs, *Biomaterials.* 37 (2015) 383–394. doi:10.1016/j.biomaterials.2014.10.026.
- [236] Y.J. Wang, L.J. Chen, L.W. Tan, Q. Zhao, F. Luo, Y.Q. Wei, Z.Y. Qian, PEG-PCL based micelle hydrogels as oral docetaxel delivery systems for breast cancer therapy, *Biomaterials.* 35 (2014) 6972–6985. doi:10.1016/j.biomaterials.2014.04.099.
- [237] Y. Zhou, L. Liu, Y. Cao, S. Yu, C. He, X. Chen, A Nanocomposite Vehicle Based on Metal–Organic Framework Nanoparticle Incorporated Biodegradable Microspheres for Enhanced Oral Insulin Delivery, *ACS Appl. Mater. Interfaces.* 12 (2020) 22581–22592. doi:10.1021/acsami.0c04303.
- [238] M.S. Falzarano, C. Passarelli, E. Bassi, M. Fabris, D. Perrone, P. Sabatelli, N.M. Maraldi, S. Donà, R. Selvatici, P. Bonaldo, K. Sparnacci, M. Laus, P. Braghetta, P. Rimessi, A. Ferlini, Biodistribution and molecular studies on orally administered nanoparticle-AON complexes encapsulated with alginate aiming at inducing dystrophin rescue in mdx mice, *Biomed Res. Int.* 2013 (2013) 4–8. doi:10.1155/2013/527418.
- [239] M.D. Bhavsar, M.M. Amiji, Gastrointestinal distribution and in vivo gene transfection studies with nanoparticles-in-microsphere oral system (NiMOS), *J. Control. Release.* 119 (2007) 339–348. doi:10.1016/j.jconrel.2007.03.006.
- [240] Z. Zhang, K.-J. Jung, R. Zhang, J.L. Muriel Mundo, D.J. McClements, In situ monitoring of lipid droplet release from biopolymer microgels under simulated gastric conditions using magnetic resonance imaging and spectroscopy, *Food Res. Int.* 123 (2019) 181–188. doi:10.1016/j.foodres.2019.04.063.
- [241] S. Javanbakht, N. Nazari, R. Rakhshaei, H. Namazi, Cu-crosslinked carboxymethylcellulose/naproxen/graphene quantum dot nanocomposite hydrogel beads for naproxen oral delivery, *Carbohydr. Polym.* 195 (2018) 453–459. doi:10.1016/j.carbpol.2018.04.103.
- [242] M.J. Barea, M.J. Jenkins, Y.S. Lee, P. Johnson, R.H. Bridson, Encapsulation of Liposomes within pH Responsive Microspheres for Oral Colonic Drug Delivery, *Int. J. Biomater.* 2012 (2012) 1–8. doi:10.1155/2012/458712.
- [243] T.K. Giri, S. Bhowmick, S. Maity, Entrapment of capsaicin loaded nanoliposome in pH responsive hydrogel beads for colonic delivery, *J. Drug Deliv. Sci. Technol.* 39 (2017) 417–422. doi:10.1016/j.jddst.2017.05.002.
- [244] L. Hou, Y. Shi, G. Jiang, W. Liu, H. Han, Q. Feng, J. Ren, Y. Yuan, Y. Wang, J. Shi, Z. Zhang, Smart nanocomposite hydrogels based on azo crosslinked graphene oxide for oral colon-specific drug delivery, *Nanotechnology.* 27 (2016) 315105. doi:10.1088/0957-4484/27/31/315105.
- [245] T.K. Giri, S. Bhowmick, S. Maity, Entrapment of capsaicin loaded nanoliposome in pH

- responsive hydrogel beads for colonic delivery, *J. Drug Deliv. Sci. Technol.* 39 (2017) 417–422. doi:10.1016/j.jddst.2017.05.002.
- [246] Q. Zhu, J. Talton, G. Zhang, T. Cunningham, Z. Wang, R.C. Waters, J. Kirk, B. Eppler, D.M. Klinman, Y. Sui, S. Gagnon, I.M. Belyakov, R.J. Mumper, J.A. Berzofsky, Large intestine-targeted, nanoparticle-releasing oral vaccine to control genitorectal viral infection, *Nat. Med.* 18 (2012) 1291–1296. doi:10.1038/nm.2866.
- [247] M. Naeem, U.A. Awan, F. Subhan, J. Cao, S.P. Hlaing, J. Lee, E. Im, Y. Jung, J.-W. Yoo, Advances in colon-targeted nano-drug delivery systems: challenges and solutions, *Arch. Pharm. Res.* 43 (2020) 153–169. doi:10.1007/s12272-020-01219-0.
- [248] M. Dhyani, N. Joshi, W.A. Bemelman, M.S. Gee, V. Yajnik, A. D’Hoore, G. Traverso, M. Donowitz, G. Mostoslavsky, T.K. Lu, N. Lineberry, H.G. Niessen, D. Peer, J. Braun, C.P. Delaney, M.C. Dubinsky, A.N. Guillory, M. Pereira, N. Shtraizent, G. Honig, D.B. Polk, A. Hurtado-Lorenzo, J.M. Karp, F. Michelassi, Challenges in IBD Research: Novel Technologies, *Inflamm. Bowel Dis.* 25 (2019) S24–S30. doi:10.1093/ibd/izz077.
- [249] M. Zhang, C. Xu, D. Liu, M.K. Han, L. Wang, D. Merlin, Oral Delivery of Nanoparticles Loaded With Ginger Active Compound, 6-Shogaol, Attenuates Ulcerative Colitis and Promotes Wound Healing in a Murine Model of Ulcerative Colitis, *J. Crohn’s Colitis.* 12 (2018) 217–229. doi:10.1093/ecco-jcc/jjx115.
- [250] J.M. Knipe, L.E. Strong, N.A. Peppas, Enzyme- and pH-Responsive Microencapsulated Nanogels for Oral Delivery of siRNA to Induce TNF- α Knockdown in the Intestine, *Biomacromolecules.* 17 (2016) 788–797. doi:10.1021/acs.biomac.5b01518.
- [251] N. Iglesias, E. Galbis, M.J. Díaz-Blanco, R. Lucas, E. Benito, M.V. De-Paz, Nanostructured Chitosan-based biomaterials for sustained and colon-specific resveratrol release, *Int. J. Mol. Sci.* 20 (2019). doi:10.3390/ijms20020398.
- [252] B. Duan, M. Li, Y. Sun, S. Zou, X. Xu, Orally Delivered Antisense Oligodeoxyribonucleotides of TNF- α via Polysaccharide-Based Nanocomposites Targeting Intestinal Inflammation, *Adv. Healthc. Mater.* 8 (2019). doi:10.1002/adhm.201801389.
- [253] W. Li, Y. Li, Z. Liu, N. Kerdsakundee, M. Zhang, F. Zhang, X. Liu, T. Bauleth-Ramos, W. Lian, E. Mäkilä, M. Kemell, Y. Ding, B. Sarmiento, R. Wiwattanapatapee, J. Salonen, H. Zhang, J.T. Hirvonen, D. Liu, X. Deng, H.A. Santos, Hierarchical structured and programmed vehicles deliver drugs locally to inflamed sites of intestine, *Biomaterials.* 185 (2018) 322–332. doi:10.1016/j.biomaterials.2018.09.024.
- [254] Q. Zhu, J. Talton, G. Zhang, T. Cunningham, Z. Wang, R.C. Waters, J. Kirk, B. Eppler, D.M. Klinman, Y. Sui, S. Gagnon, I.M. Belyakov, R.J. Mumper, J.A. Berzofsky, Large intestine-targeted, nanoparticle-releasing oral vaccine to control genitorectal viral infection, *Nat. Med.* 18 (2012) 1291–1296. doi:10.1038/nm.2866.
- [255] H. Laroui, G. Dalmasso, H.T.T. Nguyen, Y. Yan, S. V. Sitaraman, D. Merlin, Drug-Loaded Nanoparticles Targeted to the Colon With Polysaccharide Hydrogel Reduce Colitis in a Mouse Model, *Gastroenterology.* 138 (2010) 843–853. doi:10.1053/j.gastro.2009.11.003.
- [256] G. Leonaviciute, O. Zupančič, F. Prüfert, J. Rohrer, A. Bernkop-Schnürch, Impact of lipases on the protective effect of SEDDS for incorporated peptide drugs towards intestinal peptidases, *Int. J. Pharm.* 508 (2016) 102–108. doi:10.1016/j.ijpharm.2016.04.044.
- [257] S. Hauptstein, F. Prüfert, A. Bernkop-Schnürch, Self-nanoemulsifying drug delivery systems as novel approach for pDNA drug delivery, *Int. J. Pharm.* 487 (2015) 25–31. doi:10.1016/j.ijpharm.2015.03.064.
- [258] J. Griesser, G. Hetényi, H. Kadas, F. Demarne, V. Jannin, A. Bernkop-Schnürch, Self-emulsifying peptide drug delivery systems: How to make them highly mucus permeating, *Int. J. Pharm.* 538 (2018) 159–166. doi:10.1016/j.ijpharm.2018.01.018.
- [259] J. Griesser, S. Burtscher, S. Köllner, I. Nardin, F. Prüfert, A. Bernkop-Schnürch, Zeta potential changing self-emulsifying drug delivery systems containing phosphorylated polysaccharides, *Eur. J. Pharm. Biopharm.* 119 (2017) 264–270. doi:10.1016/j.ejpb.2017.06.025.
- [260] H. Friedl, S. Dünnhaupt, F. Hintzen, C. Waldner, S. Parikh, J.P. Pearson, M.D. Wilcox, A. Bernkop-Schnürch, Development and evaluation of a novel mucus diffusion test system approved by self-nanoemulsifying drug delivery Systems, *J. Pharm. Sci.* 102 (2013) 4406–4413. doi:10.1002/jps.23757.

- [261] W. Song, Y. Yang, M. Yu, Q. Zhu, M.S. Damaneh, H. Zhong, Y. Gan, Enhanced digestion inhibition and mucus penetration of F127-modified self-nanoemulsions for improved oral delivery, *Asian J. Pharm. Sci.* 13 (2018) 326–335. doi:10.1016/j.ajps.2018.03.001.
- [262] E. Kontogiannidou, T. Meikopoulos, C. Virgiliou, N. Bouropoulos, H. Gika, I.S. Vizirianakis, A. Müllertz, D.G. Fatouros, Towards the development of Self-Nano-Emulsifying Drug Delivery Systems (SNEDDS) containing trimethyl chitosan for the oral delivery of amphotericin B: In vitro assessment and cytocompatibility studies, *J. Drug Deliv. Sci. Technol.* 56 (2020) 101524. doi:10.1016/j.jddst.2020.101524.
- [263] A. Mahmood, F. Prüfert, N.A. Efiana, M.I. Ashraf, M. Hermann, S. Hussain, A. Bernkop-Schnürch, Cell-penetrating self-nanoemulsifying drug delivery systems (SNEDDS) for oral gene delivery, *Expert Opin. Drug Deliv.* 13 (2016) 1503–1512. doi:10.1080/17425247.2016.1213236.
- [264] G. Hetényi, J. Griesser, M. Moser, F. Demarne, V. Jannin, A. Bernkop-Schnürch, Comparison of the protective effect of self-emulsifying peptide drug delivery systems towards intestinal proteases and glutathione, *Int. J. Pharm.* 523 (2017) 357–365. doi:10.1016/j.ijpharm.2017.03.027.
- [265] G. Leonaviciute, N.T. Adamovic, H.T. Lam, J. Rohrer, A. Partenhauser, A. Bernkop-Schnürch, Self-emulsifying drug delivery systems (SEDDS): Proof-of-concept how to make them mucoadhesive, *Eur. J. Pharm. Biopharm.* 112 (2017) 51–57. doi:10.1016/j.ejpb.2016.11.019.
- [266] G. Hetényi, J. Griesser, I. Nardin, A. Bernkop-Schnürch, Combination of SEDDS and Preactivated Thiomers Technology: Incorporation of a Preactivated Thiolated Amphiphilic Polymer into Self-Emulsifying Delivery Systems, *Pharm. Res.* 34 (2017) 1171–1179. doi:10.1007/s11095-017-2131-5.
- [267] I.A. Elbahwy, N. Lupo, H.M. Ibrahim, H.R. Ismael, A.A. Kasem, C. Caliskan, B. Matuszczak, A. Bernkop-Schnürch, Mucoadhesive self-emulsifying delivery systems for ocular administration of econazole, *Int. J. Pharm.* 541 (2018) 72–80. doi:10.1016/j.ijpharm.2018.02.019.
- [268] J. Rohrer, A. Partenhauser, S. Hauptstein, C.M. Gallati, B. Matuszczak, M. Abdulkarim, M. Gumbleton, A. Bernkop-Schnürch, Mucus permeating thiolated self-emulsifying drug delivery systems, *Eur. J. Pharm. Biopharm.* 98 (2016) 90–97. doi:10.1016/j.ejpb.2015.11.004.
- [269] N.A. Efiana, T.N.Q. Phan, A.J. Wicaksono, A. Bernkop-Schnürch, Mucus permeating self-emulsifying drug delivery systems (SEDDS): About the impact of mucolytic enzymes, *Colloids Surfaces B Biointerfaces.* 161 (2018) 228–235. doi:10.1016/j.colsurfb.2017.10.032.
- [270] S. Zaichik, C. Steinbring, C. Menzel, L. Knabl, D. Orth-Höller, H. Ellemunter, K. Niedermayr, A. Bernkop-Schnürch, Development of self-emulsifying drug delivery systems (SEDDS) for ciprofloxacin with improved mucus permeating properties, *Int. J. Pharm.* 547 (2018) 282–290. doi:10.1016/j.ijpharm.2018.06.005.
- [271] M.I. Cardona, N.M. Nguyen Le, S. Zaichik, D.M. Aragón, A. Bernkop-Schnürch, Development and in vitro characterization of an oral self-emulsifying delivery system (SEDDS) for rutin fatty ester with high mucus permeating properties, *Int. J. Pharm.* 562 (2019) 180–186. doi:10.1016/j.ijpharm.2019.03.036.
- [272] B.J. Boyd, C.A.S. Bergström, Z. Vinarov, M. Kuentz, J. Brouwers, P. Augustijns, M. Brandl, A. Bernkop-Schnürch, N. Shrestha, V. Prétat, A. Müllertz, A. Bauer-Brandl, V. Jannin, Successful oral delivery of poorly water-soluble drugs both depends on the intraluminal behavior of drugs and of appropriate advanced drug delivery systems, *Eur. J. Pharm. Sci.* 137 (2019) 104967. doi:10.1016/j.ejps.2019.104967.
- [273] S. Xu, W.-G. Dai, Drug precipitation inhibitors in supersaturable formulations, *Int. J. Pharm.* 453 (2013) 36–43. doi:10.1016/j.ijpharm.2013.05.013.
- [274] J. Brouwers, M.E. Brewster, P. Augustijns, Supersaturating Drug Delivery Systems: The Answer to Solubility-Limited Oral Bioavailability?, *J. Pharm. Sci.* 98 (2009) 2549–2572. doi:10.1002/jps.21650.
- [275] M. Dias, The effect of β -cyclodextrins on the permeation of diclofenac from supersaturated solutions, *Int. J. Pharm.* 263 (2003) 173–181. doi:10.1016/S0378-5173(03)00366-1.
- [276] D.B. Warren, C.A.S. Bergström, H. Benameur, C.J.H. Porter, C.W. Pouton, Evaluation of the Structural Determinants of Polymeric Precipitation Inhibitors Using Solvent Shift Methods and Principle Component Analysis, *Mol. Pharm.* 10 (2013) 2823–2848. doi:10.1021/mp300576u.

- [277] G. Singh, R.S. Pai, In vitro and in vivo performance of supersaturable self-nanoemulsifying system of trans-resveratrol, *Artif. Cells, Nanomedicine Biotechnol.* 44 (2016) 510–516. doi:10.3109/21691401.2014.966192.
- [278] G. Quan, B. Niu, V. Singh, Y. Zhou, C.-Y. Wu, X. Pan, C. Wu, Supersaturable solid self-microemulsifying drug delivery system: precipitation inhibition and bioavailability enhancement, *Int. J. Nanomedicine.* 12 (2017) 8801–8811. doi:10.2147/IJN.S149717.
- [279] N. Zhang, F. Zhang, S. Xu, K. Yun, W. Wu, W. Pan, Formulation and evaluation of luteolin supersaturable self-nanoemulsifying drug delivery system (S-SNEDDS) for enhanced oral bioavailability, *J. Drug Deliv. Sci. Technol.* 58 (2020) 101783. doi:10.1016/j.jddst.2020.101783.
- [280] J.-H. Lee, H. Kim, Y. Cho, T.-S. Koo, G. Lee, Development and Evaluation of Raloxifene-Hydrochloride-Loaded Supersaturable SMEDDS Containing an Acidifier, *Pharmaceutics.* 10 (2018) 78. doi:10.3390/pharmaceutics10030078.
- [281] H. Han, Y. Li, Z. Peng, K. Long, C. Zheng, W. Wang, T.J. Webster, L. Ge, A Soluplus/Poloxamer 407-based self-nanoemulsifying drug delivery system for the weakly basic drug carvedilol to improve its bioavailability, *Nanomedicine Nanotechnology, Biol. Med.* 27 (2020) 102199. doi:10.1016/j.nano.2020.102199.
- [282] J. Bannow, Y. Yorulmaz, K. Löbmann, A. Müllertz, T. Rades, Improving the drug load and in vitro performance of supersaturated self-nanoemulsifying drug delivery systems (super-SNEDDS) using polymeric precipitation inhibitors, *Int. J. Pharm.* 575 (2020) 118960. doi:10.1016/j.ijpharm.2019.118960.
- [283] D.R. Lee, M.J. Ho, Y.W. Choi, M.J. Kang, A Polyvinylpyrrolidone-Based Supersaturable Self-Emulsifying Drug Delivery System for Enhanced Dissolution of Cyclosporine A, *Polymers (Basel).* 9 (2017) 124. doi:10.3390/polym9040124.
- [284] M.J. Kang, D.R. Lee, H.J. Jung, H.R. Cho, J.S. Park, S.-H. Yoon, Y.S. Choi, C.-H. Oh, M.J. Ho, Y.W. Choi, Enhanced dissolution and oral absorption of tacrolimus by supersaturable self-emulsifying drug delivery system, *Int. J. Nanomedicine.* 11 (2016) 1109. doi:10.2147/IJN.S102991.
- [285] M. Ogino, K. Yakushiji, H. Suzuki, K. Shiokawa, H. Kikuchi, Y. Seto, H. Sato, S. Onoue, Enhanced pharmacokinetic behavior and hepatoprotective function of ginger extract-loaded supersaturable self-emulsifying drug delivery systems, *J. Funct. Foods.* 40 (2018) 156–163. doi:10.1016/j.jff.2017.08.035.
- [286] N.-T. Tung, C.-S. Tran, H.-A. Nguyen, T.-D. Nguyen, S.-C. Chi, D.-V. Pham, Q.-D. Bui, X.-H. Ho, Formulation and biopharmaceutical evaluation of supersaturable self-nanoemulsifying drug delivery systems containing silymarin, *Int. J. Pharm.* 555 (2019) 63–76. doi:10.1016/j.ijpharm.2018.11.036.
- [287] M.-S. Kim, E.-S. Ha, G.-H. Choo, I.-H. Baek, Preparation and in Vivo Evaluation of a Dutasteride-Loaded Solid-Supersaturable Self-Microemulsifying Drug Delivery System, *Int. J. Mol. Sci.* 16 (2015) 10821–10833. doi:10.3390/ijms160510821.
- [288] I.H. Baek, E.S. Ha, J.W. Yoo, Y. Jung, M.S. Kim, Design of a gelatin microparticle-containing self-microemulsifying formulation for enhanced oral bioavailability of dutasteride, *Drug Des. Devel. Ther.* 9 (2015) 3231–3238. doi:10.2147/DDDT.S86458.
- [289] A. Petchsomrit, N. Sermkaew, R. Wiwattanapatapee, Hydroxypropylmethyl cellulose-based sponges loaded self-microemulsifying curcumin: Preparation, characterization, and in vivo oral absorption studies, *J. Appl. Polym. Sci.* 133 (2016) 1–10. doi:10.1002/app.42966.
- [290] E. Josef, H. Bianco-Peled, Sponges carrying self-microemulsifying drug delivery systems, *Int. J. Pharm.* 458 (2013) 208–217. doi:10.1016/j.ijpharm.2013.09.024.
- [291] Z. Četković, S. Cvijić, D. Vasiljević, Formulation and characterization of novel lipid-based drug delivery systems containing polymethacrylate polymers as solid carriers for sustained release of simvastatin, *J. Drug Deliv. Sci. Technol.* 53 (2019). doi:10.1016/j.jddst.2019.101222.
- [292] K.M. Yang, P.Y. Chiang, Preparation and evaluation of release formulation of γ -oryzanol/algae oil self-emulsified with alginate beads, *Mar. Drugs.* 17 (2019). doi:10.3390/md17030156.
- [293] Y. Seto, C. Morizane, K. Ueno, H. Sato, S. Onoue, Supersaturable Self-Emulsifying Drug Delivery System of Krill Oil with Improved Oral Absorption and Hypotriglyceridemic Function, *J. Agric. Food Chem.* 66 (2018) 5352–5358. doi:10.1021/acs.jafc.8b00693.
- [294] S. Raut, B. Karzuon, E. Atef, Using in situ Raman spectroscopy to study the drug precipitation

- inhibition and supersaturation mechanism of Vitamin E TPGS from self-emulsifying drug delivery systems (SEDDS), *J. Pharm. Biomed. Anal.* 109 (2015) 121–127. doi:10.1016/j.jpba.2015.02.027.
- [295] D. Zheng, C. Lv, X. Sun, J. Wang, Z. Zhao, Preparation of a supersaturatable self-microemulsion as drug delivery system for ellagic acid and evaluation of its antioxidant activities, *J. Drug Deliv. Sci. Technol.* 53 (2019) 101209. doi:10.1016/j.jddst.2019.101209.
- [296] D.J. Shin, B.R. Chae, Y.T. Goo, H.Y. Yoon, C.H. Kim, S. Il Sohn, D. Oh, A. Lee, S.H. Song, Y.W. Choi, Improved dissolution and oral bioavailability of valsartan using a solidified supersaturatable self-microemulsifying drug delivery system containing gelucire® 44/14, *Pharmaceutics*. 11 (2019). doi:10.3390/pharmaceutics11020058.

Experimental section

Chapter II: Development and structural characterization of dried nanoemulsion for oral drug delivery

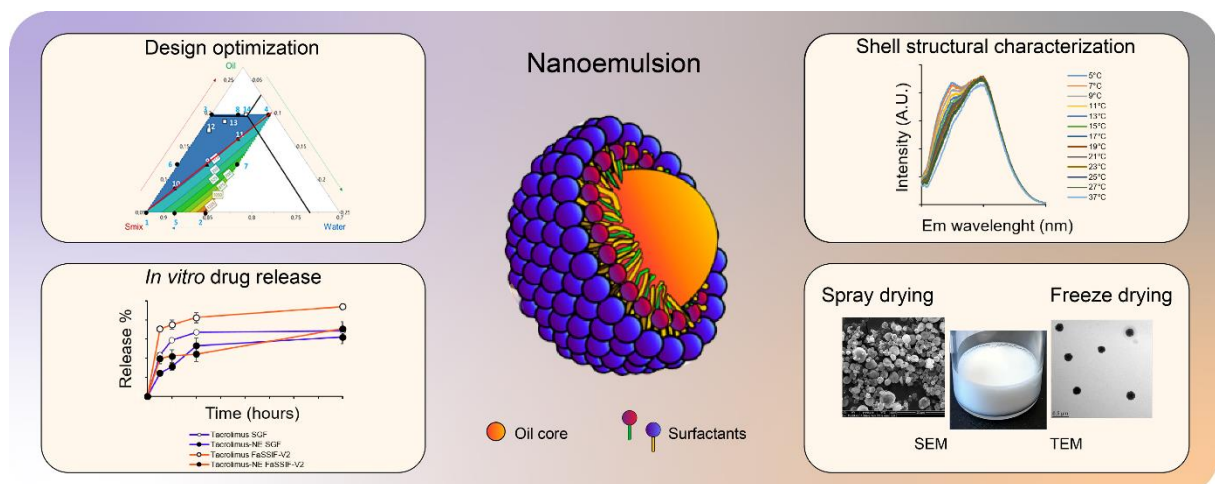
Nanoemulsions (NE), as major representative of lipid-based drug delivery systems (LBDDS), are excellent candidates for the oral delivery of poorly water-soluble drugs, owing to the ease of preparation, high drug loading, enhance solubility and protection of drugs and interaction with the intestinal epithelium which maximize drug absorption.

Main aim

The aim of this first chapter of the work was the rational development and physicochemical-structural characterisation of a novel NE intended for the oral delivery of hydrophobic drugs.

Specific objectives

- Prepare NE using a formulation approach based on the emulsion phase inversion (EPI) method coupled with a high energy input; optimize the formulation process; physicochemically characterize the system; load the NE with a hydrophobic model drug; assess the stability in simulated gastrointestinal environment;
- Convert the NE in a solid dosage form by both freeze- and spray-drying;
- Characterise the structure of the NE with a main focus on the NE shell using a new methodology based on X-ray diffraction, differential scanning calorimetry (DSC) and fluorescent spectroscopy by labelling NE with the Dioll probe.



Highlights of the chapter

- The design and optimization of a NE composed of a medium chain triglyceride (MCT, Miglyol® 812) oil core stabilized by a mixture of PEGylated hydrophilic (Myrj® 52) and hydrophobic (Labrafil® M1944CS) surfactants has been presented. This NE possess a high colloidal stability with a size of around 100 nm, PdI of 0.2 and slightly negative surface charge (−9 mV).
- The NE obtained were able to efficiently load the hydrophobic model drug tacrolimus. Moreover, upon incubation with simulated gastrointestinal fluids they increased the stability of the associated compound and released it in a sustained manner, proving their relevance as oral delivery device.
- Freeze-drying technique has been identified as the technique of choice to convert NE in a solid dosage. Upon re-dispersion, NE maintained their physicochemical attributes with minimal alteration of their size.
- An in depth analyses of the particle shell was proposed. By means of X-ray diffraction, DSC and fluorescent spectroscopy studies, the NE was proved to possess a fluid shell which is amorphous when in colloidal suspension and crystalline when dried.

The studies presented in this chapter have been published as research article on the journal *Colloids and Surfaces A*, <https://doi.org/10.1016/j.colsurfa.2020.124614>.

The text is reproduced below.

Development and structural characterization of a novel nanoemulsion for oral drug delivery

Annalisa Rosso¹, Giovanna Lollo¹, Yves Chevalier¹, Nam Troung¹, Claire Bordes¹, Sandrine Bourgeois¹, Ofelia Maniti², Thierry Granjon², Pierre-Yves Dugas³, Sebastien Urbaniak¹, Stephanie Briançon¹

¹ University of Lyon, Université Claude Bernard Lyon 1, CNRS, LAGEPP UMR 5007, 43 bd 11 Novembre 1918, 69622 Villeurbanne, France.

² University of Lyon, Université Lyon 1, CNRS, Institut de Chimie et Biochimie Moléculaires et Supramoléculaires, ICBMS UMR 5246, 43 bd 11 Novembre 1918, 69622 Villeurbanne, France.

³ University of Lyon, Université Lyon 1, CNRS, C2P2 UMR 5265, 43 bd 11 Novembre 1918, 69622 Villeurbanne, France.

II. Abstract

The objective of this work has been to develop a template for the design and characterization of dried nanoemulsion (NE) for oral administration of hydrophobic compounds. A rational optimization of the nanosystem using an experimental design was performed to achieve stable NE of 100 nm with a neutral surface potential. NE were able to efficiently encapsulate the model drug tacrolimus, providing a sustained drug release in both SGF (simulated gastric fluid) and FaSSIF-V2 fluid (simulated intestinal fluid in fasted state). To improve their long-term physical stability, NE were dried using spray-drying and freeze-drying. Following reconstitution in water, they maintain their physicochemical properties without alteration. The highest process yield was obtained by freeze-drying using very low amount of cryoprotectant, overcoming major challenges related with the production of dry powders from oil based systems. Then, in order to improve the current structural analysis of nanocarriers an original structural characterization of the NE, with an in-depth focus on the NE shell nature was then performed. Through X-ray diffraction and differential scanning calorimetry (DSC) measurements we demonstrated that the NE shell was amorphous when in colloidal suspension and crystalline upon drying. We also developed a novel polarity-sensitive fluorophore to assess the NE shell fluidity when in colloidal suspension. Globally, in the work here presented a relationship between the fluidity of the NE shell and the structure of used excipients was established. The gained evidences on the NE structure will contribute to a more rational design of nanosystems, opening the way to novel applications in oral drug delivery.

II.1. Introduction

Lipid-based drug delivery systems (LBDDS) have drawn increasing attention in the last decade for their great potential to improve oral delivery of poorly water-soluble drugs [1]. Their main advantages rely on the ability i) to increase the solubility of hydrophobic compounds, ii) to protect the associated drug from the harsh conditions of the GI tract, iii) to prolong drug intestinal residence time and iv) to promote interactions with intestinal epithelium resulting in enhanced intestinal absorption [2]. Moreover, they can be obtained using easy and transposable techniques of production that allow the translation of LBDDS to pre-clinical studies and clinical applications. LBDDS are core-shell structures composed of an inner oil core in which the drug is solubilized and an external layer which stabilizes the aqueous suspension. They are made of inert, biocompatible and biodegradable FDA-approved materials having

well-established safety profiles for oral administration of pharmaceuticals [3]. LBDDS include a wide range of nanosystems that can be classified as: vesicular systems (i.e. liposomes, niosomes), fluid emulsified systems such as nanoemulsions (NE) and self-emulsifying drug delivery systems (SEDDS), and solid lipid particulate systems such as solid lipid nanoparticles (SLN), nanostructured lipid carrier (NLC) and lipid nanocapsules (LNC) [4,5]. All these LBDDS are structurally different though they are based on emulsion formulation processes. Thus, mastery over emulsion formation phenomena is crucial towards the development of nanosystems having definite specifications of their therapeutic properties depending on the drug to be loaded [6].

NE are thermodynamically unstable emulsions with mean droplet diameters lower than 200 nm made of an inner oil core stabilized by an external surfactant shell [7]. Their advantage over other LBDDS arises from the large drug loading capacity provided by the high oil content of the system [8–10]. NE can be obtained using either high-energy or low-energy approaches. These methods differ for the physicochemical mechanisms that govern nanosystem formation. High-energy approaches are based on the use of specific equipment (high-pressure homogenizers, ultrasound dispersers) that dissipate intense mechanical power into the sample, mixing water and oil phases and breaking droplets down to smaller sizes [11]. In contrast, low-energy approaches relying on “spontaneous emulsification” processes, such as the phase inversion composition (PIC), emulsion phase inversion (EPI), and phase inversion temperature (PIT) techniques which allow the formation of ultrafine droplets [8,12]. Among low-energy approaches, EPI method is an isothermal technique in which emulsification is performed by changes in system composition [13]. It has been widely studied for the production of NE [6,8,13,14]. However, major drawbacks such as the limited types of surfactants which can be used compared to high-energy method and the propensity to Ostwald ripening due to the high Laplace pressure inside small NE droplets, limits the use of EPI technique for the production of suitable NE [15].

Based on the previous background, the present work aims at the rational design and development of a novel NE. The EPI technique and homogenization process were combined to broaden the spectra of excipients that can be used to formulate NE by low energy methods. A case-specific optimization of the system was performed using an experimental design. The influence of composition (surfactant amount and surfactant-to-oil ratio SOR) on physicochemical properties of NE was studied. The transposability of the system was evaluated and the optimized NE formulation was scaled up 10-fold. Tacrolimus, a BCS Class II immunomodulatory agent used in the treatment of various diseases, was chosen as hydrophobic model drug to be encapsulated into NE. Stability studies and *in vitro* release behaviour were carried out in relevant GI media as simulated gastric fluid (SGF) and simulated intestinal fluid in fasted state (FaSSIF-V2). The procedure here presented for nanoemulsion formulation and characterization can be used as template for a rational design of lipid nanosystems. Then, NE were dried using spray-drying and freeze-drying to preserve their long term stability. While NE formulations have already been reported for oral drug delivery, to our knowledge, drying processes to obtain a powder as final product are still lacking in the literature [32,33]. The shell surrounding NE droplets was characterized exploiting a unique methodology. X-ray diffraction and differential scanning calorimetry (DSC) were used to assess the shell crystalline or amorphous state. Finally, an innovative method based on a specific fluorescence spectroscopy analysis by labelling NE with a Laurdan derivative, was set up to investigate the shell fluid or rigid nature. The ultimate goal was to offer a way of correlating the shell composition and rigidity with nanoparticle stability, drug encapsulation efficacy and release behaviour.

II.2. Materials and methods

II.2.1. Materials

Medium chain triglycerides, MCT (Miglyol®812) purchased from CREMER OLEO GmbH & Co. KG (Hamburg, Germany) was used as oil. Polyoxyethylene(40) stearate (Myrj®52) from Sigma-Aldrich (St Quentin-Fallavier, France) and oleoyl polyoxyl-6 glycerides (Labrafil®M1944CS) from Gattefossé (Saint-Priest, France) were used as non-ionic surfactants. The aqueous phase used to prepare emulsions was sodium phosphate buffer solution (5 mM; pH 7.4). Tacrolimus was purchased from LC Laboratories (Woburn, MA, USA). Hydrochloric acid 37%, AnalaR NORMAPUR® Reag. Ph. Eur. was from VWR International (Fontenay-sous-Bois, France). Dichloromethane, methanol, acetonitrile (HPLC grade), dodecyl sulfate sodium salts pure, sodium taurocholate hydrate 96% and sodium hydroxide were purchased from Fisher Scientific (Illkirch, France). Egg phospholipids with 70% phosphatidylcholine (Lipoid E80S) was from Lipoid GmbH (Ludwigshafen am Rhein, Germany). Acetic acid was obtained from Chem-Lab NV (Zedelgem, Belgium). Maltodextrin MD (Glucidex® 12D) from Roquette Frères (Lestrem, France) and trehalose 100 (TR) as a gift of Hayashibara Co. Ltd (Okayama, Japan) were used as cryoprotectants in the drying studies. Milli-Q water, used to prepare all solutions and buffers, was obtained using a Milli-Q Academic System (Millipore, Saint Quentin, Yvelines France).

II.2.2. Nanoemulsion preparation

Nanoemulsions (NE) were prepared by emulsion phase inversion (EPI) technique [13]. The oil phase was prepared by mixing the oil (MCT) and surfactants (Polyoxyethylene(40) stearate: S1 and oleoyl polyoxyl-6 glycerides: S2) under magnetic stirring (750 rpm) at 80 °C. Then, the aqueous phase (PBS 5 mM), heated at 80 °C as well, was added into the organic melt phase. Stirring was performed using a rotor-stator disperser (T25 digital Ultra-Turrax® equipped with a S25N-8G shaft. IKA®-Werke GmbH & Co. KG, Staufen, Germany) at 11,000 rpm. Two cycles of stirring of 10 min each were performed. The resulting colloidal system was cooled to room temperature under magnetic stirring during 30 min. The process was designed so that the final emulsion always had a total mass of 5 g. Finally, NE were scaled up to 50 g (10 times larger than the optimization step scale) by adaptation of the shaft of the rotor-stator disperser.

2.2.1. Influence of formulation: ternary phase diagram and mixture design

To investigate the NE region, three ternary phase diagrams were designed using 23 formulations for each diagram. The ternary mixtures were composed of oil, water and three different surfactant mixtures (S1 + S2) called Smix. Smix was characterized by the Surfactant Mass Ratio (*SMR*) of S1 to S2

$$SMR = \frac{\text{mass of S1}}{\text{mass of S2}} \quad \text{Eq. 1}$$

The NE area was identified by varying the Smix/Oil/Water amount at fixed *SMR* of 1, 2.5, and 5.

Another parameter of the formulation was the Surfactant-to-Oil ratio (*SOR*) defined as

$$SOR = \frac{\text{mass of Smix}}{\text{mass of MCT}} \quad \text{Eq. 2}$$

II.2.3. Physicochemical and morphological measurements

Electrical conductivity was measured using a portable conductivity meter (CDM210 Conductivity Meter, MeterLabTM, Radiometer Analytical SAS, Lyon, France). Shear viscosity measurements were

performed using a controlled shear-rate rheometer (MCR 302 rheometer, Anton Paar, Les Ulis, France). All measurements were carried over a range of different shear rates (0.1–100 s⁻¹) at 25 °C. The crystalline characteristics of NE were determined through X-ray powder diffraction (XRPD) analysis at the “Centre de Diffractométrie Henri Longchambon” facility of the University Lyon 1 using a Bruker AXS D8 Advance X-ray diffractometer operating in the Bragg θ - 2θ configuration using Cu K α radiation (1.54 Å wavelength) in an angular domain from 10° to 70° at scanning rates of 0.25°·min⁻¹.

Size distribution and surface electrical potential of NE were measured using Malvern Zetasizer® NanoZS (Malvern Instruments S.A., Worcestershire, UK). Particle size and polydispersity index (PDI) were determined by Dynamic Light Scattering (DLS) diluting all samples with Milli-Q water to ensure correct calculation of size distribution by the method of cumulants. Analyses were carried out at 25 °C with an angle of detection of 173°. ζ -potentials were measured by electrophoresis technique after dilution of samples in KCl 1 mM. Analyses were performed in triplicate.

NE morphology was analysed by transmission electron microscopy (TEM), cryogenic-transmission electron microscopy (Cryo-TEM) and scanning electron microscopy (SEM) at the “Centre Technologique des Microstructures” (CT μ) facility of the University of Lyon. TEM was performed with a Philips CM120 microscope. Diluted NE (10 μ L) was deposited on a microscope grid (copper support coated with carbon) and slowly dried in open air. The dry samples were observed by TEM under 120 kV acceleration voltage. For Cryo-TEM analysis diluted samples of NE were dropped onto 300 mesh holey carbon films (Quantifoil R2/1) and quench-frozen in liquid ethane using a cryo-plunge workstation (made at Laboratoire de Physique des Solides-LPS, Orsay, France). The specimens were then mounted on a precooled Gatan 626 sample holder, transferred into the microscope (Phillips CM120) and observed at an accelerating voltage of 120 kV. Moreover, TEM microscope grids, on which NE were deposited and slowly dried in open air overnight, were plunged frozen in liquid ethane (following the Cryo-TEM protocol of sample preparation) and NE were observed by TEM (cold TEM).

Scanning electron microscopy (SEM) was performed on dried samples following spray-drying with a FEI Quanta 250 FEG microscope. A drop of diluted aqueous suspension of re-hydrated spray-dried NE was deposited on a flat steel holder and dried at room temperature. Then samples were coated under vacuum by cathodic sputtering with copper. The samples were observed by SEM under an accelerating voltage of 15 kV.

The structural characterizations of NE aqueous suspensions and dried NE were performed by differential scanning calorimetry (DSC) using a Q200® instrument from TA Instruments (New Castle, DE, USA). A nitrogen purge of 50 mL·min⁻¹ was used for all measurements. The temperature range was -80 °C to +160 °C. Samples (about 10 mg) were accurately weighed and sealed in 40 μ L aluminium pans close with either a hermetic lid for DSC of excipients and NE powders, or perforated aluminium lids DSC of NE and S1 in water that gradually released water when heated above 40 °C.

The fluidity of the NE shell was determined by mean of a newly synthesized Laurdan derivative, Dioll (patent pending EPO19306175.1-1118). The Dioll probe was dissolved in ethanol (263 μ M). NE was diluted 1:100 (0.27% w/v). The Dioll solution (10 μ L) was added to 1 mL NE to reach a 2.6 μ M final concentration of Dioll, corresponding to a Dioll-NE ratio of 1:2900 (w/w). The sample was incubated for 20 min at room temperature. As controls, the fluorescence of Dioll solutions (2.6 μ M) in MCT and in water, and the fluorescence of blank NE (without Dioll) were recorded. For the blank NE control, 10 μ L of ethanol were added to 1 mL NE. Fluorescence data were obtained using a FP-8500

spectrofluorimeter (JASCO applied science, Halifax, Canada). The excitation wavelength was 390 nm and the emission spectra were recorded between 400 and 600 nm at several temperatures ranging from 5 to 27 °C in steps of 2 °C and at 37 °C (2.5 nm bandwidth). The generalized polarization (*GP*) parameter was calculated from emission intensities according to:

$$GP = \frac{I_{440} - I_{490}}{I_{440} + I_{490}} \quad \text{Eq. 3}$$

where I_{440} and I_{490} are recorded fluorescence intensities at wavelengths of 440 nm and 490 nm, respectively, as previously described for Laurdan [16].

II.2.4. Tacrolimus-loaded nanoemulsion development

II.2.4.1. Solubility study of tacrolimus

Tacrolimus (50 mg) was dissolved in 1 mL of MCT, S2 or S1, stirred (750 rpm) at 80 °C during 3 h and left overnight to reach equilibrium. Then, samples were centrifuged at 14000 rpm for 20 min and the supernatant was collected and mixed with 1 mL of a methanol-dichloromethane mixture (1:1) and 2 mL of acetonitrile. Following filtration with 0.22 µm Nylon syringe filter (Whatman GmbH, Dassel, Germany), samples were injected into the HPLC system for tacrolimus detection. The apparatus consisted of Agilent 1200 Series G1311A Quat Pump, Agilent 1200 Series G1367B HIP-ALS High Performance Autosampler, equipped with Agilent 1200 Series G1315D Dad Diode Array Detector HPLC (Agilent, Santa Clara, CA, United States). Tacrolimus was separated on a RP-C18 column (Kinetex 5 µm C18 100 Å, 150 × 4.6 mm, Phenomenex, Torrance, CA, USA), with temperature set to 60 °C, using acetonitrile-deionized water 0.5% acetic acid (70:30) as mobile phase at a flow rate of 1.0 mL·min⁻¹. The injection volume was 20 µL and the detection wavelength was 213 nm [17]. The retention time of tacrolimus was at 3.99 ± 0.02 min. The system was managed by OpenLab CDS ChemStation Edition software (Agilent, Santa Clara, CA, United States). The calibration curve was linear ($R^2 = 0.999$) in the concentration range of 10–250 µg·mL⁻¹. The method was validated according to ICH Q2(R1) guidelines. Detection and quantification limits (*LOD* and *LOQ*) were 7.6 µg·mL⁻¹ and 23 µg·mL⁻¹, respectively [18].

II.2.4.2. Tacrolimus encapsulation efficiency and drug loading in nanoemulsions

To determine the encapsulation efficiency (*EE*) of tacrolimus into the system, tacrolimus-loaded NE (2 mg·mL⁻¹) was separated from the aqueous medium by size exclusion chromatography. Separation was performed on PD-10 Desalting Columns, containing 8.3 mL of Sephadex™ G-25 resin (GE Healthcare Bio-Sciences AB, Uppsala, Sweden), using BPS 5 mM as the eluent. Fractions containing NE were identified and collected in microtubes owing to their milky appearance. Tacrolimus was extracted from fractions containing NE as previously described (section 2.4.1) and analysed by HPLC. Total NE was analysed to determine the total amount of tacrolimus present in the initial formulation. The encapsulation efficiency (*EE*) was calculated following Eq. 4:

$$EE(\%) = \frac{\text{mass of tacrolimus in NE}}{\text{mass of tacrolimus feeding}} \times 100 \quad \text{Eq. 4}$$

The drug loading (*DL*) was calculated as the ratio of the mass of tacrolimus detected in the purified NE to the total mass of NE:

$$DL(\%) = \frac{\text{mass of tacrolimus in NE}}{\text{mass of NE}} \times 100 \quad \text{Eq. 5}$$

Analyses were done in triplicate.

II.2.5. *In vitro* NE stability and release study of tacrolimus in simulated GI fluids

The simulated gastric fluid (SGF, pH 1.2, 0.5% Sodium Lauryl Sulfate (SLS)) and simulated intestinal fluid in fasted state (FaSSIF-V2, pH 6.5) were prepared according to Zhang et al. [19] and Jantravid et al. [20] respectively. The colloidal stability of tacrolimus-loaded NE in simulated gastric and intestinal fluids was evaluated by DLS analysis. To this aim, 250 μL of NE were diluted in 1 mL of either simulated gastric fluid without pepsin (SGF) or simulated intestinal fluid without pancreatin (SIF), prepared in accordance with the guidelines of the Ph. Eur. 9th ed. and then incubated at 37 °C. The sample (1 mL) was collected at different time points for the determination of the average hydrodynamic diameter and polydispersity index by DLS. Each analysis was performed in triplicate in three different batches.

The *in vitro* release study of tacrolimus from drug-loaded NE was performed in gastric (SGF-SLS) and intestinal (FaSSIF-V2) fluids, under sink condition (2 $\mu\text{g}\cdot\text{mL}^{-1}$ tacrolimus concentration), using the dialysis method. A dialysis bag (Spectrum™ Spectra/Por™ dialysis membrane, MWCO: 6-8 kDa, Fisher Scientific, Illkirch, France) containing 400 μL of loaded NE (1.0 $\text{mg}\cdot\text{mL}^{-1}$) was placed in 200 mL of release medium and incubated at 37 °C under a stirring rate of 150 rpm. Tacrolimus-loaded NE were withdrawn from dialysis bags at predetermined time intervals (up to 8 h in SGF and up to 72 h in FaSSIF-V2) and total tacrolimus content was determined by HPLC. In the case of release into FaSSIF-V2, analysis was also performed at 50 °C, which is above S1 excipient melting point (43 °C–48 °C). Tacrolimus dissolved in a mixture of ethanol and water (30:70) at 1 $\text{mg}\cdot\text{mL}^{-1}$ was used as control.

II.2.6. Drying techniques

II.2.6.1. Spray-drying of nanoemulsions

The spray-drying technique was used to dry blank NE mixed with Maltodextrin (MD). Concentrations of maltodextrin of 5, 7.5 and 10% w/w and concentration of nanoemulsion of 5, 10 and 15% w/w were investigated. Prior to spray-drying, the compatibility of blank NE with MD solutions was examined visually for checking against possible phase separation, both at room temperature and under centrifugation acceleration of 2300 g for 5 min. Rheological measurements for the NE/excipients suspensions were performed using a MCR 302 rheometer (Anton Paar, Les Ulis, France) at controlled temperature (20 \pm 2 °C). Then, 50 g of mixture of NE and MD were spray-dried with a Mini Spray-dryer Büchi B191 (Büchi, Rungis, France) (NAM: Flawil, Switzerland), which had a two-fluid nozzle with cap-orifice diameter of 0.7 mm and operated in a co-current mode. The applied process parameters were: inlet temperature = 120 °C, aspirator setting = 50% of the maximum capacity, pump rate = 3 mL/min. The spray-dried powder was recovered and kept in closed vials (room temperature) to avoid moisture sorption.

II.2.6.2. Freeze-drying of nanoemulsions

NE was freeze-dried without or with trehalose (TR) as a cryoprotectant. Concentrations of trehalose of 1, 2.5, 5 and 10% w/w and concentration of nanoemulsion of 3.4, 6.8, 13.5 and 27% w/w were investigated. Samples (2 mL) were transferred into 6 mL volume glass vials and the lyophilization was carried out in a Cryonext pilot freeze-dryer (Cryonext, Saint-Aunès, France). The freeze-drying technology was as follow: freezing at -50 °C for 6 h in the freeze-dryer chamber; primary drying from

-50 °C to 0 °C in 24 h; secondary drying at 20 °C for 12 h. Finally, the vials were sealed with rubber caps and stored at 4 °C until further analysis.

II.2.6.3. Dried nanoemulsion physicochemical and morphological characterization and reconstitution

Residual moisture content was determined by thermogravimetric analysis (TGA) using a TG 209 F1 Libra thermogravimetric analyser (Netzsch, Selb, Germany) at a heating rate of 10 °C·min⁻¹ and temperature range from 20 °C to 150 °C. Following freeze-drying, the dry powders were re-hydrated by progressive addition of milli-Q water. The reconstitution time was evaluated and particle size and polydispersity index (PDI) were measured by DLS. The morphological analysis of freeze-dried NE was performed by transmission electronic microscopy (TEM). Spray-dried NE were examined by scanning electron microscopy (SEM). The impact of drying on the loaded NE (2 mg·mL⁻¹) was determined by HPLC. The drug content and the encapsulation efficiency were measured before and after the freeze-drying in order to detect any leakage during the process.

II.2.7. Statistical analysis

All data were expressed as mean ± SD. For NE mixture design, data were statistically analysed by multiple linear regression calculations, analysis of variance (ANOVA) and residual analysis with Modde® software (Umetrics, Sartorius-Stedim, Sweden). A P-value lower than 0.05 was considered as indicating statistical significance.

II.3. Results and discussion

II.3.1. Design and development of nanoemulsion

NE were prepared using the emulsion phase inversion (EPI) technique and homogenization process (using a rotor-stator disperser). The principle of EPI technique is based on the catastrophic phase inversion that occurs when water is titrated over the organic phase constituted by the mixture of oil and surfactants. In our case the organic phase was made of medium chain caprylic/capric triglycerides (MCT) stabilized by a mixture of non-ionic hydrophilic and hydrophobic surfactants, polyoxyethylene(40) stearate (S1) (HLB 16.9) and oleoyl polyoxyl-6 glycerides (S2) (HLB 4). The hydrophilic surfactant, S1, was chosen among PEGylated stearates to form a steric barrier against droplet coalescence and allow formation of small particle size [12]. S2 was used as hydrophobic surfactant [21]. The selected NE components are common lipid ingredients available in the market, approved by FDA for the oral route. Worthy of mention is that for the first time they were combined in this study to create a delivery system in the nanometric range. The emulsion phase inversion region for the O/W to W/O transition was studied in selected NE prepared by adding the aqueous phase to the oil phase (Fig. 1). The oil phase had a transparent appearance, a low electrical conductivity (0.39 μS·cm⁻¹) and a relatively low shear viscosity (52 mPa·s). After the first water addition (14%), the formulation became turbid. Then the addition of more water (20%) led to formation of a milky suspension that quickly turned into a viscous gel. At this point the electrical conductivity slightly increased and the viscosity increased steeply, reaching its maximum value (12000 mPa·s) at a water content of 28%. The increase in conductivity was less pronounced (from 30 to 800 μS·cm⁻¹) in the range of maximum viscosity value, supporting the formation of an intermediate gel-like material. Then, when more water was added (>

28%), the viscosity strongly decreased (3200 mPa·s), the conductivity increased (up to 3000 $\mu\text{S}\cdot\text{cm}^{-1}$) and the formulation presented the milky white aspect typical of O/W emulsions [13]. The intermediate highly viscous gel might be a multiple emulsion (W/O/W). At this stage, additional water made the catastrophic phase inversion to take place (W/O/W to O/W) when the small internal water droplets coalesced at the external surface of the double emulsion. The formation of a highly viscous double emulsion during formulation of NE using EPI method has previously been described [14,35].

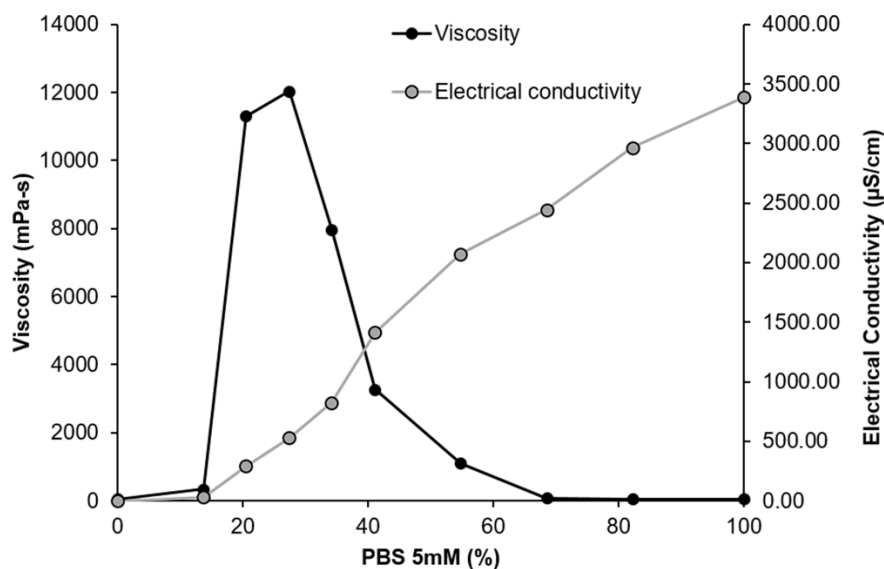


Fig. 12 Effect of water titration (phosphate buffer 5 mM, pH 7.4) on the viscosity (black line) and electrical conductivity (grey line) of NE at 80 °C.

II.3.2. Influence of formulation: ternary diagram and mixture design

An exhaustive study on the influence of NE composition and method of preparation on NE physicochemical properties, drug loading, structure and stability was developed. The design of the NE formulation was carried out using ternary phase diagrams.

The apices of the phase diagram were oil (MCT), water and surfactant mixture (Smix). Three different Smix compositions (1, 2.5 and 5) were studied (data can be found in the Supplementary Information file). For all diagrams, three domains were identified: solid state, liquid-gel state, and liquid state in which the domain of interest for NE formation was found. The area of the solid state domain increased with respect to *SMR* (from 1 to 5), which was attributed to the high content of S1. High viscosity is related to the large amount of hydrophilic PEG chains swollen by water via hydrogen bonding. This effect was correlated with an increase in the liquid-gel state formation observed at *SMR* of 2.5 and 1. A NE domain was present for all *SMR*. It was attained when the water content ranged from 0.7 to 0.95, the oil ranged from 0.02 to 0.15 and Smix ranged from 0.02 to 0.30. At *SMR* = 5 the NE area was smaller than at *SMR* = 1 and 2.5 and NE were highly viscous, which made the formation of NE more difficult [8, 23]. At *SMR* = 1 and 2.5, the extent of the NE area was higher; it was the largest at *SMR* = 2.5.

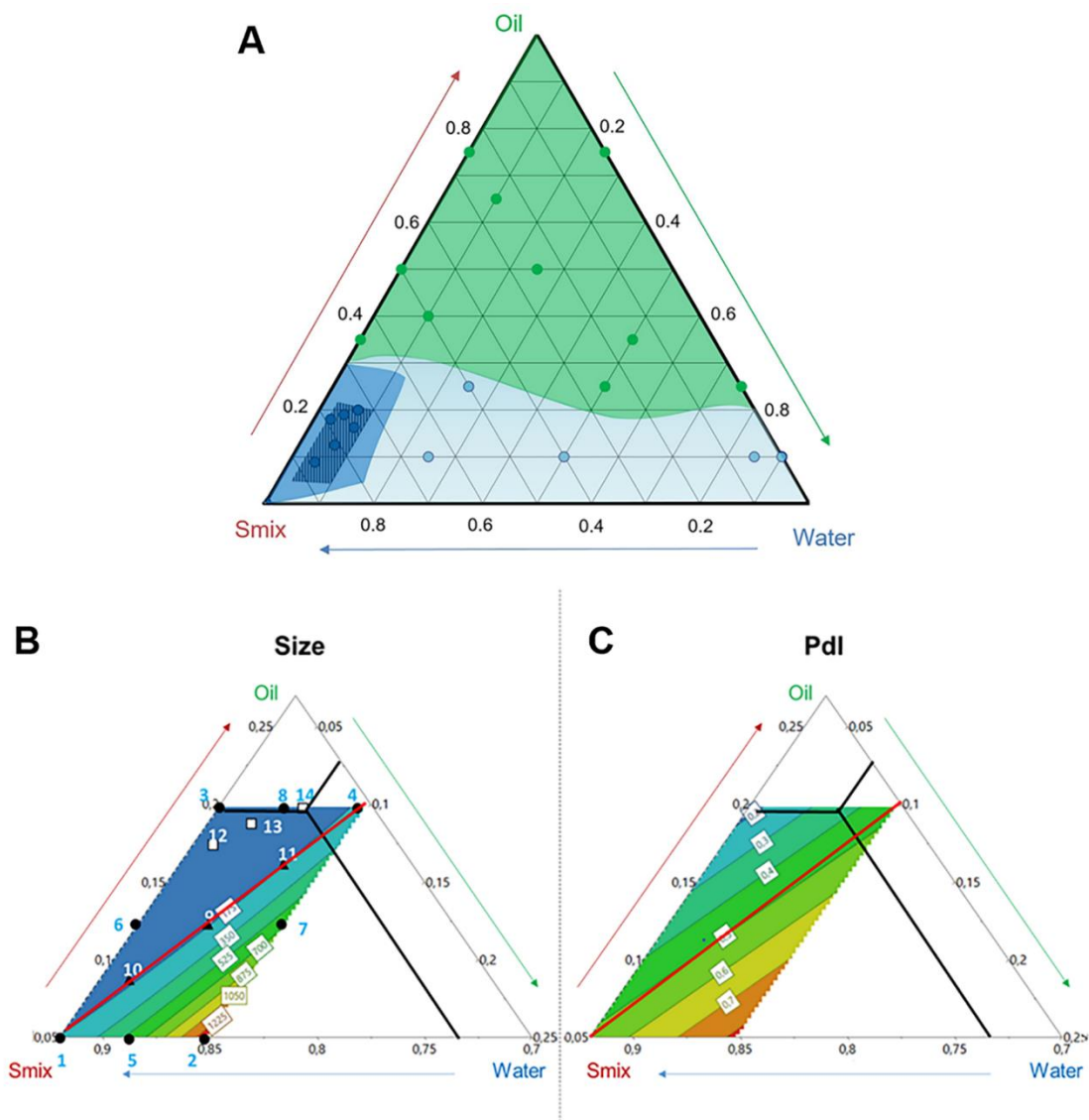


Fig. 2 A) Ternary phase diagram at $SMR=2.5$. The green area corresponds to formulations in the solid state, the two blue areas to formulations in the liquid state. The dark blue region corresponds to formulations containing NE. The trapezoid-shaped area is the selected reduced region of interest (ROI) for refined analysis. B and C) Pseudoternary phase diagram at $SMR=2.5$. Contour plots of the predicted droplet mean size (B) and Pdl (C) in the triangle defined by the lower bounds of mass fractions of oil, water and Smix ($SMR=2.5$) with design points (●), check points (▲) and optimized formulations (□). The composition of the selected optimized formulation (formulation number 14) is indicated by black lines. The red line corresponds to $SOR=2$.

The system at $SMR = 2.5$ was selected for optimization purpose (Fig. 2). Thus, the relation between the organic phase composition and the size characteristics of the resulting NE was more in-depth investigated by means of an experimental design in a pseudo-ternary phase diagram. Upper and lower bounds on the proportions of the NE components were defined according to the ternary phase diagram results (trapezoid-shaped area in Fig. 2A). The resulting set of constraints on the component mass fractions was: $0.03 < x_{oil} < 0.1$, $0.05 < x_{Smix} < 0.2$ and $0.7 < x_{water} < 0.92$. The constrained experimental

domain consisting of four vertices and four edges is shown in Fig. 2A. It is represented in the triangle whose vertices were obtained from the lower bounds of the NE components.

The eight design points corresponding to the 4 extreme vertices and the midpoints of the four edges of the constrained region (runs 1 to 8 in Table 1) were chosen in order to fit the second-degree Scheffé polynomial:

$$Y = \sum_{i=1}^3 b_i x_i + \sum_{i < j}^3 b_{ij} x_i x_j \quad \text{Eq. 6}$$

According to Scheffé [22], the vertices of the experimental domain are the most useful points for estimating the coefficients of the linear blending terms b_i , while the midpoints of the edges are better useful for estimating the binary blending parameters b_{ij} [22,23]. The overall centroid of the constrained experimental domain (run 9) was used as a validation point to check the predictive performance of the developed model (Table 1).

Table 1 Mixture design and size distribution results.

Run		x_{oil}	x_{Smix}	x_{water}	<i>SOR</i>	<i>d</i> (nm)	PdI
1	Design Point (vertex)	0.030	0.050	0.920	1.7	193	0.51
2	Design Point (vertex)	0.100	0.050	0.850	0.5	1500	0.82
3	Design Point (vertex)	0.030	0.200	0.770	6.7	108	0.27
4	Design Point (vertex)	0.100	0.200	0.700	2.0	245	0.42
5	Design Point (edge midpoint)	0.065	0.050	0.885	0.8	507	0.66
6	Design Point (edge midpoint)	0.030	0.125	0.845	4.2	124	0.30
7	Design Point (edge midpoint)	0.100	0.125	0.775	1.3	596	0.77
8	Design Point (edge midpoint)	0.065	0.200	0.735	3.1	141	0.23
9	Check point (centroid)	0.065	0.125	0.810	1.9	199	0.58
10	Check point	0.048	0.088	0.865	1.8	182	0.42
11	Check point	0.083	0.163	0.755	2.0	185	0.43
12	Optimized formulation	0.030	0.180	0.790	6.0	107	0.30
13	Optimized formulation	0.050	0.190	0.760	3.8	131	0.25
14	Optimized formulation	0.070	0.200	0.730	2.9	137	0.20

The results (Table 1) showed very large variations of NE size distribution with a mean size ranging from about 100 to 1500 nm and PdI comprised between 0.23 and 0.82. The eight first experiments were used to determine the regression model coefficients in Equation 6. Only the regression coefficients significant at the 5% level (*t*-test) were kept in the model. The ANOVA results indicated the high significance of the developed model ($p < 0.05$). The determination coefficients (R^2 and R^2 adjusted) above 0.9 also proved the satisfactory adequacy of the model. Moreover, runs 9, 10 and 11 were used as a check points to evaluate the model-predictive performance: as example, the estimated mean size and PdI for run 9 were 173 nm and 0.48 respectively, which were similar to the experimental values (199 nm and 0.58) indicating adequacy of model.

The estimated surface contours for the mean size (Fig. 2B) and PdI were plotted in pseudoternary phase diagrams (Fig. 2C). The region of interest corresponding to a mean diameter less than 140 nm is coloured in dark blue in Fig. 2B. The area where PdI < 0.3 (Fig. 2C) was larger than that where $D < 140$ nm, so that the whole dark blue region of Fig. 2A corresponded to satisfactory formulations with regards to the PdI criterion. The amounts of Smix and oil in the formulations greatly influenced both the mean size and PdI. As expected, low PdI's were obtained at large x_{Smix} and low x_{oil} and small droplet mean diameters required x_{oil} less than 0.08. From these results, three optimized formulations were identified on the basis of two selection criteria: i) stability, ii) high oil content: runs 12, 13 and 14. The

optimized NE that had maximum oil content was run 14 (indicated by black lines in Fig. 2B and 2C); its composition contained oil, Smix and water mass fractions of 0.07, 0.2 and 0.73, respectively.

Besides, the surfactant-to-oil ratio (*SOR*) was studied for *SMR* = 2.5. Nanometric droplets smaller than 200 nm were formed at $SOR \geq 2$. High surfactant concentrations allowed the formation of smallest droplets. However, at the highest surfactant concentrations tested (*SOR* = 6), a bimodal particle size distribution was observed.

The stability of formulations was estimated using homogeneity and size measurements as readouts. After 4 days of storage at 20 °C, stable and monodispersed NE (*PdI* < 0.2) were obtained at *SMR* = 2.5 and *SOR* = 2.86, 4.04 and 5. The results confirmed the interdependency between *SOR* and overall surfactant amount in NE. In fact, stability was achieved when there was a sufficient surfactant amount to cover droplet surfaces [24].

Overall, the goal of developing a stable NE, maximizing the oil content (7%), was achieved by setting *SMR* = 2.5 (HLB 13.2) and *SOR* = 2.86 (Fig. 2B and 2C). The use of an experimental design provided a rigorous methodology for optimization of formulation, which is much more suitable than the “classical” method based on trial-and-error. The full region of interest, expressed in terms of practical formulation parameters such as *SMR*, x_{oil} and *SOR*, was disclosed. Then, the optimum formulation with regards to stability, size and polydispersity criteria was selected by a minimum number of experiments. Previous studies demonstrated that the development, physicochemical attributes and stability of NE may be improved by using associations of two or more different emulsifiers, rather than an individual type [25]. TEM observations of emulsions prepared with S1 alone showed that droplets exhibited a clear tendency to aggregate (images can be found in the supplementary section). Thus, the presence of a hydrophobic surfactant (S2) in Smix (*SMR* = 2.5, *SOR* = 2.86) was mandatory for ensuring stability.

The Smix that yielded stable NE had a hydrophilic-lipophilic balance (HLB) close to the required HLB of the oil phase (13.2) [26]. The HLB values of the surfactant mixture were 10.5, 13.2 and 14.3 at *SMR* = 1, 2.5 and 5, respectively. Based on this assumption, the NE at *SMR* = 2.5 matched the required HLB of MCT.

The stability of NE in colloidal suspension was assessed at 20 °C and 37 °C, over 28 days (supplementary materials). No creaming or sample degradation were observed during the studied period and the mean size and polydispersity index (*PdI*) measured by DLS remained stable.

The robustness of the formulation process was evaluated by scaling up the NE. A batch 10 times bigger than the optimized one was produced. NE (scaled $\times 10$) maintained their initial physicochemical properties in terms of size and polydispersity (data not shown), indicating that the process can be transposed to a larger scale production.

II.3.3. Physicochemical and morphological characterization of optimized nanoemulsions

Optimized NE had mean droplet size of around 104 ± 3 nm, a low *PdI* (0.2) and a neutral/slightly negative ζ -potential (-9 ± 1 mV). This neutral surface charge derived from the PEGylated surfactant (S1) shell hinders interactions with intestinal contents and mucus layer, thus enhancing NE diffusion to the epithelium and translocation through the mucosa [52].

Transmission electron microscopy (TEM) and Cryo-TEM observations (Fig. 3A to 3D) were performed to study their morphology. TEM images showed a monodispersed population of spherical droplets with a smooth surface. However, to perform TEM observations, samples were dried on the grid and the

interaction of NE with the electron beam may cause structural alteration of particles, leading to a misinterpretation of results. Cryo-TEM was thus performed to directly investigate NE in the frozen-hydrated state, very close to their native state [27]. Moreover, Cryo-TEM observation allows the discrimination of smaller and bigger particles. Finally, it confirmed that NE formulations presented quite monodispersed population of spherical droplets.

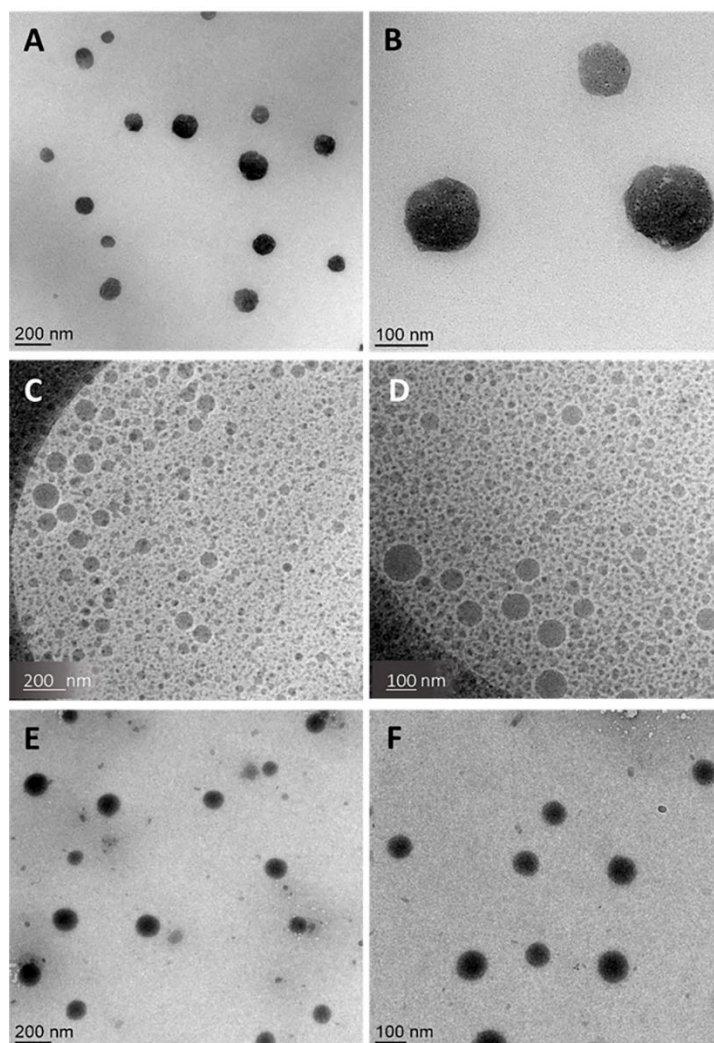


Fig. 3 A and B) TEM of blank NE, C and D) Cryo-TEM of blank NE, E and F) Cold TEM of tacrolimus-loaded NE. All images are at magnification of 200 nm and 100 nm.

II.3.4. Tacrolimus-loaded nanoemulsion formulation and physicochemical characterization

Tacrolimus, an immunomodulatory agent used in the treatment of various diseases [19], was encapsulated into the NE as hydrophobic model drug. The fundamental prerequisite to obtain a high encapsulation efficiency of the drug in nanosystems is a high solubility of the active compound in excipients. The solubility of tacrolimus was $11.9 \pm 0.01 \text{ mg}\cdot\text{mL}^{-1}$ in MCT, $29.9 \pm 0.003 \text{ mg}\cdot\text{mL}^{-1}$ in S2 and $30.6 \pm 0.01 \text{ mg}\cdot\text{mL}^{-1}$ in S1, suggesting the feasible encapsulation of the drug in NE.

Thus, tacrolimus was mixed with the NE oil phase ($2 \text{ mg}\cdot\text{mL}^{-1}$, $SMR = 2.5$, $SOR = 2.86$) by magnetic stirring (750 rpm) at $80 \text{ }^\circ\text{C}$ for 2 h to reach equilibrium, and NE were prepared performing two cycles of 10 min stirring at $80 \text{ }^\circ\text{C}$. Physicochemical characteristics of tacrolimus-loaded NE and blank NE were

the same: mean diameter was 96 nm against 104 nm, PdI was 0.23 vs 0.22 and ζ -potential was -8.7 mV vs -9.1 mV. Moreover, owing to the high lipophilic character of tacrolimus, encapsulation efficiency was close to 100% (99.5% was measured), with a drug loading of around 0.74%. This encapsulation efficiency is higher than for tacrolimus-loaded ethosomes (around 80%) [28] and lipid nanocapsules (over 90%) [29]. Moreover, the drug content ($2 \text{ mg}\cdot\text{mL}^{-1}$) was higher when compared to lipid system previously developed for the oral delivery of tacrolimus ($0.79 \pm 0.05 \text{ mg}\cdot\text{mL}^{-1}$ in lipid-core nanocapsules [53]) highlighting the interest of exploiting such formulation to further enhance drug deliver across the oral absorption barrier. DLS measurements were confirmed by “cold TEM” observations (Fig. 3E and 3F). After preparing TEM grids and let sample dry overnight, TEM grids were frozen in liquid ethane and observed by Cryo-TEM. Cold TEM images showed that loaded NE formed monodispersed population with a spherical shape.

The stability of loaded NE in colloidal suspension, upon storage at both at 20°C and 37°C , was followed over 28 days (supplementary materials). Three parameters were assessed at different time points: i) macroscopic aspect (presence of aggregates, cream formation or changes in colour); ii) particle size, polydispersity and ζ -potential; and iii) tacrolimus concentration in the preparation and leakage of the drug. No sample degradation was observed and mean size, polydispersity index (PdI) and surface potential remained stable during the studied period. Moreover, 75% of encapsulated tacrolimus was retained in the NE upon 28 days of storage at 20°C .

II.3.5. Stability and *in vitro* release of tacrolimus-loaded nanoemulsion in simulated GI fluids

The stability of loaded NE in terms of size evolution was assessed upon incubation during 3 h in SGF and 8 h in SIF media (data presented in the supplementary materials). Results indicated that loaded NE maintained their initial size in the experimental conditions tested.

Release behaviour of loaded NE was evaluated *in vitro* under sink conditions in SLS-SGF and in FaSSIF-V2 (Fig. 4). Tacrolimus dissolved in a mixture of ethanol and water (30:70) was used as a control.

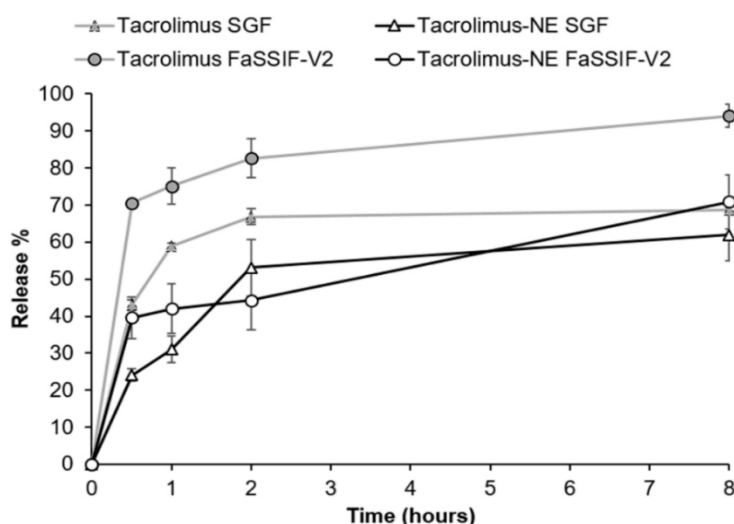


Fig. 4 *In vitro* release profiles of tacrolimus from ethanol/water solution and loaded NE in SGF (pH 1.2) or FaSSIF-V2 (pH 6.5). Mean \pm SD, n=3. SGF: simulated gastric fluid in presence of sodium lauryl sulfate (SLS 0.5% w/v); FaSSIF-V2: simulated intestinal fluid in fasted state.

Upon 30 min of incubation in SLS-SGF, 25% of the drug was released from the NE, reaching 50% during 2 h. Then, no further release was detected in the following 8 h. In FaSSIF-V2, 39% of tacrolimus was released during the first 30 min, then, 45% until 2 h. A plateau was reached following 10 h of incubation, with 75% of tacrolimus released up to 72 h (data shown in the supplementary section).

Controls showed that the release rate was not due to diffusion through the dialysis membrane. Tacrolimus solubilized in ethanol/water mixture was rapidly released in SGF, reaching 40% in 30 min followed by 60% of release in 8 h. In FaSSIF-V2, the release was faster, reaching 70% in 30 min, and 94% in 8 h. Tacrolimus was released in a sustained manner once encapsulated in the NE compared to drug solutions. This behaviour was correlated to the high affinity of the drug with the oil core of NE, which resulted from the high hydrophobicity of tacrolimus. Overall, around 40% of drug would be available upon 1 h of oral administration and the complement would be released within 24 h in a controlled sustained manner, thereby acting as maintenance dose. In accordance with previous studies, this profile might be beneficial to overcome fluctuations in drug plasma levels [54].

II.3.6. Conversion into dry solid powders

To increase the stability of the system both spray-drying and freeze-drying techniques were exploited. The drying of nanosystems allows to overcome limitations of conventional (liquid) formulations (as storage instability, particle aggregation, drug leakage and microorganism growth over time [30]) and favor the oral administration of dry NE in a powder form (i.e. capsules, Tablets).

Spray-drying is a single step procedure for drying liquid formulations by rapid water evaporation in a hot gas flow [31]. While, in the case of freeze-drying, the conversion into a solid powder involves removal of water by sublimation of ice crystals from frozen material at low pressure and low temperature [32]. The use of heat is avoided, therefore making the freeze-drying the most common processing method for removing moisture from biopharmaceuticals and for producing high quality powder for thermosensitive drugs. However, freeze-drying is still challenging for the production of dry emulsions and NE due to several critical steps (cryoprotectant choice, freezing rate and conditions, primary and secondary drying process) which need to be controlled [32].

The use of drying excipients (trehalose, maltose, sucrose, glucose, maltodextrin or mannitol) is highly recommended in both processes. During the spray drying process, excipients are added to provide a matrix to the dry product while it is heated to high temperatures [31]. Using specific excipients such as lactose or maltodextrin, several dispersed systems, as emulsions, liposomes and nanocapsules, have been successfully spray-dried with preservation of their initial properties that allows reconstitution of an aqueous suspension [31]. While, in freeze-drying, cryoprotectants and lyoprotectants (i.e. trehalose, sucrose, lactose) are used to prevent the disruption of the droplets during freezing and drying steps [32]. Both spray-drying and freeze-drying technologies were evaluated with regards to obtain dry powders of NE. Firstly, the feasibility of both processes was assessed and maltodextrin (MD) and trehalose (TR) were rationally selected as drying excipients to improve spray-drying and freeze-drying performance, respectively. The dry powders were characterized in terms of moisture content, product yield and macroscopic properties. Then, following reconstitution by rehydration, NE physicochemical properties were assessed.

II.3.6.1. Nanoemulsions spray-drying and characterization

During the spray-drying process, the prevention of phase separation between NE and excipients before the feed pumping step is crucial to prepare homogeneous powders and to ensure effective NE protection [31,33]. In this study, NE were spray-dried in presence of maltodextrin (MD) as drying excipient based on both maltodextrin finest attributes, as from the literature [31], and on preliminary studies comparing the homogenization properties of NE with maltodextrin, lactose and hydroxypropyl methylcellulose (HPMC) (results not shown). Phase separation of NE/MD mixtures was studied at equilibrium as well as under centrifugal forces. When the MD solution was mixed with the NE at different ratios (Table 2), no spontaneous phase separation occurred in all studied samples up to 2 h. However, after 6 h, creaming occurred in samples whose MD concentration exceeded 7.5%. Creaming was also observed after centrifugation of samples at high MD concentrations (MD > 7.5%).

Table 2 Compatibility of NE with different concentration of maltodextrin (MD) “–” “No separation; “+” Light separation, with very thin upper cream layer; “+++” Obvious separation, with upper creamed layer. % expressed as% w/v.

NE (% w/v)	MD (% w/v)	Equilibrium			Centrifugation (2300 g, 5 min)	Viscosity at 20 °C (mPa·s)
		15 min	2 h	6 h		
5	5	–	–	–	–	2.1
5	10	–	–	–	+	3.3
10	5	–	–	–	–	3.6
10	10	–	+	+++	+++	6.2
15	7.5	–	+	+++	+++	8.2
15	10	–	+	+++	+++	11.7

Emulsions mixed with MD solutions show an enhance rate of creaming when a critical MD concentration, defined as critical flocculation concentration (CFC), is exceeded. Above the CFC the non-adsorbed MD molecules in the aqueous phase cause depletion flocculation of NE droplets [34]. In our experiment the critical flocculation concentration (CFC) was identified at MD concentrations \geq 7.5%.

Too high viscosity of the initial solution hinders homogenous atomization and correct drop formation [48]. An increase of MD and NE concentrations (from 5 to 15%) led to a slight increase of viscosity (from 2 to 12 mPa·s). However, the overall viscosity remained low (< 12 mPa·s) and spray-drying could be performed even at high NE concentration (15% w/v). Following the spray-drying process, powders were recovered both from the cyclone wall and bottom. Macroscopic characteristics of powder obtained are presented in Table 3.

Table 3 Characteristics of spray-dried NE powders.

NE (% w/v)	MD (% w/v)	Ratio NE/MD	Macroscopic properties	Moisture content (% w/v)	Yield (% w/v)
5	5	1	White powder, good flowability	3.1	77.3
5	10	0.5	White powder, good flowability	4.5	90.2
10	5	2	White powder, sticky	1.7	–
10	10	1	White powder, good flowability	3.7	89.7
15	7.5	2	White powder, quite sticky	2.4	73.2
15	10	1.5	White powder, good flowability	2.6	92.8

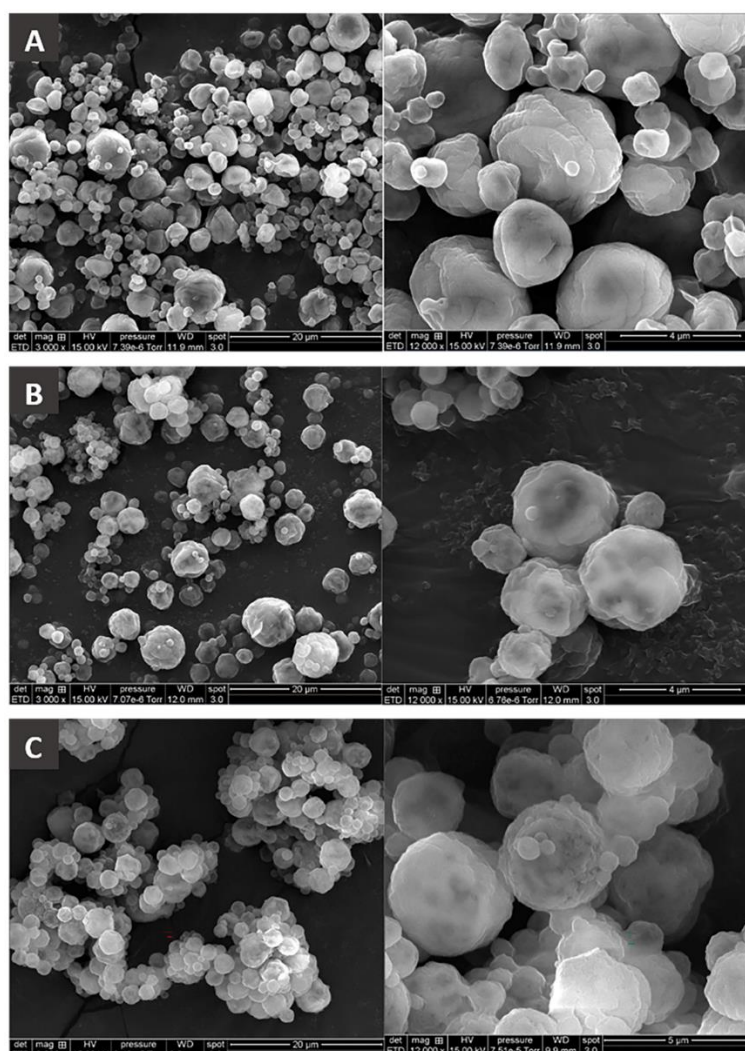


Fig. 5 SEM images of spray-dried NE at different NE and MD concentrations (% w/v). NE:MD = A) 5:10; B) 10:10; C) 15:10.

Powders were pasty and stuck to the cyclone bottom when spray-dried with a NE/MD ratio of 2. Formulations with lower NE/MD ratios of 1.5, 1 and 0.5 resulted in smooth powders, which could be collected at the cyclone wall. Residual moisture content of all obtained powders was very low, varying from 1.7% to 4.5% (Table 3). It is worthy to notice that two sticky powders, corresponding to formulations with an NE/MD ratio of 2, showed the lowest value of relative humidity (1.67% and 2.4%, respectively). Their sticky state resulted from the exposure of the oil phase of droplets, due to the low amount of MD present in the powder. The sticky state of the formulation having NE-MD concentration of 10%-5% hampered the powder collection for further analysis. Process yields were satisfying, with values ranging from 70 to 93%, for all other mixtures (Table 3). 90% yield was reached for the mixture containing 10% of MD and NE at 5%. Such yields are much higher than the ones reported in the literature. In fact, previous works reported process yields between 30% and 40% for lipid-core nanocapsules (1%) spray-dried in presence of lactose (10% w/v) [35]. Also, nanocapsules (1%) were spray-dried in presence of MD (10% w/v) and the process yield was 66.9% [31].

SEM observations of NE powders (Fig. 5) revealed particles with a spherical shape and a folded surface with a broad size distribution, ranging from 500 nm to 6 μ m (Fig. 5). The powders obtained for NE:MD concentrations of 5:10 (Fig. 5A) and 10:10 (B) (Fig. 5B) were composed of single particles while, in the case of powder obtained from higher NE:MD concentrations of 15:10 (Fig. 5C) particles looked like irregular agglomerates. Agglomeration was probably related to a phenomenon of interparticle adhesion during drying process, caused by the low amount of MD that did not provide an effective protective shell against sticking.

The stability after spray-drying was assessed by evaluating the ability of NE to recover their initial physicochemical properties following reconstitution in water (Fig. 6A). When NE (concentration 15-10-5%) was spray dried in presence of MD at 10%, no variation in terms of NE size and PdI were detected. While, for powders prepared using NE at 15 and 5% and MD at 7.5 and 5% respectively, an increase of NE hydrodynamic diameter (from 102 nm to 260 nm and 225 nm, respectively) and of PdI (from 0.15 to 0.4) were observed following resuspension in water.

Overall, best results in terms of production yield, moisture content and stability following reconstitution were obtained for the mixture prepared at NE concentration of 5% and MD concentration of 10%.

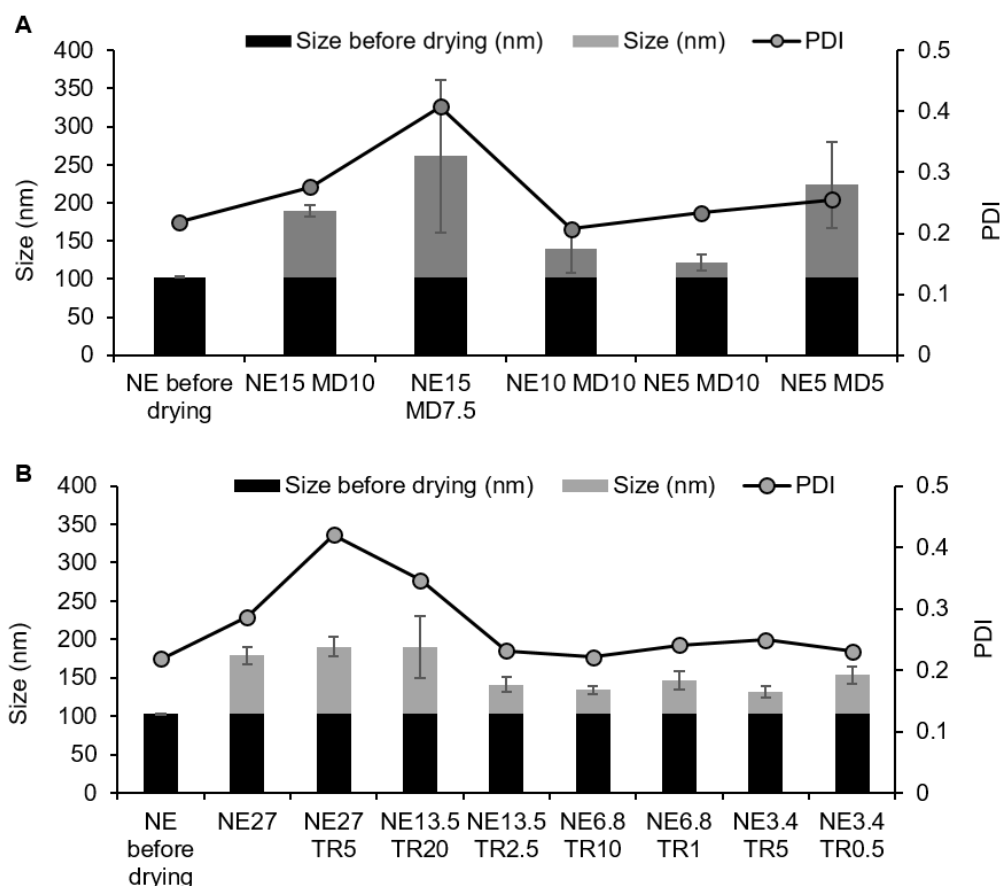


Fig. 6 Particle size and polydispersity index (PDI) of : A) re-hydrated spray-dried NE at different NE and MD concentrations (% w/v); B) re-hydrated freeze-dried NE at different NE and TR concentrations (% w/v).

II.3.6.2. Nanoemulsions freeze-drying and characterization

Prior to lyophilization study, a freeze-thawing experiment was performed. The choice of trehalose as drying excipient was dictated by its reported superiority in the freeze-drying process because of its reduced hygroscopy, low chemical reactivity and high glass transition temperature [32,33]. Moreover, better maintaining of NE physicochemical properties was observed with trehalose when compared to maltodextrin (results not shown). NE was mixed with TR at different concentrations (Table 4) and the stability of mixtures was evaluated upon 24 h of storage at 4 °C. No phase separation was observed for all NE-TR mixtures.

Samples were then frozen in the freeze-drying chamber at slow freezing rate that avoided TR trapping into ice crystals [36]. Frozen NE were thawed and their physicochemical properties were analysed by DLS. Though particle sizes of all samples slightly increased (Table 4), they remained in the acceptable nanometer range (< 200 nm). Size increase was more pronounced (around 70 nm) in samples with NE/TR ratio higher than 10. Smaller and highly monodisperse (PDI = 0.1) particles were obtained for NE/TR ratio \leq 6.8.

Table 4 Physicochemical characterization of NE mixed with trehalose (TR) at different ratio following the freeze-thawing study. NE original size = 103.9 ± 2.7 nm; PDI = 0.20.

NE (% w/v)	TR (% w/v)	Ratio NE/TR	Size (nm)	PdI
27			146 ± 3	0.13
	1	27	174 ± 5	0.24
27	2.5	10.8	165 ± 2	0.21
	5	5.4	128 ± 2	0.12
13.5	1	13.5	176 ± 3	0.26
	2.5	5.4	154 ± 2	0.16
6.8	1	6.8	151 ± 2	0.14
	10	0.68	128 ± 1	0.17
3.4	5	0.68	111 ± 1	0.12

The freeze-thawing experiment showed that the freezing stage of the lyophilization process did not affect the stability of the droplets, though this is considered as one of the most critical step. On this basis, freeze-drying was performed for the samples prepared at NE/TR ratio lower than 10.

Representative pictures of the lyophilized cakes are shown in Fig. 7. The NE lyophilized without cryoprotectant resulted in elegant cakes with no defects (Fig. 7A and Table 5). White snow-like, smooth and elegant cakes were obtained for samples prepared at NE concentration of 13.5% and 2.5% of TR (Fig. 7B). While, at low NE content (3.4%) (Fig. 7D and Table 5) cakes resulted of poorest quality, with partial shrinkage and cracks.

The residual moisture content of all obtained powders was low, varying from 0.3% to 3.3% (Table 5). The highest TR concentration tested (10%, 20%) contained more moisture ($> 3\%$). This was due to unfrozen water remaining trapped in the sugar matrix during the sublimation step. Process yields were satisfactory, with values ranging from 87% (NE:TR = 6.8%:10%) to 100% (NE 27%) (Table 5).

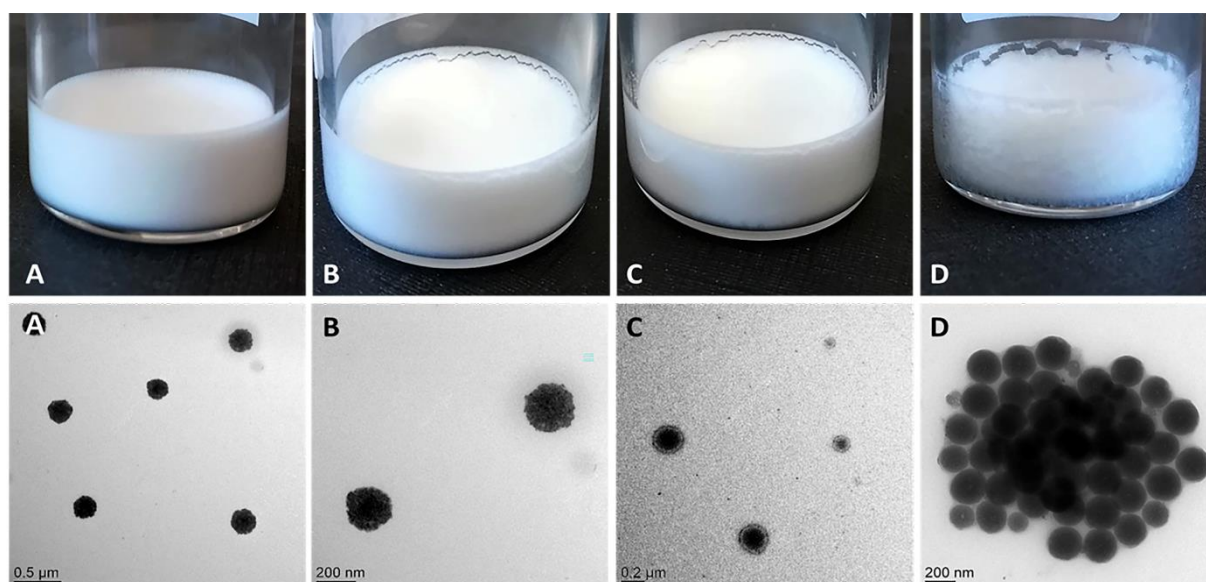


Fig. 7 Visual appearance of NE cakes and TEM images of NE after lyophilization and reconstitution in water. A) Blank NE without cryoprotectant; B) Blank-NE:TR=13.5:2.5; C) Tacrolimus-loaded NE:TR=13.5:2.5; D) Blank NE:TR=3.4:5.

Table 5 Characteristics of freeze-dried NE powders.

NE (% w/v)	TR (% w/v)	Ratio NE/TR	Macroscopic properties	Moisture content (% w/v)	Yield (% w/v)
27.0			White snow like smooth oily cake	0.3	103.6
27.0	5	5.4	White snow like smooth elegant cake	1.2	97.2
13.5	2.5	5.4	White snow like smooth elegant cake	0.9	99.2
13.5	20	0.7	White snow like smooth elegant cake	2.9	97.5
6.8	1	6.8	White brittle cake	0.9	97.9
6.8	10	0.7	White brittle cake	3.4	86.5
3.4	0.5	6.8	White brittle cake, shrinkage	0.4	97.8
3.4	5	0.7	White brittle cake	3.3	90.0

The ability of dried NE to recover their initial physicochemical properties upon reconstitution in water was also evaluated. All the dried samples were rehydrated with pure water under gentle shaking and analysed for droplet size by DLS (Fig. 6B). NE without cryoprotectant (27%) showed acceptable increase in size (from 103 nm to 173 nm) and PDI (0.3). However, their rehydration was difficult and slow (> 10 min). NE at different concentrations were mixed with TR solutions or with the powder of TR before drying. When TR solutions (13.5% and 6.8%) were mixed with NE, the lyophilized cakes were easily and rapidly rehydrated (less than 1 min). Physicochemical properties of NE at 13.5% (size = 141 nm, PDI = 0.2) were better preserved at TR amount of 2.5% (Fig. 6B). TEM observations (Fig. 7B) revealed that particles were spherical and presented a rough surface. NE formed a monodispersed population and no visible aggregates were present. However, at the lowest NE (3.4%) and TR (0.5%) concentrations an increase in particle size (154 nm) was observed. TEM (Fig. 7D) showed that particles were highly agglomerated. Low NE content formulations exhibited a poor aptness to freeze-drying. When the powder of TR (5%) was dissolved in NE suspension (27%), large (190 nm) and highly polydisperse (PDI = 0.4) particles were obtained, revealing a partial destabilization of the emulsion by TR. These results highlight the importance of the addition method (TR solution versus powder), which had to be considered as relevant during the freezing and drying steps.

In order to study whether the freeze-drying process could cause the leakage of the loaded drug, loaded NE were formulated, diluted at final NE concentration of 13.5%, mixed with TR solution (2.5%) and freeze-dried. A snow-like, smooth, elegant cake (Fig. 7C), with a low moisture content (0.8%) was obtained. After rehydration, loaded NE physicochemical properties were maintained and corresponded to the ones of the freeze-dried blank NE (size = 146 nm, PDI = 0.3). *EE* was 80%, demonstrating the feasibility of freeze-drying loaded NE without drug leakage.

Overall, the highest yield of NE while preserving physicochemical properties was reached when 13.5% NE was freeze-dried in presence of 2.5% TR.

Recent studies report the successful lyophilisation of MCT-lecithin nanoemulsions at TR-NE ratio 10/1, while in this work same results were obtained at TR-NE ratio of 1/5 [55]. Our freeze-drying protocol benefits from using a low amount of cryoprotectant to dry a highest amount of lipid system. Such attribute cannot be found in previous research and can broaden the use of nanoemulsions in pharmaceutical applications. Globally, both freeze-drying and spray-drying were efficient in the conversion of NE into a dry powder. Although spray-drying is faster and less expensive than freeze-

drying, the high processing temperatures and the lowest quality of the dried products make the freeze-drying the preferred method for preserving the present pharmaceutical formulations. The highest process yields were obtained by freeze-drying. Indeed, there is no product collection step required after freeze-drying, thus avoiding product loss and contamination. A higher concentration of NE (13.5% by freeze-drying versus 5% by spray-drying) was dried using lower amount of excipient (TR 2.5%).

II.3.7. Structural characterization of nanoemulsions in colloidal suspension and reconstituted following drying processes

A unique structural characterization of the NE, with an in-depth focus on the NE shell nature was performed. The shell composition, thickness and rigidity can affect nanoparticles stability and drug encapsulation efficacy [6]. So far, many studies on lipid-based systems focused on the characterization of crystalline or amorphous state of the oil core and on the link between drug loading efficacy and core properties [37]. The fluid or rigid nature of liposomes [38] and the rigid character of SLN or LNC composed of PEGylated surfactants [39] have been previously reported, but to our knowledge few studies have addressed the core-shell structure of NE [40]. The state of the shell (crystalline or amorphous) was presently investigated by means of DSC and XRPD measurements and the fluidity of the NE shell was assessed by fluorescence using a polarity-sensitive fluorophore. DSC analysis of the crystalline state of NE ($SMR = 2.85$, $SOR = 2.86$) is shown in Fig. 8.3.

Only evaporation of water was visible as NE was heated from room temperature up to 160 °C (step 1). Once the sample was dry in the DSC pan, cooling caused crystallization, as revealed by an exotherm starting at 30 °C (step 2). Finally heating again caused melting at 40 °C (step 3). The exothermic and endothermic heats in the cooling step and heating steps were identical. DSC scans of single and physical mixtures of NE components were run in order to disclose which materials were involved in such thermal events.

Typical thermograms of NE and single components (after water evaporation) are displayed in Fig. 8.1 and 8.2. The solid crystalline hydrophilic surfactant S1, analysed as a powder, showed a melting endotherm at 43.1 °C and a crystallization exotherm at 28.9 °C upon cooling (Fig. 8.1 and 8.2, sample A). The same pattern was observed when S1 was dissolved in water, at a concentration of 14.28% (Fig. 8.1 and 8.2, sample B). Once S1 powder was mixed with liquid S2, no variation in the melting point was found for S1 (Fig. 8.1, sample C and Table 6). In addition to the main peak, a second peak at lower temperatures (38 °C) was observed in mixtures of S1 and S2 (Fig. 8.1, sample C), S1 and MCT (Fig. 8.1, sample D) and in the oil phase of the NE (Fig. 8.1, sample E), suggesting the presence of a second crystalline phase, attributable to a polymorphic form of the stearic acid of S1. Polymorphism resulted from the different molecular packing of S1 when mixed with S2 and MCT excipients [37].

DSC was also employed to study the MCT behaviour. In the mixture of S1 and MCT upon cooling, the MCT crystallized at -25.5 °C (Fig. 8.2, sample D). The melting of the frozen MCT occurred at -12.5 °C (Fig. 8.1, sample D). While when the MCT were in the oil phase (sample E) and in the NE (sample F), a decrease of its crystallization peak (-37.9 °C) and an appearance of a second melting peak (-27.2 °C) were observed. Such behaviour can be referred to MCT polymorphism [37,41]. However, the assignment of polymorphs to MCT needs further investigation.

Overall, the major characteristic peaks for S1 were still observed in melting and crystallization patterns of NE (Fig. 8.1 and 8.2, sample F), proving the crystalline nature of the PEGylated NE shell. While the

liquid amorphous state of S2 and MCT was supposedly maintained after NE formulation. In accordance with our results, previous studies proved how surfactants used to stabilize LNC and SLN maintained their crystallinity upon interaction with the oil core composed of medium chain triglycerides [37,42]. Moreover, dried NE powders and dried NE rehydrated were analysed to examine the influence of the drying process on the structure of NE. Once water had been evaporated, the melting and crystallization peaks of S1 were visible in NE dried with both spray-drying and freeze-drying (Table 6), while rehydrated NE were amorphous in colloidal suspension. A shift in the melting and crystallization peaks of the spray-dried NE (Table 6) was observed due to the presence of MD cryoprotectant in the sample. Instead, in both freeze-dried NE powders and NE rehydrated (analysed in absence of cryoprotectant), the crystallinity of the NE shell was maintained, without significant variations compared to the formulation before drying, as shown in Fig. 8.1 and 8.2, samples G and H. The degree of crystallinity was calculated from the ratio of the enthalpy of S1 in the NE to bulk S1 enthalpy. The use of raw S1 not 100% crystalline and the formation of polymorphs not present in the bulk material might explain the degree of crystallinity values higher than 100%, as the melting enthalpy of the raw S1 was taken as reference (Table 6).

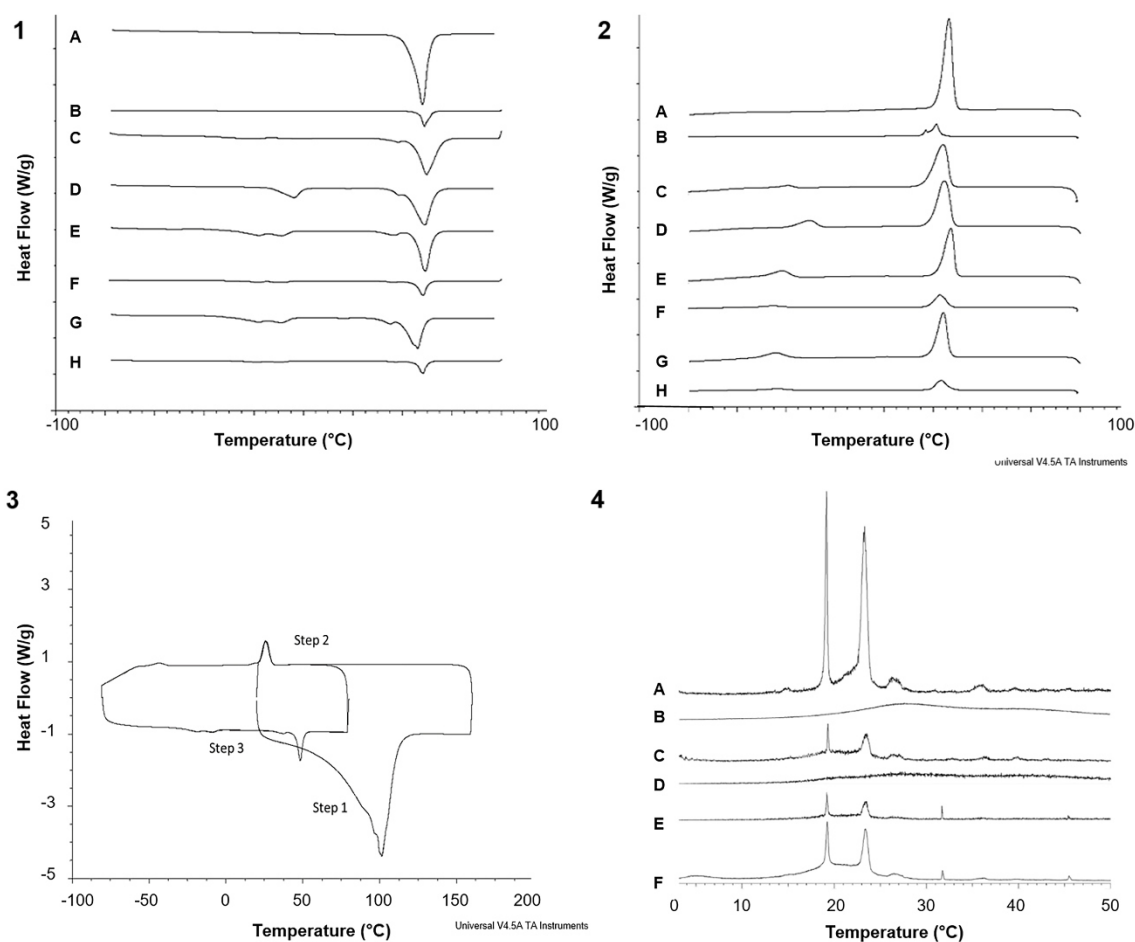


Fig. 8.1 and 2) DSC thermograms of: (A) S1 powder, (B) S1 in water solution, (C) mixture of S1 and S2 (SMR=2.5), (D) mixture of S1 and MCT, (E) oil phase: S1, S2 and MCT, (F) blank NE, (G) freeze-dried blank NE powder and (H) freeze-dried blank NE re-suspended in water. Analysis performed from $-80\text{ }^{\circ}\text{C}$ to $+80\text{ }^{\circ}\text{C}$ at a $10\text{ }^{\circ}\text{C min}^{-1}$ rate. Data corresponding to the second cooling (1) and third heating (2) steps. 3) DSC thermogram of blank NE. Step 1: heating scan from $+20\text{ }^{\circ}\text{C}$ to $+160\text{ }^{\circ}\text{C}$; step 2: cooling

scan from +80 °C to -80 °C; step 3: heating scan from -80 °C to +80 °C. 4) XRPD patterns of: (A) S1 powder, (B) S1 in water solution, (C) mixture of dry S1 and S2 (SMR=2.5), (D) blank NE in colloidal suspension, (E) blank NE after complete water evaporation, (F) freeze-dried blank NE powder.

Table 6 DSC analysis from -80 °C to +160 °C at a 10 °C·min⁻¹ heating rate. NE were analyzed at the second heating scan.

Sample	T_m (°C)	T_c (°C)	ΔE_m (J·g ⁻¹)	ΔE_c (J·g ⁻¹)	Crystallinity (%)
S1	43.1	28.9	128.6	128.6	100.0
S1 + S2	44.4	27.4	123.7	128.2	96.2
S1 + MCT	41.1	28.2	137.2	133.6	106.7
Full oil phase	45.1	29.4	136.3	137.3	105.9
NE	45.4	29.7	155.3	148.9	120.8
Freeze-dried NE powder	39.1	26.9	131.7	129.9	102.4
Freeze-dried NE rehydrated	45.4	27.2	111.1	109.5	86.4
Spray-dried NE powder	34.8	- 5.7	85.9	62.9	77.8
Spray-dried NE rehydrated	39.9	- 2.3	4.7	6.0	77.8

However, information about the crystalline state of NE while in colloidal suspension could not be provided due to the lack of sensitivity of the DSC technique in analysing samples in their wet state.

Thus, XRPD experiments (Fig. 8.4) were performed to further study the state of S1 in the NE shell and confirm the components behaviour established by DSC measurements. Bulk S1 (Fig. 8.4A) exhibited several diffraction reflections with two major sharp peaks at diffraction angles ($2\theta = 19.1^\circ$ and 23.2°), indicating its crystalline state. The same peaks were observed in the mixture of S1 and S2 and in the NE after complete water evaporation (Fig. 8.4C and E, respectively). Similar peaks were also observed in the freeze-dried NE powder (Fig. 8.4F), demonstrating the aptness to freeze-drying of developed nanosystem. However, there were no characteristic peaks for crystalline S1 in colloidal suspension of NE (Fig. 8.4D), suggesting the amorphous state of S1 in wet state after the EPI process.

The nature of the NE shell was highly influenced by the presence of water. The dry hydrophilic shell was crystalline (after water evaporation and for lyophilized samples) and it became amorphous when hydrated. In line with previous studies, the formation of a bulky amorphous PEG-water complex in colloidal NE suspension decreases the packing density of the surfactant to such an extent that the stearic chains are no longer crystalline. This is a possible explanation for the observed behaviour [43].

NE were stabilized using a surfactant (S1) which is solid at room and physiological temperature (T_m of S1 = 43 °C) rising doubts about the fluid or rigid nature of the amorphous NE shell.

Firstly, an *in vitro* release study of tacrolimus was carried out at 50 °C. No differences in release pattern were observed compared to 37 °C, though these temperatures were below and above surfactant melting point (43 °C). Thus, the surfactant shell should have been in its molten state at both temperatures, such that it did not significantly act as a barrier against drug release [44].

To confirm this result, fluorescence measurements using polarity sensitive fluorophores were performed. Laurdan (6-dodecanoyl-2-dimethylaminonaphthalene) is a polarity-sensitive fluorophore commonly used for the assessment of liposomes rigidity and the study of biological membranes. Yet, when incubated with NE solution, its fluorescence emission spectrum with a single peak at 440 nm was characteristic of a highly hydrophobic environment, suggesting that the fluorophore was inserted in the hydrophobic core of the NE. Therefore, we presently used a home-made derivative of Laurdan called Dioll (patent pending EPO19306175.1-1118) having an enhanced polarity allowing better insertion in

the NE shell. Dioll was post-inserted in the NE shell by simple mixing the probe with the NE suspension (Dioll-NE). Insertion of Dioll in the NE shell was checked by measurements of emission spectra of controls. Due to the lack of fluorescence activity in hydrophilic environment, no fluorescence emission was detected when the probe was dissolved in water. Neither blank NE emitted fluorescence. A single peak at 440 nm was observed when Dioll was dissolved in MCT related to the radiative de-excitation of a “locally excited” state of Dioll in oil [16] (detailed information can be found in the supplementary section). Emission spectra of Dioll-NE at temperatures ranging from 5 °C to 37 °C showed two peaks at 440 nm and 490 nm, (Fig. 9), which, based on literature data on Laurdan [16], corresponded to fluorophore inserted into a rigid or a fluid environment, respectively, each band depending on the physical state of the medium and on the capacity of the probe to undergo interactions with the surrounding water molecules. So, we could conclude that Dioll was emitting from NE surfactant shell and not from the MCT core of NE. Indeed, the Dioll hydrophobic tail could be oriented towards the NE oil core, while the hydrophilic and fluorescent naphthalene moiety could be aligned with the PEG components of S1, towards the surrounding water phase. NE size, Pdl and surface charge did not vary upon insertion of the probe (size: 105 ± 1 nm, Pdl: 0.21, ζ -potential: -18 ± 1 mV).

Decreasing the temperature from 37 °C to 5 °C led to the progressive increase of peak intensity at 440 nm (Fig. 9A). To quantify membrane fluidity state at each temperature, the GP values were calculated as described in Materials and methods section. GP increased as temperature was lowered (Fig. 9B), proving decreased fluidity of the NE shell. However, GP values remained negative (fluid state) and no significant phase transition from fluid to rigid state occurred over the full temperature range. The NE shell was in its fluid state, even at low temperature (5 °C).

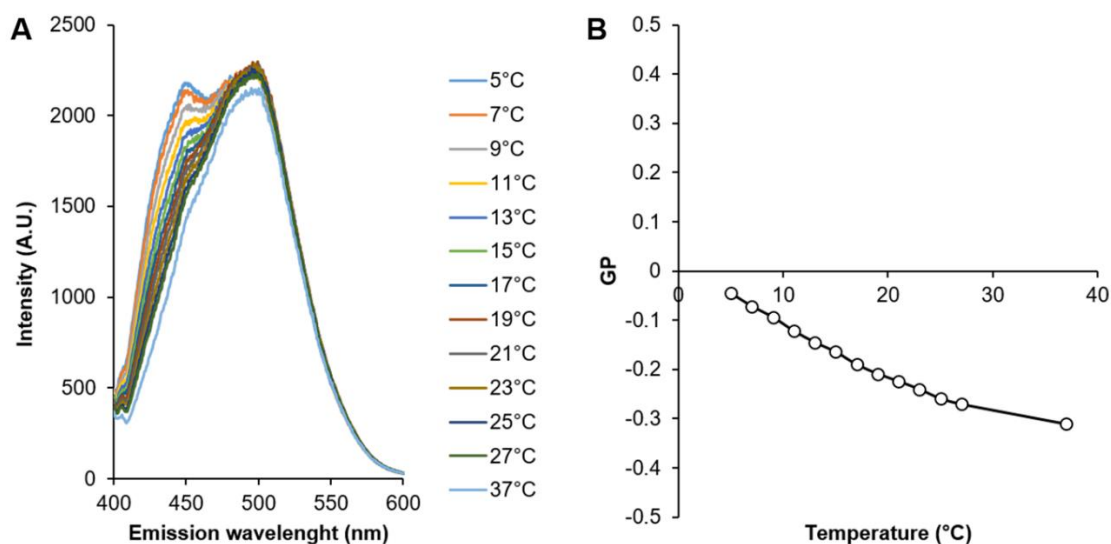


Fig. 9 A) Effect of temperature on fluorescence emission of Dioll-NE; B) Generalized Polarization of probes inserted in Dioll-NE as a function of temperature.

NE differs from other LBDDS, such as LNC for the nature of the shell, which is fluid for NE and fairly rigid for LNC. The rigidity of the system is related to i) the presence of PEG as the outmost particle coating (i.e. lipidots, NLC, modified matrix SLN and mRNA-LNP [39,40,45,46]) and the density of PEG chains (PEG density is usually low for NE (< 10 wt%) and rather high (> 10 wt%) for LNC

[29,47]); ii) the use of a solid excipient whose melting point is higher than the storage temperature [48]; iii) the overconcentration of surfactant on the NE surface, thanks to the stirring cycles performed, while formulating particles by the PIT method [48]. The presented NE should be rigid with regards to these three criteria. However, it was fluid according to fluorescence measurement. The fluidity of the NE shell is ascribed to the chemical structure of the S1 PEGylated surfactant that has a bulky head group that lowers the surfactant packing density in the membrane. S1 head groups weakened hydrophobic interactions between surfactant tails, thus constraining alkyl chains in a disordered configuration in order to fill the full space set by lateral steric repulsions between bulky PEG moieties [49]. Similar impact of the structure of system components on the final fluidity of the system has been described for liposomes. Liposomes composed of phosphatidic acid, which has a small head group, are rigid, while liposomes composed of phosphatidylcholine, which has a larger head group, are more fluid [50]. Moreover, the presence of the second surfactant (S2), which intercalates S1 in the NE shell, may further reduce the packing density of PEG chains [25,51].

We move that the latter shell characterization be performed on several lipid-based nanocarriers. Gained information on shell properties would patch the current structural analysis, whose main objective is the lipid core, leading to a better understanding of correlations between particle composition and stability, drug encapsulation efficacy, drug release behaviour. The whole set of physicochemical properties allows a proposal for the NE structure as described in Fig. 10.

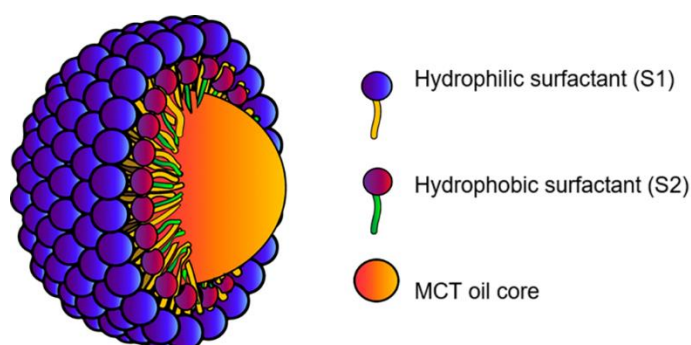


Fig. 10 Representation of the NE structure with oil core and mixed surfactant shell.

The oil liquid core corresponding to MCT, was surrounded by a surfactant shell composed of a mixture of S1 and S2. S2 was located inside the mixed surfactant layer and its hydrophobic part interacts with the oil phase while the hydrophilic part of S1 was oriented to water.

II.4. Conclusion

In this work a novel approach of producing NE, based on the EPI method coupled with high energy input to shape droplets' size, was proposed. Through this innovative procedure, NE physicochemical properties were tuned to obtain systems which best suit the desired application.

Once the formulation criterion settled, the system composition was varied and optimized by mean of a robust experimental design over the full ternary phase diagram. The region of interest of suitable formulations was selected through the evaluation of parameters as the *S_{mix}* surfactant ratio (*SMR*) and the surfactant-to-oil ratio (*SOR*). The ability of NE to efficiently encapsulate hydrophobic drug molecules (tacrolimus) and to modulate the release behaviour of the associated drug in biorelevant GI

fluids was proven. To increase the shelf-life of the finished product by preserving it in a more stable dry state, NE were successfully converted into dry powders, using spray-drying and freeze-drying techniques. Finally, the freeze-drying resulted as the most adequate technique, overcoming major challenges related with the production of dry powders from oil based systems. To study the shell nature (crystallinity and fluidity) of lipid nanocarriers, we have exploited an original methodology, based on combining DSC, XRD and an innovative fluorescence analysis. While, the fluidity of the NE shell was closely related to the structure of used excipients. Such structural analysis will supplement the usual characterization of nanocarriers, which is mostly focusing on the system core and loaded drug. Overall, the methodology and results here presented provide a template for developing a rational design of nanoemulsion-based systems intended for oral delivery of hydrophobic drugs.

Acknowledgements

The research leading to these results has received funding from Agence Nationale de la Recherche, HyDNano project (ANR-18-CE18-0025-01) and from the Ministère de l'Enseignement Supérieur et de la Recherche (France)

II. References

- [1] H. Mu, R. Holm, A. Müllertz, Lipid-based formulations for oral administration of poorly water-soluble drugs., *Int. J. Pharm.* 453 (2013) 215–24. doi:10.1016/j.ijpharm.2013.03.054.
- [2] A. Müllertz, A. Ogonna, S. Ren, T. Rades, New perspectives on lipid and surfactant based drug delivery systems for oral delivery of poorly soluble drugs, *J. Pharm. Pharmacol.* 62 (2010) 1622–1636. doi:10.1111/j.2042-7158.2010.01107.x.
- [3] N. Matougui, L. Boge, A.-C. Groo, A. Umerska, L. Ringstad, H. Bysell, P. Saulnier, Lipid-based nanoformulations for peptide delivery, *Int. J. Pharm.* 502 (2016) 80–97. doi:10.1016/j.ijpharm.2016.02.019.
- [4] H. Shrestha, R. Bala, S. Arora, Lipid-Based Drug Delivery Systems, *J. Pharm.* 2014 (2014) 1–10. doi:10.1155/2014/801820.
- [5] F.U. Rehman, K.U. Shah, S.U. Shah, I.U. Khan, G.M. Khan, A. Khan, From nanoemulsions to self-nanoemulsions, with recent advances in self-nanoemulsifying drug delivery systems (SNEDDS), *Expert Opin. Drug Deliv.* 14 (2017) 1325–1340. doi:10.1080/17425247.2016.1218462.
- [6] N. Anton, J.-P. Benoit, P. Saulnier, Design and production of nanoparticles formulated from nano-emulsion templates—A review, *J. Control. Release.* 128 (2008) 185–199. doi:10.1016/j.jconrel.2008.02.007.
- [7] C. Solans, I. Solé, Nano-emulsions: Formation by low-energy methods, *Curr. Opin. Colloid Interface Sci.* 17 (2012) 246–254. doi:10.1016/j.cocis.2012.07.003.
- [8] J. Komaiko, D.J. McClements, Optimization of isothermal low-energy nanoemulsion formation: Hydrocarbon oil, non-ionic surfactant, and water systems, *J. Colloid Interface Sci.* 425 (2014) 59–66. doi:10.1016/j.jcis.2014.03.035.
- [9] D.J. McClements, Edible nanoemulsions: fabrication, properties, and functional performance, *Soft Matter.* 7 (2011) 2297–2316. doi:10.1039/C0SM00549E.
- [10] N. Sadurní, C. Solans, N. Azemar, M.J. García-Celma, Studies on the formation of O/W nano-emulsions, by low-energy emulsification methods, suitable for pharmaceutical applications, *Eur. J. Pharm. Sci.* 26 (2005) 438–445. doi:10.1016/j.ejps.2005.08.001.
- [11] A. Maali, M.T.H. Mosavian, Preparation and Application of Nanoemulsions in the Last Decade (2000–2010), *J. Dispers. Sci. Technol.* 34 (2013) 92–105. doi:10.1080/01932691.2011.648498.
- [12] J.S. Komaiko, D.J. McClements, Formation of Food-Grade Nanoemulsions Using Low-Energy Preparation Methods: A Review of Available Methods, *Compr. Rev. Food Sci. Food Saf.* 15 (2016) 331–352. doi:10.1111/1541-4337.12189.
- [13] F. Ostertag, J. Weiss, D.J. McClements, Low-energy formation of edible nanoemulsions: Factors

- influencing droplet size produced by emulsion phase inversion, *J. Colloid Interface Sci.* 388 (2012) 95–102. doi:10.1016/j.jcis.2012.07.089.
- [14] S. Mayer, J. Weiss, D.J. McClements, Vitamin E-enriched nanoemulsions formed by emulsion phase inversion: Factors influencing droplet size and stability, *J. Colloid Interface Sci.* 402 (2013) 122–130. doi:10.1016/j.jcis.2013.04.016.
- [15] M.M. Fryd, T.G. Mason, Advanced Nanoemulsions, *Annu. Rev. Phys. Chem.* 63 (2012) 493–518. doi:10.1146/annurev-physchem-032210-103436.
- [16] C.C. De Vequi-Suplicy, C.R. Benatti, M.T. Lamy, Laurdan in fluid bilayers: Position and structural sensitivity, *J. Fluoresc.* 16 (2006) 431–439. doi:10.1007/s10895-005-0059-3.
- [17] A. Lamprecht, N. Ubrich, H. Yamamoto, U. Schäfer, H. Takeuchi, C.M. Lehr, P. Maincent, Y. Kawashima, Design of rolipram-loaded nanoparticles: Comparison of two preparation methods, *J. Control. Release.* 71 (2001) 297–306. doi:10.1016/S0168-3659(01)00230-9.
- [18] International Conference on Harmonization of Technical Requirements for Registration of Pharmaceuticals for Human Use. Validation of Analytical Procedures: Text and Methodology, Q2 (R1), (2005).
- [19] D. Zhang, X. Pan, S. Wang, Y. Zhai, J. Guan, Q. Fu, X. Hao, W. Qi, Y. Wang, H. Lian, X. Liu, Y. Wang, Y. Sun, Z. He, J. Sun, Multifunctional Poly(methyl vinyl ether-co-maleic anhydride)-graft-hydroxypropyl- β -cyclodextrin Amphiphilic Copolymer as an Oral High-Performance Delivery Carrier of Tacrolimus, *Mol. Pharm.* 12 (2015) 2337–2351. doi:10.1021/acs.molpharmaceut.5b00010.
- [20] E. Jantratid, N. Janssen, C. Reppas, J.B. Dressman, Dissolution Media Simulating Conditions in the Proximal Human Gastrointestinal Tract: An Update, *Pharm. Res.* 25 (2008) 1663–1676. doi:10.1007/s11095-008-9569-4.
- [21] K.-O. Choi, N.P. Aditya, S. Ko, Effect of aqueous pH and electrolyte concentration on structure, stability and flow behavior of non-ionic surfactant based solid lipid nanoparticles, *Food Chem.* 147 (2014) 239–244. doi:10.1016/j.foodchem.2013.09.095.
- [22] H. Scheffe, The Simplex-Centroid Design for Experiments with Mixtures, *J. R. Stat. Soc. Ser. B.* 25 (1963) 235–263. www.jstor.org/stable/2984294.
- [23] H. Scheffé, Experiments with Mixtures, *J. R. Stat. Soc. Ser. B.* 21 (1959) 238–238. doi:10.1111/j.2517-6161.1959.tb00335.x.
- [24] A.H. Saberi, Y. Fang, D.J. McClements, Fabrication of vitamin E-enriched nanoemulsions: Factors affecting particle size using spontaneous emulsification, *J. Colloid Interface Sci.* 391 (2013) 95–102. doi:10.1016/j.jcis.2012.08.069.
- [25] D.J. McClements, S.M. Jafari, Improving emulsion formation, stability and performance using mixed emulsifiers: A review, *Adv. Colloid Interface Sci.* 251 (2018) 55–79. doi:10.1016/j.cis.2017.12.001.
- [26] T. Schmidts, D. Dobler, A.C. Guldán, N. Paulus, F. Runkel, Multiple W/O/W emulsions-Using the required HLB for emulsifier evaluation, *Colloids Surfaces A Physicochem. Eng. Asp.* 372 (2010) 48–54. doi:10.1016/j.colsurfa.2010.09.025.
- [27] J. Kuntsche, J.C. Horst, H. Bunjes, Cryogenic transmission electron microscopy (cryo-TEM) for studying the morphology of colloidal drug delivery systems, *Int. J. Pharm.* 417 (2011) 120–137. doi:10.1016/j.ijpharm.2011.02.001.
- [28] G. Li, Y. Fan, C. Fan, X. Li, X. Wang, M. Li, Y. Liu, Tacrolimus-loaded ethosomes: Physicochemical characterization and *in vivo* evaluation, *Eur. J. Pharm. Biopharm.* 82 (2012) 49–57. doi:10.1016/j.ejpb.2012.05.011.
- [29] N.T. Huynh, C. Passirani, P. Saulnier, J.P. Benoit, Lipid nanocapsules: A new platform for nanomedicine, *Int. J. Pharm.* 379 (2009) 201–209. doi:10.1016/j.ijpharm.2009.04.026.
- [30] Y. Wang, Y. Zheng, L. Zhang, Q. Wang, D. Zhang, Stability of nanosuspensions in drug delivery, *J. Control. Release.* 172 (2013) 1126–1141. doi:10.1016/j.jconrel.2013.08.006.
- [31] P. Tewa-Tagne, S. Briañçon, H. Fessi, Preparation of redispersible dry nanocapsules by means of spray-drying: Development and characterisation, *Eur. J. Pharm. Sci.* 30 (2007) 124–135. doi:10.1016/j.ejps.2006.10.006.
- [32] A.R.D.V. Morais, É.D.N. Alencar, F.H. Xavier Júnior, C.M. De Oliveira, H.R. Marcelino, G. Barratt, H. Fessi, E.S.T. Do Egito, A. Elaissari, Freeze-drying of emulsified systems: A review, *Int. J. Pharm.* 503 (2016) 102–114. doi:10.1016/j.ijpharm.2016.02.047.

- [33] H.H. Myat, G.C. Ritthidej, Impact of formulation parameters on physical characteristics of spray dried nanoemulsions and their reconstitutions, *Asian J. Pharm. Sci.* 11 (2016) 197–198. doi:10.1016/j.ajps.2015.11.038.
- [34] U. Klimesorn, P. Sophanodora, P. Chinachoti, D. McClements, Stability and rheology of corn oil-in-water emulsions containing maltodextrin, *Food Res. Int.* 37 (2004) 851–859. doi:10.1016/j.foodres.2004.05.001.
- [35] M.C.L. Marchiori, A.F. Ourique, C. de B. da Silva, R.P. Raffin, A.R. Pohlmann, S.S. Guterres, R.C.R. Beck, Spray-Dried Powders Containing Tretinoin-Loaded Engineered Lipid-Core Nanocapsules: Development and Photostability Study, *J. Nanosci. Nanotechnol.* 12 (2012) 2059–2067. doi:10.1166/jnn.2012.5192.
- [36] N.-O. Chung, M.K. Lee, J. Lee, Mechanism of freeze-drying drug nanosuspensions, *Int. J. Pharm.* 437 (2012) 42–50. doi:10.1016/j.ijpharm.2012.07.068.
- [37] V. Jennings, A.F. Thünemann, S.H. Gohla, Characterisation of a novel solid lipid nanoparticle carrier system based on binary mixtures of liquid and solid lipids, *Int. J. Pharm.* 199 (2000) 167–177. doi:10.1016/S0378-5173(00)00378-1.
- [38] M. Hirai, R. Kimura, K. Takeuchi, Y. Hagiwara, R. Kawai-Hirai, N. Ohta, N. Igarashi, N. Shimizu, Structure of liposome encapsulating proteins characterized by X-ray scattering and shell-modeling, *J. Synchrotron Radiat.* 20 (2013) 869–874. doi:10.1107/S0909049513020827.
- [39] M. Garcia-Fuentes, M.J. Alonso, D. Torres, Design and characterization of a new drug nanocarrier made from solid–liquid lipid mixtures, *J. Colloid Interface Sci.* 285 (2005) 590–598. doi:10.1016/j.jcis.2004.10.012.
- [40] C.L. Dora, L.F.C. Silva, J.-L. Putaux, Y. Nishiyama, I. Pignot-Paintrand, R. Borsali, E. Lemos-Senna, Poly(ethylene glycol) Hydroxystearate-Based Nanosized Emulsions: Effect of Surfactant Concentration on Their Formation and Ability to Solubilize Quercetin, *J. Biomed. Nanotechnol.* 8 (2012) 202–210. doi:10.1166/jbn.2012.1380.
- [41] A.P.B. Ribeiro, M.H. Masuchi, E.K. Miyasaki, M.A.F. Domingues, V.L.Z. Stroppa, G.M. de Oliveira, T.G. Kieckbusch, Crystallization modifiers in lipid systems, *J. Food Sci. Technol.* 52 (2015) 3925–3946. doi:10.1007/s13197-014-1587-0.
- [42] B. Heurtault, P. Saulnier, B. Pech, J.-E. Proust, J.-P. Benoit, A novel phase inversion-based process for the preparation of lipid nanocarriers., *Pharm. Res.* 19 (2002) 875–80. doi:10.1023/a:1016121319668.
- [43] N.S. Murthy, Z. Zhang, S. Borsadia, J. Kohn, Nanospheres with a smectic hydrophobic core and an amorphous PEG hydrophilic shell: structural changes and implications for drug delivery, *Soft Matter.* 14 (2018) 1327–1335. doi:10.1039/C7SM02472J.
- [44] V. Karavelidis, D. Giliopoulos, E. Karavas, D. Bikiaris, Nanoencapsulation of a water soluble drug in biocompatible polyesters. Effect of polyesters melting point and glass transition temperature on drug release behavior., *Eur. J. Pharm. Sci.* 41 (2010) 636–43. doi:10.1016/j.ejps.2010.09.004.
- [45] M.A. Schubert, M. Harms, C.C. Müller-Goymann, Structural investigations on lipid nanoparticles containing high amounts of lecithin, *Eur. J. Pharm. Sci.* 27 (2006) 226–236. doi:10.1016/j.ejps.2005.10.004.
- [46] M. Yanez Arteta, T. Kjellman, S. Bartesaghi, S. Wallin, X. Wu, A.J. Kvist, A. Dabkowska, N. Székely, A. Radulescu, J. Bergenholtz, L. Lindfors, Successful reprogramming of cellular protein production through mRNA delivered by functionalized lipid nanoparticles, *Proc. Natl. Acad. Sci.* 115 (2018) E3351–E3360. doi:10.1073/pnas.1720542115.
- [47] S. Hirsjärvi, S. Dufort, J. Gravier, I. Texier, Q. Yan, J. Bibette, L. Sancey, V. Jossierand, C. Passirani, J.-P. Benoit, J.-L. Coll, Influence of size, surface coating and fine chemical composition on the *in vitro* reactivity and *in vivo* biodistribution of lipid nanocapsules versus lipid nanoemulsions in cancer models, *Nanomedicine Nanotechnology, Biol. Med.* 9 (2013) 375–387. doi:10.1016/j.nano.2012.08.005.
- [48] N. Anton, P. Gayet, J.-P. Benoit, P. Saulnier, Nano-emulsions and nanocapsules by the PIT method: An investigation on the role of the temperature cycling on the emulsion phase inversion, *Int. J. Pharm.* 344 (2007) 44–52. doi:10.1016/j.ijpharm.2007.04.027.
- [49] A. Dickey, R. Faller, Examining the contributions of lipid shape and headgroup charge on bilayer behavior, *Biophys. J.* 95 (2008) 2636–2646. doi:10.1529/biophysj.107.128074.

- [50] N. Kato, A. Ishijima, T. Inaba, F. Nomura, S. Takeda, K. Takiguchi, Effects of lipid composition and solution conditions on the mechanical properties of membrane vesicles, *Membranes (Basel)*. 5 (2015) 22–47. doi:10.3390/membranes5010022.
- [51] C. Zylberberg, S. Matosevic, Pharmaceutical liposomal drug delivery: a review of new delivery systems and a look at the regulatory landscape, *Drug Deliv.* 23 (2016) 3319–3329. doi:10.1080/10717544.2016.1177136.
- [52] S. Hua, E. Marks, J.J. Schneider, S. Keely, Advances in oral nano-delivery systems for colon targeted drug delivery in inflammatory bowel disease: Selective targeting to diseased versus healthy tissue, *Nanomedicine Nanotechnology, Biol. Med.* 11 (2015) 1117–1132. doi:10.1016/j.nano.2015.02.018.
- [53] R.B. Friedrich, F.A. Dimer, S.S. Guterres, R.C.R. Beck, A.R. Pohlmann, Nanoencapsulation of tacrolimus in lipid-core nanocapsules showed similar immunosuppressive activity after oral and intraperitoneal administrations, *J. Biomed. Nanotechnol.* 10 (2014) 1599–1609. doi:10.1166/jbn.2014.1842.
- [54] S. Khan, M. Shaharyar, M. Fazil, S. Baboota, J. Ali, Tacrolimus-loaded nanostructured lipid carriers for oral delivery – Optimization of production and characterization, *Eur. J. Pharm. Biopharm.* 108 (2016) 277–288. doi:10.1016/j.ejpb.2016.07.017.
- [55] S. Guerrero, M. Inostroza-Riquelme, P. Contreras-Orellana, V. Diaz-Garcia, P. Lara, A. Vivanco-Palma, A. Cárdenas, V. Miranda, P. Robert, L. Leyton, M.J. Kogan, A.F.G. Quest, F. Oyarzun-Ampuero, Curcumin-loaded nanoemulsion: a new safe and effective formulation to prevent tumor recurrence and metastasis, *Nanoscale.* 10 (2018) 22612–22622. doi:10.1039/C8NR06173D.

II. Supplementary Information

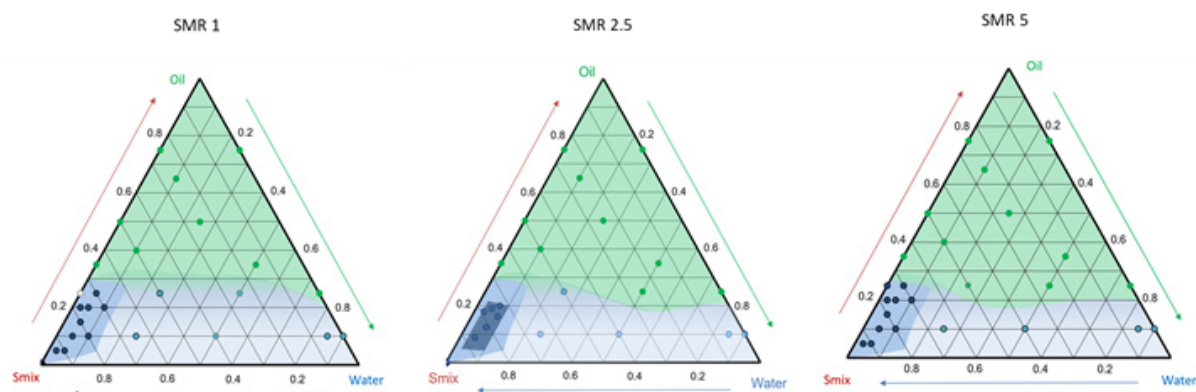


Fig. S1. Ternary phase diagram at $SMR =$ (A) 1, (B) 2.5, (C) 5. The green area corresponds to formulations in the solid state, the two blue areas to formulations in the liquid state. The dark blue region corresponds to formulations containing NE.

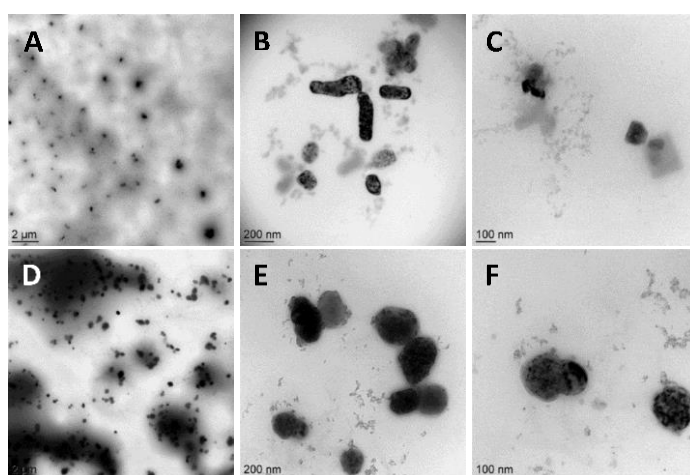


Fig. S2. TEM images of blank NE composed of S1 and S2 (without MCT) (A, B and C) and blank NE composed of S1 and MCT (without S2) (D, E, and F) at different magnifications (scales bars are 2 μm (A and D), 200 nm (B and E) and 100 nm (C and F)).

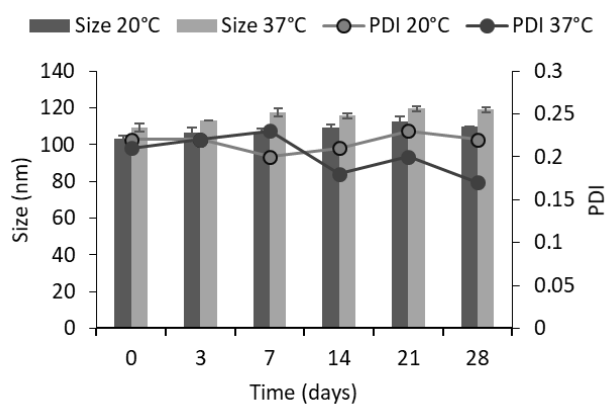


Fig. S3. Stability study of blank NE upon storage at 20 $^{\circ}\text{C}$ and 37 $^{\circ}\text{C}$ for 28 days. Data are shown as mean \pm S.D., $n = 3$.

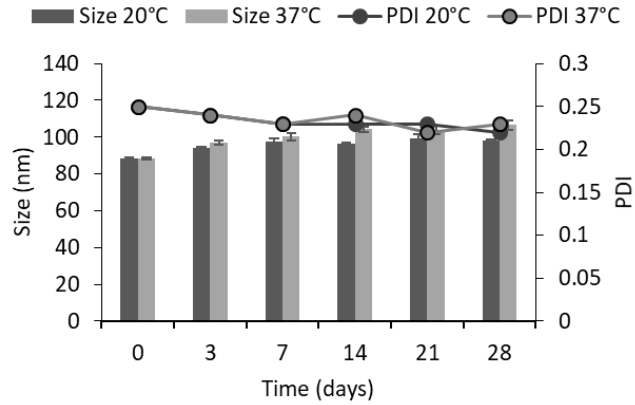


Fig. S4. Stability study of tacrolimus-NE upon storage at 20 °C and 37 °C for 28 days. Data are shown as mean \pm S.D., $n = 3$.

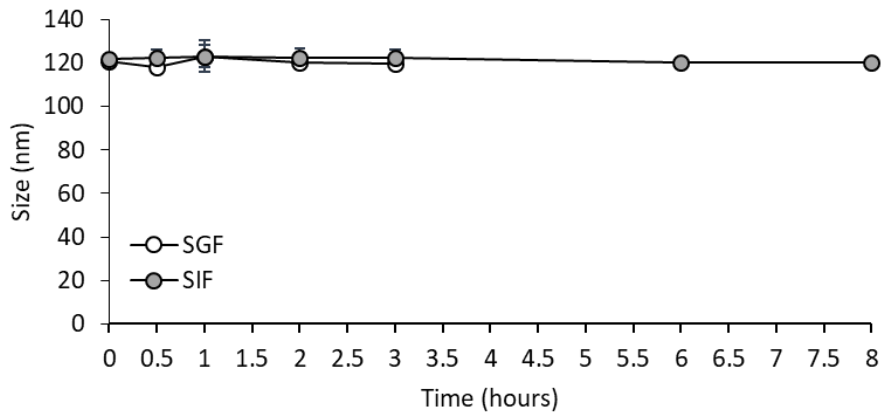


Fig. S5. Evolution of the particle size of tacrolimus-NE upon incubation in SGF and SIF media at 37 °C. The attenuator of the DLS instrument was fixed at 6 in the whole series of experiments. Mean \pm S.D., $n = 3$. Original size of the formulation: 120.9 ± 0.8 nm. SGF: simulated gastric fluid; SIF: simulated intestinal fluid.

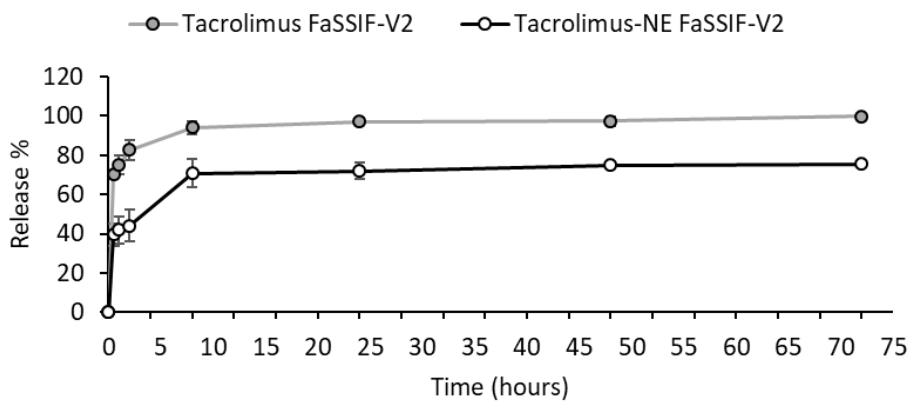


Fig. S6. *In vitro* release profiles of tacrolimus from solutions and loaded NE in FaSSIF-V2 (pH 6.5) up to 72 h. Mean \pm SD, $n = 3$. FaSSIF-V2: simulated intestinal fluid in fasted state.

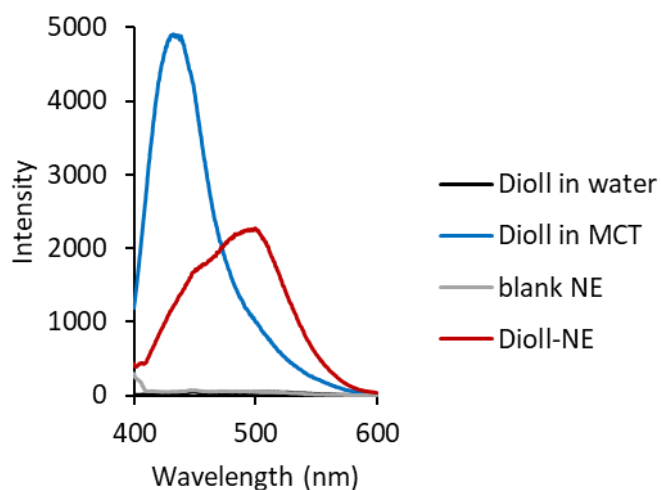


Fig. S7. Fluorescence emission spectra of Dioll-NE in control media at 21 °C used as references for assessment of the effective insertion of Dioll in the NE shell.

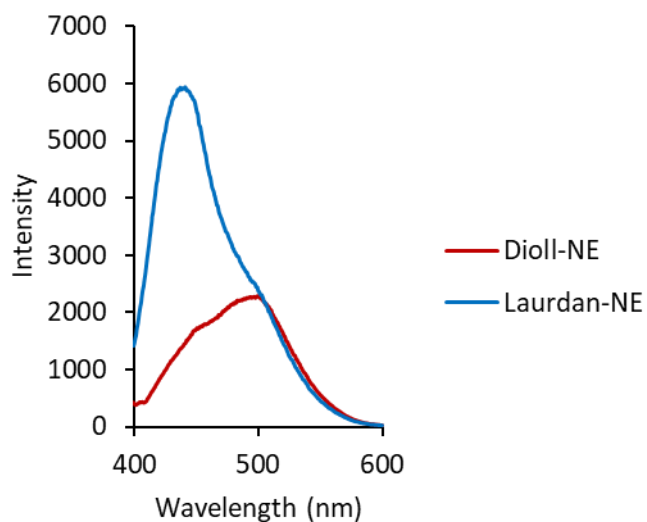


Fig. S8. Fluorescence emission spectra of Laurdan-NE versus Dioll-NE, showing the poor adequacy of the Laurdan probe in performing fluorescence measurements. Laurdan mostly inserted in the NE MCT core because of its highest hydrophobicity compared to Dioll, while Dioll was located in the NE shell.

Chapter III: Nanocomposite sponges for enhancing intestinal residence time following oral administration

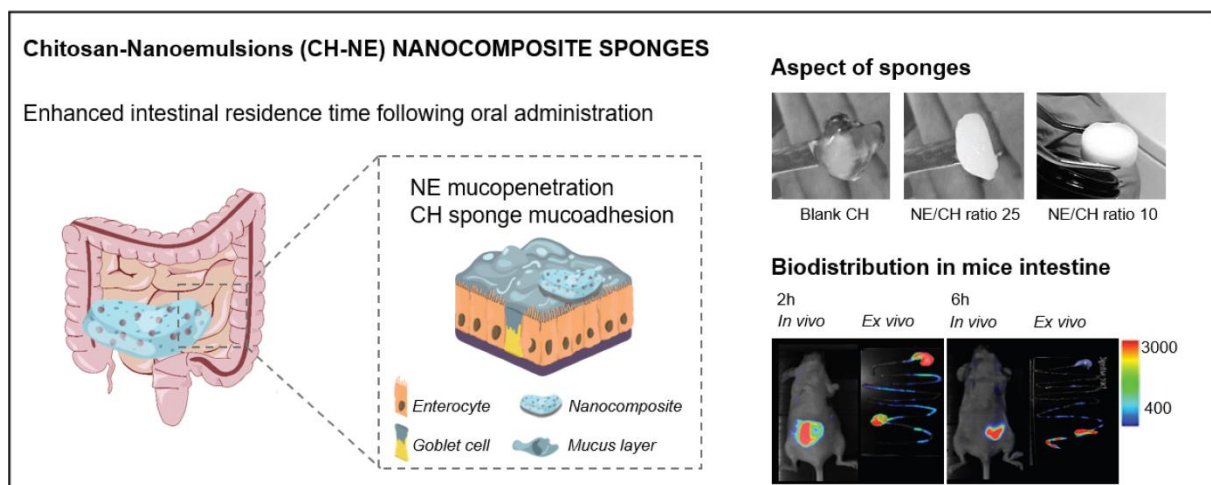
The oral administration of drugs faces several biological hurdles, notably the presence of the intestinal mucus gel layer that hinders drug delivery to the underlying epithelium, and the rapid mucus turnover that enhance drug excretion. Hybrid systems based on the combination of nanoparticles and polymers in a single device have been proposed as a promising strategy for prolonged retention and controlled drug release at the intestinal epithelial surface.

Main aim

The aim of this second chapter of the thesis was the design of a nanocomposite, by loading mucopenetrating PEGylated nanoemulsions (NEs) in a mucoadhesive chitosan (CH) sponge, to prolong intestinal residence time following oral administration.

Specific objectives

- Assess the mucopenetrating ability of NEs;
- Produce nanocomposite sponges by the freeze-drying technique and evaluate the NEs release in biorelevant intestinal fluids;
- Study the system cytocompatibility *in vitro* on models of intestinal cells (HCT 116 and Caco-2 cells)
- Compare the intestinal residence time of the NEs and the nanocomposite sponge via *in vivo* biodistribution studies in healthy mice.



Highlights of the chapter

- The NEs are promising mucopenetrating candidates. They showed only weak surface affinity interactions with reconstituted mucins and they penetrated in a preformed mucin network rapidly.
- A nanocomposite was efficiently designed by embedding of NEs in a CH sponge via the freeze-drying technique, without altering the NE physicochemical properties. Being in a dry form such system possesses a high storage stability.
- Nanocomposite sponges with diverse structural properties were obtained by modulation of NE and CH concentrations. These structural differences allowed to tune the sponge pH-dependent stability and the NE release profile in simulated intestinal environment.
- The nanocomposite sponge showed increased intestinal residence time after oral administration to healthy mice. Thanks to the mucoadhesive ability of the CH, the sponge acted as a reservoir to localize NEs at the intestinal site. This opens the way for its future exploitation as systemic or local drug delivery system.

Nanocomposite sponges for enhancing intestinal residence time following oral administration

Annalisa Rosso¹, Valentina Andretto¹, Yves Chevalier¹, David Kryza¹, Jacqueline Sidi-Boumedine¹, Ana Grenha², Filipa Guerreiro², Adem Gharsallaoui¹, Veronica La Padula³, Alexandra Montembault⁴, Laurent David⁴, Stéphanie Briançon¹ and Giovanna Lollo¹

1. Univ Lyon, Université Claude Bernard Lyon 1, CNRS, LAGEPP UMR 5007, 43 boulevard du 11 Novembre 1918, F-69622, Villeurbanne, France
2. Centre for Marine Sciences (CCMAR), Universidade do Algarve, Campus de Gambelas, 8005-139 Faro, Portugal
3. Centre Technologique des Microstructures (CT μ), Université Claude Bernard Lyon 1, France
4. Univ Lyon, Université Claude Bernard Lyon 1, CNRS, Ingénierie des Matériaux Polymères (IMP) UMR 5223, 15 boulevard Latarjet, F-69622, Villeurbanne, France

III. Abstract

In this work, nanocomposites that combine mucopenetrating and mucoadhesive properties in a single system are proposed as innovative strategy to increase drug residence time in the intestine following oral administration. To this aim, a novel mucoadhesive chitosan (CH) sponge loaded with mucopenetrating PEGylated nanoemulsions (NEs) was developed via the freeze-casting technique. The NEs mucopenetration ability was determined studying the surface affinity and thermodynamic binding of the nanosystem with mucins. The ability of nanoparticles to penetrate across preformed mucins layers was validated by 3D-time laps CLSM imaging. Microscopy observation (Scanning Electron Microscopy and Optical Microscopy) of CH-NE sponges revealed that the structure of sponge is highly impacted by CH and NE concentrations. *In vitro* release kinetics of NEs from re-hydrated sponges towards a biorelevant intestinal fluid (FaSSIF-V2) revealed a sustained release over the whole intestinal pH range (5–7.4). To assess the cytocompatibility of the system, the NEs were incubated with HCT 116 and Caco-2 cell lines. A time- and concentration-dependent loss of cell viability was observed on HCT 116 cells, while NEs revealed a non-toxic behaviour on Caco-2 cells at all concentrations tested. Finally, the *in vivo* biodistribution of the nanocomposite was evaluated after oral gavage in healthy mice. The intestinal retention of NEs was highly enhanced when loaded in the sponge compared to NEs suspension. Overall, our results demonstrated that the developed nanocomposite sponges are promising systems for sustained drug intestinal delivery.

III.1. Introduction

The development of drug delivery strategies able to control and sustain drug release after oral administration must be achieved using systems that are biocompatible, mechanically flexible, and steady over time [1–3]. Upon oral administration, drugs face stomach acidic environment and enzymatic degradation before reaching the intestine, which limits their availability. Once in the intestine, further obstacles to be considered are i) the presence of the intestinal mucus gel layer that hinders drug delivery to the underlying epithelium, and ii) mucus turnover, that enhance drug excretion [4]. To overcome these biological hurdles and increase the residence time of active compounds in the gastro-intestinal (GI) tract, mucoadhesive and mucopenetrating drug delivery nanosystems have been extensively

explored [5,6]. Mucoadhesive systems obtained by coating the nanosystems with bioadhesive polymers (chitosans, alginates, and acrylic polymers) are able to interact with the mucus layer through several mechanisms, including electrostatic, H-bonding and/or hydrophobic interactions [1,7–9]. This strategy allows the nanosystems to remain intimately attached to the mucins gel, however premature cargo release and/or accumulation inside the mucosal layer could occur [10]. On the contrary, mucopenetrating nanocarriers can spread over the mucosa, penetrate deep mucus regions and reach the intestinal epithelium [11,12]. A reduction of interactions with mucins is provided by a neutral surface charge of the particles, resulting from the coating with non-ionic polymers such as poly(ethylene glycol) (PEG) [13–15]. A further improvement strategy consists in the development of nanocomposites made of mucopenetrating nanoparticles integrated into a biocompatible mucoadhesive macro-structure. Exploiting this strategy, nanosystems can be released from the composite in a controlled and “on-demand” fashion, assisting site-specific drug targeting, and finally interacting with the epithelial surface [6]. For the development of such mucoadhesive macro-systems, physical hydrogels based on polysaccharides have been extensively studied [3,16–19]. However, because of their semi-solid properties and hydrated nature, hydrogels presented practical concerns such as the limited stability during storage and the dependence of the hydrogel network properties on the physiological conditions (pH, enzymes). This can shorten the *in vivo* residence time or trigger burst drug release [17,20]. To address this issue, dry porous 3D systems such as sponges have been designed. Sponges are obtained via the controlled solidification of polymers and colloidal suspensions by mean of the freeze-casting technique. [21–23]. Sponges can improve mucoadhesion thanks to their porous structure, while providing a sustained drug release [24,25]. Moreover, the dry state guarantees a high system stability for storage and offers an *in situ* activable platform upon hydration in biological fluids [26]. The incorporation of a drug delivery systems inside sponge macro or micro-structures can refine intestinal targeting ability [27]. Nanocomposites have been proved to enhance the systemic absorption [2,28] or maximize the local effect of drugs [3]. Their exploitation is currently under investigation for the treatment of different pathological conditions including obesity, diabetes, colon cancer and inflammatory disorders, such as ulcerative colitis and Crohn’s disease [3,20,29,30].

We recently developed novel nanoemulsions (NEs), composed of an oil core surrounded by a non-ionic PEGylated surfactant shell, which holds promising features as mucopenetrating drug delivery system [31]. In this work, we aimed at developing chitosan (CH) sponges loaded with NEs as novel nanocomposites to control and prolong drug intestinal delivery. To reach this objective our strategy was focused on increasing the intestinal residence time of such nanocomposite via the combination of mucopenetrating (NEs) and mucoadhesive (CH sponge) properties in a single delivery system.

Chitosan is a high mucoadhesive polysaccharide regarded as non-toxic, biocompatible and biodegradable. Its adhesion capacity to the mucosal epithelium has been largely described and arises mainly from the electrostatic binding with anionic glycoproteins of mucins in the intestine [32,33]. In particular, the low pH of inflamed zones can favour such interactions increasing its mucoadhesive ability [18].

We hypothesized that the CH sponge can prolong the drug retention time in the intestine by adhering to the mucus allowing a controlled release of the embedded NEs. To validate our approach, we firstly assessed the mucopenetrating ability of NEs. Then, NE-loaded CH sponges (CH-NE) obtained by freeze-casting technique, were characterized regarding their structural and mechanical properties. The

impact of the CH sponge on NEs release kinetics was investigated after sponge re-hydration in a simulated intestinal fluid. The cytocompatibility of the system was assessed on human colorectal carcinoma cells (HCT 116 and Caco-2). Finally, *in vivo* biodistribution studies of both fluorescent NEs and CH-NE after oral gavage of mice were performed to assess the ability of nanocomposite to increase the residence time of NEs in the intestine.

III.2. Material and methods

III.2.1. Materials

Medium chain triglycerides, MCT (Miglyol®812), was purchased from Cremer Oleo GmbH & Co. KG (Hamburg, Germany). Polyoxyethylene (40) stearate (Myrj®52), Nile red (NR), curcumin (CCM), formic acid, sodium dodecyl sulphate (SDS), mucin from porcine stomach Type II and Dulbecco's modified Eagle's medium (DMEM) were purchased from Sigma-Aldrich (St Quentin-Fallavier, France). Oleoyl polyoxyl-6 glycerides (Labrafil®M1944CS) was provided by Gattefossé (Saint-Priest, France). Egg phospholipids with 70% phosphatidylcholine (Lipoid E80S) were obtained from Lipoid GmbH (Ludwigshafen am Rhein, Germany). Potassium dihydrogen phosphate (KH_2PO_4) and potassium chloride (KCl) were purchased from Riedel-de-Haën AG (Seelze, Germany). Di-sodium hydrogen orthophosphate dihydrate ($\text{Na}_2\text{HPO}_4 \cdot 2\text{H}_2\text{O}$) was purchased from Serva Electrophoresis GmbH (Heidelberg, Germany). Sodium chloride (NaCl), hydrochloric acid (HCl) 37%, phosphate buffered saline (PBS) tablets (pH 7.4), 3-(4,5-dimethylthiazol-2-yl)-2,5-diphenyltetrazolium (MTT) was obtained from VWR International (Fontenay-sous-Bois, France). Penicillin/streptomycin ($10000 \text{ U} \cdot \text{mL}^{-1}$), foetal bovine serum (FBS, South America) and nanomycopolitine from Dutscher SAS (Brumath, France). Acetic acid was obtained from Chem-Lab NV (Zedelgem, Belgium). Dichloromethane, methanol, acetonitrile (HPLC grade), sodium taurocholate hydrate 96%, sodium hydroxide (NaOH), DiI₁₈(5) solid, 1,1'-dioctadecyl-3,3,3',3'-tetramethylindodicarbocyanine, 4-chlorobenzene sulfonate salt (DiD) and Promega CellTiter 96™ AQueous One Solution Cell Proliferation Assay (3-(4,5-dimethylthiazol-2-yl)-5-(3-carboxymethoxyphenyl)-2-(4-sulfophenyl)-2H-tetrazolium), MTS) were purchased from Thermo Fisher Scientific (Illkirch, France). Milli-Q® water was obtained using a Milli-Q® Academic System from Merck-Millipore (Saint-Quentin-en-Yvelines, France). The aqueous phase used to prepare NEs was phosphate buffer saline solution (PBS 5 mM, pH 7.4). The aqueous phase used to prepare mucin gels was Sorenson's phosphate buffer containing Na_2HPO_4 and KH_2PO_4 (0.2 M, pH 7.4). The chitosan used in this study was produced from N-deacetylation of chitin extracted from squid pens and was purchased from Mahtani Chitosan (batch type 114). Its structural properties are the following: a degree of acetylation of $4.0 \pm 0.5\%$, a weight-average molar mass M_w of $550 \pm 50 \text{ kg} \cdot \text{mol}^{-1}$ and a dispersity \mathcal{D} of 1.5 ± 0.3 . ^1H NMR analysis was used to determine the degree of acetylation (DA) of chitosan [34]. M_w and \mathcal{D} were determined as previously described [35], using size exclusion chromatography (SEC) coupled online with a differential refractometer (Optilab T-rEX, Wyatt; $\lambda=658 \text{ nm}$) and with a multi-angle laser light scattering detector (Dawn-HELOES II, Wyatt; $\lambda=664 \text{ nm}$).

III.2.2. Process of nanoemulsions formulation

NEs were prepared by emulsion phase inversion (EPI) technique coupled with high stirring energy input as previously described [31]. Briefly, NEs were composed of an MCT oil core stabilized by a surfactant

shell, made of a mixture of hydrophilic and hydrophobic surfactants, namely polyoxyethylene (40) stearate (Myrj 52) and oleoyl polyoxyl-6 glycerides (Labrafil M1944CS), respectively. To prepare the oil phase, MCT (0.35 g) and surfactants (1 g) were mixed and magnetically stirred (750 rpm) using a thermostated bath at 80 °C. The aqueous phase (PBS 5 mM, 3.65 mL), heated up to 80 °C as well, was added into the organic melt phase. Stirring was then performed by two cycles of 10 min using a rotor-stator disperser (T25 digital Ultra-Turrax® equipped with a S25N-10G shaft, IKA®-Werke GmbH & Co. KG, Staufen, Germany) rotating at 11000 rpm at 80 °C. Hydrophobic dyes as Nile red (NR), curcumin (CCM) and DiD were added to the oil phase during NEs preparation for their encapsulation in NE droplets. The final fluorescent probe concentrations in the NEs were NR 200 $\mu\text{g}\cdot\text{mL}^{-1}$, CCM 500 $\mu\text{g}\cdot\text{mL}^{-1}$, DiD 50 $\mu\text{g}\cdot\text{mL}^{-1}$. NR or CCM were solubilized in the oil phase and magnetically stirred (750 rpm) for 2 h at 80 °C to obtain a homogeneous mixture. NEs were then formulated as explained above. Regarding the lipophilic carbocyanine dye DiD, 125 μL of its stock solution in ethanol (2 $\text{mg}\cdot\text{mL}^{-1}$) were mixed with the oil phase and the NEs were formulated keeping the temperature below the DiD melting point (68 °C) in order to avoid dye decomposition.

III.2.3. Physico-chemical characterization of nanoemulsions

The size distribution and surface potential of the NE droplets were determined using Malvern Zetasizer® Nano ZS instrument (Malvern Instruments S.A., Worcestershire, UK). The particle sizes were measured by Dynamic Light Scattering (DLS) at 25 °C at a scattering angle of 173 °. The ζ -potential was calculated from the mean electrophoretic mobility measured for samples diluted in 0.1 mM KCl. Measurements were performed in triplicate.

The stability of blank and CCM-NEs in as produced colloidal suspension was followed during 28 days upon storage at 20 °C. At scheduled time points, particle size, polydispersity index (PdI) and ζ -potential were measured. Moreover, dye leakage (CCM and NR) from NE was assessed at day 28. Free dye was separated from the suspending aqueous medium by size exclusion chromatography on PD-10 Desalting Columns containing 8.3 mL of Sephadex™ G-25 resin (GE Healthcare Bio-Sciences AB, Uppsala, Sweden). The NE containing fractions were easily identified thanks to their turbidity and collected in microtubes. For NR-loaded NEs, 200 mg of isolated NE were dissolved in ethanol (1 g) and analysed by UV-vis absorbance at 549 nm. The CCM-loaded NE fraction was analysed by HPLC equipped with an UV-vis detector using the method described by Liu et al. [36,37]. In order to quantify CCM, 300 mg of isolated NEs were dissolved in methanol (1 g) and the samples were vortexed for 5 min. The samples were filtered using Nylon filter 0.22 μm (Whatman GmbH, Dassel, Germany) before injection in the HPLC system. The HPLC apparatus consisted of Agilent 1200 Series G1311A Quat Pump, Agilent 1200 Series G1367B HIP-ALS High Performance Autosampler, equipped with Agilent 1200 Series G1315D Dad Diode Array Detector HPLC (Agilent, Santa Clara, CA, United States). CCM was detected using a RP-C18 column (Kinetex 5 μm C18 100 Å, 150 \times 4.6 mm, Phenomenex, Torrance, CA, USA), set at 30 °C, using acetonitrile and deionized water 0.1% formic acid (50:50) as mobile phase at a flow rate of 1.0 $\text{mL}\cdot\text{min}^{-1}$. The injection volume was 10 μL , the detection wavelength 423 nm and the total run time 8 min. The chromatogram of CCM exhibited a characteristic peak at a retention time 6.6 min. Peak areas were recorded and processed on the OpenLab CDS ChemStation Edition software (Agilent, Santa Clara, CA, United States). The HPLC calibration curve was linear ($R^2 = 0.99$) in the concentration range of

0.04–40 $\mu\text{g}\cdot\text{mL}^{-1}$. The method was validated according to ICH Q2(R1) guidelines. Detection and quantification limits (LOD and LOQ) were 2.17 $\mu\text{g}\cdot\text{mL}^{-1}$ and 7.24 $\mu\text{g}\cdot\text{mL}^{-1}$, respectively.

The encapsulation efficiency was calculated as the ratio of dye detected in the isolated NE (NE purified: NEp) to the amount of dye initially loaded in the NE (NE initial: NEi):

$$\text{Encapsulation efficiency (\%)} = \frac{\text{NEp}}{\text{NEi}} \times 100 \quad \text{Eq. 1}$$

III.2.4. Mucins-nanoemulsions interaction

III.2.4.1. Colloidal stability of nanoemulsions in mucins

Mucin solution from porcine stomach Type II (1% w/v) was prepared by suspending 40 mg of mucin powder in 4 mL of Sorenson's phosphate buffer (pH 7.4). The solution was magnetically stirred (750 rpm) for 2 h in an ice bath and left for equilibration overnight at 4 °C. Then, mucin solution and blank NE were mixed to obtain a final mucin concentration of 0.5% w/v and NE concentration of 0.5% w/v. Samples were magnetically stirred at 300 rpm for 4 h in a water bath at 37 °C. At predetermined time points (0.5, 1, 2, 3, and 4 h) an aliquot (1 mL) was retrieved and centrifuged at 7000 rpm for 5 min to separate mucin and entrapped NEs from the supernatant. Then, the supernatant was collected and NEs size distribution and ζ -potential were measured at 37 °C. The ζ -potential of NEs (0.1% w/v) and mucin solutions (0.1% w/v) in PBS 5 mM was separately analysed at pH values ranging from 2 to 9. The pH was varied by titration of NaOH (0.1 M) or HCl (0.1 M). Measurements were performed in triplicate.

III.2.4.2. Microcalorimetric studies

The thermodynamics of the interaction between mucin and NE were assessed by isothermal titration calorimetry (VP-ITC, MicroCal, Northampton, MA). 0.1 g of mucin from porcine stomach (type II) were dissolved in 1 L of PBS (5 mM pH 7.4) to obtain a final concentration of 0.01% w/v and NE were diluted with the same PBS to 0.1% w/v. Both solutions were degassed while stirring for 10 min before the loading. 1.42 mL of the mucin solution were placed into the calorimetric cell equilibrated at 25 °C and titrated by the injection of 283 μL of NE loaded in the syringe (3 μL for the first injection, followed by 28 injections of 10 μL each) under continuous stirring at 307 rpm. The duration of each injection was 20 s, and the time interval between them was 200 s. Control titrations were performed by injecting the same concentration of NE into the reaction cell containing the dilution buffer, using the same injection parameters. The raw data obtained with the control titration were then subtracted to the mucin-nanoemulsion raw data.

III.2.4.3. 3D-time laps imaging using confocal laser scanning microscopy

The penetration of NE (10% w/v) in artificial gastric mucin type II (10% w/v) was verified by 3D time laps imaging using Confocal Laser Scanning Microscopy (CLSM, Confocal Zeiss LSM 800) available at the Centre Technologique des Microstructures (CT μ) of the University Lyon 1 (Villeurbanne, France). A constant volume of mucin solution (50 μL) was filled in a chamber slide resulting in equally thick mucins layers (3 mm). At time zero, 10 μL of DiD-loaded NEs were added on the top of the mucin layer (Fig. S1). Z-stacks (51 images of planes at various depths) within the mucin sample were obtained at a constant distance of 20 μm from the bottom of the slide. The wavelength for DiD excitation was set at 640 nm and the emission was measured between 646 and 700 nm. Particle penetration was tracked and z-stacks images starting from time 10 min and at time intervals of 10 min up to 3 h were recorded. A

sample of mucin alone was examined as control. Images were analysed with the Fiji ImageJ software [38] for fluorescence intensity and 3D visualisation of image stacks.

III.2.5. Preparation of chitosan sponges and nanoemulsion incorporation process

CH solutions were prepared by dissolving CH in an aqueous solution of acetic acid at 1% w/w under magnetic stirring (375 rpm) for 24 h at room temperature. Mass % of CH reported in Table 1 included ~8% of residual water content. The final CH concentrations were 0.1% w/w (CH A) and 1% w/w (CH B) (Table 1).

Table 1. Formulated chitosan (CH) and nanoemulsion-loaded chitosan (CH-NE) sponges.

Sample	% (w/w) in CH-NE mixture		% (w/w) in CH-NE sponge		NE/CH ratio (w/w)	Apparent density (g/cm ³)
	CH	NE	CH	NE		
CH A	0.1	–	100	–	–	0.02 ± 0.01
CH B	1	–	100	–	–	0.04 ± 0.01
CH-NE A	0.1	2.5	3.9	96.1	25	0.44 ± 0.03
CH-NE B	1	2.5	28.6	71.4	2.5	0.10 ± 0.05
CH-NE C	1	10	9.1	90.9	10	0.21 ± 0.01

In order to prepare CH-NE mixtures, NEs were added to CH solutions and the samples were magnetically stirred at 375 rpm for 3 h at room temperature until complete homogenization. CH-NE mixtures at CH concentrations of 0.1% and 1% w/w and NEs concentrations of 2.5% and 10% w/w were obtained (CH-NE A, B, C in Table 1). The samples were then transferred to lyophilisation vials to be converted into dry sponges by freeze-casting technique [24]. The freezing and drying steps were carried out in a Cryonext pilot freeze-dryer (Cryonext, Saint-Aunès, France). The freeze-drying process consisted in 3 steps: i) freezing at -50 °C for 6 h in the freeze-dryer chamber (cooling speed of 0.3°C·min⁻¹ during the first 3h); ii) primary drying from -50 °C to 0 °C in 20 h (0.1 mbar); iii) secondary drying at 20 °C for 12 h (0.1 mbar for 6h, then 0.01 mbar for other 6h). Finally, the vials were sealed with rubber caps and stored at 20 °C.

III.2.6 Microscopy observations of sponges: scanning electron microscopy (SEM) and optical images

Sponge morphology was assessed by scanning electron microscopy (SEM) using a FEI Quanta 250 FEG microscope at the Centre Technologique des Microstructures (CTμ) of the University Lyon 1 (Villeurbanne, France). Surface and cross-sectional morphology of the sponges were analysed. The samples were coated under vacuum by cathodic sputtering with copper and observed by SEM under an accelerating voltage of 15 kV. Transmission electron microscopy (TEM) was performed with a Philips CM120 microscope at the Centre Technologique des Microstructures (CTμ) of the University Lyon 1 (Villeurbanne, France). Diluted NE (10 μL) was deposited on a microscope grid (copper support coated with carbon) and slowly dried in open air. The dry samples were observed by TEM under 120 kV acceleration voltage. Optical images of sponge surfaces were collected using a Keyence VHX-6000

series digital microscope (Keyence, Jonage, France). Pictures of the depth of pores across a large area of the sponge surface were captured in real-time and combined by 3D image stitching.

III.2.7. Rehydration and water uptake capacity

The water uptake capacity of CH and CH-NE sponges was evaluated at pH 5, 5.5 and 7.5 in two different media: PBS (5 mM) and simulated GI fluid in fasted state (FaSSIF-V2). Pre-weighed freeze-dried sponges (initial mass M_0) were submerged in the media. At predetermined time points, the excess of medium was gently removed using a micropipette, and hydrated sponges were weighed (M_s). The water uptake was calculated as follows:

$$\text{water uptake \%} = \frac{M_s - M_0}{M_0} \times 100 \quad \text{Eq. 2}$$

The study was performed in triplicate.

III.2.8. Rheological characterization

Oscillatory rheological tests were carried out through a MCR 302 rheometer (Anton Paar, Les Ulis, France) fitted with a 25 mm plate-plate geometry. CH and CH-NE sponges were rehydrated in PBS at pH 7.5 for 15 min. The temperature was set at 22 °C. The applied strain ($\gamma\%$) was fixed at 1% within the linear viscoelastic regime on the basis of a previous amplitude sweep test. The apparent storage and loss moduli of rehydrated CH and CH-NE sponges were measured by mean of frequency sweep tests over an angular frequency range of 100–0.05 $\text{rad}\cdot\text{s}^{-1}$. Measurements were performed in triplicate.

III.2.9. In vitro release studies

The *in vitro* release of NEs from the CH sponges was evaluated in PBS and FaSSIF-V2 at pH of 5, 5.5 and 7.5 by mean of two different studies: destructive and cumulative test.

The influence of the composition and pH of the release medium was assessed by a destructive study. NR-loaded NEs were embedded into CH-NE A sponges (52 mg) and 3 mL of release medium were added on the top of sponges. Two different media at three different pH were tested: i) PBS at pH 5, pH 5.5, and pH 7.5 ii) FaSSIF-V2 at pH 5, 5.5 and 7.5. At scheduled time points (5 min, 30 min, 2 h, 8 h and 24 h), the release media were retrieved and the amount of NEs released (NR-loaded NEs) was measured by UV-vis spectroscopy.

Then, the influence of CH and NE concentrations on NE release from the sponges was assessed in FaSSIF-V2 by mean of a cumulative study. To this aim, 5 mL of medium FaSSIF-V2 were added on top of the sponges containing CCM-loaded NE (weight of the dry sponge CH-NE A: 52 mg, B: 70 mg, C: 55 mg and D: 60 mg, at constant CCM concentration of 50 $\mu\text{g}\cdot\text{g}^{-1}$) and the pH was varied over time. FaSSIF-V2 was prepared at pH 7.5 and this pH was maintained for the first 24 h of the study. Then, the pH was decreased to 5.5 for the following 48 h. Finally, the pH value was set at 5 to 72 h. At predetermined time points (30 min, 1, 2, 3, 4, 5, 6, 7, 8, 24, 48, and 72 h), the entire volume of medium was removed and replaced with fresh medium. The amount of CCM released was quantified by HPLC-UV as described above. Data were normalized based on the dry weight of the NE in the sponge. Studies were performed in triplicate.

III.2.10. *In vitro* cell viability studies

III.2.10.1 Cell culture conditions

Human colorectal carcinoma (HCT 116) cells were used to perform the MTT assays, being cultured in 75 cm² flasks, at 37 °C in a humidified atmosphere 5% CO₂ and 95% air incubator. Cell culture medium was DMEM, supplemented with 10% (v/v) FBS and 1% (v/v) penicillin/streptomycin. The medium was exchanged every two days.

Human colon carcinoma (Caco-2) cells were used to perform MTS assays. Caco-2 cells were cultured in 75 cm² flasks, at 37 °C in a humidified atmosphere 5% CO₂ and 95% air incubator. Cell culture medium was DMEM, supplemented with 10% (v/v) FBS, 2% (v/v) penicillin/streptomycin and 1% nanomycopulitine. The medium was exchanged every two days.

III.2.10.2 Toxicological evaluation of NE

The effect of blank NEs on the viability of HCT 116 cells was evaluated by the MTT colorimetric assay. To do so, 1x10⁴ cells/well were seeded in 96-well plates and maintained overnight at 37 °C, 5% CO₂. Then, the culture medium was removed, and cells were treated with increasing concentration of blank NE (ranging from 10 to 1250 µg·mL⁻¹) diluted with pre-warmed DMEM supplemented with 2% of FBS (v/v). DMEM was used as positive control (100% viability), while SDS (2%, w/v) as negative control. Cells were exposed to the formulations for 3 and 24 h at 37 °C. After the considered period, samples were replaced with 100 µL of fresh medium added of 25 µL of MTT solution (0.5 mg·mL⁻¹ in PBS pH 7.4) in each well. The plates were incubated for 4 h at 37 °C. The formazan purple crystals formed by the reaction of MTT with NAD(P)H of metabolically active cells were dissolved in 100 µL SDS (10%, w/v) and the plates incubated overnight at 37 °C. The absorbance was measured spectrophotometrically (Infinite M200; Tecan, Austria) at 570 nm, with background correction at 650 nm.

The effect of blank NEs on the viability of Caco-2 cells was evaluated by the MTS assay. To this end, 2x10⁴ cells/well were seeded in 96-well plates and maintained for 48 h at 37 °C, 5% CO₂. Then, the culture medium was removed, and cells were treated with increasing concentration of blank NE (ranging from 10 to 1250 µg·mL⁻¹) diluted with pre-warmed DMEM supplemented with 10% of FBS (v/v). DMEM was used as positive control (100% viability), while SDS (3%, w/v) as negative control. Cells were exposed to the formulations for 3 and 24 h at 37 °C. After the considered period, samples were replaced with 100 µL of fresh medium added of 20 µL of MTS solution (Promega CellTiter 96™ AQueous One Solution Cell Proliferation Assay) in each well. The plates were incubated for 4 h at 37 °C. The absorbance was measured spectrophotometrically (Multiskan EX, Thermo Fisher Scientific, France) at 492 nm, with background correction at 620 nm.

Cell viability was calculated by the following formula (Abs = absorbance):

$$\text{Cell viability (\%)} = \frac{\text{Abs sample} - \text{Abs SDS}}{\text{Abs DMEM} - \text{Abs SDS}} \times 100 \quad \text{Eq. 3}$$

The IC₅₀ were calculated using GraphPad Prism version 8.0.0 for Windows (GraphPad Software, San Diego, California, USA). The study was performed in triplicate.

III.2.11. *In vivo* biodistribution study of fluorescent NE-loaded sponges following oral administration

All animal experiments were approved by the local animal ethics of University Claude Bernard Lyon 1, and carried out in compliance with current French guidelines. Female nude mice (average body weight

of 20 g, n = 45) used for the experiment were obtained from Charles River Laboratories (Saint-Germain-Nuelles, France). The animals were fasted for 12 h before the oral gavage. Three different systems were administered: i) DiD-loaded NEs (NE 10% w/w), ii) DiD-loaded NEs mixed with CH solution (CH dissolved in acetic acid), named CH-NE mixture (CH-NE C, CH 1%- NE 10% w/w), and iii) DiD-loaded NEs embedded in the CH sponge, defined as CH-NE sponge (CH-NE C, CH 1%- NE 10% w/w). NEs and CH-NEs mixture were administered as liquid colloidal suspensions, while CH-NE sponges were re-hydrated with water and filled in the feeding tube. Mice were randomly divided into three groups: NE (n = 15), CH-NE mixture (n = 15), CH-NE sponge (n = 15). Each formulation contained NEs at a concentration of $100 \text{ mg} \cdot \text{mL}^{-1}$, corresponding to a dose of $\approx 1.25 \text{ mg} \cdot \text{kg}^{-1}$ of body weight. At scheduled time points (1, 2, 3, 4, and 6 h), anesthetized animals were placed prone in a light-tight chamber where a controlled flow of 1.5% isoflurane in air was administered through a nose cone to maintain anaesthesia. Fluorescence images as well as black and white pictures of mice whole body (ventral view) were acquired via a back-thinned CCD-cooled camera ORCAIIBT-512G (Hamamatsu Photonics Deutschland GmbH, Herrsching am Ammersee, Germany) using a coloured glass long-pass RG 665 filter (Melles Griot, Voisins les Bretonneaux, France), which cuts off all excitation light. Optical excitation was carried out at 644 nm, and the emission wavelength was detected at 664 nm. At each time point (1, 2, 3, 4, and 6 h), n = 3 mice for time point were sacrificed and the organs (GI, liver, spleen, heart, kidneys, lungs, bone, brain, muscle) were harvested. *Ex vivo* fluorescent measurements were performed immediately after organ collection to determine the accumulation of the dye. Images were analysed using the Wasabi software (Hamamatsu Photonics Deutschland GmbH, Herrsching am Ammersee, Germany). The fluorescence intensities of the different intestinal segments were normalized to the fluorescence intensity of the whole intestinal tract in each mouse. Then, comparisons between normalized signals were made at all the time points for all different groups.

III.2.12. Statistical analysis

The normality of data distribution of the *in vitro* cytotoxicity and *in vivo* studies was assessed by mean of the Shapiro-Wilk test ($\alpha > 0.05$). *In vitro* cytotoxicity data were analysed by mean of a Student's t-test to compare different groups. *In vivo* data were analysed by a Two Way ANOVA multiple comparison (Tukey test). A p-value less than 0.05 indicated statistical significance ($p < 0.05 = *$; $p < 0.01 = **$; $p < 0.001 = ***$; $\geq 0.05 =$ not significant). Statistical analysis of the data was performed using GraphPad Prism version 8.0.0 for Windows (GraphPad Software, San Diego, California, USA). The data are the mean \pm SD for n = 3.

III.3. Results and discussion

III.3.1. Nanoemulsions formulation, physicochemical characterization, and stability

Monodisperse lipid nanosystems, namely NEs with neutral/slightly negative surface charge have been designed and obtained combining emulsion phase inversion (EPI) technique and homogenization process [31]. They presented a mean droplet size of $104 \pm 3.1 \text{ nm}$, a low PdI (0.2) and a ζ -potential of $-9 \pm 1.1 \text{ mV}$ (Table 2). Due to the presence of the hydrophobic core, Nile red (NR) and curcumin (CCM) dyes were efficiently loaded, with encapsulation efficiencies around 100% ($99.7 \pm 1.2\%$ for NR-NEs and $99.9 \pm 4.3\%$ for CCM-NEs). Furthermore, no alterations in particle hydrodynamic diameter and PdI were observed for loaded systems ($92.9 \pm 5.4 \text{ nm}$ for NR-loaded NE and $97.7 \pm 8.2 \text{ nm}$ for CCM-loaded

NE; PDI 0.2) (see Table 2). The ζ -potential of the NEs was shifted towards more negative values after NR and CCM loading (-20.1 ± 2.9 mV for NR-loaded NEs and -19.4 ± 5.3 mV for CCM-loaded NEs) (Table 2).

The stability of blank and loaded NEs in colloidal suspension (27% w/w, pH 6.8), upon storage at 20 °C, was followed over 28 days (Fig. S2 in supplementary information). The mean hydrodynamic size and PDI remained stable during the examined period. Moreover, no leakage of the dyes was detected upon 28 days (maintenance of encapsulation of $100.1 \pm 3.2\%$ for NR-loaded NEs, $98.6 \pm 5.3\%$ for CCM-loaded NEs, see table 2). We showed in our previous work that the selected NEs formulation was stable in both SGF (simulated gastric fluid) and FaSSIF-V2 fluid (simulated intestinal fluid in fasted state), making them a good system candidate for oral delivery [31].

Table 2. Physicochemical characteristics of blank and loaded nanoemulsions (NEs). NR-NE: Nile red-loaded NE; CCM-NE: curcumin-loaded NE.

Sample	Size (nm)	PDI	ζ -potential (mV)	Encapsulation efficiency (%)	
				Day 0	Day 28
Blank NE	104 ± 3.1	0.2	-9 ± 1.1	–	–
NR-NE	92.9 ± 5.4	0.2	-20 ± 2.9	99.7 ± 1.2	100.1 ± 3.2
CCM-NE	97.7 ± 8.2	0.2	-19 ± 5.3	99.9 ± 4.3	98.6 ± 5.3

III.3.2. Mucopenetrating properties of nanoemulsions

To target the intestinal epithelium, delivery systems must diffuse across the mucus layer either to interact with surface receptors of the epithelial cells, or to pass through the epithelium to reach the blood circulation [11]. To predict mucus permeation behaviour, we carried out an in-depth physicochemical characterization of mucin-NEs interactions using different techniques: Dynamic Light Scattering (DLS), Isothermal Titration Calorimetry (ITC) and Confocal Laser Scanning Microscopy (CLSM) analysis.

As a first approach, we studied the surface ionic interactions of PEGylated NEs in presence of reconstituted intestinal mucins by monitoring hydrodynamic diameter and surface charge of the system using DLS over the time. As described by Bernkop-Schnürch group, the contact between negatively charged mucins and nanoparticles can result in a possible adsorption of mucins onto the NEs surface through electrostatic interactions, affecting the physicochemical properties of the nanosystem [12]. No increase in particle size (around 100 nm) and no modification of NEs ζ -potential (around -8 mV) was observed after incubation of NEs (0.5% w/v) with mucins (0.5% w/v) in Sorenson's phosphate buffer (pH 7.4) at 37 °C during 4 h (Fig. S3 A in supplementary information). Due to the neutral surface charge of the NEs, the interaction with mucins was avoided.

The DLS analysis was further exploited to analyse the pH-dependent behaviour of both mucins and NEs. In fact, the pH of mucus can vary based on its location. The mucus at the luminal surface is usually more acidic than the mucin firmly adherent layer near the epithelial interface. Such variation of pH can lead to conformational changes in the mucin structure that could consequently induce possible interactions with NEs at certain pH ranges [32]. The ζ -potential of NEs (0.1% w/v) and mucin solutions (0.1% w/v) was separately analysed at pH values ranging from 2 to 9 in PBS 5 mM at room temperature (Fig. S3 B in supplementary information).

Under strongly acidic conditions (pH < 2) mucin pH shifted toward neutrality (-0.4 mV) due to the protonation of carboxylic acid residues and NE followed the same behaviour showing a surface charge close to -0.4 mV [39]. The absence of electrostatic charge and electrostatic repulsions between NE nanoparticles implied that steric forces alone imparted colloidal stabilisation.

At neutral pH, NEs and mucins showed a similar weak negative ζ -potential (-13 ± 1 and -11.1 ± 1 mV respectively). In basic conditions (pH 9), ζ -potential values of -15.7 ± 2 mV were recorded for mucins and of -14.8 ± 1 mV for NEs. This slightly negative surface charge NEs and mucins suggested the presence of repulsive electrostatic forces between the two systems showing that strong polyelectrolyte association will not occur.

After establishing that NEs and mucins exhibited only weak interactions, the thermodynamics of specific mucins-nanoparticles interaction were investigated using ITC [40]. In this case, we tested whether nanoparticles and mucins were able to interact and the nature of the possible non-covalent interactions (electrostatic interactions, van der Waals forces and hydrophobic interactions) [13]. When a mucin solution (0.01% w/v) was titrated with NEs dispersion (0.1% w/v) only the presence of low energy peaks was evidenced, a pattern similar to the one obtained during the control titration analysis (Fig. S3 C in supplementary information). We concluded that these low-energy effects were mainly due to the dilution of the NEs in the sample cell. In good agreement with the ζ -potential analysis of NEs surface properties, this finding suggested the presence of only weak interactions between mucins and NEs.

Along with DLS and ITC experiments, monitoring the NEs displacement in mucins is fundamental to get insights into the particles behaviour in complex biological environments. Hence, we monitored the diffusion of NEs in mucins using 3D-time laps CLSM imaging (Fig. 1). To minimize the errors, the study was performed in a dedicated chamber slide containing the mucin solution. At the beginning of the analysis (time point 10 min in Fig. 1 A and B), the majority of NEs were present in upper layers, as demonstrated by the high fluorescent signal. Over the three h of the analysis, NEs diffused to the underneath layers at a speed of $1.34 \mu\text{m} \cdot \text{min}^{-1}$. After 180 min of analysis, fluorescence could be observed across the whole mucin sample, meaning that NEs were distributed in all the sample height (600 μm). (Fig. 1 A and B, video S1 in supplementary information).

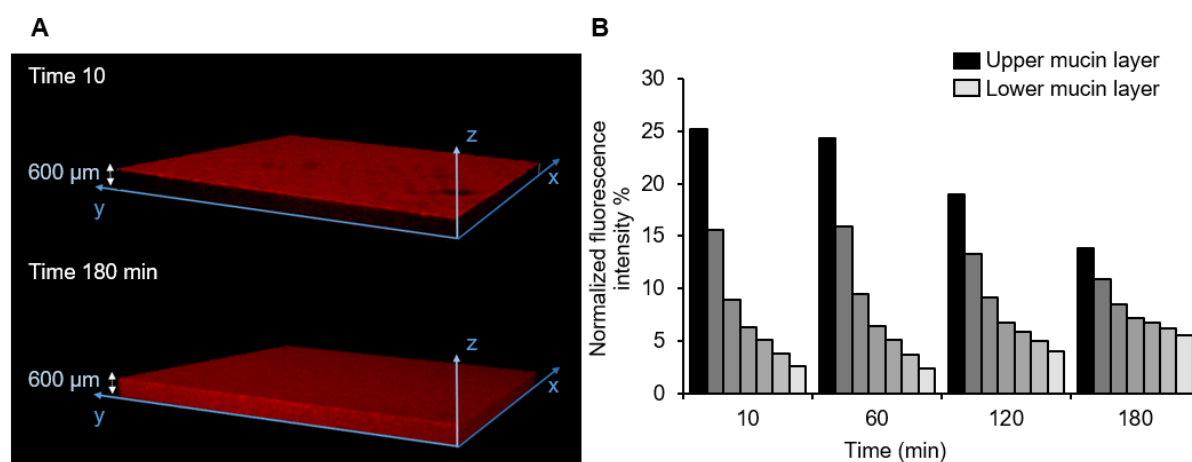


Fig. 1. A) Z-stacks of NE penetration (red) in the mucin layer (10% w/v, 600 μm thickness) at time point 10 and 180 min; B) total fluorescence signal of NE in the mucin layer (10% w/v) as a function of time as determined by image analysis software.

The developed NEs were endowed with penetrating ability by their PEGylated shell (PEG (40) stearate surfactant). The PEGylation strategy aimed at conferring neutral surface properties to the nanocarriers to reduce their association with mucus. Modifications of the nanoparticle surface with hydrophilic polymers, such as polydopamine [11], dextran-containing polymers [4] or PEG [13] have been described as successful strategies to facilitate mucus penetration. In the design of poly(lactic-co-glycolic acid-polyethylene glycol (PLGA-PEG) NP [13] and PEG-based lipid-polymer hybrid vesicles [17] the authors observed that molecular weight (M_w) of PEG, neutral ζ -potential and PEG density were key parameters controlling mucopenetration. In the case of PLGA-PEG NPs, 5% w/w of PEG (5 kDa) was needed to decrease the interactions with mucins. While in the case of hybrid vesicles, the displacement through reconstituted porcine mucus was observed only at a copolymer poly(ethylene glycol)-b-poly(cholesterol methacrylate (PEG-b-PCMA) concentration of 25% w/w [17]. In our study, the mucopenetration ability of NEs was conferred by PEG-40 stearate as PEGylated surfactant at a concentration of 14.3% w/w. By avoiding the entrapment in the mucosal barriers, the developed NEs show promising results for reaching the intestinal epithelium and improve drug delivery efficacy.

III.3.3. Development of chitosan and nanoemulsion-loaded chitosan sponges

An original nanocomposite system made of mucopenetrating NEs loaded in a mucoadhesive CH sponge was designed with the final aim to increase the intestinal residence time.

CH of low degree of acetylation (DA 4%) and high molecular weight (M_w 500 kg·mol⁻¹) was used. High M_w CH has been selected as it provides greater mucoadhesion ability because of the higher molecular interactions with mucins and the increased entanglement of CH molecules in the mucin layer [33]. The preparation of CH-NEs sponges is illustrated in Fig. 2.

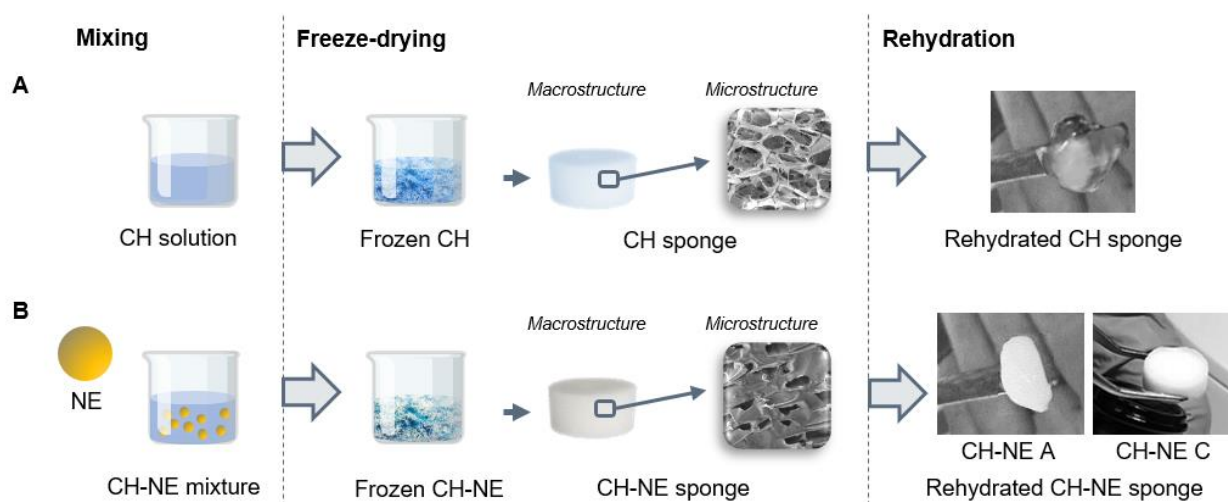


Fig. 2. Formulation process of A) chitosan (CH) sponges and B) nanoemulsion-loaded chitosan (CH-NE) sponges and their aspect after re-hydration. CH-NE A: sponge at low CH concentration (CH 0.1%- NE 2.5% w/w), CH-NE C: sponge at high CH concentration (CH 1%- NE 10% w/w). CH: chitosan (500 kg·mol⁻¹, DA 4%); NE: nanoemulsion.

Firstly, CH was solubilized in an acetic acid solution concentrated at 1% w/w. Then, NEs were added to CH solution and the CH-NEs mixture was stirred to obtain a homogeneous suspension. To produce

CH sponges (Fig. 2 A) and nanocomposite sponges (Fig. 2 B), the isotropic freeze-casting method was used [22]. By freezing the CH solution or the CH-NE mixture, a solid phase is segregated by the moving freezing front and accumulated between the growing ice crystals, thus determining the structural configuration of the final system. Dry sponges were obtained once ice has been removed by sublimation. The porosity is thus a replica of the frozen aqueous crystals. The morphology of CH sponges was examined by SEM analysis (Fig. 3).

At low CH concentration (0.1% w/w CH A series I in figure 3), CH sponges were soft and unconsolidated, presenting smooth surfaces. Entangled and non-continuous inter-pore membranes were present both at the surface (Fig. 3 I1 and 3 I2) and in the bulk (Fig. 3 I3 and 3 I4) of the sponge. As chitosan concentration increased (1% w/w CH B series III in figure 3), consolidated sponges presenting a well-defined cellular structure, interconnected pores and smooth walls were obtained (Fig. 3 III1 to 3 III4).

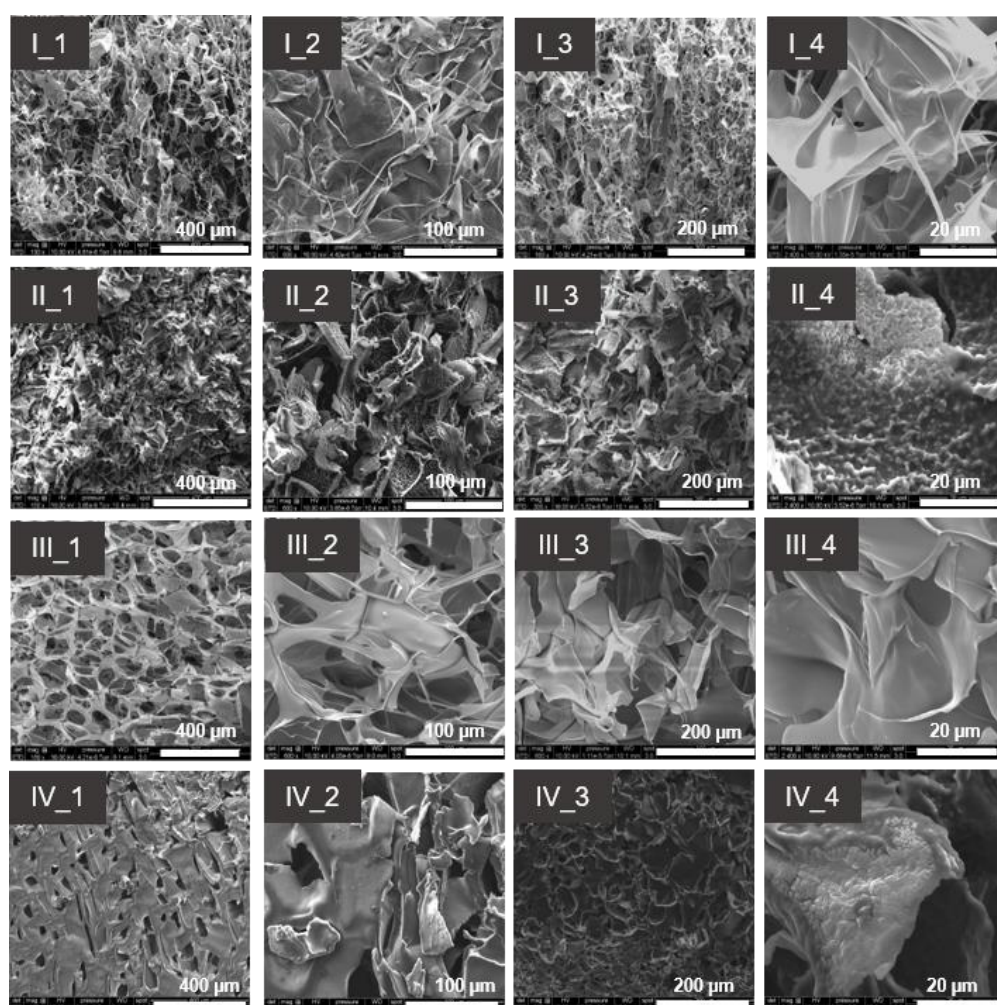


Fig. 3. SEM images of CH and CH-NE sponges. I: CH A; II: CH-NE A; III: CH B; IV: CH-NE C as defined in table 1. 1: sample surface at low magnification (scale bar: μm); 2: sample surface at higher magnification (scale bar: $100\ \mu\text{m}$); 3: Bulk of the sponge sample at intermediate magnification (scale bar: $200\ \mu\text{m}$); 4 Bulk of the sponge sample at high magnification (scale bar: $20\ \mu\text{m}$).

Upon the loading of NEs in CH, sponges presented a different organization characterized by a dense structure and rough surface (Fig. 3 II and 3 IV). Such roughness was ascribed to the accumulation of NEs on the sponge surface, as previously reported [41,42]. A further proof of concept of the NE presence in the nanocomposite sample was obtained through TEM images (Fig. S4 in supplementary information), showing NE with hydrodynamic size of around 100 nm and spherical shape. At high NE/CH ratio of 25 (CH 0.1% w/w, CH-NE A) the CH inter-pore membranes were entirely covered in NEs because of the excess of NE present (Fig. 3 II). In turn, at NE/CH ratio of 10 (CH 1% w/w, CH-NE C) the NE accumulated on CH walls while maintaining the sponge porous structure (Fig. 3 IV). Optical images showed that the depth of the pores at the sponge surface decreased in presence of NE in a NEs concentration-dependent manner (535 μm in CH B vs 146 μm in CH-NE B and 90 μm in CH-NE C sponges, Fig. 4). Apparently, the presence of NEs was concomitant with a higher ice nucleation during the freezing process which led to the formation of small ice crystals and consequently small pores in the sponges [43].

Overall, the amount of CH and NEs played an important role in determining the final morphology of systems. CH concentration determined the porous structure of sponges (CH B), while the NEs were adsorbed onto the CH walls of the sponge network.

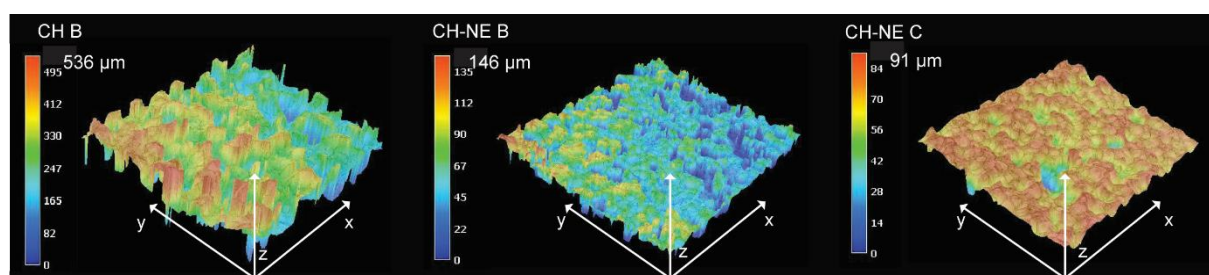


Fig. 4. Optical images of CH B and CH-NE sponges (CH-NE B and CH-NE C). The z-axis values 535 μm , 146 μm and 90 μm represent the maximum depth of the pores on the sponge surface.

III.3.4. Sponges rehydration: water uptake capacity

CH and CH-NEs sponges were rehydrated in PBS and FaSSIF-V2. PBS was used to mimic ion concentration, osmolarity, and pH of human body fluids and FaSSIF-V2 to mimic the physiological composition of human intestinal fluid [44]. The pH was set at 5, 5.5 and 7.5 for both media: such pH range covers the apparent pKa of CH (~6.2) and simulates *in vitro* the human intestinal luminal pH in both healthy (pH of 5.5 in the small bowel and 7.5 in the colon) and inflammatory conditions (reduced pH values mostly in the colon) [3].

Upon rehydration in PBS media, pure CH sponges (0.1% w/w CH A and 1% w/w CH B) dissolved at pH values (pH 5 and 5.5) below the pKa CH (Fig. 5 A). The protonation of amine groups of chitosan allowed its progressive re-dissolution in such acidic aqueous solutions. On the other hand, at pH 5.5 in FaSSIF-V2 medium and at pH of 7.5 in both PBS and FaSSIF-V2, CH sponges (CH A and CH B) turned into hydrogel-like structure able to take-up high water amounts (85% water uptake in PBS at pH 7.5; 70% in FaSSIF-V2 at pH 7.5 and 5.5) (Fig. 5 A and Fig. 2).

A different trend was observed for NE-loaded sponges. When CH-NE sponges prepared at high NE/CH ratio of 25 (CH 0.1% w/w CH-NE A) were rehydrated, the macrostructure of the dry sponge collapsed and turned into a dense, aggregated system (Fig. 2). The swelling was immediate, and no further water

uptake occurred over time (Fig. 5 B). Unlike pure CH sponges (0.1% w/w CH A), CH-NE A did not dissolve at any pH up to 8 h and the complete dissolution only occurred after 24 h at pH 5, in both PBS and FaSSIF-V2 (Fig. 5 B). Instead, at lower CH-NE ratio of 2.5 and 10 (CH 1% w/w CH-NE B and CH-NE C), the macrostructure of the sponges was not altered upon rehydration (Fig. 2) and all systems became non pH- responsive, as described in details in section 3.6. NEs loading impaired the ability of the polymeric structure to retain water: 10% of water, on average, was taken-up by CH-NE sponge A (Fig. 5 B). This behaviour was related to the high apparent density and low porosity of the nanocomposite system (table 1) and it could be ascribed to the presence of NEs, which enhanced the hydrophobicity of the systems. In previous studies, the incorporation of a hydrophobic component in hydrogels was shown to decrease water uptake [45,46]. The slight reduction in water uptake over time (Fig. 5 B) could be associated with the release of the NE absorbed on the sponge surface in the rehydration medium, as highlighted in section 3.6.

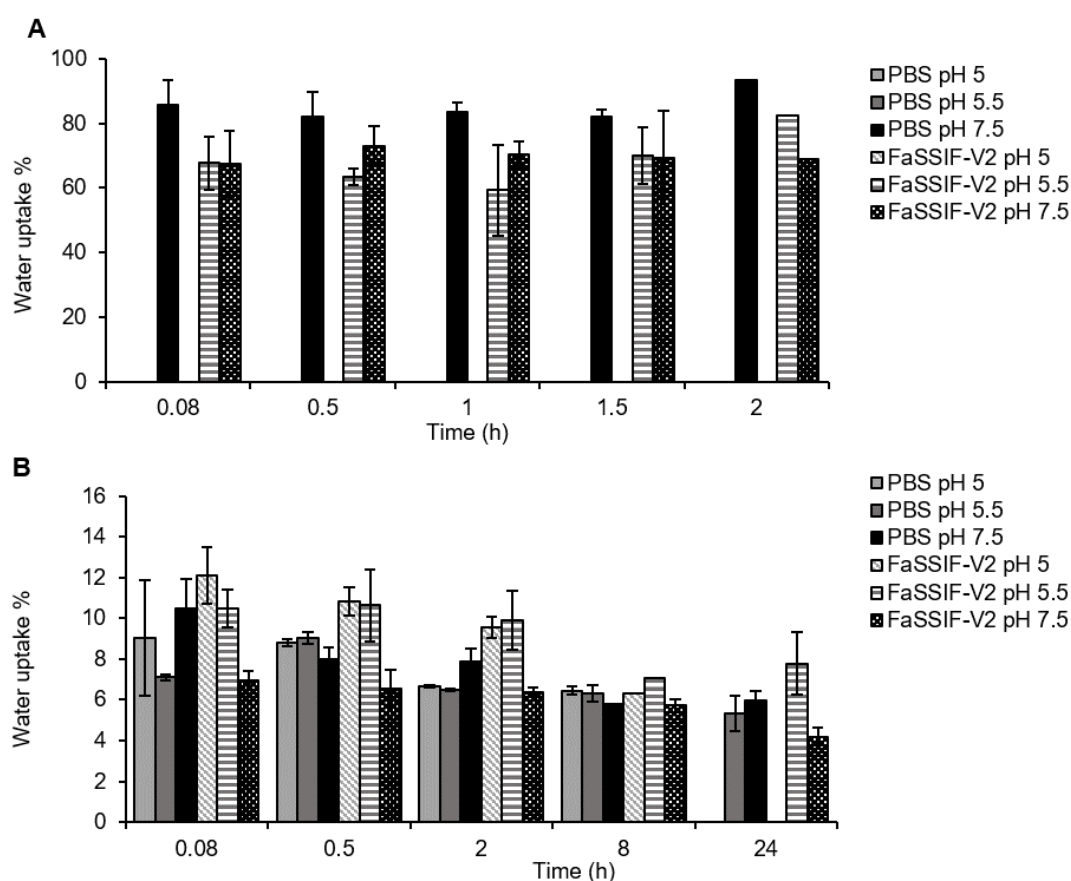


Fig. 5 A) Water uptake capacity of CH A sponge at pH 5, 5.5 and 7.5 in both PBS and FaSSIF-V2; B) Water uptake capacity of CH-NE A sponge at pH 5, 5.5 and 7.5 in both PBS and FaSSIF-V2.

III.3.5. Rheological analysis

The viscoelastic properties of rehydrated sponges were assessed through rheological measurements in dynamic mode. From amplitude sweep measurements, the linear viscoelastic region was identified at a shear strain ($\gamma\%$) range of 0.01%–100%, at angular frequency (ω) = 10 $\text{rad}\cdot\text{s}^{-1}$ and temperature of 22 °C). Thus, frequency sweep measurements were performed at $\gamma\%$ 1%, ω = 0.05–100 $\text{rad}\cdot\text{s}^{-1}$. The results obtained for sponges with and without NEs are given for ω = 1 $\text{rad}\cdot\text{s}^{-1}$ in Fig. 6.

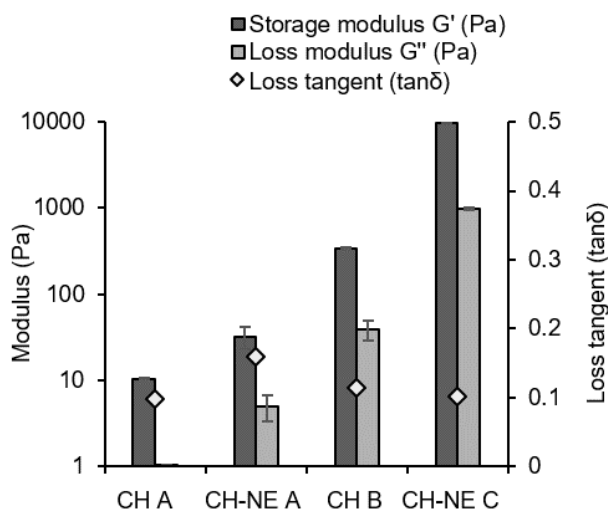


Fig. 6. Variation of G' and G'' moduli and loss tangents of rehydrated CH and CH-NE sponges (PBS pH 7.5) at different CH and NE concentrations at an angular frequency $\omega = 1 \text{ rad}\cdot\text{s}^{-1}$

The frequency sweeps always presented the same trend: the apparent moduli were nearly frequency-independent, G' was much higher than G'' , the loss tangent was always lower than 1 (Table S1), conditions that define gel-like rheological behaviour [47]. For samples obtained from CH solutions at low concentration (0.1% w/w CH A and CH-NE A), at high angular frequency ($> 10 \text{ rad}\cdot\text{s}^{-1}$), the G' and G'' moduli increased with frequency (Fig. S5). This behavior is typical of that of softer gels [48]. The G' and G'' apparent moduli were higher at higher CH concentration (CH B versus CH A Fig. 7), indicative of the improved connectivity of the sponge network (see figure 3). Moreover, values of apparent moduli were higher when CH was loaded with NEs, with increasing values at the highest NEs concentrations (10% w/w CH-NE C). In line with previous findings [49], the increase in the system stiffness along with NEs addition suggested that NEs were able to interact with CH, preventing the relaxation of CH chains under shear stress. NEs also bring hydrophobicity to the sponges and limit water uptake, thus limiting plasticization effects of chitosan by water.

In view of an intestinal delivery, the mechanical strength of rehydrated sponges is a major asset. A cohesive system, as CH-NE C, might be suitable to increase the retention time at the intestinal site by avoiding product flow together with enhancing mucoadhesion [50].

III.3.6. *In vitro* release studies

In vitro release studies of NEs from nanocomposite sponges following rehydration were carried out in PBS and FaSSIF-V2 at pH 5, 5.5 and 7.5 in order to investigate i) the role of pH and composition of release medium (destructive release studies), and ii) the influence of the sponge composition (NE/CH ratio) on the nanosystem release kinetics (cumulative release studies).

Fig. 7 A shows how pH and composition of the release medium affected NEs release (destructive release studies). The study was performed on samples at NE/CH ratio of 25 (CH-NE A). When NEs were incubated with PBS at pH 5 and 5.5, 65% of NEs were released within 8 h (Fig. 7 A). In the case of PBS at pH 7.5, only 47% of NEs were released over the same experimental period. This release behaviour at

pH values lower than the pKa of CH (6.2) can be related to the protonation of CH amino groups, resulting in the increase of CH solubility, which weakens the structure of the sponge.

In the release study performed in FaSSIF-V2 at pH 5, 5.5 and 7.5, 50% of NEs were released over 8h of incubation irrespective of the medium pH. After 24 h the CH sponge completely dissolved and 100% of NEs were released at pH 5 in both PBS and FaSSIF-V2 (Fig. 7 A). Lower release rates were observed at the two other pH: 80% release at pH 5.5 in PBS, 50% release at pH 5.5 and pH 7.5 in FaSSIF-V2 (Fig. 7 A). From these results, we determined the impact of the intestinal medium composition on the system behaviour. FaSSIF-V2 contains amphiphilic molecules, such as sodium taurocholate (NaTC) and lecithin, able to interact with the nanocomposites, thus increasing the hydrophobicity of the sponge and slowing down the release rate. Lecithin can have affinity for the hydrophobic regions formed by the hydrophobic interactions NEs-CH and NEs-NEs [51,52]. Diversely, NaTC binds strongly to the nanocomposite thanks to hydrophobic and electrostatic interactions between the negatively charged sulfonate groups of the surfactant and the amino groups of CH, which are partly protonated at pH 5 and 5.5, forming insoluble micelle-like clusters within CH beads [40].

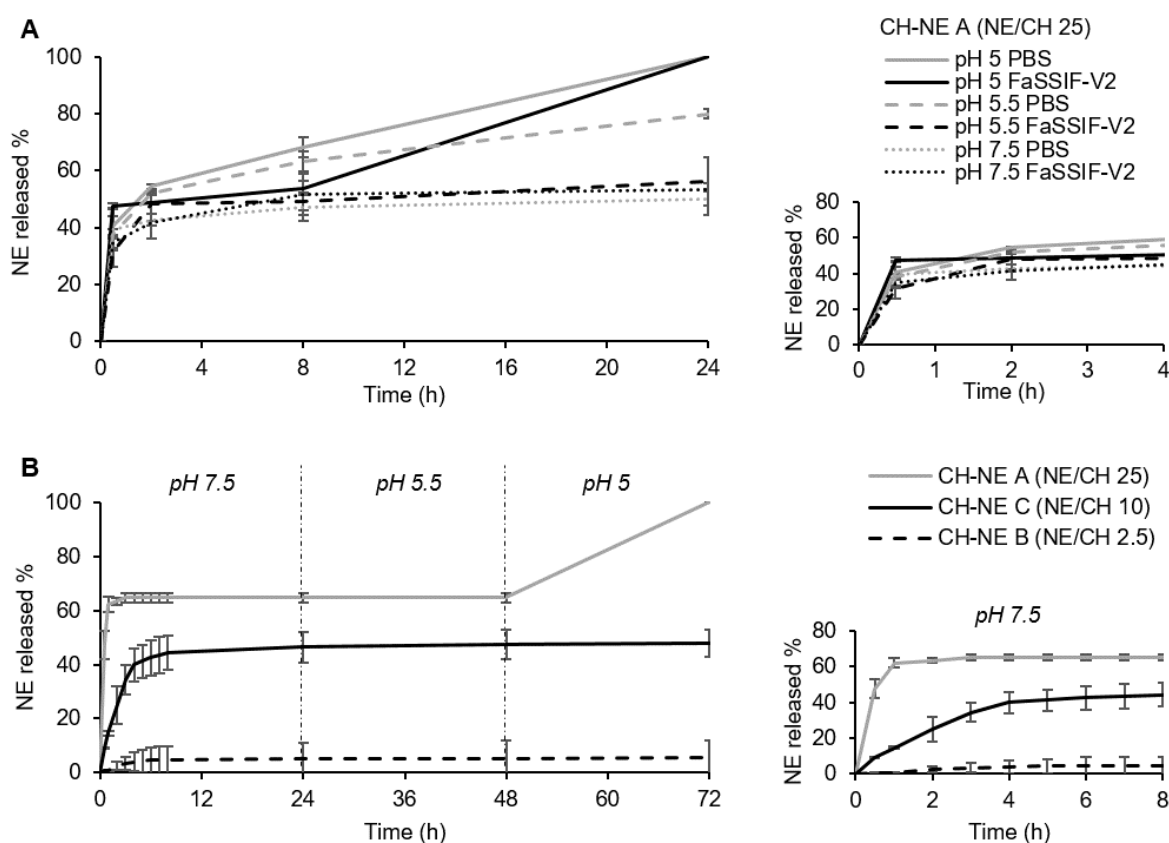


Fig. 7. A) NEs release (Nile Red-loaded NE (NR-NE), $20 \mu\text{g}\cdot\text{mL}^{-1}$) from the nanocomposite sponge CH-NE A in PBS and FaSSIF-V2 at pH 5, 5.5 and 7.5 up to 24 h; destructive release study to evaluate the effect of pH and release medium; B) NEs release (curcumin-loaded NEs (CCM-NEs), CCM $50 \mu\text{g}\cdot\text{mL}^{-1}$) from nanocomposite sponges at different NEs and CH concentrations in FaSSIF-V2 at pH 7.5 up to 24 h, pH 5.5 up to 48 h and pH 5 up to 72 h; cumulative release study to evaluate the effect of chitosan and nanoemulsions concentration.

The physicochemical properties of NEs released from the rehydrated nanocomposites were also investigated (in PBS at pH 7.5). NEs showed a slight increase in the hydrodynamic diameter (128 ± 3 nm vs 104 ± 3 nm), while ζ -potential values shifted from -9 ± 1 mV to -1.7 ± 1 mV, indicative of the absorption of some chitosan chains on the particle surface. A cumulative release study was performed to investigate the influence of the sponge composition expressed as NE/CH ratio on the release kinetic of NEs. Release studies were performed in FaSSiF-V2 and the pH was decreased from 7.5 to 5 over 72 h. As reported in Fig. 7 B, the sponge at high NE/CH ratio of 25 (CH-NE A) fastly released 47% of NEs in 30 min, reaching 65% after 3 h. When the NE/CH ratio was decreased to 10 (CH-NE C) the release became sustained. 9% of NE was released in 30 min, 34% in 3 h and a plateau at 46% was reached at 8 h. The further decrease in the NE/CH ratio at 2.5 (CH-NE B) prevented the NE release. After 24 h, the pH was lowered at 5.5 and no changes in the release profile were observed up to 48 h. Thus, at time point 48 h, the pH was further decreased until 5. The sponge at NE/CH ratio of 25 (CH-NE A) dissolved in one day and 100% of NEs was released. Instead, in the sponges at NE/CH ratio of 2.5 and 10 (CH-NE B and C) the release rate remained constant (plateau at 50% for CH-NE C). These observations suggested that part of the NE was on the bulk of the membranes constituting the pores of the sponges, while part of the NE was located at the sponge surface (see figure 3). NE could interact with the CH polymer chains via hydrogen bonding but also via hydrophobic interactions, since the CH used in this study (4% DA in the neutralized state) exhibits hydrophobicity [52]. In the sponge at high NE/CH ratio of 25 an excess of NE was present at the sponge surface and the NE completely covered the CH membranes and the sponge lost its porous nature, as highlighted by the SEM images (Fig. 3 series II). This excess of NE was easily and rapidly released from the sponge surface once in contact with the medium [53]. Then, the remaining NE was constantly released by diffusion trough the sponge creating a plateau. Instead, at a NE/CH ratio of 10, a lower amount of NE accumulated on the surface, in fact the sponge maintained its porous structure (SEM images Fig. 3 series IV and optical images Fig. 4). The main mechanism of NE release was the diffusion of the NE present in the bulk of the pore walls. The hydrogen bonds and hydrophobic interactions between CH and NEs together with the interconnected 3D network of the sponge microstructure supported the NE diffusion and led to a controlled and prolonged release over time. Similarly, Kassem et al. described a sustained release of the hydrophilic drug buspirone hydrochloride from chitosan sponges by increasing the polymer concentration from 0.5% to 2% thus decreasing the ratio between drug and polymer [23]. The absence of release in CH-NE B sponge suggested that when the NE/CH ratio was low (NE/CH 2.5) all the NE were entrapped in the sponge structure, supposedly strongly interacting with the CH polymer chains. Complete NE release of 100% was achieved only in the sponge at high NE/CH ratio of 25 (CH-NE A) when the pH was shifted towards acidic value of 5 due to the sponge dissolution and massive release of particles from the surface of the sponge walls. Possible reasons of the CH-NE A sponge dissolution are i) the lower CH concentration in the initial suspension that led to lower thickness of the interpore membranes and to a higher amount of NE in the bulk of pore membranes, and ii) the modification of the crystalline structure of CH in presence of NE governed by the NE/CH ratio [52]. Further evaluation of the nanocomposite crystallinity will assist in gaining a better understanding of the NE release kinetics. Thus, in sponges CH-NE B and C, 100% of release could be achieved only after degradation in the colon by bacterial enzymes and human chitinases [2].

Overall, these results showed that by varying the NE/CH ratio we were able to modulate the release rate of NEs. Several strategies have been reported in the literature to tune the release of nanosystems from their composite systems as i) the modulation of the degree of cross-linking in polymeric hydrogels [54,55], ii) the *in situ* hydrogelation of polymers followed by their selective pH triggered degradation [18], iii) the chemically-driven erosion of the nanocomposite hydrogel network at the site of action [56]. In this work a sustained release was obtained by loading NEs in CH sponges at NE/CH ratio of 10 (CH-NE C). These CH sponges offer the advantages of protecting NEs from the harsh environment of the GI tract and they can tackle shortcomings related to the pH-dependent strength of CH-based materials, such as the rapid dissolution and the immediate release of the associated nanosystem [57]. The sustained NE release and the mechanical strength provided by the NE presence in the bulk of the pore walls, the stability over the full intestinal pH range (5 to 7.5) and the CH mucoadhesive potential made the developed nanocomposite sponges (CH-NE C) the preferred candidate for enhancing the intestinal residence and the delivery performance *in vivo*.

III.3.7. *In vitro* cytotoxicity

Cell viability assays were carried out in order to evaluate the cytocompatibility of blank NEs on two separate intestinal cell lines, the HCT 116 and the Caco-2. Human colon carcinoma Caco-2 cells are commonly used as a model of intestinal barrier since upon differentiation they express a phenotype comparable to enterocytes [58]. Human colorectal carcinoma HCT 116 cells are considered a model of colon cancer primary cells [59]. The *in vitro* cell viability assay was conducted by exposing both cell lines to NEs for 3 and 24 h in concentrations ranging from 1250 to 0.62 $\mu\text{g}\cdot\text{mL}^{-1}$ (Fig. 8). The minimum level acceptable of cell viability in cytotoxicity tests was fixed at 70% according to ISO 10993 [60].

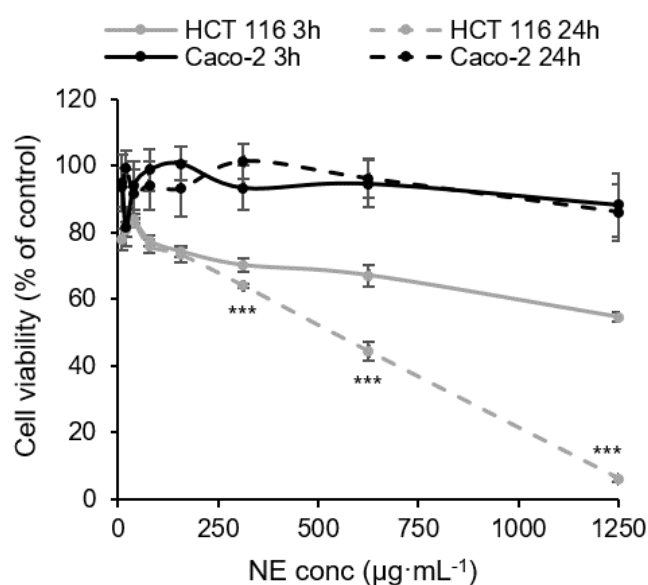


Fig. 8. Cell viability of HCT-116 and Caco-2 cells after exposure to blank NE for 3h and 24h. Statistical data analysis: $p < 0.05 = *$; $p < 0.01 = **$; $p < 0.001 = ***$; $\geq 0.05 =$ not significant.

After the first 3 h, for the HCT 116 cells, blank NEs did not show signs of cytotoxicity with a cell viability above 80% up to 625 $\mu\text{g}\cdot\text{mL}^{-1}$, while NEs were toxic at the higher concentration used (1250 $\mu\text{g}\cdot\text{mL}^{-1}$, $p=0.01$). A time-dependent decrease in the viability of HCT 116 cells was observed. After 24

h blank NE showed toxicity at concentration higher than $156 \mu\text{g}\cdot\text{mL}^{-1}$, being the IC₅₀ value of $336 \mu\text{g}\cdot\text{mL}^{-1}$. The value of IC₅₀ of the blank NE was similar to the ones previously reported for lipid nanocapsules [59], polymeric nanocapsules [61,62] and solid lipid nanoparticles [63] when evaluated on the same colon cancer cell line (HCT-116).

Regarding to the Caco-2 cell line, their viability remained higher than 80% even at higher NE concentrations ($1250 \mu\text{g}\cdot\text{mL}^{-1}$) for both time points tested, in accordance with other studies [15,64].

The difference in cytotoxicity between the two cell lines can be ascribed to the different % of FBS used. In the case of HCT 116 cells a 2% of FBS was required to ensure cell growth. While in the case of Caco-2 cells the % of FBS was 10%.

Overall results showed that the cytocompatibility of the NE here developed was in an acceptable range and opened the way to its future use as delivery system for systemic or localized treatment. Since the cell viability might be altered by the shielding effect of the CH sponge, future studies will investigate the toxicity profile of the developed nanocomposite.

III.3.8. *In vivo* biodistribution and transit studies in mice

A variety of methods has been reported in the literature for assessing GI transit times, motility, and drug release. *In vivo* biodistribution studies using fluorescent or radio-labelled nanoparticles have been largely described to localize the nanosystems in the GI tract [62]. In this work, we evaluated the residence time of fluorescent DiD-labelled CH-NE mixture (before freeze-drying) and CH-NE sponges in the GI tract by near-infrared fluorescence imaging following oral administration to healthy mice. DiD-loaded NEs were also used as control. Observations were made at 1, 2, 3, 4, and 6 h to anesthetized mice. Due to the short duration of the anaesthesia and the rapid recovery time, the effect of anaesthesia on GI motility was not expected. Time points were chosen according to previous studies considering that mice have a total GI transit time of about 6 h and that the majority of the intestinal content is located in small intestines and cecum after 3 h [65]. The *in vivo* biodistribution profiles of formulations following oral administration are shown in Fig. 9 A. A wide distribution of the fluorescent signal in the mice GI region was observed for all the systems. After 6 h, the fluorescent signal still was detected in the mice GI tract and it was more intense for CH-NE mixture and CH-NE sponge than for the NEs.

In order to perform a semi-quantitative analysis of the fluorescent dye distribution, organs were harvested and *ex vivo* images were taken (Fig. 9 B). The images collected at the different time points were processed to extract different information on residence time, targeting ability and potential toxic effect of the formulations. It was noticed that 1 h after oral gavage, NEs entered the stomach because of the intense fluorescence of almost the entire loop of small intestines and cecum. At 3 h, NEs were visualized mainly in the cecum, ascending, transverse and descending tract of the colon, and the rectum. After 6 h, only a weak fluorescent signal was still present in the small intestine while the most intense fluorescence was found in the rectum (Fig. 9 B and 10 A). A different transit time was observed when the NEs were mixed with the CH solution (CH-NE mixture). After 2 h and 3 h, an intense fluorescence signal was located in the cecum. NEs were retained up to 4 h in cecum and colon and no fluorescent signal was detected in the rectum up to 6 h (Fig. 9 B and 10 A). On the other hand, when the CH-NE-sponge was administered the intestinal residence time was considerably enhanced. The highest level of fluorescent signal was detected in the cecum up to 6 h (Fig. 9 B and 10 A). However, the fluorescence signal coming from NEs embedded in the sponge was less intense as compared to those obtained with

the NEs or CH-NE mixture. This observation suggested that the DiD fluorescence was quenched and that the NEs fluorescence intensity was underestimated in the composite formulation. Quenching typically occurs when lipophilic fluorescent labels are tightly packed together in the nanoparticle core, as previously observed for other nanocarriers [66], and it can be further enhanced by the shield effects of the macro-system [29].

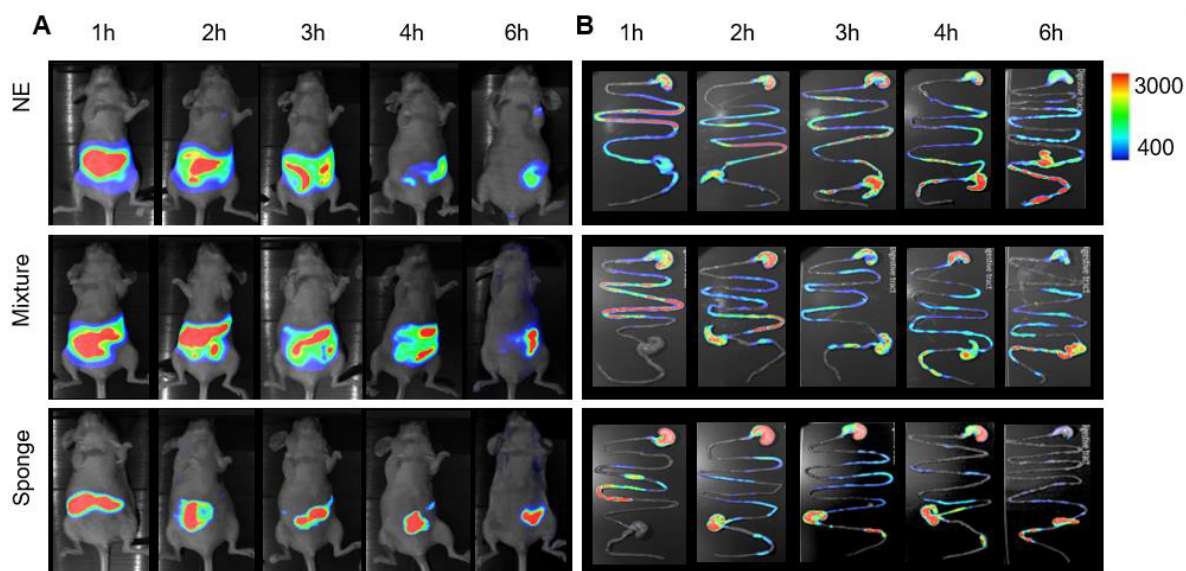


Fig. 9. A) Fluorescent images of mice whole body; B) representative *ex vivo* fluorescence images of intestines of mice sacrificed at 1, 2, 3, 4 and 6 h after oral administration of nanoemulsions (NE), CH-NE mixture (Mixture), CH-NE sponge (Sponge).

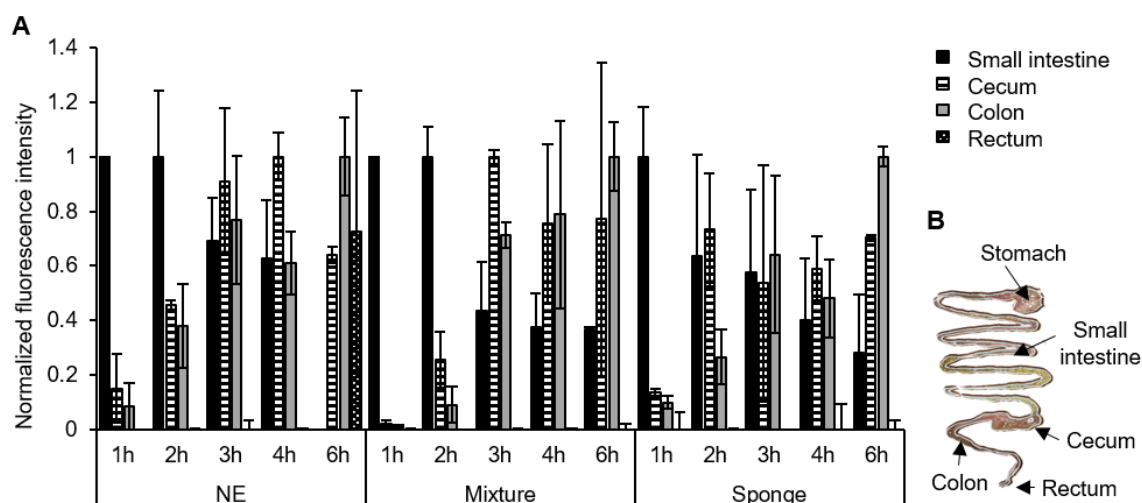


Fig. 10. A) Contents of nanoemulsion (NE), NE-loaded chitosan mixture (Mixture), NE-loaded chitosan sponge (Sponge) in different parts of the intestinal tract following oral administration at time 1, 2, 3, 4 and 6 h; B) Dissection scheme of the mouse GI tract. Statistical data analysis in supplementary information Fig. S6.

We also verified by visual inspection the absence of alteration of the intestinal mucosa indicating absence of toxicity, and preservation of the physiology and gastrointestinal integrity. Moreover, using

IVIS technique no NEs fluorescent signal was observed in other organs but the GI (no NEs detected in kidneys, liver, spleen, heart, brain, muscles, lungs, bones, skin and urine). These data suggest that the developed nanocomposite sponge can be investigated for prolonging the intestinal residence time of associated drugs thus allowing for their sustained systemic absorption or enhanced local therapeutic efficacy in the case of inflammatory intestinal pathologies [67].

Targeting of nanoparticles to the intestine has been extensively studied as a method to potentially enhance drug systemic absorption or maximize delivery in a specific GI site. However, due to the unique and diverse physiology of the GI tract, including mucus thickness and structure, numerous cell types and various physiological functions, the oral delivery of drug-loaded nanocarriers is still an open challenge. Thanks to the enhancement in the targeting ability and intestinal residence, nanocomposite can be considered as a valid candidate to boost the local effect or to enhance the systemic absorption of drugs and biologics following oral administration. Similar findings have been previously reported for nanoparticle-loaded hydrogels. Laroui et al. synthesized a cross-linked chitosan and alginate hydrogel to encapsulate nanoparticles containing the anti-inflammatory tripeptide Lys-Pro-Val (KPV) that ameliorated mucosal inflammation *in vivo* [18]. Nanoparticles containing CD98 siRNA or plasmid DNA embedded in hydrogel were also used target small and large intestine [2,3]. Finally, similar nanocomposite structure made of alginate loaded nanoparticles has been described for improving the systemic absorption of oral insulin [20].

In the present work, the mucoadhesive properties of CH were combined with the mucopenetrating ability of NEs in a single delivery system. By adhering to the mucins, CH enhanced the NEs residence time in the intestine and prolonged their retention at the mucosal surface. Hence, the NEs might act as depot, that may deliver the encapsulated drug, promoting a high drug concentration and a reduction in dosage and frequency of administration. Future examinations of nanocomposite sponge residence time in the intestinal tract will require bigger animals, such as pigs, with transit times more similar to humans [65].

III.4. Conclusions

Nanocomposites combining mucopenetrating NEs and mucoadhesive CH sponges aimed at the prolonged intestinal drug delivery by oral administration were successfully developed. The combination of mucopenetrating entities encapsulated in a mucoadhesive carrier just started to be explored. The loading of nanoparticles in a macrostructure that offers protection from the harsh GI environment and enhances the intestinal retention is still an open challenge.

In this work, NEs, synthesized via the emulsion phase inversion technique, were selected as mucopenetrating nanocarrier. The absence of surface affinity and thermodynamic interactions with mucins, together with the rapid penetration in a preformed mucin network suggested their mucopenetrating potential *in vitro*. Hence, a freeze-casting process was used to produce highly porous nanocomposite CH sponges. The structural and mechanical properties of the latter were found to be tweakable by varying CH and NEs concentration, leading to the formation of a pore-wall structure at CH amount of 1% w/w and NE/CH ratio lower than 10 (namely CH-NE C). *In vitro* release studies in a biorelevant intestinal fluid (FaSSIF-V2) highlighted the ability of sponges to release NEs in a sustained manner irrespectively of the pH of the media. This behaviour represents a great advantage for maximizing drug delivery in the intestine. The cytocompatibility of NEs was assessed on Caco-2 and HCT 116 cells. NEs proved to be non-toxic on Caco-2 cells at concentration higher than 1 mg·mL⁻¹,

while a time- and concentration-dependent inhibition of cell viability was observed on HCT 116 cells being the threshold of toxicity at $313 \mu\text{g}\cdot\text{mL}^{-1}$ after 24 h. The *in vivo* biodistribution studies in mice showed that the nanocomposite sponge greatly increased the intestinal residence time of NEs. Overall, these results proved the benefits offered by nanocomposite sponges as intestinal delivery system with a view to the local or systemic improvement in therapeutic effect.

Acknowledgements:

The research leading to these results has received funding from National Research Agency (ANR), HyDNano project (ANR-18-CE18-0025-01), the PHC Pessoa Programme between ANR and Fundação para a Ciência e Tecnologia (FCT): NanoSpeed, (N° 42306YB) and from FCT project UID/Multi/04326/2019 and from the Ministère de l'Enseignement Supérieur et de la Recherche (France).

III. References

- [1] X. Liu, C. Steiger, S. Lin, G.A. Parada, J. Liu, H.F. Chan, H. Yuk, N. V. Phan, J. Collins, S. Tamang, G. Traverso, X. Zhao, Ingestible hydrogel device, *Nat. Commun.* 10 (2019) 493. doi:10.1038/s41467-019-08355-2.
- [2] M.D. Bhavsar, M.M. Amiji, Gastrointestinal distribution and *in vivo* gene transfection studies with nanoparticles-in-microsphere oral system (NiMOS), *J. Control. Release.* 119 (2007) 339–348. doi:10.1016/j.jconrel.2007.03.006.
- [3] H. Laroui, D. Geem, B. Xiao, E. Viennois, P. Rakhya, T. Denning, D. Merlin, Targeting Intestinal Inflammation With CD98 siRNA/PEI-loaded Nanoparticles, *Mol. Ther.* 22 (2014) 69–80. doi:10.1038/mt.2013.214.
- [4] Y. Song, Y. Shi, L. Zhang, H. Hu, C. Zhang, M. Yin, L. Chu, X. Yan, M. Zhao, X. Zhang, H. Mu, K. Sun, Synthesis of CSK-DEX-PLGA Nanoparticles for the Oral Delivery of Exenatide to Improve Its Mucus Penetration and Intestinal Absorption, *Mol. Pharm.* 16 (2019) 518–532. doi:10.1021/acs.molpharmaceut.8b00809.
- [5] E. Taipaleenmäki, B. Städler, Recent Advancements in Using Polymers for Intestinal Mucoadhesion and Mucopenetration, *Macromol. Biosci.* 20 (2020) 1900342. doi:10.1002/mabi.201900342.
- [6] S. Merino, C. Martín, K. Kostarelos, M. Prato, E. Vázquez, Nanocomposite Hydrogels: 3D Polymer–Nanoparticle Synergies for On-Demand Drug Delivery, *ACS Nano.* 9 (2015) 4686–4697. doi:10.1021/acs.nano.5b01433.
- [7] S.F. Pantze, J. Parmentier, G. Hofhaus, G. Fricker, Matrix liposomes: A solid liposomal formulation for oral administration, *Eur. J. Lipid Sci. Technol.* 116 (2014) 1145–1154. doi:10.1002/ejlt.201300409.
- [8] B. Menchicchi, J.P. Fuenzalida, K.B. Bobbili, A. Hensel, M.J. Swamy, F.M. Goycoolea, Structure of Chitosan determines its interactions with mucin, *Biomacromolecules.* 15 (2014) 3550–3558. doi:10.1021/bm5007954.
- [9] S. Kootala, L. Filho, V. Srivastava, V. Linderberg, A. Moussa, L. David, S. Trombotto, T. Crouzier, Reinforcing Mucus Barrier Properties with Low Molar Mass Chitosans, *Biomacromolecules.* 19 (2018) 872–882. doi:10.1021/acs.biomac.7b01670.
- [10] W. Niebel, K. Walkenbach, A. Béduneau, Y. Pellequer, A. Lamprecht, Nanoparticle-based clodronate delivery mitigates murine experimental colitis, *J. Control. Release.* 160 (2012) 659–665. doi:10.1016/j.jconrel.2012.03.004.
- [11] B. Poinard, S. Kamaluddin, A.Q.Q. Tan, K.G. Neoh, J.C.Y. Kah, Polydopamine Coating Enhances Mucopenetration and Cell Uptake of Nanoparticles, *ACS Appl. Mater. Interfaces.* 11 (2019) 4777–4789. doi:10.1021/acsami.8b18107.
- [12] I. Pereira de Sousa, C. Steiner, M. Schmutzler, M.D. Wilcox, G.J. Veldhuis, J.P. Pearson, C.W. Huck, W. Salvenmoser, A. Bernkop-Schnürch, Mucus permeating carriers: formulation and characterization of highly densely charged nanoparticles, *Eur. J. Pharm. Biopharm.* 97 (2015)

- 273–279. doi:10.1016/j.ejpb.2014.12.024.
- [13] Q. Xu, L.M. Ensign, N.J. Boylan, A. Schön, X. Gong, J.-C. Yang, N.W. Lamb, S. Cai, T. Yu, E. Freire, J. Hanes, Impact of Surface Polyethylene Glycol (PEG) Density on Biodegradable Nanoparticle Transport in Mucus ex Vivo and Distribution in Vivo, *ACS Nano*. 9 (2015) 9217–9227. doi:10.1021/acsnano.5b03876.
- [14] R. Nunes, F. Araújo, J. Tavares, B. Sarmiento, J. das Neves, Surface modification with polyethylene glycol enhances colorectal distribution and retention of nanoparticles, *Eur. J. Pharm. Biopharm.* 130 (2018) 200–206. doi:10.1016/j.ejpb.2018.06.029.
- [15] A. Jaradat, M.H. Macedo, F. Sousa, K. Arkill, C. Alexander, J. Aylott, B. Sarmiento, Prediction of the enhanced insulin absorption across a triple co-cultured intestinal model using mucus penetrating PLGA nanoparticles, *Int. J. Pharm.* 585 (2020) 119516. doi:10.1016/j.ijpharm.2020.119516.
- [16] S. Peers, P. Alcouffe, A. Montembault, C. Ladavière, Embedment of liposomes into chitosan physical hydrogel for the delayed release of antibiotics or anaesthetics, and its first ESEM characterization, *Carbohydr. Polym.* 229 (2020) 115532. doi:10.1016/j.carbpol.2019.115532.
- [17] E. Taipaleenmäki, G. Christensen, E. Brodzkij, S.A. Mouritzen, N. Gal, S. Madsen, M.S. Hedemann, T.A. Knudsen, H.M. Jensen, S.L. Christiansen, F.V. Sparsø, B. Städler, Mucopenetrating polymer – Lipid hybrid nanovesicles as subunits in alginate beads as an oral formulation, *J. Control. Release*. 322 (2020) 470–485. doi:10.1016/j.jconrel.2020.03.047.
- [18] H. Laroui, G. Dalmasso, H.T.T. Nguyen, Y. Yan, S. V. Sitaraman, D. Merlin, Drug-Loaded Nanoparticles Targeted to the Colon With Polysaccharide Hydrogel Reduce Colitis in a Mouse Model, *Gastroenterology*. 138 (2010) 843–853. doi:10.1053/j.gastro.2009.11.003.
- [19] M. Moaddab, J. Nourmohammadi, A.H. Rezayan, Bioactive composite scaffolds of carboxymethyl chitosan-silk fibroin containing chitosan nanoparticles for sustained release of ascorbic acid, *Eur. Polym. J.* 103 (2018) 40–50. doi:10.1016/j.eurpolymj.2018.03.032.
- [20] M. Alfatama, L.Y. Lim, T.W. Wong, Alginate–C18 Conjugate Nanoparticles Loaded in Tripolyphosphate-Cross-Linked Chitosan–Oleic Acid Conjugate-Coated Calcium Alginate Beads as Oral Insulin Carrier, *Mol. Pharm.* 15 (2018) 3369–3382. doi:10.1021/acs.molpharmaceut.8b00391.
- [21] H.A. Hazzah, R.M. Farid, M.M.A. Nasra, M.A. EL-Massik, O.Y. Abdallah, Lyophilized sponges loaded with curcumin solid lipid nanoparticles for buccal delivery: Development and characterization, *Int. J. Pharm.* 492 (2015) 248–257. doi:10.1016/j.ijpharm.2015.06.022.
- [22] M. Wang, Y. Ma, Y. Sun, S.Y. Hong, S.K. Lee, B. Yoon, L. Chen, L. Ci, J.-D. Nam, X. Chen, J. Suhr, Hierarchical Porous Chitosan Sponges as Robust and Recyclable Adsorbents for Anionic Dye Adsorption, *Sci. Rep.* 7 (2017) 18054. doi:10.1038/s41598-017-18302-0.
- [23] M.A.A. Kassem, A.N. ElMeshad, A.R. Fares, Lyophilized Sustained Release Mucoadhesive Chitosan Sponges for Buccal Bupirone Hydrochloride Delivery: Formulation and In Vitro Evaluation, *AAPS PharmSciTech.* 16 (2015) 537–547. doi:10.1208/s12249-014-0243-3.
- [24] T. De Witte, A.M. Wagner, L.E. Fratila-Apachitei, A.A. Zadpoor, N.A. Peppas, Immobilization of nanocarriers within a porous chitosan scaffold for the sustained delivery of growth factors in bone tissue engineering applications, *J. Biomed. Mater. Res. Part A*. 108 (2020) 1122–1135. doi:10.1002/jbm.a.36887.
- [25] R.C. Feitosa, D.C. Geraldés, V.L. Beraldo-de-Araújo, J.S.R. Costa, L. Oliveira-Nascimento, Pharmacokinetic Aspects of Nanoparticle-in-Matrix Drug Delivery Systems for Oral/Buccal Delivery, *Front. Pharmacol.* 10 (2019) 1057. doi:10.3389/fphar.2019.01057.
- [26] A. Martín-Illana, F. Notario-Pérez, R. Cazorla-Luna, R. Ruiz-Caro, M.D. Veiga, Smart Freeze-Dried Bigels for the Prevention of the Sexual Transmission of HIV by Accelerating the Vaginal Release of Tenofovir during Intercourse, *Pharmaceutics*. 11 (2019) 232. doi:10.3390/pharmaceutics11050232.
- [27] T. Kim, J.U. Kim, K. Yang, K. Nam, D. Choe, E. Kim, I.-H. Hong, M. Song, H. Lee, J. Park, Y.H. Roh, Nanoparticle-Patterned Multicompartmental Chitosan Capsules for Oral Delivery of Oligonucleotides, *ACS Biomater. Sci. Eng.* 4 (2018) 4163–4173. doi:10.1021/acsbiomaterials.8b00806.
- [28] Q. Zhu, J. Talton, G. Zhang, T. Cunningham, Z. Wang, R.C. Waters, J. Kirk, B. Eppler, D.M. Klinman, Y. Sui, S. Gagnon, I.M. Belyakov, R.J. Mumper, J.A. Berzofsky, Large intestine–

- targeted, nanoparticle-releasing oral vaccine to control genitoretal viral infection, *Nat. Med.* 18 (2012) 1291–1296. doi:10.1038/nm.2866.
- [29] L. Hou, Y. Shi, G. Jiang, W. Liu, H. Han, Q. Feng, J. Ren, Y. Yuan, Y. Wang, J. Shi, Z. Zhang, Smart nanocomposite hydrogels based on azo crosslinked graphene oxide for oral colon-specific drug delivery, *Nanotechnology*. 27 (2016) 315105. doi:10.1088/0957-4484/27/31/315105.
- [30] M.N. Corstens, C.C. Berton-Carabin, P.T. Elichiry-Ortiz, K. Hol, F.J. Troost, A.A.M. Masclee, K. Schroën, Emulsion-alginate beads designed to control in vitro intestinal lipolysis: Towards appetite control, *J. Funct. Foods*. 34 (2017) 319–328. doi:10.1016/j.jff.2017.05.003.
- [31] A. Rosso, G. Lollo, Y. Chevalier, N. Troung, C. Bordes, S. Bourgeois, O. Maniti, T. Granjon, P.-Y. Dugas, S. Urbaniak, S. Briançon, Development and structural characterization of a novel nanoemulsion for oral drug delivery, *Colloids Surfaces A Physicochem. Eng. Asp.* 593 (2020) 124614. doi:10.1016/j.colsurfa.2020.124614.
- [32] B. Menchicchi, J.P. Fuenzalida, A. Hensel, M.J. Swamy, L. David, C. Rochas, F.M. Goycoolea, Biophysical Analysis of the Molecular Interactions between Polysaccharides and Mucin, *Biomacromolecules*. 16 (2015) 924–935. doi:10.1021/bm501832y.
- [33] A. Mendes, J. Sevilla Moreno, M. Hanif, T. E.L. Douglas, M. Chen, I. Chronakis, Morphological, Mechanical and Mucoadhesive Properties of Electrospun Chitosan/Phospholipid Hybrid Nanofibers, *Int. J. Mol. Sci.* 19 (2018) 2266. doi:10.3390/ijms19082266.
- [34] A. Hirai, H. Odani, A. Nakajima, Determination of degree of deacetylation of chitosan by ¹H NMR spectroscopy, *Polym. Bull.* 26 (1991) 87–94. doi:10.1007/BF00299352.
- [35] A. Montebault, C. Viton, A. Domard, Physico-chemical studies of the gelation of chitosan in a hydroalcoholic medium, 26 (2005) 933–943. doi:10.1016/j.biomaterials.2004.03.033.
- [36] Y. Liu, M. Siard, A. Adams, M.L. Keowen, T.K. Miller, F. Garza, Jr., F.M. Andrews, N.P. Seeram, Simultaneous quantification of free curcuminoids and their metabolites in equine plasma by LC-ESI-MS/MS, *J. Pharm. Biomed. Anal.* 154 (2018) 31–39. doi:10.1016/j.jpba.2018.03.014.
- [37] G. Lollo, G. Ullio-Gamboa, E. Fuentes, K. Matha, N. Lautram, J.-P. Benoit, In vitro anti-cancer activity and pharmacokinetic evaluation of curcumin-loaded lipid nanocapsules, *Mater. Sci. Eng. C*. 91 (2018) 859–867. doi:10.1016/j.msec.2018.06.014.
- [38] J. Schindelin, I. Arganda-Carreras, E. Frise, V. Kaynig, M. Longair, T. Pietzsch, S. Preibisch, C. Rueden, S. Saalfeld, B. Schmid, J.-Y. Tinevez, D.J. White, V. Hartenstein, K. Eliceiri, P. Tomancak, A. Cardona, Fiji: an open-source platform for biological-image analysis, *Nat. Methods*. 9 (2012) 676–682. doi:https://doi.org/10.1016/j.jconrel.2017.12.034.
- [39] G. Ramírez-García, L. Trapiella-Alfonso, F. D’Orlyé, A. Varenne, Electrophoretic Methods for Characterizing Nanoparticles and Evaluating Their Bio-interactions for Their Further Use as Diagnostic, Imaging, or Therapeutic Tools, in: *Capill. Electromigr. Sep. Methods*, Elsevier, 2018: pp. 397–421. doi:10.1016/B978-0-12-809375-7.00019-8.
- [40] M. Thongngam, D.J. McClements, Isothermal titration calorimetry study of the interactions between chitosan and a bile salt (sodium taurocholate), *Food Hydrocoll.* 19 (2005) 813–819. doi:10.1016/j.foodhyd.2004.11.001.
- [41] T. Furst, G.R. Dakwar, E. Zagato, A. Lechanteur, K. Remaut, B. Evrard, K. Braeckmans, G. Piel, Freeze-dried mucoadhesive polymeric system containing pegylated lipoplexes: Towards a vaginal sustained released system for siRNA, *J. Control. Release*. 236 (2016) 68–78. doi:10.1016/j.jconrel.2016.06.028.
- [42] R. Ikono, N. Li, N.H. Pratama, A. Vibriani, D.R. Yuniarni, M. Luthfansyah, B.M. Bachtiar, E.W. Bachtiar, K. Mulia, M. Nasikin, H. Kagami, X. Li, E. Mardliyati, N.T. Rochman, T. Nagamura-Inoue, A. Tojo, Enhanced bone regeneration capability of chitosan sponge coated with TiO₂ nanoparticles, *Biotechnol. Reports*. 24 (2019). doi:10.1016/j.btre.2019.e00350.
- [43] S. Deville, Freeze-casting of porous biomaterials: Structure, properties and opportunities, *Materials (Basel)*. 3 (2010) 1913–1927. doi:10.3390/ma3031913.
- [44] D.M. Mudie, N. Samiei, D.J. Marshall, G.E. Amidon, C.A.S. Bergström, Selection of In Vivo Predictive Dissolution Media Using Drug Substance and Physiological Properties, *AAPS J.* 22 (2020) 34. doi:10.1208/s12248-020-0417-8.
- [45] M. Dai, X. Zheng, X. Xu, X. Kong, X. Li, G. Guo, F. Luo, X. Zhao, Y.Q. Wei, Z. Qian, Chitosan-Alginate Sponge: Preparation and Application in Curcumin Delivery for Dermal Wound Healing

- in Rat, *J. Biomed. Biotechnol.* 2009 (2009) 1–8. doi:10.1155/2009/595126.
- [46] C.A. Schoener, H.N. Hutson, N.A. Peppas, pH-responsive hydrogels with dispersed hydrophobic nanoparticles for the delivery of hydrophobic therapeutic agents, *Polym. Int.* 61 (2012) 874–879. doi:10.1002/pi.4219.
- [47] K. Almdal, J. Dyre, S. Hvidt, O. Kramer, Towards a phenomenological definition of the term ‘gel’, *Polym. Gels Networks.* 1 (1993) 5–17. doi:10.1016/0966-7822(93)90020-I.
- [48] A. Montembault, C. Viton, A. Domard, Rheometric study of the gelation of chitosan in a hydroalcoholic medium, *Biomaterials.* 26 (2005) 1633–1643. doi:10.1016/j.biomaterials.2004.06.029.
- [49] H. Liu, K. Nakagawa, D. Chaudhary, Y. Asakuma, M.O. Tadé, Freeze-dried macroporous foam prepared from chitosan/xanthan gum/montmorillonite nanocomposites, *Chem. Eng. Res. Des.* 89 (2011) 2356–2364. doi:10.1016/j.cherd.2011.02.023.
- [50] A.D. Woolfson, M.L. Umrethia, V.L. Kett, R.K. Malcolm, Freeze-dried, mucoadhesive system for vaginal delivery of the HIV microbicide, dapivirine: Optimisation by an artificial neural network, *Int. J. Pharm.* 388 (2010) 136–143. doi:10.1016/j.ijpharm.2009.12.042.
- [51] P. Knoos, A. V. Svensson, S. Ulvenlund, M. Wahlgren, Release of a poorly soluble drug from hydrophobically modified poly (acrylic acid) in simulated intestinal fluids, *PLoS One.* 10 (2015) 1–16. doi:10.1371/journal.pone.0140709.
- [52] J. Becerra, G. Sudre, I. Royaud, R. Montserret, B. Verrier, C. Rochas, T. Delair, L. David, Tuning the Hydrophilic/Hydrophobic Balance to Control the Structure of Chitosan Films and Their Protein Release Behavior, *AAPS PharmSciTech.* 18 (2017) 1070–1083. doi:10.1208/s12249-016-0678-9.
- [53] M. Goldberg, A. Manzi, E. Aydin, G. Singh, P. Khoshkenar, A. Birdi, B. LaPorte, A. Krauskopf, G. Powell, J. Chen, R. Langer, Development of a Nanoparticle-Embedded Chitosan Sponge for Topical and Local Administration of Chemotherapeutic Agents, *J. Nanotechnol. Eng. Med.* 5 (2014) 040905. doi:10.1115/1.4030899.
- [54] W. Gao, D. Vecchio, J. Li, J. Zhu, Q. Zhang, V. Fu, J. Li, S. Thamphiwatana, D. Lu, L. Zhang, Hydrogel Containing Nanoparticle-Stabilized Liposomes for Topical Antimicrobial Delivery, *ACS Nano.* 8 (2014) 2900–2907. doi:10.1021/nn500110a.
- [55] L. Racine, A. Guliyeva, I. Wang, V. Larreta-Garde, R. Auzély-Velty, I. Texier, Time-Controllable Lipophilic-Drug Release System Designed by Loading Lipid Nanoparticles into Polysaccharide Hydrogels, *Macromol. Biosci.* 17 (2017) 1700045. doi:10.1002/mabi.201700045.
- [56] W. Zhu, Y. Li, L. Liu, Y. Chen, C. Wang, F. Xi, Supramolecular Hydrogels from Cisplatin-Loaded Block Copolymer Nanoparticles and α -Cyclodextrins with a Stepwise Delivery Property, *Biomacromolecules.* 11 (2010) 3086–3092. doi:10.1021/bm100889j.
- [57] A. Worthen, K. Irving, Y. Lapitsky, Supramolecular Strategy Effects on Chitosan Bead Stability in Acidic Media: A Comparative Study, *Gels.* 5 (2019) 11. doi:10.3390/gels5010011.
- [58] Y. Sambuy, I. De Angelis, G. Ranaldi, M.L. Scarino, A. Stammati, F. Zucco, The Caco-2 cell line as a model of the intestinal barrier: influence of cell and culture-related factors on Caco-2 cell functional characteristics, *Cell Biol. Toxicol.* 21 (2005) 1–26. doi:10.1007/s10565-005-0085-6.
- [59] G. Lollo, K. Matha, M. Bocchiardo, J. Bejaud, I. Marigo, A. Virgone-Carlotta, T. Dehoux, C. Rivière, J.-P. Rieu, S. Briançon, T. Perrier, O. Meyer, J.-P. Benoit, Drug delivery to tumours using a novel 5-FU derivative encapsulated into lipid nanocapsules, *J. Drug Target.* 27 (2019) 634–645. doi:10.1080/1061186X.2018.1547733.
- [60] International Organization for Standardization, ISO 10993-1 Biological Evaluation of Medical Devices—Part, Vol. 5, Tests for in Vitro Cytotoxicity, Geneva Switz. (2009).
- [61] I. Štaka, A. Cadete, B.T. Surikutchi, H. Abuzaid, T.D. Bradshaw, M.J. Alonso, M. Marlow, A novel low molecular weight nanocomposite hydrogel formulation for intra-tumoural delivery of anti-cancer drugs, *Int. J. Pharm.* 565 (2019) 151–161. doi:10.1016/j.ijpharm.2019.04.070.
- [62] G. Lollo, A. Gonzalez-Paredes, M. Garcia-Fuentes, P. Calvo, D. Torres, M.J. Alonso, Polyarginine Nanocapsules as a Potential Oral Peptide Delivery Carrier, *J. Pharm. Sci.* 106 (2017) 611–618. doi:10.1016/j.xphs.2016.09.029.
- [63] L. Ferreira, Carneiro, Silva, Pacheco, Souza-Fagundes, Goes, Oliveira, Correa, Formation of ion

- pairing as an alternative to improve encapsulation and anticancer activity of all-trans retinoic acid loaded in solid lipid nanoparticles, *Int. J. Nanomedicine*. 7 (2012) 6011–6020. doi:10.2147/IJN.S38953.
- [64] T.J. Wooster, S.C. Moore, W. Chen, H. Andrews, R. Addepalli, R.B. Seymour, S.A. Osborne, Biological fate of food nanoemulsions and the nutrients they carry – internalisation, transport and cytotoxicity of edible nanoemulsions in Caco-2 intestinal cells, *RSC Adv*. 7 (2017) 40053–40066. doi:10.1039/C7RA07804H.
- [65] P. Padmanabhan, J. Grosse, A.B.M.A. Asad, G.K. Radda, X. Golay, Gastrointestinal transit measurements in mice with ^{99m}Tc-DTPA-labeled activated charcoal using NanoSPECT-CT, *EJNMMI Res*. 3 (2013) 60. doi:10.1186/2191-219X-3-60.
- [66] H. Zhang, S.C. De Smedt, K. Remaut, Fluorescence Correlation Spectroscopy to find the critical balance between extracellular association and intracellular dissociation of mRNA complexes, *Acta Biomater*. 75 (2018) 358–370. doi:10.1016/j.actbio.2018.05.016.
- [67] P. Luciani, A.E.H. de Mendoza, T. Casalini, S. Lang, K. Atrott, M.R. Spalinger, A. Pratsinis, J. Sobek, I. Frey-Wagner, J. Schumacher, J.C. Leroux, G. Rogler, Gastroresistant oral peptide for fluorescence imaging of colonic inflammation, *Journal of Controlled Release*. 262 (2017) 118-126. <https://doi.org/10.1016/j.jconrel.2017.07.024>

III. Supplementary information

Table S1 Viscoelastic properties of rehydrated CH and CH-NE sponges (PBS pH 7.5) at angular frequency of $1 \text{ rad}\cdot\text{s}^{-1}$.

Sample	CH-NE% (w/w)	Storage modulus G' (Pa)	Loss modulus G'' (Pa)	Loss tangent ($\tan\delta$)	Complex modulus G^*
CH A	0.1	10.5 ± 0.2	1.0 ± 0.1	0.10 ± 0.0	10.6
CH-NE A	0.1–2.5	32.3 ± 9	5.0 ± 2	0.16 ± 0.1	32.7
CH B	1	340.9 ± 13	38.9 ± 10	0.11 ± 0.1	343.1
CH-NE C	1–10	9563.4 ± 72	977.5 ± 23	0.10 ± 0.0	9613.2

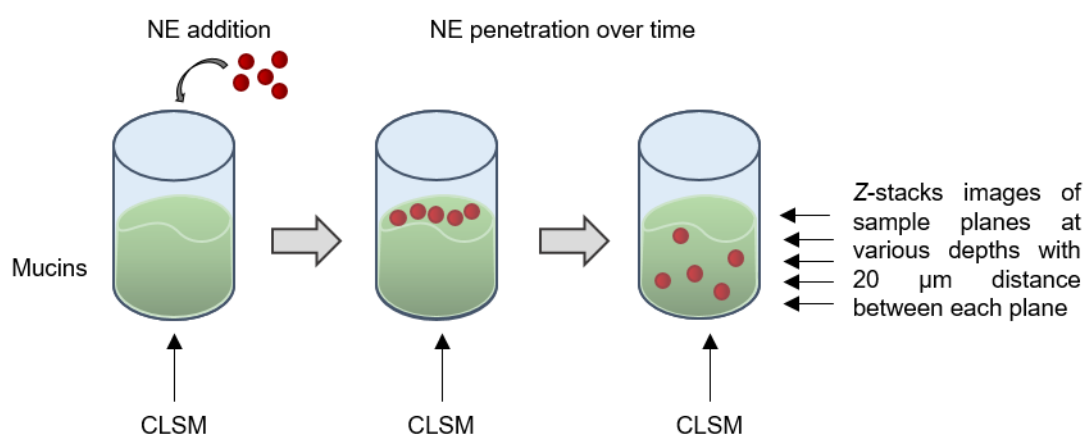


Fig. S1 Experimental setup to study the diffusion of DiD labelled-NEs (10% w/v) in artificial gastric mucin type II (10% w/v) by 3D time laps imaging using confocal laser scanning microscopy (CLSM). A defined volume of mucin solution was filled in a chamber slides resulting in an equally thick mucin layer (3 mm). Then, a predetermined volume of DiD labelled-NEs was added on the top of ASM. Z-stacks (images of planes at various depths) within the mucin sample were obtained over time at constant distance of $20 \mu\text{m}$ from the bottom of the slide.

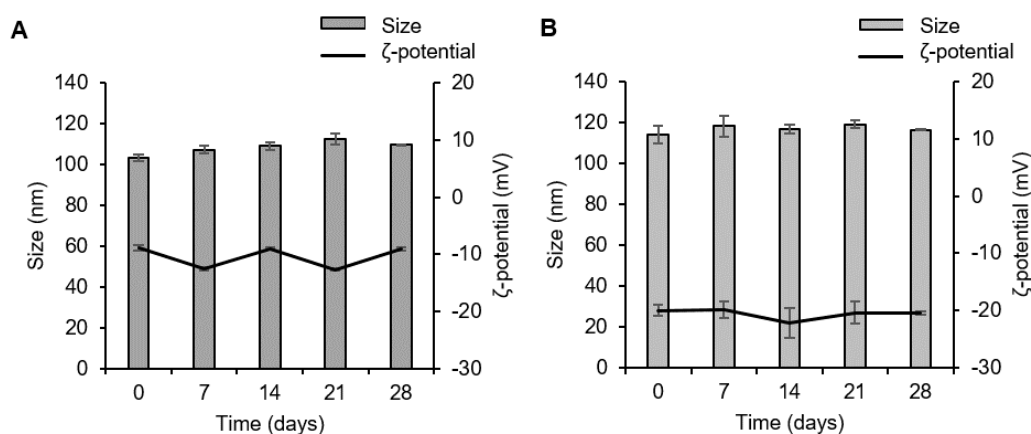


Fig. S2 Physicochemical stability over time of A) blank nanoemulsion, B) curcumin-loaded nanoemulsion ($0.5 \text{ mg}\cdot\text{mL}^{-1}$).

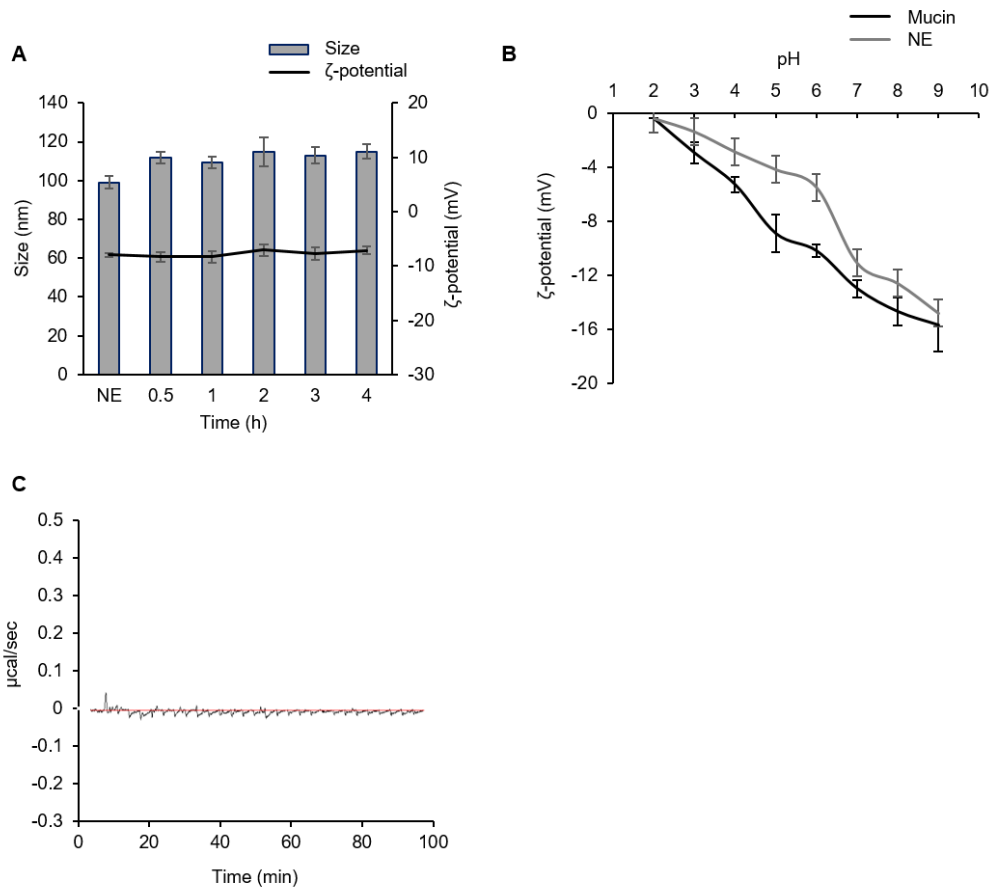


Fig. S3 A) Colloidal stability of NE (0.5% w/v) upon incubation with mucin (0.5% w/v); B) Surface charge of NEs (0.1% w/v) and mucin solutions (0.1% w/v) as assessed by DLS analysis at pH values ranging from 2 to 9 in PBS 5 mM at room temperature. The pH was varied by titration of NaOH (0.1 M) or HCl (0.1 M); C) Calorimetric raw data recorded over time by the titration of NE with mucin solutions.

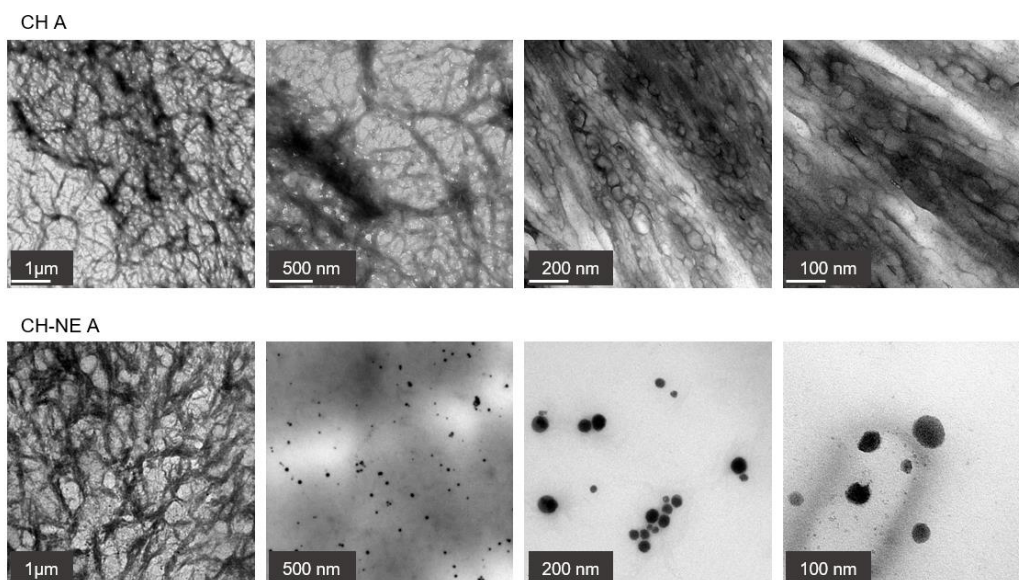


Fig. S4 TEM images of CH A and CH-NE A sponges with sample surface at 1 μm , 500 nm, 200 nm and 100 nm.

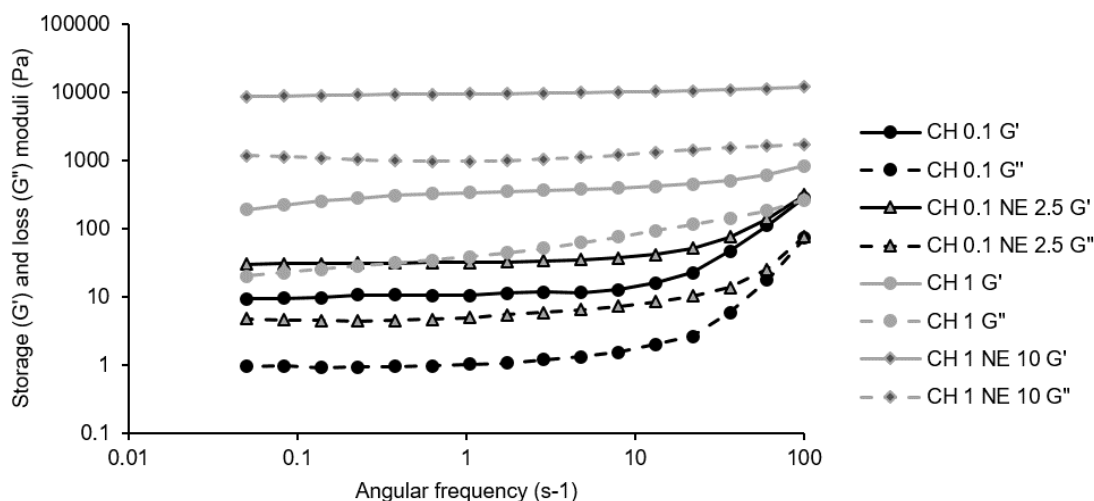


Fig. S5 Variation of G' (full lines) and G'' (dashed lines) moduli versus frequency for CH and CH-NE sponges at different CH and NE concentrations.

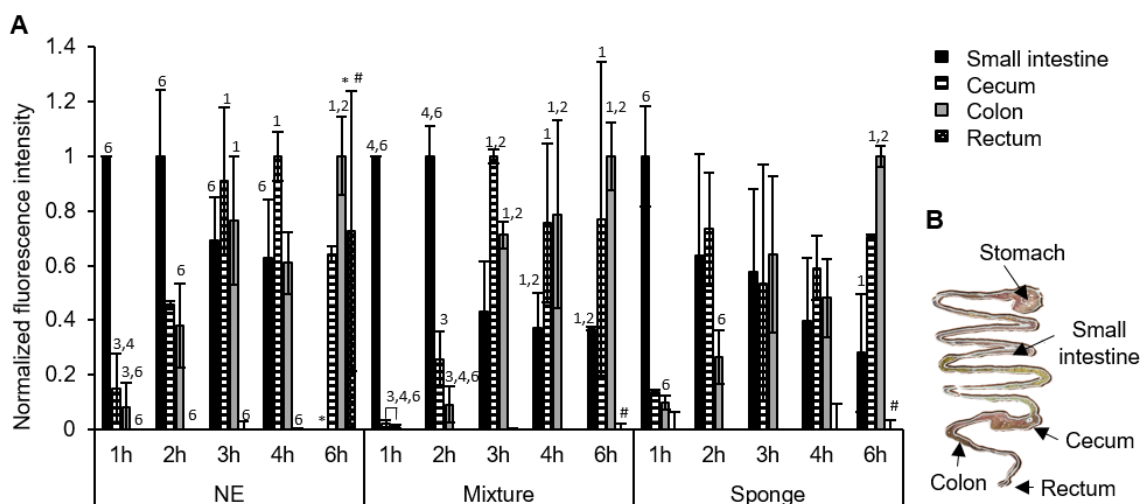


Fig. S6 A) Contents of nanoemulsion (NE), NE-loaded chitosan mixture (Mixture), NE-loaded chitosan sponge (Sponge) in different parts of the intestinal tract following oral administration at time 1, 2, 3, 4 and 6 h; B) Dissection scheme of the mouse GI tract. Statistical data analysis: * = significant difference ($p < 0.05$) from all time points within one sample (NE or Mixture or Sponge); 2 = significant difference ($p < 0.05$) from the time point 2 h within one sample (NE or Mixture or Sponge); 3,6 = significant difference ($p < 0.05$) from time points 3 h and 6 h within one sample (NE or Mixture or Sponge); # = significant difference ($p < 0.05$) from other samples at the same time point.

Chapter IV: Supersaturable self-microemulsifying delivery systems enhance oral bioavailability of a benzimidazole derivative anticancer drug.

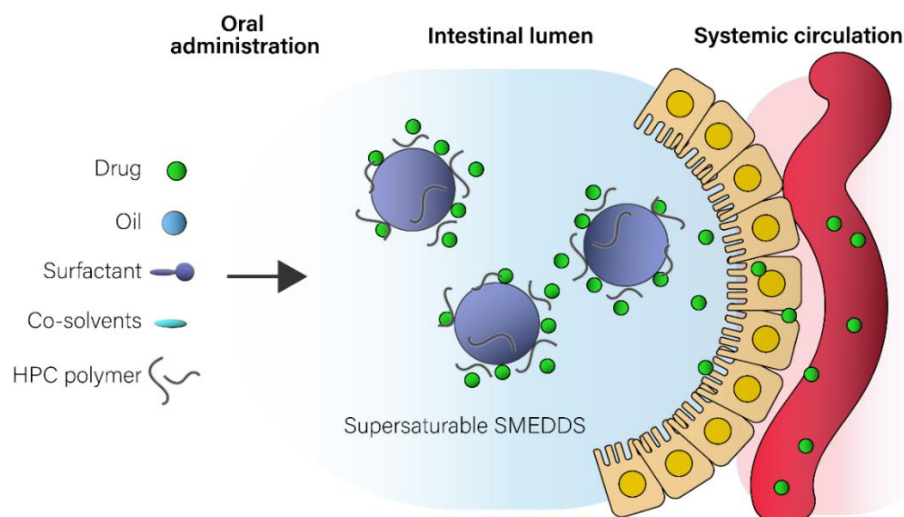
Self-microemulsifying drug delivery systems (SMEDDS) are isotropic mixtures of oil, surfactants and co-solvents that exploit the intestinal intraluminal fluids to spontaneously form microemulsions. Their combination with precipitation inhibitors in supersaturable systems can allow to increase the drug payload and to maximize and prolong intestinal absorption by balancing the need for high intraluminal drug concentrations with the guarantee of sufficient stability.

Main aim

The aim of this third chapter of the work was the design of a supersaturable SMEDDS (S-SMEDDS) to address the poor solubility and oral bioavailability of a novel lipophilic anticancer drug, BI.

Specific objectives

- Formulate and optimize SMEDDS and S-SMEDDS;
- Evaluate their stability in simulated gastrointestinal fluids;
- Study cytocompatibility and transport on the Caco2 cell line;
- Assess SMEDDS and S-SMEDDS pharmacokinetic profile following oral administration in healthy mice.



Highlights of the chapter

- SMEDDS made of Miglyol® 812, Kolliphor® RH40, Transcutol® HP, EtOH and Klucel™ EF (1%) were designed and optimized. S-SMEDDS showed a size of 19 nm, a good self-microemulsification ability and 2- to 4-folds higher drug loading capacity than SMEDDS.
- The SMEDDS and S-SMEDDS not only enhanced drug solubility, but also ameliorate intestinal permeability. They were proved to increase paracellular transport by inducing a transient opening of tight junctions on Caco-2 cell monolayers.
- A liquid chromatography-mass spectrometry (LC-MS) method for the detection of the drug in plasma was established. The method allowed to quantify low drug concentrations of $1.4 \text{ ng}\cdot\text{mL}^{-1}$ and study the pharmacokinetic profile of drug-loaded systems following oral administration in healthy mice.
- The S-SMEDDS prolonged the drug plasmatic circulation time compared to free drug and SMEDDS.

Supersaturable self-microemulsifying delivery systems enhance oral bioavailability of a benzimidazole anticancer drugs

Annalisa Rosso¹, E. Almouazen¹, J. Pontes², V. Andretto¹, M. Leroux¹, E. Romasko¹, C. Bordes¹, S. Azzouz-Maache¹, I. Coste³, T. Renno³, S. Giraud³, S. Briancon¹ and G. Lollo¹

5. University of Lyon, Université Claude Bernard Lyon 1, CNRS, LAGEPP UMR 5007, 43 Boulevard du 11 Novembre 1918, F-69622, Villeurbanne, France
6. Centre for Marine Sciences (CCMAR), Universidade do Algarve, Campus de Gambelas, 8005-139 Faro, Portugal
7. Centre de Recherche en Cancérologie de Lyon (CRCL), INSERM U1052, CNRS UMR_5286, Centre Léon Bérard, Université de Lyon (UCBL1), Lyon, France.

IV. Abstract

This study explored the design of a supersaturable SMEDDS (S-SMEDDS) to address the poor solubility and oral bioavailability of a novel benzimidazole derivative anticancer drug, BI. The SMEDDS formulation made of Miglyol® 812, Kolliphor® RH40, Transcutol® HP and ethanol, was established by a careful selection of the components through drug solubility studies and optimisation of the system via a mixture design. By adding hydroxypropyl cellulose (1% KluCEL™ EF) in conventional SMEDDS, the supersaturable system with two-fold higher loading capacity for BI was obtained. Upon dispersion in aqueous media, SMEDDS and S-SMEDDS created neutrally charge droplets of 19 nm, showing a good self-microemulsification ability and high robustness to dilution. The *in vitro* stability of the system evaluated in simulated gastric (SGF) and intestinal (SIF) fluids, highlighted the ability of S-SMEDDS to recover their physicochemical properties and avoid drug precipitation once moved from gastric to intestinal basic pH. An *in vitro* cell viability study using the Caco-2 cell line indicated the safety of the formulations up to 1 mg·mL⁻¹. Investigations on the permeability of SMEDDS and S-SMEDDS across a model of intestinal epithelium (Caco-2 monolayer) via TEER and fluorescent tracking coupled with confocal scanning laser microscopy (CLSM) analysis indicated the ability of the formulations to induce the transient opening of tight junctions. Moreover, *in vivo* studies after oral gavage in healthy mice depicted a prolonged drug plasmatic circulation time with S-SMEDDS compared to free-drug and SMEDDS. Overall, this data highlight the potential of using S-SMEDDS as alternative to conventional SMEDDS for improving the oral systemic absorption of water-insoluble drugs.

IV.1. Introduction

Pharmaceutical pipelines are highly populated with poorly water-soluble drug candidates that require novel formulation strategies to provide adequate bioavailability following oral administration. These drugs mainly belong to the Biopharmaceutical Classification System (BCS) class II (low solubility, high permeability) and IV (low solubility, low permeability) [1]. To overcome their limited solubility and bioavailability, lipid-based drug delivery systems (LBDDS) have attracted considerable attention due to their capacity to present the drug in a solubilized state in their lipid excipients, facilitating gastrointestinal absorption [2–4]. LBDDS design ranges from oil solutions to more complex systems as nanoemulsions, lipid nanocapsules and self-nano and microemulsifying drug delivery systems

(SNEDDS and SMEDDS) [5]. SNEDDS and SMEDDS are isotropic mixtures of oil, surfactants and co-solvents, that rapidly and spontaneously self-emulsify once entering in contact with aqueous fluids in the gastrointestinal tract [6–8]. Upon dispersion SNEDDS form two-phases kinetically stable nanoemulsions, while SMEDDS form one-phase thermodynamically stable microemulsions [9]. Numerous advantages are offered by SMEDDS, including i) thermodynamic stability [10], ii) small droplet size which provide a high contact surface between the drug and the intestinal mucosa maximising absorption [11], iii) simple manufacturing process and ease of scale-up [12] and iv) possible formulation into soft or hard gelatine capsule or tablets that are easy to administer orally [13,14]. Up to date SMEDDS have been exploited as delivery platform for many poorly water-soluble drugs such as the benzimidazole derivatives albendazol and olmesartan [13,15]. In particular, more than ten drugs, notably cyclosporine (Sandimmune®, Neoral®), ritonavir (Norvir®), and saquinavir (Fortovase®) are available in the market as SEDDS to improve their oral bioavailability [16]. Despite all these positive features, low drug loading, loss of drug solubilisation capacity upon dilution with body fluids, pH variations or intestinal digestion which leads to drug precipitation prior to absorption limit their application [17–19]. Therefore, supersaturable formulations have been developed by adding precipitation inhibitors to conventional SMEDDS [20,21]. The aim of the supersaturable approach is to create a supersaturated drug state upon dispersion in the GI fluids and last such condition enough to maximize absorption [16]. Pharmaceutical polymers as hydroxypropyl methylcellulose (HPMC), polyvinylpyrrolidone (PVP), hydroxypropyl cellulose (HPC), poly (acrylic acid) (PAA), polyethylene glycol (PEG) and polyvinyl caprolactam–polyvinyl acetate–polyethylene glycol graft copolymer (Soluplus®), have been used as precipitation inhibitors to kinetically or thermodynamically maintain supersaturation by inhibiting drug nucleation and crystal growth [18,19,22,23]. Their stabilisation mechanism is mainly based on the formation of hydrogen bonds or hydrophobic interactions, together with the increased system viscosity [16,20]. Previous studies with poorly water-soluble drugs such as cyclosporine A, fenofibrate, paclitaxel support the notion that supersaturable SEDDS (S-SEDDS) offer higher oral bioavailability than conventional SEDDS [19,22,24].

Based on this knowledge, we aimed at developing supersaturable SMEDDS to enhance the oral absorption of new therapeutic molecules, such as the anticancer agent BI. BI is a benzimidazole derivative with antitumor activity able to interfere with the MAPK/ERK pathway, leading to the suppression of proliferation and of resistance to apoptosis of cancer cells. Its efficacy has been proved in human cancer cell lines of lung, colon, pancreas, melanoma and sarcoma, while no activity has been observed in normal cells, highlighting its high selectivity [25]. BI belongs to BCS Class II, making it an optimal candidate for its formulation in such lipid systems.

The rationale behind this work is that by enabling higher drug load and promoting supersaturation after self-emulsification in the intestine, BI-loaded S-SMEDDS improve drug absorption and hence plasma concentrations compared to free drug and conventional SMEDDS. Firstly, SMEDDS were formulated and optimized by mean of a mixture design. Then, high payload supersaturable systems (S-SMEDDS) were prepared by incorporating HPC as viscosity enhancer and inhibitor of drug precipitation in SMEDDS. SMEDDS and S-SMEDDS were characterized in terms of physicochemical and rheological properties, self-emulsification ability, stability to dilution and efficacy in encapsulating the drug BI. *In vitro* stability tests and pH-shift experiments in simulated gastric (SGF, pH 1.2) and intestinal (SIF, pH 6.8) fluids were performed to evaluate if S-SMEDDS increased the drug concentration in solution and

hindered drug precipitation compared to conventional SMEDDS. The systems cytocompatibility and the ability to permeate across the epithelial barrier were studied *in vitro* on Caco-2 cells. Lastly, *in vivo* pharmacokinetic studies were performed after oral administration to healthy mice to determine the advantage of S-SMEDDS in enhancing the systemic absorption of BI.

IV.2. Materials and methods

IV.2.1. Materials

BI was provided by the Center for Drug Discovery and Development (C3D) platform (Centre de recherche en cancérologie de Lyon (CRCL), Lyon, France). Medium chain triglycerides, MCT (Miglyol® 812) was purchased from Cremer Oleo GmbH & Co. KG (Hamburg, Germany). Polyoxyl 40 hydrogenated castor oil (Kolliphor® RH40) and Polyoxyl 35 hydrogenated castor oil (Kolliphor® EL) were purchased from BASF SE (Ludwigshafen, Germany). Polyoxyethylene 40 stearate (Myrj® 52), formic acid (98% - 100%, LC-MS grade), glacial acetic acid, ethanol (EtOH) 96%, dimethyl sulfoxide (DMSO), sodium dodecyl sulphate (SDS), Dulbecco's modified Eagle's medium (DMEM) and Hanks' Balanced Salt solution (HBSS, modified, with sodium bicarbonate, without phenol red, calcium chloride and magnesium sulfate) were provided by Sigma-Aldrich (St Quentin-Fallavier, France). Oleoyl polyoxyl-6 glycerides (Labrafil® M1944CS), linoleoyl polyoxyl-6 glycerides (Labrafil® M2125CS), diethylene glycol monoethyl ether (Transcutol® HP) were provided by Gattefossé (Saint-Priest, France). Hydroxypropyl cellulose (HPC, Klucel™ LF and EF grades) was purchased from Ashland (Wilmington, Delaware, United States). Potassium dihydrogen phosphate and potassium chloride were purchased from Riedel-de-Haën AG (Seelze, Germany). Di-sodium hydrogenorthophosphate dihydrate was purchased from Serva Electrophoresis GmbH (Heidelberg, Germany). Hydrochloric acid 37% and sodium chloride were obtained from VWR International (Fontenay-sous-Bois, France). Dichloromethane (DCM), methanol (MeOH, HPLC grade and LC/MS grade), sodium hydroxide, DiIC₁₈(5) solid, 1,1'-dioctadecyl-3,3',3'-tetramethylindodicarbocyanine, 4-chlorobenzenesulfonate salt (DiD), 4',6-Diamidino-2-Phenylindole, Dihydrochloride (DAPI) and Promega CellTiter 96™ AQueous One Solution Cell Proliferation Assay (3-(4,5-dimethylthiazol-2-yl)-5-(3-carboxymethoxyphenyl)-2-(4-sulfophenyl)-2H-tetrazolium), MTS) were purchased from Fisher Scientific (Illkirch, France). Penicillin/streptomycin (10,000 U·mL⁻¹), foetal bovine serum (FBS), nanomycopultine from Dutscher SAS (Brumath, France). Phalloidin-iFluor™ 488 Conjugate was purchased from AAT Bioquest -Interchim (Montluçon, France). Milli-Q® water was obtained using a Milli-Q® Academic System from Merck Millipore (Saint-Quentin-en-Yvelines, France).

IV.2.2. Solubility studies of BI

Various oils, surfactants and co-solvents were screened for their ability to dissolve BI. Saturated solutions were prepared by adding an excess of BI powder (25 mg) to 500 µL of each excipient (Kolliphor® RH40, Kolliphor® EL, Myrj® 52, Transcutol® HP, EtOH, DMSO, Miglyol® 812, Labrafil® M1944CS, Labrafil® M2125CS), stirred at 750 rpm for 3 h at 37 °C and then left for 24 h to reach the equilibrium. Moreover, the solubility of BI was evaluated in phosphate buffer at pH 7.4 and 6.8, in acetate buffer at pH 4.5. An excess of BI powder was added to each solvent and samples were stirred at 600 rpm for 30 min at 37 °C. The excipients and buffers were then centrifuged at 14,000 rpm

for 15 min at room temperature to separate the precipitated drug. The supernatant (50 mg) was diluted with 2 mL of MeOH/DCM mixture (50/50 w/w) and filtered through 0.22 µm nylon syringe filter (Whatman GmbH, Dassel, Germany). The concentration of BI was determined in each of the excipients by validated high-performance liquid chromatography (HPLC) method as described in the following section (2.3.4).

IV.2.3. Development of SMEDDS formulations

IV.2.3.1. SMEDDS formulation and optimization using mixture design

The ternary phase diagram of the selected oil, surfactant, and co-solvents, each one representing an apex of the triangle, was constructed by mixing the excipients at various proportions. The self-microemulsifying region was identified by adding 900 µL of ultrapure water over 100 mg of each formulation (dilution factor 10) in a glass beaker and magnetically stirring at 100 rpm for 5 min at 37 °C in a water bath. The size of the resultant microemulsions was measured by DLS analysis.

Preliminary experiments were performed to identify the self-microemulsifying region in the ternary diagram. In this region, further investigations were achieved by the means of a mixture design in order to optimize the SMEDDS mean size. A series of 25 SMEDDS with varied concentrations of oil (Miglyol® 812: 5–70% w/w), surfactant (Kolliphor® RH40: 10–70% w/w), and co-solvents (Transcutol® HP and EtOH: 15–25% w/w at Transcutol® HP/ EtOH ratio of 50/50) were thus prepared. Aiming at a thorough investigation of the area of formation of SMEDDS droplets and at determining formulations showing the desired physicochemical attributes, a mixture design was used to model results of experiments. The upper and lower bounds on the component proportions x_i were defined according to the ternary phase diagram preliminary results and the resulting set of constraints was: $0.05 < x_{oil} < 0.30$, $0.45 < x_{surfactant} < 0.80$ and $0.15 < x_{co-solvents} < 0.25$. According to Scheffé [A], the nine design points corresponding to the 4 extreme vertices, the midpoints of the four edges and the centroid of the constrained region were chosen as the most useful points for estimating the coefficients of the special cubic polynomial:

$$\hat{Y} = \sum_{i=1}^3 b_i x_i + \sum_{i < j}^3 b_{ij} x_i x_j + b_{123} x_1 x_2 x_3 \quad \text{Eq. 1}$$

where the variable \hat{Y} corresponds to the microemulsion mean size predicted by the model.

Moreover, additional runs regularly spread over the constrained experimental domain were used as check points to assess the predictive performance of the developed model. Multiple linear regression calculations, analysis of variance (ANOVA) and residual analysis were performed with Modde® software (Umetrics, Sartorius-Stedim, Sweden).

IV.2.3.2. Supersaturable SMEDDS formulation

To prepare supersaturable SMEDDS (S-SMEDDS), two different HPC (Klucel™ LF and Klucel™ EF) at concentration of 1% and 3% (w/w) were added in the optimized SMEDDS system (F12, Table 1) by replacing the surfactant Kolliphor® RH40 (S-SMEDDS I). A second type of S-SMEDDS (S-SMEDDS II) was then prepared by substituting EtOH with DMSO. Firstly, SMEDDS were optimized on the base of the developed ternary phase diagram in order to have a limited amount of DMSO (5%) and maintain unvaried the physicochemical properties of the formed microemulsions. The optimized SMEDDS was composed of 79% Kolliphor® RH40, 7.5% Miglyol® 812, 7.5% Transcutol® HP and 5% DMSO (%)

w/w). Then, S-SMEDDS were formulated by adding Klucel™ EF at concentration of 1% (w/w) while reducing the amount of surfactant Kolliphor® RH40 (S-SMEDDS II).

IV.2.3.3. Preparation of BI-loaded SMEDDS

BI was loaded in the optimized SMEDDS (F12 Table 1) at different concentrations (SMEDDS a: 0.5 mg·mL⁻¹; b: 0.9 mg·mL⁻¹; c: 1.4 mg·mL⁻¹; d: 1.9 mg·mL⁻¹). BI was also loaded in S-SMEDDS I (Klucel™ EF 1% w/w) at a concentration of 3 mg·mL⁻¹ and in S-SMEDDS II (Klucel™ EF 1% w/w and DMSO) of 5.5 mg·mL⁻¹. Briefly, BI was dissolved in the oil-surfactant-co-solvents mixture and the system was magnetically stirred at 100 rpm for 10 min at 37 °C until a clear solution was obtained. Then microemulsions were formed by dilution with water and the droplet size was measured immediately after formulation. The samples were observed for turbidity or phase separation over a period of 48 h. The concentration of BI in SMEDDS excipients was determined by diluting 50 mg of freshly prepared mixture in 2 mL of MeOH/DCM mixture (50/50 w/w) and analysed by HPLC.

The drug loading (*DL*) was calculated as the ratio of the mass of BI loaded in SMEDDS to the total mass of SMEDDS:

$$DL(\%) = \frac{\text{mass of BI in SMEDDS}}{\text{mass of SMEDDS}} \times 100 \quad \text{Eq. 2}$$

To assess the drug encapsulation efficiency in microemulsions, which represented the solubility of BI in the microemulsion droplets, the samples were centrifuged at 10,000 rpm for 5 min at room temperature to separate the non-encapsulated drug. Then, 200 mg of the supernatant were retrieved, dissolved in 2 mL of MeOH/DCM mixture (50/50 w/w) and analysed by HPLC as described in section 2.3.4. The encapsulation efficiency (*EE*) was calculated as following:

$$EE(\%) = \frac{\text{mass of BI in microemulsion}}{\text{mass of feeding BI}} \times 100 \quad \text{Eq. 3}$$

Analyses were done in triplicate.

IV.2.3.4. HPLC determination of BI

The HPLC system for BI detection consisted of Agilent 1200 Series G1311A Quat Pump, Agilent 1200 Series G1367B HIP-ALS High Performance Autosampler, equipped with Agilent 1200 Series G1315D Dad Diode Array Detector HPLC (Agilent, Santa Clara, CA, United States). BI was separated on a reverse phase C18 column (Kinetex 5 µm C18 100 Å, 150 × 4.6 mm, Phenomenex, Torrance, CA, USA), with temperature set to 23 °C. The mobile phase was composed of MeOH/0.1% formic acid and ultrapure water/0.1% formic acid, in gradient elution mode, at a flow rate of 0.6 mL·min⁻¹. The injection volume was 5 µL and the detection wavelength was 354 nm. The total run time was 20 min. The system was managed by OpenLab CDS ChemStation Edition software (Agilent, Santa Clara, CA, United States). The HPLC method was linear ($R^2 = 0.9996$) in the concentration range of 2.5–150 µg·mL⁻¹. The method was validated according to ICH Q2(R1) guidelines [26]. Detection and quantification limits (*LOD* and *LOQ*) were 3.82 µg·mL⁻¹ and 12.74 µg·mL⁻¹, respectively.

IV.2.4. SMEDDS characterization

IV.2.4.1. Droplet size and ζ-potential measurements

Size distribution and surface potential of microemulsions were determined using Malvern Zetasizer® Nano ZS instrument (Malvern Instruments S.A., Worcestershire, UK). Particle sizes were measured by

Dynamic Light Scattering (DLS) at 25 °C at a scattering angle of 173 °. The ζ -potential was calculated from the mean electrophoretic mobility measured for samples diluted in 0.1 mM KCl. Measurements were performed in triplicate.

IV.2.4.2. Rheological analysis

The rheological tests were carried out through an MCR 302 rheometer (Anton Paar, Les Ulis, France) fitted with a 25 mm cone-plate geometry. The temperature was set at 25 °C. Approximately 300 μ L of the formulation was added to the steel Peltier plate and the head was lowered to the measurement gap of 49 μ m. Flow sweep experiments were performed with a shear rate in the range of 1 to 100 s^{-1} to measure the viscosity of blank SMEDDS, S-SMEDDS I containing Klucel™ LF or Klucel™ EF at concentration of 1% and 3% (w/w) and S-SMEDDS II. All measurements were performed in triplicates.

IV.2.4.3. Determination of self-emulsification time

The emulsification time of SMEDDS and S-SMEDDS was assessed by measuring the time (s) required to obtain a clear dispersion. Ultrapure water was added dropwise onto the SMEDDS mixture (dilution factor 10) under gentle magnetic stirring (100 rpm) in a water bath at 37 °C.

IV.2.4.4. Effect of dilution on SMEDDS

The impact of SMEDDS dilution on microemulsion formation was studied by diluting SMEDDS 5, 10, 20 and 100 times with ultrapure water. Experiments were performed under gentle magnetic stirring (100 rpm) in a water bath at 37 °C. The droplet diameter of microemulsions was determined and samples were observed for any sign of phase separation over 24 h.

IV.2.5. Stability studies in simulated gastrointestinal fluids

The colloidal stability of BI-loaded SMEDDS a, SMEDDS b, SMEDDS c, S-SMEDDS I and S-SMEDDS II was evaluated in simulated gastric fluid (SGF) at pH 1.2 (dilution factor 10).

The colloidal stability of BI-loaded SMEDDS c, S-SMEDDS I and S-SMEDDS II was evaluated in simulated intestinal fluid (SIF) at pH 6.8 (dilution factor 10). Both SGF and SIF did not contained enzymes and were prepared in accordance with the guidelines of the Ph. Eur. 9th. All samples were kept under continuous stirring (100 rpm) in a water bath at 37 °C for the whole period of analysis. The droplet size and PDI of microemulsions in both SGF and SIF were measured by DLS analysis at time points 0, 60, 120 and 180 min.

In the case of microemulsions in SGF, the BI encapsulation efficiency was also assessed at time points 0, 60, 120 and 180 min by mean of HPLC, as explained in section 2.3.4.

Subsequently, the pH was shifted from acid to alkaline to simulate the pH changes in the GI tract. BI-loaded SMEDDS c), S-SMEDDS I and S-SMEDDS II were dispersed in SGF at pH 1.2 (dilution factor 10, time point 0). Then, the pH was increased by titration with 1M NaOH solution (final pH of 11, time point 10 min). At predetermined time points (0, 10, 30, 60, 120, 180 and 360 min) the samples were withdrawn, the microemulsions size was analysed by DLS, and the BI encapsulation efficiency was assessed by HPLC, as explained in section 2.3.4.

IV.2.6. *In vitro* studies on Caco-2 cells

IV.2.6.1 Cell culture conditions

Human colon carcinoma (Caco-2) cells were used to perform the MTS (3-(4,5-dimethylthiazol-2-yl)-5-(3-carboxymethoxyphenyl)-2-(4-sulfophenyl)-2H-tetrazolium) assay. Caco-2 cells were cultured in 75 cm² flasks, at 37 °C in a humidified atmosphere 5% CO₂ and 95% air incubator. Cell culture medium was DMEM, supplemented with 10% (v/v) FBS, 2% (v/v) penicillin/streptomycin and 1% nanomycopulitine. The medium was exchanged every two days.

IV.2.6.2 *In vitro* cell viability studies

The effect of drug-loaded SMEDDS and S-SMEDDS I on the viability of Caco-2 cells was evaluated by the MTS assay. 1x10⁴ cells/well were seeded in 96-well plates and maintained for 48 h at 37 °C, 5% CO₂. Then, the culture medium was removed and cells were treated with increasing concentration of drug-loaded SMEDDS c, S-SMEDDS I and free drug in ethanol diluted with pre-warmed DMEM supplemented with 10% of FBS (v/v) to obtain a drug concentration range from 0.63 to 10 µM. Blank SMEDDS and S-SMEDDS I were also tested to assess the cytocompatibility of systems without the drug. DMEM was used as positive control (100% viability), while SDS (3%, w/v) as negative control. Cells were exposed to the formulations for 24 h at 37 °C, 5% CO₂. After the considered period, samples were replaced with 100 µL of fresh medium added of 20 µL of MTS solution in each well. The plates were incubated for 4 h at 37 °C. The absorbance was measured spectrophotometrically (Multiskan EX, Thermo Fisher Scientific, France) at 492 nm, with background correction at 620 nm. The study was performed in triplicate.

Cell viability was calculated by the following formula (*Abs* = absorbance):

$$\text{Cell viability (\%)} = \frac{\text{Abs sample} - \text{Abs SDS}}{\text{Abs DMEM} - \text{Abs SDS}} \times 100 \quad \text{Eq. 4}$$

IV.2.6.3 Transport of SMEDDS and S-SMEDDS across Caco-2 cell monolayers

Caco-2 cells were seeded at a density of 2.5x10⁴ cells/cm² onto Transwell inserts (1 x 10/8 cm² pore density, 0.4 µm pore size, polyethylene terephthalate (PET) membrane, ThinCert™ Greiner Bio-One, Les Ulis, France) in 24-well tissue culture plates (Cellstar® Greiner Bio-One, Les Ulis, France). The cells were grown in a DMEM culture media containing 10% FBS for 21 to 26 days at 37 °C, 5 % CO₂ for them to differentiate so as to morphologically resemble the enterocytes of the small intestine, presenting the characteristic tight junctions, microvilli and brush-border [27-28]. During the period of growth, the media was initially replaced after 5 days and subsequently it was changed every 2 days. Cell differentiation was evaluated by transepithelial electrical resistance (TEER) measurements in an apical to basolateral direction using a Millicell® ERS-2 Voltohmmeter (Merck Millipore, Darmstadt, Germany). Caco-2 monolayers were used when TEER values were around 300 Ω·cm².

Apical-to-basolateral transport experiments across the Caco-2 monolayers were carried out. To this aim the growth medium was removed, replaced with HBSS and cells were incubated for 30 min at 37 °C, 5% CO₂. The HBSS medium was supplemented with glucose (25 mM). The SMEDDS and S-SMEDDS were stained with the fluorescent dye DiD (2 mg·mL⁻¹) in order to quantify the transport by fluorescence spectroscopy. DiD-stained SMEDDS and DiD-stained S-SMEDDS microemulsions were formulated in HBSS with SMEDDS and S-SMEDDS final concentrations of 1 mg·mL⁻¹, selected on the base of cell viability studies, and DiD concentrations of 1 µg·mL⁻¹. Then, 150 µL of HBSS containing the DiD-

stained SMEDDS or DiD-stained S-SMEDDS microemulsions were added to the apical compartment of the inserts. The basolateral compartment was filled with 1 mL of HBSS. The experiments were performed in triplicate.

After 2 h and 4 h of incubation at 37 °C 5% CO₂, the medium in the basolateral compartment was collected and the amount of DiD-stained SMEDDS and DiD-stained S-SMEDDS was quantified via fluorescent measurements using a Spark® multimode microplate reader (Tecan Trading AG, Männedorf, Switzerland). The excitation and emission wavelengths were 635 nm and 720 nm respectively. HBSS was used as negative control, while DiD-stained SMEDDS and DiD-stained S-SMEDDS were used as positive control.

IV.2.6.4 Measurement of the Transepithelial Electrical Resistance

TEER measurements were performed all along the transport studies. in order to gain information on the potential route of transport (transcellular or paracellular). As a reference, TEER values of the cell monolayers were measured just before adding the formulations. Then, once the cells incubated with DiD-stained SMEDDS and DiD-stained S-SMEDDS, TEER values were recorded at 2 and 4 h. The TEER of monolayers incubated with HBSS were measured as a control. After 4 h, the tested formulations were removed and replaced by fresh DMEM in order to check the TEER values at 24 h after exposure to SMEDDS and S-SMEDDS. Each TEER value was calculated as a percentage of the initial TEER value. The experiments were performed in triplicate.

IV.2.6.5 Localization of SMEDDS and S-SMEDDS in Caco-2 cell monolayers

DiD-stained SMEDDS and S-SMEDDS were tested for their cell association and internalization across the Caco-2 cell monolayers. The localization of samples in Caco-2 cell monolayers was studied qualitatively by confocal laser scanning microscopy (CLSM). The inserts obtained from the permeability studies were fixed in 4% (v/v) paraformaldehyde (PFA). After 24 h storage at 4 °C, the cells were washed with PBS and permeabilized with 0.1% Triton X-100 (Sigma Aldrich, USA) in PBS for 5 min. The tight junctions were then stained with Phalloidin-iFluor™ 488 Conjugate in PBS (16 µM) for 20 min. After 5 cycles of washing, nuclei were stained with DAPI in PBS (25 µg/mL) for 10 min. Cells were rinsed with PBS twice. The inserts were then cut and stained cells were imaged on a Leica TCS SP5 X confocal microscope (Leica Microsystems, Mannheim, Germany). Images were analysed with the Fiji ImageJ software [29] for background correction.

IV.2.7. *In vivo* pharmacokinetic study

IV.2.7.1. SMEDDS and S-SMEDDS administration and blood collection

Mouse experiments were conducted in agreement with the local ethics committee (CECCAPP, Comité d'Evaluation Commun au PBES, à AniCan, au laboratoire P4, à l'ENS, à l'IGFL), authorization number #10386. Female nude mice (average body weight of 19-20 g) used for the *in vivo* pharmacokinetic study were obtained from Charles River Laboratories (Saint-Germain-Nuelles, France). Mice were housed in clean polypropylene cages (5 mice/cage) with the commercial pellet diet and water *ad libitum* at 22 ± 2 °C and kept on a 12 h light/dark cycle. Prior to oral gavage, animals were fasted for 12 h. The mice were randomly divided into four groups (n= 3 for each group) corresponding to 4 formulations: i) BI-loaded SMEDDS c (14 mg·kg⁻¹ of BI), ii) BI-loaded S-SMEDDS I (30 mg·kg⁻¹ of BI), iii) BI-loaded S-

SMEDDS II (55 mg·kg⁻¹ of BI), iv) BI dispersion in HPC (40 mg·kg⁻¹ of BI). After oral gavage mice were housed one per cage and food was given them back. At time points 0, 0.25, 0.5, 1, 3, 6, 8, and 24 h blood samples (100 µL) were collected intracardially or retro-orbitally. Experiments were ended at time point 6 h for the mice receiving HPC dispersion and SMEDDS c (groups iv and i). Blood samples were immediately centrifuged at 40,000 rpm for 15 min at 4 °C, and the separated plasma was stored at -20 °C until analysis.

IV.2.7.2. Plasma sample extraction and analysis

Prior to extraction, frozen plasma samples were thawed at ambient temperature. Mouse plasma (50 µL) was mixed with 450 µL of MeOH and samples were vortexed for 20 s. The mixture was centrifuged at 10,000 rpm for 10 min at 4 °C. The supernatant was filtered on a 0.22 µm Nylon filter and injected in HPLC-MS for the analysis using the same conditions as in section 2.7.2.

IV.2.7.3. Development of LC-MS analysis of plasma samples

The LC-MS method was established to quantify BI in plasma, using an Agilent InfinityLab Liquid Chromatography/Mass Selective Detector (LC/MSD) system equipped with an electrospray ionization (ESI) source (Agilent, Santa Clara, CA, United States). Chromatographic separation was achieved on a HPLC reversed phase C18 column (Zorbax RRHD SB-C18, 2.1×50 mm, 1.8 µm, Agilent, Santa Clara, CA, United States) maintained at 40 °C. The separation was accomplished using water as mobile phase A (30%) and MeOH as mobile phase B (70%) in isocratic elution mode at a flow rate of 0.4 mL·min⁻¹. The injection volume was 5 µL and the total run time 10 min. The mass spectrometer was operated in positive ionization mode with fragmentation and capillary voltage set at 240 and 4 kV, respectively. Protonated BI was quantified in the selected-ion monitoring (SIM) mode at m/z 388.2 (M+H)⁺. The system was controlled by OpenLab CDS ChemStation Edition for LC&LC/MS Systems software (Agilent, Santa Clara, CA, United States). In order to prepare standard curves, 50 µL of BI stock solution in MeOH were mixed with 50 µL of blank plasma, samples were vortexed for 20 s, then 400 µL of MeOH were added and samples were vortexed again for 20 s. The mixture was centrifuged at 10,000 rpm for 10 min at 4 °C. The supernatant was filtered on a 0.22 µm nylon filter and injected in HPLC-MS for the analysis. Analysis were done in triplicate. The BI calibration curve was linear ($r^2 = 0.997$) over the concentration range 1.4–240 ng·mL⁻¹.

IV.2.7.4. Pharmacokinetic data analysis

Pharmacokinetic data were treated by non-compartmental analysis of the percentage of the administered dose versus time profiles with Kinetica 5.1 software (Thermo Fischer Scientific, France). The maximum BI plasma concentration (C_{\max}) and the time taken to reach the maximum plasma concentration (T_{\max}) were determined from the individual plasma concentration vs time curves. The elimination half-life ($t_{1/2}$) was calculated as follows:

$$t_{1/2} = \frac{\ln 2}{K_e} \times 100 \quad \text{Eq. 5}$$

where K_e is the elimination rate constant.

The trapezoidal equation was used to calculate the area under the curve (AUC) during the whole experimental period (AUC [0 - ∞]). The mean residence time (MRT) was calculated by dividing the area under the first moment of the concentration/time integral (AUMC) by the AUC.

IV.2.8. Statistical analysis

The normality of data distribution of *in vitro* cell viability study was assessed by mean of the Shapiro-Wilk test ($\alpha > 0.05$). Data were analysed by mean of a Student's *t*-test to compare different groups using GraphPad Prism version 8.0.0 for Windows (GraphPad Software, San Diego, California, USA). A *p*-value less than 0.05 indicated statistical significance. The data are the mean \pm SD for $n = 3$.

IV.3. Results and discussion

IV.3.1. Solubility studies

BI is a lipophilic BCS class II drug, showing a logP value of 3.7 and very weak basic properties [25]. BI is not soluble in aqueous media as it was not detected in phosphate buffer at pH 7.4, pH 6.8 and in acetate buffer at pH 4.5 because below the HPLC *LOQ* ($12.7 \mu\text{g}\cdot\text{mL}^{-1}$). Solubility study of BI in oils, surfactants and co-solvents was the primary pre-formulation test to select the suitable SMEDDS excipients and define the amount of drug that can be loaded in the system. Fig. 1 illustrates the drug chemical structure and the results of solubility studies.

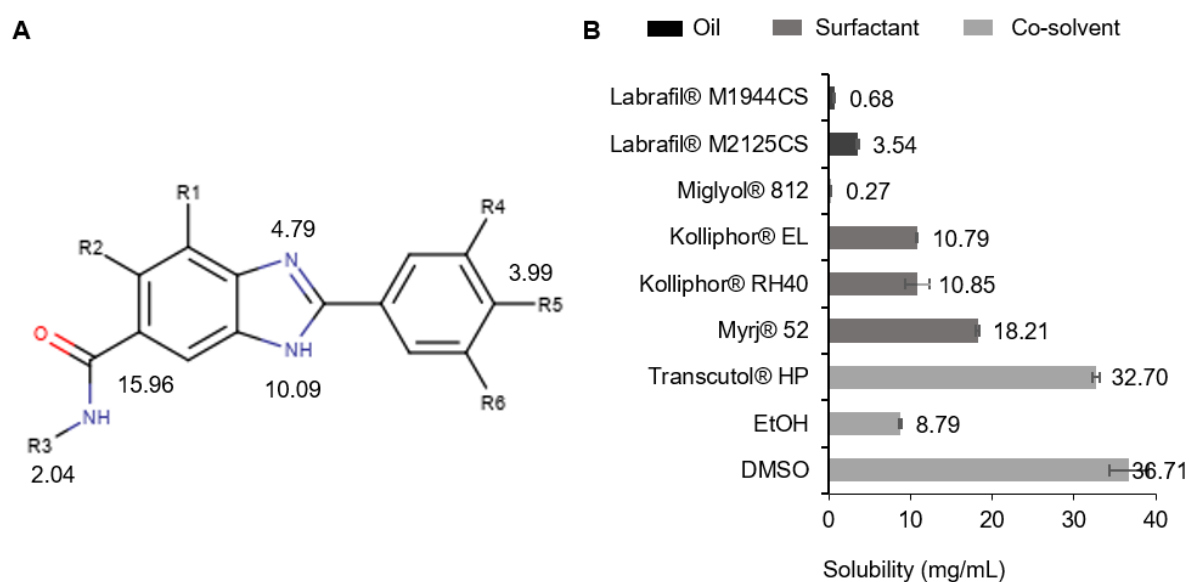


Fig. 1 A) BI chemical structure and pKa values; B) Maximum solubility of BI in various excipients expressed in $\text{mg}\cdot\text{mL}^{-1}$.

The drug solubility was low in all the tested oils with values of $0.7 \text{ mg}\cdot\text{mL}^{-1}$ in Labrafil® M1944CS, $3.5 \text{ mg}\cdot\text{mL}^{-1}$ in Labrafil® M2125CS and $0.3 \text{ mg}\cdot\text{mL}^{-1}$ in Miglyol® 812. The surfactants Kolliphor® EL (and Kolliphor® RH40 showed similar values of solubility ($10.8 \text{ mg}\cdot\text{mL}^{-1}$ and $10.9 \text{ mg}\cdot\text{mL}^{-1}$ respectively), while the solubility was two times higher in the surfactant Myrj® 52 ($18.2 \text{ mg}\cdot\text{mL}^{-1}$). The greatest solubility capacity was provided by Transcutol® HP ($32.7 \text{ mg}\cdot\text{mL}^{-1}$) and DMSO ($36.7 \text{ mg}\cdot\text{mL}^{-1}$), while the solubility in EtOH was of $8.8 \text{ mg}\cdot\text{mL}^{-1}$.

These results pointed out that BI solubility is highly dependent on fatty acid chain length, on HLB value and on the presence of ethylene oxide moieties in excipients. The lowest solubility was observed in Miglyol® 812, a medium chain triglyceride having an HLB value of 6. Labrafil® M1944CS and M2125CS, partially PEGylated long chain triglycerides, also showed low solubility because of their low HLB value of 9. Among all tested surfactants, the highest solubility was detected in Kolliphor® RH40

(10.9 mg·mL⁻¹) and Myrj® 52 (18.2 mg·mL⁻¹), that possess higher content of ethylene oxide moieties (PEG40) than Kolliphor® EL (PEG35) and higher HLB values (16.9 for Myrj® 52, 14–16 for Kolliphor® RH40, 12–14 for Kolliphor® EL). Transcutol® HP, ETOH and DMSO were evaluated as co-solvents. The higher solubilisation capacity of DMSO (36.7 mg·mL⁻¹) compared to the one of ethanol (8.8 mg·mL⁻¹) lies on its higher polarity, while the higher solubility in Transcutol® HP (32.7 mg·mL⁻¹) was ascribable to the ethylene oxide moiety. In accordance with previous studies on the solubility of lipophilic drugs in lipid excipients [30,31], a key to increase the solubility of BI was the high polarity and the H-bond interactions between drug and oxygen/hydroxyl functional groups of PEGylated excipients while non-polar and double bond π - π interactions played a minor role in triggering solubilisation.

Taking into account the solubility study, Miglyol® 812, Kolliphor® RH40, Transcutol® HP and EtOH were selected as components of SMEDDS for the delivery of the anticancer agent BI. In the formulation of SMEDDS, the selection of the oil has to be a compromise between the solubilizing potential and the ability to facilitate the microemulsions formation, since the drug solubility can be enhanced by the microemulsification of oil with surfactants. [9] Unsaturated fatty acids like Labrafil® M1944CS and M2125CS are known for their susceptibility to oxidation that can disturb the stability of the system [32], while medium chain triglycerides are resistant to oxidation and possess high emulsifying capacity [33]. For these reasons, Miglyol® 812 was selected as the oil component in SMEDDS. Kolliphor® RH40 was the surfactant of choice based on its good solubilizing capacity for BI and on the fact that it has efficient self-emulsification capacity when combined with Miglyol® 812 [34]. Besides, Kolliphor® RH40 showed low digestion and ability to inhibit the intestinal efflux transporter P-glycoprotein (P-gp), resulting in enhanced drug absorption and bioavailability [35,36]. Co-solvents addition is required to reduce the interfacial tension between oil and aqueous phases, promoting nanodroplet formation and stability, and to partially substitute surfactants, thus limiting intestinal local irritation [37]. In order to maximize drug loading Transcutol® HP was selected, while DMSO or EtOH were used to further improve the molecular dispersion of BI in the mixture. EtOH was chosen over DMSO because FDA approved for food products and widely use in the design of lipid-based systems [19,23,38].

IV.3.2. SMEDDS optimization through mixture design

The ternary phase diagram was constructed to identify the self-microemulsifying region and to select SMEDDS formulations. The phase diagram consisted of 100% of oil, surfactant and co-solvents (ratio 50/50) in each apex of the triangle (Fig. 2A). The use of co-solvents at ratios other than 50/50 was also investigated but failed to provide a satisfactory outcome. Each microemulsion was formulated by addition of water over the oily excipients (dilution factor 10) and the microemulsifying ability was assessed by DLS analysis. Visually, the turbid appearance of samples indicated the formation of coarse emulsions, while clear solutions corresponded to microemulsions. It was observed that a decrease in the oil content led to a decrease in droplet size and PdI. Microemulsions with an average size lower than 35 nm and PdI lower than ≤ 0.3 were obtained at oil content lower than 30% (blue dots in Fig. 2A). Thus, a set of constraints on the component mass fractions of $0.05 < X_{oil} < 0.30$, $0.45 < X_{surfactant} < 0.80$ and $0.15 < X_{co-solvents} < 0.25$ was defined for SMEDDS optimization through a mixture design. Only the regression coefficients significant at the 5% level (*t*-test) were kept in the model: the coefficients b_{12} and b_{23} were thus removed from Eq. 1. The ANOVA results indicated the high significance of the fitting with a *p*-

value of 0.03 (F -test). The determination coefficient $R^2=0.89$ proved the satisfactory adequacy of the model. Finally, its good predictive performance was assessed by the residuals at the test points: they were determined for each experiment as the difference between the experimental size and the one predicted by the model and were below 8 nm, i.e. in good accordance with the experimental error determined from repeated runs (standard deviation = 2.2 nm). Once validated, the developed model was used to plot the estimated surface contours for the mean size in a pseudoternary phase diagram (Fig. 2B). A progressive increase in size from 15 up to 30 nm was observed in samples at the lowest oil content ($x_{oil} < 10\%$) when the amount of co-solvents was increased from 15 to 25% (blue regions at the bottom right in Fig 2B), supposedly because of the destructuring of microemulsion droplets. For $x_{oil} > 0.2$, the amount of surfactant greatly influenced the microemulsion droplet mean size which ranges from 20 to 85 nm with $x_{surfactant}$ decreasing from 65 down to 45% while no significant influence was observed for $x_{oil} < 0.2$. At intermediate oil contents in between 10 and 15%, SMEDDS formulations appeared quite robust since characterized by similar mean size of less than 20 nm (dark blue region in Fig 2B). The width of this area corresponded to the feasibility domain. Experimentally, microemulsions in the feasibility domain showed an average size of around 20 nm and PDI lower than 0.1 (green dots in Fig. 2A, formulations F12, F17, F18, F19, F23 in Table 1).

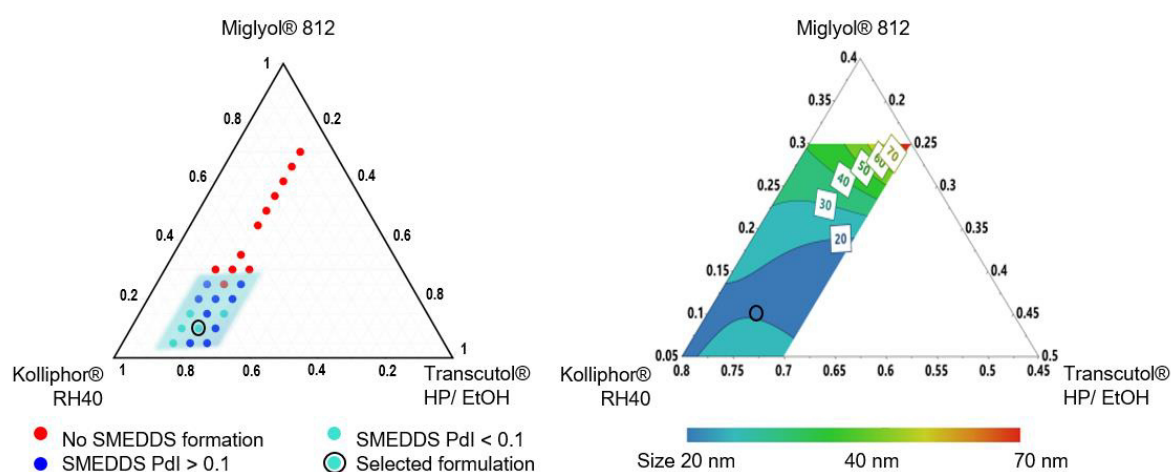


Fig. 2 A) Ternary phase diagram of SMEDDS composed of Miglyol® 812, Kolliphor® RH40 and Transcutol® HP/ EtOH (50/50). Red dots correspond to unsuitable formulations. Blue dots correspond to formulations having a nanometric size and PDI lower than 0.3. Green dots correspond to the feasibility domain showing microemulsion droplets of around 20 nm and PDI lower than 0.1. The selected formulation is highlighted with a black circle (F12, size 19 nm, PDI 0.1); B) Pseudoternary phase diagram. Contour plots of the predicted droplet mean size in the triangle defined by the lower and upper bounds of mass fractions of oil, surfactant and co-solvents with the selected optimized formulation (F12) indicated by a black circle.

Table 1 Composition and physicochemical properties of SMEDDS in the feasibility domain composed of Miglyol® 812, Kolliphor® RH40, Transcutol® HP and EtOH.

SMEDDS	Miglyol® 812 (% w/w)	Kolliphor® RH40 (% w/w)	Transcutol® HP (% w/w)	EtOH (% w/w)	Size (nm)	PdI
F12	10	70	10	10	18.6 ± 2.2	< 0.1
F17	15	70	7.5	7.5	21.5 ± 1.6	< 0.1
F18	10	75	7.5	7.5	18.7 ± 2.6	< 0.1
F19	5	80	7.5	7.5	16.4 ± 1.2	< 0.1
F23	15	60	12.5	12.5	21.9 ± 1.3	< 0.1

The criteria for the selection of the optimal formulation were: i) surfactant content that had to be lower than 70% in order to minimize system toxicity *in vivo* [39,40], ii) EtOH content that should not exceed the approved limit in medicinal products [41], iii) oil content that had to be high enough to emulsify the system but low enough to guarantee a high drug loading since the BI solubility in the oil was very low. On this basis, the SMEDDS F12, composed of 70% surfactant, 10% oil, 10% co-solvent Transcutol® HP and 10% EtOH (Table 1 and Fig. 2), was selected for further studies.

The SMEDDS F12 microemulsions had an average size of 18.6 ± 2.2 nm, low PdI and neutral ζ -potential of -1.0 ± 0.8 mV. Despite the neutral surface charge, SMEDDS showed high stability up to 21 days (Fig. S1 in supplementary information). This might be ascribed to SMEDDS thermodynamical stability and to the presence of Kolliphor® RH40 and Transcutol® HP, non-ionic surfactants which sterically stabilize the system by forming a shell around the droplet surface, as previously evidenced by Nasr et al. [15]. The developed SMEDDS were diluted to a maximum of 100-fold and a minimum of 5-fold in order to mimic the process of dilution in the intestinal tract [42]. As already observed in previous studies [7,43], dilutions did not cause any alteration in the system physicochemical properties (Fig. S2), any change in visual clarity, and no phase separation was observed within 24 h. The preservation of microemulsions integrity was attributed to the high amount of surfactant Kolliphor® RH40, which never fell below the critical micelle concentration (CMC of Kolliphor® RH40: 0.03% w/w at 37 °C) even in high diluted conditions (100-fold).

IV.3.3. Supersaturable SMEDDS formulation and optimisation

S-SMEDDS were developed to promote drug solubilisation and to prolong supersaturation in the gastrointestinal fluids, providing an opportunity to increase drug absorption [16,21]. S-SMEDDS formulations were prepared by adding the two different cellulose derivatives Klucel™ EF and Klucel™ LF at concentrations of 1% or 3% (w/w) to the optimized SMEDDS formulation F12. The self-emulsifying process of this system is illustrated in Fig. 3A, and the systems physicochemical properties in Fig. 3B.

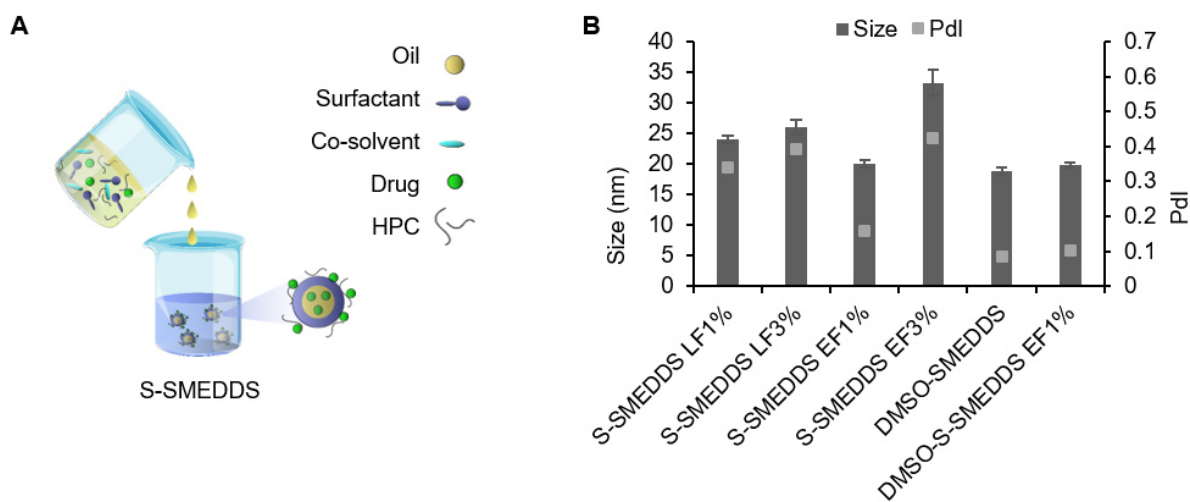


Fig. 3 A) Formulation of S-SMEDDS; B) Physicochemical properties of blank supersaturable SMEDDS (S-SMEDDS).

The optimisation was performed through the evaluation of both physicochemical properties of microemulsions by DLS analysis (Fig. 3B) and rheological properties of S-SMEDDS by flow sweep measurements at 25 °C (Fig. S3). From the rheological analysis it was observed that both S-SMEDDS I and II showed a shear thinning behaviour, meaning that the viscosity decreased at increasing shear rate, while SMEDDS (F12), analysed as control, displayed a Newtonian behaviour and a constant viscosity value of 150 mPa·s. S-SMEDDS at Klucel™ EF concentration of 1% (w/w) had an apparent viscosity of 17,583 mPa·s (shear rate 5 s⁻¹) and maintained the physicochemical characteristics of conventional SMEDDS (size 20.5 ± 1 nm, PDI 0.2) upon dilution in water (Fig. 3B), indication of good self-emulsification ability. On the other hand, S-SMEDDS containing Klucel™ EF3%, LF1% and LF3%, presented higher apparent viscosity of 168,135 mPa·s, 73,407 mPa·s and 95,907 mPa·s respectively (shear rate 5 s⁻¹) and their microemulsions showed high polydispersity (PDI > 0.3), meaning that their self-emulsification was hindered by the too high viscosity. The different self-emulsifying properties of S-SMEDDS containing Klucel™ EF and LF could be ascribed to the Klucel™ different viscosity grades (EF and LF) used in this study. Klucel™ LF is a medium viscosity grade HPC, with a MW of 95,000 Dalton, while Klucel™ EF has lower viscosity and MW (80,000 Dalton), that make it more easily soluble in organic liquids [20,44]. Only when using the low viscosity grade Klucel™ EF at the lower concentration of 1% (w/w), the emulsifying ability and the physicochemical properties of the system were preserved. Similar effect of the precipitator inhibitor concentration on self-emulsification was previously reported for S-SMEDDS containing HPC intended for the delivery of raloxifene. When the amount of HPC was increased from 1 to 5% (w/w), the high viscosity of the system was shown to hinder the microemulsion formation [45]. Thus, 1% Klucel™ EF was selected to create the supersaturable system. Then, in order to further enhance the drug loading, a second S-SMEDDS system was developed. EtOH was replaced with DMSO, in which BI was highly soluble (36.7 ± 2.0 mg·mL⁻¹). DMSO is considered a non-toxic solvent with oral Permitted Daily Exposure (PDE) limit of 50 mg·day⁻¹ according to the FDA, and previous studies reported the use of DMSO in SNEDDS for the oral route [46–48]. The feasibility of obtaining DMSO-SMEDDS by substituting EtOH in the SMEDDS F12 formulation was

firstly assessed. Therefore, the amount of excipients was optimized using the developed ternary phase diagrams to prevent alteration of the system physicochemical properties. When using 79% Kolliphor® RH40, 7.5% Miglyol® 812 and 7.5% Transcutol® HP and 5% DMSO (% w/w), a microemulsion with same size (18.8 ± 0.6 nm) and PdI (0.1) of SMEDDS microemulsions were obtained (Fig. 3B). S-SMEDDS containing Klucel™ EF at 1% (w/w) and DMSO were prepared (DMSO-S-SMEDDS EF 1%). DMSO-S-SMEDDS EF1% presented an apparent viscosity of 81,194 mPa·s (shear rate 5 s^{-1} , Fig. S3), value that was higher than the one of S-SMEDDS EF1% (17,583 mPa·s). However, the microemulsion physicochemical properties were not altered being the hydrodynamic diameter of 19.8 ± 0.5 nm and PdI of 0.1 (Fig. 3B).

Overall, two S-SMEDDS, containing 1% Klucel™ EF and EtOH or DMSO, were selected as supersaturable systems for further studies, henceforth referred to as S-SMEDDS I (containing EtOH) and S-SMEDDS II (containing DMSO).

IV.3.4. Determination of self-emulsification time

The emulsification time is an important parameter for assessing the emulsification potential of the formulations without the use of any external thermal or mechanical energy.

SMEDDS F12 showed an emulsification time of 68 s and S-SMEDDS I of 127 s, which indicate their ability to quickly disperse when subjected to aqueous dilution under mild agitation. The reason behind the rapid emulsification is the fast water penetration in the shell of surfactant and co-solvents surrounding the oil droplets [49]. A longer emulsification time of 481 s was recorded for S-SMEDDS II and was ascribed to the higher system viscosity.

IV.3.5. BI loading in SMEDDS and S-SMEDDS

BI was added to the SMEDDS mixture at drug loading (DL) up to 0.19% (Table 2). High drug encapsulation efficiency was obtained for SMEDDS a ($92.7 \pm 0.1\%$), b ($92.2 \pm 3.8\%$) and c ($83.9 \pm 0.1\%$). When a higher amount of drug was loaded in the system (SMEDDS d, DL 0.19%), the microemulsion presented a cloudy appearance and an orange solid crystalline precipitate of BI was observed, meaning that the saturation solubility of BI was exceeded. The addition of BI did not influence droplet size (19.1 ± 0.9 nm), PdI (< 0.1) and surface charge (-0.4 ± 0.9 mV) for the SMEDDS a, b and c (Table 2).

Table 2 Physicochemical properties of blank and BI-loaded microemulsion and encapsulation efficiency in SMEDDS, s-SMEDDS I and s-SMEDDS II by HPLC analysis. *drug precipitation.

Sample	Drug loading (%)	Size (nm)	PdI	ζ-potential (mV)	Encapsulation efficiency (%)
SMEDDS a	0.05	18.4 ± 0.4	< 0.1		92.7 ± 0.1
SMEDDS b	0.09	18.7 ± 0.2	< 0.1	-1.5 ± 1.0	92.2 ± 3.8
SMEDDS c	0.14	19.1 ± 0.9	< 0.1		83.8 ± 0.1
SMEDDS d	0.19	18.5 ± 0.2	< 0.1	-0.4 ± 0.8	*
S-SMEDDS I	0.30	20.2 ± 0.8	< 0.2	-0.3 ± 0.2	90.5 ± 12
S-SMEDDS II	0.55	20.1 ± 0.7	< 0.2	-2.2 ± 0.5	92.7 ± 7.3

The addition of Klucel™ EF as precipitation inhibitor allowed to increase 2-folds the BI loading in S-SMEDDS I compared to conventional SMEDDS (DL from 0.14% in SMEDDS c to 0.30% in S-SMEDDS I), without variation of the physicochemical properties (droplet size 20.2 ± 0.8 nm, PDI < 0.2 , ζ -potential -0.3 ± 0.2 mV). The encapsulation efficiency was high ($90.5 \pm 12\%$) and no drug precipitation occurred. S-SMEDDS II allowed to further increase the drug loading up to 0.55% (encapsulation efficiency $92.7 \pm 7.3\%$) while maintaining droplet size (20.1 ± 0.7 nm, PDI < 0.2) and surface charge (-2.2 ± 0.5 mV, Table 2). Previous studies already demonstrated that the use of HPC in S-SMEDDS allowed to maintain the lipophilic drug raloxifene in a supersaturated state above its equilibrium level [45].

The S-SMEDDS here developed solubilised higher BI amounts and hindered BI precipitation from microemulsions after dispersion in water due to the higher viscosity of the system and the creation of hydrogen bonds between BI and HPC (Klucel™ EF). The HPC is adsorbed and accumulated onto the BI crystal surface, delaying the crystallization and nucleation process that would have led to precipitation.

IV.3.6. Stability studies in simulated gastrointestinal fluids

In sight of their oral administration, the stability of developed formulations was evaluated in simulated gastric fluid (SGF) at pH 1.2 and in simulated intestinal fluid (SIF) at pH 6.8.

Firstly, drug-loaded SMEDDS a, SMEDDS b, SMEDDS c, S-SMEDDS I and S-SMEDDS II were dispersed in SGF at pH 1.2 (10-fold dilution) and the physicochemical properties of the formed microemulsions (Fig. 4 A) and their drug encapsulation efficiency (Table S1) were studied over 3 h.

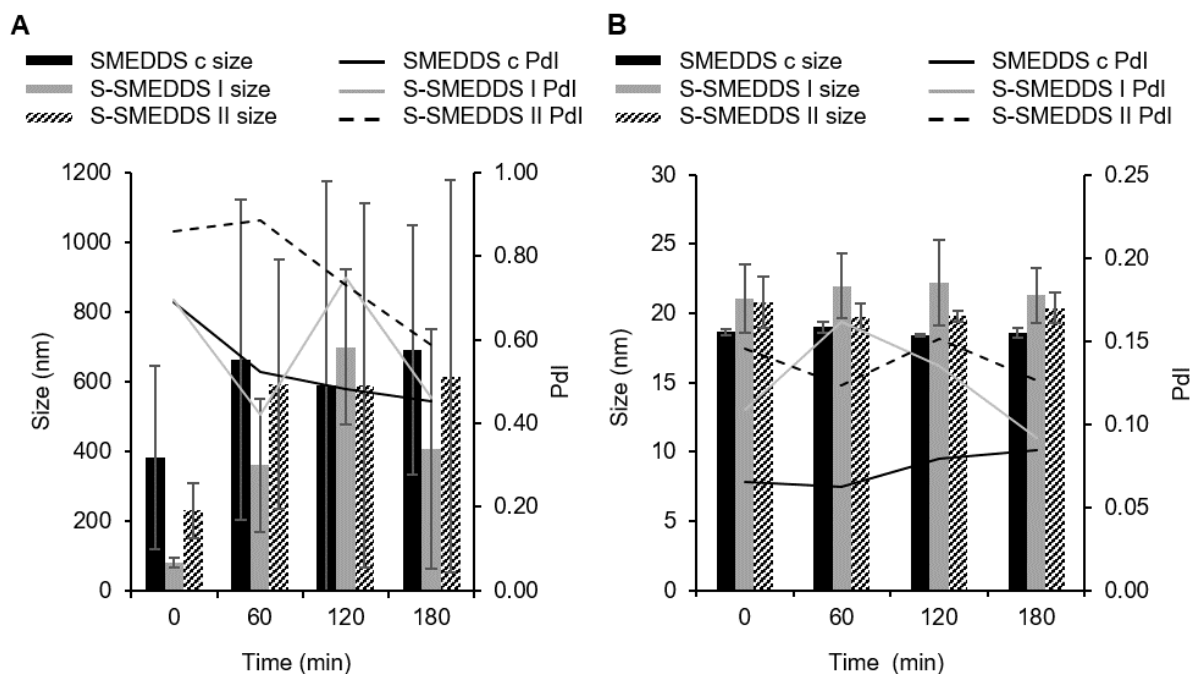


Fig. 4 Stability studies of BI-loaded SMEDDS c, S-SMEDDS I and S-SMEDDS II microemulsions in A) simulated gastric fluids (SGF) and B) simulated intestinal fluids (SIF) up to 3h. Stability was evaluated by mean of DLS analysis.

Upon dispersion in SGF, SMEDDS a (DL 0.05%) and SMEDDS b (DL of 0.09%) microemulsions maintained the physicochemical properties (size < 20 nm PdI 0.1), but their encapsulation efficiency decreased after 3 h (from $87.5 \pm 1.9\%$ to $64.8 \pm 5.8\%$ in SMEDDS a and from $78.2 \pm 6.3\%$ to $36.7 \pm 4.0\%$ in SMEDDS b, Table S1). Instead, SMEDDS c (DL 0.14%) microemulsion turned yellow and turbid, the size and PdI increased dramatically (size > 500 nm, PdI > 0.3 in Fig. 4A). Visible BI precipitation was observed and only the $21.7 \pm 0.1\%$ of BI was still encapsulated in the formulation (Table S1). When the stability of blank SMEDDS was evaluated in SGF (10-fold dilution) no alteration in size and PdI were observed (size 19 nm, PdI of 0.1), sign of the excipient stability in gastric environment. It was concluded that the drug precipitation process from SMEDDS in SGF was drug-concentration dependent and the maximum drug solubility in SMEDDS a, b and c microemulsions at acidic pH was $0.03 \text{ mg}\cdot\text{mL}^{-1}$.

Then, S-SMEDDS were dispersed in SGF. S-SMEDDS I (DL 0.30%) formed an emulsion with a yellowish reflection and a size of $80.3 \pm 4.9 \text{ nm}$ (Fig. 4A) that destabilized after 1 h (particle size above 360 nm) leading to visible drug precipitation. S-SMEDDS II (DL 0.55%) suspension developed opacity immediately, particle size and PdI drastically increased ($230.6 \pm 79 \text{ nm}$, PdI 0.9), and a visible yellow solid crystalline precipitate of BI appeared. Upon dilution, only $21.7 \pm 0.1\%$ of BI was detected in S-SMEDDS I, and $13.7 \pm 0.1\%$ in S-SMEDDS II (Table S1). Despite system instability, the maximum drug concentration in S-SMEDDS I and II microemulsions upon dilution in SGF was $0.07 \text{ mg}\cdot\text{mL}^{-1}$, 2.3-fold higher than the one of SMEDDS ($0.03 \text{ mg}\cdot\text{mL}^{-1}$). Thanks to the presence of Klucel™ EF (1% w/w), S-SMEDDS maintained the drug in a supersaturated state in simulated acidic conditions. Similar reduction of drug precipitation in gastric environment was observed for S-SMEDDS containing HPMC [23] and Eudragit® E [50]. The partial precipitation in strong acidic conditions was ascribed to the BI ionisation (pKa 4.97, 3.99, 2.04), that hindered the association with the non-ionic excipients generating supersaturation at lower drug concentration. The effect of drug ionisation state on inefficient association with lipids leading to drug precipitation at gastric pH was previously reported for cinnarizine [17] [38] and haloperidol [51].

Subsequently, BI-loaded SMEDDS c, S-SMEDDS I and S-SMEDDS II were dispersed in SIF at pH 6.8 (10-fold dilution) and the physicochemical properties of the formed microemulsions were studied by DLS analysis over 3 h (Fig. 4B). No alteration of particle size (< 25 nm) and PdI (< 0.2) were observed during the experimental period, indicative of the system stability.

The rate of precipitation and supersaturation in the stomach might affect the performance of SMEDDS in the intestine and reduce drug absorption [21]. With the aim of mimicking the system fate *in vivo*, we adjusted the microemulsion pH from acid to alkaline in a pH-shift study and we evaluated the ability of SMEDDS c, S-SMEDDS I and S-SMEDDS II to recover their physicochemical properties and avoid drug precipitation at intestinal pH (Fig. 5).

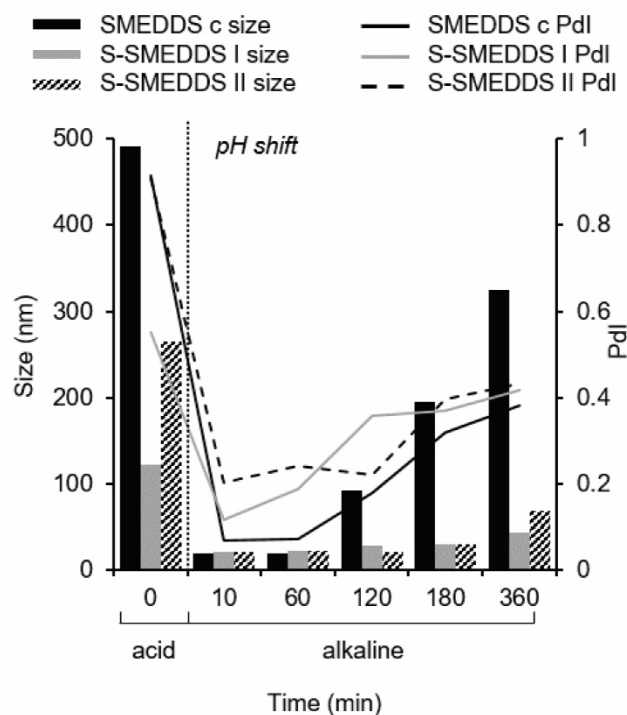


Fig. 5 Physicochemical properties of BI-loaded SMEDDS c and S-SMEDDS I and II following pH adjustment from acid (time point 0 min) to alkaline (from time point 10 min to 360 min).

Systems were firstly dispersed in SGF, where drug precipitation occurred. Afterwards, alkalisation was produced by adding NaOH (time point 10 min in Fig. 5). In consequence of the pH shift the BI precipitate immediately re-dissolved, formulations turned clear and the physicochemical properties of microemulsions were re-established. Moreover, all BI was solubilized in the lipid droplets, as demonstrated by the high values of encapsulation efficiency ($78.4 \pm 1.7\%$ in SMEDDS c, $83.4 \pm 0.6\%$ in S-SMEDDS I and $90.9 \pm 1.0\%$ in S-SMEDDS II at time point 10 min). SMEDDS c recovered their properties and remained stable up to 2h. Then, their hydrodynamic diameter progressively augmented and the system became highly polydispersed at 6 h (size 324 nm, PdI 0.4, Fig. 5). S-SMEDDS were more stable. No alteration in particle size was observed, but PdI increased at 2 h in S-SMEDDS I and at 3 h in S-SMEDDS II, indicating the presence of aggregated particles. Even after 6 h BI was still encapsulated in all the systems (encapsulation efficiency of $79.80 \pm 1.5\%$ in SMEDDS c, $83.01 \pm 1.6\%$ in S-SMEDDS I and $91.85 \pm 2.5\%$ in S-SMEDDS II). In accordance with previous research [18], when the lipophilic drug was in its non-ionised form the interactions with the lipid excipients were maximized. At time point 3 h, S-SMEDDS I maintained $0.24 \text{ mg} \cdot \text{mL}^{-1}$ and S-SMEDDS II $0.46 \text{ mg} \cdot \text{mL}^{-1}$ of BI in a supersaturated state and ready to be absorbed. The ability of developed S-SMEDDS microemulsions to regain their properties and to maintain the drug in a high supersaturated state in the intestinal environment is a major prerequisite to enhance drug systemic absorption.

IV.3.7 Cytotoxicity assessment of the SMEDDS and S-SMEDDS formulations

The cytocompatibility of blank and drug-loaded SMEDDS and S-SMEDDS I was assessed in the human colon carcinoma (Caco-2) cell model after 24 h exposure via MTS cell viability assays. The minimum level acceptable of cell viability in cytotoxicity tests was fixed at 70% according to ISO 10993 [52]. Fig.

6A shows that the self-emulsifying systems did not affect the Caco-2 cell viability, whereas the free drug was highly toxic at all concentrations tested. Cell viability values higher than 70% were observed for blank SMEDDS c and S-SMEDDS I and their drug-loaded counterparts at system concentrations up to $1.3 \text{ mg}\cdot\text{mL}^{-1}$. Such system concentration ensured that the Kolliphor® RH40 amount was below the reported limit of toxicity, since Kolliphor® RH40 in high amount was reported to damage Caco-2 cells by promoting oxidative stress and inhibition of the cardiac mitochondrial respiration [53]. Besides, the ability of SMEDDS c and S-SMEDDS I to significantly reduce the drug toxicity on intestinal cells is a major advantage in sight of an oral administration, as previously reported [50].

IV.3.8 *In vitro* transepithelial permeability and cellular uptake studies

Transepithelial permeability assays were performed to evaluate if the developed systems could also exert an effect on the epithelial permeability. Studies were carried out on Caco-2 monolayers by labelling the blank SMEDDS and S-SMEDDS I with the fluorescent dye DiD.

Analysis of DiD fluorescence showed that after 2h and 4h the fluorescence intensity was halved in the apical compartment compared to the sample fed solution at time point 0. No fluorescent signal was detected in the basolateral compartment. This was probably due to the high diluted conditions and suggested the system accumulation within or inside intestinal cells.

TEER values of the Caco-2 cell monolayers were monitored upon exposure to DiD-labelled SMEDDS, DiD-labelled S-SMEDDS and the corresponding control (HBSS) for up to 4 h. The results in Fig. 6B indicated that the TEER values of the monolayer were not modified upon incubation with the HBSS medium, while in the case of SMEDDS and S-SMEDDS I a decrease in the TEER of around 25% was observed at 2 and 4 h. Interestingly, the standard TEER values could be re-established after removal of the samples. In fact, the TEER values observed at 24 h were very similar to the initial ones. Taking into account that the SMEDDS and S-SMEDDS concentrations used in this experiment ($1 \text{ mg}\cdot\text{mL}^{-1}$) did not compromise the cell viability, this TEER reduction could be directly associated with the system ability to modify the paracellular permeability by transitory opening of the tight junctions. These results are in line with those obtained by Aktas et al. who proved the ability of Exendin-4 loaded SNEDDS composed of Cremophor® EL, Labrasol®, propylene glycole to reversibly decrease the TEER values of Caco-2 cell monolayers and to enhance drug permeability compared to the free drug solution [54].

CLSM analysis confirmed TEER and basolateral fluorescence results. Fig. 6C shows the confocal micrographs of Caco-2 cells monolayer on Transwell® inserts after exposure to SMEDDS and S-SMEDDS for 2 h and 4 h. Untreated cells in presence of HBSS were imaged as a control.

Red stained fluorescent structures consistent with DiD-labelled nanosystems was visible for all tested formulations at 2 h and 4 h. The red signal was not visible in the images of cell monolayers treated with the HBSS control. At time point of 2 h, systems accumulated in correspondence of tight junctions. After 4 h the distribution of the fluorescent signal was more uniform, less intense and mainly present within the cell membrane and nucleus. This was an sign of the possible permeation across the monolayer or of the partial internalization into intestinal cells. In accordance with the decrease in TEER values, a clear disruption of tight junctions was observed upon incubation with both SMEDDS and S-SMEDDS I compared to the HBSS control, as indicated by the discontinuity in cell membrane green signal. Such enhancement of the paracellular transport across Caco-2 cell monolayers was ascribed to the small droplet size of SMEDDS and S-SMEDDS and to the amphiphilic non-ionic surfactants present in the

formulation which were previously reported to exert a membrane fluidifying effect and to transiently and reversibly open tight junctions [50,55–58]. Previous studies also stated that the co-solvent Transcutol HP can have a permeation enhancing effect [6,59].

The ability of the developed SMEDDS and S-SMEDDS of opening tight junctions highlights their potential for the oral administration of hydrophobic drugs.

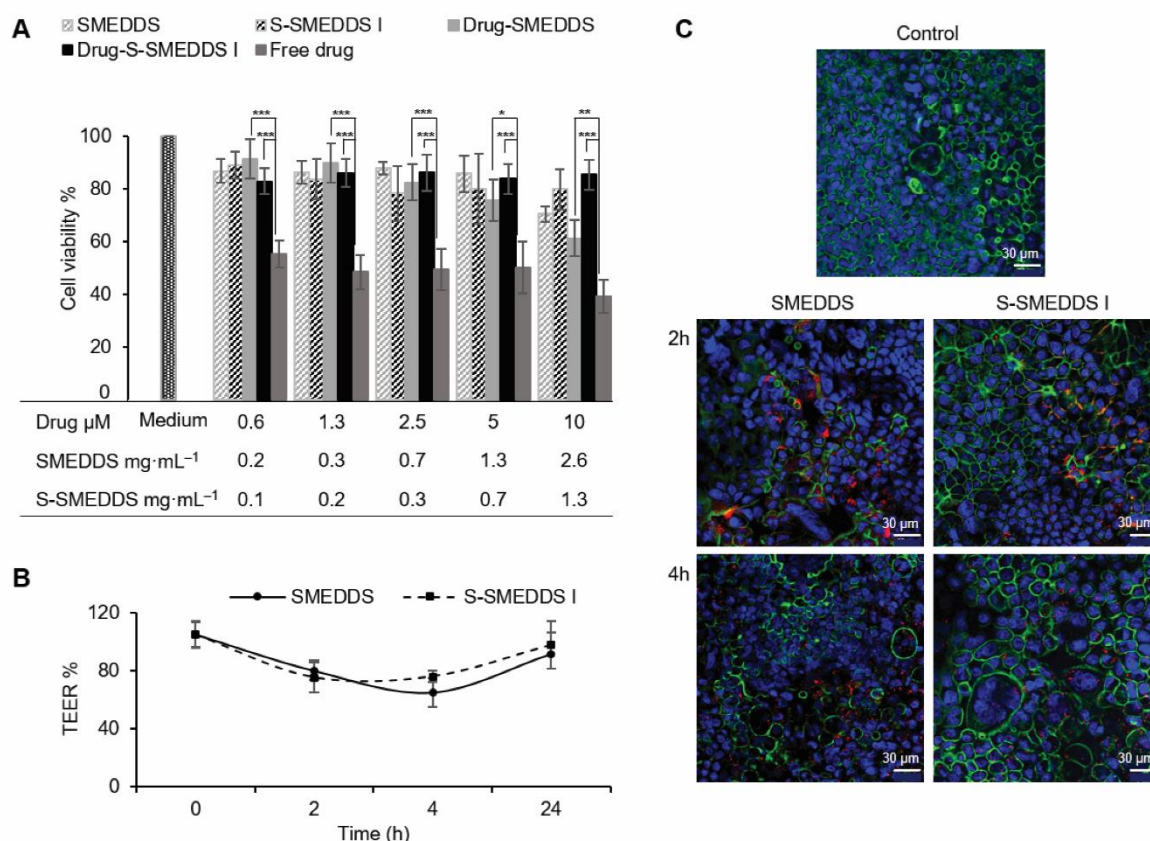


Fig. 6. A) Viability of Caco-2 cells after incubation with blank SMEDDS, blank S-SMEDDS, drug-loaded SMEDDS, drug-loaded S-SMEDDS, free drug solution in EtOH for 24 h. Data are shown as mean \pm SD, $n = 3$. Statistical data analysis: $p < 0.05 = *$; $p < 0.01 = **$; $p < 0.001 = ***$; $\geq 0.05 =$ not significant. B) TEER values of Caco-2 monolayer upon incubation with DiD-labelled SMEDDS and S-SMEDDS ($1 \text{ mg}\cdot\text{mL}^{-1}$). C) Confocal microscope images of fixed and stained Caco-2 cell monolayers grown on transwell membranes for 21 days prior to 2 h and 4 h exposure to DiD-labelled SMEDDS and DiD-labelled S-SMEDDS I (red). Fixed cells were stained with DAPI (blue nuclei) and Phalloidin-iFluor™ 488 Conjugate (green tight junctions). Scale bar: 30 μm .

IV.3.9 Pharmacokinetic studies

Pharmacokinetic studies were performed to evaluate the oral absorption of BI loaded SMEDDS and S-SMEDDS following oral administration in healthy mice. BI dispersion in HPC was used as a control. BI blood concentration was quantified by LC-MS analysis after the development and optimization of plasma extraction and plotted as a function of time (Fig. 7 A and B). The pharmacokinetic parameters are summarized in Table 3.

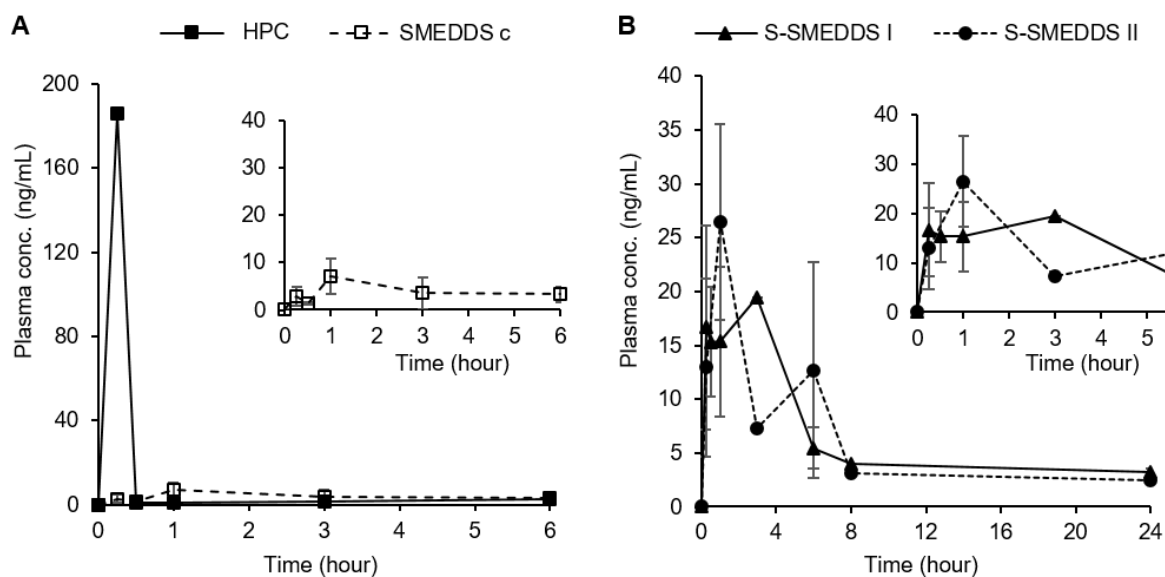


Fig. 7 Plasma concentrations vs time profile after oral administration of A) drug dispersion in HPC and SMEDDS c (up to 6 h) and B) S-SMEDDS I and S-SMEDDS II (up to 24 h).

Table 3 Pharmacokinetic parameters of BI following oral administration to mice.

Sample	BI administered	C_{max}	T_{max}	AUC	$t_{1/2}$	MRT
	dose					
	$mg \cdot kg^{-1}$	$ng \cdot mL^{-1}$	h	$ng \cdot mL^{-1} \cdot h$	h	h
HPC	40	186.2	0.25	66.8	2.6	2.3
SMEDDS c	14	7.1	1	47.6	4.9	7.8
S-SMEDDS I	30	19.5	3	295.1	30.0	36.1
S-SMEDDS II	55	26.5	1	171.9	8.5	12.2

When BI was administered as dispersion in HPC the drug intestinal absorption was immediate, the peak plasma concentration was $186.2 \text{ ng} \cdot \text{mL}^{-1}$ and occurred at 15 min (Fig. 7 A and Table 3).

The encapsulation of BI in SMEDDS c provided lower plasma concentration as compared to HPC dispersion, being the C_{max} below $10 \text{ ng} \cdot \text{mL}^{-1}$ (Fig. 7 A).

When S-SMEDDS I and II were administered, the peak plasma concentration was three times higher compared to SMEDDS (Fig. 7 B). Longer T_{max} were observed when the drug was associated to the delivery systems, notably in S-SMEDDS I (1 h for SMEDDS c and S-SMEDDS II; 3 h for S-SMEDDS I). The Area Under the Curve (AUC) was lower for SMEDDS ($47.6 \text{ ng} \cdot \text{mL}^{-1} \cdot \text{h}$) than for BI dispersion in HPC ($66.8 \text{ ng} \cdot \text{mL}^{-1} \cdot \text{h}$). While the AUC of S-SMEDDS I was $295.1 \text{ ng} \cdot \text{mL}^{-1} \cdot \text{h}$ and of S-SMEDDS II was $171.9 \text{ ng} \cdot \text{mL}^{-1} \cdot \text{h}$, about 4.5-fold and 2.5-fold greater than that obtained with the reference formulation.

The half-life ($t_{1/2}$) was longer for S-SMEDDS I, being its value 12-fold higher than for BI dispersion, 6-fold higher than SMEDDS c and 4-fold higher than S-SMEDDS II. In line with the AUC values, the medium residence time (MRT) increased when the drug loaded in the delivery systems, particularly in the case of S-SMEDDS I (36 h).

The variation of the dose-dependent pharmacokinetics parameters (C_{max} , AUC and MRT) suggested that the loading in S-SMEDDS had a positive impact on the drug concentration-time profile. While the increase of the dose-independent pharmacokinetics parameters (T_{max} , $t_{1/2}$) proved the ability of S-

SMEDDS I to prolong the blood circulation time of the drug. Such behaviour was ascribed to the presence of HPC in s-SMEDDS I that induced and maintained the drug in a supersaturated state over time. S-SMEDDS too were less efficient in prolonging the drug blood circulation time. We suggested that the behaviour of S-SMEDDS II was related to the long emulsification time and high viscosity of S-SMEDDS II, that prevented drug absorption.

Conventional SMEDDS systems have been previously developed for benzimidazole derivatives such as albendazol, leading to a marked increase in the absorption of the drugs [13]. Albendazol was also formulated in supersaturated SMEDDS, containing polyethylene glycol 400 (PEG 400) as solubility enhancer, and a 63% improvement of its relative bioavailability was observed when orally administered to rabbit ($10 \text{ mg}\cdot\text{kg}^{-1}$) [11]. Compared to the latter system the S-SMEDDS here developed will enable the administration of a higher amount of drug ($30 \text{ mg}\cdot\text{kg}^{-1}$ in mice).

Overall, by combining the attributes of small SMEDDS microemulsions, that have a large surface area for intestinal absorption, together with the supersaturable characteristics, the S-SMEDDS formulation approach proved to be a successful strategy for the oral delivery of lipophilic drug molecules.

IV.4. Conclusions

In the present study the oral administration of the new benzimidazole derivative anticancer agent BI was challenged by its formulation in supersaturable self-microemulsifying drug delivery systems (S-SMEDDS). Firstly, SMEDDS made of Miglyol® 812, Kolliphor® RH40, Transcutol® HP and EtOH (or DMSO) were developed and optimized by means of a mixture design to generate microemulsions having a size of 19 nm, low PdI (0.1) and neutral ζ -potential (around 1 mV) upon dispersion in water under mild agitation. Then, the drug payload was boosted by formulating two supersaturable systems (S-SMEDDS) in which 1% Klucel™ EF was added as precipitation inhibitor. For efficient drug dissolution, S-SMEDDS I contained 10% EtOH as co-solvent and S-SMEDDS II 5% DMSO. The systems physicochemical properties were not affected by the dilution rate and both SMEDDS and S-SMEDDS showed good emulsification ability upon dispersion in water, being the time for dispersion faster in presence of EtOH than DMSO. When stability studies were performed in simulated gastrointestinal fluids, both SMEDDS and S-SMEDDS presented instability in the gastric environment (pH 1.2). However, S-SMEDDS recovered their physicochemical properties and avoided drug precipitation once moved to the intestinal basic pH, indicating their potential as oral delivery systems. The SMEDDS and S-SMEDDS were cytocompatible with Caco-2 cells up to $1.3 \text{ mg}\cdot\text{mL}^{-1}$ and by carrying the drug in their oil core they markedly reduced its toxicity. Transport and uptake studies on Caco-2 cell monolayers proved the ability of SMEDDS and S-SMEDDS to increase the epithelial permeability by the transient opening of tight junctions without signs of cytotoxicity. The *in vivo* evaluation after oral administration to healthy mice highlighted how S-SMEDDS prolonged the drug plasmatic circulation time, compared to free drug and conventional SMEDDS, by maintaining the drug in its supersaturated state in the intestine.

Globally in this work we demonstrated that the application of supersaturation to self-emulsifying systems lead to the development of improved formulations for the oral administration of other lipophilic BCS Class II drugs.

Acknowledgements:

The research leading to these results has received funding from National Research Agency (ANR), HyDNano project (ANR-18-CE18-0025-01), the PHC Pessoa Programme between ANR and Fundação para a Ciência e Tecnologia (FCT): NanoSpeed, (N° 42306YB) and from FCT project UID/Multi/04326/2019, from the Ministère de l'Enseignement Supérieur et de la Recherche (France) and from the Center for Drug Discovery and Development (C3D) platform (Centre de recherche en cancérologie de Lyon (CRCL), Lyon, France.

IV. References

- [1] K.J. Filipowski, M. V. Varma, A.F. El-Kattan, C.M. Ambler, R.B. Ruggeri, T.C. Goosen, K.O. Cameron, Intestinal Targeting of Drugs: Rational Design Approaches and Challenges, *Curr. Top. Med. Chem.* 13 (2013) 776–802. doi:10.2174/1568026611313070002.
- [2] A. Rosso, G. Lollo, Y. Chevalier, N. Troung, C. Bordes, S. Bourgeois, O. Maniti, T. Granjon, P.-Y. Dugas, S. Urbaniak, S. Briançon, Development and structural characterization of a novel nanoemulsion for oral drug delivery, *Colloids Surfaces A Physicochem. Eng. Asp.* 593 (2020) 124614. doi:10.1016/j.colsurfa.2020.124614.
- [3] G. Lollo, A. Gonzalez-Paredes, M. Garcia-Fuentes, P. Calvo, D. Torres, M.J. Alonso, Polyarginine Nanocapsules as a Potential Oral Peptide Delivery Carrier, *J. Pharm. Sci.* 106 (2017) 611–618. doi:10.1016/j.xphs.2016.09.029.
- [4] S. Gupta, R. Kesarla, A. Omri, Formulation Strategies to Improve the Bioavailability of Poorly Absorbed Drugs with Special Emphasis on Self-Emulsifying Systems, *ISRN Pharm.* 2013 (2013) 1–16. doi:10.1155/2013/848043.
- [5] C. Dumont, S. Bourgeois, H. Fessi, V. Jannin, Lipid-based nanosuspensions for oral delivery of peptides, a critical review, *Int. J. Pharm.* 541 (2018) 117–135. doi:10.1016/j.ijpharm.2018.02.038.
- [6] A.B. Buya, B. Ucar, A. Beloqui, P.B. Memvanga, V. Pr at, Design and evaluation of self-nanoemulsifying drug delivery systems (SNEDDSs) for senicapoc, *Int. J. Pharm.* 580 (2020) 119180. doi:10.1016/j.ijpharm.2020.119180.
- [7] P. Desai, A. Thakkar, D. Ann, J. Wang, S. Prabhu, Loratadine self-microemulsifying drug delivery systems (SMEDDS) in combination with sulforaphane for the synergistic chemoprevention of pancreatic cancer, *Drug Deliv. Transl. Res.* 9 (2019) 641–651. doi:10.1007/s13346-019-00619-0.
- [8] P. Patel, S.R. Pailla, N. Rangaraj, H.S. Cheruvu, S. Dodoala, S. Sampathi, Quality by Design Approach for Developing Lipid-Based Nanoformulations of Gliclazide to Improve Oral Bioavailability and Anti-Diabetic Activity, *AAPS PharmSciTech.* 20 (2019) 45. doi:10.1208/s12249-018-1214-x.
- [9] C.W. Pouton, Lipid formulations for oral administration of drugs: Non-emulsifying, self-emulsifying and 'self-microemulsifying' drug delivery systems, *Eur. J. Pharm. Sci.* 11 (2000) 93–98. doi:10.1016/S0928-0987(00)00167-6.
- [10] E. Ruckenstein, The origin of thermodynamic stability of microemulsions, *Chem. Phys. Lett.* 57 (1978) 517–521. doi:10.1016/0009-2614(78)85311-1.
- [11] T. Mukherjee, F.M. Plakogiannis, Development and oral bioavailability assessment of a supersaturated self-microemulsifying drug delivery system (SMEDDS) of albendazole, *J. Pharm. Pharmacol.* 62 (2010) 1112–1120. doi:10.1111/j.2042-7158.2010.01149.x.
- [12] S. Dokania, A.K. Joshi, Self-microemulsifying drug delivery system (SMEDDS)-challenges and road ahead, *Drug Deliv.* 22 (2015) 675–690. doi:10.3109/10717544.2014.896058.
- [13] S. Sawatdee, A. Atipairin, A.S. Yoon, T. Srichana, N. Changsan, T. Suwandecha, Formulation development of albendazole-loaded self-microemulsifying chewable Tablets to enhance dissolution and bioavailability, *Pharmaceutics.* 11 (2019). doi:10.3390/pharmaceutics11030134.
- [14] B. Chatterjee, S. Hamed Almurisi, A. Ahmed Mahdi Dukhan, U.K. Mandal, P. Sengupta, Controversies with self-emulsifying drug delivery system from pharmacokinetic point of view, *Drug Deliv.* 23 (2016) 3639–3652. doi:10.1080/10717544.2016.1214990.

- [15] A. Nasr, A. Gardouh, M. Ghorab, Novel solid self-nanoemulsifying drug delivery system (S-SNEDDS) for oral delivery of olmesartan medoxomil: Design, formulation, pharmacokinetic and bioavailability evaluation, *Pharmaceutics*. 8 (2016). doi:10.3390/pharmaceutics8030020.
- [16] H. Park, E. Ha, M. Kim, Current Status of Supersaturable Self-Emulsifying Drug Delivery Systems, *Pharmaceutics*. 12 (2020) 365. doi:10.3390/pharmaceutics12040365.
- [17] A.T. Larsen, A.G. Ohlsson, B. Polentarutti, R.A. Barker, A.R. Phillips, R. Abu-Rmaileh, P.A. Dickinson, B. Abrahamsson, J. Østergaard, A. Müllertz, Oral bioavailability of cinnarizine in dogs: Relation to SNEDDS droplet size, drug solubility and in vitro precipitation, *Eur. J. Pharm. Sci.* 48 (2013) 339–350. doi:10.1016/j.ejps.2012.11.004.
- [18] S. Raut, B. Karzuon, E. Atef, Using in situ Raman spectroscopy to study the drug precipitation inhibition and supersaturation mechanism of Vitamin E TPGS from self-emulsifying drug delivery systems (SEDDS), *J. Pharm. Biomed. Anal.* 109 (2015) 121–127. doi:10.1016/j.jpba.2015.02.027.
- [19] G. Quan, B. Niu, V. Singh, Y. Zhou, C.-Y. Wu, X. Pan, C. Wu, Supersaturable solid self-microemulsifying drug delivery system: precipitation inhibition and bioavailability enhancement, *Int. J. Nanomedicine*. 12 (2017) 8801–8811. doi:10.2147/IJN.S149717.
- [20] S. Xu, W.-G. Dai, Drug precipitation inhibitors in supersaturable formulations, *Int. J. Pharm.* 453 (2013) 36–43. doi:10.1016/j.ijpharm.2013.05.013.
- [21] B.J. Boyd, C.A.S. Bergström, Z. Vinarov, M. Kuentz, J. Brouwers, P. Augustijns, M. Brandl, A. Bernkop-Schnürch, N. Shrestha, V. Prémat, A. Müllertz, A. Bauer-Brandl, V. Jannin, Successful oral delivery of poorly water-soluble drugs both depends on the intraluminal behavior of drugs and of appropriate advanced drug delivery systems, *Eur. J. Pharm. Sci.* 137 (2019) 104967. doi:10.1016/j.ejps.2019.104967.
- [22] D.R. Lee, M.J. Ho, Y.W. Choi, M.J. Kang, A Polyvinylpyrrolidone-Based Supersaturable Self-Emulsifying Drug Delivery System for Enhanced Dissolution of Cyclosporine A, *Polymers (Basel)*. 9 (2017) 124. doi:10.3390/polym9040124.
- [23] P. Gao, B.D. Rush, W.P. Pfund, T. Huang, J.M. Bauer, W. Morozowich, M.S. Kuo, M.J. Hageman, Development of a Supersaturable SEDDS (S-SEDDS) Formulation of Paclitaxel with Improved Oral Bioavailability, *J. Pharm. Sci.* 92 (2003) 2386–2398. doi:10.1002/jps.10511.
- [24] P. Gao, B.D. Rush, W.P. Pfund, T. Huang, J.M. Bauer, W. Morozowich, M.S. Kuo, M.J. Hageman, Development of a Supersaturable SEDDS (S-SEDDS) Formulation of Paclitaxel with Improved Oral Bioavailability, *J. Pharm. Sci.* 92 (2003) 2386–2398. doi:10.1002/jps.10511.
- [25] T. Renno, I. Coste-Invernizzi, S. Giraud, S. Lebecque, Benzoimidazole derivatives as anticancer agents. PATENT WO/2018/054989A1, WO/2018/054989A1, 2018.
- [26] International Conference on Harmonization of Technical Requirements for Registration of Pharmaceuticals for Human Use. Validation of Analytical Procedures: Text and Methodology, Q2 (R1), (2005).
- [27] Y. Sambuy, I. De Angelis, G. Ranaldi, M.L. Scarino, A. Stammati, F. Zucco, The Caco-2 cell line as a model of the intestinal barrier: influence of cell and culture-related factors on Caco-2 cell functional characteristics, *Cell Biol. Toxicol.* 21 (2005) 1–26. doi:10.1007/s10565-005-0085-6.
- [28] A. Beloqui, A. des Rieux, V. Prémat, Mechanisms of transport of polymeric and lipidic nanoparticles across the intestinal barrier, *Adv. Drug Deliv. Rev.* 106 (2016) 242–255. doi:10.1016/j.addr.2016.04.014.
- [29] J. Schindelin, I. Arganda-Carreras, E. Frise, V. Kaynig, M. Longair, T. Pietzsch, S. Preibisch, C. Rueden, S. Saalfeld, B. Schmid, J.-Y. Tinevez, D.J. White, V. Hartenstein, K. Eliceiri, P. Tomancak, A. Cardona, Fiji: an open-source platform for biological-image analysis, *Nat. Methods*. 9 (2012) 676–682. doi:https://doi.org/10.1016/j.jconrel.2017.12.034.
- [30] Y.-C. Lee, C. Dalton, B. Regler, D. Harris, Drug solubility in fatty acids as a formulation design approach for lipid-based formulations: a technical note, *Drug Dev. Ind. Pharm.* 44 (2018) 1551–1556. doi:10.1080/03639045.2018.1483395.
- [31] P.A. Makoni, J. Ranchhod, K. WaKasongo, S.M. Khamanga, R.B. Walker, The use of quantitative analysis and Hansen solubility parameter predictions for the selection of excipients for lipid nanocarriers to be loaded with water soluble and insoluble compounds, *Saudi Pharm. J.* 28 (2020) 308–315. doi:10.1016/j.jsps.2020.01.010.

- [32] V.J. Stella, Chemical Drug Stability in Lipids, Modified Lipids, and Polyethylene Oxide-Containing Formulations, *Pharm. Res.* 30 (2013) 3018–3028. doi:10.1007/s11095-013-1051-2.
- [33] P.P. Constantinides, J.-P. Scalart, Formulation and physical characterization of water-in-oil microemulsions containing long- versus medium-chain glycerides, *Int. J. Pharm.* 158 (1997) 57–68. doi:10.1016/S0378-5173(97)00248-2.
- [34] B. Jing, Z. Wang, R. Yang, X. Zheng, J. Zhao, S. Tang, Z. He, Enhanced oral bioavailability of felodipine by novel solid self-microemulsifying tablets, *Drug Dev. Ind. Pharm.* 42 (2016) 506–512. doi:10.3109/03639045.2015.1058816.
- [35] N.-T. Tung, C.-S. Tran, T.-M.-H. Pham, H.-A. Nguyen, T.-L. Nguyen, S.-C. Chi, D.-D. Nguyen, T.-B.-H. Bui, Development of solidified self-microemulsifying drug delivery systems containing l-tetrahydropalmatine: Design of experiment approach and bioavailability comparison, *Int. J. Pharm.* 537 (2018) 9–21. doi:10.1016/j.ijpharm.2017.12.027.
- [36] Y. Tayrouz, Pharmacokinetic and pharmaceutic interaction between digoxin and Cremophor RH40, *Clin. Pharmacol. Ther.* 73 (2003) 397–405. doi:10.1016/S0009-9236(03)00059-6.
- [37] R.L. Oberle, T.J. Moore, D.A.P. Krummel, Evaluation of mucosal damage of surfactants in rat jejunum and colon, *J. Pharmacol. Toxicol. Methods.* 33 (1995) 75–81. doi:10.1016/1056-8719(94)00060-H.
- [38] S.D. Siqueira Jørgensen, T. Rades, H. Mu, K. Graeser, A. Müllertz, Exploring the utility of the Chasing Principle: influence of drug-free SNEDDS composition on solubilization of carvedilol, cinnarizine and R3040 in aqueous suspension, *Acta Pharm. Sin. B.* 9 (2019) 194–201. doi:10.1016/j.apsb.2018.07.004.
- [39] L. Kiss, F.R. Walter, A. Bocsik, S. Veszeka, B. Ózsvári, L.G. Puskás, P. Szabó-Révész, M.A. Deli, Kinetic Analysis of the Toxicity of Pharmaceutical Excipients Cremophor EL and RH40 on Endothelial and Epithelial Cells, *J. Pharm. Sci.* 102 (2013) 1173–1181. doi:10.1002/jps.23458.
- [40] M. Ogino, K. Yakushiji, H. Suzuki, K. Shiokawa, H. Kikuchi, Y. Seto, H. Sato, S. Onoue, Enhanced pharmacokinetic behavior and hepatoprotective function of ginger extract-loaded supersaturable self-emulsifying drug delivery systems, *J. Funct. Foods.* 40 (2018) 156–163. doi:10.1016/j.jff.2017.08.035.
- [41] J.A. Kraut, M.E. Mullins, Toxic Alcohols, *N. Engl. J. Med.* 378 (2018) 270–280. doi:10.1056/NEJMra1615295.
- [42] M. Vertzoni, P. Augustijns, M. Grimm, M. Koziolk, G. Lemmens, N. Parrott, C. Pentafragka, C. Reppas, J. Rubbens, J. Van Den Abeele, T. Vanuytsel, W. Weitschies, C.G. Wilson, Impact of regional differences along the gastrointestinal tract of healthy adults on oral drug absorption: An UNGAP review, *Eur. J. Pharm. Sci.* 134 (2019) 153–175. doi:10.1016/j.ejps.2019.04.013.
- [43] H. Liao, Y. Gao, C. Lian, Y. Zhang, B. Wang, Y. Yang, J. Ye, Y. Feng, Y. Liu, Oral absorption and lymphatic transport of baicalein following drug–phospholipid complex incorporation in self-microemulsifying drug delivery systems, *Int. J. Nanomedicine.* Volume 14 (2019) 7291–7306. doi:10.2147/IJN.S214883.
- [44] N.N. Mohammed, S. Majumdar, A. Singh, W. Deng, N.S. Murthy, E. Pinto, D. Tewari, T. Durig, M.A. Repka, Klucel™ EF and ELF polymers for immediate-release oral dosage forms prepared by melt extrusion technology, *AAPS PharmSciTech.* 13 (2012) 1158–1169. doi:10.1208/s12249-012-9834-z.
- [45] J.-H. Lee, H. Kim, Y. Cho, T.-S. Koo, G. Lee, Development and Evaluation of Raloxifene-Hydrochloride-Loaded Supersaturable SMEDDS Containing an Acidifier, *Pharmaceutics.* 10 (2018) 78. doi:10.3390/pharmaceutics10030078.
- [46] A.A. Kassem, A.M. Mohsen, R.S. Ahmed, T.M. Essam, Self-nanoemulsifying drug delivery system (SNEDDS) with enhanced solubilization of nystatin for treatment of oral candidiasis: Design, optimization, in vitro and in vivo evaluation, *J. Mol. Liq.* 218 (2016) 219–232. doi:10.1016/j.molliq.2016.02.081.
- [47] D. Sakloetsakun, S. Dünnhaupt, J. Barthelmes, G. Perera, A. Bernkop-Schnürch, Combining two technologies: Multifunctional polymers and self-nanoemulsifying drug delivery system (SNEDDS) for oral insulin administration, *Int. J. Biol. Macromol.* 61 (2013) 363–372. doi:10.1016/j.ijbiomac.2013.08.002.
- [48] Food and Drug Administration, Dimethyl Sulfoxide (DMSO), (n.d.). <https://www.fda.gov/>.

- [49] N. Parmar, N. Singla, S. Amin, K. Kohli, Study of cosurfactant effect on nanoemulsifying area and development of lercanidipine loaded (SNEDDS) self nanoemulsifying drug delivery system, *Colloids Surfaces B Biointerfaces*. 86 (2011) 327–338. doi:10.1016/j.colsurfb.2011.04.016.
- [50] P. Jaisamut, K. Wiwattanawongsa, P. Graidist, Y. Sangsen, R. Wiwattanapatapee, Enhanced Oral Bioavailability of Curcumin Using a Supersaturatable Self-Microemulsifying System Incorporating a Hydrophilic Polymer; In Vitro and In Vivo Investigations, *AAPS PharmSciTech*. 19 (2018) 730–740. doi:10.1208/s12249-017-0857-3.
- [51] S. Li, P. Madan, S. Lin, Effect of ionization of drug on drug solubilization in SMEDDS prepared using Capmul MCM and caprylic acid, *Asian J. Pharm. Sci.* 12 (2017) 73–82. doi:10.1016/j.ajps.2016.10.001.
- [52] International Organization for Standardization, ISO 10993-1 Biological Evaluation of Medical Devices—Part, Vol. 5, Tests for in Vitro Cytotoxicity, Geneva Switz. (2009).
- [53] L. Kiss, F.R. Walter, A. Bocsik, S. Veszeka, B. Ózsvári, L.G. Puskás, P. Szabó-Révész, M.A. Deli, Kinetic Analysis of the Toxicity of Pharmaceutical Excipients Cremophor EL and RH40 on Endothelial and Epithelial Cells, *J. Pharm. Sci.* 102 (2013) 1173–1181. doi:10.1002/jps.23458.
- [54] Y. Aktas, M. Celik Tekeli, N. Celebi, Development and characterization of exendin-4 loaded self-nanoemulsifying system and in vitro evaluation on Caco-2 cell line, *J. Microencapsul.* 37 (2020) 41–51. doi:10.1080/02652048.2019.1692945.
- [55] A. Beloqui, P.B. Memvanga, R. Coco, S. Reimondez-Troitiño, M. Alhouayek, G.G. Muccioli, M.J. Alonso, N. Csaba, M. de la Fuente, V. Préat, A comparative study of curcumin-loaded lipid-based nanocarriers in the treatment of inflammatory bowel disease, *Colloids Surfaces B Biointerfaces*. 143 (2016) 327–335. doi:10.1016/j.colsurfb.2016.03.038.
- [56] M.H. Patel, K.K. Sawant, Self microemulsifying drug delivery system of lurasidone hydrochloride for enhanced oral bioavailability by lymphatic targeting: In vitro, Caco-2 cell line and in vivo evaluation, *Eur. J. Pharm. Sci.* 138 (2019) 105027. doi:10.1016/j.ejps.2019.105027.
- [57] J. Zhao, M.H. Stenzel, Entry of nanoparticles into cells: the importance of nanoparticle properties, *Polym. Chem.* 9 (2018) 259–272. doi:10.1039/C7PY01603D.
- [58] E. Nottingham, V. Sekar, A. Mondal, S. Safe, A.K. Rishi, M. Singh, The Role of Self-Nanoemulsifying Drug Delivery Systems of CDODA-Me in Sensitizing Erlotinib-Resistant Non-Small Cell Lung Cancer, *J. Pharm. Sci.* 109 (2020) 1867–1882. doi:10.1016/j.xphs.2020.01.010.
- [59] Y.-M. Yin, F.-D. Cui, C.-F. Mu, M.-K. Choi, J.S. Kim, S.-J. Chung, C.-K. Shim, D.-D. Kim, Docetaxel microemulsion for enhanced oral bioavailability: Preparation and in vitro and in vivo evaluation, *J. Control. Release*. 140 (2009) 86–94. doi:10.1016/j.jconrel.2009.08.015.

IV. Supplementary information

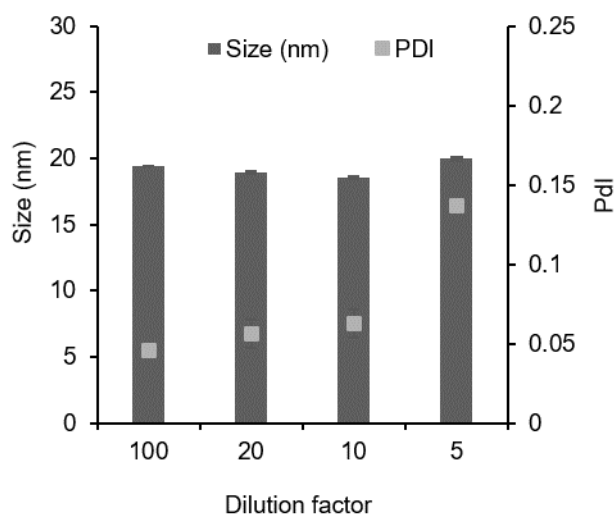


Fig. S1 BI-loaded SMEDDS b ($0.9 \text{ mg}\cdot\text{mL}^{-1}$) microemulsion stability over time in milliQ® water at 37 °C.

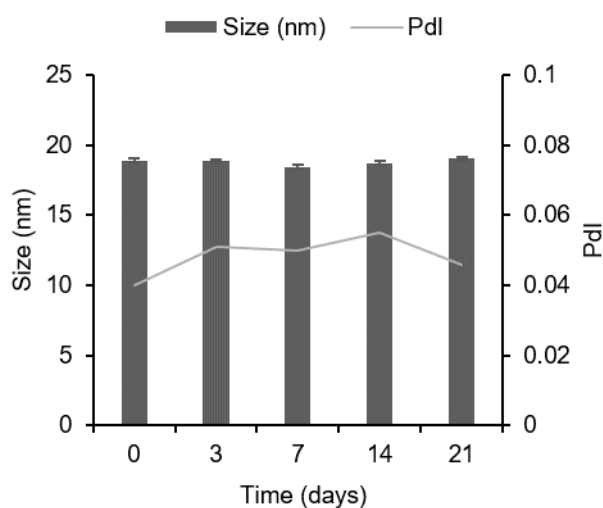


Fig. S2 Effect of the dilution factor on SMEDDS physicochemical properties.

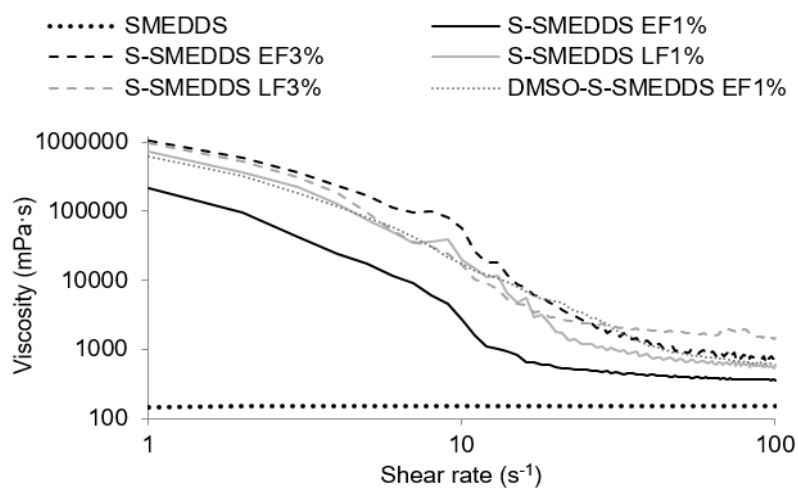


Fig. S3 Flow sweep experiments (viscosity vs. shear rate response) of SMEDDS and S-SMEDDS at 25 °C.

Table S1 BI-loaded SMEDDS and S-SMEDDS microemulsions stability in simulated gastric fluids (SGF) at time point 0 and 180 min, detected by HPLC analysis.

Sample	Drug loading (%)	Time (hours)	Encapsulation efficiency (%)
SMEDDS a	0.05	0	87.5 ± 1.9
		180	64.7 ± 5.8
SMEDDS b	0.09	0	78.1 ± 6.3
		180	36.7 ± 4.0
SMEDDS c	0.14	0	21.7 ± 2.3
		180	32.7 ± 2.4
S-SMEDDS I	0.30	0	21.5 ± 0.1
		180	18.4 ± 0.1
S-SMEDDS II	0.55	0	13.6 ± 0.1
		180	11.9 ± 1.2

Chapter V. General discussion

The aim of the present research thesis has been the development of hybrid polymeric-lipid systems based on nanoemulsions (NEs) loaded into a chitosan sponges and supersaturable self-microemulsifying drug delivery systems (S-SMEDDS). Both systems were designed for improving intestinal residence time following oral administration and for increasing local or systemic drug absorption.

To this aim, a first part of this work was dedicated to the formulation and the physicochemical-structural characterization of the nanosystems, NE and SMEDDS, and then of their hybrid polymeric counterparts, sponges and S-SMEDDS. A second part was focused on the evaluation *in vitro* and *in vivo*.

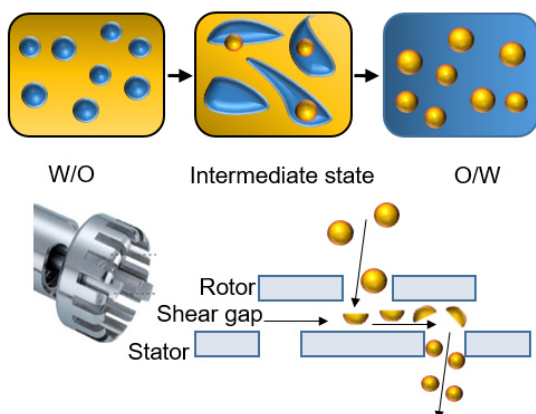
V.1 Formulation and characterization

In this work, two types of lipid-based formulations were developed: NE, prepared by emulsion phase inversion (EPI) method, were intended for an improved oral drug delivery, and SMEDDS, created by self-emulsification, aimed at the solubility enhancement of poorly-water soluble molecules in the intestinal tract (Fig. 1).

Nanoemulsion

Formulation method

Emulsion phase inversion (EPI) + high energy input (UltraTurrax®)



Composition

Oil: MCT (Miglyol 812)
Surfactants hydrophilic PEG(40)stearate (Myrj 52); hydrophobic Oleoyl polyoxyl-6 glycerides (Labrafil M1944CS)

Physicochemical properties

Dependent on the formulation process
Size around 100 nm
Pdl < 0.2
Surface charge neutral

Stability

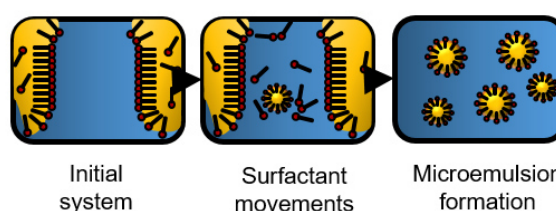
Kinetically stable

Purpose

Drug delivery

SMEDDS

Self-microemulsification



Oil: MCT (Miglyol 812)
Surfactants: hydrophilic Polyoxyl 40 hydrogenated castor oil (Kolliphor RH40)
Co-solvents: diethylene glycol monoethyl ether (Transcutol HP) + EtOH/DMSO

Dependent on the system composition
Size < 20 nm
Pdl < 0.1
Surface charge neutral

Thermodynamically stable

Drug solubility enhancement

Fig. 1 Comparison between the two developed nanosystems, nanoemulsions (NE) and SMEDDS, as for their formulation process, composition and physicochemical attributes.

V.1.1 Nanosystems

NE were formulated by mean of EPI method coupled with a high energy input via a rotor-stator disperser. The choice of excipients was based on their common use in lipid-based formulations and their FDA status for the oral route. The NE core was composed of medium chain caprylic/capric triglycerides (MCT, Miglyol® 812) and stabilized by a mixture of non-ionic hydrophilic and hydrophobic surfactants, polyoxyethylene (PEG)-40 stearate (Myrj® 52, HLB 16.9) and oleoyl polyoxyl-6 glycerides (Labrafil® M1944CS, HLB 4). The hydrophilic PEGylated surfactant was selected because of i) the reported stabilizing properties, ii) the emulsification ability, iii) the related biological advantages, such as the neutral surface potential optimal to permeate across the intestinal mucus layer [1,2]. The hydrophobic surfactant was added to the formulation to strengthen the NE structure by positioning between the oil core and the PEGylated shell, thus conferring stability [3]. Worthy of mention is that the combination of these excipients in a nanometric system is for the first time described.

NE was optimized using an experimental design in ternary and pseudo-ternary diagrams [4]. The selected formulation had an oil content of 7% (w/w), a surfactant to oil (SOR) ratio of 2.86 and HLB of 13.2. NE presented a size of 100 nm, they were quite monodispersed (PDI 0.2) and neutrally charged (ζ -potential -9 mV). The avoidance of organic solvents for NE formulation makes the EPI provides an additional benefit over other techniques for toxicity reasons [5].

The EPI was previously used for the development of food-grade NE. By simple water addition over the oil phase (MCT, vitamin E acetate, Tween® 80, SOR 1) McClements research group obtained NE showing a size of 90 nm and low PDI (0.22) at SOR value of 1 [6].

In the present study, the EPI alone turned out not to be the optimal method for the development of NE, and additional energy was needed to refine the droplet size. Possible reason was the solid nature of the excipient which needed to be solubilized at high temperature (80 °C) for homogeneous mixing with other excipients. The issue was simply overcome by furnishing additional energy to the system via rotor-stator dispersers. This technique was already presented by Ragelle et al. who prepared 146 nm NE (PDI < 0.1), made of a MCT oil core (Miglyol® 812, Lipoid E80®) stabilised by a surfactant mixture (Labrasol®, Tween®), intended for fisetin delivery by water titration heated at 70 °C followed by a cycle of high shear mixing (UltraTurrax®, 21,500 rpm) for 10 min and an additional cycle of sonication for 15 min [7]; and by Rutckeviski et al. who developed bullfrog oil NE stabilized by a surfactant blend of Tween® 20 and Span® 80 of 410 nm (PDI 0.2) via one UltraTurrax® cycle of 10 min at 11,000 rpm [8]. Also the UltraTurrax® was used when formulating NE in presence of small amount of surfactants, as in the case of NE, composed of Eugenia brejoensis essential oil and Tween® 80 as surfactant, that were homogenized at 12,000 rpm for 4 min, obtaining droplets of 143 nm [9].

Overall, the formulation process here proposed may recall the widely exploited high-pressure homogenization or microfluidization, in which coarse emulsions are formed and their droplets subsequently broken down into nanometric particles [10]. Its advantage lies i) in the production of droplets with high kinetic stability and ii) in the lower amount of energy and time required that makes it economically beneficial and environmentally sustainable [11].

The robustness of the formulation process was demonstrated by the efficiency in scaling up the NE 10 times. A further scale up in light of a future industrialisation has to take account of difficulties in obtaining homogeneity in large volumes.

The use of alternative and newer formulation processes, namely the microfluidics [12], could be envisaged to further shape the system monodispersity or decrease the surfactant amount.

Conversely, the formulation process of SMEDDS was much simpler and required the addition of water on the lipid phase under gentle stirring at physiological temperature (37 °C). The microemulsion droplet formation and physicochemical characteristics did not depend upon the formulation method but on the composition of the system. The range of exploitable excipient was limited and their careful selection was the fundamental step for optimal SMEDDS development. A literature search was performed to identify the components that were exploitable for the design of a self-emulsifying formulation [13,14], then oil, surfactant and co-solvents were selected on the base of their solubilisation capacity for the drug. The optimal system in terms of physicochemical attributes (size < 20 nm, PdI < 0.1) was chosen after thorough optimisation using a mixture design. Recently, Nottingham et al. exploited this methodology to optimize SNEDDS particle size, drug content and drug release [15].

The final system was composed of 10% (w/w) oil (MCT, Miglyol® 812), 70% (w/w) surfactant (Polyoxyl 40 hydrogenated castor oil, Kolliphor® RH40) and 20% (w/w) co-solvents (diethylene glycol monoethyl ether Transcutol® HP and ethanol or DMSO). The surfactant to oil (SOR) ratio was 7 and the HLB 12.2.

SMEDDS had a 2.6-fold lower oil content than NE. This is typical of LFCS class IIIB systems (microemulsions). The choice of designing a SMEDDS system with a low oil content was driven by the low solubility of the concerned drug in oils and by its high solubility in compounds possessing high content of ethylene oxide moieties (PEG40) and high HLB values, such as Kolliphor® RH40. Besides, the feasibility of loading the drug in NE was assessed prior to the creation of the SMEDDS system with poor results (i.e. complete drug precipitation within 24 h from NE at drug loading of 1 mg·mL⁻¹, results not reported).

Upon water addition under gentle agitation the optimized SMEDDS led to the formation of microemulsions droplets of 18.52 ± 0.02 nm, low PdI and neutral surface charge (-1.03 ± 0.82 mV). The self-emulsification occurred in 68 s due to the fast water penetration in the shell of surfactant and co-solvents surrounding the oil droplets [16].

The system was highly stable upon dilution due to the high amount of surfactant Kolliphor® RH40, which never fell below the critical micelle concentration (CMC of Kolliphor® RH40: 0.03% w/w at 37 °C, as reported by the technical specifications [17]) even in the highest diluted conditions (100-fold).

The selected excipients Miglyol® 812, Kolliphor® RH40, Transcutol® HP and EtOH (or DMSO) were already used in self-emulsifying formulations in previous works [18–20]. However, their efficient combination as SMEDDS was reported for the first time in this study.

Co-solvents EtOH or DMSO were used as vehicle for the drug in order to facilitate its homogeneous dispersion in the mixture. In accordance with previous studies reporting their use in SEDDS, their content was kept at values lower than the reported limit of toxicity for the oral route, ensuring the safety of the developed formulation [18,21–24].

V.1.2 Conversion of the nanoemulsions in solid dosage forms

Further step in the formulation process of the nanosystems was the conversion of NEs in solid dosage forms using both freeze- and spray-drying. The purpose was to increase the NE storage stability, and to test the process feasibility in sight of the NE loading in the dry nanocomposite sponge.

Both freeze-drying and spray-drying were efficient in the conversion of NE into a dry powder and they allowed to preserve NE physicochemical and structural properties, but the freeze-drying turned out to be the preferred technique (Fig. 6 Chapter II).

Previous research compared freeze- and spray-drying for the solidification of NE, concluding that the spray-drying should be the technique of choice. Their criteria of selection were the dry samples quality, stability and morphology and the maintainance of the nanoparticle physicochemical properties upon reconstitution on water [25–27] (Table 2 in section I.4.3 introduction). In the present work, NE were spray-dried in presence of maltodextrin (MD) as drying excipients. A NE:MD ratio of 0.5, corresponding to a NE concentration of 5% (w/v) and MD of 10% (w/v), guaranteed the obtainment of dry powders showing all the required characteristics in terms of visual aspect, physicochemical properties, yield and morphological characteristics. These results are in accordance with previous studies on the drying of NE using MD that showed an increase in the NE size when using a low excipient amount (i.e. MD at 3% [28]) or when no drying agents were used [27] (Table 2 in section I.4.3 introduction). While it was proved that the physicochemical properties of nanosystems were completely preserved when the excipient were added in a large excess (23.9% w/w of a 70:30 lactose: sucrose mixture [29] and 57.7% w/w of lactose [30]).

Freeze-drying of NE was performed in presence of trehalose (TR) as cryoprotectant. We could conclude that i) NE complied with all freeze dried requirements when the NE amount was high and the cryoprotectant amount was low (NE 13.5% TR 2.5% at NE: TR ratio of 5:1); ii) an excessive dilution of the nanosystem (NE < 5% w/v) resulted in poor drying performance in terms of cake appearance and NE physicochemical properties after reconstitution; iii) the method of cryoprotectant addition should be considered as relevant as the freezing and drying steps: the cryoprotectant should be added in the colloidal suspension as a solution rather than a powder since its direct addition as powder can lead to partial droplet destabilisation (higher size and PDI); iv) the freeze-drying in absence of cryoprotectant was feasible: despite the long reconstitution time, NE showed an acceptable increase in size (of 70 nm) and PDI (from 0.2 to 0.3).

Commonly, when freeze-drying NE, the tendency is to use a high cryoprotectant amount and low NE amount to ensure an efficient protection of the nanosystem from the freezing and drying stresses [31–34] (Table 2 in section I.4.3 introduction), not always resulting in an optimal drying performance. Moreover, high cryoprotectant incorporation also lead to higher residual moisture content due to unfrozen water remaining trapped in the sugar matrix during the sublimation step [35].

The NE conversion in a solid dosage form also challenges the current research on the spray- and freeze-drying of other lipid-based systems than NE. The spray-drying procedure here presented allowed the obtainment of higher process yield (90%) compared to previous research on lipid-core nanocapsules (1% w/v) spray-dried in presence of lactose (10% w/v) (yields between 30% and 40%) [36], and nanocapsules (1% w/v) spray-dried in presence of MD (10% w/v) (yield 66.9%) [37]. As for freeze-drying, Morais et al. achieved the task of freeze-drying microemulsions using maltose at 5% (w/w), with a reduction in the droplet size (from 54 to 32 nm) and no changes in the content of the loaded drug

Amphotericin B [38]. Instead, the lyophilisation of other lipid-based systems such as LNC is still demanding a thorough investigation of the formulation and the process conditions in order to ensure the long-term stability of these systems. Briot et al. reported an attempt to freeze-dry LNC loaded with decitabine in presence of 40% w/w sucrose solution added in a 1:1 v/v ratio. Their protocol allowed for the maintenance of the nanoparticle physicochemical characteristics, however the residual moisture was high (25% of the initial quantity) and the drug payload was drastically decreased of 9-fold indicating that this method could not be selected to stabilize the formulation [39].

The findings of the drying study here reported can be helpful for the future design of dry lipid-based systems.

V.1.3 Polymer hybrid nanosystems: nanocomposite sponges and S-SMEDDS

In order to improve the pharmaceutical performance of the developed nanocarriers, matrix structured hybrid systems (polymeric nanocomposite sponges) and self-emulsifying polymer hybrid systems were formulated. The two hybrids differed for structural and functional properties (Fig.2).

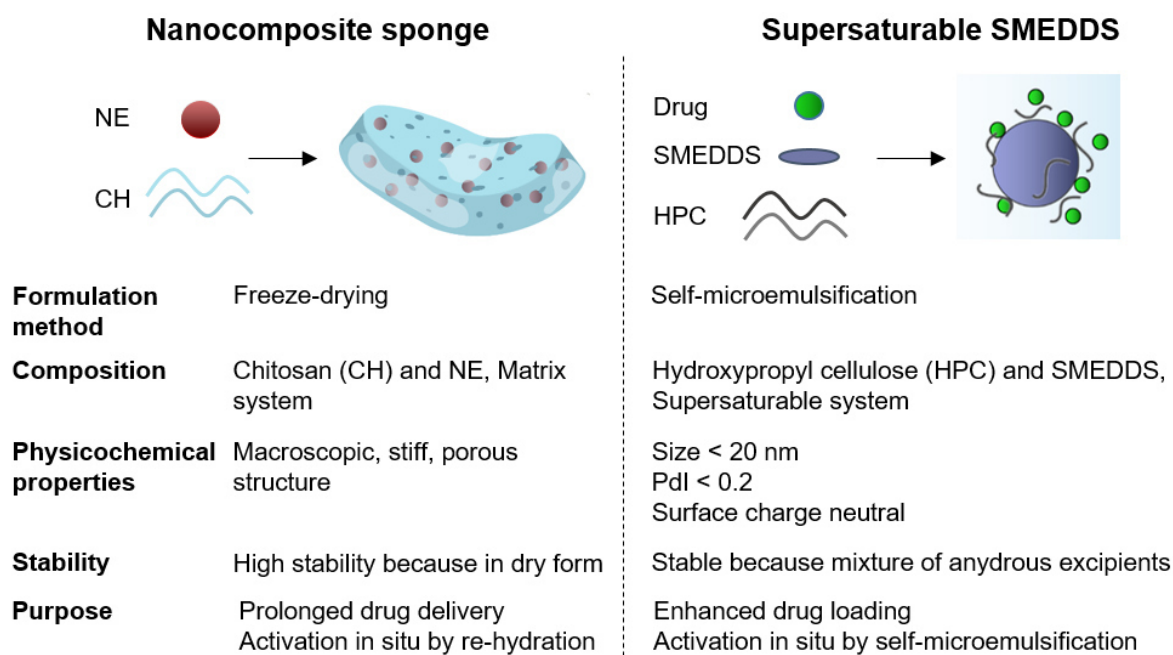


Fig. 2 Comparison between the two developed hybrid nanosystems, nanocomposite sponges and supersaturable SMEDDS, as for their formulation process, composition, physicochemical and structural attributes.

Nanocomposites consisted in NE embedded in the matrix of a chitosan (CH) sponge.

Unlike S-SMEDDS in which the polymer is in simple dispersion, in the nanocomposite the polymer creates a matrix in which the NE is embedded. This matrix protects the nanosystem from the external environment, stabilizes it and modulates its release and interactions with the environment. A point in common with the S-SMEDDS is that both systems were created to be activated in situ: the S-SMEDDS via the generation of microemulsions starting from the polymer-lipid mixture and the sponges via rehydration once in contact with intestinal fluids.

Chitosan (CH, $550 \text{ kg}\cdot\text{mol}^{-1} M_w$, 4% DA) was selected as polymer to create the nanocomposite matrix. CH has been widely exploited in nanocomposites [40–49] because of its favourable properties including biocompatibility, biodegradability, antibacterial and biological activity [50,51]. Besides, several studies proved its superiority as mucoadhesive cationic polymer owing to its ability to develop molecular attraction forces by electrostatic interactions with the negative charges of intestinal mucin depending on the environmental pH [52–54]. A key limitation in the use of CH is its low mechanical strength, its tendency to dissolve at pH lower than its pKa (6.2) and its difficulty to promote a sustained release [55,56]. We overcame these shortcomings by producing nanocomposite CH sponges via freeze-drying. NE were loaded in sponges by mixing of the NE colloidal suspension with the chitosan solution prior to the creation of the final system (Fig. 2 Chapter III). This method of nanoparticle addition was also used by Laroui et al. to produce chitosan-alginate hydrogels containing tripeptide Lys-Pro-Val (KPV)-loaded NPs [49] and by Javanbakht et al. to produce chitosan beads containing graphene quantum dot nanoparticles [44]. A different procedure was used by Cui et al. who loaded freeze-dried nanoparticles into pre-formed chitosan-ethylenediaminetetraacetic acid (EDTA) hydrogels and subsequently converted them into films [43]. However, most studies reported that the nanoparticle mixing with the polymer precursor rather than its loading in preformed polymeric network is preferable since it allows for a more homogenous dispersion of NP in the polymeric matrix [57].

The presence of the NE conferred stiffness and reinforced the structure of sponges. The porous structure was primarily defined by the morphology of the growing solvent crystals, and secondarily by the ability of the particles and CH chains to pack between the crystals. NE could interact with the CH polymer chains via hydrogen bonding but also via hydrophobic interactions, being the nature of the CH used (4% DA in the neutralized state) hydrophobic [58]. Consequently, part of the NE was present on the bulk of the membranes constituting the pores of the sponges, and part of the NE was located at the sponge surface (Fig. 3. Chapter III). Following rehydration, the presence of the NE hindered the conversion of the dry sponge in a gel-like structure ($\text{pH} > 6.5$) or its dissolution ($\text{pH} < 6.5$) and preserved its solid state as wet sponge in the whole intestinal pH range (from 5 to 7.5), while ensuring water absorption capacity (Fig. 5 Chapter III).

The evaluation of the physicochemical properties of NE after sponge rehydration (increase in NE size of around 20 nm, unvaried PDI and shift towards neutral values of surface charge) pointed out that the CH polymer acted as drying excipient protecting the NE against the drying stress. In fact, the reported increase in particle size was comparable to the one observed for the NE dried in presence of trehalose (NE13.5%-TR2.5%) and lower than the one of NE freeze-dried alone (NE27%).

The production of a dry macro-structure in a single step by freeze-casting was already reported for chitosan alone [59] and for nanocomposite aimed at tissue engineering purposes [60] or at buccal and vaginal delivery [61,62]. Only few examples of the application of the freeze-drying technique to intestinal nanocomposites can be found, where the freeze-drying was merely used for the conversion of the nanocomposite in a dry form (dry hydrogel or dry microsphere), but not as formulation process *per se*. Casadei et al. designed a nanocomposite through the freeze-drying of a dextran methacrylate hydrogel prepared by UV irradiation and loaded with SLN. The system was dried in absence of cryoprotectants exploiting the dextran methacrylate matrix for SLN stabilisation purposes. Upon rehydration the system recovered its gel-like characteristics and allowed for a sustained release [63]. Also microspheres of mPEG-b-PLLA (biodegradable methoxy poly(ethylene glycol)-block-poly(L-

lactide) embedded with nanoparticles for insulin oral delivery were produced by means of a double emulsification process followed by lyophilisation. The rehydrated matrix maintained its structure in the gastric acidic pH, while decomposing at intestinal pH ensuring for a targeted delivery [64].

Lastly, the interest in the use of the freeze-casting arises from the possibility of modulating the system properties not only by varying the system composition but also by varying the process parameters. In this study we used a freeze-casting process to produce sponges with a cellular structure. It would be interesting to vary the drying parameters, such as the freezing temperature and the freezing rate in order to modulate the size of the ice crystals and consequently the size of the resulting pores [65]. Additionally, the direction of the solidification front could be varied during the freezing step to create systems with a lamellar or columnar pore structure [66], and compare the impact of in terms of rehydration performance, drug release and efficacy *in vivo*.

The other type of developed hybrid nanosystem was self-emulsifying polymer hybrid systems, which consisted in SMEDDS combined with the polymeric precipitator inhibitor HPC. These supersaturable-SMEDDS (S-SMEDDS) are a mixture of polymer and lipid excipients. Upon dispersion in aqueous medium, the lipid excipients create microemulsions, while the polymers prevent drug precipitation by maintaining the drug in a supersaturated state above the equilibrium solubility. Most of the studies on supersaturable systems exploit PIs that are insoluble in the lipid excipients and once in the GI tract got dispersed in the aqueous phase or positioned themselves at the interface of the lipid droplets maintaining the drug in a supersaturated state. Examples are HPMC [67–70], Poloxamer 407 [20,71,72] and Soluplus® [18,73,74]. They supposedly act by creating H-bonds and hydrophobic interactions with the drug or by absorbing the drug crystals thanks to their rigidity and high molecular weight [13]. Also HPC has been proved an effective lipid-insoluble PIs with respect to the kinetic stabilization of supersaturation thanks to the formation of H-bonds with the drug and to the decrease in drug crystal diffusion due to an increase in the system viscosity [75]. In the present study, HPC mechanism of drug precipitation inhibition was ascribed to the enhancement in system viscosity and to interactions between polymer and drug molecules.

In the design of S-SMEDDS, three are the main objectives: (i) to achieve maximal drug loading, (ii) to shorten the system self-emulsification time, and (iii) to minimize drug degradation under *in vivo* physiological conditions.

Two different S-SMEDDS were prepared: S-SMEDDS I containing 10% EtOH and 1% HPC and S-SMEDDS II containing 5% DMSO and 1% HPC (% w/w). The drug loading performance of conventional SMEDDS was enhanced 2-fold through S-SMEDDS I and of 4-fold through S-SMEDDS II. However, the self-microemulsification time of S-SMEDDS II was longer (> 8 min) than in S-SMEDDS I (2 min) because of the too high viscosity of the system that delayed the components homogenous mixing and the water penetration in the shell of surfactant and co-solvents surrounding the oil droplets. Thus, S-SMEDDS I was the system of choice from a technological point of view.

The amount of precipitator inhibitor added was lower than previously reported in the literature. Lee et al. designed S-SMEDDS, composed of a surfactant mixture of Capryol™ 90 and Labrasol® and of PEG 200 as co-solvent, complemented with 5% of the precipitator inhibitor HPC-L [75]. The S-SMEDDS prepared by Singh, containing a propylene glycol non-ionic lipophilic surfactant (Lauroglycol® FCC) and an ethoxylated co-solvent (Transcutol® P) contained 5% of HPMC as precipitator inhibitor [67].

While an even higher content of precipitator inhibitor was used by Bannow et al., who supplemented the conventional SNEDDS, made of a MCT oil core (Capmul® MCM) stabilized by surfactants (Captex® 300 Kolliphor® RH40) with 20% w/w PVP/VA 64 to create S-SNEDDS [76]. The addition of PI in such high amount can cause variations in the nanodroplet physicochemical properties that can jeopardise the system performance. In HPMC S-SNEDDS [67] the size increased from 57 nm to 213 nm showing three distinctive particle measurements in the DLS analysis and a high PDI value of 0.47, thereby indicating a heterogeneous dispersion. Instead, Quan et al. succeeded in designing S-SEDDS containing 15% of the precipitation inhibitor polyvinyl caprolactam–polyvinyl acetate–polyethylene glycol graft copolymer (Soluplus®) without significant alteration of the droplet size and PDI, which suggest the well-retained self-emulsifying ability. The slight increase in the mean droplet size compared to conventional SEDDS (from 125 nm to 132 nm) was attributed to the absorption of Soluplus® on the particle surfaces and the enhanced steric stabilization generated by the strongly hydrated polymer chain [18]. These observations suggest that we might try to use another precipitator inhibitor, such as HPMC, Soluplus® or Poloxamer, in view of maximizing its amount and consequently decreasing the amount of surfactant (Kolliphor® RH40), though bearing in mind that the system physicochemical properties must not be compromised.

Furthermore, the developed S-SMEDDS can be converted in solid dosage forms with a view to further improve their storage stability. Among all the exploitable methods presented in section I.5.2 of the manuscript introduction, spray-drying and freeze-drying look valuable approaches. As a first trial the protocols developed for the NE could be applied to S-SMEDDS. Alternatively, S-SMEDDS could be embedded in polymers such as chitosan to generate sponges combining the advantages of a dry form with the ones of a matrix for a sustained release, enhanced mucoadhesion and improved stabilisation of supersaturation.

V.1.4 Highlights on the nanoemulsion structure

Part of this PhD work was devoted to the structural characterization of the NE, with an in-depth focus on the NE shell nature (Fig. 3).

The NE shell was crystalline when the NE dry and amorphous when in colloidal suspension, supposedly because of the formation of a bulky amorphous PEG-water complex in colloidal NE suspension that decreased the packing density of the surfactant to such an extent that the Myrj® 52 surfactant stearic chains were no longer crystalline (Fig. 8 Chapter II).

The fluid nature of the NE shell can be ascribed to the low surfactant packing density in the shell, since the bulky head group of the PEGylated surfactant weakened the hydrophobic interactions between surfactant tails, thus constraining alkyl chains in a disordered configuration to fill the space between PEG moieties. Besides, the hydrophobic surfactant by intercalating the hydrophilic one can further reduce the packing density of PEG chains (Fig. 9 Chapter II).

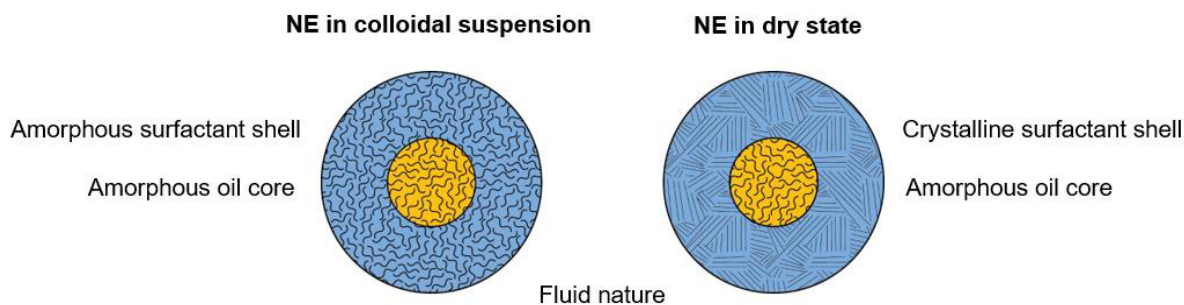


Fig. 3 Characteristics of the NE shell.

These observations are in accordance with studies performed on liposomes showing that liposomes are fluid when composed of large head group excipients such as phosphatidylcholine and rigid when composed of small ones such as phosphatidic acid [77,78]. Dora et al. reported that the addition of PEG 660-stearate (Solutol® HS15) to hydrogenated soybean lecithin with 70% phosphatidylcholine (Lipoid® S75-3N) in the formulation of nanosized emulsions increased the flexibility of the shell layer because of the prevention of a close packing of the molecules at the interface. Whereas the shell was rigid when the Lipoid® S75-3N was used as the sole surfactant [79].

The analysis here presented can be useful to provide a proof of concept of the structural differences between NE and other lipid based systems and shed more light on their complexity. Up to date the rigidity of a system has been stated based on observations regarding components amount, properties and physico state and on the exploited formulation method. LNC are thought to possess a rigid shell because of the surfactant used, which have a melting point higher than the storage temperature, because of the high density of PEG chains (> 10% versus < 10% in NE) and because of the overconcentration of surfactant on the particle surface thanks to the temperature cycles performed while formulating by PIT method [80]. While the rigidity of NLC, modified matrix SLN and mRNA-LNP has been related to the presence of PEG as the outmost particle coating [81–83].

A more rational approach for the characterisation of their fluid or rigid nature is therefore needed.

The use of the polarity sensitive Dioll is a novelty in nanotechnology. Dioll (patent EPO19306175.1–1118) is a newly synthesized derivative of the fluorophore Laurdan (6-dodecanoyl-2-dimethylaminonaphthalene). It was selected for this study because of its enhanced polarity that allowed better insertion in the NE shell compared to Laurdan. Up to date Laurdan and its derivatives were only used for the assessment of liposomes rigidity and the study of biological membranes [84,85].

The exploitation of this technique in association with conventional ones, namely small-angle X-ray scattering (SAXS) [86], ¹H nuclear magnetic resonance (NMR) spectroscopy [87], and 1,6-di-phenyl-1,3,5-hexatriene (DPH) fluorescence anisotropy [88] can provide useful information on the structural properties of lipid-based nanosystem over a broad range of conditions.

NE developed in this study are intended to deliver hydrophobic drugs. The presence of an amorphous oil core in NE state is highly beneficial to maximise the drug loading since an amorphous state facilitates the incorporation of the drug [89,90]. Moreover, the preservation of the amorphous state also when the NE in its dry state ensure the maintenance of a high drug encapsulation efficiency [86].

The nature of the shell plays a primary role on drug release. A sustained release of the loaded hydrophobic drug is ensured by the PEG-water complex in the shell which increases the hydrophilic character of the outer NE layer and slows down the drug diffusion through the PEG corona [86].

The crystallinity of the NE shell may underlie the NE aptness to freeze-drying. The crystallisation of the PEGylated Myrj® 52 surfactant upon water sublimation might strengthen the shell ensuring system stability during all drying steps. This is consistent with previous finding on nanocapsules in which the system aptness to freeze-drying was ascribed to crystallization of lecithin upon drying [91].

The crystallinity of the shell when the NE in its dry form further contribute to enhance the system stability upon storage since a particle crystalline state is more stable than an amorphous one [92].

Lastly, the fluid nature of the NE shell might impact the NE biological performance and in particular its cellular internalisation pathway. We will make a point on this biological aspect in section V.2.6.

V.2 *In vitro* and *in vivo* evaluation

In vitro and *in vivo* studies aimed at assessing the biological attributes of the developed formulations. Firstly, we evaluated the potential of NE, SMEDDS and S-SMEDDS systems to maintain a good stability in simulated gastric and intestinal fluids. *In vitro* release studies in simulated GI media aimed at evaluating the ability of the NE to control the release of the loaded drug were carried out.

Secondly, we examined the cytocompatibility of the NE and of SMEDDS and S-SMEDDS on intestinal cell models (Caco-2 and HCT 116). Then, we studied the mucopenetrating properties of the NE and the efficiency of the mucoadhesive chitosan sponge to increase the NE intestinal residence time after oral administration to mice. Lastly, SMEDDS and S-SMEDDS were evaluated as for their cellular permeability across Caco-2 monolayers and for their ability to increase drug bioavailability *in vivo* in healthy mice.

V.2.1 Considerations on stability in simulated gastrointestinal fluids

In view of their oral administration the stability of developed systems was evaluated in simulated gastric fluid (SGF) at pH 1.2 and simulated intestinal fluid (SIF) at pH 6.8, without enzymes, at 37 °C.

In the case of the NE, the stability was mirrored by the capacity of the drug-loaded delivery system (tacrolimus-loaded NE) to maintain its initial size and PDI in both SGF up to 3h and SIF up to 6h without showing drug leakage.

Instead, in the case of SMEDDS, the stability assessment implied the ability of the formulation to self-emulsify in the gastrointestinal environment and to keep the drug in a solubilized state (SMEDDS) or supersaturated state (S-SMEDDS). BI precipitate in acidic SGF from both SMEDDS and S-SMEDDS probably due to the drug ionized state that hampered hydrophobic and H-bond interactions with the non-ionic excipients. The precipitation was partially reduced by S-SMEDDS because of the ability of HPC to interact with the drug and maintain it in a supersaturated state (Fig. 4 Chapter IV).

Both SMEDDS and S-SMEDDS II were stable in the SIF alkaline pH, where the drug interactions with the system excipients were favoured thanks to the drug non-ionised form. Noteworthy, when the pH was shifted from acidic to alkaline values, with a view to mimic the pH variations in the GI tract, systems reclaimed their properties and all the drug re-dissolved in the oil droplets, being S-SMEDDS I the most stable (Fig. 5 Chapter IV). The avoidance of system instability while transiting in the stomach is for formulation scientist a primary concern. In the case of a neutrally charged drug, such as curcumin, the

prevention of precipitation in SGF was easily achieved thanks to the addition of a small amount of Eudragit® E PO (5% w/w) as a precipitation inhibitor in S-SMEDDS. The hydrogen bonding between the carbonyl group of the Eudragit® E PO polymer and the hydroxyl (OH) group of curcumin facilitated the drug-polymer interaction independently from the acidic pH environment [93].

In the aim of stabilize the SMEDDS suspension in SGF, Lee et al. proposed pH-modified S-SMEDDS incorporating a precipitation inhibitor (HPC-L) and an acidifier (phosphoric acid) to increase the solubility of raloxifene hydrochloride. This system, showing a pH of 2.5, improved the dissolution of the drug when in SGF at pH 1.2 (> 80%) compared to non-pH-modified S-SMEDDS, indicating that the drug precipitation can be limited by modulating the pH of S-SMEDDS [75]. Further studies reported the efficient inhibition of precipitation of indomethacin, a weak acid lipophilic drug, in SGF by supplementing SEDDS with Vitamin E TPGS (20% w/w), thanks to the creation of hydrogen bonding with the drug. By using Raman spectroscopy, the authors were able to correlate the structure and physicochemical properties of the drugs and surfactants to their ability to prevent drug precipitation, suggesting the importance that the careful selection of system components can have on the overall performance [94]. In a similar research on SMEDDS loaded with the lipophilic drug itraconazole, the authors observed that the surfactants (2.5%) ability to stabilize the drug supersaturation in acidic medium was limited to a rather short time period (5 min in case of Tween® 20 and Kolliphor® RH40, 40 min in case of Vitamin E TPGS). Whereas, a non-polymeric precipitator inhibitor like hydrophilic cyclodextrins was much more effective. This finding opens the way for the possible exploitation of precipitator inhibitors other than the polymeric ones [95].

Alternatively, system disturbance and drug low solubilisation in gastric environment were avoided by filling SEDDS in enteric coated capsules. Al-Nimry et al. proved that the capsule protected the solid-SNEDDS at pH 1.2, while complete omeprazole solubilisation was achieved after capsule dissolution at intestinal basic pH of 7.4 [96]. We suggest to exploit this easy, technically and economically favourable approach which consists in the loading in enteric capsules also for the developed S-SMEDDS (Fig.4). SMEDDS can be solidified prior to filling [97] or newer technologies such as the enteric coated softgels (<https://consumerhealth.catalent.com/over-the-counter/softgel/enteric-coated-softgels/>) or the liquid-filled hard capsules (LFHCs) composed of a hydroxypropyl methylcellulose (HPMC) shell (<https://www.capsugel.com/service-suites/hpmc-gelatin-and-alternate-polymer-capsules>) can be used to fill the liquid S-SMEDDS. The HPMC coating will ensure protection in the stomach environment and release at pH higher than 6.8.

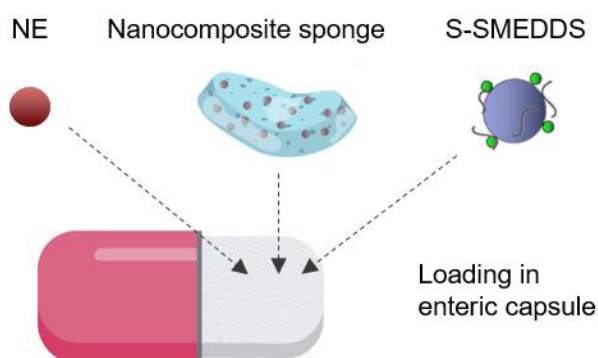


Fig. 4 Suggestion of the loading of nanoemulsion (NE), nanocomposite sponge and S-SMEDDS in enteric capsules.

In addition, enteric capsules could be exploited for the delivery of the developed NE dried powders and nanocomposite sponges. In order to achieve a targeted small intestinal or colonic delivery the avoidance of system instability or degradation in the stomach is essential. Examples of nanocomposites stabilized by a gastro-resistant protection have been mentioned in Table 5 and 6, section I.6.1 of the introduction. Santos et al. research group designed enteric nanocomposite microspheres by loading chitosan-coated liposomes in an hydroxypropyl methylcellulose acetate succinate matrix. The polymer conferred total protection from the harsh gastric conditions, then its dissolution at pH higher than 6.8 allowed for system activation specifically in the intestine [98]. Similarly, sodium dodecyl sulphate modified-metal-organic framework nanoparticles (Ins@MIL100/SDS) were embedded in microsphere composed of the enteric methoxy poly(ethylene glycol)-block-poly(L-lactide) (mPEG-b-PLLA) polymer that protect them from rapid degradation under acidic conditions in the stomach allowing for specific nanoparticle delivery in the intestine at pH higher than 6.8 [64]. While, Nanoparticle-in-Microparticle Delivery System (NiMDS) designed to exert a mucoadhesion activity in the intestine were filled in enteric capsules prior to oral administration to dogs. The strategy allowed to avoid the impairment of the NiMDS integrity and to prevent the release of the encapsulated drug in the stomach leading to high system effectiveness *in vivo* [41]. Also other nanocomposite systems would benefit from a delivery via enteric capsules. Antisense oligonucleotide (ASO)-chitosan nanoparticles were embedded in a chitosan-phytic acid matrix shaped as microparticles that were subsequently coated with phytic acid protective shell creating multicompartimental capsules. The double chitosan and phytic acid layers protected the encapsulated ASO from nuclease digestion and acidic environment, but a burst release (between 25% and 50% depending on the capsule size) of ASO occurred upon incubation in SGF over 2h. Despite this partial premature release of the cargo as assessed *in vitro*, the multicompartimental capsules were efficient to deliver high amount of ODN to the small intestine or the colon of rats *in vivo* [40]. A gastro-resistant coating would further ameliorate the system performance.

As regards the present work, the use of enteric capsules will be favourable to protect the system and to avoid any premature release of the NE from the sponge and/or of the drug from the NE in the stomach, while guaranteeing complete system efficiency at its intestinal site of action.

V.2.2 Insights into release mechanisms

The determination of drug release *in vitro* is important for the characterization of the dosage form performance. The experimental conditions, such as pH, temperature, medium volume, sample volume and time points, are usually defined and kept constant. However, the lack of a standardized method makes the results be highly subjective.

Two types of release were described in this work: the release of the model hydrophobic drug tacrolimus from NE, and the release of NE from the sponge matrix.

The release study of the drug from NE was performed under sink conditions, in both SGF (pH 1.2) and FaSSIF-V2 (pH 6.5). The sustained release of tacrolimus from NE was correlated to the high affinity of the drug with the oil core of NE, which resulted from the high hydrophobicity of tacrolimus (Fig. 4 Chapter II). We suggested that the release occurred by a simple diffusion process of the drug to the surface of the oily droplets [99].

The release study of NE from sponges was carried out in PBS or FaSSIF-V2 at pH 5, 5.5 and 7.5 under non-sink conditions. The aim was to better mimic the physiological intestinal environment and to avoid

the premature release of the dye loaded in the NE core (curcumin or Nile red were loaded in NE for the HPLC or UV quantification of the NE release) thus seeking to evaluate the behaviour of the nanosystem *per se*.

The release of NE from sponges was affected by the type of medium and by the sponge composition (ratio NE/CH) (Fig. 7 Chapter III).

The slower release in simulated intestinal media (FaSSIF-V2) compared to PBS might have been caused by the hydrophobic and electrostatic interactions of FaSSIF-V2 components (sodium taurocholate and lecithin) with the sponge structure that generated a more lipophilic environment from which NE release was less favoured [100,101].

The variation of the NE/CH ratio led to three different types of release mechanisms: desorption, diffusion and dissolution (Fig. 5).

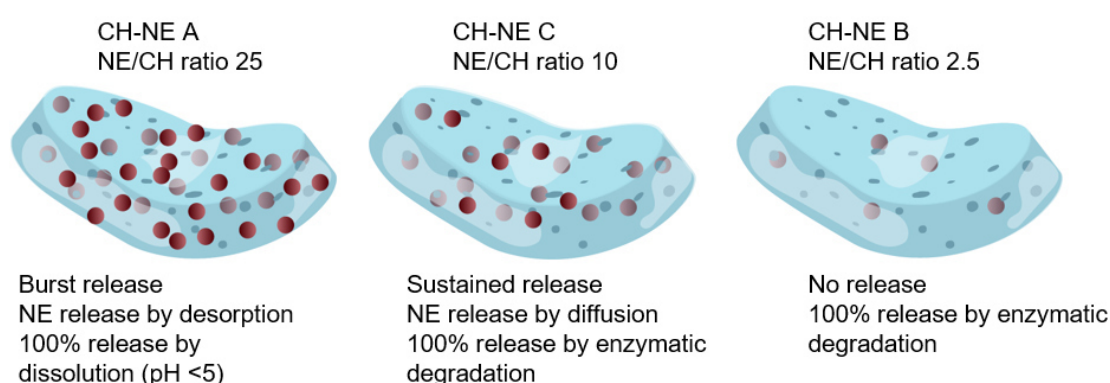


Fig. 5 Summary of the mechanisms of NE release from the nanocomposite sponges of different composition, expressed as NE/CH ratio (CH-NE A: NE/CH ratio 25, CH-NE C: NE/CH ratio 10, CH-NE B: NE/CH ratio 2.5).

At high NE/CH mass ratio of 25 (CH-NE A) the release mainly occurred by desorption of the NE associated to the sponge surface and it was burst, because of the excess of NE present. At intermediate NE/CH ratio of 10 (CH-NE C) the release was sustained and due to diffusion of the NE through the sponge 3D network. Complete release (100%) occurred by dissolution of the sponge matrix at pH 5 in the case of sponges at low CH amount and different crystalline structure governed by the ratio NE/CH (CH-NE A), as from [58]. CH-NE sponges B and C were not affected by the acidic pH of 5, making us suppose that 100% of release would be achieved only after sponge enzymatic degradation [102].

Overall, the CH-NE C sponge (NE/CH ratio of 10) was the system of choice from a technological point of view, because it provided a sustained NE release and was stable in the whole intestinal pH range, properties that are hardly found in CH-based materials because of their pH-dependent strength [55,56]. Several strategies have been reported in the literature to tune the release of nanosystems from their nanocomposites. A mechanism of release similar to the one of the sponges here presented was provided by the micelle-loaded chitosan-carballylic acid hydrogels for colonic resveratrol delivery designed by Iglesias et al. Their results proved that only a 40% of active was released by desorption or diffusion after 48h incubation in simulated colonic medium suggesting that a complete release can be provided through the selective chitosan degradation by the colon microflora [47].

Bhavsar et al. designed nanocomposite microspheres composed of a PCL matrix in which gelatin nanoparticles containing plasmid DNA were embedded. The release mechanism was based on a chemically-driven erosion pattern. Once in the intestine the lipases degraded the PCL matrix of the microsphere and then the proteases digested the gelatin nanoparticles causing their degradation and the release of plasmid DNA resulting in complete drug release in 5 h [102]. A drawback of the strategy above mentioned could be the long latency of release onset due to interpersonal variability in enzyme expression. A system which exploits several release mechanisms as the sponge here developed could offer better performance.

Other nanocomposites were designed to release the nanoparticle and their loaded active by means of pH-triggered dissolution mechanism. It is the case of NE-loaded microgels of alginate and carrageenan whose matrix is intended to prevent lipid digestion in the stomach and to subsequently dissolve at intestinal pH releasing the NE [103].

The release can also be modulated via a swelling mechanism. Alginate hydrogels were designed to specifically swell at pH 7.4 in the intestine and release the loaded NE, but to stay intact at pH 1.2 or 2.5 in the stomach ensuring NE protection. 80% released was observed within 30 min at pH due to the quick swelling and breakdown of hydrogels [104]. The advantage of our system compared to the latter is the possibility of a higher control of the NE release over time. In fact, the latter two types of system will act merely as delivery platform for the NE without providing the additional advantage of prolonging the NE residence time at the site of action.

For a better understanding of NE release dynamics, the effective diffusion coefficients of NE droplets inside different sponges should be estimated by modelling their diffusion process. We are currently developing a mathematical model based on the monodimensional unsteady Fick's second law of diffusion, with appropriate initial and boundary conditions, to fit the experimental release data [105,106].

The aim of our study was the evaluation of the release of the nanosystem, as done also by [43,107].

The majority of studies in the literature report the release of the drug from the nanocomposite rather than of the nanosystem [41,42,45,98,108–113]. We believe that these approaches should complement each other. In the future, the release kinetics of a model drug (previously loaded in the NE) from the nanocomposite sponges will be assessed to take a wider view of the whole release process in sight of a therapeutic application.

As regards the developed SMEDDS, the drug release behaviour was not evaluated. The study of the release from SEDDS is particularly troublesome since the process is much more controlled by external factors than by the formulation *per se*, as opposed to all other delivery devices. Several causes can affect the release, such as the time needed by the system to self-emulsify, the tendency of the drug to precipitate in the medium, the drug absorption rate from the intestinal mucosal layer or the changes in system composition over time due to the release of surfactants and solvents as well as due to the digestion of lipids by lipases [99]. In light of the system characteristics it can be inferred that the release would be based on a simple diffusion process. Furthermore, a more sustained release can be expected from the S-SMEDDS compared to SMEDDS because of the incorporation of the polymeric PI that could provide polymer-drug interactions.

V.2.3 Evaluation of the cytocompatibility of the developed formulations

The aim of the cell viability studies was the preliminary screening of the cytocompatibility of developed formulations. All nanosystems (NE, SMEDDS and S-SMEDDS) were not toxic at concentration of $1 \text{ mg}\cdot\text{mL}^{-1}$ on Caco-2 cells (Fig. 8 Chapter III, Fig. 6 Chapter IV). These results are in line with what reported in the literature for similar lipid-based nanosystems [25,114, 115]. Interestingly, previous research showed that the incorporation of precipitator inhibitors in S-SMEDDS allowed to significantly reduced the toxicity of the corresponding SMEDDS thanks to a 15% reduction in the surfactant concentration (Kolliphor® EL) [93]. In this study, similar values of toxicity were found for both blank SMEDDS and S-SMEDDS. This was probably due to the minimal difference in the amount of Kolliphor® RH40 present in SMEDDS (70% w/w) and S-SMEDDS (69% w/w).

When the cell viability after exposure to NE was evaluated on HCT 116 cells, the NE showed higher toxicity compared to Caco-2. The reason was the different concentration of FBS used (2% for HCT 116 and 10% for Caco-2), which can have formed a different protein corona on the particle surface [116].

The toxicity profile of the nanocomposite sponges was not studied. Because of the possible shielding effect of the NEs by the CH sponge that might alter the cell viability profile of the NE, such evaluation is needed.

The cytocompatibility screening presented in this work was performed by mean of a widely exploited cell viability screening assays (MTS) and on a simple monoculture of Caco-2 cells. This cell prototype does not completely mimic the complex intestinal physiology [117]. In the future, we must consider using advanced intestinal *in vitro* and/or *ex vivo* models for the obtainment of more predictive data [117]. In particular, a co-culture model Caco-2 and HT29-MTX cells will be useful to assess the impact of the mucus barrier on the nanosystem behaviour, while a co-culture Caco-2/HT29-MTX with Raji B cells, mimicking intestinal microfold (M) cells can represent a physiologically relevant model to evaluate particle uptake [98,118–120]. Also, advanced 3D *in vitro* models of the intestine can be used, such as organoids, microfluidic intestine-on-chip, 3D bioprinted or microengineered intestinal models [121–124].

V.2.4 Observations on developed nanoparticles cellular uptake and intestinal permeability

Once nanosystems have reached their intestinal target, the ability to cross the cellular barrier defines their fate. Three are the possible scenarios: i) the system does not interact with the cells and releases the drug in the intestine, ii) the system is uptaken by epithelial cells and iii) the system is transported through the epithelium via transcellular or paracellular transport. The release of the loaded drug can occur at any time and varies from device to device and from drug to drug, leading to a local or systemic therapeutic effect.

Self-emulsifying systems are usually intended to increase the drug solubility. However, in recent years several studies reported their ability to exert a beneficial effect on the intestinal permeability too [15,115,125–128].

The developed SMEDDS and S-SMEDDS enhanced the paracellular transport across Caco-2 cell monolayers by opening of tight junctions (Fig. 6 Chapter IV). This behaviour was ascribed to the system small droplet size of and to the presence of amphiphilic non-ionic surfactants and medium chain fatty acids, which were previously reported to exert a membrane fluidifying effect and to reversibly open tight junctions [93,126,129–131]. Interestingly, almost all commonly employed surfactants, and the

Kolliphor surfactant family in particular, have been suggested to show some inhibitory activity against efflux transporters. The inhibition mechanism apparently involves alterations in membrane transporter structure or changes to transporter expression [132]. Further investigations are needed to evaluate any activity on efflux transporters by the developed SMEDDS and S-SMEDDS which contain around 70% of Kolliphor RH40.

Moreover, the observed enhancement of the paracellular transport could explain the reduced cytotoxicity of the drug when loaded in SMEDDS because of its reduced intracellular uptake.

Experiments are planned to assess the interactions between NE and Caco-2 cells. As mentioned in section V.1.4, the fluid nature of the NE shell might impact the NE cellular internalisation pathway. In a recent study we found that by modulating the liposome composition and thus its membrane fluidity, selective targeting on cancer cells could be achieved. Rigid-state liposomes targeted the stiffer control cells, whereas fluid-state liposomes targeting the flexible and metastatic cells and were internalized via a fusion process with the tumour membranes which become increasingly fluid with cancer progression [133]. The possibility of NE fusion with the targeted membrane will have to be carefully evaluated. Despite the fluid state of the NE shell, the NE possess a PEGylated surfactant as outer layer. PEG is known to inhibit liposome fusion and to promote liposome internalisation by endocytosis but also to reduce the interactions of lipid-based formulation with the intestinal epithelium [134,135]. The results of NE transport studies may reveal valuable information for a better understanding of the NE *in vivo* behavior and for a smart modulation of its properties in sight of a therapeutic application.

V.2.5 Considerations on nanosystems mucopenetrating ability

To diffuse efficiently through the mucus, nanoparticles need to minimize the interactions between them and mucin [2]. The preliminary *in vitro* studies performed in this work suggested that NE were a good mucopenetrating candidate. The NE penetrating ability was ascribed to their PEGylated shell provided by the hydrophilic PEGylated surfactant PEG-40 stearate (Myrj® 52).

The NE had a PEGylated surfactant concentration of 14.3%, which is lower than what previously reported. Zaichik et al. successfully designed mucopenetrating NE by incorporation of the PEGylated surfactant polyethoxylated-35 castor at concentrations of 30% [136]. While the PEG-based lipid-polymer hybrid vesicles developed by Taipaleenmäki et al. diffused only at a copolymer poly(ethylene glycol)-*b*-poly(cholesterol methacrylate (PEG-*b*-PCMA) concentration of 25% w/w [118].

The NE was composed of a low molecular mass PEG with an average PEG chain length of 2 kDa (PEG-40 stearate), which can favour mucopenetration. A study by Inchaurrega et al. showed that nanoparticles coated with 2 kDa PEG better permeated the intestinal mucus layer than nanoparticles coated with 10 kDa PEG. In fact, at such high molecular mass PEG (> 10 kDa) the particles exhibited mucoadhesive properties [137].

Further evaluation is recommended to confirm the reported observations on NE mucopenetration. Firstly, a more appropriate mucus model should be used. The commercial reconstituted mucins exploited (mucins from porcine stomach type II, Sigma Aldrich commercial product) are very different from the mucus freshly collected from porcine organs like stomach or intestine, in terms of structure, physicochemical behaviour and possible interactions [52,54]. The time of the analysis should also be increased to better evaluate the possibility of NE complete penetration through the mucus layer. Lastly, the experimental conditions should be optimized to ensure the maintenance of a constant humid

microenvironment thus preventing NE and mucins from drying out over time. For a future evaluation, we suggest to use more predictive techniques and conditions, such as multiple particle tracking (MPT) on freshly collected porcine intestinal mucus and Ussing chambers on intestinal segments *ex vivo* [41,43,138].

Self-emulsifying systems were not evaluated for their mucopenetrating properties in the present work. The developed SMEDDS and S-SMEDDS might possess good mucopenetrating potential. In a study by Friedl et al., Kolliphor RH 40 and triacetin were identified as promising excipients for SNEDDSs to overcome the mucus barrier and therefore facilitate contact with epithelial cells [139]. Being the developed SMEDDS composed of 70% Kolliphor RH40, the possibility of it being mucopenetrating is high.

V.2.6 Combination of mucoadhesion and mucopenetration and analysis of the *in vivo* biodistribution following oral administration

The assessment of the system behaviour *in vivo* after oral administration to mice was the last stage of the biological evaluation. (Fig. 9-10 Chapter III and Fig. 6). The sponge ability to enhance the intestinal residence time constitutes a step forward in confirming our hypothesis that the combination of mucopenetrating and mucoadhesive properties in a single delivery device is a winning delivery strategy.

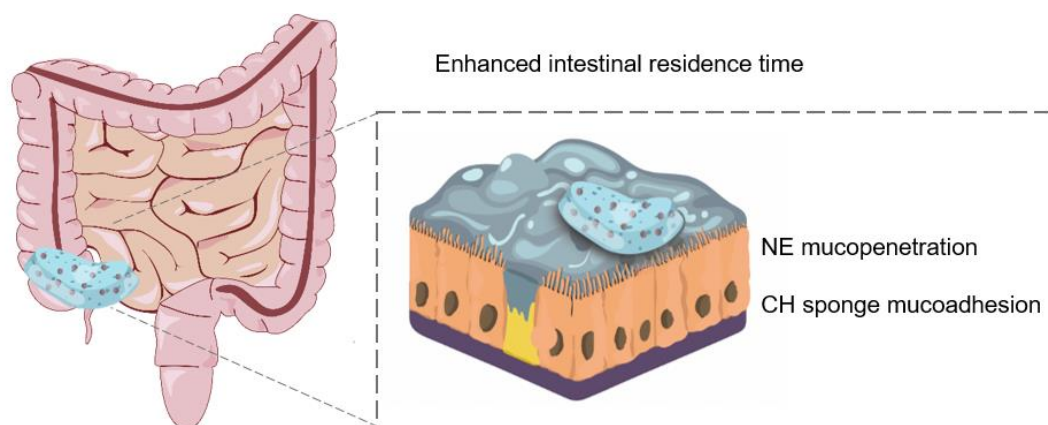


Fig. 6 Combination of mucoadhesion and mucopenetration properties in nanocomposite sponges.

Up to date only few studies reported the combination of mucoadhesion and mucopenetration in a single delivery platform. Recently, Taipaleenmäki et al. developed mucoadhesive alginate microgels loaded with mucopenetrating PEG-based lipid-polymer hybrid vesicles. When orally administered to rats, the alginate beads protected the NE from the harsh environment of the GI tract but they were not efficient in extended the intestinal retention of the vesicles because of their fast dissolution at intestinal pH. The authors concluded that alginate might not have been the ideal choice as a mucoadhesive polymer and using either a positively charged hydrogel or thiolation might have resulted in longer retention times [118].

Our nanocomposite sponge can overcome the current lack of effective intestinal targeting approaches. In this work we suggested that the sponge protected the NE and provided a sustained NE release *in vivo*. The NE then penetrated across the mucus layer to reach the underlying epithelium.

Despite the absence of DiD fluorescent signal in organs other than the GI, we cannot exclude that no NE passed in circulation because of the detection limit of the technique that we used.

We demonstrated the enhanced intestinal local retention of the nanocomposite and we ascribed it to the chitosan mucoadhesive properties [53,140]. The mucoadhesive characteristics of nanocomposite polymeric matrix were previously exploited for prolonged retention [40,43,98]. Indinavir nanoparticles produced by drug nanonization were loaded in alginate-chitosan microparticles. After dissolution of the enteric Eudragit coating, the microparticles adhered to the intestinal mucus and the nanoparticles were retained in the intestinal mucosa by physical entrapment leading to enhanced bioavailability [41].

Our system can be exploited to enhance the efficacy of a localized treatment for inflammatory disorders, such as ulcerative colitis and Crohn's disease [47]. The therapeutic potential of the nanocomposite sponge could be maximised in inflamed intestinal conditions, where the pH is lower and CH is protonated, being the electrostatic complexation with mucins favoured at a pH between 2.4 and 6.3 [141]. This strategy was previously exploited by Iglesias et al. with chitosan-carballylic acid nanocomposite hydrogels loaded with resveratrol micelles and by Duan et al. Chitosan-Alginate hydrogels embedded with antisense oligodeoxyribonucleotide nanoparticles for inflammatory bowel disease (IBD) treatment [47,142]. Alternatively, delivery systems took advantage of the inflammatory state to increase residence time via a bioadhesion mechanism. It is the case of hydroxypropyl methylcellulose acetate succinate microparticles that protected the loaded NPs from the acidic environment and deliver them in the intestine; then, at the intestinal site, the negatively charged hyaluronic acid present on the nanoparticle surface brought the nanoparticles at the inflammation site, rich in positively charged proteins, where the nanoparticles gradually released their cargo by enzymatic degradation [143].

Finally, investigations in bigger animals, such as pigs, with physiology and transit times more similar to humans [144], will be preferable to facilitate the sponge administration procedure and collect more predictive data. By using a more appropriate *in vivo* model, it will be also possible to administer sponges at different NE/CH ratio (CH-NE A, B and C) and to evaluate the effect of the nanocomposite composition and structure on the biodistribution.

V.2.7 Analysis of the SMEDDS and S-SMEDDS *in vivo* behaviour

Preliminary studies were carried out to assess the S-SMEDDS pharmacokinetic profile after oral administration to healthy mice. The drug dispersion in HPC and the SMEDDS were used as a control (Fig.7 Chapter IV).

The systems contained different drug concentrations which corresponded to the maximum drug loading in the self-emulsifying systems, being the administered dose of $14 \text{ mg}\cdot\text{kg}^{-1}$ for SMEDDS, $30 \text{ mg}\cdot\text{kg}^{-1}$ for S-SMEDDS I and $55 \text{ mg}\cdot\text{kg}^{-1}$ for S-SMEDDS II. The free drug was at a dose of $40 \text{ mg}\cdot\text{kg}^{-1}$ as dispersion in HPC that was prepared right before administration. Such differences in the administered drug amount allowed to observe the behaviour of the different formulations. The variation in C_{\max} together with the higher values of AUC and MRT when administering S-SMEDDS I and II highlighted the positive impact of the supersaturable delivery system on the drug pharmacokinetic profile. However, the direct comparison of the dose-dependent parameters (C_{\max} , AUC and MRT) between systems was hindered.

Instead, we could compare the dose-independent pharmacokinetics parameters (T_{max} , $t_{1/2}$) which proved the ability of S-SMEDDS I to prolong the blood circulation time of the drug compared to all other formulations. In fact, S-SMEDDS I thanks to the presence of the precipitation inhibitor HPC were able to maintain the drug in a supersaturated state in the intestine for long time periods, supposedly promoting sustained drug absorption in the systemic circulation. S-SMEDDS II were not as much effective as S-SMEDDS I. This was surprising as the administered dose of drug was 1.8-times higher with S-SMEDDS II than S-SMEDDS I. We believe that such behaviour can be due to the longer emulsification time and to the higher viscosity of S-SMEDDS II that prevented drug absorption. The use of DMSO in S-SMEDDS II did not turn out to be the ideal choice.

In line with our results, a multitude of S-SNEDDS/S-SMEDDS have demonstrated potential to improve the pharmacokinetic performance of lipophilic drugs [20,67,69–73,145]. By incorporating 2% (w/w) HPMC in S-SNEDDS, Zhang et al. increased 2.2-fold the oral AUC_{0-24h} of the drug luteolin in rats compared to conventional SNEDDS [69]. Also Quan et al. achieved a 1.4-fold greater AUC and a 40% improvement of the oral relative bioavailability of fenofibrate by using solid S-SEDDS compared to conventional solid SEDDS. Their vivo pharmacokinetic study conducted in beagle dogs and the S-SEDDS contained 15% (w/w) of Soluplus® as precipitation inhibitor [18]. The above mentioned systems led to a marked enhancement of the AUC. The advantage of the S-SMEDDS here developed is the prolonged blood circulation time of the drug. In a future therapeutic application this will allow to lengthen the dosing interval and ameliorate patient compliance.

V.2.8 Perspectives on the evaluation of system digestion

Orally administered lipid-based systems are submitted to the same digestive process as dietary fat. Depending on their composition, particle size and surface properties, they can be digested forming secondary vesicles in the small intestine, or they can be indigested remaining intact for absorption [146]. The impact of the triglyceride chain length on the system digestion was highlighted by Christophersen et al. while studying the release mechanism of a model protein, lysozyme, encapsulated in solid lipid microparticles. They observed that the presence of longer chains slowed down the digestion process and consequently the release [147]. Not only the chain length, but also the surfactant can have an impact on degradation velocity of lipid-based nanoparticles by lipases. The incorporation of non-ionic surfactants containing stealth PEG head groups in lipid-based nanoparticles provided enhanced resistance to digestion and reduced drug precipitation in comparison to the digestible non-PEGylated counterpart [148]. Besides, the number of ethylene oxide functionalities on surfactants chains was found to affect the velocity of degradation in the intestine by lipase/co-lipase. Olbrich et al. showed that a high number of ethylene oxide groups of the surfactant hindered the anchoring of the enzyme on the particle and consequently its degradation/digestion [149].

It can be suggested that the developed NE and SMEDDS would undergo a slow digestion process because of the presence of PEGylated surfactants in their shell (13.5% Myrj® 52 in NE and 70% Kolliphor® RH40 in SMEDDS). A prompt evaluation of the digestion process of the developed nanosystems and of the possible protective effect of the sponges will be the object of future studies.

V. References

- [1] J.S. Komaiko, D.J. McClements, Formation of Food-Grade Nanoemulsions Using Low-Energy Preparation Methods: A Review of Available Methods, *Compr. Rev. Food Sci. Food Saf.* 15 (2016) 331–352. doi:10.1111/1541-4337.12189.
- [2] Q. Xu, L.M. Ensign, N.J. Boylan, A. Schön, X. Gong, J.-C. Yang, N.W. Lamb, S. Cai, T. Yu, E. Freire, J. Hanes, Impact of Surface Polyethylene Glycol (PEG) Density on Biodegradable Nanoparticle Transport in Mucus *ex vivo* and Distribution *in vivo*, *ACS Nano.* 9 (2015) 9217–9227. doi:10.1021/acsnano.5b03876.
- [3] K.-O. Choi, N.P. Aditya, S. Ko, Effect of aqueous pH and electrolyte concentration on structure, stability and flow behavior of non-ionic surfactant based solid lipid nanoparticles, *Food Chem.* 147 (2014) 239–244. doi:10.1016/j.foodchem.2013.09.095.
- [4] G. Lefebvre, J. Riou, G. Bastiat, E. Roger, K. Frombach, J.-C. Gimel, P. Saulnier, B. Calvignac, Spontaneous nano-emulsification: Process optimization and modeling for the prediction of the nanoemulsion's size and polydispersity, *Int. J. Pharm.* 534 (2017) 220–228. doi:10.1016/j.ijpharm.2017.10.017.
- [5] D.J. McClements, J. Rao, Food-Grade Nanoemulsions: Formulation, Fabrication, Properties, Performance, Biological Fate, and Potential Toxicity, *Crit. Rev. Food Sci. Nutr.* 51 (2011) 285–330. doi:10.1080/10408398.2011.559558.
- [6] S. Mayer, J. Weiss, D.J. McClements, Vitamin E-enriched nanoemulsions formed by emulsion phase inversion: Factors influencing droplet size and stability, *J. Colloid Interface Sci.* 402 (2013) 122–130. doi:10.1016/j.jcis.2013.04.016.
- [7] H. Ragelle, S. Crauste-Manciet, J. Seguin, D. Brossard, D. Scherman, P. Arnaud, G.G. Chabot, Nanoemulsion formulation of fisetin improves bioavailability and antitumour activity in mice, *Int. J. Pharm.* 427 (2012) 452–459. doi:10.1016/j.ijpharm.2012.02.025.
- [8] R. Rutckeviski, F.H. Xavier, A.R.D.V. Morais, L. Amaral-Machado, E.D.N. Alencar, J. Genre, A.A. De Souza Araujo, E.S.T. Do Egito, Therapeutic bullfrog oil-based nanoemulsion for oral application: Development, characterization and stability, *Acta Pharm.* 69 (2019) 33–48. doi:10.2478/acph-2019-0001.
- [9] J.F. Mendes, H.H.A. Martins, C.G. Otoni, N.A. Santana, R.C.S. Silva, A.G. Da Silva, M.V. Silva, M.T.S. Correia, G. Machado, A.C.M. Pinheiro, R.H. Piccoli, J.E. Oliveira, Chemical composition and antibacterial activity of *Eugenia brejoensis* essential oil nanoemulsions against *Pseudomonas fluorescens*, *LWT.* 93 (2018) 659–664. doi:10.1016/j.lwt.2018.04.015.
- [10] S. Kentish, T.J. Wooster, M. Ashokkumar, S. Balachandran, R. Mawson, L. Simons, The use of ultrasonics for nanoemulsion preparation, *Innov. Food Sci. Emerg. Technol.* 9 (2008) 170–175. doi:10.1016/j.ifset.2007.07.005.
- [11] H.-R. Wu, C.-Q. Wang, J.-X. Wang, J.-F. Chen, Y. Le, Engineering of Long-Term Stable Transparent Nanoemulsion Using High-Gravity Rotating Packed Bed for Oral Drug Delivery, *Int. J. Nanomedicine.* Volume 15 (2020) 2391–2402. doi:10.2147/IJN.S238788.
- [12] J. Riewe, P. Erfle, S. Melzig, A. Kwade, A. Dietzel, H. Bunjes, Antisolvent precipitation of lipid nanoparticles in microfluidic systems – A comparative study, *Int. J. Pharm.* 579 (2020) 119167. doi:10.1016/j.ijpharm.2020.119167.
- [13] H. Park, E. Ha, M. Kim, Current Status of Supersaturable Self-Emulsifying Drug Delivery Systems, *Pharmaceutics.* 12 (2020) 365. doi:10.3390/pharmaceutics12040365.
- [14] I. Nardin, S. Köllner, Successful development of oral SEDDS: screening of excipients from the industrial point of view, *Adv. Drug Deliv. Rev.* 142 (2019) 128–140. doi:10.1016/j.addr.2018.10.014.
- [15] E. Nottingham, V. Sekar, A. Mondal, S. Safe, A.K. Rishi, M. Singh, The Role of Self-Nanoemulsifying Drug Delivery Systems of CDODA-Me in Sensitizing Erlotinib-Resistant Non-Small Cell Lung Cancer, *J. Pharm. Sci.* 109 (2020) 1867–1882. doi:10.1016/j.xphs.2020.01.010.
- [16] N. Parmar, N. Singla, S. Amin, K. Kohli, Study of cosurfactant effect on nanoemulsifying area and development of lercanidipine loaded (SNEDDS) self nanoemulsifying drug delivery system, *Colloids Surfaces B Biointerfaces.* 86 (2011) 327–338. doi:10.1016/j.colsurfb.2011.04.016.
- [17] BASF SE Care Chemicals Division Pharma Ingredients & Services, Kolliphor RH 40, 2011.
- [18] G. Quan, B. Niu, V. Singh, Y. Zhou, C.-Y. Wu, X. Pan, C. Wu, Supersaturable solid self-

- microemulsifying drug delivery system: precipitation inhibition and bioavailability enhancement, *Int. J. Nanomedicine*. 12 (2017) 8801–8811. doi:10.2147/IJN.S149717.
- [19] N.-T. Tung, C.-S. Tran, T.-M.-H. Pham, H.-A. Nguyen, T.-L. Nguyen, S.-C. Chi, D.-D. Nguyen, T.-B.-H. Bui, Development of solidified self-microemulsifying drug delivery systems containing l-tetrahydropalmatine: Design of experiment approach and bioavailability comparison, *Int. J. Pharm.* 537 (2018) 9–21. doi:10.1016/j.ijpharm.2017.12.027.
- [20] N.-T. Tung, C.-S. Tran, H.-A. Nguyen, T.-D. Nguyen, S.-C. Chi, D.-V. Pham, Q.-D. Bui, X.-H. Ho, Formulation and biopharmaceutical evaluation of supersaturable self-nanoemulsifying drug delivery systems containing silymarin, *Int. J. Pharm.* 555 (2019) 63–76. doi:10.1016/j.ijpharm.2018.11.036.
- [21] A.A. Kassem, A.M. Mohsen, R.S. Ahmed, T.M. Essam, Self-nanoemulsifying drug delivery system (SNEDDS) with enhanced solubilization of nystatin for treatment of oral candidiasis: Design, optimization, *in vitro* and *in vivo* evaluation, *J. Mol. Liq.* 218 (2016) 219–232. doi:10.1016/j.molliq.2016.02.081.
- [22] D. Sakloetsakun, S. Dünnhaupt, J. Barthelmes, G. Perera, A. Bernkop-Schnürch, Combining two technologies: Multifunctional polymers and self-nanoemulsifying drug delivery system (SNEDDS) for oral insulin administration, *Int. J. Biol. Macromol.* 61 (2013) 363–372. doi:10.1016/j.ijbiomac.2013.08.002.
- [23] P. Gao, B.D. Rush, W.P. Pfund, T. Huang, J.M. Bauer, W. Morozowich, M.S. Kuo, M.J. Hageman, Development of a Supersaturable SEDDS (S-SEDDS) Formulation of Paclitaxel with Improved Oral Bioavailability, *J. Pharm. Sci.* 92 (2003) 2386–2398. doi:10.1002/jps.10511.
- [24] S.D. Siqueira Jørgensen, T. Rades, H. Mu, K. Graeser, A. Müllertz, Exploring the utility of the Chasing Principle: influence of drug-free SNEDDS composition on solubilization of carvedilol, cinnarizine and R3040 in aqueous suspension, *Acta Pharm. Sin. B.* 9 (2019) 194–201. doi:10.1016/j.apsb.2018.07.004.
- [25] R. Nunes, B.D.A. Pereira, M.A. Cerqueira, P. Silva, L.M. Pastrana, A.A. Vicente, J.T. Martins, A.I. Bourbon, Lactoferrin-based nanoemulsions to improve the physical and chemical stability of omega-3 fatty acids, *Food Funct.* 11 (2020) 1966–1981. doi:10.1039/c9fo02307k.
- [26] T.M. El-Messery, U. Altuntas, G. Altin, B. Özçelik, The effect of spray-drying and freeze-drying on encapsulation efficiency, *in vitro* bioaccessibility and oxidative stability of krill oil nanoemulsion system, *Food Hydrocoll.* 106 (2020). doi:10.1016/j.foodhyd.2020.105890.
- [27] Q. Hu, H. Gerhard, I. Upadhyaya, K. Venkitanarayanan, Y. Luo, Antimicrobial eugenol nanoemulsion prepared by gum arabic and lecithin and evaluation of drying technologies, *Int. J. Biol. Macromol.* 87 (2016) 130–140. doi:10.1016/j.ijbiomac.2016.02.051.
- [28] H.H. Myat, G.C. Ritthidej, Impact of formulation parameters on physical characteristics of spray dried nanoemulsions and their reconstitutions, *Asian J. Pharm. Sci.* 11 (2016) 197–198. doi:10.1016/j.ajps.2015.11.038.
- [29] P.G. Maher, Y.H. Roos, M.A. Fenelon, Physicochemical properties of spray dried nanoemulsions with varying final water and sugar contents, *J. Food Eng.* 126 (2014) 113–119. doi:10.1016/j.jfoodeng.2013.11.001.
- [30] P.G. Maher, M.A.E. Auty, Y.H. Roos, L.M. Zychowski, M.A. Fenelon, Microstructure and lactose crystallization properties in spray dried nanoemulsions, *Food Struct.* 3 (2015) 1–11. doi:10.1016/j.foostr.2014.10.001.
- [31] H.-Y. Wu, C.-B. Sun, N. Liu, Effects of different cryoprotectants on microemulsion freeze-drying, *Innov. Food Sci. Emerg. Technol.* 54 (2019) 28–33. doi:10.1016/j.ifset.2018.12.007.
- [32] G.A. Ledet, S. Biswas, V.P. Kumar, R.A. Graves, D.M. Mitchner, T.M. Parker, L.A. Bostanian, S.P. Ghosh, T.K. Mandal, Development of orally administered γ tocotrienol (GT3) nanoemulsion for radioprotection, *Int. J. Mol. Sci.* 18 (2017). doi:10.3390/ijms18010028.
- [33] M.T. Orr, R.M. Kramer, L. V. Barnes, Q.M. Dowling, A.L. Desbien, E.A. Beebe, J.D. Laurance, C.B. Fox, S.G. Reed, R.N. Coler, T.S. Vedvick, Elimination of the cold-chain dependence of a nanoemulsion adjuvanted vaccine against tuberculosis by lyophilization, *J. Control. Release.* 177 (2014) 20–26. doi:10.1016/j.jconrel.2013.12.025.
- [34] F. Li, T. Wang, H.B. He, X. Tang, The properties of bufadienolides-loaded nano-emulsion and submicro-emulsion during lyophilization, *Int. J. Pharm.* 349 (2008) 291–299. doi:10.1016/j.ijpharm.2007.08.011.

- [35] J.H. Crowe, B.J. Spargo, L.M. Crowe, Preservation of dry liposomes does not require retention of residual water., *Proc. Natl. Acad. Sci.* 84 (1987) 1537–1540. doi:10.1073/pnas.84.6.1537.
- [36] M.C.L. Marchiori, A.F. Ourique, C. de B. da Silva, R.P. Raffin, A.R. Pohlmann, S.S. Guterres, R.C.R. Beck, Spray-Dried Powders Containing Tretinoin-Loaded Engineered Lipid-Core Nanocapsules: Development and Photostability Study, *J. Nanosci. Nanotechnol.* 12 (2012) 2059–2067. doi:10.1166/jnn.2012.5192.
- [37] P. Tewa-Tagne, S. Briançon, H. Fessi, Preparation of redispersible dry nanocapsules by means of spray-drying: Development and characterisation, *Eur. J. Pharm. Sci.* 30 (2007) 124–135. doi:10.1016/j.ejps.2006.10.006.
- [38] A. Rochelle do Vale Morais Morais, F.H. Xavier-Jr., É. do Nascimento Alencar, C. Melo de Oliveira, N. Dantas Santos, A. Antônio Silva-Júnior, G. Barratt, E. Sócrates Tabosa do Egitto, Optimization of the freeze-drying process for microemulsion systems, *Dry. Technol.* 37 (2019) 1745–1756. doi:10.1080/07373937.2018.1536883.
- [39] T. Briot, E. Roger, N. Lautram, A. Verger, A. Clavreul, F. Lagarce, Development and *in vitro* evaluations of new decitabine nanocarriers for the treatment of acute myeloid leukemia, *Int. J. Nanomedicine*. Volume 12 (2017) 8427–8442. doi:10.2147/IJN.S147659.
- [40] T. Kim, J.U. Kim, K. Yang, K. Nam, D. Choe, E. Kim, I.-H. Hong, M. Song, H. Lee, J. Park, Y.H. Roh, Nanoparticle-Patterned Multicompartmental Chitosan Capsules for Oral Delivery of Oligonucleotides, *ACS Biomater. Sci. Eng.* 4 (2018) 4163–4173. doi:10.1021/acsbiomaterials.8b00806.
- [41] J.C. Imperiale, P. Nejamkin, M.J. del Sole, C. E. Lanusse, A. Sosnik, Novel protease inhibitor-loaded Nanoparticle-in-Microparticle Delivery System leads to a dramatic improvement of the oral pharmacokinetics in dogs, *Biomaterials*. 37 (2015) 383–394. doi:10.1016/j.biomaterials.2014.10.026.
- [42] R. Augustine, D.L. Ashkenazi, R.S. Arzi, V. Zlobin, R. Shofti, A. Sosnik, Nanoparticle-in-microparticle oral drug delivery system of a clinically relevant darunavir/ritonavir antiretroviral combination, *Acta Biomater.* 74 (2018) 344–359. doi:10.1016/j.actbio.2018.04.045.
- [43] F. Cui, C. He, L. Yin, F. Qian, M. He, C. Tang, C. Yin, Nanoparticles incorporated in bilaminated films: A smart drug delivery system for oral formulations, *Biomacromolecules*. 8 (2007) 2845–2850. doi:10.1021/bm070339e.
- [44] S. Javanbakht, A. Shaabani, Encapsulation of graphene quantum dot-crosslinked chitosan by carboxymethylcellulose hydrogel beads as a pH-responsive bio-nanocomposite for the oral delivery agent, *Int. J. Biol. Macromol.* 123 (2019) 389–397. doi:10.1016/j.ijbiomac.2018.11.118.
- [45] M. Alfatama, L.Y. Lim, T.W. Wong, Alginate–C18 Conjugate Nanoparticles Loaded in Tripolyphosphate-Cross-Linked Chitosan–Oleic Acid Conjugate-Coated Calcium Alginate Beads as Oral Insulin Carrier, *Mol. Pharm.* 15 (2018) 3369–3382. doi:10.1021/acs.molpharmaceut.8b00391.
- [46] M. Zhang, C. Xu, D. Liu, M.K. Han, L. Wang, D. Merlin, Oral Delivery of Nanoparticles Loaded With Ginger Active Compound, 6-Shogaol, Attenuates Ulcerative Colitis and Promotes Wound Healing in a Murine Model of Ulcerative Colitis, *J. Crohn’s Colitis*. 12 (2018) 217–229. doi:10.1093/ecco-jcc/jjx115.
- [47] N. Iglesias, E. Galbis, M.J. Díaz-Blanco, R. Lucas, E. Benito, M.V. De-Paz, Nanostructured Chitosan-based biomaterials for sustained and colon-specific resveratrol release, *Int. J. Mol. Sci.* 20 (2019). doi:10.3390/ijms20020398.
- [48] B. Duan, M. Li, Y. Sun, S. Zou, X. Xu, Orally Delivered Antisense Oligodeoxyribonucleotides of TNF- α via Polysaccharide-Based Nanocomposites Targeting Intestinal Inflammation, *Adv. Healthc. Mater.* 8 (2019). doi:10.1002/adhm.201801389.
- [49] H. Laroui, G. Dalmasso, H.T.T. Nguyen, Y. Yan, S. V. Sitaraman, D. Merlin, Drug-Loaded Nanoparticles Targeted to the Colon With Polysaccharide Hydrogel Reduce Colitis in a Mouse Model, *Gastroenterology*. 138 (2010) 843–853. doi:10.1053/j.gastro.2009.11.003.
- [50] N. Sereni, A. Enache, G. Sudre, A. Montembault, C. Rochas, P. Durand, M.H. Perrard, G. Bozga, J.P. Puaux, T. Delair, L. David, Dynamic Structuration of Physical Chitosan Hydrogels, *Langmuir*. 33 (2017) 12697–12707. doi:10.1021/acs.langmuir.7b02997.
- [51] F.M. Goycoolea, F. Brunel, N.E.E. Gueddari, A. Coggiola, G. Lollo, B.M. Moerschbacher, C. Remuñán-López, T. Delair, A. Domard, M.J. Alonso, Physical Properties and Stability of Soft

- Gelled Chitosan-Based Nanoparticles, *Macromol. Biosci.* 16 (2016) 1873–1882. doi:10.1002/mabi.201600298.
- [52] B. Menchicchi, J.P. Fuenzalida, A. Hensel, M.J. Swamy, L. David, C. Rochas, F.M. Goycoolea, Biophysical Analysis of the Molecular Interactions between Polysaccharides and Mucin, *Biomacromolecules*. 16 (2015) 924–935. doi:10.1021/bm501832y.
- [53] B. Menchicchi, J.P. Fuenzalida, K.B. Bobbili, A. Hensel, M.J. Swamy, F.M. Goycoolea, Structure of Chitosan determines its interactions with mucin, *Biomacromolecules*. 15 (2014) 3550–3558. doi:10.1021/bm5007954.
- [54] S. Kootala, L. Filho, V. Srivastava, V. Linderberg, A. Moussa, L. David, S. Trombotto, T. Crouzier, Reinforcing Mucus Barrier Properties with Low Molar Mass Chitosans, *Biomacromolecules*. 19 (2018) 872–882. doi:10.1021/acs.biomac.7b01670.
- [55] A. Worthen, K. Irving, Y. Lapitsky, Supramolecular Strategy Effects on Chitosan Bead Stability in Acidic Media: A Comparative Study, *Gels*. 5 (2019) 11. doi:10.3390/gels5010011.
- [56] A. Martín-Illana, F. Notario-Pérez, R. Cazorla-Luna, R. Ruiz-Caro, M.D. Veiga, Smart Freeze-Dried Bigels for the Prevention of the Sexual Transmission of HIV by Accelerating the Vaginal Release of Tenofovir during Intercourse, *Pharmaceutics*. 11 (2019) 232. doi:10.3390/pharmaceutics11050232.
- [57] P. Thoniyot, M.J. Tan, A.A. Karim, D.J. Young, X.J. Loh, Nanoparticle–Hydrogel Composites: Concept, Design, and Applications of These Promising, Multi-Functional Materials, *Adv. Sci.* 2 (2015) 1–13. doi:10.1002/advs.201400010.
- [58] J. Becerra, G. Sudre, I. Royaud, R. Montserret, B. Verrier, C. Rochas, T. Delair, L. David, Tuning the Hydrophilic/Hydrophobic Balance to Control the Structure of Chitosan Films and Their Protein Release Behavior, *AAPS PharmSciTech*. 18 (2017) 1070–1083. doi:10.1208/s12249-016-0678-9.
- [59] M. Wang, Y. Ma, Y. Sun, S.Y. Hong, S.K. Lee, B. Yoon, L. Chen, L. Ci, J.-D. Nam, X. Chen, J. Suhr, Hierarchical Porous Chitosan Sponges as Robust and Recyclable Adsorbents for Anionic Dye Adsorption, *Sci. Rep.* 7 (2017) 18054. doi:10.1038/s41598-017-18302-0.
- [60] T. Ikeda, K. Ikeda, K. Yamamoto, H. Ishizaki, Y. Yoshizawa, K. Yanagiguchi, S. Yamada, Y. Hayashi, Fabrication and Characteristics of Chitosan Sponge as a Tissue Engineering Scaffold, *Biomed Res. Int.* 2014 (2014) 1–8. doi:10.1155/2014/786892.
- [61] T. De Witte, A.M. Wagner, L.E. Fratila-Apachitei, A.A. Zadpoor, N.A. Peppas, Immobilization of nanocarriers within a porous chitosan scaffold for the sustained delivery of growth factors in bone tissue engineering applications, *J. Biomed. Mater. Res. Part A*. 108 (2020) 1122–1135. doi:10.1002/jbm.a.36887.
- [62] T. Furst, G.R. Dakwar, E. Zagato, A. Lechanteur, K. Remaut, B. Evrard, K. Braeckmans, G. Piel, Freeze-dried mucoadhesive polymeric system containing pegylated lipoplexes: Towards a vaginal sustained released system for siRNA, *J. Control. Release*. 236 (2016) 68–78. doi:10.1016/j.jconrel.2016.06.028.
- [63] M.A. Casadei, F. Cerreto, S. Cesa, M. Giannuzzo, M. Feeney, C. Marianecchi, P. Paolicelli, Solid lipid nanoparticles incorporated in dextran hydrogels: A new drug delivery system for oral formulations, *Int. J. Pharm.* 325 (2006) 140–146. doi:10.1016/j.ijpharm.2006.06.012.
- [64] Y. Zhou, L. Liu, Y. Cao, S. Yu, C. He, X. Chen, A Nanocomposite Vehicle Based on Metal–Organic Framework Nanoparticle Incorporated Biodegradable Microspheres for Enhanced Oral Insulin Delivery, *ACS Appl. Mater. Interfaces*. 12 (2020) 22581–22592. doi:10.1021/acsami.0c04303.
- [65] I. Nelson, S.E. Naleway, Intrinsic and extrinsic control of freeze casting, *J. Mater. Res. Technol.* 8 (2019) 2372–2385. doi:10.1016/j.jmrt.2018.11.011.
- [66] K.L. Scotti, D.C. Dunand, Freeze casting – A review of processing, microstructure and properties via the open data repository, FreezeCasting.net, *Prog. Mater. Sci.* 94 (2018) 243–305. doi:10.1016/j.pmatsci.2018.01.001.
- [67] G. Singh, R.S. Pai, *In vitro* and *in vivo* performance of supersaturable self-nanoemulsifying system of trans-resveratrol, *Artif. Cells, Nanomedicine Biotechnol.* 44 (2016) 510–516. doi:10.3109/21691401.2014.966192.
- [68] Y. Seto, C. Morizane, K. Ueno, H. Sato, S. Onoue, Supersaturable Self-Emulsifying Drug Delivery System of Krill Oil with Improved Oral Absorption and Hypotriglyceridemic Function,

- J. Agric. Food Chem. 66 (2018) 5352–5358. doi:10.1021/acs.jafc.8b00693.
- [69] N. Zhang, F. Zhang, S. Xu, K. Yun, W. Wu, W. Pan, Formulation and evaluation of luteolin supersaturable self-nanoemulsifying drug delivery system (S-SNEDDS) for enhanced oral bioavailability, *J. Drug Deliv. Sci. Technol.* 58 (2020) 101783. doi:10.1016/j.jddst.2020.101783.
- [70] M. Ogino, K. Yakushiji, H. Suzuki, K. Shiokawa, H. Kikuchi, Y. Seto, H. Sato, S. Onoue, Enhanced pharmacokinetic behavior and hepatoprotective function of ginger extract-loaded supersaturable self-emulsifying drug delivery systems, *J. Funct. Foods.* 40 (2018) 156–163. doi:10.1016/j.jff.2017.08.035.
- [71] D.J. Shin, B.R. Chae, Y.T. Goo, H.Y. Yoon, C.H. Kim, S. Il Sohn, D. Oh, A. Lee, S.H. Song, Y.W. Choi, Improved dissolution and oral bioavailability of valsartan using a solidified supersaturable self-microemulsifying drug delivery system containing gelucire® 44/14, *Pharmaceutics.* 11 (2019). doi:10.3390/pharmaceutics11020058.
- [72] Y.T. Goo, S.H. Song, D.W. Yeom, B.R. Chae, H.Y. Yoon, C.H. Kim, S.Y. Park, T.H. Kang, S. Lee, Y.W. Choi, Enhanced oral bioavailability of valsartan in rats using a supersaturable self-microemulsifying drug delivery system with P-glycoprotein inhibitors, *Pharm. Dev. Technol.* 25 (2020) 178–186. doi:10.1080/10837450.2019.1683749.
- [73] H. Han, Y. Li, Z. Peng, K. Long, C. Zheng, W. Wang, T.J. Webster, L. Ge, A Soluplus/Poloxamer 407-based self-nanoemulsifying drug delivery system for the weakly basic drug carvedilol to improve its bioavailability, *Nanomedicine Nanotechnology, Biol. Med.* 27 (2020) 102199. doi:10.1016/j.nano.2020.102199.
- [74] M.J. Kang, D.R. Lee, H.J. Jung, H.R. Cho, J.S. Park, S.-H. Yoon, Y.S. Choi, C.-H. Oh, M.J. Ho, Y.W. Choi, Enhanced dissolution and oral absorption of tacrolimus by supersaturable self-emulsifying drug delivery system, *Int. J. Nanomedicine.* 11 (2016) 1109. doi:10.2147/IJN.S102991.
- [75] J.-H. Lee, H. Kim, Y. Cho, T.-S. Koo, G. Lee, Development and Evaluation of Raloxifene-Hydrochloride-Loaded Supersaturable SMEDDS Containing an Acidifier, *Pharmaceutics.* 10 (2018) 78. doi:10.3390/pharmaceutics10030078.
- [76] J. Bannow, Y. Yorulmaz, K. Löbmann, A. Müllertz, T. Rades, Improving the drug load and *in vitro* performance of supersaturated self-nanoemulsifying drug delivery systems (super-SNEDDS) using polymeric precipitation inhibitors, *Int. J. Pharm.* 575 (2020) 118960. doi:10.1016/j.ijpharm.2019.118960.
- [77] N. Kato, A. Ishijima, T. Inaba, F. Nomura, S. Takeda, K. Takiguchi, Effects of lipid composition and solution conditions on the mechanical properties of membrane vesicles, *Membranes (Basel).* 5 (2015) 22–47. doi:10.3390/membranes5010022.
- [78] A. Dickey, R. Faller, Examining the contributions of lipid shape and headgroup charge on bilayer behavior, *Biophys. J.* 95 (2008) 2636–2646. doi:10.1529/biophysj.107.128074.
- [79] C.L. Dora, L.F.C. Silva, J.-L. Putaux, Y. Nishiyama, I. Pignot-Paintrand, R. Borsali, E. Lemos-Senna, Poly(ethylene glycol) Hydroxystearate-Based Nanosized Emulsions: Effect of Surfactant Concentration on Their Formation and Ability to Solubilize Quercetin, *J. Biomed. Nanotechnol.* 8 (2012) 202–210. doi:10.1166/jbn.2012.1380.
- [80] N. Anton, P. Gayet, J.-P. Benoit, P. Saulnier, Nano-emulsions and nanocapsules by the PIT method: An investigation on the role of the temperature cycling on the emulsion phase inversion, *Int. J. Pharm.* 344 (2007) 44–52. doi:10.1016/j.ijpharm.2007.04.027.
- [81] M. Garcia-Fuentes, M.J. Alonso, D. Torres, Design and characterization of a new drug nanocarrier made from solid–liquid lipid mixtures, *J. Colloid Interface Sci.* 285 (2005) 590–598. doi:10.1016/j.jcis.2004.10.012.
- [82] M.A. Schubert, M. Harms, C.C. Müller-Goymann, Structural investigations on lipid nanoparticles containing high amounts of lecithin, *Eur. J. Pharm. Sci.* 27 (2006) 226–236. doi:10.1016/j.ejps.2005.10.004.
- [83] M. Yanez Arteta, T. Kjellman, S. Bartesaghi, S. Wallin, X. Wu, A.J. Kvist, A. Dabkowska, N. Székely, A. Radulescu, J. Bergenholtz, L. Lindfors, Successful reprogramming of cellular protein production through mRNA delivered by functionalized lipid nanoparticles, *Proc. Natl. Acad. Sci.* 115 (2018) E3351–E3360. doi:10.1073/pnas.1720542115.
- [84] M. Cheniour, D. Gueyraud, P.G. Goekjian, T. Granjon, O. Marcillat, A convenient and versatile synthesis of Laurdan-like fluorescent membrane probes: Characterization of their fluorescence

- properties, *RSC Adv.* 6 (2016) 5547–5557. doi:10.1039/c5ra20369d.
- [85] C.C. De Vequi-Suplicy, C.R. Benatti, M.T. Lamy, Laurdan in fluid bilayers: Position and structural sensitivity, *J. Fluoresc.* 16 (2006) 431–439. doi:10.1007/s10895-005-0059-3.
- [86] N.S. Murthy, Z. Zhang, S. Borsadia, J. Kohn, Nanospheres with a smectic hydrophobic core and an amorphous PEG hydrophilic shell: structural changes and implications for drug delivery, *Soft Matter.* 14 (2018) 1327–1335. doi:10.1039/C7SM02472J.
- [87] S. Takegami, K. Ueyama, A. Konishi, T. Kitade, Combination of 1H nuclear magnetic resonance spectroscopy and principal component analysis to evaluate the lipid fluidity of flutamide-encapsulated lipid nanoemulsions, *Anal. Bioanal. Chem.* 410 (2018) 5033–5042. doi:10.1007/s00216-018-1154-z.
- [88] R. Gharib, S. Fourmentin, C. Charcosset, H. Greige-Gerges, Effect of hydroxypropyl- β -cyclodextrin on lipid membrane fluidity, stability and freeze-drying of liposomes, *J. Drug Deliv. Sci. Technol.* 44 (2018) 101–107. doi:10.1016/j.jddst.2017.12.009.
- [89] V. Jennings, A.F. Thünemann, S.H. Gohla, Characterisation of a novel solid lipid nanoparticle carrier system based on binary mixtures of liquid and solid lipids, *Int. J. Pharm.* 199 (2000) 167–177. doi:10.1016/S0378-5173(00)00378-1.
- [90] A. Zielińska, N.R. Ferreira, A. Feliczak-Guzik, I. Nowak, E.B. Souto, Loading, release profile and accelerated stability assessment of monoterpenes-loaded solid lipid nanoparticles (SLN), *Pharm. Dev. Technol.* 25 (2020) 832–844. doi:10.1080/10837450.2020.1744008.
- [91] C. Dulieu, D. Bazile, Influence of lipid nanocapsules composition on their aptness to freeze-drying., *Pharm. Res.* 22 (2005) 285–92. doi:10.1007/s11095-004-1196-0.
- [92] D.H. Alshora, M.A. Ibrahim, F.K. Alanazi, Nanotechnology from particle size reduction to enhancing aqueous solubility, in: *Surf. Chem. Nanobiomaterials*, 2016: pp. 163–191. doi:10.1016/B978-0-323-42861-3.00006-6.
- [93] P. Jaisamut, K. Wiwattanawongsa, P. Graidist, Y. Sangsen, R. Wiwattanapatapee, Enhanced Oral Bioavailability of Curcumin Using a Supersaturable Self-Microemulsifying System Incorporating a Hydrophilic Polymer; *In vitro* and *In vivo* Investigations, *AAPS PharmSciTech.* 19 (2018) 730–740. doi:10.1208/s12249-017-0857-3.
- [94] S. Raut, B. Karzoon, E. Atef, Using in situ Raman spectroscopy to study the drug precipitation inhibition and supersaturation mechanism of Vitamin E TPGS from self-emulsifying drug delivery systems (SEDDS), *J. Pharm. Biomed. Anal.* 109 (2015) 121–127. doi:10.1016/j.jpba.2015.02.027.
- [95] M.E. Brewster, R. Vandecruys, J. Peeters, P. Neeskens, G. Verreck, T. Loftsson, Comparative interaction of 2-hydroxypropyl- β -cyclodextrin and sulfobutylether- β -cyclodextrin with itraconazole: Phase-solubility behavior and stabilization of supersaturated drug solutions, *Eur. J. Pharm. Sci.* 34 (2008) 94–103. doi:10.1016/j.ejps.2008.02.007.
- [96] S.S. Al-Nimry, K.A. Alkhamis, B.M. Altaani, Solid self-nanoemulsifying drug delivery system filled in enteric coated hard gelatin capsules for enhancing solubility and stability of omeprazole hydrochloride, *Pharm. Dev. Technol.* 7450 (2020). doi:10.1080/10837450.2020.1721536.
- [97] J.A.C. Barbosa, M.M. Al-Kauraiishi, A.M. Smith, B.R. Conway, H.A. Merchant, Achieving gastroresistance without coating: Formulation of capsule shells from enteric polymers, *Eur. J. Pharm. Biopharm.* 144 (2019) 174–179. doi:10.1016/j.ejpb.2019.09.015.
- [98] C. Costa, Z. Liu, J.P. Martins, A. Correia, P. Figueiredo, A. Rahikkala, W. Li, J. Seitsonen, J. Ruokolainen, S.-P. Hirvonen, A. Aguiar-Ricardo, M.L. Corvo, H.A. Santos, All-in-one microfluidic assembly of insulin-loaded pH-responsive nano-in-microparticles for oral insulin delivery, *Biomater. Sci.* 8 (2020) 3270–3277. doi:10.1039/D0BM00743A.
- [99] A. Bernkop-Schnürch, A. Jalil, Do drug release studies from SEDDS make any sense?, *J. Control. Release.* 271 (2018) 55–59. doi:10.1016/j.jconrel.2017.12.027.
- [100] P. Knoos, A. V. Svensson, S. Ulvenlund, M. Wahlgren, Release of a poorly soluble drug from hydrophobically modified poly (acrylic acid) in simulated intestinal fluids, *PLoS One.* 10 (2015) 1–16. doi:10.1371/journal.pone.0140709.
- [101] M. Thongngam, D.J. McClements, Isothermal titration calorimetry study of the interactions between chitosan and a bile salt (sodium taurocholate), *Food Hydrocoll.* 19 (2005) 813–819. doi:10.1016/j.foodhyd.2004.11.001.
- [102] M.D. Bhavsar, M.M. Amiji, Gastrointestinal distribution and *in vivo* gene transfection studies

- with nanoparticles-in-microsphere oral system (NiMOS), *J. Control. Release.* 119 (2007) 339–348. doi:10.1016/j.jconrel.2007.03.006.
- [103] Z. Zhang, K.-J. Jung, R. Zhang, J.L. Muriel Mundo, D.J. McClements, In situ monitoring of lipid droplet release from biopolymer microgels under simulated gastric conditions using magnetic resonance imaging and spectroscopy, *Food Res. Int.* 123 (2019) 181–188. doi:10.1016/j.foodres.2019.04.063.
- [104] L. Lei, Y. Zhang, L. He, S. Wu, B. Li, Y. Li, Fabrication of nanoemulsion-filled alginate hydrogel to control the digestion behavior of hydrophobic nobiletin, *LWT - Food Sci. Technol.* 82 (2017) 260–267. doi:10.1016/j.lwt.2017.04.051.
- [105] P.L. Ritger, N.A. Peppas, A simple equation for description of solute release I. Fickian and non-fickian release from non-swellable devices in the form of slabs, spheres, cylinders or discs, *J. Control. Release.* 5 (1987) 23–36. doi:10.1016/0168-3659(87)90034-4.
- [106] D. Caccavo, An overview on the mathematical modeling of hydrogels' behavior for drug delivery systems, *Int. J. Pharm.* 560 (2019) 175–190. doi:10.1016/j.ijpharm.2019.01.076.
- [107] R. Sun, Q. Xia, Release mechanism of lipid nanoparticles immobilized within alginate beads influenced by nanoparticle size and alginate concentration, *Colloid Polym. Sci.* 297 (2019) 1183–1198. doi:10.1007/s00396-019-04538-x.
- [108] S. Peers, P. Alcouffe, A. Montembault, C. Ladavière, Embedment of liposomes into chitosan physical hydrogel for the delayed release of antibiotics or anaesthetics, and its first ESEM characterization, *Carbohydr. Polym.* 229 (2020) 1–10. doi:10.1016/j.carbpol.2019.115532.
- [109] M.A. Casadei, F. Cerreto, S. Cesa, M. Giannuzzo, M. Feeney, C. Marianecchi, P. Paolicelli, Solid lipid nanoparticles incorporated in dextran hydrogels: A new drug delivery system for oral formulations, *Int. J. Pharm.* 325 (2006) 140–146. doi:10.1016/j.ijpharm.2006.06.012.
- [110] L. Soudry-Kochavi, N. Naraykin, T. Nassar, S. Benita, Improved oral absorption of exenatide using an original nanoencapsulation and microencapsulation approach, *J. Control. Release.* 217 (2015) 202–210. doi:10.1016/j.jconrel.2015.09.012.
- [111] U.M. Musazzi, L.S. Dolci, B. Albertini, N. Passerini, F. Cilurzo, A new melatonin oral delivery platform based on orodispersible films containing solid lipid microparticles, *Int. J. Pharm.* 559 (2019) 280–288. doi:10.1016/j.ijpharm.2019.01.046.
- [112] Y.J. Wang, L.J. Chen, L.W. Tan, Q. Zhao, F. Luo, Y.Q. Wei, Z.Y. Qian, PEG-PCL based micelle hydrogels as oral docetaxel delivery systems for breast cancer therapy, *Biomaterials.* 35 (2014) 6972–6985. doi:10.1016/j.biomaterials.2014.04.099.
- [113] R. Sun, Q. Xia, Nanostructured lipid carriers incorporated in alginate hydrogel: Enhanced stability and modified behavior in gastrointestinal tract, *Colloids Surfaces A Physicochem. Eng. Asp.* 574 (2019) 197–206. doi:10.1016/j.colsurfa.2019.04.082.
- [114] T.J. Wooster, S.C. Moore, W. Chen, H. Andrews, R. Addepalli, R.B. Seymour, S.A. Osborne, Biological fate of food nanoemulsions and the nutrients they carry – internalisation, transport and cytotoxicity of edible nanoemulsions in Caco-2 intestinal cells, *RSC Adv.* 7 (2017) 40053–40066. doi:10.1039/C7RA07804H.
- [115] A.B. Buya, B. Ucar, A. Beloqui, P.B. Memvanga, V. Pr at, Design and evaluation of self-nanoemulsifying drug delivery systems (SNEDDSs) for senicapoc, *Int. J. Pharm.* 580 (2020) 119180. doi:10.1016/j.ijpharm.2020.119180.
- [116] V. Francia, K. Yang, S. Deville, C. Reker-Smit, I. Nelissen, A. Salvati, Corona Composition Can Affect the Mechanisms Cells Use to Internalize Nanoparticles, *ACS Nano.* 13, 10 (2019) 11107–11121. DOI:10.1021/acsnano.9b03824
- [117] J.S. Dutton, S.S. Hinman, R. Kim, Y. Wang, N.L. Allbritton, Primary Cell-Derived Intestinal Models: Recapitulating Physiology, *Trends Biotechnol.* 37 (2019) 744–760. doi:10.1016/j.tibtech.2018.12.001.
- [118] E. Taipaleenm aki, G. Christensen, E. Brodskij, S.A. Mouritzen, N. Gal, S. Madsen, M.S. Hedemann, T.A. Knudsen, H.M. Jensen, S.L. Christiansen, F.V. Spars , B. St dler, Mucopenetrating polymer – Lipid hybrid nanovesicles as subunits in alginate beads as an oral formulation, *J. Control. Release.* 322 (2020) 470–485. doi:10.1016/j.jconrel.2020.03.047.
- [119] C. Schimpel, B. Teubl, M. Absenger, C. Meindl, E. Fr hlich, G. Leitinger, A. Zimmer, E. Roblegg, Development of an Advanced Intestinal *in vitro* Triple Culture Permeability Model To Study Transport of Nanoparticles, *Mol. Pharm.* 11 (2014) 808–818. doi:10.1021/mp400507g.

- [120] M. Diop, N. Auberval, A. Viciglio, A. Langlois, W. Bietiger, C. Mura, C. Peronet, A. Bekel, D. Julien David, M. Zhao, M. Pinget, N. Jeandidier, C. Vauthier, E. Marchioni, Y. Frere, S. Sigrist, Design, characterisation, and bioefficiency of insulin–chitosan nanoparticles after stabilisation by freeze-drying or cross-linking, *Int. J. Pharm.* 491 (2015) 402–408. doi:10.1016/j.ijpharm.2015.05.065.
- [121] L.R. Madden, T. V. Nguyen, S. Garcia-Mojica, V. Shah, A. V. Le, A. Peier, R. Visconti, E.M. Parker, S.C. Presnell, D.G. Nguyen, K.N. Retting, Bioprinted 3D Primary Human Intestinal Tissues Model Aspects of Native Physiology and ADME/Tox Functions, *IScience*. 2 (2018) 156–167. doi:10.1016/j.isci.2018.03.015.
- [122] Y. Wang, D.B. Gunasekara, M.I. Reed, M. DiSalvo, S.J. Bultman, C.E. Sims, S.T. Magness, N.L. Allbritton, A microengineered collagen scaffold for generating a polarized crypt-villus architecture of human small intestinal epithelium, *Biomaterials*. 128 (2017) 44–55. doi:10.1016/j.biomaterials.2017.03.005.
- [123] S. Yoshida, H. Miwa, T. Kawachi, S. Kume, K. Takahashi, Generation of intestinal organoids derived from human pluripotent stem cells for drug testing, *Sci. Rep.* 10 (2020) 5989. doi:10.1038/s41598-020-63151-z.
- [124] V. De Gregorio, B. Corrado, S. Sbrescia, S. Sibilio, F. Urciuolo, P.A. Netti, G. Imparato, Intestine-on-chip device increases ECM remodeling inducing faster epithelial cell differentiation, *Biotechnol. Bioeng.* 117 (2020) 556–566. doi:10.1002/bit.27186.
- [125] T. Vasconcelos, F. Araújo, C. Lopes, A. Loureiro, J. das Neves, S. Marques, B. Sarmento, Multicomponent self nano emulsifying delivery systems of resveratrol with enhanced pharmacokinetics profile, *Eur. J. Pharm. Sci.* 137 (2019). doi:10.1016/j.ejps.2019.105011.
- [126] M.H. Patel, K.K. Sawant, Self microemulsifying drug delivery system of lurasidone hydrochloride for enhanced oral bioavailability by lymphatic targeting: *In vitro*, Caco-2 cell line and *in vivo* evaluation, *Eur. J. Pharm. Sci.* 138 (2019) 105027. doi:10.1016/j.ejps.2019.105027.
- [127] Y. Aktas, M. Celik Tekeli, N. Celebi, Development and characterization of exendin-4 loaded self-nanoemulsifying system and *in vitro* evaluation on Caco-2 cell line, *J. Microencapsul.* 37 (2020) 41–51. doi:10.1080/02652048.2019.1692945.
- [128] E. Kontogiannidou, T. Meikopoulos, C. Virgiliou, N. Bouropoulos, H. Gika, I.S. Vizirianakis, A. Müllertz, D.G. Fatouros, Towards the development of Self-Nano-Emulsifying Drug Delivery Systems (SNEDDS) containing trimethyl chitosan for the oral delivery of amphotericin B: *In vitro* assessment and cytocompatibility studies, *J. Drug Deliv. Sci. Technol.* 56 (2020) 101524. doi:10.1016/j.jddst.2020.101524.
- [129] A. Beloqui, P.B. Memvanga, R. Coco, S. Reimondez-Troitiño, M. Alhouayek, G.G. Muccioli, M.J. Alonso, N. Csaba, M. de la Fuente, V. Préat, A comparative study of curcumin-loaded lipid-based nanocarriers in the treatment of inflammatory bowel disease, *Colloids Surfaces B Biointerfaces*. 143 (2016) 327–335. doi:10.1016/j.colsurfb.2016.03.038.
- [130] J. Zhao, M.H. Stenzel, Entry of nanoparticles into cells: the importance of nanoparticle properties, *Polym. Chem.* 9 (2018) 259–272. doi:10.1039/C7PY01603D.
- [131] T. Lindmark, Y. Kimura, P. Artursson, Absorption enhancement through intracellular regulation of tight junction permeability by medium chain fatty acids in Caco-2 cells., *J. Pharmacol. Exp. Ther.* 284 (1998) 362–9.
- [132] O.M. Feeney, M.F. Crum, C.L. McEvoy, N.L. Trevaskis, H.D. Williams, C.W. Pouton, W.N. Charman, C.A.S. Bergström, C.J.H. Porter, 50 years of oral lipid-based formulations: Provenance, progress and future perspectives, *Adv. Drug Deliv. Rev.* 101 (2016) 167–194. doi:10.1016/j.addr.2016.04.007.
- [133] J. Bompard, A. Rosso, L. Brizuela Madrid, S. Mebarek, L.J. Blum, A.-M.T. Trunfio-Sfarghiu, G. Lollo, T. Granjon, A. Girard-Egrot, O. Maniti, Membrane Fluidity as a New Mean to Selectively Target Cancer Cells with Fusogenic Lipid Carriers, *Langmuir*. (2020) acs.langmuir.0c00262. doi:10.1021/acs.langmuir.0c00262.
- [134] F. Sun, M. Adrian, N. Beztsinna, J.B. van den Dikkenberg, R.F. Maas-Bakker, P.M. van Hasselt, M.J. van Steenberg, X. Su, L.C. Kapitein, W.E. Hennink, C.F. van Nostrum, Influence of PEGylation of Vitamin-K-Loaded Mixed Micelles on the Uptake by and Transport through Caco-2 Cells, *Mol. Pharmaceutics*. 15 (2018) 3786–3795. doi:10.1021/acs.molpharmaceut.8b00258.

- [135] B. Pelaz, P. del Pino, P. Maffre, R. Hartmann, M. Gallego, S. Rivera-Fernández, J.M. de la Fuente, G.U. Nienhaus, W.J. Parak, Surface Functionalization of Nanoparticles with Polyethylene Glycol: Effects on Protein Adsorption and Cellular Uptake, *ACS Nano*. 9 (2015) 6996–7008. doi:10.1021/acs.nano.5b01326.
- [136] S. Zaichik, C. Steinbring, M. Jelkmann, A. Bernkop-Schnürch, Zeta potential changing nanoemulsions: Impact of PEG-corona on phosphate cleavage, *Int. J. Pharm.* 581 (2020) 119299. doi:10.1016/j.ijpharm.2020.119299.
- [137] L. Inchaurrega, N. Martín-Arbella, V. Zabaleta, G. Quincoces, I. Peñuelas, J.M. Irache, *In vivo* study of the mucus-permeating properties of PEG-coated nanoparticles following oral administration, *Eur. J. Pharm. Biopharm.* 97 (2015) 280–289. doi:10.1016/j.ejpb.2014.12.021.
- [138] L.M. Ensign, A. Henning, C.S. Schneider, K. Maisel, Y.-Y. Wang, M.D. Porosoff, R. Cone, J. Hanes, *Ex vivo* Characterization of Particle Transport in Mucus Secretions Coating Freshly Excised Mucosal Tissues, *Mol. Pharm.* 10 (2013) 2176–2182. doi:10.1021/mp400087y.
- [139] H. Friedl, S. Dünnhaupt, F. Hintzen, C. Waldner, S. Parikh, J.P. Pearson, M.D. Wilcox, A. Bernkop-Schnürch, Development and evaluation of a novel mucus diffusion test system approved by self-nanoemulsifying drug delivery Systems, *J. Pharm. Sci.* 102 (2013) 4406–4413. doi:10.1002/jps.23757.
- [140] A. Mendes, J. Sevilla Moreno, M. Hanif, T. E.L. Douglas, M. Chen, I. Chronakis, Morphological, Mechanical and Mucoadhesive Properties of Electrospun Chitosan/Phospholipid Hybrid Nanofibers, *Int. J. Mol. Sci.* 19 (2018) 2266. doi:10.3390/ijms19082266.
- [141] Collado-González, González Espinosa, Goycoolea, Interaction Between Chitosan and Mucin: Fundamentals and Applications, *Biomimetics*. 4 (2019) 32. doi:10.3390/biomimetics4020032.
- [142] B. Duan, M. Li, Y. Sun, S. Zou, X. Xu, Orally Delivered Antisense Oligodeoxyribonucleotides of TNF- α via Polysaccharide-Based Nanocomposites Targeting Intestinal Inflammation, *Adv. Healthc. Mater.* 8 (2019) 1801389. doi:10.1002/adhm.201801389.
- [143] W. Li, Y. Li, Z. Liu, N. Kerdsakundee, M. Zhang, F. Zhang, X. Liu, T. Bauleth-Ramos, W. Lian, E. Mäkilä, M. Kemell, Y. Ding, B. Sarmiento, R. Wiwattanapatapee, J. Salonen, H. Zhang, J.T. Hirvonen, D. Liu, X. Deng, H.A. Santos, Hierarchical structured and programmed vehicles deliver drugs locally to inflamed sites of intestine, *Biomaterials*. 185 (2018) 322–332. doi:10.1016/j.biomaterials.2018.09.024.
- [144] P. Padmanabhan, J. Grosse, A.B.M.A. Asad, G.K. Radda, X. Golay, Gastrointestinal transit measurements in mice with 99mTc-DTPA-labeled activated charcoal using NanoSPECT-CT, *EJNMMI Res.* 3 (2013) 60. doi:10.1186/2191-219X-3-60.
- [145] T. Mukherjee, F.M. Plakogiannis, Development and oral bioavailability assessment of a supersaturated self-microemulsifying drug delivery system (SMEDDS) of albendazole, *J. Pharm. Pharmacol.* 62 (2010) 1112–1120. doi:10.1111/j.2042-7158.2010.01149.x.
- [146] T. Wang, Y. Luo, Biological fate of ingested lipid-based nanoparticles: current understanding and future directions, *Nanoscale*. 11 (2019) 11048–11063. doi:10.1039/C9NR03025E.
- [147] P.C. Christophersen, L. Zhang, M. Yang, H.M. Nielsen, A. Müllertz, H. Mu, Solid lipid particles for oral delivery of peptide and protein drugs I – Elucidating the release mechanism of lysozyme during lipolysis, *Eur. J. Pharm. Biopharm.* 85 (2013) 473–480. doi:10.1016/j.ejpb.2013.07.017.
- [148] O.M. Feeney, H.D. Williams, C.W. Pouton, C.J.H. Porter, ‘Stealth’ lipid-based formulations: Poly(ethylene glycol)-mediated digestion inhibition improves oral bioavailability of a model poorly water soluble drug, *J. Control. Release*. 192 (2014) 219–227. doi:10.1016/j.jconrel.2014.07.037.
- [149] C. Olbrich, R. Müller, Enzymatic degradation of SLN—effect of surfactant and surfactant mixtures, *Int. J. Pharm.* 180 (1999) 31–39. doi:10.1016/S0378-5173(98)00404-9.

Conclusions

In this thesis work we proposed hybrid nanosystems that combine nanoparticles and polymeric systems as a new class of biomaterials unleashing unique synergistic properties with significant potential to prolong intestinal residence and improve drug delivery efficiency.

The study proved the technological feasibility of formulating lipid-based nanosystems and their hybrid polymeric counterparts, and provided for the preliminary evaluation of the systems biological attributes *in vitro* and *in vivo*.

In a first part, polymeric hybrid nanocomposites, made of NE embedded in CH sponges, were developed aiming at the exploitation of the intestinal mucus barrier to prolong the delivery. We presented a comprehensive characterisation of the nanosystem from a physicochemical and structural point of view. The successful embedding of NE in chitosan sponges, that guaranteed the NE sustained release without alteration of its physicochemical properties, gave a proof of the feasibility of designing the nanocomposite. The preliminary studies performed *in vitro* suggested that the NE possess mucopenetrating properties that will allow it to reach the targeted intestinal epithelium *in vivo*, and that the NE loading in the sponge will promote the NE sustained release in the intestinal site of action. Lastly, the nanocomposite oral administration to mice proved the effectiveness in increasing the intestinal residence time, thus confirming our hypothesis. Despite the noticeable progress in the development of hybrid nanosystem done in this work, there is still a need for further detailed studies on sponge structure and interactions with the NE which will provide a sound base for a better understanding of its biological attributes. While the mucoadhesive and mucopenetrating attributes of the systems should be further evaluated *ex vivo* and/or *in vivo* with more performant techniques.

The second part of this work presented the design of a hybrid nanosystem in the form of supersaturable S-SMEDDS for the intestinal delivery of a benzimidazole derivative anticancer drug. In this frame we took advantage of the intestinal fluids to generate the nanosystem *in situ*. The addition of precipitation inhibitor HPC was intended to increase the drug loading in the formulation and to minimize the drug precipitation in the gastrointestinal fluids. HPC maintained the drug in a supersaturated state over a long time period prolonging the drug blood circulation time. The systems were cytocompatible on Caco-2 cells and had a positive impact on the intestinal permeability by improving the paracellular transport. The S-SMEDDS loading in enteric capsules or the optimisation of the composition by substitution of the precipitator inhibitor are suggested to tackle the stability shortcoming in the gastric environment and further improve the drug therapeutic efficacy.

The findings of this work can serve the domain from different perspectives. From a technological viewpoint it offers a better understanding of the formulation process of lipid-based nanocarriers and their hybrid polymeric counterparts, highlighting the importance of rational design in order to obtain nanocomposites with appropriate physicochemical and morphological characteristics. From a biological viewpoint it suggests the potential of the develop nanocomposite as intestinal drug delivery device for a future exploitation for both the treatment of local pathologies and the systemic delivery of active molecules. Further investigations are highly recommended to uncover the possibilities of these formulations.

Résumé substantiel

La voie orale est la plus courante des voies d'administration des principes actifs pharmaceutiques (API). Ses avantages découlent de la grande surface intestinale pour l'absorption des médicaments, de la possibilité d'auto-administration qui améliore l'observance du patient et des faibles coûts de production [1,2]. Cependant, la précipitation ou la dégradation du principe actif ainsi que le temps de résidence relativement court au niveau intestinal sont des obstacles majeurs à l'administration orale [3]. Dans ce cadre, les nanosystèmes de délivrance lipidiques (LBDDS), comme les nanoémulsions (NE) et les systèmes auto-émulsionnables, sont une approche prometteuse pour améliorer l'efficacité thérapeutique locale ou systémique des médicaments [4,5]. Les NE sont des dispersions colloïdales, thermodynamiquement instables, composées majoritairement de deux liquides non miscibles (eau et huile). L'un des liquides est dispersé sous forme de gouttelettes nanométriques stabilisées par un tensioactif dans l'autre liquide [6]. Les systèmes auto-émulsionnables sont des mélanges d'huile, tensioactif et co-solvants capables de former spontanément des nano- (SNEDDS) ou des microémulsions (SMEDDS) lors de leur dispersion dans une phase aqueuse telle que les liquides intestinaux sous légère agitation [7]. Malgré les progrès technologiques, certaines limites biologiques empêchent encore ces systèmes de délivrance de répondre aux nombreuses exigences thérapeutiques. Parmi eux figurent un faible taux d'encapsulation du principe actif, une capacité de ciblage limitée et un temps de résidence au niveau intestinal court. Des systèmes hybrides associant les nanoparticules à des polymères ont été proposés pour dépasser ces limites. [8]. Parmi ces systèmes hybrides on trouve : i) les systèmes hybrides à matrice, également appelés nanocomposites polymériques, où le polymère forme une matrice 3D dans laquelle les nanoparticules sont englobées ; ii) les systèmes hybrides auto-émulsionnables constitués d'une suspension de nanoparticules dans une solution de polymère [9].

Ce travail de thèse consiste à développer des nanosystèmes hybrides pour augmenter le temps de résidence intestinale après administration orale, en vue d'augmenter l'effet local ou encore l'absorption systémique des médicaments.

À ces fins, deux nanosystèmes hybrides différents ont été conçus : i) des nanocomposites polymériques composés de NE chargées dans une éponge de chitosane (CH) ii) des systèmes auto-émulsionnables sursaturables (S-SMEDDS) obtenus par la combinaison de SMEDDS conventionnels avec un inhibiteur de précipitation polymérique, l'hydroxypropylcellulose (HPC).

L'objectif spécifique de la conception des nanocomposites polymères était de protéger les NEs et de moduler la libération du principe actif tout en prolongeant le temps de résidence du système au niveau intestinal. Ces nanocomposites peuvent être envisagés dans l'optique d'une administration systémique ou locale de médicaments. L'objectif spécifique de la conception de S-SMEDDS était d'améliorer la solubilité et l'absorption orale d'un médicament anticancéreux hydrophobe modèle.

Dans un premier temps, les nanosystèmes (NE et SMEDDS) ont été préparés, optimisés et caractérisés d'un point de vue physico-chimique et structurel. Ensuite, les nanosystèmes ont été combinés avec les polymères (CH ou HPC) pour obtenir leurs homologues hybrides. Enfin, leurs efficacités *in vitro* et *in vivo* ont été évaluées.

La première partie de ce travail de thèse met en avant les études de formulation et caractérisation des NE. Les NE ont été formulées par la méthode d'inversion de phase de l'émulsion (EPI), couplée à un

apport d'énergie élevé pour affiner la taille des gouttelettes (disperseur Ultraturax®). Les NE sont composées de triglycérides à chaîne moyenne (MCT, Miglyol® 812, esters des acides caprylique/caprique) stabilisés par un mélange de tensioactifs hydrophiles et hydrophobes non ioniques, le stéarate de polyoxyéthylène (Myrj® 52, HLB 16.9) et le glycéride d'oléoyl polyoxyl-6 (Labrafil® M1944CS, HLB 4). La formulation a été optimisée à l'aide d'un plan d'expériences pour obtenir les paramètres suivants : une teneur en huile 7% (p/p), un rapport massique des agents tensioactifs (SMR) de 2.5 et un rapport agent tensioactif/huile (surfactant-to-oil ratio SOR) de 2.86. Les NE possèdent une taille de 100 nm, un PDI de 0.2 et une charge de surface neutre (-9 mV). Un principe actif modèle hydrophobe, le tacrolimus, a été encapsulé dans les NE, avec une excellente efficacité d'encapsulation (99.5%) et sans altération des propriétés physicochimiques. La libération prolongée du principe actif dans un milieu gastrique simulé le SGF (pH 1.2) et un milieu intestinal simulé le FaSSIF-V2 (pH 6.5) a été prouvée.

Ensuite, les NE ont été séchées en utilisant les procédés de lyophilisation et de spray-drying afin d'augmenter leur stabilité au stockage. Des additifs ont été ajoutés pour préserver la structure des systèmes au séchage : maltodextrine (MD) pour le spray-drying et tréhalose (TR) pour la lyophilisation. La lyophilisation s'est avérée être le procédé à privilégier en raison d'un rendement plus élevé (90 % en spray-drying contre 99 % en lyophilisation) et de la possibilité de sécher les formulations avec une concentration élevée en NE (13.5% en lyophilisation contre 5% en spray drying) et un rapport NE/excipient supérieur (5.4 en lyophilisation contre 0.5 en spray drying).

La caractérisation structurale de la NE a été effectuée en se concentrant sur la nature de la surface de la NE. Tout d'abord, l'état cristallin ou amorphe de la NE a été évalué par DSC et par diffraction de rayons X. Les analyses ont montré que le cœur huileux reste amorphe, alors que la coque est amorphe lorsque la NE est liquide mais possède une structure cristalline lorsque la NE est à l'état sec. Ce point est particulièrement intéressant car la présence d'un noyau huileux amorphe maximise le taux d'encapsulation [10] et la cristallinité de l'enveloppe à l'état sec améliore la stabilité du système lors du stockage [11]. Deuxièmement, la nature fluide de la coque de la NE a été montrée par des mesures de fluorescence, à l'aide d'un fluorophore dérivé du Laurdan sensible à la polarité. La fluidité peut être expliquée par la faible densité de tassement du tensioactif Myrj® 52 dans la coque.

Les propriétés mucopénétrantes des NE ont été évaluées en utilisant des mucines reconstituées, provenant d'estomacs de porc, pour simuler la barrière de mucus intestinal (chapitre III). L'analyse DLS a démontré que la taille et la charge des NE n'étaient pas affectées en présence de mucines, ce qui démontre la présence de faibles interactions de surface entre les deux [12]. L'analyse l'ITC a, en outre, confirmé l'absence d'interactions additionnelles entre les mucines et les NE. Enfin, par microscopie confocale à balayage laser (CLSM) on a observé que les NE pénétraient efficacement dans les mucines, se répartissant sur toute l'épaisseur de l'échantillon en 3 h. Les propriétés mucopénétrantes ont été attribués à la présence du surfactant PEGylé (PEG-40 stéarate) dans la coque de la NE [13–15].

Ensuite, ce travail s'est intéressé au développement de nanocomposite hybrides CH-NE (chapitre III). Les éponges nanocomposites ont été produites par lyophilisation. Trois éponges ont été préparées :

- CH-NE A (CH 0.1%-NE 2.5%, rapport NE/CH de 25)
- CH-NE B (CH 1%-NE 2.5%, rapport NE/CH de 2.5)

- CH-NE C (CH 1%-NE 10%, rapport NE/CH de 10).

Les propriétés structurales et mécaniques des éponges varient en fonction de la concentration en CH et en NE, comme le montrent les images en microscopie optique et électronique. En comparaison avec des éponges de CH seul, la présence des NE entraîne un renforcement de la structure, par interactions entre la NE et les chaînes de CH par liaison hydrogène et interactions hydrophobe, une autre partie des NE est retrouvée à la surface des éponges [54].

La cinétique de libération des NE a été étudiée après réhydratation de l'éponge dans un liquide intestinal simulé (FaSSIF-V2) à différents pH (5, 5.5, 7.5) [16]. Dans l'éponge avec un rapport NE/CH élevé (de 25), c'est-à-dire avec un excès de NE situé à la surface de l'éponge, la NE est facilement et rapidement libérée une fois en contact avec le milieu. Au contraire, à un rapport NE/CH de 10, la NE doit d'abord diffuser à travers la matrice de l'éponge, entraînant une libération contrôlée et prolongée dans le temps. Aucune libération n'a été retrouvée dans l'échantillon CH-NE B (NE/CH 2.5) car toute la NE participait à la formation de la structure de l'éponge. La libération complète des NE n'a été atteinte que dans l'éponge à un rapport NE/CH élevé de 25 (CH-NE A), suite à la dissolution de l'éponge à pH 5. Les raisons possibles sont la faible teneur en CH (0.1%) et la modification de la structure cristalline du CH en fonction du rapport NE/CH [17].

La cytocompatibilité des NE a été évaluée *in vitro* sur des cellules Caco-2. Les NE se sont révélées non toxiques à une concentration supérieure à 1 mg·mL⁻¹.

Les études de biodistribution *in vivo* chez la souris ont montré que l'éponge nanocomposite (CH-NE C) augmente considérablement le temps de séjour intestinal grâce à la capacité mucoadhésive du CH [18,19]. Le système s'accumule dans le cæcum à partir de 2 h et un signal fluorescent élevé est toujours détecté dans le cæcum et le côlon après 6 h. Au contraire lorsque la NE est administrée seule, un transit à travers le GI en 4 h est observé et la plupart de la formulation est excrétée à 6 h. Aucun signal fluorescent n'a été détecté dans les autres organes, ce qui indique que le système est bien retenu au niveau intestinal. De plus, aucune altération de la muqueuse intestinale n'a été observée.

Dans l'ensemble, ces résultats prouvent les avantages offerts par les éponges nanocomposites en tant que système de livraison intestinale pour un effet du médicament encapsulé au niveau local ou systémique.

La deuxième partie de la thèse (chapitre IV) concerne la formulation et la caractérisation des SMEDDS et des S-SMEDDS pour l'administration orale d'un médicament anticancéreux appartenant à la classe de benzimidazoles, le BI. Les excipients des SMEDDS (huile, tensioactif et co-solvants) ont été sélectionnés sur la base de leur capacité de solubilisation du principe actif et un plan d'expérience a permis l'optimisation du système. Le système final était composé de 10% (p/p) d'huile (MCT, Miglyol® 812), 70% (p/p) d'agent tensioactif (Polyoxyl 40 huile de ricin hydrogénée, Kolliphor® RH40) et 20% (p/p) de co-solvants (diéthylène glycol monoéthyléther Transcutol® HP et éthanol ou DMSO). Après ajout d'eau, les SMEDDS conduisent à la formation de microémulsions de taille 18.52 ± 0.02 nm, avec un faible Pdl, une charge de surface neutre (-1.03 ± 0.82 mV) et une bonne capacité d'auto-émulsification vérifiée par le temps nécessaire à cette émulsification (68 s).

Ensuite, les S-SMEDDS ont été formulés par ajout d'hydroxypropylcellulose (HPC, Klucel® EF) dans les SMEDDS. Deux S-SMEDDS différents ont été préparés : S-SMEDDS I contenant 10% d'EtOH et 1% de HPC et S-SMEDDS II contenant 5% de DMSO et 1% de HPC (% p/p). Comparée au SMEDDS

classique, a charge en principe actif a été doublée avec le S-SMEDDS I et quadruplée avec le S-SMEDDS II.

Les essais en milieu gastrique simulé (SGF, pH 1.2) ont montré une précipitation du principe actif depuis les SMEDDS et les S-SMEDDS, mais, grâce à la présence de l'hydroxypropylcellulose (Klucel™ EF, 1% p/p) jouant le rôle d'inhibiteur de précipitation, la concentration du principe actif dans les S-SMEDDS reste 2.3 fois plus élevée que dans les SMEDDS. . En milieu liquide intestinal simulé (SIF, pH 6.8), tous les systèmes sont stables, il n'y a pas de précipitation et tout le principe actif reste dissous. La cytocompatibilité des NE a été évaluée sur la lignée cellulaire Caco-2. Les SMEDDS et S-SMEDDS sont cytocompatibles jusqu'à 1.3 mg·mL⁻¹ et elles permettent une réduction de la toxicité du BI, avantage majeur en vue d'une administration orale [20]. Ensuite la capacité des SMEDDS et S-SMEDDS à augmenter la perméabilité intestinale a été évaluée sur des monocouches de cellules Caco-2 en utilisant trois techniques différentes : CLSM, TEER et mesures de fluorescence. Tous les systèmes augmentent la perméabilité paracellulaire en ouvrant les jonctions serrées. Cette ouverture est transitoire et réversible comme en témoigne le retour à l'état initial des valeurs de TEER après 24 h, ce qui confirme l'absence de toxicité du système, conformément aux études précédentes [20–23].

Enfin, le profil pharmacocinétique des SMEDDS et des S-SMEDDS a été évalué in vivo sur la souris après administration orale. Par rapport au BI seul et au SMEDDS, les S-SMEDDS I prolongent le temps de circulation plasmatique avec un Tmax plus long et un t1/2 plus important. L'ajout de l'inhibiteur de précipitation HPC a permis de maintenir le principe actif dans un état sursaturé pendant une longue période, induisant une circulation prolongée. Les résultats obtenus sont conformes à ceux précédemment observé pour d'autres S-SMEDDS [24–30] [31].

Dans l'ensemble, ce travail de thèse démontre que les nanosystèmes hybrides sont des systèmes prometteurs pour améliorer la délivrance intestinale des médicaments.

Dans le cas de nanocomposites polymères, la synergie entre nanosystème et polymère a donné lieu à des propriétés physico-chimiques et biologiques exclusives, notamment une meilleure résistance mécanique, une modulation intelligente de la cinétique de libération des nanoparticules et une augmentation du temps de résidence intestinale après administration orale.

Alors que, dans le cas des S-SMEDDS, le nanocomposite a permis d'améliorer le taux d'encapsulation du médicament anticancéreux hydrophobe BI et de prolonger son temps de présence dans la circulation systémique.

Références

- [1] L.M. Ensign, R. Cone, J. Hanes, Oral drug delivery with polymeric nanoparticles: The gastrointestinal mucus barriers, *Adv. Drug Deliv. Rev.* 64 (2012) 557–570. doi:10.1016/j.addr.2011.12.009.
- [2] P. Long, Q. Zhang, M. Xue, G. Cao, C. Li, W. Chen, F. Jin, Z. Li, R. Li, X. Wang, W. Ge, Tomato lectin-modified nanoemulsion-encapsulated MAGE1-HSP70/SEA complex protein vaccine: Targeting intestinal M cells following peroral administration, *Biomed. Pharmacother.* 115 (2019) 108886. doi:10.1016/j.biopha.2019.108886.
- [3] B. Homayun, X. Lin, H.-J. Choi, Challenges and Recent Progress in Oral Drug Delivery Systems for Biopharmaceuticals, *Pharmaceutics*. 11 (2019) 129. doi:10.3390/pharmaceutics11030129.
- [4] T. Lindmark, Y. Kimura, P. Artursson, Absorption enhancement through intracellular regulation of tight junction permeability by medium chain fatty acids in Caco-2 cells., *J. Pharmacol. Exp. Ther.* 284 (1998) 362–9.

- [5] K. Koga, Y. Kusawake, Y. Ito, N. Sugioka, N. Shibata, K. Takada, Enhancing mechanism of Labrasol on intestinal membrane permeability of the hydrophilic drug gentamicin sulfate, *Eur. J. Pharm. Biopharm.* 64 (2006) 82–91. doi:10.1016/j.ejpb.2006.03.011.
- [6] S. Mayer, J. Weiss, D.J. McClements, Vitamin E-enriched nanoemulsions formed by emulsion phase inversion: Factors influencing droplet size and stability, *J. Colloid Interface Sci.* 402 (2013) 122–130. doi:10.1016/j.jcis.2013.04.016.
- [7] T. Vasconcelos, F. Araújo, C. Lopes, A. Loureiro, J. das Neves, S. Marques, B. Sarmento, Multicomponent self nano emulsifying delivery systems of resveratrol with enhanced pharmacokinetics profile, *Eur. J. Pharm. Sci.* 137 (2019). doi:10.1016/j.ejps.2019.105011.
- [8] S. Merino, C. Martín, K. Kostarelos, M. Prato, E. Vázquez, Nanocomposite Hydrogels: 3D Polymer–Nanoparticle Synergies for On-Demand Drug Delivery, *ACS Nano.* 9 (2015) 4686–4697. doi:10.1021/acsnano.5b01433.
- [9] C. Desfrancois, R. Auzély, I. Texier, Lipid nanoparticles and their hydrogel composites for drug delivery: A review, *Pharmaceuticals.* 11 (2018). doi:10.3390/ph11040118.
- [10] N.S. Murthy, Z. Zhang, S. Borsadia, J. Kohn, Nanospheres with a smectic hydrophobic core and an amorphous PEG hydrophilic shell: structural changes and implications for drug delivery, *Soft Matter.* 14 (2018) 1327–1335. doi:10.1039/C7SM02472J.
- [11] D.H. Alshora, M.A. Ibrahim, F.K. Alanazi, Nanotechnology from particle size reduction to enhancing aqueous solubility, in: *Surf. Chem. Nanobiomaterials*, 2016: pp. 163–191. doi:10.1016/B978-0-323-42861-3.00006-6.
- [12] B. Menchicchi, J.P. Fuenzalida, A. Hensel, M.J. Swamy, L. David, C. Rochas, F.M. Goycoolea, Biophysical Analysis of the Molecular Interactions between Polysaccharides and Mucin, *Biomacromolecules.* 16 (2015) 924–935. doi:10.1021/bm501832y.
- [13] L. Inchaurrega, N. Martín-Arbella, V. Zabaleta, G. Quincoces, I. Peñuelas, J.M. Irache, In vivo study of the mucus-permeating properties of PEG-coated nanoparticles following oral administration, *Eur. J. Pharm. Biopharm.* 97 (2015) 280–289. doi:10.1016/j.ejpb.2014.12.021.
- [14] M.J. Santander-Ortega, M. Plaza-Oliver, V. Rodríguez-Robledo, L. Castro-Vázquez, N. Villaseca-González, J. González-Fuentes, E.L. Cano, P. Marcos, M. V. Lozano, M.M. Arroyo-Jiménez, PEGylated Nanoemulsions for Oral Delivery: Role of the Inner Core on the Final Fate of the Formulation, *Langmuir.* 33 (2017) 4269–4279. doi:10.1021/acs.langmuir.7b00351.
- [15] Q. Xu, L.M. Ensign, N.J. Boylan, A. Schön, X. Gong, J.-C. Yang, N.W. Lamb, S. Cai, T. Yu, E. Freire, J. Hanes, Impact of Surface Polyethylene Glycol (PEG) Density on Biodegradable Nanoparticle Transport in Mucus ex Vivo and Distribution in Vivo, *ACS Nano.* 9 (2015) 9217–9227. doi:10.1021/acsnano.5b03876.
- [16] M. Goldberg, A. Manzi, E. Aydin, G. Singh, P. Khoshkenar, A. Birdi, B. LaPorte, A. Krauskopf, G. Powell, J. Chen, R. Langer, Development of a Nanoparticle-Embedded Chitosan Sponge for Topical and Local Administration of Chemotherapeutic Agents, *J. Nanotechnol. Eng. Med.* 5 (2014) 040905. doi:10.1115/1.4030899.
- [17] J. Becerra, G. Sudre, I. Royaud, R. Montserret, B. Verrier, C. Rochas, T. Delair, L. David, Tuning the Hydrophilic/Hydrophobic Balance to Control the Structure of Chitosan Films and Their Protein Release Behavior, *AAPS PharmSciTech.* 18 (2017) 1070–1083. doi:10.1208/s12249-016-0678-9.
- [18] B. Menchicchi, J.P. Fuenzalida, K.B. Bobbili, A. Hensel, M.J. Swamy, F.M. Goycoolea, Structure of Chitosan determines its interactions with mucin, *Biomacromolecules.* 15 (2014) 3550–3558. doi:10.1021/bm5007954.
- [19] S. Kootala, L. Filho, V. Srivastava, V. Linderberg, A. Moussa, L. David, S. Trombotto, T. Crouzier, Reinforcing Mucus Barrier Properties with Low Molar Mass Chitosans, *Biomacromolecules.* 19 (2018) 872–882. doi:10.1021/acs.biomac.7b01670.
- [20] P. Jaisamut, K. Wiwattanawongsa, P. Graidist, Y. Sangsen, R. Wiwattanapatapee, Enhanced Oral Bioavailability of Curcumin Using a Supersaturatable Self-Microemulsifying System Incorporating a Hydrophilic Polymer; In Vitro and In Vivo Investigations, *AAPS PharmSciTech.* 19 (2018) 730–740. doi:10.1208/s12249-017-0857-3.
- [21] A. Beloqui, P.B. Memvanga, R. Coco, S. Reimondez-Troitiño, M. Alhouayek, G.G. Muccioli, M.J. Alonso, N. Csaba, M. de la Fuente, V. Prétat, A comparative study of curcumin-loaded lipid-based nanocarriers in the treatment of inflammatory bowel disease, *Colloids Surfaces B*

- Biointerfaces. 143 (2016) 327–335. doi:10.1016/j.colsurfb.2016.03.038.
- [22] M.H. Patel, K.K. Sawant, Self microemulsifying drug delivery system of lurasidone hydrochloride for enhanced oral bioavailability by lymphatic targeting: In vitro, Caco-2 cell line and in vivo evaluation, *Eur. J. Pharm. Sci.* 138 (2019) 105027. doi:10.1016/j.ejps.2019.105027.
- [23] J. Zhao, M.H. Stenzel, Entry of nanoparticles into cells: the importance of nanoparticle properties, *Polym. Chem.* 9 (2018) 259–272. doi:10.1039/C7PY01603D.
- [24] G. Singh, R.S. Pai, In vitro and in vivo performance of supersaturable self-nanoemulsifying system of trans-resveratrol, *Artif. Cells, Nanomedicine Biotechnol.* 44 (2016) 510–516. doi:10.3109/21691401.2014.966192.
- [25] Y.T. Goo, S.H. Song, D.W. Yeom, B.R. Chae, H.Y. Yoon, C.H. Kim, S.Y. Park, T.H. Kang, S. Lee, Y.W. Choi, Enhanced oral bioavailability of valsartan in rats using a supersaturable self-microemulsifying drug delivery system with P-glycoprotein inhibitors, *Pharm. Dev. Technol.* 25 (2020) 178–186. doi:10.1080/10837450.2019.1683749.
- [26] H. Han, Y. Li, Z. Peng, K. Long, C. Zheng, W. Wang, T.J. Webster, L. Ge, A Soluplus/Poloxamer 407-based self-nanoemulsifying drug delivery system for the weakly basic drug carvedilol to improve its bioavailability, *Nanomedicine Nanotechnology, Biol. Med.* 27 (2020) 102199. doi:10.1016/j.nano.2020.102199.
- [27] N. Zhang, F. Zhang, S. Xu, K. Yun, W. Wu, W. Pan, Formulation and evaluation of luteolin supersaturable self-nanoemulsifying drug delivery system (S-SNEDDS) for enhanced oral bioavailability, *J. Drug Deliv. Sci. Technol.* 58 (2020) 101783. doi:10.1016/j.jddst.2020.101783.
- [28] M. Ogino, K. Yakushiji, H. Suzuki, K. Shiokawa, H. Kikuchi, Y. Seto, H. Sato, S. Onoue, Enhanced pharmacokinetic behavior and hepatoprotective function of ginger extract-loaded supersaturable self-emulsifying drug delivery systems, *J. Funct. Foods.* 40 (2018) 156–163. doi:10.1016/j.jff.2017.08.035.
- [29] N.-T. Tung, C.-S. Tran, H.-A. Nguyen, T.-D. Nguyen, S.-C. Chi, D.-V. Pham, Q.-D. Bui, X.-H. Ho, Formulation and biopharmaceutical evaluation of supersaturable self-nanoemulsifying drug delivery systems containing silymarin, *Int. J. Pharm.* 555 (2019) 63–76. doi:10.1016/j.ijpharm.2018.11.036.
- [30] D.J. Shin, B.R. Chae, Y.T. Goo, H.Y. Yoon, C.H. Kim, S. Il Sohn, D. Oh, A. Lee, S.H. Song, Y.W. Choi, Improved dissolution and oral bioavailability of valsartan using a solidified supersaturable self-microemulsifying drug delivery system containing gelucire® 44/14, *Pharmaceutics.* 11 (2019). doi:10.3390/pharmaceutics11020058.
- [31] T. Mukherjee, F.M. Plakogiannis, Development and oral bioavailability assessment of a supersaturated self-microemulsifying drug delivery system (SMEDDS) of albendazole, *J. Pharm. Pharmacol.* 62 (2010) 1112–1120. doi:10.1111/j.2042-7158.2010.01149.x.

Annexes

Membrane Fluidity as a New Means to Selectively Target Cancer Cells with Fusogenic Lipid Carriers

Julien Bompard, Annalisa Rosso, Leyre Brizuela, Saïda Mebarek, Loïc J. Blum, Ana-Maria Trunfio-Sfarghiu, Giovanna Lollo, Thierry Granjon, Agnès Girard-Egrot, and Ofelia Maniti*



Cite This: *Langmuir* 2020, 36, 5134–5144



Read Online

ACCESS |



Metrics & More

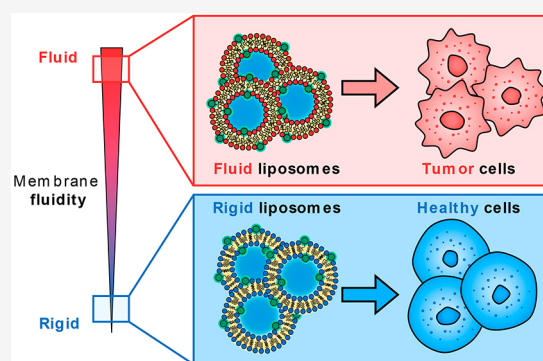


Article Recommendations



Supporting Information

ABSTRACT: Lipid-based carriers such as liposomes represent one of the most advanced classes of drug delivery systems. Their clinical success relies on their composition, similar to that of the cell membrane. Their cellular specificity often relies on a ligand–receptor interaction. Although differences in the physicochemical properties of the cell membrane between tumor and nontumor cells have been reported, they are not systematically used for drug delivery purposes. In this report, a new approach was developed to ensure selective targeting based on physical compatibility between the target and the carrier membranes. By modulating the liposome composition and thus its membrane fluidity, we achieved selective targeting on four cancer cell lines of varying aggressiveness. Furthermore, using membrane-embedded and inner core-encapsulated fluorophores, we assessed the mechanism of this interaction to be based on the fusion of the liposome with the cell membranes. Membrane fluidity is therefore a major parameter to be considered when designing lipid drug carriers as a promising, lower cost alternative to current targeting strategies based on covalent grafting.



INTRODUCTION

The lack of specificity of cancer chemotherapy drugs is a major clinical concern in the development of effective treatments.¹ In the search for new drug delivery strategies, innovative solutions based on nanocarriers occupy an important place.^{2–5} The main advantages of drug nanocarriers rely on their ability to accumulate in tumors, avoiding indiscriminate biodistribution, and to release the drug in an adjustable manner.⁶ By improving drug distribution and bioavailability, this results in a better-tolerated therapy allowing the administration of higher doses, with reduced frequency.⁷ Among the various types of nanoparticles, liposomes have been already used as drug carriers, and several formulations are currently marketed or in clinical trials.^{8–10}

The clinical interest of liposomes relies on their composition: they are nanosized vesicles made of lipid bilayers surrounding a hydrophilic aqueous core.^{11,12} In addition to being nontoxic, biocompatible, and biodegradable, their amphiphilic properties allow them to encapsulate both hydrophilic and hydrophobic drugs.

Like most submicrometer-sized drug carriers, liposomes attain the tumor site through a passive targeting mechanism based on the enhanced permeability and retention (EPR) effect, as the high vascularization of tumors increases the particle uptake when compared with healthy cells.¹³ Yet, recent studies have shown that at least in the case of gold nanoparticles extravasation across endothelial cells is possi-

ble.¹⁴ The passive targeting mechanism is in many cases high enough to reduce the side effects of chemotherapy treatments but suffers from a lack of selectivity toward capillary leakage. Passive targeting is dependent on many factors that may vary with different cancer types, such as a poor vascularization or a high interstitial pressure for solid tumors.^{15,16}

To improve liposome attachment and interaction with target cells, active targeting strategies have been explored. So far, whatever the active or passive targeting strategy, nanoparticles reach the tumor site through passive accumulation (e.g., via the EPR effect). Most current strategies use the modification in membrane protein composition by grafting liposomes with ligands specific to an overexpressed membrane protein.^{17–19} Some strategies alternatively use liposomes grafted with lectins to target a change in the carbohydrate composition of the membrane.²⁰ Cancer development also induces profound modifications of the membrane lipid composition, which invariably led to alterations of membrane physicochemical properties.^{21–28} Additionally, changes in the membrane fluidity of the tumor cells have been reported and are thought to be

Received: January 30, 2020

Revised: April 24, 2020

Published: April 27, 2020

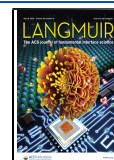
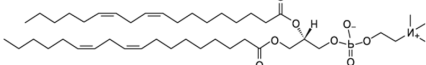
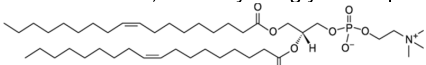
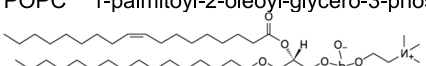
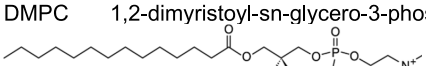

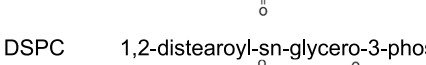
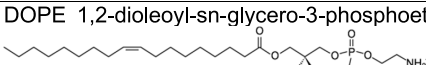


Table 1. Lipids Used for Liposome Preparations, with the Lipid Names, Fatty Acid Compositions, Structure, and Phase Transition Temperatures (T_m)

	Liposome preparation	Acyl chain composition	Lipid name and structure	T_m
Main lipid (80 %)	DL	18:2 (Cis) PC	DLPC 1,2-dilinoleoyl-sn-glycero-3-phosphocholine 	-57°C
	DO	18:1 (Δ 9-Cis) PC	DOPC 1,2-dioleoyl-sn-glycero-3-phosphocholine 	-17°C
	PO	16:0-18:1 PC	POPC 1-palmitoyl-2-oleoyl-glycero-3-phosphocholine 	-4°C
	DM	14:0 PC	DMPC 1,2-dimyristoyl-sn-glycero-3-phosphocholine 	24°C
	DP	16:0 PC	DPPC 1,2-dipalmitoyl-glycero-3-phosphocholine 	41°C
	DS	18:0 PC	DSPC 1,2-distearoyl-sn-glycero-3-phosphocholine 	55°C
Fusogenic lipid (20 %)	All preparations	18:1 (Δ 9-Cis) PE	DOPE 1,2-dioleoyl-sn-glycero-3-phosphoethanolamine 	-16°C

associated with cancer progression, the tumor membranes becoming increasingly fluid.^{29–32}

Such membrane physicochemical modifications have not been used for a drug delivery purpose. One reason is that most of the current active targeting strategies using liposomes rely on the functionalization of PEGylated liposomes with small molecules. Hence, the membrane fusion pathway remains largely unexplored in drug delivery applications, as the presence of a hydrophilic shell will inhibit membrane–membrane interactions and promote endocytosis mechanisms instead.^{33,34} Alternative strategies to PEGylation exist, allowing for longer-lasting drug carriers relying on the modulation of liposome properties such as size, surface hydrophilicity, and surface charge via lipid composition.^{35,36} Surface charge in particular is a key parameter when considering liposome blood stability, as the liposome binding by serum proteins relies on electrostatic interactions.³⁷ Moreover, it has been demonstrated on two animal models, rodent and zebra fish, that plasma protein association to liposomes also depended on lipid chain composition, with liposomes in a gel-like state being more easily covered with plasma proteins than their fluid counterparts.^{38,39} This results in increased circulation times for fluid state liposomes. All these considerations open the possibility of obtaining long-lasting non-PEGylated liposomes with a strong propensity to fuse with the target membrane.

Differences in membrane fluidity were exploited for the delivery of hybrid liposomes (constituted of 90% DMPC and 10% polyoxyethylene dodecyl ethers), and the growth inhibitory effects were correlated to the membrane fluidity of cancer cells.⁴⁰ Additionally, hybrid liposomes discriminated between human hepatocellular carcinoma cells, with more fluid membranes, and normal hepatocytes, with the more rigid membranes, which could provide perspective of targeting the cell membrane by using differences in biophysical characteristics between tumor and normal cells.⁴¹

On the basis of the above-mentioned literature, in this work we decided to explore a novel concept based on liposome membrane fluidity to promote selective targeting. To validate our hypothesis, three prostatic tumor cell lines of increasing aggressiveness were used. Differences in liposome uptake were recorded in comparison to nontumor cells and between the metastatic lines. Such differences were related to the liposome membrane fluidity. The mechanism of this interaction was also investigated by following the internalization pathways of two fluorophores: calcein encapsulated in the liposome hydrophilic compartment and a fluorescent lipid embedded in the liposome membrane. The results revealed pronounced liposome fusion with target membranes.

■ EXPERIMENTAL SECTION

Materials and Cells. Lipids and polycarbonate membranes were purchased from Avanti Polar Lipids (Alabaster, AL). Fetal bovine serum (FBS), Dulbecco's Modified Eagle Medium (DMEM), Roswell Park Memorial Institute (RPMI) medium, penicillin/streptomycin, phosphate buffered saline (PBS) composed of 10 mM phosphate, 137 mM NaCl, and 2.7 mM KCl, pH 7.4, dimethyl sulfoxide (DMSO), calcein, paraformaldehyde (PFA), and 3-(4,5-dimethylthiazol-2-yl)-2,5-diphenyltetrazolium bromide (MTT) were purchased from Sigma-Aldrich (St. Louis, MO).

Liposome Preparation. Liposomes were prepared by using the thin film hydration method. Briefly, lipids dissolved in chloroform with a total lipid mass of 5 mg were mixed in a round flask. The solvent was dried under vacuum at 50 °C on a rotatory evaporator. The lipid film obtained was hydrated by 1 mL of sterile PBS while stirring and heated above the lipid melting point. This resulted in the formation of multilamellar vesicles (MLVs) with various sizes and number of layers. Six freeze–thaw cycles in liquid nitrogen were then applied to the prepared liposomes to burst the MLVs into large unilamellar vesicles (LUVs). The LUVs' size was defined by extrusion through a porous membrane with a mini-extruder (Avanti Polar Lipids, Alabaster, AL). Liposomes were heated above their phase-transition temperature (T_m) and extruded through a 400 nm and then a 100 nm pore diameter polycarbonate membrane by using a mini-extruder apparatus (Avanti Polar Lipids). The final liposome solution was stored at 4 °C for 4 weeks, without further extrusion.

Liposomes with different lipid compositions were prepared (Table 1). A constant percentage (20%) of fusogenic lipid DOPE was used to promote the fusogenicity of the prepared liposomes. The remaining 80% of the lipid composition was made of phosphatidylcholines (PCs) with various acyl chain lengths and degrees of saturation and thus different phase transition temperatures. Six different PCs were used: DSPC, DPPC, DMPC, POPC, DOPC, and DLPC. This led to the creation of a range of liposome membrane compositions.

Fluorescent liposomes were prepared either with nitrobenzoxadiazole-grafted DOPE (NBD-PE) embedded in the liposome membrane or calcein internalized in the liposome hydrophilic core. NBD-PE was added at a 2% molar ratio to the flask prior to drying. Mass NBD-PE percentages ranged from 2.4% for DS, DO, PO, and DL liposomes to 2.5% for DP and 2.7% for DM liposomes. When hydrating the lipid film, the NBD-PE molecules were then directly incorporated in the membrane of the forming vesicles. Calcein-loaded liposomes were prepared by using calcein dissolved in PBS at a 500 μ M concentration. One milliliter of this buffer was used in lieu and place of the regular PBS when hydrating the lipid films. This resulted in the encapsulation of calcein in liposomes. Free calcein was eliminated from calcein-loaded liposomes through exclusion chromatography on PD-10 desalting columns (GE Healthcare, Chicago, IL).

Liposome Characterization. The membrane fluidity of liposomes was assessed by using an in-house Laurdan-derivative probe sensitive to the membrane polarity (DiIol, Patent pending EPO19306175.1).⁴² Liposomes at a concentration of 0.1 g/L were incubated with the probe at 2 μ M for 15 min, and then the fluorescence emission spectrum was recorded on a FP-8500 spectrofluorometer (JASCO Applied Science, Halifax, Canada), with emission and excitation slits set at 2.5 nm. Spectra were recorded from 400 to 600 nm at 37 °C, with an excitation λ_{max} set at 390 nm. The generalized polarization (GP) parameter was calculated as indicated in eq 1, where I_{440} is the fluorescence emission intensity at 440 nm (gel phase) and I_{490} is the fluorescence emission intensity at 490 nm (liquid crystalline phase).⁴³ Results were expressed as mean \pm standard deviation of three independent experiments.

$$GP = (I_{440} - I_{490}) / (I_{440} + I_{490}) \quad (1)$$

The liposome distribution and surface charge were analyzed by using a Malvern Zetasizer Nano ZS (Malvern Instruments S.A., Worcestershire, UK). Particle size and polydispersity index (PDI) were determined by dynamic light scattering (DLS) at a concentration of 1 mg/mL liposomes in PBS. Analyses were

performed at 25 °C with an angle of detection of 173 °C. The ζ -potential values were measured by the electrophoresis technique. For ζ -potential measurements, liposomes were prepared in a low ionic salt buffer (HEPES, 20 mM, pH 7.4). The stability of the particles was investigated by following the size and PDI of the preparations 1, 2, 3, and 4 weeks after preparation. Liposome size results were expressed as mean \pm standard deviation of three independent liposome preparations. Liposome PDI results were expressed as the mean PDI of the preparations and were measured concurrently with liposome size on three independent liposomes preparations.

Liposome morphology was analyzed by cryogenic transmission electron microscopy (Cryo-TEM) at the "Centre Technologique des Microstructures" (CT μ) facility of the University of Lyon. Diluted samples of liposomes were dropped onto 300 mesh holey carbon films (Quantifoil R2/1) and quench-frozen in liquid ethane by using a cryo-plunge workstation (made at Laboratoire de Physique des Solides-LPS, Orsay, France). The specimens were then mounted on a precooled Gatan 626 sample holder, transferred into the microscope (Phillips CM120), and observed at an accelerating voltage of 120 kV.

Cell Culture. Four human cell lines were used as *in vitro* models: WPMY-1, LNCaP, C4-2B, and PC-3. The WPMY-1 cell line was originally obtained from healthy prostate tissue surrounding a tumor.⁴⁴ LNCaP is a hormone-sensitive cell line obtained from a lymph node metastasis derived from a prostate tumor.⁴⁵ The C4-2B cell line was obtained as a subline of LNCaP xenografts in castrated mice, resulting in the formation of a hormonal independent bone metastasis.⁴⁶ The PC-3 cell line was isolated from a vertebral metastasis stemming from a prostate tumor and entirely composed of carcinoma cells.⁴⁷ WPMY-1 and LNCaP cell lines were purchased from ATCC (Manassas, VA). PC-3 and C4-2B cell lines were a kind gift from Dr. Olivier Cuvillier (Institute of Pharmacology and Structural Biology, Toulouse, France).

WPMY-1 cells were cultured in DMEM supplemented with 5% (v/v) FBS, 100 U/mL penicillin, and 100 μ g/mL streptomycin. The LNCaP, C4-2B, and PC-3 cells were cultured in RPMI medium supplemented with 10% (v/v) FBS, 100 U/mL penicillin, and 100 μ g/mL streptomycin. All cells were cultured in a humidified incubator at 37 °C with 5% CO₂. After standard trypsinization, cells were seeded to the adapted density for cell viability and cytotoxicity assays and for liposome–cell interaction characterization.

Cell Viability Assay. The number of adherent viable cells was assessed by using the MTT assay, which is based on the reaction of a colorless tetrazolium salt with cellular reductases to form purple formazan crystals.⁴⁸ Cells (6×10^4 cells/cm² for WPMY-1 and LNCaP, 3×10^4 cells/cm² for C4-2B and PC-3) seeded in 12-well plates were treated with liposomes for 2 h 30 min, washed with PBS, and cultured in fresh medium for an additional 72 h. Afterward, MTT was added at a final concentration of 0.125 g/L. The plate was further incubated for 3 h at 37 °C, after which the culture medium was removed, and the formed formazan crystals were dissolved in 1 mL of DMSO. After 20 min incubation, the absorbance of the plate was measured at 570 nm. Absorbance measurements were conducted on an Infinite-M200 Pro plate reader (TECAN, Männedorf, Switzerland). Results were expressed as mean \pm standard deviation of three independent experiments.

Cytotoxicity Assay. Cell death was assessed by using the lactate dehydrogenase (LDH) assay that relies on the detection of a cytosolic enzyme, the LDH, in the culture medium as an indicator of membrane disruption upon cell death. Cells (6×10^4 cells/cm² for WPMY-1 and LNCaP, 3×10^4 cells/cm² for C4-2B and PC-3) seeded in 12-well plates were treated with liposomes for 2 h 30min, washed with PBS, and cultured in fresh medium for an additional 72 h. LDH was detected in 50 μ L of culture medium by using an LDH cytotoxicity assay kit (Sigma-Aldrich), as described by the manufacturer. Results were expressed as mean \pm standard deviation of three independent experiments.

Liposome–Cell Interaction Characterization. WPMY-1, LNCaP, C4-2B, and PC-3 cells were plated overnight in 96-well plates with a cell density of 6×10^4 cells/cm² for WPMY-1 and LNCaP and 3×10^4 cells/cm² for C4-2B and PC-3. The amount of

cell per well was chosen to ensure 80% surface coverage prior to liposome addition. NBD-PE or calcein fluorescent liposomes were added at a final concentration of 0.25 g/L, and the plate was further incubated for 2 h 30 min at 37 °C. The plates were rinsed three times with PBS, fixed with PFA 3.7% in PBS for 10 min, and then rinsed three more times with PBS. Finally, the plates were visualized by using an AxioObserverZ.1 (Zeiss, Oberkochen, Germany) epifluorescence microscope.

The fluorescence signal was quantified by calculating a corrected total cell fluorescence (CTCF) parameter by using ImageJ software. The cell surface was delimited, and the intensity of pixels contained in the cell was summed. The resulting total cell fluorescence was divided by the area occupied by the cells to obtain a mean cell light density. CTCF was obtained after equalization of the mean cell light density against the mean density of background readings in the same field of view, following eq 2.

$$\text{CTCF} = \text{mean cell density} - \text{mean background density} \quad (2)$$

For each cell line/liposome composition couple, the CTCF was calculated on a total of 30 cells, spread over six independent cell culture wells. To allow further comparison between cell lines, results were expressed as a percentage of targeting, with the strongest interaction corresponding to 100% targeting. Data followed a normal distribution. The Student's *t* test was used to analyze the data. Results were expressed as mean \pm standard deviation and were considered significant when $p < 0.05$ (*) and highly significant when $p < 0.01$ (**).

RESULTS

Design of Liposomes of Controlled Membrane Fluidity. To target cancer cell membranes, liposomes covering a wide range of membrane fluidity were prepared as detailed in Table 1. For all liposome preparations, 20 mol % of fusogenic lipid DOPE (1,2-dioleoyl-*sn*-glycero-3-phosphoethanolamine) was used to favor membrane fusion mechanisms between liposomes and plasma membranes. The membrane order degree (membrane fluidity) was dictated by the remaining 80%, which were constituted of phosphatidylcholines presenting various acyl chain lengths and degrees of unsaturation. DSPC, DPPC, and DMPC are phospholipids with saturated chains (18, 16, and 14 carbons, respectively). These preparations were denoted as DS, DP, and DM. POPC is a phospholipid with a saturated 16-carbon and an unsaturated 18-carbon chain (PO preparation); DOPC and DLPC possess two unsaturated 18-carbon chains with one and two double bonds, respectively (DO and DL preparations).

To ensure that the membrane composition range translated in a membrane fluidity range at 37 °C, the degree of membrane ordering (fluidity) was quantified by using an in-house Laurdan derived sensitive to membrane polarity, inserted in the liposome membrane (Dioll, patent pending EPO19306175.1). This probe spontaneously inserts in the bilayer, and its fluorescence emission is sensitive to the viscosity of its environment (e.g., Dioll inserted in DMPC liposomes shifted its maximum emission fluorescence (Figure S1) from 440 nm at low temperature (gel state) to 490 nm (liquid crystalline state)). A generalized polarization (GP) parameter can be calculated from the spectra as described in the Experimental Section (eq 1). GP evolution as a function of temperature presents an inflection point around 24 °C, which is in line with T_m values characteristic from DMPC (Figure S1). In our case, we used the fluorescence spectra of Dioll (Figure S2) and the resulting GP parameter to quantify the fluidity state of the six liposome preparations used (Figure 1) at 37 °C.

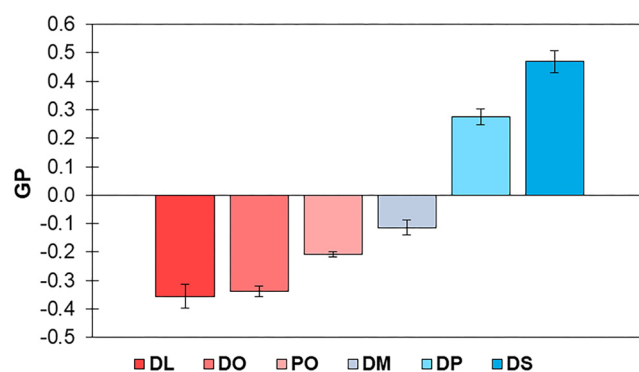


Figure 1. Lipid composition dictates liposome fluidity. GP values are calculated for each liposome composition as mean \pm SD of at least three independent experiments at 37 °C.

At 37 °C, membranes of DL and DO liposomes made of phospholipids with long and unsaturated acyl chains were in a fluid state as indicated by the negative GP values of -0.36 ± 0.04 and -0.34 ± 0.02 , respectively. Membranes of PO and DM liposomes reached a more rigid but still fluid state, as revealed by the higher but still negative GP values of -0.21 ± 0.01 and -0.11 ± 0.03 , respectively. Membranes of DP and DS liposomes were at a more rigid state as shown by GP positive values of 0.27 ± 0.03 and 0.47 ± 0.04 , respectively. As expected, the fluidity state of the liposomal membrane depends on the lipid chain length and the acyl chain degree of unsaturation and was quantitatively evaluated by the GP value (Figure 1).

To check the quality of the preparation in view of *in cellulo* use, the size and polydispersity of liposomes were measured (Figure 2a). Except DS, all liposome preparations showed an average size between 120 and 160 nm, constant for 4 weeks at least, with a rather low polydispersity index (PDI) and a typical size distribution histogram showing a single peak. For the very rigid DS preparation, two populations are present on the size distribution histogram: a population with an average diameter of 160 nm, which is consistent with that evidenced for PO liposomes (Figure 2d), and another population with a larger size, higher than 1 μm (Figure 2e). This results in a high PDI value (0.4). Yet, even for this more disperse preparation, the population of nanoparticles with a diameter lower than 200 nm was systematically present in the preparation for 4 weeks. These findings were confirmed by Cryo-TEM analysis (Figure 2b,c) which show typical unilamellar vesicles of 100–200 nm. No micrometer-sized vesicles were observed. We can attribute the peak situated at 1 μm on the size histogram of DS liposomes to vesicle aggregation in this rigid preparation.

The ζ -potential measurements showed a slightly negative surface potential around -10 mV, which can be attributed to the presence of the heads of PC groups which are oriented through the external water phase. This has been demonstrated also for other PC-based nanosystems.^{49–51} This value is lower than that obtained for liposomal carriers containing positively charged components (DOTAP).⁵² Even though the liposomes were made of zwitterionic lipids such as PC and PE, the global surface charge was not neutral: the charge delocalization at the lipid headgroup creates weak charge repulsion forces between liposomes, preventing them from coalescing or fusing into larger vesicles over the course of 4 weeks.

Calcein was loaded in the six liposome preparations, and calcein fluorescence intensity was plotted as a function of the

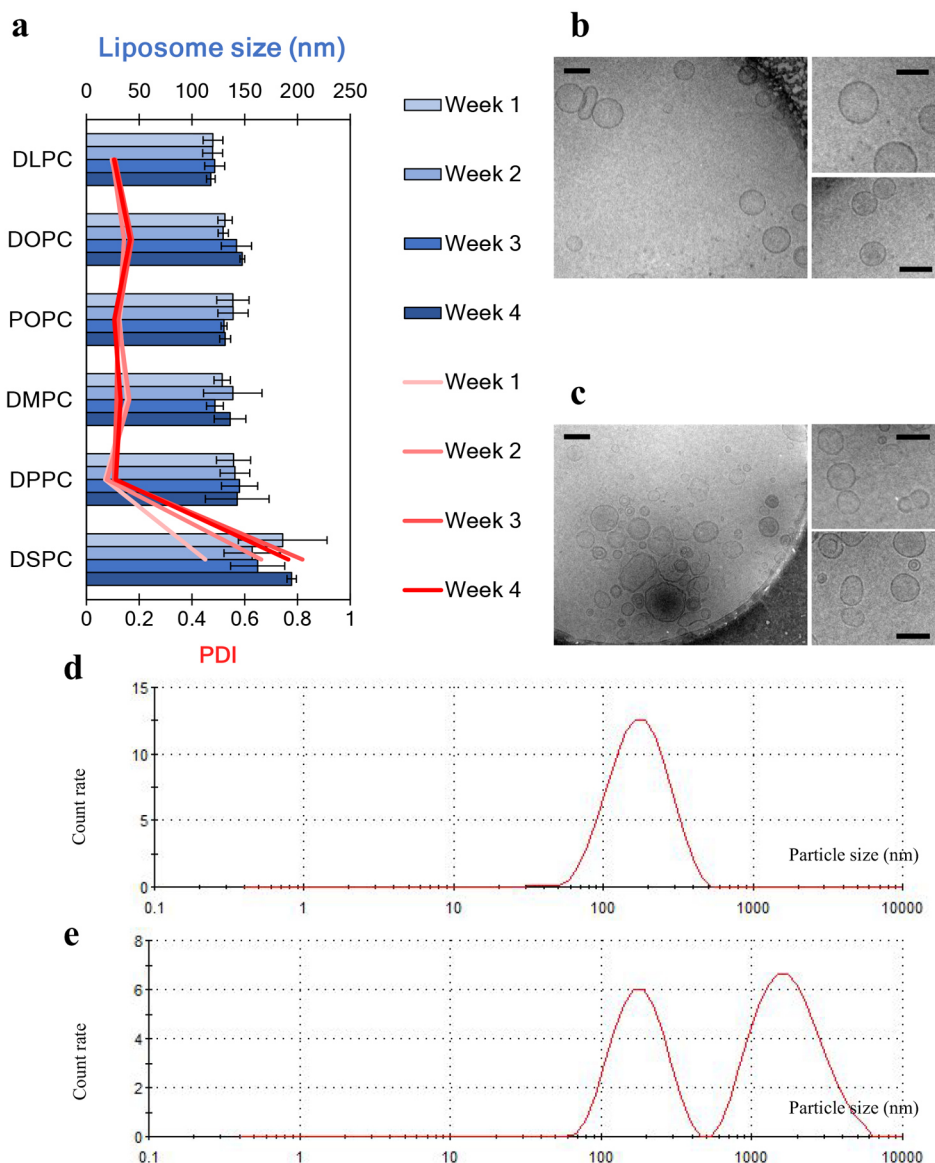


Figure 2. Monodisperse liposomes show a good stability over 4 weeks. (a) Liposome average size in blue and polydispersity index (PDI) in red. Plot of representative means (\pm SD) of three independent experiments per liposome preparation over the course of 4 weeks. Isolated PO (b) and DS (c) liposomes visualized by Cryo-TEM. Scale bars: 200 nm. Size distribution plots of PO (d) and DS (e) liposomes.

liposome preparation after removal of excess molecules by size exclusion chromatography (Figure S3). All liposome preparations encapsulated the fluorophore, but fluid liposomes such as DL and DO preparations were the most efficient.

Liposome Fluidity and Active Cell Targeting. The selective interaction of liposomes modulated by their membrane fluidity was tested on four cell lines chosen as models of human prostate cancer: WPMY-1, a nontumor control; LNCaP, lymph node hormone-sensitive low-aggressiveness metastasis; C4-2B, hormone-independent bone metastasis of intermediate aggressiveness; and PC-3, highly aggressive bone metastasis.⁵³

To monitor the liposome–cell interactions, nitrobenzoxadiazole-grafted DOPE (NBD-PE), a fluorescent lipid, was embedded in the liposomal lipid bilayer at a 2% molar ratio. The liposome preparations were incubated with adherent cells, and the internalization was followed by epifluorescence microscopy (Figure 3a). Liposome stability in the cell culture

medium was checked with calcein-leakage experiments (Figure S4), and all the preparations used were found to be stable over several hours in cell culture medium supplemented with FBS. The extent of the interaction was quantified by calculating the corrected total cell fluorescence (Figure 3b). The interaction pattern was different for each cell line. For the control WPMY-1 cells, an efficient targeting was achieved with the most rigid DS liposomes. Of note, DA liposomes (composed of 78% of DAPC (C20:0), 20% DOPE and 2% NBD-PE) also strongly interacted with WPMY-1, but not with PC-3 cells, which confirmed that control cells preferentially interact with rigid liposomes. The fluorescence intensity quantified on fluorescence images of WPMY-1 cells incubated with DA liposomes was lower than that obtained for DS liposomes (Figure S5), which indicated that an optimal composition for WPMY-1 targeting was DS. LNCaP cells were targeted by DM, PO, DO, and, more marginally, DL liposomes. C4-2B cells interacted with PO and DM and showed a weaker signal with DO and

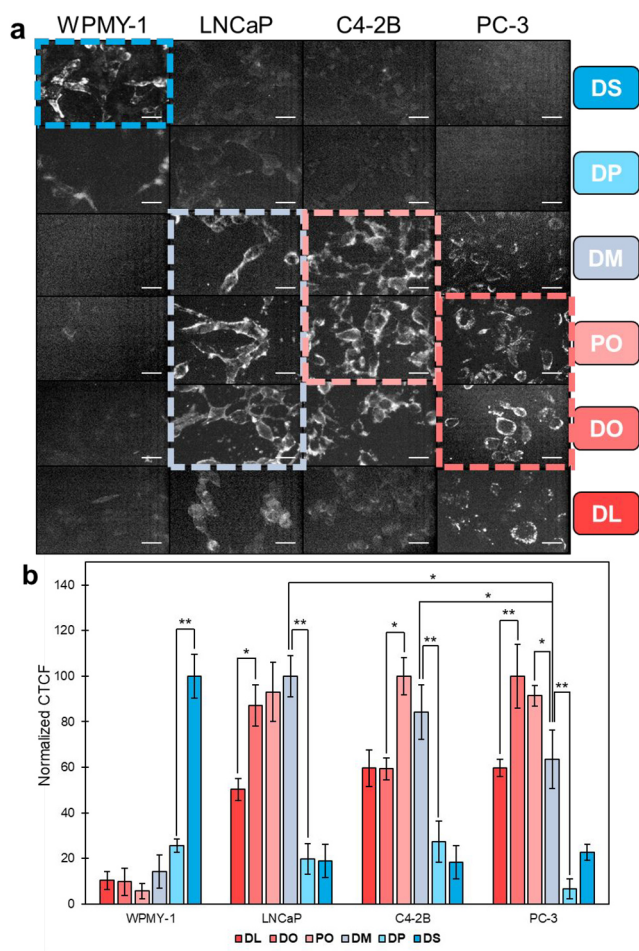


Figure 3. Lipid composition dictates cell uptake of liposomes. (a) Epifluorescence microscopy images of the interaction of WPMY-1, LNCaP, C4-2B, and PC-3 cells with six liposome preparations detailed in Table 1 after 2 h 30 min incubation. Scale bars: 20 μm . (b) Fluorescence intensity quantification using the CTCF method. Plot of means (\pm SD) of 30 individual cell measurements spread over six independent assays. Results expressed as a percentage of targeting, with the strongest interaction corresponding to 100% targeting. * $p < 0.05$ and ** $p < 0.01$ (Student's t test).

DL. PC-3 cells strongly interacted with DO and PO preparations and more modestly with DM and DL; none of the metastatic cell lines showed an interaction with the rigid DP and DS liposomes. Hence, the difference in the signal obtained shows the influence of the liposomal lipid composition on the targeting pattern: liposomes primarily made of fluid-state lipids target the tumor cells, while liposomes made of rigid-state lipids target the control cells.

Among fluid liposomes, if we look more precisely to behavior DM liposomes discriminate PC-3 cells from C4-2B cells ($p = 0.045$) and LNCaP cells ($p = 0.014$).

Cell Viability and Cytotoxicity of Liposomes. To check the biocompatibility of the liposome in a 2D cell culture model, we performed cytotoxicity and cell viability assays on the four cell lines immediately after 2 h 30 min treatment with liposomes to check for immediate toxicity or 72 h post-liposome treatment to exclude toxicity effects through activation of metabolic pathways. Figure 4a shows the cell viability evaluated by the MTT metabolic test after 72 h incubation, which was very little affected by liposome

incubation. A similar conclusion was drawn from LDH cytotoxicity test: no LDH leakage was observed after incubation with liposomes (Figure 4b). No toxic effects were observed after 2 h 30 min incubation with liposomes (Figure S6). Therefore, the prepared liposomes make excellent drug carriers, as they have no toxic effect on cells.

Liposome–Cell Interaction Mechanism. The mechanism of the liposome–membrane interaction was investigated by using two fluorophores: NBD-PE, a fluorescent lipid integrated into the liposomal membrane (Figure 5a), and calcein, a fluorescent probe encapsulated in liposomes (Figure 5b). Based on the targeting patterns presented in Figure 3, two liposome compositions were tested: POPC/DOPE 80:20 (PO), as it interacts with the three cancer cell lines, and DSPC/DOPE 80:20 (DS), as it interacts with the control cell line.

The results revealed a strong difference in the fluorescence distribution inside the cell depending on the encapsulated fluorophore. Liposomes incorporating NBD-PE led to a fluorescent signal localized at the cell membrane (Figure 5a). Yet, at the microscope resolution, it is difficult to see whether the fluorophore is distributed inside the plasma membrane or in the membrane of liposomes attached to the cells. We can, however, exclude an endocytosis pattern in which liposomes and fluorophore would be distributed in the inner compartments of the cell (endocytic vesicles, endosomes, etc.). The NBD-PE distribution pattern was therefore indicative of either liposome adhesion to the cell membrane or liposome fusion with the membrane and consequent distribution of the fluorophore in the plasma membrane (Figure 5a). To discriminate between these two possibilities, we used calcein-loaded liposomes. In this case, calcein is a hydrophilic fluorophore which is expected to be encapsulated in the inner compartment of the liposomes. Indeed, this fluorophore is readily released upon liposome-burst experiments.⁵⁴ After incubation with calcein-containing liposomes, the fluorophore was mainly distributed in the cytoplasm (Figure 5b). Therefore, calcein-containing liposomes either are internalized through endocytosis pathways or release their internal content in the cytoplasm upon membrane fusion processes. Yet, in the case of vesicle internalization the two fluorophores are expected to colocalize. This is not the case, as the two fluorophores show different distributions inside the cell: NBD-PE, which is of hydrophobic nature, remains at the cell membrane, whereas calcein, which is hydrophilic, is distributed in the cytoplasm. Therefore, among the main mechanisms proposed—endocytosis, membrane fusion, or liposome adhesion to the cell membrane—the results supported a membrane fusion process leading to the distribution of the fluorescent lipid in the cell membrane and the release of calcein in the cytosol.

DISCUSSION

The process of tumor development modifies in a major way all cellular physiological pathways.⁵⁵ This leads to many adaptations that enable tumor cells to survive, proliferate, and invade surrounding tissues. Among these, changes in membrane lipid composition resulting in membrane fluidity modifications have been widely reported.^{21,27–29} In this study, we used membrane fluidity modulations as a new way to selectively target tumor cells with liposomal carriers. We prepared liposomes using PCs with various acyl chains to obtain a membrane fluidity scale ranging from rigid to fluid, as

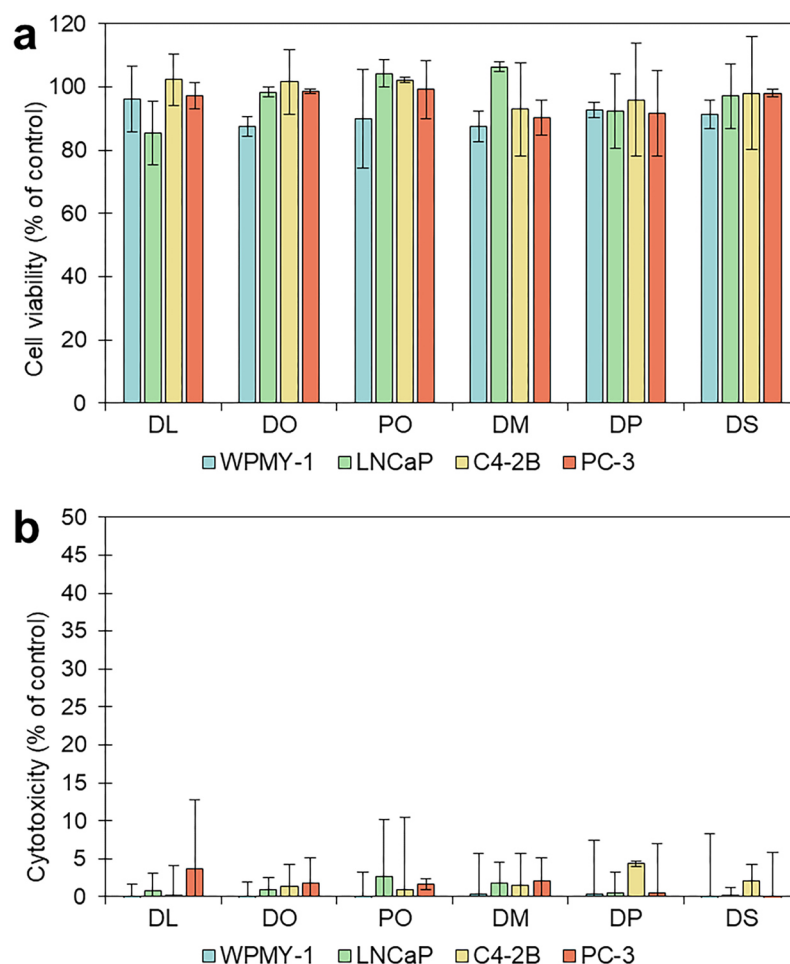


Figure 4. Liposomes do not affect cell viability and show no cytotoxic effect. (a) Cell viability quantification, assessed on plated cells with the MTT assay 3 days after liposome treatment. Results expressed as a percentage of cell viability relative to an untreated control corresponding to 100% viability. (b) Cytotoxicity quantification, assessed on the same cells than (a) with the LDH assay. Results expressed as a percentage of cell death relative to an untreated control corresponding to 0% toxicity and a control treated with 10% Triton X-100 corresponding to 100% toxicity.

reported by a polarity-sensitive probe (Figure 1). Except for the DS preparation, which was very rigid and in which the T_m difference between DSPC and the much lower melting DOPE may induce significant demixing, the liposome preparations used were monodisperse and stable for several weeks (Figure 2). By tracking the fluorescent lipid NBD-PE incorporated in the liposome membrane, we investigated the interaction of these liposomes with a nontumoral (control) and three different tumor cell lines and show that prepared liposomes achieve specific targeting of tumor or control cells solely on the basis of their lipid composition (Figure 5). The intrinsic membrane fluidity of the liposomes seems therefore to be determinant for liposome–cell interaction specificity. Yet, as discussed above, DS liposome preparation shows a high dispersity in terms of size and may contain a large proportion of larger particles; therefore, a size effect cannot be excluded. A thorough study of the influence of the size of liposomes should be considered in the future to better understand the fusion mechanism and the cell specificity.

Moreover, the interaction of fluid-state liposomes with tumor cells showed a different signal between the low-aggressive LNCaP and C4-2B cells, on one hand, and the highly aggressive PC-3 cells on the other hand. While DM liposomes interact strongly with LNCaP and C4-2B cells, they

interact less efficiently with PC-3 cells. This suggests that the fluidity of the liposomal membrane is, along with liposome size, surface charge, and hydrophilicity, one of the physicochemical parameters that affect liposome uptake by promoting liposome–cell interactions and the subsequent liposome fusion with the plasma membrane. It is interesting to notice that fluid liposomes were the most selective not only in terms of uptake but also in terms of amount of fluorophore encapsulated (Figure S3).

To explore the mechanism of liposome–cell membrane interaction, we used liposomes embedding NBD-PE in the lipid bilayer or encapsulating calcein in the hydrophilic core to follow the internalization profile. The NBD-PE fluorescence profile was restricted to the cell membrane whereas calcein showed a cytoplasm diffuse pattern. Considering three possible mechanisms of interaction—adhesion of liposomes to the cell, fusion of the liposome with the cell plasma membrane, and internalization through endocytosis—the profile obtained with both NBD-PE- and calcein-loaded liposomes (Figure 5) matched the expected signal for a liposome–cell membrane fusion. This points out that the internalization is mainly based on fusion phenomena. This fusion mechanism, which appears controlled by the match of the membrane fluidity between the cell and the liposomes membranes, is probably favored by the

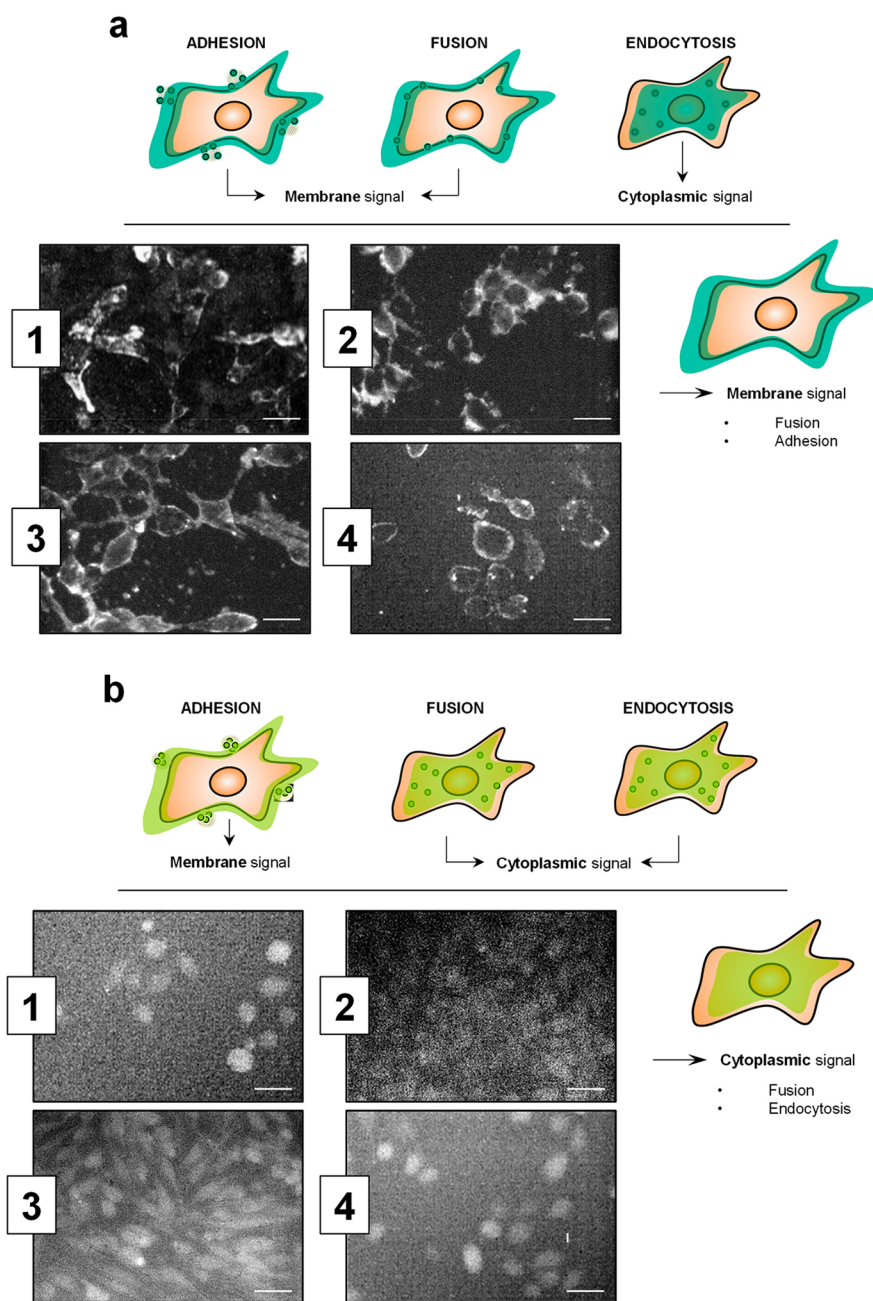


Figure 5. Two fluorophore interaction pattern highlights a fusion mechanism. (a) Predicted and experimental interaction patterns for liposomes incorporating NBD-PE in the liposomal membrane. Epifluorescence images of WPMY-1 (1), LNCaP (2), C4-2B (3), and PC-3 (4) cells, incubated with liposomes containing 2% of NBD-PE. (b) Predicted and experimental interaction patterns for liposomes encapsulating calcein. Epifluorescence images of WPMY-1 (1), LNCaP (2), C4-2B (3), and PC-3 (4) cells, incubated with liposomes encapsulating 500 μM calcein. Images shown are representative of three independent measurements on each cell line. In both cases, cells were incubated with the liposome composition that exhibited maximal interaction, i.e., DS for WPMY-1 cells and PO for LNCaP, C4-2B, and PC-3 cells. Scale bars: 20 μm .

presence of DOPE, a fusogenic lipid in the liposome membrane, as its conical geometry promotes the formation of inverted hexagonal intermediate structures that lead to the formation of fusion pores.⁵⁶ For drug delivery purposes, such a mechanism is very promising, since fusion leads to the release of the entrapped drug directly in the cytosol of the targeted cells. Indeed, liposomes adhering to the cell surface exhibit poor drug release, and endocytic pathways lead to the early and late stages of endosomes that fuse with lysosomes, often leading to a lower activity of the encapsulated drug. Additionally, cytotoxicity and cell viability assays revealed no

toxic effect of liposomes on all cell lines tested (Figure 4). This highlights the drug delivery potential of these liposomes, as they specifically target tumor cells while remaining nontoxic to the control cells. It must be stressed here that instead of relying on the difference in membrane carbohydrate or protein composition usually used in current targeting strategies, these liposomes achieve specific targeting based on membrane fluidity differences.

Membrane fluidity is one of the key parameters for membrane fusion, since it determines the mobility of lipids, proteins, and water molecules that cooperate in the

reorganization and the assembly required and induced by the membrane fusion.⁵⁷ As it is directly dependent on the membrane lipid composition, any modification of the lipid metabolism results in a membrane fluidity change. Many studies found a link between membrane lipid composition, membrane physicochemical state, and pathologies, especially in the case of cancers where higher unsaturation of acyl chains is associated with an elevated membrane fluidity and metastasis aggressiveness.^{21,58} A previous study of PC-3 and WPMY-1 cells, the two extremes in the range of aggressiveness of the cell lines used, revealed that the membrane of the highly aggressive and metastatic PC-3 cells is less viscous and more prone to deformation than that of the control WPMY-1 cells.³² In this study, we found that the liposome–cell interaction is sensitive to the membrane lipid composition, with fluid-state liposomes targeting the flexible and metastatic cells, whereas rigid-state liposomes target the stiffer control cells. In addition, we determined that the interaction mechanism is mainly based on a membrane fusion process, which supports the idea that targeting relies on a difference in the physicochemical properties of the membrane and, in particular, on differences in membrane fluidity.

The role of lipid composition in liposome design has been widely studied. However, until now, it was generally recognized as a parameter affecting the global liposome stability and the drug encapsulation efficiency.⁵⁹ A recent study shows that tailoring the lipid composition of nanoparticles modulates their cellular uptake in triple negative breast cells (4 T1).⁶⁰ In addition to the lipid headgroup, acyl chain length and unsaturation also largely influence cellular uptake in triple negative 4 T1 breast cancer cells, with an increased uptake for liposomes constituted of C18:1 acyl chains. Moreover, membrane fluidity of the liposomes seems to play an important part in determining the liposome uptake as a major effect of cholesterol, a modulator of membrane fluidity of the liposomes, is observed. In our case, POPC and DOPC liposomes, which contain C18:1 chains, largely and selectively interact with prostate tumor cell lines. Yet, intrinsic differences between breast and prostate cancer cell lines seem to exist in terms of membrane composition and/or metabolic pathways and determine liposome uptake. No uptake was measured for long and saturated chains as C18:0 and C16:0 in prostate cancer cell lines, and cell viability was affected by C12:0-containing liposomes (not shown), but not by C14:0 (DM) liposomes (Figure 4) as it was the case for breast cancer cells. Two other previous studies also found that the lipid composition of a nanoparticle could affect its interaction with cells.^{61,62}

In the present report, we show that targeting can be achieved by modulating the liposome physical state. Yet, the use of liposomes as drug carriers cannot be discussed without considering factors related to circulation *in vivo*, such as blood protein binding, interaction with circulatory cells, or cholesterol transfer. Tailoring lipid composition by modulating particle global charge may yield hydrophilic vesicles, and thus limit plasma protein binding, while maintaining fluidity state. Studies of association of plasma proteins with liposomes have also shown that liposome membrane properties such as its fluidity state, above or below lipid melting points, determines particle circulation properties, as plasma protein binding depends on the fluidity state of the membrane.^{38,39} Altogether, fine-tuning of the lipid composition of carriers is a promising strategy to promote specific drug delivery. These findings shed

new light on liposome membrane composition, which in turn modulates membrane fluidity, by highlighting its role as a key targeting parameter.

CONCLUSION

Selective drug delivery strategies is a Holy Grail in cancer therapy. Here, we report for the first time a valid alternative targeting based on liposome membrane fluidity. Using this approach, we can easily tune liposomes to promote liposome fusion with the target membrane. This strategy has been proved successful in selective targeting of four prostatic cell lines. Unlike conventional approaches, it does not rely on proteins or carbohydrates functionalization and constitutes a cost-effective alternative to promote membrane fusion and consequently avoid endocytosis and lysosomal degradation. Altogether, the carrier's ability to target a particular cell type according to its membrane fluidity and its fusion with the target membrane are assets that should make it possible to reduce the doses of active ingredients injected into the body to limit the unwanted side effects of chemotherapy.

ASSOCIATED CONTENT

Supporting Information

The Supporting Information is available free of charge at <https://pubs.acs.org/doi/10.1021/acs.langmuir.0c00262>.

Phase transition of DMPC liposomes reported with Dioll fluorescence; Dioll fluorescence spectra in DS, DP, DM, PO, DO, and DL liposomes; calcein load in liposome preparations; liposome stability in cell culture medium; DA liposome interaction with WPMY-1 and PC-3 cells; liposomes do not affect cell viability and show no cytotoxic effect (PDF)

AUTHOR INFORMATION

Corresponding Author

Ofelia Maniti – Institut de Chimie et Biochimie Moléculaires et Supramoléculaires, ICBMS UMR 5246, CNRS, Univ Lyon, Université Lyon 1, Lyon, France; orcid.org/0000-0001-9371-9580; Email: ofelia.maniti@univ-lyon1.fr

Authors

Julien Bompard – Institut de Chimie et Biochimie Moléculaires et Supramoléculaires, ICBMS UMR 5246, CNRS, Univ Lyon, Université Lyon 1, Lyon, France; orcid.org/0000-0001-8057-9144

Annalisa Rosso – Laboratoire d'Automatique, de Génie des Procédés et de Génie Pharmaceutique LAGEPP UMR 5007, CNRS, Univ Lyon, Université Lyon 1, Lyon, France

Leyre Brizuela – Institut de Chimie et Biochimie Moléculaires et Supramoléculaires, ICBMS UMR 5246, CNRS, Univ Lyon, Université Lyon 1, Lyon, France

Saïda Mebarek – Institut de Chimie et Biochimie Moléculaires et Supramoléculaires, ICBMS UMR 5246, CNRS, Univ Lyon, Université Lyon 1, Lyon, France

Loïc J. Blum – Institut de Chimie et Biochimie Moléculaires et Supramoléculaires, ICBMS UMR 5246, CNRS, Univ Lyon, Université Lyon 1, Lyon, France

Ana-Maria Trunfio-Sfarghiu – Laboratoire de Mécanique des Contacts et Structures, LaMCoS UMR 5259, CNRS, Univ Lyon, Université Lyon 1, Lyon, France

Giovanna Lollo – Laboratoire d'Automatique, de Génie des Procédés et de Génie Pharmaceutique LAGEPP UMR 5007,

CNRS, Univ Lyon, Université Lyon 1, Lyon, France;

orcid.org/0000-0001-7030-3056

Thierry Granjon – Institut de Chimie et Biochimie Moléculaires et Supramoléculaires, ICBMS UMR 5246, CNRS, Univ Lyon, Université Lyon 1, Lyon, France; orcid.org/0000-0002-8575-3727

Agnès Girard-Egrot – Institut de Chimie et Biochimie Moléculaires et Supramoléculaires, ICBMS UMR 5246, CNRS, Univ Lyon, Université Lyon 1, Lyon, France

Complete contact information is available at:

<https://pubs.acs.org/10.1021/acs.langmuir.0c00262>

Funding

This research was supported by grants from the French National Research Agency (ANR), the French Ligue Nationale contre le Cancer Association, the and CNRS Prematuration program.

Notes

The authors declare no competing financial interest.

ACKNOWLEDGMENTS

We thank Mr. Pierre-Yves Dugas from the Chemistry, Catalysis, Polymers and Processes Institute of Lyon for the Cryo-TEM experiments, Dr. Olivier Cu villier from the Institute of Pharmacology and Structural Biology of Toulouse for the PC-3 and C4-2B cell lines, and Dr. Arnaud Vigneron from the Cancer Research Center of Lyon for helpful discussions and insights.

REFERENCES

- (1) Kuchta, R. D.; Shewach, D. S. Introduction to Cancer Chemotherapeutics. *Chem. Rev.* **2009**, *109*, 2859–2861.
- (2) Shi, J.; Kantoff, P. W.; Wooster, R.; Farokhzad, O. C. Cancer nanomedicine: progress, challenges and opportunities. *Nat. Rev. Cancer* **2017**, *17*, 20–37.
- (3) Aslan, B.; Ozpolat, B.; Sood, A. K.; Lopez-Berestein, G. Nanotechnology in cancer therapy. *J. Drug Target.* **2013**, *21*, 904–913.
- (4) Hassanzadeh, P.; Fullwood, I.; Sothi, S.; Aldulaimi, D. Cancer nanotechnology. *Gastroenterol. Hepatol. Bed. Bench.* **2011**, *4*, 63–69.
- (5) Bahrami, B.; Hojjat-Farsangi, M.; Mohammadi, H.; Anvari, E.; Ghalamfarsa, G.; Yousefi, M.; Jadidi-Niaragh, F. Nanoparticles and targeted drug delivery in cancer therapy. *Immunol. Lett.* **2017**, *190*, 64–83.
- (6) Leung, S. J.; Romanowski, M. Light-Activated Content Release from Liposomes. *Theranostics* **2012**, *2*, 1020–1036.
- (7) Tiwari, G.; Tiwari, R.; Sriwastawa, B.; Bhati, L.; Pandey, S.; Pandey, P.; Bannerjee, S. K. Drug delivery systems: An updated review. *Int. J. Pharm. Invest.* **2012**, *2*, 2–11.
- (8) Fassas, A.; Anagnostopoulos, A. The use of liposomal daunorubicin (DaunoXome) in acute myeloid leukemia. *Leuk. Lymphoma* **2005**, *46*, 795–802.
- (9) James, N. D.; Coker, R. J.; Tomlinson, D.; Harris, J. R. W.; Gompels, M.; Pinching, A. J.; Stewart, J. S. W. Liposomal Doxorubicin (Doxil): An Effective New Treatment for Kaposi's Sarcoma in AIDS. *Clin. Oncol. (R. Coll. Radiol.)* **1994**, *6*, 294–296.
- (10) Stathopoulos, G. P.; Antoniou, D.; Dimitroulis, J.; Michalopoulou, P.; Bastas, A.; Marosis, K.; Stathopoulos, J.; Provata, A.; Yiamboudakis, P.; Veldekis, D.; Lolis, N.; Georgatou, N.; Toubis, M.; Pappas, C.; Tsoukalas, G. Liposomal cisplatin combined with paclitaxel versus cisplatin and paclitaxel in non-small-cell lung cancer: a randomized phase III multicenter trial. *Ann. Oncol.* **2010**, *21*, 2227–2232.
- (11) Akbarzadeh, A.; Rezaei-Sadabady, R.; Davaran, S.; Joo, S. W.; Zarghami, N.; Hanifepour, Y.; Samiei, M.; Kouhi, M.; Nejati-Koshki,

K. Liposome: classification, preparation, and applications. *Nanoscale Res. Lett.* **2013**, *8*, 102.

(12) Sandeep, K.; Sunilkumar, K.; Sudheer, B.; Mohanvarma, M. Liposomal drug delivery system - A comprehensive review. *Int. J. Drug. Dev. Res.* **2013**, *5*, 62–75.

(13) Kobayashi, H.; Watanabe, R.; Choyke, P. L. Improving Conventional Enhanced Permeability and Retention (EPR) Effects; What Is the Appropriate Target? *Theranostics* **2014**, *4*, 81–89.

(14) Sindhvani, S.; Syed, A. M.; Ngai, J.; Kingston, B. R.; Maiorino, L.; Rothschild, J.; MacMillan, P.; Zhang, Y.; Rajesh, N. U.; Hoang, T.; Wu, J. L. Y.; Wilhelm, S.; Zilman, A.; Gadde, S.; Sulaiman, A.; Ouyang, B.; Lin, Z.; Wang, L.; Egeblad, M.; Chan, W. C. W. The entry of nanoparticles into solid tumours. *Nat. Mater.* **2020**, *19*, 566.

(15) Jain, R. K.; Stylianopoulos, T. Delivering nanomedicine to solid tumors. *Nat. Rev. Clin. Oncol.* **2010**, *7*, 653–664.

(16) Heldin, C.; Rubin, K.; Pietras, K.; Östman, A. High interstitial fluid pressure — an obstacle in cancer therapy. *Nat. Rev. Cancer* **2004**, *4*, 806–813.

(17) Zhai, G.; Wu, J.; Xiang, G.; Mao, W.; Yu, B.; Li, H.; Piao, L.; Lee, L. J.; Lee, R. J. Preparation, characterization and pharmacokinetics of folate receptor-targeted liposomes for docetaxel delivery. *J. Nanosci. Nanotechnol.* **2009**, *9*, 2155–61.

(18) Song, X.; Ju, R.; Xiao, Y.; Wang, X.; Liu, S.; Fu, M.; Liu, J.; Gu, L.; Li, X.; Cheng, L. Application of multifunctional targeting epirubicin liposomes in the treatment of non-small-cell lung cancer. *Int. J. Nanomed.* **2017**, *12*, 7433–7451.

(19) Song, Z.; Lin, Y.; Zhang, X.; Feng, C.; Lu, Y.; Gao, Y.; Dong, C. Cyclic RGD peptide-modified liposomal drug delivery system for targeted oral apatinib administration: enhanced cellular uptake and improved therapeutic effects. *Int. J. Nanomed.* **2017**, *12*, 1941–1958.

(20) Bakowsky, H.; Richter, T.; Kneuer, C.; Hoekstra, D.; Rothe, U.; Bendas, G.; Ehrhardt, C.; Bakowsky, U. Adhesion characteristics and stability assessment of lectin-modified liposomes for site-specific drug delivery. *Biochim. Biophys. Acta, Biomembr.* **2008**, *1778*, 242–249.

(21) Sok, M.; Sentjurc, M.; Schara, M. Membrane fluidity characteristics of human lung cancer. *Cancer Lett.* **1999**, *139*, 215–20.

(22) Li, M.; Yasumura, D.; Ma, A. A.; Matthes, M. T.; Yang, H.; Nielson, G.; Huang, Y.; Szoka, F. C.; Lavail, M. M.; Diamond, M. I. Intravitreal Administration of HA-1077, a ROCK Inhibitor, Improves Retinal Function in a Mouse Model of Huntington Disease. *PLoS One* **2013**, *8*, 1–8.

(23) Xia, C. F.; Boado, R. J.; Zhang, Y.; Chu, C.; Pardridge, W. M. Intravenous glial-derived neurotrophic factor gene therapy of experimental Parkinson's disease with Trojan horse liposomes and a tyrosine hydroxylase promoter. *J. Gene Med.* **2008**, *10*, 306–315.

(24) Wu, J.; Lee, A.; Lu, Y.; Lee, R. J. Vascular targeting of doxorubicin using cationic liposomes. *Int. J. Pharm.* **2007**, *337*, 329–335.

(25) Serda, R.; Ruiz-Esparza; Flores-Arredondo, J.; Segura-Ibarra; Torre, G.; Blanco; Ferrari, M. The physiology of cardiovascular disease and innovative liposomal platforms for therapy. *Int. J. Nanomed.* **2013**, *8*, 629–640.

(26) Levchenko, T. S.; Hartner, W. C.; Torchilin, V. P. Liposomes in diagnosis and treatment of cardiovascular disorders. *Methpdist. Debakey. Cardiovasc. J.* **2012**, *8*, 36–41.

(27) Yao, J. K.; van Kammen, D. P.; Gurklis, J. Red blood cell membrane dynamics in schizophrenia. III. Correlation of fatty acid abnormalities with clinical measures. *Schizophr. Res.* **1994**, *13*, 227–232.

(28) Yao, J. K.; van Kammen, D. P.; Welker, J. A. Red blood cell membrane dynamics in schizophrenia. II. Fatty acid composition. *Schizophr. Res.* **1994**, *13*, 217–226.

(29) Kuriyama, S.; Theveneau, E.; Benedetto, A.; Parsons, M.; Tanaka, M.; Charras, G.; Kabla, A.; Mayor, R. In vivo collective cell migration requires an LPAR2-dependent increase in tissue fluidity. *J. Cell Biol.* **2014**, *206*, 113–127.

(30) Zhao, W.; Prijic, S.; Urban, B. C.; Tisza, M. J.; Zuo, Y.; Li, L.; Tan, Z.; Chen, X.; Mani, S. A.; Chang, J. T. Candidate antimetastasis

drugs suppress the metastatic capacity of breast cancer cells by reducing membrane fluidity. *Cancer Res.* **2016**, *76*, 2037–2049.

(31) Nakazawa, I.; Iwazumi, M. A role of the cancer cell membrane fluidity in the cancer metastases: an ESR study. *Tohoku J. Exp. Med.* **1989**, *157*, 193–198.

(32) Zouaoui, J.; Trunfio-Sfarghiu, A. M.; Brizuela, L.; Piednoir, A.; Maniti, O.; Munteanu, B.; Mebarek, S.; Girard-Egrot, A.; Landoulsi, A.; Granjon, T. Multi-scale mechanical characterization of prostate cancer cell lines: Relevant biological markers to evaluate the cell metastatic potential. *Biochim. Biophys. Acta, Gen. Subj.* **2017**, *1861*, 3109–3119.

(33) Chem, J. M.; Tomatsu, I.; Marsden, H. R.; Rabe, M.; Versluis, F.; Zheng, T.; Zope, H.; Kros, A. Influence of pegylation on peptide-mediated liposome fusion. *J. Mater. Chem.* **2011**, *21*, 18927–18933.

(34) Hatakeyama, H.; Akita, H.; Harashima, H. The Polyethylene-glycol Dilemma: Advantage and Disadvantage of PEGylation of Liposomes for Systemic Genes and Nucleic Acids Delivery to Tumors. *Biol. Pharm. Bull.* **2013**, *36*, 892–899.

(35) Smoluchowski, M. Drei Vorträge über Diffusion, Brownsche Molekularbewegung und Koagulation von Kolloidteilchen. *Phys. Z.* **1916**, *17*, 585–599.

(36) Montaner, J.; Cano-Sarabia, M.; Simats, A.; Hernandez-Guillamon, M.; Rosell, A.; Maspoch, D.; Campos-Martorell, M. Charge effect of a liposomal delivery system encapsulating simvastatin to treat experimental ischemic stroke in rats. *Int. J. Nanomed.* **2016**, *11*, 3035–3048.

(37) Honary, S.; Zahir, F. Effect of Zeta Potential on the Properties of Nano-Drug Delivery Systems - A Review (Part 2). *Trop. J. Pharm. Res.* **2013**, *12*, 265–273.

(38) Semple, S. C.; Chonn, A.; Cullis, P. R. Influence of cholesterol on the association of plasma proteins with liposomes. *Biochemistry* **1996**, *35* (8), 2521–2525.

(39) Sieber, S.; Grossen, P.; Detampel, P.; Siegfried, S.; Witzigmann, D.; Huwyler, J. Zebrafish as an early stage screening tool to study the systemic circulation of nanoparticulate drug delivery systems in vivo. *J. Controlled Release* **2017**, *264*, 180–191.

(40) Ueoka, R.; Matsumoto, Y.; Goto, K.; Ichihara, H.; Komizu, Y. Membrane Targeted Chemotherapy with Hybrid Liposomes for Tumor Cells Leading to Apoptosis. *Curr. Pharm. Des.* **2011**, *17*, 1709–1719.

(41) Komizu, Y.; Ueoka, H.; Ueoka, R. Selective accumulation and growth inhibition of hybrid liposomes to human hepatocellular carcinoma cells in relation to fluidity of plasma membranes. *Biochem. Biophys. Res. Commun.* **2012**, *418*, 81–86.

(42) Cheniour, M.; Gueyrard, D.; Goekjian, P. G.; Granjon, T.; Marcillat, O. A convenient and versatile synthesis of Laurdan-like fluorescent membrane probes: characterization of their fluorescence properties. *RSC Adv.* **2016**, *6* (7), 5547–5557.

(43) Parasassi, T.; Krasnowska, E. K.; Bagatolli, L.; Gratton, E. Laurdan and Prodan as Polarity-Sensitive Fluorescent Membrane Probes. *J. Fluoresc.* **1998**, *8*, 365–373.

(44) Webber, M.; Trakul, N.; Thraves, P.; Bello-DeOcampo, D.; Chu, W.; Storto, P.; Huard, T.; Rhim, J.; Williams, D. A human prostatic stromal myofibroblast cell line WPMY-1: a model for stromal-epithelial interactions in prostatic neoplasia. *Carcinogenesis* **1999**, *20*, 1185–1192.

(45) Horoszewicz, J. S.; Leong, S. S.; Kawinski, E.; Karr, J. P.; Rosenthal, H.; Chu, T. M.; Mirand, E. A.; Murphy, G. P. LNCaP Model of Human Prostatic Carcinoma. *Cancer Res.* **1983**, *43*, 1809–1818.

(46) Wu, H.; Hsieh, J.; Gleave, M. E.; Brown, N. M.; Pathak, S.; Chung, L. W. K. Derivation of androgen-independent human LNCaP prostatic cancer cell sublines: role of bone stromal cells. *Int. J. Cancer* **1994**, *57*, 406–412.

(47) Kaighn, M.; Narayan, K.; Ohnuki, Y.; Lechner, J.; Jones, L. Establishment and characterization of a human prostatic carcinoma cell line (PC-3). *Invest. Urol.* **1979**, *17*, 16–23.

(48) Mosmann, T. Rapid Colorimetric Assay for Cellular Growth and Survival: Application to Proliferation and Cytotoxicity Assays. *J. Immunol. Methods* **1983**, *65*, 55–63.

(49) Lollo, G.; Rivera-Rodriguez, G. R.; Bejaud, J.; Montier, T.; Passirani, C.; Benoit, J. P.; Garcia-Fuentes, M.; Alonso, M. J.; Torres, D. Polyglutamic acid-PEG nanocapsules as long circulating carriers for the delivery of docetaxel. *Eur. J. Pharm. Biopharm.* **2014**, *87* (1), 47–54.

(50) Moya, M. L.; Lopez-Lopez, M.; Lebron, J. A.; Ostos, F. J.; Perez, D.; Camacho, V.; Beck, I.; Merino-Bohorquez, V.; Camean, M.; Madinabeitia, N.; Lopez-Cornejo, P. Preparation and Characterization of New Liposomes. Bactericidal Activity of Cefepime Encapsulated into Cationic Liposomes. *Pharmaceutics* **2019**, *11* (2), e69.

(51) Chibowski, E.; Szczes, A. Zeta potential and surface charge of DPPC and DOPC liposomes in the presence of PLC enzyme. *Adsorption* **2016**, *22*, 755–765.

(52) Takeuchi, K.-i.; Ishihara, M.; Kawaura, C.; Noji, M.; Furuno, T.; Nakanishi, M. Effect of zeta potential of cationic liposomes containing cationic cholesterol derivatives on gene transfection. *FEBS Lett.* **1996**, *397* (2–3), 207–209.

(53) Cunningham, D.; You, Z. In vitro and in vivo model systems used in prostate cancer research. *J. Biol. Methods* **2015**, *2*, 17.

(54) Katsu, T. Application of calcein-loaded liposomes for the determination of membrane channel size. *Biol. Pharm. Bull.* **1999**, *22* (9), 978–980.

(55) Devita, V. T.; Chu, E. A History of Cancer Chemotherapy. *Cancer Res.* **2008**, *68*, 8643–8654.

(56) Gruner, S. M. Intrinsic curvature hypothesis for biomembrane lipid composition: A role for nonbilayer lipids. *Proc. Natl. Acad. Sci. U. S. A.* **1985**, *82*, 3665–3669.

(57) Aeffner, S.; Reusch, T.; Weinhausen, B.; Salditt, T. Energetics of stalk intermediates in membrane fusion are controlled by lipid composition. *Proc. Natl. Acad. Sci. U. S. A.* **2012**, *109*, 1609–1618.

(58) Beloribi-Djefafia, S.; Vasseur, S.; Guillaumond, F. Lipid metabolic reprogramming in cancer cells. *Oncogenesis* **2016**, *5*, e189.

(59) Zylberberg, C.; Matosevic, S. Pharmaceutical liposomal drug delivery: a review of new delivery systems and a look at the regulatory landscape. *Drug Delivery* **2016**, *23*, 3319–3329.

(60) Abumanhal-Masarweh, H.; da Silva, D.; Poley, M.; Zinger, A.; Goldman, E.; Krinsky, N.; Kleiner, R.; Shenbach, G.; Schroeder, J. E.; Shklover, J.; Shainsky-Roitman, J.; Schroeder, A. Tailoring the lipid composition of nanoparticles modulates their cellular uptake and affects the viability of triple negative breast cancer cells. *J. Controlled Release* **2019**, *307*, 331–341.

(61) Takechi-haraya, Y.; Sakai-kato, K.; Abe, Y.; Kawanishi, T.; Okuda, H.; Goda, Y. Atomic Force Microscopic Analysis of the Effect of Lipid Composition on Liposome Membrane Rigidity. *Langmuir* **2016**, *32*, 6074–6082.

(62) Carradori, D.; dos Santos, A. G.; Masquelier, J.; Paquot, A.; Saulnier, P.; Eyer, J.; Pr eat, V.; Muccioli, G. G.; Mingeot-leclercq, M.; des Rieux, A. The origin of neural stem cells impacts their interactions with targeted-lipid nanocapsules: Potential role of plasma membrane lipid composition and fluidity. *J. Controlled Release* **2018**, *292*, 248–255.

List of communications

This PhD work was realized at the Laboratoire d'Automatique, de Génie des Procédés et de Génie Pharmaceutique (LAGEPP) laboratory at the University Claude Bernard Lyon 1, in collaboration with the Ingénierie des Matériaux Polymères (IMP) laboratory and with the C3D platform of the Centre de Recherche en Cancérologie de Lyon (CRCL). Part of the work was carried out at the University of Algarve in Portugal thanks to the exchange program Partenariat Hubert Curien (PHC) Pessoa Programme of Campus France and Fundação para a Ciência e Tecnologia (FCT): NanoSpeed (N° 42306YB). The research leading to these PhD thesis results has received funding from National Research Agency (ANR) HyDNano project (ANR-18-CE18-0025-01).

This manuscript is based on publications in the format of original research articles and on a review article:

- [A. Rosso](#), V. Andretto, Y. Chevalier, D. Kryza, J. Sidi-Boumedine, A. Grenha, F. Guerreiro, A. Gharsallaoui, A.C. Montembault, L. David, S. Briançon and G. Lollo, Nanocomposite sponges for enhancing intestinal residence time following oral administration, *Journal of Controlled Release* 2020 (submitted)
- [A. Rosso](#), E. Almouazen J. Pontes, M. Leroux, E. Romasko, S. C. Bordes, Azzouz-Maache, I. Coste, R. Touffic, S. Giraud, S. Briançon and G. Lollo, Supersaturable self-microemulsifying delivery systems: an approach to enhance oral bioavailability of benzimidazole anticancer drugs, *Drug Delivery and Translational Research* 2020 (submitted)
- V. Andretto, [A. Rosso](#), S. Briançon and G. Lollo, Nanocomposite systems for precise oral delivery of drugs and biologics, *Drug Delivery and Translational Research* 2020 (submitted)
- J. Bompard, [A. Rosso](#), L. Brizuela, S. Mebarek, L. J. Blum, AM. Trunfio-Sfarghiu, G. Lollo, T. Granjon, A. Girard-Egrot and O. Maniti, Membrane Fluidity as a New Means to Selectively Target Cancer Cells with Fusogenic Lipid Carriers, *Langmuir* 2020, 36, 19, 5134–5144
- [Rosso](#), G. Lollo, Y. Chevalier, N. Troung, C. Bordes, S. Bourgeois, O. Maniti, T. Granjon, P. Dugas, S. Urbaniak, S. Briançon, Development and structural characterization of dried nanoemulsion for oral drug delivery, *Colloids and Surfaces A* 2020, 593, 124614

The work included in this thesis was presented during international and national conferences as oral communications or as posters:

Oral communications

- 4th ChemBioInteract Conference: Innovations in Pharmaceuticals Drug Delivery, Lyon, France. 21-22 Nov 2019. Mucoadhesive chitosan sponges loaded with nanoemulsions for sustained intestinal delivery. [A. Rosso](#), G. Lollo, A. Montembault, Y. Chevalier, L. David, S. Briançon
- 24 Journée Scientifique de l'EDISS, Lyon, France. 9 Oct 2019. Nanocomposite chitosan scaffolds for local sustained intestinal drug delivery. [A. Rosso](#), G. Lollo, A. Montembault, Y. Chevalier, L. David, S. Briançon

Poster presentations

- SFNano C’Nano joint meeting 2019 –Dijon, France. 10-12 Dec 2019. Tailoring structural properties of nanoemulsion-loaded chitosan scaffold for sustained intestinal delivery. [A. Rosso](#), Y. Chevalier, A. Montembault, L. David, S. Briançon, G. Lollo
- Controlled Release Society Annual Meeting & Exposition, Valencia, Spain. 21-24 July 2019. Oral nanoemulsion prepared by phase inversion emulsification: development, optimization and evaluation of freeze drying technology. [A. Rosso](#), G. Lollo, N. Troung, Y. Chevalier, S. Briançon
- Formulation days –, Lyon, France. 10-11 Jan 2019. Rationally designed tacrolimus-loaded nanoemulsion: a novel stable oral drug delivery system. [A. Rosso](#), G. Lollo, N. Troung, Y. Chevalier, S. Briançon
- 23^{ème} Journée Scientifique de l'EDISS –, Villeurbanne, France. 11 Oct 2018. Insights into nanoemulsions: design, morphology and drying study of a novel nanocarrier for lipophilic drug encapsulation. [A. Rosso](#), G. Lollo, N. Troung, Y. Chevalier, S. Briançon

